

AD-A 191 122

①

AFOSR-TR-0210

UNITED STATES AIR FORCE
GRADUATE STUDENT SUMMER SUPPORT PROGRAM
1987
PROGRAM TECHNICAL REPORT
UNIVERSAL ENERGY SYSTEMS, INC.
VOLUME II of II

Program Director, UES
Rodney C. Darrah

Program Manager, AFOSR
Major Richard Kopka

Program Administrator, UES
Susan K. Espy

Submitted to
Air Force Office of Scientific Research
Bolling Air Force Base
Washington, DC

December 1987

DTIC
ELECTE
MAR 01 1988
S H D

DISTRIBUTION STATEMENT A

Approved for public release;
Distribution Unlimited

882 29 174

SS: 10: A-6A

TABLE OF CONTENTS

<u>Section</u>	<u>Page</u>
Preface	i
List of 1987 Graduate Student Participants	ii
Participant Laboratory Assignment	xv
Research Reports	xix



Accession For	
NTIS GRA&I	<input checked="" type="checkbox"/>
DTIC TAB	<input type="checkbox"/>
Unannounced	<input type="checkbox"/>
Justification	
By _____	
Distribution/	
Availability Codes	
Dist	Avail and/or Special
A-1	

REPORT DOCUMENTATION PAGE

Form Approved
OMB No. 0704-0188

1a. REPORT SECURITY CLASSIFICATION		1b. RESTRICTIVE MARKINGS		
2a. SECURITY CLASSIFICATION AUTHORITY		3. DISTRIBUTION/AVAILABILITY OF REPORT Approved for public release; distribution unlimited.		
2b. DECLASSIFICATION/DOWNGRADING SCHEDULE				
4. PERFORMING ORGANIZATION REPORT NUMBER(S)		5. MONITORING ORGANIZATION REPORT NUMBER(S) AFOSR-TR- 88-0210		
6a. NAME OF PERFORMING ORGANIZATION Universal Energy Systems Inc.	6b. OFFICE SYMBOL (if applicable)	7a. NAME OF MONITORING ORGANIZATION AFOSR/XOT		
6c. ADDRESS (City, State, and ZIP Code) 4401 Dayton-Xenia Road Dayton, OH 45432		7b. ADDRESS (City, State, and ZIP Code) Building 410 Bolling AFB DC 20332-6448		
8a. NAME OF FUNDING / SPONSORING ORGANIZATION Same as #7	8b. OFFICE SYMBOL (if applicable)	9. PROCUREMENT INSTRUMENT IDENTIFICATION NUMBER F49620-85-C-0013		
8c. ADDRESS (City, State, and ZIP Code) Same as #7		10. SOURCE OF FUNDING NUMBERS		
		PROGRAM ELEMENT NO. 61102F	PROJECT NO. 3396	TASK NO. D5
11. TITLE (Include Security Classification) USAF Graduate Student Summer Support Program - Volume 2 - 1987				
12. PERSONAL AUTHOR(S) Rodney C. Darrah, Susan K. Espy				
13a. TYPE OF REPORT Annual	13b. TIME COVERED FROM _____ TO _____	14. DATE OF REPORT (Year, Month, Day) December 1987	15. PAGE COUNT	
16. SUPPLEMENTARY NOTATION				
17. COSATI CODES		18. SUBJECT TERMS (Continue on reverse if necessary and identify by block number)		
FIELD	GROUP			SUB-GROUP
19. ABSTRACT (Continue on reverse if necessary and identify by block number) See Attached				
20. DISTRIBUTION/AVAILABILITY OF ABSTRACT <input checked="" type="checkbox"/> UNCLASSIFIED/UNLIMITED <input type="checkbox"/> SAME AS RPT <input type="checkbox"/> DTIC USERS		21. ABSTRACT SECURITY CLASSIFICATION IMC: ASSOFOED		
22a. NAME OF RESPONSIBLE INDIVIDUAL LT. COL. CLAUDE CAVENDER		22b. TELEPHONE (Include Area Code) 202-767-4970	22c. OFFICE SYMBOL XOT	

I. INTRODUCTION

AFOSR-TR. 88-0210

Universal Energy Systems, Inc. (UES) was awarded the United States Air Force Summer Faculty Research Program on August 15, 1984. The contract is funded under the Air Force Systems Command by the Air Force Office of Scientific Research.

The program has been in existence since 1978 and has been conducted by several different contractors. The success of the program is evident from its history of expansion since 1978.

The Summer Faculty Research Program (SFRP) provides opportunities for research in the physical sciences, engineering, life sciences, business, and administrative sciences. The program has been effective in providing basic research opportunities to the faculty of universities, colleges, and technical institutions throughout the United States.

The program is available to faculty members in all academic grades: instructor, assistant professor, professor, department chairman, and research facility directors. It has proven especially beneficial to young faculty members who are starting their academic research programs and to senior faculty members who have spent time in university administration and are desirous of returning to scholarly research programs.

Beginning with the 1982 program, research opportunities were provided for 17 graduate students. The 1982 pilot student program was highly successful and was expanded in 1983 to 53 students; there were 84 graduate students in the 1984 program.

In the previous programs, the graduate students were selected along with their professors to work on the program. Starting with the 1985 program, the graduate students were selected on their own merits. They were assigned to be supervised by either a professor on the program or by an engineer at the Air Force Laboratories participating in the program. There were 92 graduate students selected for the 1985 program.

Again in the 1986 program, the graduate students were selected on their own merits, and assigned to be supervised by either a professor on the program or by an engineer at the participating Air Force Laboratory. There were 100 graduate students selected for the 1986 program.

Follow-on research opportunities have been developed for a large percentage of the participants in the Summer Faculty Research Program in 1979-1983 period through an AFOSR Minigrant Program.

On 1 September 1983, AFOSR replaced the Minigrant Program with a new Research Initiation Program. The Research Initiation Program provides follow-on research awards to home institutions of SFRP participants. Awards were made to approximately 50 researchers in 1983. The awards were for a maximum of \$12,000 and a duration of one year or less. Substantial cost sharing by the schools contributes significantly to the value of the Research Initiation Program. In 1984 there were approximately 80 Research Initiation awards.

PREFACE

U.S. AF

The ~~United States Air Force~~ Graduate Student Summer Support Program (USAF-GSSSP) is conducted under the United States Air Force Summer Faculty Research Program. The program provides funds for selected graduate students to work at an appropriate Air Force Facility with a supervising professor who holds a concurrent Summer Faculty Research Program appointment or with a supervising Air Force Engineer. This is accomplished by the students being selected on a nationally advertised competitive basis for a ten-week assignment during the summer intersession period to perform research at Air Force laboratories/centers. Each assignment is in a subject area and at an Air Force facility mutually agreed upon by the students and the Air Force. In addition to compensation, travel and cost of living allowances are also paid. The USAF-GSSSP is sponsored by the Air Force Office of Scientific Research, Air Force Systems Command, United States Air Force, and is conducted by Universal Energy Systems, Inc.

The specific objectives of the 1987 USAF-GSSSP are:

- (1) To provide a productive means for the graduate students to participate in research at the Air Force Weapons Laboratory;
- (2) To stimulate continuing professional association among the Scholars and their professional peers in the Air Force;
- (3) To further the research objectives of the United States Air Force; *and*
- (4) To enhance the research productivity and capabilities of the graduate students especially as these relate to Air Force technical interests.

During the summer of 1987, 101 graduate students participated. These researchers were assigned to 25 USAF laboratories/centers across the country. This two volume document is a compilation of the final reports written by the assigned students members about their summer research efforts.

LIST OF 1987 GRADUATE STUDENT PARTICIPANTS

NAME/ADDRESS	DEGREE, SPECIALTY, LABORATORY ASSIGNED
Antoinne C. Able Meharry Medical College School of Medicine Nashville TN 37208 (615) 361-5303	<u>Degree:</u> M.S., Biology, 1982 <u>Specialty:</u> Biology <u>Assigned:</u> SAM
Mark T. Anater Dept. of Polymer Science University of Akron Akron, OH 44311 (216) 434-1844	<u>Degree:</u> B.S., Chemistry, 1986 <u>Specialty:</u> Chemistry <u>Assigned:</u> ML
Petar Arsenovic Dept. of Materials Science John Hopkins University Baltimore, MD 21218 (301) 338-8970	<u>Degree:</u> M.S., Mechanical & Aerospace Sciences, 1985 <u>Specialty:</u> Chemistry <u>Assigned:</u> ML
Catherine Aubertin Dept. of Educational Psychology Southern Illinois University Carbondale, IL 62901 (618) 536-7763	<u>Degree:</u> M.S., Environmental Design 1982 <u>Specialty:</u> Environmental Design <u>Assigned:</u> HRL/MO
David R. Bosch Dept. of Mechanical/Aero. Eng. Arizona State University Tempe, AZ 85287 (602) 965-3291	<u>Degree:</u> B.S., Mechanical Engineering 1987 <u>Specialty:</u> Mechanical Engineering <u>Assigned:</u> APL
Steven W. Bucey Dept. of Physics Kent State University Kent, OH 44240 (216) 673-1255	<u>Degree:</u> M.S., Physics, 1986 <u>Specialty:</u> Mechanical Engineering <u>Assigned:</u> ML
John N. Bullock Dept. of Electrical Engineering Univ. of Missouri-Rolla Rolla, MO 65401 (314) 341-3123	<u>Degree:</u> B.S., Electrical Eng., 1987 <u>Specialty:</u> Electrical Engineering <u>Assigned:</u> APL

Robyn A. Butcher
Wright State University
Dept. of Biology
Dayton, OH 45435
(513) 886-1784

Degree: B.S., Biology, 1987
Specialty: Biology
Assigned: AAMRL

Kevin P. Cahill
Dept. of Electrical/Comp. Eng.
University of Cincinnati
Cincinnati, OH 45221
(513) 475-4461

Degree: B.S., Physics, 1987
Specialty: Physics
Assigned: AL

David C. Carpenter
Dept. of Nuclear Engineering
Texas A&M University
College Station, TX 77843
(409) 845-4161

Degree: M.S., Nuclear Eng., 1986
Specialty: Nuclear Engineering
Assigned: WL

Andrew D. Carson
Dept. of Educational Psychology
University of Texas-Austin
Austin, TX 78712-1296
(512) 471-4155

Degree: M.S., Human Development 1986
Specialty: Nuclear Engineering
Assigned: HRL/MO

Kyunam Choi
Dept. of Physics and Astronomy
University of New Mexico
Albuquerque, NM 87131
(505) 277-6317

Degree: M.S., Physics, 1984
Specialty: Physics
Assigned: WL

Otis Cosby Jr.
Meharry Medical College
School of Medicine
Nashville, TN 37208
(615) 321-6413

Degree: B.S., Natural Science, 1983
Specialty: Natural Science
Assigned: SAM

Richard B. Davidson
Dept. of Mathematics
University of Alabama
Birmingham, AL 35205
(215) 934-3720

Degree: B.S., Math & Computer Sci.
1987
Specialty: Mathematics
Assigned: ML

Tamara Della-Rodolfa
Dept. of Psychology
Indiana Univ. of Pennsylvania
Indiana, PA 15705
(412) 357-2426

Degree: B.S., Psychology, 1986
Specialty: Psychology
Assigned: AAMRL

Steve Dixon
Dept. of Chemistry
Wright State University
Dayton, OH 45435
(513) 873-2855

Degree: B.S., Chemistry, 1986
Specialty: Chemistry
Assigned: AAMRL

James Drakes
Dept. of Physics
Tennessee Space Institute
Tullahoma, TN 37388
(615) 455-0631

Degree: B.S., Physics, 1987
Specialty: Physics
Assigned: AEDC

Susan M. Dumbacher
Dept. of Aerospace Eng.
University of Cincinnati
Cincinnati, OH 45219
(513) 621-0095

Degree: B.S., Aerospace Engr., 1986
Specialty: Aerospace Engineering
Assigned: FDL

Donna N. Edwards
School of Pharmacy
Florida A&M University
Tallahassee, FL 32307
(904) 599-3302

Degree: M.S., Chemistry, 1982
Specialty: Chemistry
Assigned: OEHL

Kathy S. Enlow
Dept. of Health, Physical Ed.
University of Alabama
Tuscaloosa, AL 35487-1967
(205) 348-6075

Degree: B.S., Community Health Care
1985
Specialty: Health Care
Assigned: SAM

Thomas Enneking
Dept. of Civil Engineering
University of Notre Dame
Notre Dame, IN 46556
(219) 283-1497

Degree: M.S., Civil Eng., 1978
Specialty: Civil Engineering
Assigned: FDL

Gloria Fisher
Dept. of Psychology
University of Mississippi
University, MS 38677
(601) 232-5077

Degree: M.S., Industrial/Org. Psych.
1987
Specialty: Industrial Psychology
Assigned: DEOMI

Inge Ford-Belgrave
Texas Southern University
University, MS 38677
(601) 232-5077

Degree: B.S., Biology, 1984
Specialty: Environmental Pollutants
Assigned: OEHL

Beverley Gable
Dept. of Psychology
Ohio University
Lancaster, OH 43130
(614) 654-0602

Degree: M.S., Psychology, 1987
Specialty: Psychology
Assigned: AAMRL

Deborah Gagnon
Dept. of Psychology
State University of New York
Amherst, NY 14260
(716) 689-7553

Degree: B.S., Psychology, 1987
Specialty: Psychology
Assigned: AAMRL

Edward Gellenbeck
Dept. of Computer Science
Oregon State University
Corvallis, OR 97330
(503) 752-1977

Degree: M.S., Computer Science, 1985
Specialty: Computer Science
Assigned: SAM

James A. Gerald
Dept. of Electrical Eng.
University of Mississippi
University, MS 38677
(601) 232-3752

Degree: B.S., Electrical Engr., 1987
Specialty: Electrical Engineering
Assigned: WL

Maurice Gilbert
Dept. of Medicine
Meharry Medical College
Nashville, TN 37208
(615) 327-6111

Degree: M.S., Biomedical Sci., 1983
Specialty: Biomedical Sciences
Assigned: SAM

Jeffrey Girard
Dept. of Mechanical Eng.
Washington State University
Pullamn WA 99164
(509) 335-8654

Degree: M.S., Mechanical Engr., 1982
Specialty: Mechanical Engineering
Assigned: ESC

Beverly Girten
Dept. of Exercise Physiology
Ohio State University
Columbus, OH 43210
(614) 292-1223

Degree: M.S., Exercise Physiology
1983
Specialty: Exercise Physiology
Assigned: AAMRL

Laura Giusti
Dept. of Psychology
San Diego State University
San Diego, CA 92182
(412) 833-3912

Degree: B.S., Psychology, 1986
Specialty: Psychology
Assigned: AAMRL

Nadia Greenridge
Dept. of Anthropology
New York University
New York City, NY 07631
(212) 598-3258

Degree: M.S., Anthropology, 1984
Specialty: Anthropology
Assigned: AAMRL

Thomas Harkins
Dept. of Mechanical Eng.
Louisiana State University
Baton Rouge, LA 70808
(505) 766-3671

Degree: B.S., Mech. Engr., 1986
Specialty: Mechanical Engineering
Assigned: AD

Deborah Hollenbach
Dept. of Biology
University of Dayton
Dayton, OH 45432
(513) 259-2135

Degree: B.S., Biology, 1986
Specialty: Biology
Assigned: AAMRL

Adrienne Hollis
Dept. of Biomedical Sciences
Meharry Medical College
Nashville, TN 37208
(615) 327-6221

Degree: B.S., Biology, 1986
Specialty: Biology
Assigned: SAM

Stephen Huyer
Dept. of Aerospace Engineering
University of Colorado
Boulder, CO 80309
(303) 444-63-68

Degree: B.S., Aerospace Engr., 1986
Specialty: Aerospace Engineering
Assigned: FJSRL

David James
Dept. of Math
Eastern Illinois University
Charleston, IL 61920
(217) 581-2028

Degree: B.S., Computer Sci., 1985
Specialty: Computer Science
Assigned: AEDC

George James, III
Dept. of Aerospace Eng.
Texas A&M University
College Station, TX 77843-3141
(409) 845-3947

Degree: M.S., Aerospace Engr., 1986
Specialty: Aerospace Engineering
Assigned: RPL

Stephen R. Jenei
Dept. of Biology
University of Dayton
Dayton, OH 45469-0001
(513) 229-2135

Degree: B.S., Biology, 1986
Specialty: Biology
Assigned: AAMRL

<p>Kenneth Jenks Dept. of Aero/Astronautical Eng. University of Illinois Urbana, IL 61801 (217) 244-0743</p>	<p><u>Degree:</u> B.S., Computer Sci., 1985 <u>Specialty:</u> Computer Science <u>Assigned:</u> WL</p>
<p>Michele Johnson School of Electrical Engr. Cornell University Ithaca, NY 14853 (607) 255-4304</p>	<p><u>Degree:</u> B.S., Electr. Eng., 1984 <u>Specialty:</u> Electrical Engineering <u>Assigned:</u> RADC</p>
<p>Scharine Kirshoff Dept. of Geology University of Alaska Fairbanks, AL 99503 (907) 474-7274</p>	<p><u>Degree:</u> M.S., Geology, 1986 <u>Specialty:</u> Geology <u>Assigned:</u> AFGL</p>
<p>Gary Lake Dept. of Industrial Eng. University of Houston Houston, TX 77035 (713) 749-2538</p>	<p><u>Degree:</u> M.S., Industrial Engr., 1985 <u>Specialty:</u> Industrial Engineering <u>Assigned:</u> OEHL</p>
<p>David Landis Dept. of Civil Engineering Auburn University Auburn, AL 36849 (205) 826-4320</p>	<p><u>Degree:</u> B.S., Civil Eng., 1986 <u>Specialty:</u> Civil Engineering <u>Assigned:</u> ESC</p>
<p>Sharon Landis Dept. of Computer Sci./Eng. Auburn University Auburn, AL 36849 (205) 826-4330</p>	<p><u>Degree:</u> B.S., Computer Engr., 1986 <u>Specialty:</u> Computer Engineering <u>Assigned:</u> ESC</p>
<p>Craig Langenfeld Dept. of Mechanical Eng. Ohio State University Columbus, OH 43210 (614) 268-2176</p>	<p><u>Degree:</u> B.S., Mechanical Engr., 1986 <u>Specialty:</u> Mechanical Engineering <u>Assigned:</u> APL</p>
<p>Christopher Leger Dept. of Mechanical Eng. Louisiana State University Baton Rouge, LA 70893 (504) 334-2453</p>	<p><u>Degree:</u> B.S., Mechanical Engr., 1986 <u>Specialty:</u> Mechanical Engineering <u>Assigned:</u> AD</p>

Bruce Liby
Dept. of Physics/Astronomy
University of New Mexico
Albuquerque, NM 87107
(505) 277-2616

Degree: M.S., Physics, 1984
Specialty: Physics
Assigned: WL

A. Jeannine Lincoln
Dept. of Biomedical Sciences
Wright State University
Dayton, OH 45435
(513) 873-2504

Degree: B.S., Biochemistry, 1987
Specialty: Biochemistry
Assigned: AAMRL

Yolanda Malone
School of Medicine
Meharry Medical College
Nashville, TN 37208
(615) 321-0939

Degree: B.S., Chemistry, 1985
Specialty: Chemistry
Assigned: SAM

Randal Mandock
Dept. of Mechanical Eng.
Georgia Institute of Tech.
Atlanta, GA 30332
(404) 894-3776

Degree: M.S., Atmospheric Sci., 1986
Specialty: Atmospheric Sciences
Assigned: OEHL

James W. Mattern
Dept. of Physics/Electr. Eng.
Oregon Graduate Center
Beaverton, OR 97005
(503) 690-1130

Degree: B.S., Computer Engr., 1986
Specialty: Computer Engineering
Assigned: AD

Matthew McBeth
Dept. of Elect./Biomedical Eng.
Vanderbilt University
Nashville, TN 37235
(615) 322-2767

Degree: B.S., Computer Sci., 1986
Specialty: Computer Science
Assigned: AEDC

Jennifer B. McGovern
Dept. of Psychology
University of Florida
Gainesville, FL 32611
(904) 392-0605

Degree: M.S., Psychology, 1987
Specialty: Psychology
Assigned: SAM

Roland Medellin
Dept. of Biology
Brown University
Providence, RI 02912
(401) 273-7646

Degree: B.S., Biology, 1987
Specialty: Biology
Assigned: OEHL

Otto M. Melko
Dept. of Mathematics
University of California
Santa Cruz, CA 95064
(408) 429-2085

Degree: M.S., Math, 1982
Specialty: Mathematics
Assigned: AD

Ethan S. Merrill
Dept. of Engineering
University of Mississippi
Greenville, MS 38701
(904) 283-2942

Degree: B.S., Civil Engr.
Specialty: Civil Engineering
Assigned: ESC

Veronica Minsky
Dept. of Computer Science
Middle Tennessee State Univ.
Murfreesboro, TN 37217
(615) 898-2669

Degree: B.S., Linguistics, 1978
Specialty: Linguistics
Assigned: AEDC

Frank W. Moore
Dept. of Computer Sci./Eng.
Wright State University
Dayton, OH 45435
(513) 873-3515

Degree: B.S., Computer Engr., 1986
Specialty: Computer Engineering
Assigned: AL

Stephen Morgan
Dept. of Psychology
Montclair State College
Upper Montclair, NJ 07043
(201) 893-4000

Degree: B.S., Psychology, 1984
Specialty: Psychology
Assigned: HRL/LR

Lisa Morris
Biology Department
University of Dayton
Physiology Laboratory
300 College Park Avenue
Dayton, OH 45469-0001
(513) 229-2135

Degree: B.S., Biology, 1985
Specialty: Physiology
Assigned: AAMRL

Conrad Murray
School of Medicine
Meharry Medical College
Nashville, TN 37208
(615) 321-5837

Degree: M.S., Biochemistry, 1986
Specialty: Biochemistry
Assigned: SAM

Steven Naber
Dept. of Statistics
Ohio State University
Columbus, OH 43201
(614) 421-6647

Degree: M.S., Statistics, 1984
Specialty: Statistics
Assigned: OEHL

Jerome Nadel
Dept. of Psychology
University of Kansas
Manhattan, KS 66506
(913) 532-6850

Degree: B.S., Psychology, 1980
Specialty: Psychology
Assigned: HRL/OT

Victoria Nasman
Dept. of Psychology
Northwestern University
Evanston, IL 60201
(312) 491-7643

Degree: M.S., Psychology, 1984
Specialty: Psychology
Assigned: SAM

Mark Neumeier
Dept. of Mechanical Systems
Wright State University
Dayton, OH 45435
(513) 873-2476

Degree: M.S., Psychology, 1984
Specialty: Psychology
Assigned: SAM

Khan Nguyen
Dept. of Mechanical Eng.
University of Chicago-Illinois
Chicago, IL 60607
(312) 849-1362

Degree: M.S., Mathematics, 1984
Specialty: Mathematics
Assigned: APL

Wendy Nguyen
Dept. of Biology
Trinity University
715 Stadium Drive
San Antonio, TX 78284
(512) 736-7231

Degree: B.A., Biology, 1987
Specialty: Biology
Assigned: SAM

Bernadette Njoku
Dept. of Chemistry
Meharry Medical College
Nashville, TN 37208
(615) 327-4098

Degree: B.S., Chemistry, 1982
Specialty: Chemistry
Assigned: SAM

Charles Norfleet
Dept. of Civil Eng./Mechanics
Southern Illinois University
Carbondale, IL 62901
(618) 536-2368

Degree: B.S., Engineering Mechanics,
1986
Specialty: Engineering Mechanics
Assigned: ML

Douglas Phillipott
Dept. of Management
Auburn University
Auburn, AL 36830
(205) 887-3889

Degree: B.S., Chemical Engr., 1984
Specialty: Chemical Engineering
Assigned: LMC

Susan Poppens
Dept. of Computer Science
University of Missouri
Rolla, MO 65401
(314) 341-4491

Degree: B.S., Math/Comp. Sci., 1985
Specialty: Math/Computer Science
Assigned: ESMC

Mark Prazak
Dept. of Chemistry
Wright State University
Dayton, OH 45371
(513) 873-2855

Degree: B.S., Chemistry, 1986
Specialty: Chemistry
Assigned: ML

Mark Reavis
Aerospace Dept.
University of Colorado
College of Engineering
Campus Box 429
Boulder, CO 80309

Degree: B.S., Aerospace, 1987
Specialty: Aerospace
Assigned: FJSRL

Peter Riddiford
Dept. of Electrical Eng.
Ohio State University
Columbus, OH 43210
(614) 292-1752

Degree: B.S., Electrical Eng., 1987
Specialty: Electrical Engineering
Assigned: FDL

Keith Riese
Dept. of Electrical Eng.
University of Nebraska
Lincoln, NE 68588-0511
(402) 472-3771

Degree: M.S., Electrical Eng., 1972
Specialty: Electrical Engineering
Assigned: SAM

Mary Robinson
Dept. of Health
University of Alabama
Scottsboro, AL 35768
(205) 259-5342

Degree: B.S., Sociology, 1976
Specialty: Sociology/Psychology
Assigned: SAM

Filiberto Santiago
Dept. of Mechanical Eng.
University of Puerto Rico
Mayaguez, PR 00708
(809) 834-4040

Degree: M.S., Mechanical Eng., 1987
Specialty: Mechanical Engineering
Assigned: AEDC

Gregory Schoeppner
Dept. of Civil Engineering
Ohio State University
Columbus, OH 43210
(614) 436-3392

Degree: M.S., Civil Engr., 1984
Specialty: Civil Engineering
Assigned: FDL

James Seaba
Dept. of Mechanical Eng.
University of Iowa
Iowa City, IA 52242
(319) 335-5681

Degree: M.S., Mechanical Engr., 1986
Specialty: Mechanical Engineering
Assigned: APL

Jon Shupe
Dept. of Mechanical Eng.
University of Houston
Houston, TX 77004
(713) 749-7497

Degree: M.S., Mechanical Engr., 1985
Specialty: Mechanical Engineering
Assigned: ML

Christopher Sierra
Dept. of Mechanical Eng.
University of Iowa
Iowa City, IA 52241
(319) 337-6205

Degree: B.S., Mechanical Engr., 1986
Specialty: Mechanical Engineering
Assigned: FDL

Gregory Sloan
Dept. of Physics/Astronomy
University of Wyoming
Laramie, WY 82071
(307) 766-6150

Degree: B.S., Physics/Astronomy 1985
Specialty: Physics/Astronomy
Assigned: AFGL

Elisabeth Smela
Dept. of Electrical Eng.
University of Pennsylvania
Philadelphia, PA 19104
(215) 898-8548

Degree: B.S., Physics, 1985
Specialty: Physics
Assigned: ML

Rita Smith
Dept. of Mechanical Eng.
University of New Mexico
Albuquerque, NM 87111
(505) 275-2061

Degree: B.S., Mechanical Engr., 1979
Specialty: Mechanical Engineering
Assigned: WL

Brian Spielbusch
Dept. of Electrical Eng.
University of Missouri
Independence, MO 64050
(816) 476-1250

Degree: B.S., Electrical Engr., 1985
Specialty: Electrical Engineering
Assigned: WL

Louise Stark
Dept. of Computer Engineering
University of South Florida
Tampa, FL 33612
(813) 971-9625

Degree: B.S., Computer Engr., 1986
Specialty: Computer Engineering
Assigned: RADC

Steven Steinsaltz
Dept. of Math
John Hopkins University
Baltimore, MD 21218
(301) 338-8000

Degree: M.S., Mathematics, 1985
Specialty: Mathematics
Assigned: RADC

John Stewman
Dept. of Computer Sci./Eng.
University of South Florida
St. Petersburg, FL 33702
(813) 577-9029

Degree: B.S., Computer Engr., 1986
Specialty: History
Assigned: RADC

Tod Strohmayer
Dept. of Physics/Astronomy
University of Rochester
Rochester, NY 14608
(716) 325-3019

Degree: M.S., Physics, 1987
Specialty: Physics/Astronomy
Assigned: AFGL

Teresa Taylor
Dept. of Civil & Environ. Eng.
University of Washington
Pullman, WA 99164-2902
(509) 335-8546

Degree: M.S., Geological Engr., 1984
Specialty: Geological Engineering
Assigned: ESC

Tien Tran
Dept. of Electr. & Comp. Eng.
University of Cincinnati
Cincinnati, OH 45221
(513) 851-7350

Degree: B.S., Electrical Engr., 1980
Specialty: Electrical Engineering
Assigned: RADC

John Usher
Dept. of Industrial Eng.
Louisiana State University
Baton Rouge, LA 70816
(504) 388-5112

Degree: M.S., Industrial Engr., 1986
Specialty: Chemical Engineering
Assigned: ML

Pretta VanDible
Dept. of Chemical Engineering
Prairie View A&M University
Houston, TX 77446
(713) 857-2827

Degree: M.S., Chemical Engr., 1986
Specialty: Chemical Engineering
Assigned: RPL

William VanValkenburgh
Dept. of Computer Science
Western Michigan University
Kalamazoo, MI 49008
(616) 385-5961

Degree: B.S., Computer Science, 1986
Specialty: Computer Science
Assigned: AL

Joseph Varga
Dept. of Physics
Kent State University
Kent, OH 44242
(216) 672-2246

Degree: M.S., Physics, 1978
Specialty: Physics
Assigned: ML

Deborah Vezie
Dept. of Chemical, Biomedical
Materials Engineering
University of Arizona
Tempe, AZ 85281
(602) 784-8221

Degree: B.S., Biomedical Engr., 1987
Specialty: Biomedical Engineering
Assigned: ML

James Wade
Dept. of Astronautical Eng.
University of Illinois
Urbana, IL 61801
(217) 244-0743

Degree: B.S., Physics, 1986
Specialty: Astronautical Engineering
Assigned: WL

Randall Westhoff
Dept. of Mathematics
Eastern Washington University
Cheney, WA 99004
(509) 359-6225

Degree: B.S., Mathematics, 1986
Specialty: Mathematics
Assigned: AD

Terri Wilkerson
School of Medicine
Wright State University
Dayton, OH 45324
(513) 873-2934

Degree: B.S., Electrical Eng., 1985
Specialty: Electrical Engineering
Assigned: AAMRL

Douglas Wise
Dept. of Mechanical Eng.
University of Dayton
Oakwood, OH 45419
(513) 298-9073

Degree: B.S., Mechanical Engr., 1986
Specialty: Mechanical Engineering
Assigned: ML

PARTICIPANT LABORATORY ASSIGNMENT

C. PARTICIPANT LABORATORY ASSIGNMENT (Page 1)

1987 USAF/UES GRADUATE STUDENT SUMMER SUPPORT PROGRAM

AERO PROPULSION LABORATORY (AFWAL/APL)
(Wright-Patterson Air Force Base)

- | | |
|------------------------|-------------------|
| 1. David R. Bosch | 4. Khan V. Nguyen |
| 2. John N. Bullock | 5. James P. Seaba |
| 3. Craig A. Langenfeld | |

ARMAMENT LABORATORY (AD)
(Eglin Air Force Base)

- | | |
|----------------------|------------------------|
| 1. Thomas K. Harkins | 3. Otto M. Melko |
| 2. Christopher Leger | 4. Randall F. Westhoff |

ARMSTRONG AEROSPACE MEDICAL RESEARCH LABORATORY (AAMRL)
(Wright-Patterson Air Force Base)

- | | |
|-------------------------|--------------------------|
| 1. Robyn A. Butcher | 8. Nadia C. Greenidge |
| 2. Tamara Della-Rodolfa | 9. Deborah E. Hollenbach |
| 3. Steve L. Dixon | 10. Stephen R. Jenei |
| 4. Beverley A. Gable | 11. A. Jeannine Lincoln |
| 5. Deborah Gagnon | 12. Lisa M. Morris |
| 6. Beverly E. Girten | 13. Terri L. Wilkerson |
| 7. Laura M. Giusti | |

ARNOLD ENGINEERING DEVELOPMENT CENTER (AEDC)
(Arnold Air Force Station)

- | | |
|----------------------|-----------------------|
| 1. James A. Drakes | 4. Veronica L. Minsky |
| 2. David L. James | 5. Filiberto Santiago |
| 3. Matthew B. McBeth | |

AVIONICS LABORATORY (AFWAL/AL)
(Wright-Patterson Air Force Base)

- | | |
|---------------------|------------------------------|
| 1. Kevin Cahill | 3. Frank W. Moore |
| 2. James W. Mattern | 4. William B. VanValkenburgh |

DEFENSE EQUAL OPPORTUNITY MANAGEMENT INSTITUTE (DEOMI)
(Patrick Air Force Base)

1. Gloria Z. Fisher

EASTERN SPACE AND MISSILE CENTER (ESMC)
(Patrick Air Force Base)

1. Susan A. Poppens

ENGINEERING SERVICE CENTER (ESC)
(Tyndall Air Force Base)

- | | |
|---------------------|---------------------|
| 1. Jeffrey Girard | 4. Ethan S. Merrill |
| 2. David W. Landis | 5. Teresa A. Taylor |
| 3. Sharon K. Landis | |

C. PARTICIPANT LABORATORY ASSIGNMENT (Page 2)

FLIGHT DYNAMICS LABORATORY (AFWAL/FDL)
(Wright-Patterson Air Force Base)

- | | |
|-----------------------|--------------------------|
| 1. Susan M. Dumbacher | 4. Bryan P. Riddiford |
| 2. Thomas J. Enneking | 5. Gregory A. Schoeppner |
| 3. Mark E. Neumeier | 6. Christopher Sierra |

FRANK J. SEILER RESEARCH LABORATORY (FJSRL)
(USAF Academy)

1. Stephen A. Huyer
2. Mark A. Reavis

GEOPHYSICS LABORATORY (AFGL)
(Hanscom Air Force Base)

1. Scharine Kirchoff
2. Gregory C. Sloan
3. Tod E. Strohmayer

HUMAN RESOURCES LABORATORY/LR (HRL/LR)
(Wright-Patterson Air Force Base)

1. Stephen Morgan

HUMAN RESOURCES LABORATORY/MO (HRL/MO)
(Brooks Air Force Base)

1. Catherine A. Aubertin
2. Andrew D. Carson

HUMAN RESOURCES LABORATORY/OT (HRL/OT)
(Williams Air Force Base)

1. Jerome I. Nadel

LOGISTICS MANAGEMENT CENTER (LMC)
(Gunter Air Force Station)

1. Douglas E. Phillipott

MATERIALS LABORATORY (AFWAL/ML)
(Wright-Patterson Air Force Base)

- | | |
|------------------------|----------------------|
| 1. Mark T. Anater | 7. Jon A. Shupe |
| 2. Petar Arsenovic | 8. Elisabeth Smela |
| 3. Steven W. Bucey | 9. John M. Usher |
| 4. Richard B. Davidson | 10. Joseph C. Varga |
| 5. Charles W. Norfleet | 11. Deborah L. Vezie |
| 6. Mark Prazak | 12. Douglas L. Wise |

OCCUPATIONAL AND ENVIRONMENT HEALTH LABORATORY (OEHL)
(Brooks Air Force Base)

- | | |
|--------------------------|-----------------------|
| 1. Donna N. Edwards | 4. Randal L. Mandock |
| 2. Inge B. Ford-Belgrave | 5. Roland A. Medellin |
| 3. Gary F. Lake | 6. Steven J. Naber |

C. PARTICIPANT LABORATORY ASSIGNMENT (Page 3)

ROCKET PROPULSION LABORATORY (RPL)
(Edwards Air Force Base)

1. George H. James, III
2. Pretta L. VanDible

ROME AIR DEVELOPMENT CENTER (RADC)
(Griffiss Air Force Base)

1. Michele E. Johnson
2. Louise Stark
3. Steven J. Steinsaltz
4. John H. Stewman
5. Tien N. Tran

SCHOOL OF AEROSPACE MEDICINE (SAM)
(Brooks Air Force Base)

1. Antoine C. Able
2. Otis Cosby, Jr.
3. Kathy S. Enlow
4. Edward M. Gellenbeck
5. Maurice B. Gilbert
6. Adrienne L. Hollis
7. Yolanda A. Malone
8. Jennifer B. McGovern
9. Conrad R. Murray
10. Victoria T. Nasman
11. Wendy T. Nguyen
12. Bernadette Patricia Njoku
13. Keith A. Riese
14. Mary C. Robinson

WEAPONS LABORATORY (WL)
(Kirtland Air Force Base)

1. David C. Carpenter
2. Kyunam Choi
3. James A. Gerald
4. Kenneth C. Jenks
5. Bruce Liby
6. Rita Smith
7. Brian K. Spielbusch
8. James W. Wade

RESEARCH REPORTS

RESEARCH REPORTS

1987 GRADUATE STUDENT SUMMER SUPPORT PROGRAM

<u>Technical Report Number</u>	<u>Title</u>	<u>Graduate Researcher</u>
Volume I		
1	Effect of Repeated Low Dose Soman On Acetylcholinesterase Activity *** Same Report as Prof. Maleque ***	Antoinne C. Able
2	Synthesis of an Aromatic Heterocyclic Terphenyl Monomer	Mark T. Anatar
3	Characterization of Graphite Fibers by X-ray Diffraction	Petar Arsenovic
4	An Eight-Domain Framework for Understanding Intelligence and Predicting Intelligent Performance ***Same Report as Prof. Dillon***	Catherine A. Aubertin
5	Configuration Factors for Spacecraft/Expansible Radiator Interaction	David R. Bosch
6	Computer Evaluation of Ion-Implanted Dopant Profile Evolution During Annealing	Steven W. Bucey
7	The Interface Contribution to GaAs/Ge Heterojunction Solar Cell Efficiency ***Same Report as Prof. Wu***	John N. Bullock
8	Isolation of Osteogenic Cells From The Trauma-Activated Periosteum	Robyn A. Butcher
9	A Test Chip for Evaluation of MBE Epitaxial Layers for Novel Device Applications ***Same Report as Prof. Roenker***	Kevin Cahill
10	Preliminary Thermal Analysis of a Bimodal Nuclear Rocket Core	David C. Carpenter
11	Air Force Officer Selection Revisited: Entertaining The Possibilities for Improvement ***Same Report as Dr. Appel***	Andrew D. Carson

- | | | |
|----|--|-----------------------|
| 12 | Construction of a Phase Conjugate Laser Resonator Using Brillouin Enhanced Four Wave Mixing | Kyunam Choi |
| 13 | Effect of Repeated Low Dose Soman On Acetylcholinesteease Activity
Same Report as Prof. Maleque | Otis Cosby, Jr. |
| 14 | Ten Weeks of Literature Searches and Copying | Richard B. Davidson |
| 15 | Ambiguity and Probabilistic Inference in a Missile Warning Officer Task
Same Report as Prof. Robertson | Tamara Della-Rodolfa |
| 16 | Modeling Rates of Halocarbon Metabolism (VMAX) Using Quantitative Structure-Activity Relationships (QSAR) | Steve L. Dixon |
| 17 | Directed Motion Doppler Shift Effects on Mitric Oxide (0,0) Gamma Band Resonance Absorption | James A. Drakes |
| 18 | Preliminary Applications of Decentralized Estimation to Large Flexible Space Structures | Susan M. Dumbacher |
| 19 | Disposal of Chemotherapeutic Wastes
Same Report as Dr. Masingale | Donna N. Edwards |
| 20 | Validity of Heat Index as Indicator of Level of Heat Storage for Personnel Wearing Protective Clothing in Hot Environments | Kathy S. Enlow |
| 21 | Investigation into the Applicability of Fracture Mechanics Techniques to Aircraft Wheel Life Studies | Thomas J. Enneking |
| 22 | Construction and Preliminary Validation of an Equal Opportunity Climate Assessment Instrument
Same Report as Prof. Landis | Gloria Z. Fisher |
| 23 | An Analysis of the Mutagenicity of Beryllium Compounds Using the Ames Test | Inge B. Ford-Belgrave |
| 24 | The Effects of High Noise Levels on the Acoustic-Phonetic Structure of Speech: A Preliminary Investigation | Beverley A. Gable |

25	The Effect of Attentional Focus Level on Task Performance Utilizing Information From Different Stimulus Structure Levels	Deborah Gagnon
26	Providing On-Line Guidance To Computer Users	Edward M. Gellenbeck
27	Mode Extraction From an Electromagnetic Slow Wave System	James A. Gerald
28	Mesopic Visual Performance With and Without Glare in Contact Lense Wearers	Maurice B. Gilbert
29	Ground Run-Up Afterburner Detection and Noise Suppression	Jeffrey Girard
30	Alterations of Segmental Volume During Orthostatic Stress in Nonhuman Primates	Beverly E. Girten
31	Designing Simulator Tasks to Study the High Speed, Low Altitude Environment	Laura M. Giusti
32	A Comparative Study of the Thoraco-Lumbar Transition Vertebrae In MACACA Mulatta and PAPIO Anubis	Nadia C. Greenidge
33	Six Degree of Freedom Simulation Computer Program for Aeroelastic Free-Flight Projectiles	Thomas K. Harkins
34	Sustained Delivery of Volatile Chemicals By Means of Ceramics ***Same Report as Dr. Bajpai***	Deborah E. Hollenbach
35	The Effects of Hyperbaric Oxygen and Antioxident Deficiencies on Rat Retinal Ultrastructure	Adrienne L. Hollis
36	A Comparative Study of Differing Vortex Structures Arising in Unsteady Separated Flows	Stephen A. Huyer
37	Perturbed Functional Iteration Applied to the Navier-Stokes Equations	David L. James
38	An Optical Sensor System for Monitoring Structural Dynamics with Applications to System Identification	George H. James, III

39	Delivery of Inhibin by ALCAP Drug Delivery Capsules	Stephen R. Jenei
40	No Report Submitted	Kenneth C. Jenks
41	A System to Investigate Synthesized Voice Feedback in Man-Machine Interfaces	Michele E. Johnson
42	A Study of Small, Shallow Earthquakes and Quarry Blasts in Healy, Alaska	Scharine Kirchoff
43	A Study of Service Demand Distribution and Task Organization for the Analysis of Environmental Samples and Associated Support Services at the USAF Occupational and Environmental Health Laboratory - Brooks AFB, San Antonio, TX ***Same Report as Dr. Deal***	Gary F. Lake
44	Wave Propagation in Layered Structures	David W. Landis
45	Installation of the Adina FEM Computer Programs	Sharon K. Landis
46	Experimental Study of Isothermal Flows in a Dump Combustor	Craig A. Langenfeld
47	A Computer Simulation of a Plasma Armature Railgun	Christopher Leger
48	Investigation of Laser Diode Coupling Using Nonlinear Optics	Bruce Liby
49	Isolation of Osteogenic Cells From The Trauma-Activated Periosteum	A. Jeannine Lincoln
50	The Effects of Cataract Surgery on Pupillary Response	Yolanda A. Malone
51	Liquid Scintillation Counting with the Packard 1500 Analyzer	Randal L. Mandock
52	De-embedding S-parameter Measurements Using TSD Technique	James W. Mattern
53	An Expert System for Diagnosis and Repair of Analog Circuits	Matthew B. McBeth

Volume II

- | | | |
|----|---|----------------------|
| 54 | Physiological Monitoring Methodology in the USAFSAM Centrifuge | Jennifer B. McGovern |
| 55 | Methods of Quantifying and Enhancing Reactive Oxygen Species Production | Roland A. Medellin |
| 56 | Applications of Differential Geometry to the Shape Analysis of Gray-Value Images | Otto M. Melko |
| 57 | Ozonation of Firefighter Training Facility Wastewater and its Effect on Biodegradation
Same Report as Dr. Truax | Ethan S. Merrill |
| 58 | The Feasibility of a Laboratory Information Management System for the Analytical Chemistry Laboratory | Veronica L. Minsky |
| 59 | Investigation of the Potential Impact of New Photonic Materials on Optical Processing Systems | Frank W. Moore |
| 60 | A Review of Workload Measurement in Relation to Verbal Comprehension | Stephen Morgan |
| 61 | Development of a Long Term Solvent Delivery System | Lisa M. Morris |
| 62 | A New Sensitive Fluorometric Method for the Analysis of Submicrogram Quantities of Cholesterol
****Same Report as Prof. Price*** | Conrad R. Murray |
| 63 | Model-free Statistical Analyses of Contaminated Ground Water
Same Report as Prof. Verducci | Steven J. Naber |
| 64 | A Human Factors Evaluation of the Advanced Visual Technology System (AVTS) Eye Tracking Oculometer | Jerome I. Nadel |
| 65 | The Effects of Increased Cognitive Demands on Autonomic Self-Regulation: An Indicator of Parallel Processing in the Brain | Victoria T. Nasman |
| 66 | No Report Submitted | Mark E. Neumeier |

- | | | |
|----|---|-----------------------|
| 67 | Vaporization Behavior of Multicomponent Fuel Droplets in a Hot Air Stream
Same Report as Dr. Aggarwal | Khan V. Nguyen |
| 68 | Growth Curve and Phototaxis Assays of Axenic Chlamydomonas reinhardtii 125 | Wendy T. Nguyen |
| 69 | Microesotropia Patients Perform Well as Military Jet Pilots | Bernadette P. Njoku |
| 70 | Determination of Lumped-Mass Thermal Properties Associated with Autoclave Curing of Graphite/Epoxy Composites | Charles W. Norfleet |
| 71 | Equitable Safety Stocks for USAF Consumable Items | Douglas E. Phillpott |
| 72 | Investigation of Expert System Design Approaches for Electronic Design Environments | Susan A. Poppens |
| 73 | Thermal Stability Characteristics of a Nonflammable Chlorotrifluorethylene CTFE Base Stock Fluid | Mark Prazak |
| 74 | Control and Use of Unsteady Flows: Insect Use of Various Wing Kinematics and Related Pressure Measurements Using a Pitching Airfoil | Mark Reavis |
| 75 | Aircraft Refueling Demonstrator Using a Microbot Alpha II Robot | Bryan P. Riddiford |
| 76 | Influence of Moving Visual Environment on Saccadic Eye Movements and Fixation | Keith A. Riese |
| 77 | Thermal Stress and its Effects on Fine Motor Skill and Decoding Tasks | Mary C. Robinson |
| 78 | Design of a Mechanism to Control Wind Tunnel Turbulence | Filiberto Santiago |
| 79 | Low Velocity Impact of Graphite/Epoxy Plates
Same Report as Prof. Wolfe | Gregory A. Schoeppner |
| 80 | Experimental Research of Combustion Systems | James P. Seaba |
| 81 | The Integration of Decision Support Problems into Feature Modeling Based Design | Jon A. Shupe |

82	Optimal Control of the Wing Rock Phenomenon	Christopher Sierra
83	Calibration and Data Reduction Techniques for the AFGL Infrared Array Spectrometer	Gregory C. Sloan
84	Thermal conductivity of isotopically pure semiconductors, superlattices, semiconductor alloys, and semiconductors as a function of temperatures; control of the segregation coefficient in LEC crystal growth; and photo-Hall measurements of GaAs	Elisabeth Smela
85	Predicting Optical Degradation of a Laser Beam Through a Turbulent Shear Layer	Rita Smith
86	Experimental Verification of Imaging Correlography ***Same Report as Dr. Knopp***	Brian K. Spielbusch
87	An Aspect Graph-Based Control Strategy for 3-D Object Recognition	Louise Stark
88	Linear Programming for Air Force Decision Aiding	Steven J. Steinsaltz
89	Creating Aspect Graphs for Use in Object Recognition	John H. Stewman
90	Analysis of Emission Features in IRAS LRS Spectra	Tod E. Strohmayer
91	Centrifuge Modeling of Projectile Penetration in Dry, Granular Soil	Teresa A. Taylor
92	Optical Interconnections for Digital Image Coding	Tien N. Tran
93	An Investigation of Performance Improvement in Knowledge-Based Control Systems	John M. Usher
94	Computer Modelin for Surface Properties of Carbon Fibers	Pretta L. VanDible
95	An Advanced Vision System Testbed ***Same Report as Prof. Trenary***	William B. VanValkenburgh

96	Numerical Calculations of Dopant Diffusion involving flashlamp heating of silicon	Joseph C. Varga
97	Scanning Electron Microscopy of PBO, PBT, and Kevlar Fiber Due to sensitive nature of report cannot be published at this time	Deborah L. Vezie
98	Self Induced Deformations in a Space-Based Electromagnetic Rail Gun	James W. Wade
99	Hole Diameters in Plates Impacted by Projectiles	Randall F. Westhoff
100	Human Response to Prolonged Motionless Suspension in Four Types of Full Body Harnesses	Terri L. Wilkerson
101	Late Appointment Date No Report Submitted at this time	Douglas L. Wise

1987 USAF-UES SUMMER FACULTY RESEARCH PROGRAM/
GRADUATE STUDENT SUMMER SUPPORT PROGRAM

Sponsored by the
AIR FORCE OFFICE OF SCIENTIFIC RESEARCH

Conducted by the
Universal Energy Systems, Inc.

FINAL REPORT

PHYSIOLOGICAL MONITORING METHODOLOGY IN THE USAFSAM

CENTRIFUGE

Prepared by: Jennifer B. McGovern
Academic Rank: Graduate Student
Department and University: Psychology Department
University of Florida
Research Location: Crew Performance Lab, Aerospace
Research Branch, Crew Technology
Division, USAF School of Aerospace
Medicine
USAF Researcher: Dr. Nita L. Lewis
Date: 23 July, 1987
Contract No.: F49620-85-C-0013

PHYSIOLOGICAL MONITORING METHODOLOGY IN THE USAFSAM

CENTRIFUGE

by

Jennifer B. McGovern

ABSTRACT

Loss of consciousness due to +Gz (G-LOC) has been identified as a cause of many mishaps and loss of aircrews and aircraft. Previous studies have suggested that physiological measures, especially the EEG, would be useful to monitor pilot consciousness. This effort endeavored to define appropriate methodologies (including electrode placement and choice of electrode) for use in a USAFSAM Centrifuge study of deliberate G-LOC. Physiological signals to be monitored included EEG, EMG, EOG, ear oximetry, and respiratory sounds.

ACKNOWLEDGEMENTS

I would like to acknowledge and thank the Air Force Systems Command, the Air Force Office of Scientific Research and the Air Force School of Aerospace Medicine Crew Technology Division Aerospace Research Branch (USAFSAM/VNB) for the opportunity to work with some of the top notch people in the field of aerospace research. Special thanks to Dr. William F. Storm, Branch Chief, for allowing me to continue in the same vein of research I began with this branch in Summer 1986. I would like to acknowledge the support of the following people who helped make my summer experience a positive one: the Centrifuge Crew (a group of great guys!), Earl Cook and TSgt Ron Boone (I get a charge out of you guys!), the Centrifuge Subjects, the other contract personnel, Lt. John Cmar and Sgt. Darren Pettry (for unfailing patience), and the other people who helped me socially, politically, and technically.

More than anyone else, however, I would like to thank Dr. Nita L. Lewis who let me work like I like, do what I want, be what I am, and achieve what I can, all at her scientific expense. Her shining example, raw courage in the face of adversity, cunning, sharp scientific sense, and fantastic PR will allow me to achieve more than I might otherwise have thought

possible. She is a role model, not without faults,
but still beyond compare.

PHYSIOLOGICAL MONITORING METHODOLOGY IN THE USAFSAM

CENTRIFUGE

I. INTRODUCTION: Loss of consciousness due to +Gz (G-LOC) has been identified by the U.S. Air Force as the cause of multiple mishaps resulting in the loss of aircrew and aircraft. A previous study conducted by Lewis, et al. (1987) demonstrated changes in the electroencephalograms of subjects undergoing deliberate G-LOC on the USAFSAM Centrifuge. My work this summer was a continuation of work I began in summer 1986 which was in direct support of efforts to replicate and extend the research being conducted at USAFSAM on identification of G-LOC.

The follow-on testing included a battery of electrophysiological measures: electroencephalogram (EEG), electromyogram (EMG), electrooculogram (EOG), electrocardiogram (EKG), ear oximetry, respiratory sounds, and force of hand on stick. My participation in this study stems from my work at the University of Florida which has concentrated on electrophysiological measures (especially EEG and EMG) of information processing primarily under stressful environmental conditions. The EEG placements were selected from the International 10/20 System (a standardized montage for EEG collection). I conducted a literature search and consulted with a number

of experts in physiology and acceleration to determine the most appropriate placements for the EMG electrodes (Frost, 1987, Gillingham, 1987). Considerations for these placements included reduction of noise due to motion artefact, use of primarily large muscle groups, and use of muscles that are important to the L1 anti-G straining manoeuver. Preliminary testing of the montage included selection of electrodes for use in the centrifuge. Grass metal EEG electrodes were attached to the scalp using Collodion, a standard clinical procedure (Frost, 1987). EMG electrodes were selected from a variety of choices including Beckman plastic cup electrodes and a number of EKG electrodes differing in size, shape, and make-up. Those electrodes returning the best signals while providing optimum comfort for the subjects and strongest adhesion were selected for use in the centrifuge. EKG electrodes were placed in the standard five lead, central measure configuration. Prior to the centrifuge study I participated in training the technicians, recruitment of subjects, both into the G-LOC study and into the USAFSAM Centrifuge generic panel (a subject pool for all centrifuge studies at USAFSAM), and I aided with scheduling the preliminary study on the centrifuge. During the study itself I Instrumented subjects and oversaw the instrumentation of subjects by technicians. After the preliminary centrifuge study, I participated in

troubleshooting the electronic circuitry. There were problems in the head mounted preamplification system, the Data Inc. preamplification system, and the centrifuge slip-rings (and electrical system for removal of data from the centrifuge). Modifications included redesign of the head mounted preamplifier, removal of the Data, Inc. preamplifiers from the data collection loop, and implementation of an onboard data collection system. Dr. Lewis will continue in that vein. Options include a multiplexing data collection system and a solid state data recorder.

II. OBJECTIVES OF THE RESEARCH EFFORT: Selection of the best physiological signals to record for determination of inflight G-LOC is the primary objective of this research.

Secondary goals include finding a minimum number of required recording sites and final determination of best type of electrodes for this use as well as capability for realtime, online, inflight data collection.

III. SELECTION OF ELECTRODE SITES: EEG electrodes were placed in accordance with the International 10/20 System. Sites were chosen on the basis of accepted centers of brain activity. Five sites were recorded: a frontal (F3), two centrals (Cz and C4), a parietal (P3), and an occipital (O2). These were referenced to linked mastoids.

Electrodes were attached to the scalp with Collodion U.S.P. Aquasonic electrode gel was used. Impedances were below 4 for all subjects.

EMG electrode placements were determined by first considering the muscles required to perform a good L1 anti-G straining manoeuver. This manoeuver requires the subject to contract all the muscles in the body to increase the systemic blood pressure. Another requirement for measuring EMG included placing the electrodes such that movement artefact due to pressure against the seat (due to G or to the subject's being seated) did not interfere with recording the electrophysiological signals. Six muscle sites were chosen: Digastric (chin), Trapezius (shoulder girdle), Rectus abdominus (lateral abdomen), Biceps brachii (upper arm, front), femoral quadriceps (upper leg, front), and Gastrocnemius (lower leg, back) (Grant, 1956, Woodburne, 1957). Pre-gelled EKG electrode leads were used to record EMG because they are adhesive enough to maintain attachment under +Gz and the surface of the electrode is an appropriate size for EMG. Impedances were less than 7 for all subjects.

EOG was measured with a standard four site recording using Beckman plastic cup electrodes attached with double sided collars and filled with Aquasonic electrode gel. Impedances were less than 10 for all subjects. Respiratory sounds were recorded with a small microphone

taped to the throat at the top of the sternum. Ear oximetry was measured with an incandescent optical transducer. This transducer was placed on the lower pinna.

IV. SUBJECT PREPARATION: EEG electrode sites were prepared with OMNIPREP (a laboratory cleaner with silicon) and gauze squares or Q-Tips. Sites were further prepared with Beckman EEG Paste (a conductive material). EMG electrode sites were prepared with OMNIPREP and gauze or with alcohol and gauze. EOG sites were prepared with OMNIPREP and Q-Tips. EKG electrode sites were prepared with alcohol and gauze pads.

V. RECOMMENDATIONS: From the testing to date we know the electrode sites have met the criteria for selection. That is they fulfill the necessary measurement function with a minimum of motion artefact and a minimum of noise.

Laboratory experiments show the placements to be clean and correct. The technicians have mastered the procedures and perform placement consistently. That removes the electrode placement procedure from the troubleshooting process. The troubleshooting of the electrical circuitry is continuing. The final centrifuge testing of the system will be in September. From the data collected at that time a determination of the best indicant of G-LOC (from

the physiological signals collected) can be made.

The minimum number of signals required to make this determination will also be decided after the analysis of the data collected at that time. Without the data no further recommendations can be made.

References

- Frost, J. (1987). Personal communication, 4 June.
- Gillingham, K. (1987). Personal communication, 10 July.
- Grant, J. C. B. (1956). An Atlas of anatomy. Baltimore: The Williams and Wilkins Company.
- Lewis, N. L., McGovern, J. B., Miller, J. C., Eddy, D. R., & Forster, E. M. (1987). EEG indices of G-induced loss of consciousness (G-LOC). Paper presented to NATO-AGARD meeting, Trondheim, Norway, 25 May.
- Woodburne, R. T. (1957). Essentials of human anatomy. NY: Oxford University Press.

1987 USAF-UES SUMMER FACULTY RESEARCH PROGRAM/
GRADUATE STUDENT SUMMER SUPPORT PROGRAM

Sponsored by the
AIR FORCE OFFICE OF SCIENTIFIC RESEARCH

Conducted by
UNIVERSAL ENERGY SYSTEMS, INC.

FINAL REPORT

Methods of Quantifying and Enhancing Reactive
Oxygen Species Production

Prepared By:	Mr. Roland A. Medellin
Academic Rank:	2nd Year Medical Student
Department and University:	Division of Biology and Medicine Brown University
Research Location:	USAFSAM/RZP Brooks Air Force Base
USAF Researcher:	Major Jonathan Kiel
Date:	14 August 1987
Contract No.:	F49620-85-C-0013

I. ACKNOWLEDGEMENTS

I thank the Air Force Systems Command and the Air Force Office of Scientific Research for sponsoring my work and for availing me of USAFSAM facilities. I also thank the Radiation Science Division for providing me with this research opportunity.

I am grateful to Universal Energy Systems (UES) for the support of my work.

Major Kiel provided a friendly, professional, and safe working environment. He explained many recent findings relevant to my work. I appreciate very much his effort to assign me experiments relevant to my personal academic interests. I thank Yolanda Salmon for informing me of the GSSSP, and especially for her encouragement. AIC Gerry O'Brien, Dr. Jill Parker, Dr. Stephen Pruitt, Sgt. Dave Simmons, and AIC Angela Vallet all made invaluable suggestions and taught me important techniques. I thank Sgt. Chris McQueen for his help in preparing the graphics.

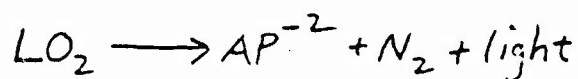
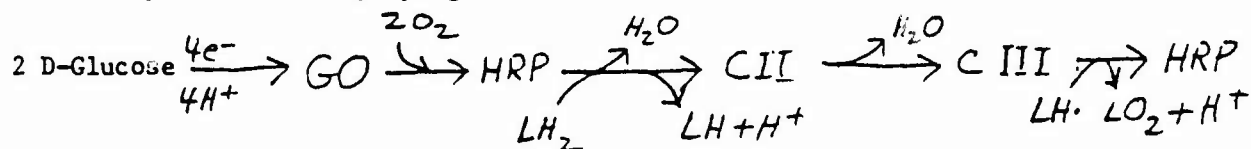
II. Methods of Quantifying and Enhancing Reactive Oxygen Species Production

by

Roland A. Medellin

ABSTRACT

... Assays were run employing the reaction summarized as follows:



in which LH_2 is Luminol, CII is electron-deficient HRP, CIII is oxy-peroxidase, LO_2 is peroxy-luminol intermediate, and AP^{-2} is Aminophthalate. Glucose Oxidase, Horseradish Peroxidase, Luminol, and Bovine Serum Albumin were immobilized on 7mm filter paper disks. These disks when assayed by adding glucose demonstrated consistent, predictable enzyme kinetics, even when various inhibitors were added to the reaction mixture. We observed 150-fold greater chemiluminescence peaks in disks to which glucose was added compared to controls. When we added Catalase, only 4.4% of this chemiluminescence was typically observed while 15% of the chemiluminescence for glucose was seen when Bovine Serum Albumin was added. Peak chemiluminescence values were observed at characteristic times after adding glucose to the disks.

We also produced virus-sized nanoparticles (Glucose Oxidase + Horseradish Peroxidase), which produced 1300-fold greater chemiluminescence over controls when a mixture of glucose and luminol was added. These nanoparticles were able to penetrate a .2 um filter, and they retained their enzymatic activity for weeks. They produced 20-fold greater chemiluminescence over controls when immobilized on gel disks. When immobilized on gel disks, nanoparticles exhibited chemiluminescence values within the same order of magnitude 80% of the time. In preliminary tests Dr. Pruitt used nanoparticles to enhance RAW and P388 macrophage-like cell line support of CTLL cytotoxic lymphocyte proliferation.

III. INTRODUCTION

Reactive Oxygen intermediates (ROI) can cause various forms of damage in living systems. They have been implicated in lipid peroxidation, enzyme inactivation, protein denaturation, and nucleic acid damage.⁽¹⁻³⁾ At the right concentrations reactive oxygen intermediates have a bactericidal effect in the host.⁴ We suspect that a protective mechanism exists in which immunocytes can mediate a transition from acute to chronic inflammation before the ROI produced in acute inflammation can accumulate to severely toxic levels. Some workers speculate that radio-frequency (RF) radiation exposure can alter the levels of ROI produced by neutrophils and macrophages leading to tissue damage. If this occurs in living organisms, a mechanism can be postulated for the allegations that RF radiation can cause certain forms of Leukemia. If true, such claims would provide a basis for implementing more thorough safety precautions in operating radar systems. The Radiation Sciences Division at the School of Aerospace Medicine is engaged in investigation designed to test these hypotheses.

As a second-year medical student, I am familiar with acute and chronic inflammation as well as basic immunology. I have had an introduction to Enzyme-linked Immunoabsorbant Assays, enzyme kinetics, and microbiology. Prior study in these areas aided me in making relevant observations in preparing cross-linked enzymes and in running chemiluminescent assays.

IV. OBJECTIVES

We intended to develop systems for measuring oxygen radical production by macrophage-like cells in an in vitro immune system. We intended to make such measurements with cells as they are exposed to RF radiation in order to determine any effects on ROI production. Also, we wanted to learn whether or not Green Heme Protein isolated from whole blood would act to enhance or inhibit any effect of RF radiation in such a cell system.

The means for achieving these objectives consisted of my work with gel disks and nanoparticles. The gel disks provide a means of immobilizing cells and the ROI-producing enzymes in close proximity to each other. This would enable us to detect levels of ROI that could not be detected before. In the living system ROI levels are maintained at undetectable concentrations by scavenger molecules such as Catalase, Superoxide Dismutase, Glutathione Peroxidase, and Ceruloplasmin.⁵ With the chemiluminescent disk assay the disk and the macrophage are so close together that we may be able to detect a rise in ROI levels before the scavenger molecules encounter the released ROI.

Nanoparticles serve a function similar to that of gel disks. With them we can modulate the amounts of ROI a cell produces at a given time. Phorbol esters can stimulate ROI production, for example, but they also stimulate the production of other mediators.⁽⁶⁻⁷⁾ Nanoparticles are more likely to be specific for ROI production. A variety of experiments can be devised taking advantage of antibodies that can link nanoparticles to cells, disks, or other molecules.

V. PROCEDURE AND RESULTS

In preparing the gel disks, we cross-linked 1 mg/ml Horseradish Peroxidase and 1 mg/ml Glucose Oxidase to each other with 30 mg/ml Bovine Serum Albumin (BSA) to which we added luminol, which intercalates within the BSA molecule. All of this was done in .01 M PBS pH 6.9. This mixture was filtered using a .2 um filter, and we then added 25% glutaraldehyde to make a 1/50, 25% glutaraldehyde/gel solution. 25 ul of this gel was added to each of 24 disks occupying wells in a microtiter plate. We placed 200 ul portions of the remaining gel in the empty wells of another microtiter plate. We used this so that we would know whether the mixture indeed became a gel. If the mixture does not gel, the disks would not hold the enzymes on their surfaces, and would release the enzymes into the surrounding medium. Both microtiter plates were wrapped in Reynolds Wrap Aluminum foil to protect the gel from light, which may catalyze unwanted reactions. The plate with the gel and plate with the disks were stored at 4°C for 48 hr.

We then activated these disks with either 200 ul .01 M PBS pH 7.4 (control), 200 ul 500 ug/ml Dextrose, 200 ul 500 ug/ml Dextrose + 200ul 10 mg/ml Superoxide Dismutase, 200 ul 500 ug/ml Dextrose + 200 ul 100mg/ml Catalase, 200 ul 500ug/ml Dextrose + 100 ul 10 µg/ml Superoxide Dismutase + 100 ul 100µg/ml Catalase, 200 ul 500 ug/ml Dextrose + 200 ul 10 µg/ml Human Serum Albumin, or 200 ul 500 ug/ml Dextrose + 200 ul 100 µg/ml Bovine Serum Albumin.

We checked for chemiluminescence with a Turner luminometer. The peak relative chemiluminescence values for 11 separate trials are tabulated in table 1. The time elapsed before peak chemiluminescence levels were reached was recorded for each trial in table 2. When each substance in the study was added to the disks, characteristic kinetics were observed as seen in Figures 1 and 1.1.(data taken from three representative trials and averaged).

Catalase and BSA consistently inhibited the chemiluminescent reaction. Superoxide Dismutase and Human Serum Albumin had no significant effect. With this data understood, we have assurance that the gel disk cross-links relatively uniform amounts of enzymes, emits uniform amounts of light energy with given reactions, and as such is useful for various chemiluminescent assays. The disks are most predictable 2 days after preparation. Any earlier the kinetics observed in the reaction with glucose are inconsistent. As the disks age, they lose their ability to produce chemiluminescence.

Table 1

Table 1 Peak Chemiluminescence Values of Glucose Oxidase-Horse Radish Peroxidase-Luminal-BSA Disks Activated by Dextrose mixed with various proteins

Substances added for activation

Experiment Number	PBS Blank	Dextrose 500µg/ml	Dextrose + SOD 500µg/ml 10µM	Dextrose + CAT 500µg/ml 10µM	Dextrose + CAT + SOD	Dextrose + HSA 10µM	Dextrose + BSA 10µM
1.	.43	60.89	70.82	2.58	2.75	49.24	3.22E/6.60L
2.	.25	56.93	45.62	1.40 early/1.98 late	2.44	32.00	1.78E/4.213L
3.	.29	84.27	40.09	2.01	1.78	2.21 early/3.76 late	2.731E/4.95L
4.	.19	45.00	86.26	2.78	4.22	12.17	4.19E/6.44L
5.	.15	49.24	56.26	2.41	4.45	29.42	6.829
6.	.20	24.32	5.31	1.87	3.05	23.56	3.03E/4.758L
7.	.36	20.74	42.12	1.68	2.34	18.83	15.81
8.	.34	40.48	31.58	1.89	3.47	68.14	2.32E/5.73L
9.	.36	38.25	56.43	2.29	3.66	26.56	6.94
10.	.42	68.24	73.04	1.77	3.18	36.18	1.43E/2.68L
11.	.37	26.61	51.57	2.01	2.50	51.58	11.81
Average ± St Dev.	.31 ± .09	46.82 ± 18.8	50.85 ± 21.0	2.06 ± .39	3.08 ± .79	31.8 ± 18.9	2.74 E (n=7) 7.00 L (n=11)

Legend

SOD Superoxide dismutase

CAT Catalase

HSA Human Serum Albumin

BSA Bovine Serum Albumin

E early peak

L late peak

n number of values used

Concentration of dextrose is always 500µg/ml in this experiment

Table 2
Kinetics of Gel Disk Activation

Values refer to the time elapsed before chemiluminescent peaks were observed after diskactivation.

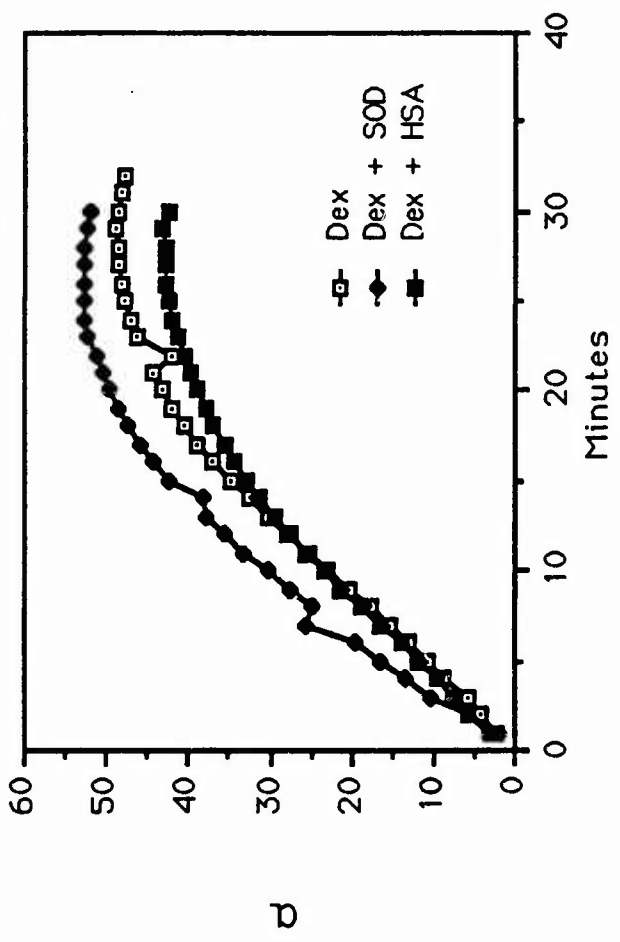
Substances Added to Activate Disks.

Experiment Number	Dextrose	Dextrose+SOD	Dextrose+CAT	Dextrose+SOD+CAT	Dextrose+HSA	Dextrose+BSA
1	20	24	2	2	20	3 38
2	30	28	2	2	25	2 43
3	20	22	2	1	16	4 38
4	23	21	2	1	32	5 NA
5	28	26	2	2	26	34
6	32	39	2	2	34	6 45
7	43	25	2	2	31	38
8	28	33	2	2	25	5 31
9	31	23	1	2	30	35
10	27	26	2	2	30	2 19
11	28	27	2	2	24	32
Average ± SD	28 ± 6	27 ± 5	2 ± .3	2 ± .4	2.7 ± 5	4 ± 2 35 ± 7 (n=7)

Legend

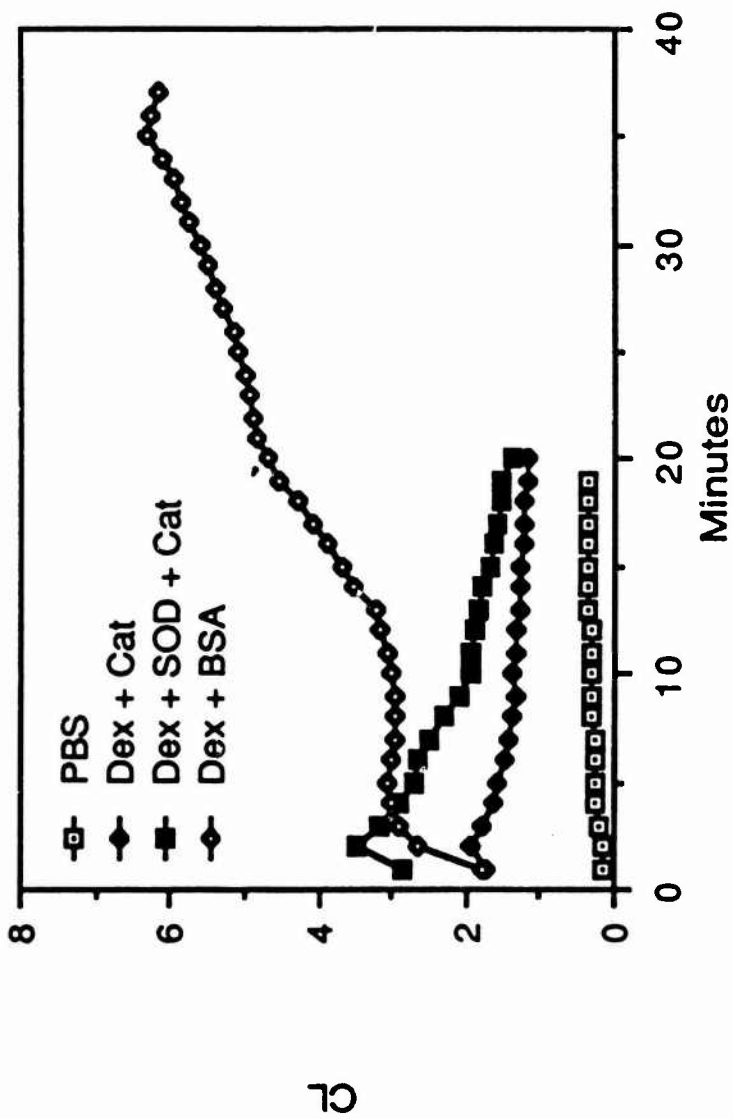
NA value not available

Fig. 1 Kinetics of Dextrose Activated Disks
With Various Proteins Added



Kinetics of Dextrose Activated Disks With Various Proteins Added

Fig. 1.1



The nanoparticles, on the other hand, produced high levels of chemiluminescence, and retained their capability for weeks. We prepared them by cross-linking Glucose Oxidase and Horseradish Peroxidase with Bovine Serum Albumin. 75% Ammonium Sulfate (w/v) was added to this solution until the absorbance at 700 nm began to rise exponentially. At this point the nanoparticles exist in a colloid state, and are suitable for recovery after purifying by means of gel filtration.

25% glutaraldehyde is added to allow continued aggregation of Glucose Oxidase-BSA-Horseradish Peroxidase particles. After one hour of refrigeration, .1 M Sodium Metabisulfite is added to the mixture in order to freeze the aggregation process ensuring that the particles remain small enough to enter cells. Gel filtration with sephadex G-25 coarse beads yields the final nanoparticle preparation as the elutant by trapping the smaller protein aggregations, particularly free Glucose Oxidase or Horseradish Peroxidase. Table 3 and Figures 1.2 and 1.3 demonstrate chemiluminescent behavior when the nanoparticles were activated with a mixture containing 1 mg/ml Dextrose, 1 mg/ml Luminol, and 1 mg/ml BSA at pH 7.4.

Table 4 and Figure 3 demonstrate the effect of filtering the nanoparticle solution with a .2 micron filter on chemiluminescent capability. The filtrate is free of bacteria as well as larger protein aggregations.

We also prepared gel disks containing 1 mg/ml Luminol, 30 mg/ml Human Serum Albumin, and 1 mg/ml Anti-Bovine Serum Albumin. We incubated this for one hour in a nanoparticle solution. Controls were incubated in PBS pH 7.4. We intended to allow the antibody to join the nanoparticle (containing BSA) to the gel, which is cross-linked to the disk. Table 5 and Figure 4 compare the chemiluminescence values of nanoparticle-treated disks to controls when 200 ul 1 mg/ml Dextrose pH 7.4 is added. We have yet to run tests that determine how much of the binding observed here is specific, and how much is nonspecific.

We were able to make one attempt at feeding nanoparticles to cells. Dr. Pruitt determined that exposing RAW or P388 macrophage-like tumor lines to 1/1000 dilutions of the nanoparticle preparations stimulated CTLL-2 lymphocyte proliferation when grown together with RAW or P388 cell lines. Concentrations greater than the 1/1000 dilution of nanoparticles tended to kill the cells. These are merely preliminary findings. More experiments

Table 3 Chemiluminescence of Nanoparticles

Table 4 Chemiluminescence of Nanoparticles Before and After Filtering

Time After Mixing (min)	1 mM Dextran pH 7.4	Nanoparticles alone	Nanoparticles + 1 mM Dextran pH 7.4
1	.006	.128	26
2	.007	.132	147.3
3	.010	.136	182.6
4	.017	.140	182.4
5	.021	.141	178.0
	n=2	n=2	n=10

Time After Mixing (min)	Before Filtering	After Filtering
1	13.47	14.88
2	OFFSC	OFFSC
3	279.85	248.4
4	295.9	280.0
5	274.8	263.0
	n=2	n=2

5.4% reduction in chemiluminescence

Fig. 1.2

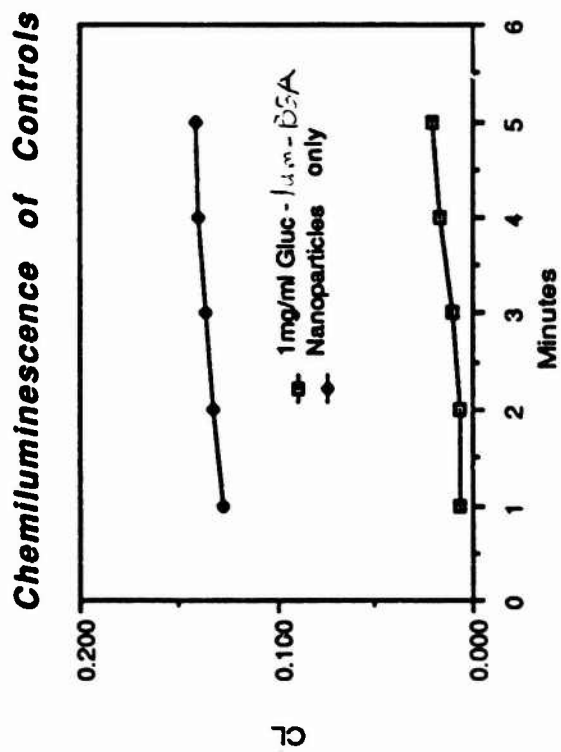


Fig. 1.3

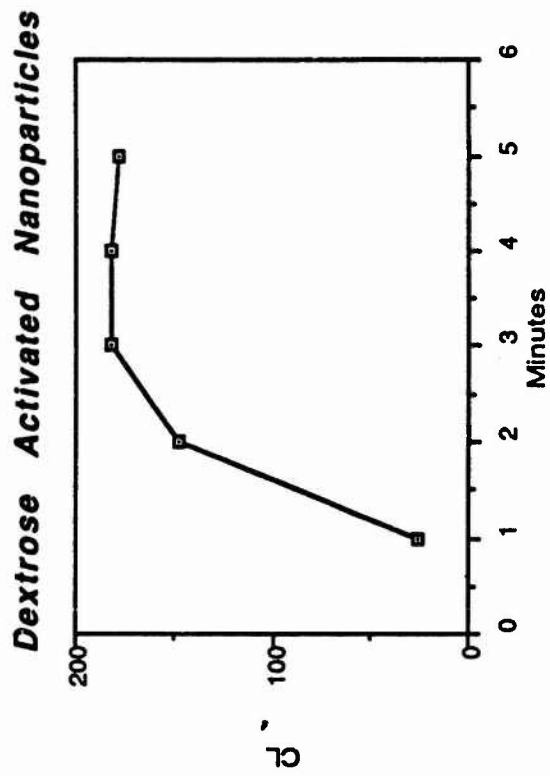
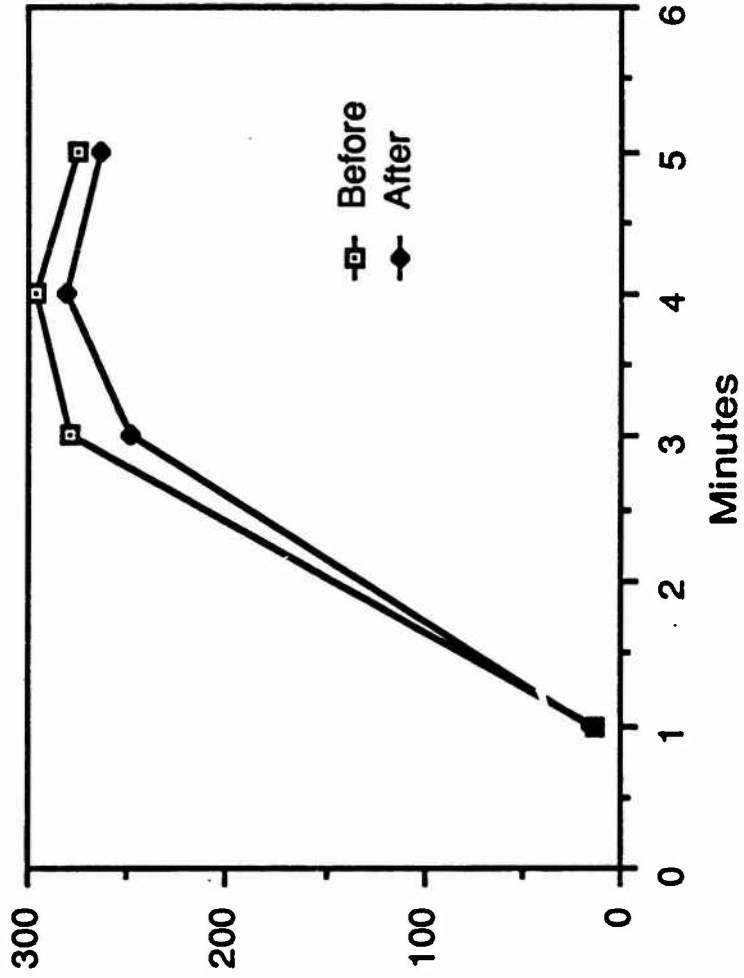


Fig. 3 Effect of Filtering On Nanoparticles



- 100 μ l of the nanoparticle preparation was activated by 100 μ l of 1mg/ml Dex-Lum-BSA pH 7.4

Table 5 Chemiluminescence of Nanoparticle Treated Disks

200 μ L 1 mg/ml dextrose pH 7.4 Added

Time (min) After Mixing	Control Disk HSA-Lum-Anti-BSA	Nanoparticle treated HSA-Lum-Anti-BSA disk
1	.015	.250
2	.017	.349
3	.012	.397
4	.003	.395
5	.011	.388
6	.005	.367
7	.008	.351
8	.004	.336
9	.010	.326
10	.004	.318
	n=1	n=4

Table 6 Chemiluminescence (CL) of Green Heme Protein Treated Disks

200 μ L 1 mg/ml dextrose pH 7.4 added

Time (min) After Mixing	Control Disk CL BSA-Lum-MetHb-GO	Green Heme Protein treated disk CL BSA-Lum-MetHb-GO
1	.151	.182
2	.191	.267
3	.190	.257
4	.182	.235
5	.172	.214
6	.165	.195
7	.153	.186
8	.148	.180
9	.144	.178
10	.140	.175
	n=2	n=9

Legend

HSA - Human Serum Albumin

Lum - Luminol

Anti-BSA - Anti-Bovine Serum Albumin

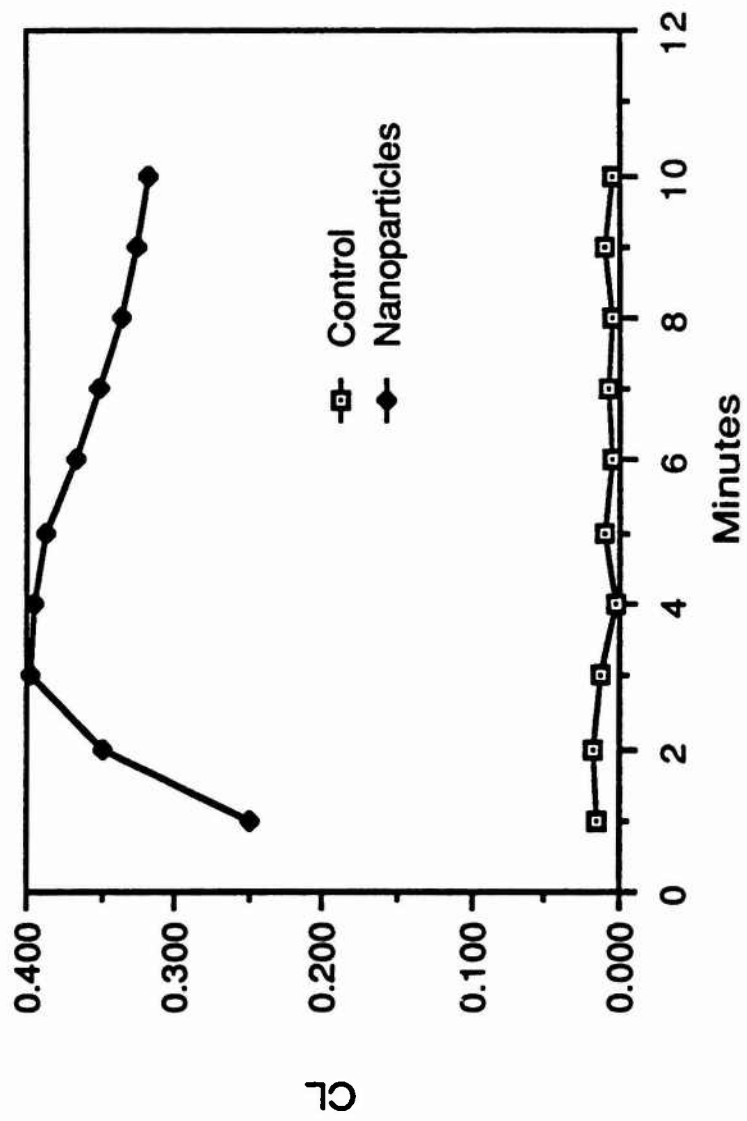
BSA - Bovine Serum Albumin

MetHb - Methemoglobin

GO - Glucose Oxidase

n - number of samples tested

Fig. 4 Chemiluminescence of Nanoparticle-Treated Disk

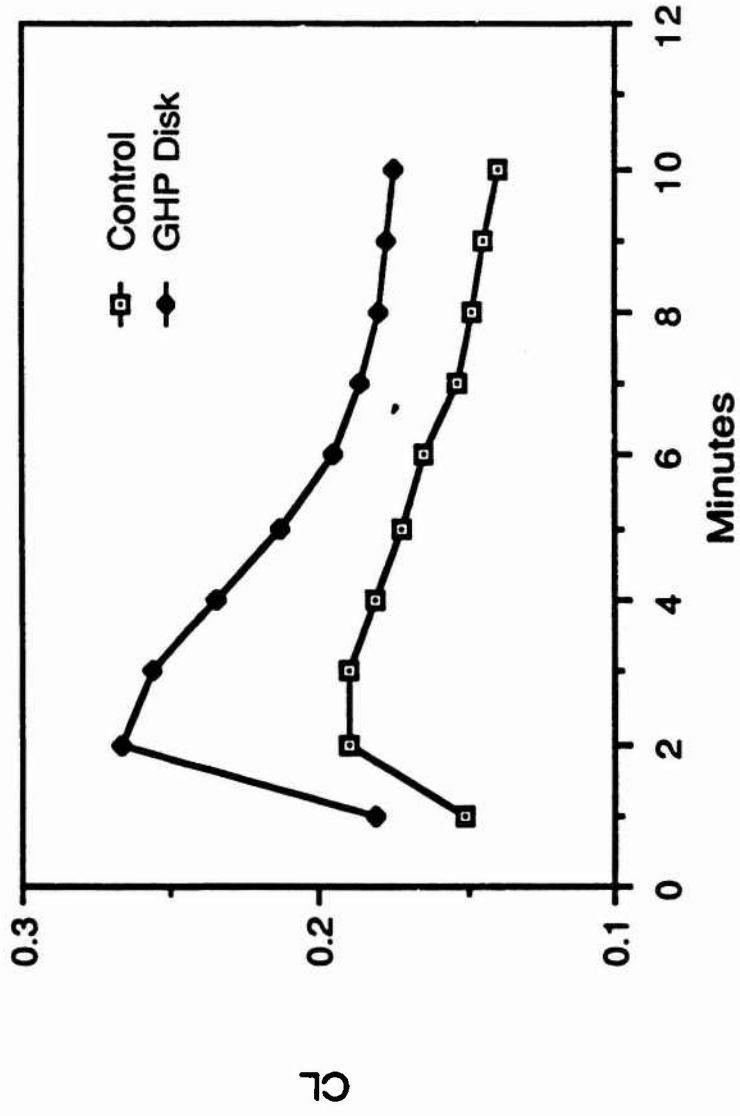


have to be run. A whole slew of immunological studies would be made possible if we can continue to demonstrate that cells can take up nanoparticles and produce measurable results.

In a separate assay, Green Heme Protein demonstrated some peroxidase activity, but the results are not altogether convincing. Table 6 and Figure 5 contain the results of this assay.

Chemiluminescence of Green Hemoprotein Treated Disks

Fig. 5



- 200µl of 1mg/ml Dextrose pH 7.4 added to disks
- Green Hemoprotein sample contaminated with Hgb

VI RECOMMENDATIONS

More tests should be run to evaluate the effects nanoparticle uptake has on immunocytes. Nanoparticle-laden macrophages may simulate macrophages activated by stimuli such as toxins, or perhaps radio-frequency radiation. Such cells provide a model for studying cell systems in which high levels of reactive oxygen intermediates are released into the medium.

The gel disk serves under some conditions as an excellent means of immobilizing proteins in assaying ROI production. I recommend an experiment in which nanoparticle-treated Human Serum Albumin-Luminol-Anti-BSA disks are run along with a control set of disks in which the disks have no antibodies. This would indicate whether antigen-antibody binding plays a role in linking nanoparticles to disks or whether the binding is nonspecific. I would recommend experiments that would determine whether the nanoparticles come to reside inside the cell or whether they bind to the surface of the cells. This could be achieved through staining techniques and microscopy.

It would be useful to run assays to determine the amounts of ROI secreted by nanoparticle-laden cells. Such cells could be added in a scintillation vial to a solution containing 1 mg/ml Dextrose, 1mg/ml Luminol, and 1 mg/ml BSA, and monitored for chemiluminescence. Such assays can be utilized in assessing whether or not toxic oxygen radicals are involved in the pathogenesis of various disease processes.

An experiment to measure the secretion of ROI by cells (RAW) attached to disks was unsuccessful. The disks contained Luminol, BSA, Horseradish Peroxidase, and Anti-Bovine Serum Albumin. It was hoped that the fc fragment of anti-BSA would attach to the RAW fc receptor as it bound by means of the fab fragment to the BSA-containing disk. With theory the NADP Oxidase system of the RAW cells would be held closely enough to the Horseradish Peroxidase and Luminol on the disk that a chemiluminescent reaction would be catalyzed. One experiment produced measurable chemiluminescence while three did not. I wonder if technical error was involved here, and would recommend a few more experiments meticulously carried out before ruling out this scheme as a possibility.

REFERENCES

1. Freeman, Bruce A. , Crapo, James D., Lab. Invest. Vol 47: pp. 412-426, 1982.
2. Slater, T.F. Biochem J, Vol. 22: pp. 1-15, 1984.
3. Cerutti, Peter A. Science Vol. 227: pp. 374-381, 1985.
4. Robbins, Stanley L., Cotran, Ramzi S., Vinay, Kumar Z., Pathological Basis of Disease, W.B. Saunders Co., Philadelphia, 1984, p. 50.
5. Ibid p. 57.
6. Aderem, Alan A., Cohen, Daniel S, Wright, Samuel D., Cohn, Z., J Exp. Med., July 1 1986, Vol. 164(1): pp. 165-179.
7. Cancer Res, November 1986, Vol 46(11): pp. 5696.

1987 USAF - UES SUMMER FACULTY RESEARCH PROGRAM /
GRADUATE STUDENT SUMMER SUPPORT PROGRAM

Sponsored by the
AIR FORCE OFFICE OF SCIENTIFIC RESEARCH

Conducted by the
Universal Energy Systems , Inc.

FINAL REPORT

APPLICATIONS OF DIFFERENTIAL GEOMETRY TO THE
SHAPE ANALYSIS OF GRAY-VALUE IMAGES

Prepared by : Otto Michael Melko
Academic Rank : M.A. in Mathematics
Department and University : Department of Mathematics
University of California
Santa Cruz , Ca. 95064
Research Location : AFATL/AGS Eglin AFB
Fort Walton Beach
Fl. 32542 - 5434
USAF Researcher : Henry Neal Urquhart
Date : 4 Sept. , 1987
Contract No : F49620 - 85 - C - 0013

APPLICATIONS OF DIFFERENTIAL GEOMETRY TO THE
SHAPE ANALYSIS OF GRAY-VALUE IMAGES

by

Otto Michael Melko

ABSTRACT

A gray-value image can be viewed as a discrete analog of a smooth surface in Euclidean space . The shape of a smooth surface can be described by the gauss curvature and mean curvature of that surface . It is therefore reasonable to expect that the discrete analogs of these curvature functions would be useful in the shape analysis of digital (gray-value) images . Two methods for discretizing these curvature functions are discussed . These methods are then used to write algorithms for shape analysis of gray-value images . Special attention is paid to the value of these algoritms for the identification of objects (such as tanks) in low resolution infrared images .

ACKNOWLEDGEMENTS

I would like to thank the Air Force Systems Command and the Air Force Office of Scientific Research for the sponsorship of this research. I would also like to thank the staff of the Advanced Guidance Air to Surface Branch of the Air Force Armament Laboratory at Eglin Air Force Base, as well as that of the Technical Library, for their assistance during my tenure as a summer fellow. I am especially indebted to Neal Urquhart, whose assistance and encouragement greatly facilitated my research.

Introduction.

The differential geometry of surfaces in three dimensional Euclidean space is a natural extension of the analytic geometry of the Euclidean plane. It is a study of the local metric and curvature properties of surfaces. In particular, the gauss curvature and mean curvature are functions that describe the shape of a surface. In digital image processing, one takes a gray-value function, which is a discretization of a real world scene, and manipulates it to extract information not readily visible. The graph of a gray-value function, called a gray-value image, is then a discretization of a surface. The curvature functions mentioned above are good candidates for image transformations because they are natural shape descriptors. One cannot, however, apply the concepts of differential geometry directly to a gray-value image, for, as the word "differential" indicates, the operations of differential geometry involve differentiation, which cannot be performed on a gray-value function. There are two ways to address this difficulty:

(i) Devise discrete analogs of the operations of differential geometry that are directly applicable as transformations of gray-value images.

(ii) Associate a surface to a gray-value image (i.e. attempt to recover the real world scene), perform the desired operations, and discretize the result.

In the sequel, after a brief overview of differential geometry, I describe methods for shape analysis on a surface, and indicate their relevance to automatic target cueing. Then I indicate how to carry out programs (i) and (ii) above, and write the associated algorithms using the Image Algebra developed by Gerhard X. Ritter for the Air Force Armament Laboratory (see [5]).

II. Objectives of the Research Effort .

My assignment as a participant in the 1987 Graduate Student Summer Support Program (GSSSP) was to determine whether the concepts of differential geometry are applicable to the problems of automatic target cueing. Having done this, the next step was to devise algorithms for image processing that would be useful to that end.

III. An Overview of Differential Geometry.

Let Q be a rectangle in the Euclidean plane, R^2 . A map, P , of Q into three dimensional Euclidean space, R^3 , is an ordered triple of real valued functions, $P(q) = (P_1(q), P_2(q), P_3(q))$, for q an element of Q . We denote the first and second order partial derivatives of P by $P_x, P_y, P_{xx}, P_{xy}, P_{yy}$.

Definition: The map $P:Q \rightarrow R^3$ is regular if its first and second order partial derivatives are continuous maps, and the cross product $P_x(q) \times P_y(q) \neq 0$ for all $q \in Q$ (note that if P is regular, then $P_{xy} = P_{yx}$). Denote by S the subset of R^3 that is the image of Q under P . If P is regular, then S is a piece of surface in R^3 . The pair (S,P) will be referred to as a regular parameterized surface. It should be noted that a surface, S , admits many different parameterizations.

The two objects that form the basis of study of surfaces are referred to as the first and second fundamental forms, they contain all the geometric information about a surface. We now give a description of these objects.

The First Fundamental Form: Let E, F, G be the functions on S defined by $E = \langle P_x, P_x \rangle, F = \langle P_x, P_y \rangle, G = \langle P_y, P_y \rangle$, where $\langle P_x, P_y \rangle$ denotes the usual inner product of vectors P_x and P_y in R^3 . Then, the first fundamental form is defined to be

$$I = E dx^2 + 2 F dx dy + G dy^2. \quad (1)$$

The Geometric Meaning of I: Let $p \in S$, and let p' be another point of S near

p. Then, if the coordinates of p are (x,y), and the coordinates of p' are (x',y'), define $\Delta x, \Delta y$ by $x' = x + \Delta x$, $y' = y + \Delta y$. The distance, d, from p to p', in S, is the length of the shortest path, γ , contained in S and connecting p to p'. A path of this type is called a geodesic. To second order (essentially, this refers to the Taylor expansion of the arc length of the geodesic as a function of its parameter, up to the second term),

$$d^2 = E (\Delta x)^2 + 2 F (\Delta x)(\Delta y) + G (\Delta y)^2. \quad (2)$$

In other words, I is the infinitesimal version of the distance function on S. If a is the point in S with coordinates (x',y), then the coordinate curves, and γ form a "curvilinear triangle". One can then interpret equation (2) as the law of cosines (from Euclidean geometry) for the curvilinear triangle $\Delta pap'$.

The Second Fundamental Form: Let $p = P(q)$, and define ν by the formula $\nu = (P_x \times P_y) / |P_x \times P_y|$ where $|P_x \times P_y|$ denotes the norm of the vector $P_x \times P_y$. We have that ν is a field of unit vectors normal (perpendicular) to the surface, S. Let L, M, N be the functions on S defined by $L = \langle \nu, P_{xx} \rangle$, $M = \langle \nu, P_{xy} \rangle$, $N = \langle \nu, P_{yy} \rangle$. Then the second fundamental form is defined to be

$$II = L dx^2 + 2 M dx dy + N dy^2. \quad (3)$$

The Geometric Meaning of II: At the point $p \in S$, II measures the degree to which the field of unit normals, ν , of S deviates from being constant near p, thus measuring the extent to which S bends at p. More precisely, let $\Delta \nu = \nu(p') - \nu(p)$, $\Delta p = p' - p$, where $\nu(p')$ is the normal at p', and $\nu(p)$ is the normal at p. The quantity $\langle \Delta \nu, \Delta p \rangle$ then measures, roughly, the change of ν in the direction Δp . This quantity obeys the formula

$$-\langle \Delta \nu, \Delta p \rangle = L (\Delta x)^2 + 2 M (\Delta x)(\Delta y) + N (\Delta y)^2. \quad (4)$$

The Gauss curvature, K, and mean curvature, H, of a surface, S, are given by :

$$K = \det \begin{bmatrix} [E & F]^{-1} [L & M] \\ [F & E] & [M & N] \end{bmatrix} = \frac{LN - M^2}{EG - F^2} \quad (5)$$

$$H = \frac{1}{2} \operatorname{tr} \begin{bmatrix} [E & F]^{-1} [L & M] \\ [F & G] & [M & N] \end{bmatrix} = \frac{1}{2} \frac{NG - 2MF - LE}{EG - F^2} \quad (6)$$

The functions K and H contain a great deal of information about the shape of the surface, S. Their meaning will be discussed in section IV. In what follows we will be interested only in surfaces that are the graphs of functions. That is, $S = \{(x,y,g(x,y)) : (x,y) \in Q\}$ where $g:Q \rightarrow R$ has continuous partial derivatives up to second order. Here $P:Q \rightarrow R^3$ is given by $P(x,y) = (x,y,g(x,y))$. In this case the formulae (5) and (6) take the form:

$$K = \frac{g_{xx}g_{yy} - (g_{xy})^2}{(1 + g_x^2 + g_y^2)^2} \quad (7)$$

$$H = \frac{(1 + g_x^2)g_{yy} - 2g_xg_yg_{xy} + (1 + g_y^2)g_{xx}}{(1 + g_x^2 + g_y^2)^{3/2}} \quad (8)$$

Finally, we state a theorem due to Gauss that will be of fundamental importance in section V. A basic fact about surfaces is that, given two points p_1, p_2 there exists a path from p_1 to p_2 in S that has minimum length. If p_1 and p_2 are close together, this path is unique. In this case we denote this path by $\overline{p_1 p_2}$, and call it the geodesic from p_1 to p_2 . Suppose we have three points p_1, p_2, p_3 in S. Then we call the domain bounded by $\overline{p_1 p_2} \cup \overline{p_2 p_3} \cup \overline{p_3 p_1}$ a geodesic triangle and denote it by $\Delta p_1 p_2 p_3$.

THEOREM(Gauss) : Let a_1, a_2, a_3 be the interior angles of the geodesic triangle $\Delta p_1 p_2 p_3$, which we denote simply as Δ , then

$$a_1 + a_2 + a_3 - \pi = \int_{\Delta} K \, dA \quad (9)$$

Here, K denotes the Gauss curvature of S , and $dA = \sqrt{E G - F^2} \, dx \, dy$ is the element of area of S . Now let p_1, \dots, p_n be n distinct points of S , and let D be the n sided geodesic polygon whose boundary consists of the set $\overline{p_1 p_2} \cup \dots \cup \overline{p_n p_1}$, immediate consequence of Gauss' theorem is that

$$a_1 + \dots + a_n - (n - 2) \pi = \int_D K \, dA \quad (10)$$

For a more detailed overview of differential geometry, the reader may wish to consult [1]. An excellent introductory textbook is [3]. Gauss' original paper, [4], is also quite readable, and intuitive in its presentation.

IV. Application of Curvature to Shape Analysis.

As an idealized model of a tank, we consider a radially symmetric point source of heat on a neutral background. The corresponding gray-value image will look like a circular bump on a plane, as in figure 1. Our goal is to devise a method that will isolate shapes such as that in figure 6 from others. A regular surface has the property that every point on that surface has a unique tangent plane. Let p be a point in S , and let T_p be the tangent plane at p , then the Gauss curvature tells us:

$K(p) > 0$; In a neighborhood of p , S is entirely to one side of T_p . In this case, we say that S is elliptic at p , there are no sections of second order contact.

$K(p) = 0$; In a neighborhood of p , there is a unique section in S of second order contact with T_p , if $L(p), M(p), N(p)$ are not all zero. Such a point is said to be parabolic at p . If $L(p), M(p), N(p)$ are all zero, then all sections have second order contact. Such a point is called planar.

$K(p) < 0$; In a neighborhood of p , S lies on both sides of T_p , such a point is called a hyperbolic point of S . Then p has precisely two sections of second order contact.

By "section", we mean a curve in S obtained by taking the intersection of S with a plane orthogonal to S at p .

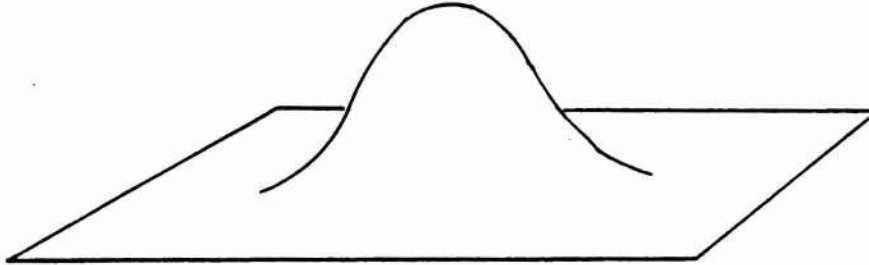


Figure 1. An idealization of a tank.

Referring to figure 1, we see that the top of the surface consists of elliptic points, and further on down, the points are hyperbolic. Once we get far away from the bump, the points are planar. Thus the curvature is, K , first positive, then negative, and then zero. Let $K'(p) = 1$, if $K(p) > 0$; $K'(p) = 0$, if $K(p) = 0$; and $K'(p) = -1$, if $K(p) < 0$. Figure 2 below displays the subregions of the domain, Q , on which K' assumes its respective values.

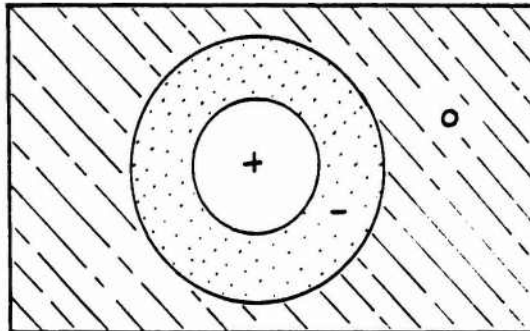


Figure 2. Segmentation of the Gauss curvature of figure 1.

The mean curvature, H , provides a measure of the rate at which the area of S changes if we expand S along its field of unit normals. The reader may wish to refer to [3] for further details.

Let $p \in S$, and suppose $K(p) > 0$. Let Π be a plane parallel to T_p , and

suppose that the distance, r , from Π to T_p is small. Then the set S is approximately an ellipse. The eccentricity, e , of this ellipse (the Dupin indicatrix, see [3], pp 148 -149) is given by the relation

$$e = 1 - k_1 / k_2 \quad (11)$$

where

$$k_1 = H - \sqrt{H^2 - K} \quad , \quad k_2 = H + \sqrt{H^2 - K} \quad (12)$$

are the principle curvatures of S (see [3] p 144). For the case $K(p) > 0$, we have assumed (without loss of generality) that $0 < k_1 \leq k_2$. For an ellipse, $0 \leq e < 1$. If e is close to zero, the ellipse is nearly circular. If e is close to 1, the ellipse is shaped like a cigar. Using equations (11) and (12), we can infer that:

- (i) If $\sqrt{H^2 - K} / |H|$ is small at p , then $\Pi \cap S$ is nearly circular.
- (ii) If $\sqrt{H^2 - K} / |H|$ is close to 1 at p , then $\Pi \cap S$ is cigar shaped.

Note that $H^2 - K = (k_1 - k_2)^2 / 4$ is always non-negative. Also, $0 < \sqrt{H^2 - K} / |H| < 1$ if and only if $K > 0$. Statements analogous to the above can be made for the cases $K(p) = 0$, $K(p) < 0$ where $\Pi \cap S$ resembles, infinitesimally, a pair of parallel lines, and a hyperbola respectively. Suppose that U is a subregion of Q (that is, an open, connected, simply connected subset of Q). Suppose that $K > 0$ on $P(U)$ where $P: Q \rightarrow R^3$ is a parameterization for S . We then have the

- Assertion: (a) If $\sqrt{H^2 - K} / |H|$ is uniformly small on $P(U)$, then U is nearly disk shaped.
- (b) If $\sqrt{H^2 - K} / |H|$ is uniformly close to one on $P(U)$, then U is oblong in shape.

By uniformly small on $P(U)$, we mean that there exists a small number $\epsilon > 0$ such that $\sqrt{H^2(p) - K(p)} / |H(p)| < \epsilon$ for all $p \in P(U)$. Similarly, uniformly close to one means that, for a small number $\epsilon > 0$, $\sqrt{H^2(p) - K(p)} / |H(p)| > 1 - \epsilon$ for all $p \in P(U)$. Figure 3, below, serves to illustrate this

assertion. Figure 3(a) represents a surface consisting of a nearly circular bump and an oblong shape. Figure 3(b) is the segmentation of the domain according as to whether the gauss curvature of 3(a) is positive, negative, or zero. The above assertion allows us to distinguish between regions A and B of figure 3(b). Region A would be considered a potential target. The smaller positive curvature regions are anomalies that occur because of the proximity of A and B.

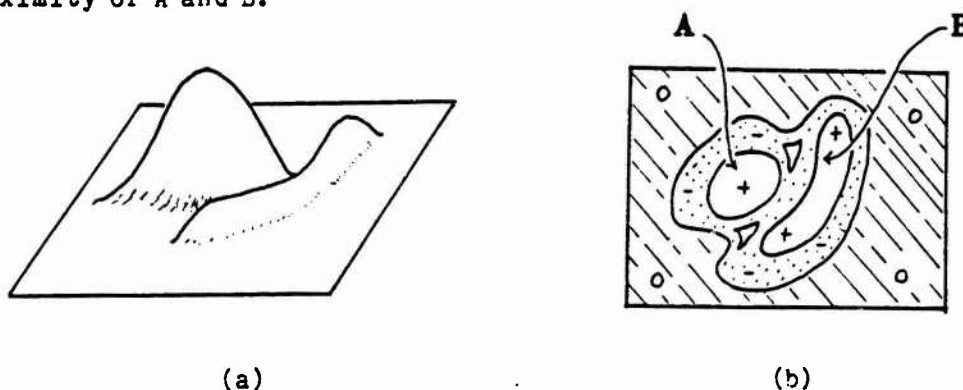


Figure 3. Illustration of the above assertion.

V. The Curvature Measure of a Piecewise Linear Surface. An Algorithm for Computing the Curvature of a Gray-value Image.

Let $Q = \{ (x,y) : a \leq x < b, c \leq y < d \}$. Set $\mu = (b - a) / m$ and $\nu = (d - c) / n$, where m, n are positive integers, and define Q_{ij} by $Q_{ij} = \{ (x,y) : a + i\mu < x < a + (i+1)\mu, c + j\nu < y < c + (j+1)\nu \}$. Each Q_{ij} is a rectangle (a square, if $\mu = \nu$) and $Q = \cup Q_{ij}$. The set $Q^0 = \{ (a + i\mu, c + j\nu) : 0 \leq i \leq m, 0 \leq j \leq n \}$ is a rectangular lattice of points in R^2 . The point $(a + i\mu, c + j\nu)$ will be denoted by q_{ij} , it is the lower left-hand corner of Q_{ij} .

Clearly, we can identify a gray-value function with a function $f: Q^0 \rightarrow R$. Each Q_{ij} prescribes the location of a pixel. Divide each rectangle Q_{ij} into two triangles by connecting the lower left hand corner of Q_{ij} with its upper right-hand corner. The upper and lower triangles

will be denoted by Q_{ij}^1 and Q_{ij}^2 respectively.

Let $f:Q \rightarrow R$ be the function on Q with the property that the restriction of f to one of the triangles Q_{ij}^r ($r = 1,2$), denoted by $f|Q_{ij}^r$, is linear and agrees with f^0 on the vertices of Q_{ij}^r .

Definition : The function, f , described above is said to be the Piecewise-Linear function (PL-function) associated to f^0 . The corresponding surface $Z = \{ (x,y,f(x,y)) : (x,y) \in Q \}$ is called the Piecewise-Linear surface (PL-surface) associated to f (or f^0). Note that f is a continuous function on Q . The PL-surface, Z , is a collection of triangles in R^3 joined together at the edges, as in figure 4.

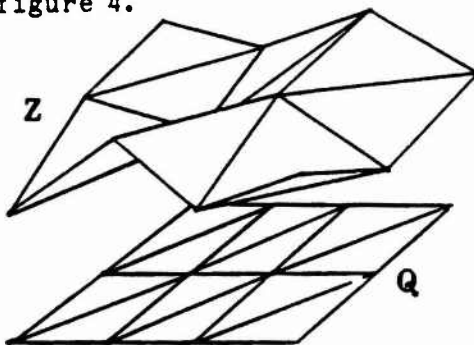


Figure 4. A PL-surface, Z , superimposed over its domain, Q .

A PL-surface is continuous, but fails to be regular at the edges and vertices in the sense presented in section III. Thus, the definition of Gauss curvature given by equation (7) doesn't apply at the edges and vertices, since f is not continuously differentiable at these points. Our problem, now, is to re-define Gauss curvature so as to admit this larger class of surfaces. A fruitful method for generalization in mathematics is to assume the properties that characterizes a mathematical object in some special situation, and use them to deduce a definition of that object that applies to more general circumstances. We proceed to do this.

The geodesics in a PL-surface, Z , are simply line segments in the individual faces of Z . Let D be a geodesic polygon in Z which contains only

one vertex, v , and which has precisely one edge in each face of Z adjacent to v . Suppose that there are t faces that meet at v and that the interior angles of these faces, at v , are $\theta_1, \dots, \theta_t$. It is easily shown that the corollary to Gauss' theorem (equation (10)) implies that

$$\int_D K \, dA = 2\pi - \theta_1 - \dots - \theta_t \quad . \quad (13)$$

The integral in equation (13) is independent of the choice of D , as long as v is the only vertex in D . This allows us to deduce that the Gauss curvature of Z is given by the Dirac measure

$$K = \sum_s \left\{ 2\pi - \sum_i \theta_{s,i} \right\} \delta_{v_s} \quad . \quad (14)$$

The index, s , runs over all vertices, v , and $\{ \theta_{s,1}, \dots, \theta_{s,t_s} \}$ is the set of interior angles at the vertex, v . The symbol δ_{v_s} denotes the (countably additive) function on (measurable) subsets of Z which assigns the value 1 to a set containing v_s , and 0 otherwise. Such a set function is also commonly referred to as a Dirac δ -function. We will refer to the number $2\pi - \theta_{s,1} - \dots - \theta_{s,t_s}$ as the measure of curvature of Z at the vertex, v_s .

Adopting the notation and terminology of [5], let K° denote the gray-value function obtained from f° by assigning to each $q_{ij} \in Q^\circ$ the measure of curvature of the associated PL-surface, Z , at the vertex $(q_{ij}, f^\circ(q_{ij}))$. We will also use f°, K° to denote the corresponding gray-value images of f°, K° respectively.

In figure 5, we have taken a point $q_{ij} \in Q^\circ$ such that q_{ij} does not lie on the boundary of Q , and labeled the points which are vertices of triangles adjacent to q_{ij} . The angles, $\theta_1, \dots, \theta_6$, are the interior angles of the corresponding triangles in Z (thus, for example, $\theta_3 \neq \pi/2$).

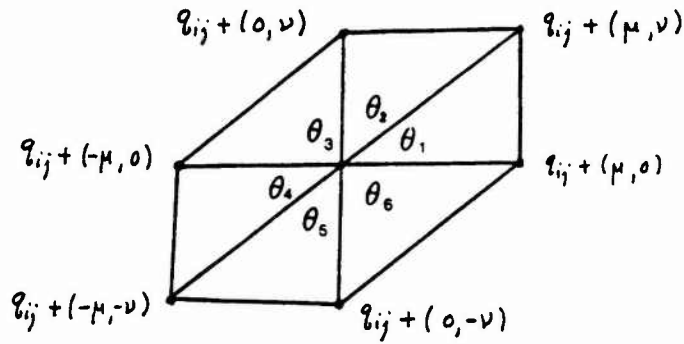


Figure 5. Points and triangles adjacent to q with respect to the above triangulation.

Let P be the parameterization of Z defined by $P(q) = (q, f(q))$. Then θ_1 is the angle between the vectors $P(q_{ij} + (\mu, \nu)) - P(q_{ij})$ and $P(q_{ij} + (\mu, 0)) - P(q_{ij})$. Thus

$$\theta_1(q_{ij}) = \cos^{-1} \left[\frac{\langle P(q_{ij} + (\mu, \nu)) - P(q_{ij}), P(q_{ij} + (\mu, 0)) - P(q_{ij}) \rangle}{|P(q_{ij} + (\mu, \nu)) - P(q_{ij})| |P(q_{ij} + (\mu, 0)) - P(q_{ij})|} \right].$$

A similar formula applies for each of the angles $\theta_2, \dots, \theta_6$. It follows that $K^0 = 2\pi - \theta_1 - \dots - \theta_6$.

Let $\Omega = \{ (1,0), (1,1), (1,0), (-1,0), (-1,-1), (0,-1) \}$. Then the points incident to q are $q_{ij} + (r\mu, s\nu)$, where $(r,s) \in \Omega$. Let Δ_{rs} denote the gray-value image $\Delta_{rs} = \{ (q_{ij}, f(q_{ij} + (r\mu, s\nu)) - f(q_{ij})) : q_{ij} \in Q^0 \}$, and let 1 denote the unit image. Define Θ_{rs}^{tu} for $(r,s) \in \Omega$, by

$$\Theta_{rs}^{tu} = \cos^{-1} \left(\frac{(r\mu 1) * (t\mu 1) + (s\nu 1) * (u\nu 1) + \Delta_{rs} * \Delta_{tu}}{\sqrt{(r\mu 1)^2 + (s\nu 1)^2 + (\Delta_{rs})^2} \sqrt{(t\mu 1)^2 + (u\nu 1)^2 + (\Delta_{tu})^2}} \right)$$

The element, (t,u) , of Ω will be said to be adjacent to (r,s) if (t,u) is to the immediate right of (r,s) in the list for Ω given above. In addition, we define the element $(1,0)$ to be adjacent to $(0,-1)$. With this convention it is easily verified that Θ_{rs}^{tu} is the gray-value image

corresponding to one of the angle functions $\theta_1, \dots, \theta_6$, if (t,u) is adjacent to (r,s) . It follows that

$$K^0 = 2\pi * 1 - \sum \theta_{rs}^{tu}, \quad (15)$$

where the sum is taken over all adjacent pairs.

Equation (15) was the goal of this section. It should be mentioned that the concepts introduced here are apparently well understood, although the author has been unable to locate any literature that adopts the same approach. Besl and Jain state a similar formula in [1], but give no indication of its derivation. The theory of convex surfaces is related to the material in this section, the reader is referred to [2] for details.

Using the geometric interpretation presented in section III, it is very likely that a definition of mean curvature can be found that applies to PL-surfaces. In this case, H will be a measure with support on the 1-skeleton (the set of edges and vertices) of Z . Because of lack of time, it was not possible to rigorously develop this idea.

VI. Computing Gauss Curvature and Mean Curvature via a Convolution Operator.

Let Q and Q_{ij} be as defined in section V. To a gray-value function, g^0 , we associate a step function $g: R^2 \rightarrow R$ by the rule $g(q) = g^0(q_{ij})$ if $q \in Q_{ij}$, and $g(q) = 0$ if $q \notin Q$. The graph of g is a discontinuous surface, \bar{Z} , consisting of horizontal rectangles. We wish to associate a smooth surface to \bar{Z} which captures its essential features, such as peaks and valleys.

Let $\phi: R^2 \rightarrow R$ be a smooth function (that is, the first and second order partial derivatives of ϕ exist and are continuous), and suppose that ϕ and all its partial derivatives to second order are integrable. Then, the convolution of g with ϕ , denoted here by $\#$, is given by

$$g \# \phi(x, y) = \iint_{\mathbb{R}^2} g(\xi, \eta) \phi(x - \xi, y - \eta) d\xi d\eta, \quad (16)$$

and the graph, S_ϕ , of $g \# \phi$ is a smooth surface. If $f = g \# \phi$, it is easily shown that $f_x = g \# (\phi_x)$, $f_y = g \# (\phi_y)$, $f_{xx} = g \# (\phi_{xx})$, $f_{xy} = g \# (\phi_{xy})$, $f_{yy} = g \# (\phi_{yy})$. The Gauss curvature, K_ϕ , and the mean curvature, H_ϕ , of S_ϕ are computed by using the formulae (7) and (8) in section III. The resulting curvature functions are very sensitive to the choice of ϕ , thus careful consideration must be given to this choice. For instance, if the support of ϕ (the set on which $\phi \neq 0$) is very small, then S_ϕ will look like a step function with rounded edges. The resulting curvature function, K_ϕ , will have huge peaks of positive and negative value at the corners of the steps, and be zero toward the middle. This will tell us nothing about how steps vary with respect to their neighbors, making K_ϕ useless. Other factors include the symmetry and ease of computability with the convolution kernel, ϕ . We require that ϕ satisfy :

- (i) The support of ϕ is roughly the size of a step and its neighbors.
- (ii) The function ϕ is radially symmetric.
- (iii) Computations with ϕ are relatively easy.

With these criteria in mind we choose ϕ to be $\phi(x, y) = \psi(x) \psi(y)$, where ψ is the Gauss probability density $\psi(x) = \exp(-x^2/2) / \sqrt{2\pi}$. This choice of ϕ does not satisfy (i), but this is easily rectified by rescaling ϕ according to the rule $\phi_\epsilon(x, y) = \phi(x/\epsilon, y/\epsilon) / \epsilon^2$. The collection of functions $\{\phi_\epsilon; \epsilon > 0\}$ is an example of an approximate identity, and has the property that $g \# \phi_\epsilon(x, y) \rightarrow g(x, y)$ as $\epsilon \rightarrow 0$ if (x, y) is a point of continuity of g .

The first and second order partial derivatives of ϕ are easily seen to be

$$\begin{aligned} \phi_x &= -x\phi, \quad \phi_y = -y\phi, \quad \phi_{xx} = (x^2 - 1)\phi, \quad \phi_{xy} = -xy\phi, \\ \phi_{yy} &= (y^2 - 1)\phi. \end{aligned}$$

Let $R = \{ (x,y) : 3 \leq x, y \leq 3 \}$ and let $R_{ab} = \{ (x,y) : -1 + 2a \leq x \leq 1 + 2a, -1 + 2b \leq y \leq 1 + 2b \}$ where a, b are elements of the set $\{ 1, 0, -1 \}$. Thus, the square, R , is the union of nine subsquares, R_{ab} . Define numbers w_{ab} by the rule

$$w_{ab} = \iint_{R_{ab}} \phi(x,y) dx dy .$$

We define $w_{ab}^x, w_{ab}^y, w_{ab}^{xx}, w_{ab}^{xy}, w_{ab}^{yy}$ similarly, for example, w_{ab}^x is the integral of ϕ_x over the set R_{ab} . All of these integrals are easily computed, using integration by parts and substitution, except for w_{ab} , which must be integrated numerically. Scaling R_{ab} down to the size of pixel domains determines the value of ϵ above. The corresponding integrals (of ϕ_ϵ , and its derivatives, over pixel domains) have the same value as those already discussed. It follows that the quantities w_{ab}^x, w_{ab}^y , etc. can be used as the weights of 3×3 templates that are discrete versions of the convolutions $g\#((\phi_\epsilon)_x), g\#((\phi_\epsilon)_y)$, etc. Let $\Phi, \Phi_x, \Phi_y, \Phi_{xx}, \Phi_{xy}, \Phi_{yy}$, denote the templates with 3×3 template configuration, and weights $w_{ab}, w_{ab}^x, w_{ab}^y, w_{ab}^{xx}, w_{ab}^{xy}, w_{ab}^{yy}$, respectively. Use g° to denote the gray-value image associated to g° . Then we have the following correspondance of smooth functions to gray-value images:

$$\begin{array}{ll} g\#\phi \rightarrow g^\circ \oplus \Phi = \Lambda & g\#\phi_{xx} \rightarrow g^\circ \oplus \Phi_{xx} = \Lambda_{xx} \\ g\#\phi_x \rightarrow g^\circ \oplus \Phi_x = \Lambda_x & g\#\phi_{xy} \rightarrow g^\circ \oplus \Phi_{xy} = \Lambda_{xy} \\ g\#\phi_y \rightarrow g^\circ \oplus \Phi_y = \Lambda_y & g\#\phi_{yy} \rightarrow g^\circ \oplus \Phi_{yy} = \Lambda_{yy} \end{array}$$

With these conventions, we define the gauss and mean curvature images of g° to be, respectively,

$$K^{\circ} = \frac{A_{xx} * A_{yy} - A_{xy}^2}{(1 + A_x^2 + A_y^2)^2} \quad (17)$$

$$H^{\circ} = \frac{(1 + A_x^2) * A_{yy} - 2 A_x * A_y * A_{xy} + (1 + A_y^2) * A_{xx}}{(1 + A_x^2 + A_y^2)^{3/2}} \quad (18)$$

Here, A^2 is understood to mean the image $A * A$. A segmentation of the Gauss curvature image is given by $\tilde{K}^{\circ} = C_{>\epsilon}(K^{\circ}) + C_{<-\epsilon}(K^{\circ})$, where $C_{>\epsilon}(K^{\circ}) = [(K^{\circ} - \epsilon) \vee 0]^{-1} * [(K^{\circ} - \epsilon) \vee 0]$, and $C_{<-\epsilon}(K^{\circ}) = [(K^{\circ} + \epsilon) \wedge 0]^{-1} * [(K^{\circ} + \epsilon) \wedge 0]$. It follows that $\tilde{K}^{\circ}(q) = 1$ if $K^{\circ}(q) > \epsilon$, 0 if $-\epsilon \leq K^{\circ}(q) \leq \epsilon$, -1 if $K^{\circ}(q) < -\epsilon$. Note that this segmentation algorithm also applies to the definition of K° given by equation (15) of section V. It can also be used on the mean curvature image, H . Whether this yields useful information is not clear.

Let $A = \sqrt{(H^{\circ})^2 - K^{\circ}} / |H^{\circ}|$, and let $\tilde{A} = C_{<\epsilon}(A)$. If ϵ is small, then A assumes the value 1 at points of nearly circular points (in the sense of section IV), and 0 otherwise. The image, A , should have the appearance of nearly circular spots. These spots could have a wide range of diameters. If $0 < \alpha < \beta$, define B to be the image $B = C_{(\alpha, \beta)}(K^{\circ}) * C_{<\epsilon}(A)$. Thus $B(q) = 1$ if $\alpha < K^{\circ}(q) < \beta$ and $A(q) < \epsilon$, and $B(q) = 0$ otherwise. Limiting the range of K° should limit the size of the corresponding spots, the spots in the image B are then likely to be targets. Obtaining good results depends on the choice of the parameters α, β, ϵ . These parameters will depend on the size and shape of the targets sought relative to the given image. Two points should be made here. First of all, we have only considered targets that are nearly circular in shape, algorithms such as the one defining B should be possible for other shapes. Secondly, experimentation will undoubtedly reveal details that have been overlooked, so that some modification of the above program may be necessary. Finally,

it should be mentioned that the author was unable to find any algorithms such as the one defining B in the literature on Image Processing.

Recommendations:

1. A second method for associating a regular surface to a grayvalue image is by means of B-splines. This method is used by Yang and Kak in [6] to compute curvature. It would be of interest to compare this method with the two described in this report for efficiency and accuracy.

2. It should be possible to establish a PL-version of mean curvature, apparently, no such notion yet exists in the literature. The author began to do this, but ran out of time.

3. It could prove useful to try other convolution kernels, perhaps one that is not radially symmetric.

4. Concepts from Topology may prove useful for distinguishing regions in the curvature images discussed above. For example, one would want a computer to be able to tell the difference between a disk and an annulus.

5. Experimentation with actual images should be performed in order to determine the strengths and weaknesses of image transformations such as A and B of section VI.

REFERENCES

1. Besl, Paul J., and Ramesh C. Jain, Invariant Surface Characteristics for 3D Object Recognition in Range Images, Comput. Vision Graphics Image Process. 33, 1986, 33 80.
2. Busemann, Herbert , Convex Surfaces, Interscience Publishers, Inc. New York, 1958.
3. do Carmo, Manfredo P., Differential Geometry of Curves and Surfaces, Prentice Hall, Inc., Englewood Cliffs, New Jersey, 1976.
4. Gauss, Karl Friedrich, General Investigations of Curved Surfaces, Raven Press, Hewlett, New York, 1965.
5. Ritter, Gerhardt X, Image Algebra , D.T.I.C. Technical Report, Defence Logistics Agency , Cameron Station , Alexandria, Virginia 22304 6145. December, 1986.
6. Yang, H.S. and A. C. Kak, Determination of the Identity, Position and Orientation of the Topmost Object in a Pile, Comput. Vision Graphics Image Process. 36, 229 255, 1986.

1987 USAF-UES SUMMER FACULTY RESEARCH PROGRAM/
GRADUATE STUDENT SUMMER SUPPORT PROGRAM

Sponsored by the
AIR FORCE OFFICE OF SCIENTIFIC RESEARCH

Conducted by the
Universal Energy Systems, Inc.

FINAL REPORT

OZONATION OF FIREFIGHTER TRAINING FACILITY WASTEWATER
AND ITS EFFECT ON BIODEGRADATION

Prepared by: Dennis D. Truax, Ph.D., P.E.
and Ethan S. Merrill, Graduate Student
Academic Rank: Assistant Professor
Department and University: Department of Civil Engineering
Mississippi State University
Research Location: Air Force Engineering and
Services Center
HQ AFESC/RDVW
Tyndall AFB, Florida 32403-6001
USAF Researcher: Mr. Bruce Nielsen
Date: 30 Sep 87
Contract No: F49620-85-C-0013

REFERENCE DR. TRUAX
SFRP FINAL REPORT NUMBER 136

1987 USAF-UES SUMMER FACULTY RESEARCH PROGRAM
GRADUATE STUDENT SUMMER SUPPORT PROGRAM

Sponsored by the
AIR FORCE OFFICE OF SCIENTIFIC RESEARCH

Conducted by the
Universal Energy Systems, Inc.

FINAL REPORT

THE FEASIBILITY OF A LABORATORY INFORMATION MANAGEMENT
SYSTEM FOR THE ANALYTICAL CHEMISTRY LABORATORY

Prepared by: Veronica S. Minsky
Academic Rank: Graduate Student
Department and University: Computer Science Department
Middle Tennessee State University
Research Location: Chemical, Metallurgical and NDE Laboratories
Arnold Engineering Development Center
Arnold Air Force Station, TN 37389-9998

USAF Reseacher:
Date: 01 Aug 87
Contract No: F49620-85-C-0073

The Feasibility of a Laboratory Information Management
System For The Analytical Chemistry Laboratory

by
Veronica S. Minsky

ABSTRACT

Microcomputer controlled laboratory instruments have accelerated the rate of sample analysis. The paperwork associated with sample processing has not kept pace. A laboratory information management system (LIMS) may improve sample processing, reporting and allow result entry directly from instruments. A LIMS system may accept results directly from most instruments with an RS-232 or IEEE 488 port. Interfacing involves two processes; first the electronic transfer of data from the instrument to the LIMS must occur, which is often an easy task, especially with newer instruments. Second the data must be transformed from the format of the instrument into the format of the LIMS database. Standardization of this process may be possible using standard forms to identify data items. Each instrument would have a custom program to identify the data items in a standard form. Each LIMS system would reformat the data from the standard form into the format of the particular LIMS database.

ACKNOWLEDGEMENTS

I wish to thank the Air Force Systems Command and the Air Force Office of Scientific Research for sponsorship of this research. Universal Energy Systems proved to be helpful and effective in all administrative aspects.

Mr. Marshall Kingery, the Effort Focal Point at AEDC, provided encouragement, enthusiasm and someone with whom to discuss ideas and directions. Whatever Mr. Kingery did not know, he knew where to find out. On more than one occasion he directed me to informative sources on the base and went out of his way to ensure the success of this project.

Mr. John Godshall's encouragement and interest in every phase of this project served as a constant source of stimulation. His intense interest in laboratory automation made this project possible. Mr. Doug Hite was an enjoyable person to work with and patiently answered my many questions. All together the laboratory staff provided an enjoyable working environment and contributed to a rewarding project.

I. INTRODUCTION:

Analytical chemistry laboratories have seen an explosion in the number of microcomputers in the laboratory. These computers enable the chemist to complete sample analyses in a fraction of the time it may have previously taken. Typically the manual system of processing paperwork associated with samples and results, however, has not kept pace. It is the weak link in the laboratory, slowing down the output of results and decreasing the overall efficiency and quality of the laboratory.

The Chemical, Metallurgical and NDE Laboratories at The Arnold Engineering Development Center are particularly concerned with the quality and efficiency of their work. A sample tracking and information system able to keep pace with the analyses would be a real asset to the laboratory. Such a system would be able to interface directly with laboratory instruments and extract test results into a laboratory information database.

My research interests have been in the area of communication software, particularly concerning microcomputers. My previous work, writing and using communication software for a wide variety of microcomputers, minicomputers and mainframes in a hospital environment, contributed to my assignment with the Chemical, Metallurgical and NDE Laboratories.

II. OBJECTIVES OF THE RESEARCH EFFORT:

Currently there are numerous laboratory information management software packages commercially available. These packages are sample tracking, report management and results entry systems. They do not generally interface with laboratory instruments automatically; communications protocols must be established and programs written to reformat test results for the LIMS database.

My assignment as a participant in the 1987 Graduate Student Summer Support Program (GSSSP) was to determine the feasibility of establishing communications between laboratory instruments and a laboratory information management system, and to study the possible standardization of these communication interfaces.

The Chemical Laboratory at AEDC has been seriously studying the possibility of purchasing a LIMS system. A goal of this research effort was to determine the needs and goals of the Chemical, Metallurgical and NDE Laboratories at AEDC, and to determine the available options and requirements of a laboratory information management systems for the lab. A result of this effort was a written specification for procurement of a LIMS system.

III.

a. The Chemical and Metallurgical Laboratories proved to be a valuable source of information during this research effort. Observing the flow of samples and paperwork thru the lab as well as interviewing the chemists, analysts, clerical staff, and managers uncovered inefficiencies in the sample paperwork process. At the First International LIMS Meeting, a users conference held in Pittsburgh, PA. June 23-25, 1987, over 40 papers were presented by users. The papers and informal discussions with conference attendees provided an additional source of information.

A visit to a laboratory with a laboratory information management systems installed was most instructive, as were to a lesser degree visits to vendor sales offices for system demonstrations. Interviews with various people at AEDC, experienced in communications hardware and software, supplemented this research effort. Finally, a review of the literature in laboratory automation added an additional source of information.

b. The Chemical, Metallurgical and NDE Laboratories are highly specialized. They provide quick sample turnaround while maintaining quality controls to insure the validity of their results. Analysts often find it necessary to by-pass the manual paperwork system in order to achieve the desired sample turnaround time. By-passing the tracking system increases chances for errors and sample loss.

One goal of the laboratory management is increased automation. They have numerous personal computers in the lab and there is a trend towards interfacing these standalone computers.

Many of the papers presented at the First International LIMS Meeting were by individuals from labs that started looking for LIMS systems before 1985. At that time few sophisticated commercial systems were available. Many of these labs elected to design and write in-house LIMS systems. Some relied on an outside person, frequently in an MIS department to design and write the system. Now two, three, or four years and thousands of dollars later, many of these labs are still modifying and revising their systems and few have integrated laboratory instruments.

There were numerous users of commercial system at the conference. Most had done some modifications to their systems, either by adding in-house programs, utilizing user configurable options, or purchasing custom programs from the vendor. Few have integrated laboratory instruments. Many users would find it necessary to pay the vendor for consulting time to begin this process of interfacing instruments.

Visits to a laboratory currently using a LIMS provided an opportunity to see first hand how LIMS managed laboratory paperwork. This lab runs a commercial LIMS package and has successfully employed user configurable options and in-house programs to customize the package. It appeared to increase the efficiency of the lab; lab reports are more timely and sample

status is easily determined. This particular lab is specialized, and the user configurable options make the system able to adapt to their ever changing needs. This lab has not interfaced any instruments with their LIMS, but plans to do so in the future. An additional observation from this visit is that the success of a LIMS depends not only on the software and hardware selected, but on the quality of the system manager overseeing the installation, customization and usage of the LIMS.

The available LIMS options will be discussed in terms of software, hardware and instrument interfaces. Software options can be broken down into in-house systems and commercially available packages. The in-house systems are typically designed with database packages. The advantage of an in-house system is the customization it allows. The disadvantage is the cost of development and maintenance.

The commercially available LIMS packages are as varied as the labs that use them. Some LIMS systems are single user systems, others are sophisticated multi-user systems. Some are particularly efficient in the large production labs, and others in small specialized labs. Choosing the best LIMS for a specific laboratory will ultimately depend upon the needs, goals and resources of that lab.

Hardware options are often dependent upon the software selected. The range of options starts with a standalone PC system and includes mainframes networked with PCs and instruments. A few software packages are available

for PC networks, allowing access to common databases and data transfers between PCs. More numerous are packages that run on minicomputers, such as the hardware from DEC VAX, Hewlett-Packard, IBM, and Concurrent. PCs may be used in place of terminals. A network can be installed in addition to or in place of the point-to-point communication between the PCs and the minicomputer. The advantage of a network is to allow the PCs operating in PC mode to access shared resources.

Instrument interfacing options depend upon the software and hardware selected. If an instrument has an RS-232 port interfacing is generally possible. There are two processes involved in instrument interfacing. The first is the electronic transfer of data from the instrument to the LIMS computer. Numerous communication packages exist, and for each instrument the communication protocol must be established. For the newer microcomputer based instruments this task is easily achieved. For the older instruments it can be a trial and error process requiring special communication software.

For some packages, the communication link must be executed in the LIMS computer and then in the instrument. Other packages such as the Hewlett-Packard LABSAM have a background program which constantly polls instruments for data transfer. The Perkin-Elmer CLAS software interfaces with chromatograms and allows the LIMS terminals to access results, raw data and initiate sample tests.

The second process is transforming data from the format used by the instrument into the format used by the LIMS database. Vendors often have example conversion programs written for the newer instruments. The user must often write these programs for the older instruments.

Beckman Instruments offers a software package, Laboratory Interface Language (LIL) allowing users to write programs for instruments which identify data items. The LIL program then reformats the identified items for the LIMS database. This prevents changes in the database from affecting the individual instrument interface programs.

This concept may assist in the standardizing of laboratory interfaces. If instrument vendors provide sample programs in FORTRAN or BASIC which identify most data items in a standard form, LIMS vendors could provide a program which accepts data items from the standard form and reformats them for their LIMS database. Most data items from an instrument would be identified in a standard form. The different LIMS would then reformat only the data items required for their particular database.

IV. RECOMMENDATIONS.

a. Based on the needs and goals of these labs, a laboratory information management system would be a valuable asset. The type of samples and tests requested by clients frequently change. The LIMS, therefore would have to

be flexible. The LIMS would have to be multi-user and have the ability to interface instruments. Support from the vendor would also be important.

The needs of the labs could be met by several commercially available packages. Requirements of the software include sample tracking and reporting, and result entry both manually and directly from instruments. It should be user configurable in the login screens, menu selections, client reports and result data. It should provide the ability to read and write directly to the database with FORTRAN or BASIC. Other desired software features include; automatic test scheduling of routine samples, batch sample entry and an easy to use query language.

The system should operate in normal office conditions, provide fast response time, and have the capacity for growth. The vendor should be able to supply software support via a telephone modem. Prior to installation of the LIMS the labs needs to identify a systems manager. This may be an additional employee or someone within the lab. This person will be involved in installing, and customizing the LIMS full time for 6 to 8 months. After this initial time period, the job should decrease to 20 percent of the systems manager's time.

b. Further study of the standardization of instrument interface could focus on determining a standard form for data items passed from the instruments. Once a standard form is established, LIMS vendors could provide a program to reformat this standard form for their specific LIMS database. This process

would simplify the instrument interface process and isolate the interface programs from variability and changes in the LIMS database. This process would involve discussions with LIMS vendors, instrument vendors, and LIMS users. A paper could be presented at the next LIMS users conference to elicit support among LIMS users. Pressure from users would be the most effective way to persuade vendors to implement interfacing standards.

REFERENCES

- Berthrong, P.G. and Mandfield, P.B. "Automation Systems For Small Laboratories: Part Two Nonchromatographic Data and LIMS Functions." American Laboratory, Vol. 18, No. 5, May 1986 pp. 82-91.
- Borman, S.A. "Laboratory Computer Networks." Analytical Chemistry, Vol. 56, No. 3, March 1984, pp. 408-413.
- Flint, D. "The Selection of a Local Communication Network." Local networks Strategy and Systems; Proceedings of Localnet'83, Online Conferences Limited, Northwood, UK, 1983, pp. 1-12.
- Jones, K. "Laboratory Information Management Systems - A Survey." Journal of Automatic Chemistry, Vol. 7, No. 3, Jul-Sep 1985, pp. 136-140.
- Liscouski, J.G. "Integrated Laboratory Automation Networks." American Laboratory, Vol. 18, No. 2, Feb. 1986, pp. 116-120.
- McKiney, K. and Lawler, G. "Exploiting PCs For Laboratory Information Management." American Laboratory, Vol. 18, No. 9, Sept. 1986, pp. 62-73.
- Ouchi, G. "How Much LIMS Does Your Lab Need." Research and Development, Vol. 28, No. 4, April 1986, pp. 78-81.
- Siemens, B.K. "Laboratory Management With Automation." American Laboratory, Vol. 19, No. 7, July 1987, pp. 54-58.

1987 USAF-UES SUMMER FACULTY RESEARCH PROGRAM/
GRADUATE STUDENT SUMMER SUPPORT PROGRAM

Sponsored by the
AIR FORCE OFFICE OF SCIENTIFIC RESEARCH

Conducted by the
Universal Energy Systems, Inc.

FINAL REPORT

Investigation of the Potential Impact of New Photonic Materials
On Optical Processing Systems

Prepared by:	Frank W. Moore
Academic Rank:	Doctoral Student
Department and University:	Computer Engineering Wright State University
Research Location:	AFWAL/AADO-2, W-PAFB, Ohio
USAF Researcher:	Mr. Joseph Brandelik
Date:	August 20, 1987
Contract No.:	F49620 - 85 - C - 0013

Investigation of the Potential Impact of New Photonic Materials
on Optical Processing Systems

by

Frank W. Moore

ABSTRACT

This report summarizes research efforts conducted during the 1987 Graduate Student Summer Support Program research term at AFWAL/AADO, Wright-Patterson Air Force Base, Ohio.

Claims for the speed and dynamic range characteristics of new photonic materials suggest that these materials could permit the development of competitive optical processors. The high resolution claimed for these materials may make them suitable for numerous information processing tasks, including memory, analog-to-digital conversion, multiplication, and two-dimensional image processing.

Non-cascadable Boolean operations have been demonstrated. Analog addition of two-dimensional images appears to be possible. Qualitative experiments suggesting uses of new photonic materials in optical systems have been performed, general properties of these materials have been determined, and future quantitative tests required for precise material characterization have been proposed. Several multiplication schemes, aimed at performance which would be competitive with state-of-the-art electronic multipliers, are also proposed.

Acknowledgements

I wish to thank the Air Force Systems Command and the Air Force Office of Scientific Research for their sponsorship of this exciting research endeavor. Specifically, the opportunity to work with the technical, managerial, and secretarial staff at the Electro-optics Technology Branch of the Avionics Laboratory at Wright-Patterson Air Force Base has been greatly appreciated. The following Avionics Laboratory personnel need to be mentioned for their invaluable support of this research effort: Joseph Brandelik for his technical guidance; and Dale Stevens for his tremendous contribution to the successful completion of the laboratory experiments. I would also like to acknowledge Universal Energy Systems, Inc. and Wright State University for their administrative support.

Most of all, I wish to thank Dr. Alastair McAulay.

I. INTRODUCTION

The general consensus among researchers of optical processing technologies is that progress in optical memories and optical logic is largely determined by the availability of new photonic materials. Until recently, materials exhibiting both the speed and the resolution necessary for optical processors to compete with existing electronics technology did not exist. Recently, however, photonic materials known as "Electron-Trapping" (ET) materials have been produced by Dr. Joseph Lindmayer and his associates at Quantex Corporation, under contract to the Aeronautical Systems Division of the United States Air Force. If Lindmayer's claims as to the speed and spatial resolution of ET materials are attainable, then an effective utilization of these materials could have a notable impact on future information processing systems.

II. OBJECTIVES OF THE RESEARCH EFFORT

The primary goals of this summer's research effort were to:

1. demonstrate fundamental Boolean operations required for the implementation of binary optical computers;
2. demonstrate principles of two-dimensional analog image addition, multiplication, and extraction;
3. determine general properties of ET materials;
4. perform qualitative experiments suggesting uses of these materials in optical systems;
5. investigate the design of high-speed optical processing systems that could exploit the full potential of ET material technology and satisfy the performance

requirements of existing and future Air Force systems.

The following sections of this report contain a summary of tests performed on Electron-Trapping material samples received by AFWAL/AADO from Quantex Corporation, together with brief discussions and assessments of test results.

III. DEMONSTRATION OF BOOLEAN LOGIC FUNCTIONS

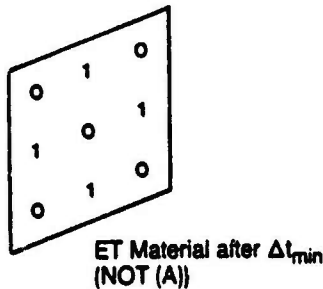
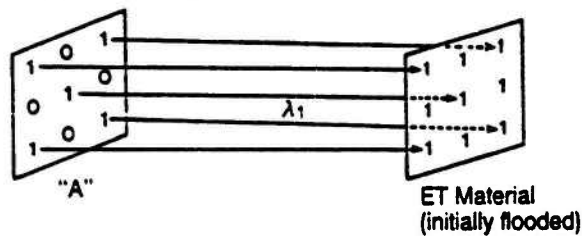
Methodologies for performing the following Boolean logic functions using ET materials have been defined: Inversion, NOR, OR, AND, NAND, XOR, and Shift. Several of these functions have been demonstrated in the laboratory. Detailed descriptions of the Inversion and NOR implementations have been included in this report; other operations are similar. Note from the feasibility of the NOR operation that every existing digital logic circuit can be constructed from photonic components.

Because the three wavelengths λ_3 (to store photonic energy in the ET material), λ_1 (to induce emission of stored energy, i.e. read the material), and λ_2 (the emission wavelength of stored photonic energy) are distinct, combinational logic circuits constructed from these gates will require "wavelength conversion" systems. Image intensifiers could be constructed that perform the conversions ($\lambda_2 \rightarrow \lambda_3$) and ($\lambda_2 \rightarrow \lambda_1$), as well as the gain and thresholding required to cascade photonic logic gates that utilize ET material technology.

Development of "complementary" ET materials with wavelength characteristic triples ($\lambda_4, \lambda_2, \lambda_3$) could provide a means of eliminating intensifiers between complementary pairs of ET material components.

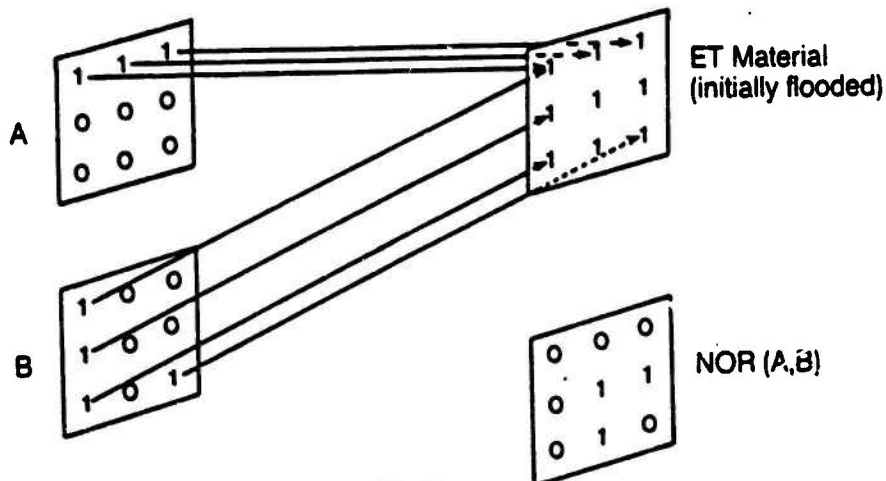
A. Inversion

1. Initially flood the surface of the ET material with λ_2 light. In effect, this step initializes all elements to a logic "1".
2. Illuminate the material with a two-dimensional light pattern (wavelength λ_1) in which bright pixels represent logical "1", and dark pixels represent logical "0", for a time Δt_{min} .
3. Subsequent reading of the material (illumination by λ_1) reveals that the only points of luminescence will be those pixels that were not exposed to λ_1 during the previous step. The resulting image will be the inverse of the two-dimensional input pattern ("not A").



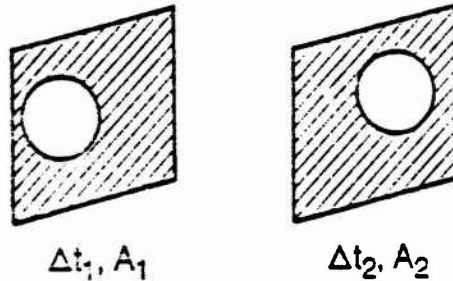
B. NOR

1. Initially flood the material surface as before.
2. Read out images A and B from the ET material. After some Δt_{min} , only those pixels not read out by either A or B will remain energized; subsequent illumination of the material by λ_1 will cause only these pixels to luminesce.



IV. DEMONSTRATION OF ANALOG ADDITION

A. Set-Up



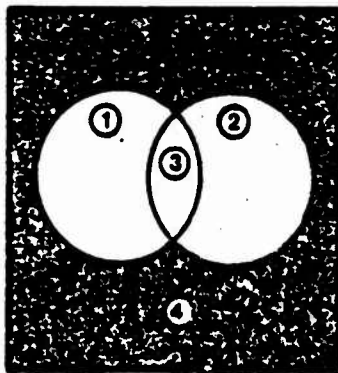
B. Procedure

1. After erasing the material surface, illuminate a small circular area of the ET material sample with λ_2 light for Δt_1 .
2. Illuminate a second small circular area of the ET material sample with λ_2 for Δt_2 . Allow part of this area A_2 to overlap the first illuminated region A_1 .
3. Read the sample using λ_1 light.

C. Result

Illumination

ET Material Sample



- | | | |
|----------|-----|----------------------------|
| Region 1 | --> | Δt_1 |
| Region 2 | --> | Δt_2 |
| Region 3 | --> | overlap of regions 1 and 2 |
| Region 4 | --) | none |

This test suggests that analog addition could be performed if the inputs and outputs remained in the linear region of the ET materials. In this event,

1. for $\Delta t_1 = \Delta t_2$: $I_1 \approx I_2 \gg I_4$; $I_3 = I_1 + I_2 = 2I_1 = 2I_2$.
2. for $\Delta t_1 = 2\Delta t_2$: $I_1 = 2I_2$; $I_2 \gg I_4$; $I_3 = I_1 + I_2 = 3I_2$.

V. GENERAL PROPERTIES OF ELECTRON-TRAPPING MATERIALS

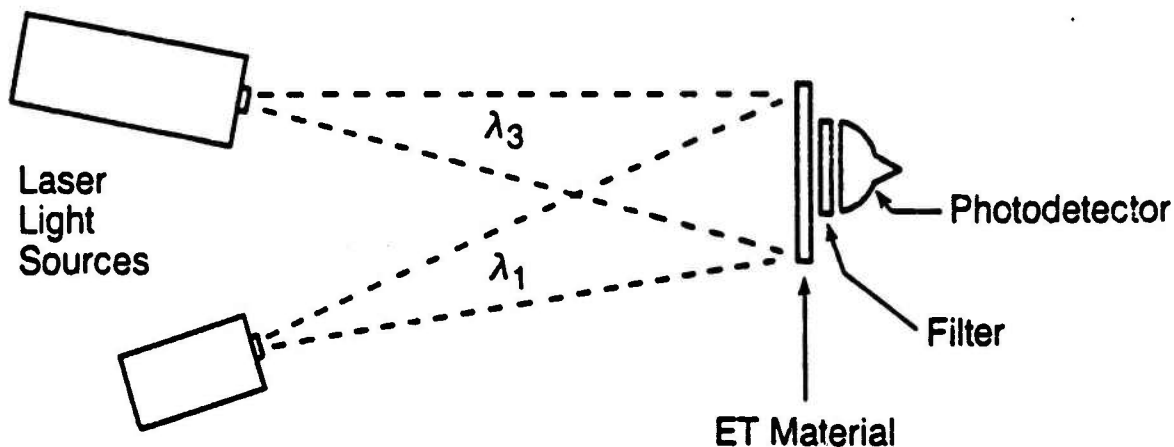
The next set of experiments described in this report demonstrated the following ET material properties:

1. The output intensity depends upon the intensity of λ_3 light used to write onto the ET material surface;
2. Output intensity also depends upon the intensity of λ_1 light used to read from the ET material surface;
3. The material has a large dynamic range. According to Quantex, this range is linear through at least three orders of magnitude, a feature that would be useful in storing one of a large number of possible analog values in a particular position on the ET material surface (Part VII).
4. The samples tested have high spatial resolution (Experiment V-3).

Laboratory experience with ET material samples indicates that the intensity of λ_2 output light is monotonically dependent upon the intensity of λ_1 light used to read it, through large ranges of stored energy and read intensity.

A. Experiment V-1

1. Set-Up:



2. Goal:

Investigate output intensity as a function of the energy at which λ_3 light was written to the ET material, as well as the intensity of λ_1 light used to read from the material.

3. Procedure:

- a. Write on the ET material for varying durations Δt with constant intensity I . The energy thus varies as $E_w = I\Delta t$.

b. After Δt , read from the material using various intensities of λ_1 light.

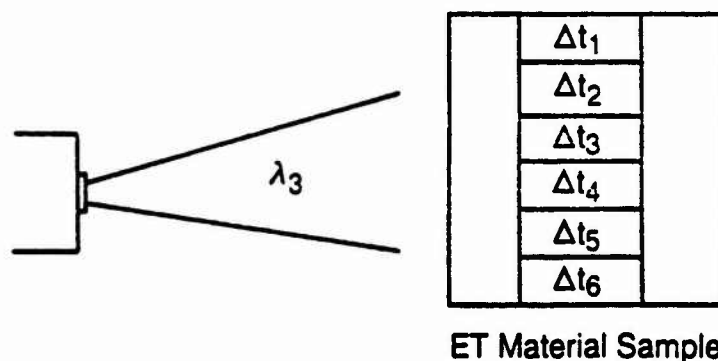
4. Results:

a. Observed that the variation in output intensity is dependent upon the increase in read light intensity as well as the amount of energy written onto the ET material.

b. Observed gradual decrease in output intensity as the sample was read by a constant λ_1 illumination.

B. Experiment V-2

1. Set-Up:



2. Goal:

Demonstrate utilization of the dynamic range of ET materials.

3. Procedure:

a. Erase the surface of the ET material with a λ_1 flood.

b. Expose adjacent sections of the material to increasing durations of constant-intensity λ_1 light.

c. Illuminate entire material with λ_1 light.

4. Results:

Observed that sections of the ET material exposed to increasingly higher energies of λ_3 light had brighter output intensities when subsequently illuminated with a uniform λ_1 wash. Furthermore, the relative brightness of these sections was maintained even while the intensity of light output was decreasing at all points on the material surface.

C. Experiment V-3

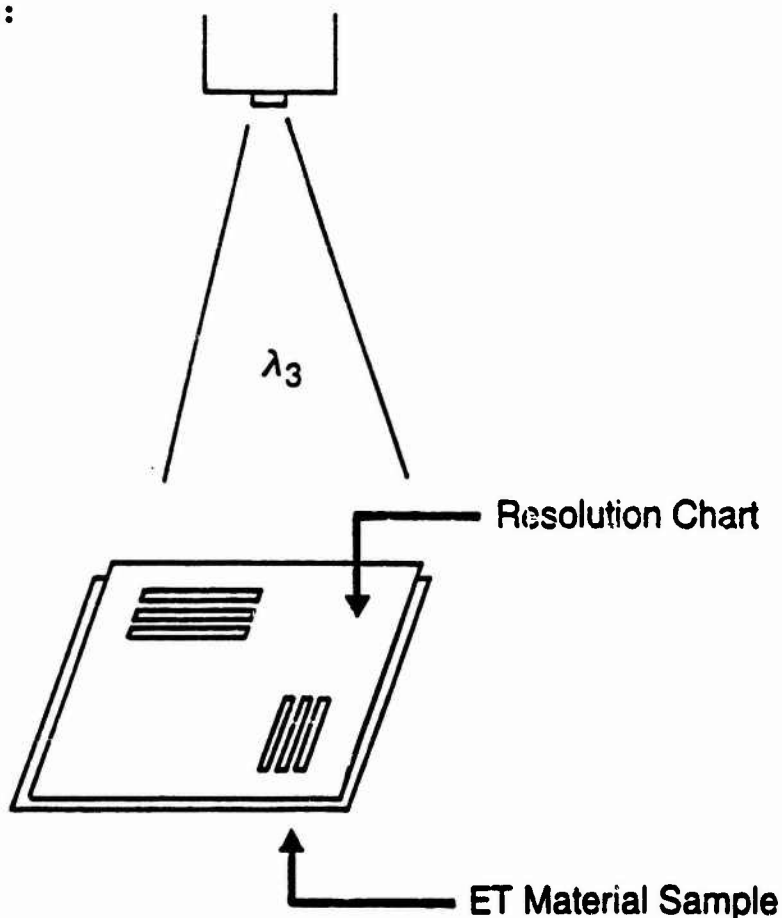
1. Goal:

Determine the resolution of ET material samples.

2. Procedure:

- a. Uniformly erase the ET material.
- b. After placing a standard resolution chart on top of the ET material sample, expose the sample to λ_2 light.
- c. Remove the resolution chart, and read the material surface using λ_1 light. A measure of the resolution of the ET material sample will be the smallest chart bar images resolved on the surface of the material.

3. Set-Up:



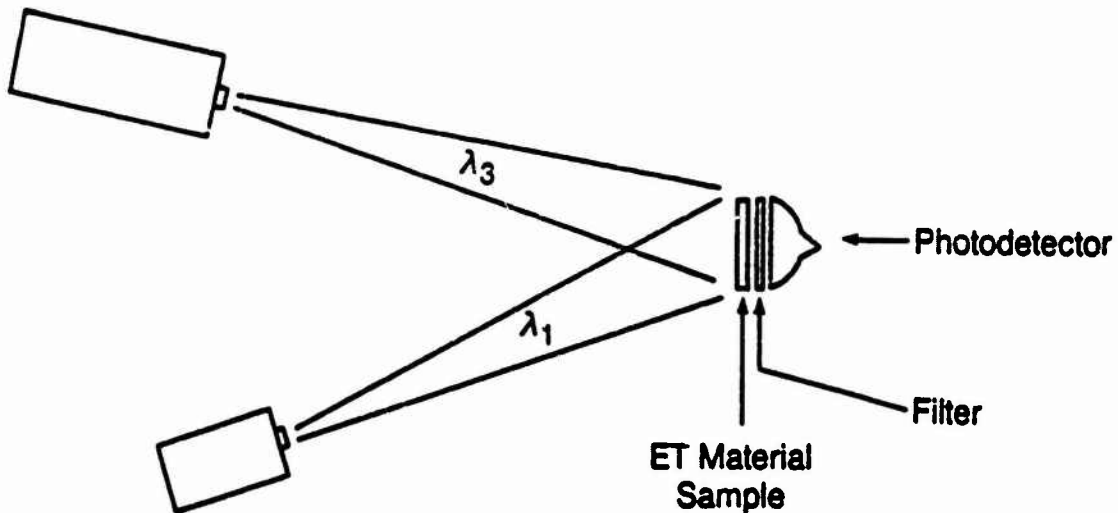
4. Result:

ET material samples produced by Quantex Corporation can be classified according to the thickness of the material on the sample surface. Experiment V-3 demonstrated that thick-film samples can resolve at least 100 lines over a 2-inch dimension of the ET material. This fact suggests that as many as 10000 elements could be stored on these relatively inexpensive devices.

Scientists at Quantex claim a much higher resolution for thin-film ET material samples (in excess of one million pixels per square mm).

VI. RECOMMENDED FUTURE QUANTITATIVE ET MATERIAL TESTS

Numerous quantitative thin-film ET material characterization tests must be performed before these materials can be used in precision high-speed processors. A typical test set-up consisting of variable-intensity λ_3 and λ_1 light sources, a band-pass filter, a λ_2 -sensitive detector, and an ET material sample is shown in the following figure:



- Test No. 1 --- Determine the saturation level of the ET material (the point at which additional energy input will not change the amount of energy stored by the material).
- Test No. 2 -- Determine the decay characteristics of the ET material during extended exposure to low levels of λ_2 -light as a function of time.
- Test No. 3 -- Determine the threshold of the ET material (the level below which the output intensity of the material remains zero, or some constant, even after additional exposure to λ_1 light).
- Test No. 4 -- Verify the effects of various wavelengths when writing to the ET material; approximate the relative write efficiencies of candidate write wavelengths.
- Test No. 5 -- Determine the effects of different wavelengths when reading and erasing the ET material; approximate

the relative read efficiencies of candidate read wavelengths.

Test No. 6 -- Determine the wavelength λ_2 at which ET material output is most intense.

Test No. 7 -- Determine the "impulse response" of the material.

- (a) What is the minimum pulse duration, for various write intensities, for which a desired change in the stored energy level can be detected?
- (b) How long, and at what intensity, will the ET material luminesce after cessation of various write excitation energies?
- (c) What is the behavior of the material in response to read pulses of various intensities and durations? What is the minimum read pulse length?

Test No. 8 -- Determine exact relationships and dependencies of λ_3 , λ_1 , and λ_2 during simultaneous illumination of the ET material by λ_1 and λ_3 light.

Test No. 9 -- Once the precise characterizations of the ET material outlined in the previous eight tests have been completed, high-speed demonstration of the Boolean functions discussed in Section (III) of this report should be performed.

VII. MULTIPLICATION ALGORITHMS USING ELECTRON-TRAPPING MATERIALS

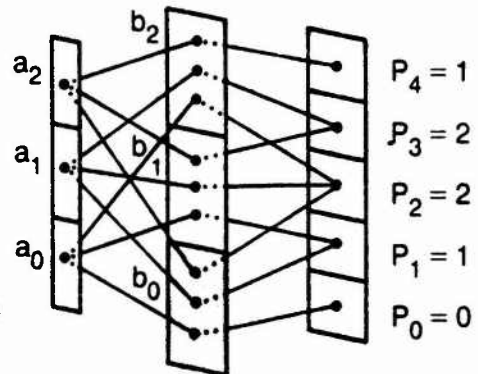
The high speed and high resolution of Electron-Trapping materials may be used when computing the product of two numbers in a binary-in-binary-out fashion (as required for interface with digital computers). In the next several pages, three schemes for performing Digital Multiplication by Analog Convolution (DMAC) are proposed:

1. Using binary multiplicands;
2. Using octal digits and medium-resolution column sums;
3. Using hexadecimal digits and high-resolution column sums.

DMAC is discussed extensively in the literature by McAulay, Rhodes and Guilfoyle, and others (see references).

Notes -- The convolution of two n-bit binary numbers can be represented by (n+1) analog levels separated by a fixed energy ΔE . Analog $((i/n) * K)$ can represent i, one of n non-zero energy levels over linear range K such that $\Delta E = ((1/n) * K)$.

The figure at right illustrates a means of performing DMAC in a single step for the simple case of $p = a * b = (111) * (110)$. Optical fiber interconnections allow the parallel projection of operand a through "transmissive elements" that pass or block light according to the values of corresponding bits in operand b. If the maximum number represented by p_i is N, then the attenuation of each fiber-optic connection from a to p must be $(1/N)$ to keep each resulting DMAC term in the linear region of ET material.



Each analog convolution, corresponding to the summation of a column of digits in a typical multiplication, must be converted to analog binary representation before being added back to the result accumulator in binary form. (This step may be performed using a small look-up table.) After $(2n-2)$ steps, $(2n)$ analog values of either 0 or 1 exist in the $(2n)$ digit positions of the result accumulator.

Predicted Performance

- t (n x n) = (time to load the first operand, n1, into an array of elements such that the transmissivity of the array corresponds to the binary values of n1 digits)
- + (time to shine copies of the second operand n2 thru the resulting n1 grid onto column sum accumulators)
- + [(2n-2) * (time to convert the resulting convolutions to binary equivalents and add these back to the result accumulator)]

Example of Binary Multiplication -- (1111111) * (1111111)

<pre> 1 1 1 1 1 1 1 * 1 1 1 1 1 1 1 ----- 1 1 1 1 1 1 1 1 1 1 1 1 1 1 1 1 1 1 1 1 1 1 1 1 1 1 1 1 1 1 1 1 1 1 1 1 1 1 1 1 1 1 1 1 1 1 1 1 1 1 1 1 1 1 1 1 ----- 1 2 3 4 5 6 7 8 7 6 5 4 3 2 1 </pre>	<p>Generation of Product Rows</p> <p>Product Rows</p> <p>DMAC Terms (Column Sums)</p>
--	---

```

0 1 2 3 4 5 6 7 8 7 6 5 4 3 2 1
                                0 0 1 0
                                -----
0 1 2 3 4 5 6 7 8 7 6 5 4 4 0
                                0 1 0 0
                                -----
0 1 2 3 4 5 6 7 8 7 6 6 4 0
                                0 1 0 0
                                -----
0 1 2 3 4 5 6 7 8 7 7 6 0
                                0 1 1 0
                                -----
0 1 2 3 4 5 6 7 8 8 8 0
                                1 0 0 0
                                -----
0 1 2 3 4 5 6 8 8 8 0
                                1 0 0 0
                                -----
0 1 2 3 4 5 7 8 8 0
                                1 0 0 0
                                -----
0 1 2 3 4 6 7 8 0
                                1 0 0 0
                                -----
0 1 2 3 5 6 7 0
                                0 1 1 1
                                -----
0 1 2 3 6 7 1
                                0 1 1 1
                                -----
0 1 2 4 7 1
                                0 1 1 1
                                -----
0 1 3 5 1
0 1 0 1
-----
0 2 3 1
0 1 1
-----
0 3 1
1 1
---
1 1

```

Column Sum Conversions

The LSB of the analog binary equivalents to the converted column replaces the analog value stored in that column, while the higher-order bits are analog-added back to the higher-order column sums of the result. A total of $(2n-2)$ sequential column conversions are required before the binary product of two binary numbers is produced.

This example illustrates a plausible technique by which the multiplication of two n -bit binary numbers can be performed via analog convolution in $2n$ total steps. The resulting product will be in binary form.

Photonic materials displaying a large linear range may be used as a substrate for the accumulation of partial products into the "column sums" required by DMAC algorithms.

Note that the "transmissive elements" shown in the diagram on the previous page need not be constructed using ET materials. A variety of existing technologies may be suitable. The only feature required by this binary multiplier for these elements is that they have the ability to either transmit or block incoming light, according to the values of the binary digits they represent.

Utilization of the Dynamic Range of ET Materials

Discussion -- the DMAC algorithm illustrated above requires conversion of base- n convolutions into binary numbers, a laborious and time-consuming task. A possibility for reducing the complexity of this chore entails a more efficient exploitation of

the large dynamic range of ET materials. Analog convolution may be performed in higher-order number bases. Fewer transformations (producing sum and carry) are required -- one per digit column in the selected number base -- at the expense of resolving higher numbers of distinct analog levels (K). Additional delay is incurred when converting product terms to binary form.

The final segments of this report illustrate a possible means of multiplying two binary operands, yielding a binary result, by convolving either 8-level (octal) or 16-level (hexadecimal) analog intermediate numerical representations. Methodologies have been developed that could exploit the large dynamic range of ET materials to perform column adjustments in higher-order number bases, thereby dramatically reducing the "column carry overhead" entailed by existing digital multiplication schemes.

A. Octal Digits (example)

Procedure --

1. Convert operand 1 from binary to octal representation via analog addition of bits, and write the analog result onto ET material;
2. Perform DMAC by reading the octal conversion of operand 1 with an octal representation of operand 2, projecting the resulting analog products onto ET material column sum accumulators;
3. Convert column sums back to analog octal values;
4. Convert octal digits back into binary form.

A multiplication scheme using octal digits in intermediate calculations is illustrated in the diagrams that follow. The numbers that have been assigned to each accumulative element represent a relative stored energy level. For a linear range of energy levels between 0 and K, the fraction ($i/7$) of the maximum energy K that may be stored in a particular accumulative element can be interpreted as an octal digit. The fractional values shown represent filter transmittances. The energy level of an input binary digit is equal either to K, representing binary 1, or to 0, representing binary 0. Conversion from binary to octal representation can be performed in a single step, with all bits of the original binary operand being projected through transmissive elements onto octal digit accumulators in parallel.

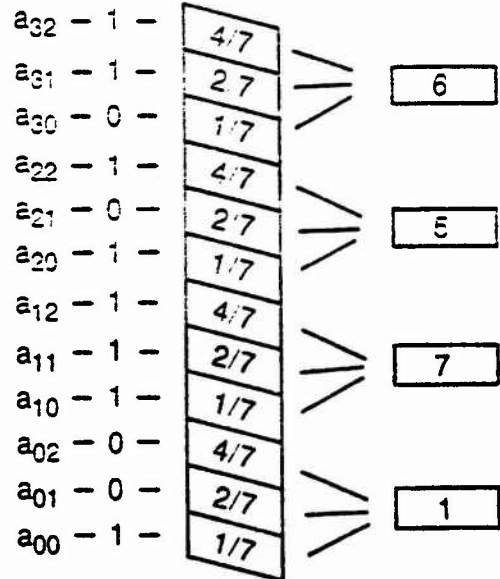
The multiplication step is similar; however, note that the ET

material output resulting from the illumination of one octal operand by a second octal operand will represent the analog product of the two operands. The resulting column sums correspond directly to the analog convolution of appropriate octal digits.

Products / Column sums

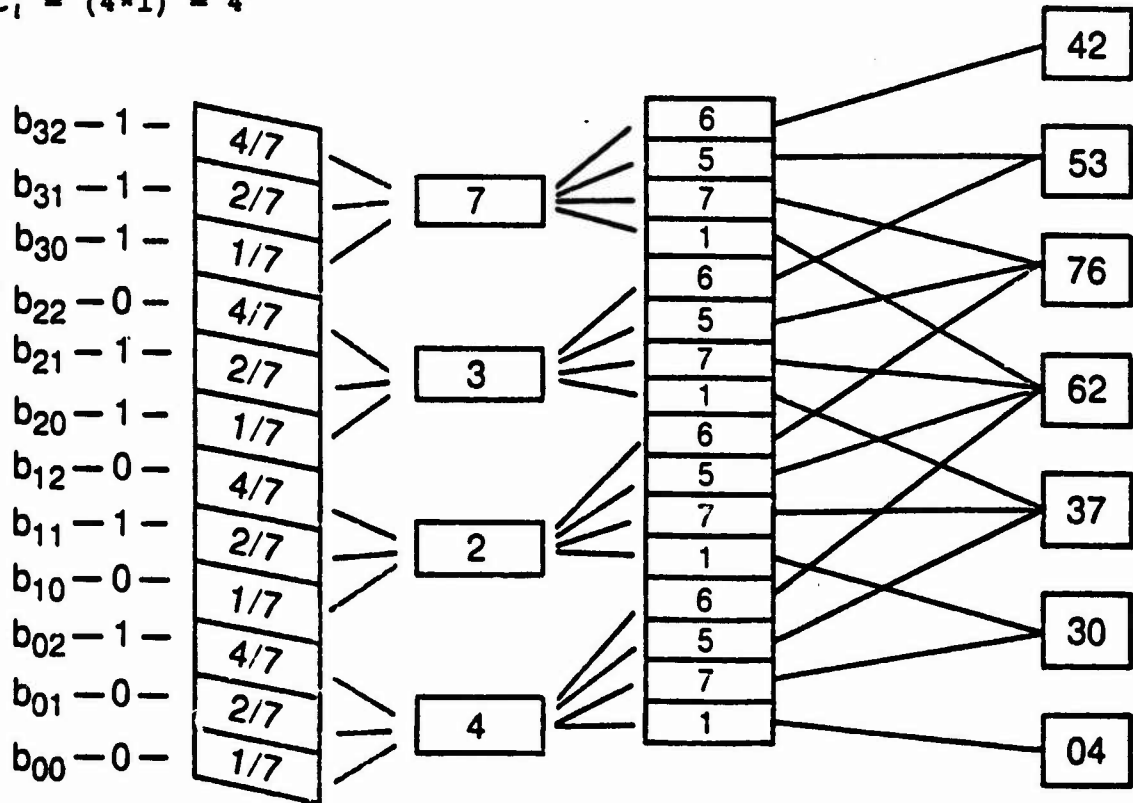
42	35	49	07			
	18	15	21	03		
		12	10	14	02	
			24	20	28	04
42	53	76	62	37	30	04

(analog convolutions)



Equivalent column sum calculations

- $C_7 = (7*6) = 42$
- $C_6 = (7*5) + (3*6) = 53$
- $C_5 = (7*7) + (3*5) + (3*6) = 36$
- $C_4 = (7*1) + (3*7) + (2*5) + (4*6) = 62$
- $C_3 = (3*1) + (2*7) + (4*5) = 37$
- $C_2 = (2*1) + (4*7) = 30$
- $C_1 = (4*1) = 4$



Column conversions (base 10 representations of column sums shown)

42 53 76 62 37 30 04

Analog convolution results

3 6 4
--

42 53 76 62 40

Illustration of the principle of Column Conversion --

5 0
--

42 53 76 67

-----> read out and erase C_i;
look up octal conversion of C_i
<----- and add this three-digit
number back to the
result accumulator.

1 0 3

42 54 76

1 1 4

43 55

6 7

49

6 1

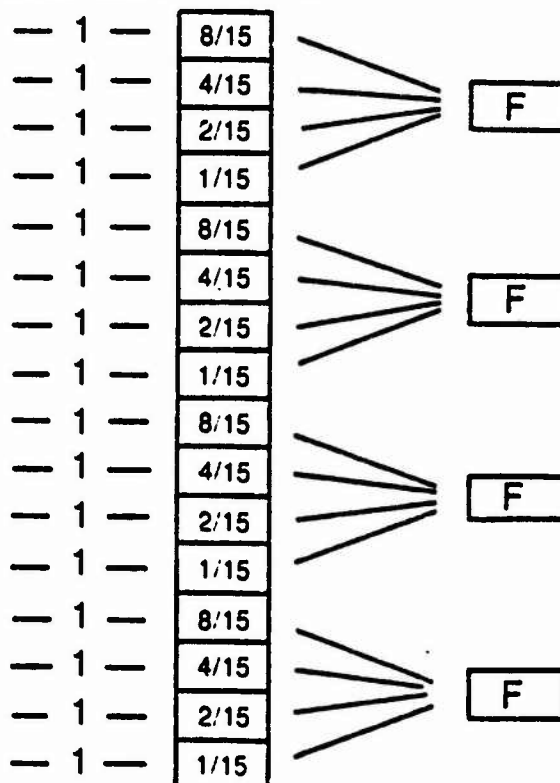
Conversion of an octal digit to binary form may be performed using a 3-bit analog-to-digital converter. Optical table look-up a-to-d converters proposed by Dr. Alastair McAulay represent an ideal solution to this conversion task (see references).

B. Hexadecimal Digits (example)

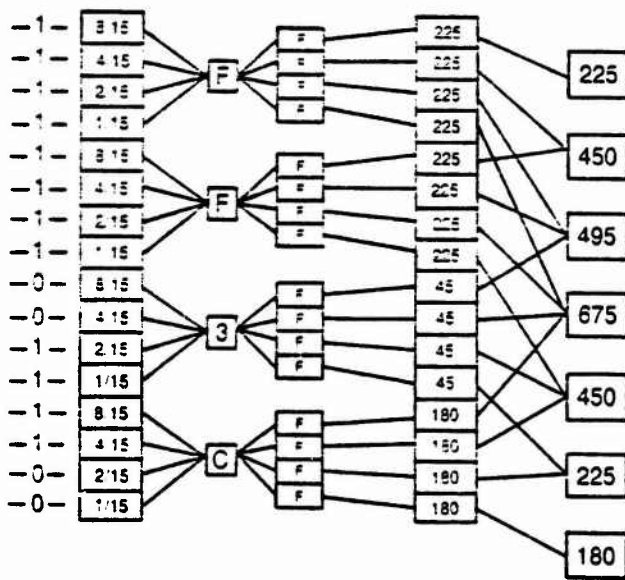
"Multiply A (1111 1111 1111 1111 = FFFFh)
times B (1111 1111 0011 1100 = FF3Ch)."

Step 1 -- Convert A to hexadecimal representation and store on an ET material surface as a hex digit H, with a corresponding energy level $E_H = ((H/15) * K)$.

Step 2 -- Convert B to hexadecimal representation and project through multiple copies of A, summing the analog products at C to form analog convolution terms, as shown.



Step 3 -- Use the analog value representing each convolution to look up a corresponding 3-digit hex sum number, which is added back to the product column sums as before.



Column conversions (base 10 representations shown)

```

225  450  495  675  450  225  180
                0  11  4
                -----
225  450  495  675  450  236
                0  14  12
                -----
225  450  495  675  464
                1  13  0
                -----
225  450  496  688
                2  11  0
                -----
225  452  507
                1  15  11
                -----
226  467
                1  13  3
                -----
1  239
                14  15
                --
15

```

```

FFFF h
* FF3C h
-----
FF3B00C4 h

```

Initial Column Summations

```

225 225 225 225
 225 225 225 225
   45  45  45  45
 180 180 180 180
-----
225 450 495 675 450 225 180

```

Analog Convolution Terms

(Total time required) =
 (time required to convert operand 1 to hexadecimal representation)
 + (time required to shine hex operand 2 through copies of operand 1 and accumulate N column sums)
 + (conversion and add-back times for resulting convolutions)
 + (final hex-binary conversion time)

Recommendations

The inherent parallelism and potential high-speed performance of optical systems offer an alternative technology for the solution of problems associated with electronics. The Air Force should continue to support the development of these systems. Two applications of immediate concern to the Air Force are analog-to-digital conversion and fast numerical calculation.

In this report, I have summarized investigations of new photonic materials and their potential impact on optical processing technology. Based on our findings, I recommend the following program of action:

1. Undertake precise characterization of Electron-Trapping materials supplied by Quantex Corporation, as discussed in section VI of this report;
2. Support the development of analog-to-digital conversion systems (such as those proposed by Dr. Alastair McAulay) utilizing new optical technology and new photonic materials;
3. Support the development of digital/optical interface devices to allow easy interconnection of electronic and optical sub-systems, thereby encouraging optical sub-system development;
4. Support development of more complex optical sub-systems, such as the fast multipliers outlined in section VII of this report.

REFERENCES

- Lindmayer, J. et. al., "New Photonic Materials for Digital Processing" (proprietary information). Contact Quantex Corporation, 2 Research Court, Rockville, Maryland 20850.
- Goutzoulis, A. P., D. K. Davies, Optical Architectures for Matrix Processing (AFWAL-TR-86-1117), November 1986.
- Huang, A. et. al., "Optical Computation Using Residue Arithmetic", Applied Optics Vol. 18 No. 2 (1979), pp. 149-161.
- Tai, A. et. al., "Optical Residue Arithmetic Computer with Programmable Computation Modules", Applied Optics Vol. 18 No. 16 (1979), pp. 2812-2823.
- Gaylord, T. K. et. al., "Optical Digital Truth Table Look-Up Processing", Optical Engineering Vol. 24 No. 1 (1985), pp. 048-058.
- McAulay, A. D., "Optical A/D Converters and Application to Digital Multiplication by Analog Convolution", SPIE Real-Time Signal Processing Conference, August 1987.
- McAulay, A. D., "Investigation of Novel Optical Table Look-Up Analog to Digital Converters", June 1987.
- Rhodes, W. T., P. S. Guilfoyle, "Acoustooptic Algebraic Processing Architectures", Proceeding of the IEEE Vol. 72, No. 7 (1984), pp.820-830.

1987 USAF-UES SUMMER FACULTY RESEARCH PROGRAM/

GRADUATE STUDENT SUMMER SUPPORT PROGRAM

Sponsored by the

AIR FORCE OFFICE OF SCIENTIFIC RESEARCH

Conducted by the

Universal Energy Systems, Inc.

FINAL REPORT

A REVIEW OF WORKLOAD MEASUREMENT IN RELATION TO VERBAL

COMPREHENSION

Prepared by:	Stephen T. Morgan
Academic Rank:	Graduate Student
Department and University:	Department of Psychology Montclair State College
Research Location:	Air Force Human Resources Laboratory Ground Operations Branch
USAF Researcher:	Lt. Michael T. Lawless
Date:	July 31, 1987
Contract No.	F49620-85-C-0013

A REVIEW OF WORKLOAD MEASUREMENT IN RELATION TO VERBAL
COMPREHENSION

by
Stephen T. Morgan

ABSTRACT

In a command and control environment, many individuals are called upon to engage in two activities simultaneously. Communication with others is often one of these tasks. It is crucial that there be no decrement in performance on either task, especially in crises situations where heavy loading on the cognitive system is apt to be present. In order to optimize an individual's performance, processing strategies need to be analyzed and the most efficient ones incorporated into appropriate training programs.

This paper reviews the literature regarding workload measurement techniques. The purpose is to investigate the most efficacious method of assessing processing load during verbal comprehension. Dual-task paradigms are found to be valid indices of mental workload. Problems associated with this technique are evaluated and a possible assessment method is offered.

ACKNOWLEDGEMENTS

I gratefully acknowledge the sponsorship of the Air Force Systems Command and the Air Force Office of Scientific Research for the opportunity to participate in the Graduate Student Summer Support Program.

I also wish to express my gratitude to the HRL/LRG staff for their affable support of my research fellowship. Dr. Larry Reed provided guidance for this project, as well as for my professional development as a whole. Also, I gained invaluable insight concerning the Air Force Human Resources Lab from thought-provoking discussions with Jeff Wampler and Mike Lawless.

I. INTRODUCTION

Many who work in technical settings are often called upon to engage in two activities at the same time. One of the most common examples of this may be seen in those who verbally communicate while devoting attention to some other task. In a command and control environment it is crucial that high performance levels be maintained on both tasks, especially in stressful situations where heavy loading on the cognitive system is apt to be present. In order to better understand the nature of time-sharing within the cognitive system, and thus keep dual task performance at optimal levels, it would be helpful to have a clear understanding of the related factors.

I am a graduate student in the field of cognitive psychology. My research interests involve the application of workload measurement to verbal communication. This resulted in my assignment to the Human Resources laboratory.

II. OBJECTIVES

In analyzing time-sharing processes, the research community has used several techniques to measure the relative mental workload required to process incoming stimuli. These measures provide data which are useful in understanding how multiple stimuli compete for limited processing resources. However, there is still some question as to how stimuli from different dimensions compete with each other. Any attempt to measure cognitive loading of two stimuli of differing dimensions must address this issue. This paper will review work done in the area of mental workload measurement. Specifically, current mental workload measurement techniques will be examined, as well as the information processing theories on which they are based. Following, the literature which deals with competition between stimuli from different dimensions will be reviewed in order to investigate their demand for processing resources.

III. THEORETICAL OVERVIEW

Any measure of cognitive loading requires the researcher to make certain assumptions regarding the nature of our processing system. These assumptions, which deal with the structure and capacity of our mental resource system, are embedded within a number of information processing theories. An overview of these theories would be helpful in order to provide the framework out of which current cognitive measurement techniques arise.

The investigation of attention has been an area of concern for many investigators since the beginnings of experimental psychology (James, 1890; Titchner, 1908). The Behaviorist and Gestalt schools of the early twentieth century went on to minimize the role of attention in their approach, however, and it wasn't until the 1950's that attention began to play a key role in the burgeoning field of cognitive psychology (Kahneman, 1973). It was at this point that some of the first comprehensive models of information processing were put forth. These models have evolved over the course of the last thirty years in order to accommodate a growing body of research in the field.

Broadbent (1958) viewed the human information processor as working within the constraints of a limited capacity. This theory, like other "bottleneck" theories, claims that when an individual is presented with a number of different stimuli simultaneously, all information is processed in parallel until it reaches some specific point (the "bottleneck") at which the system must deal with the information in a serial manner. Broadbent's filter theory posits that the stimulus which is not processed immediately is held in short term store until the processor completes perception and analysis of the first stimulus. It is only when the first stimulus has passed through the bottleneck that processing can begin for the second.

In a modification of Broadbent's (1958) theory, Treisman's (1960) model presented filtering as a matter of attenuation. That is, processing was not viewed as an all-or-none phenomenon, but as a matter of degree, whereby the unattended message is not completely ignored, but rather treated with highly reduced sensitivity within the processing system. This model allowed for some results obtained on dichotic listening tasks which indicate that the unattended ear does indeed pick up a certain degree of information (Moray, 1959).

Whereas Broadbent's (1958) theory places the bottleneck just prior to perceptual analysis, Deutsch and Deutsch (1963) claim that the bottleneck occurs after perceptual analysis, but prior to rehearsal and response selection. Interference is caused not simply by competition for recognition of the stimuli, but by competition for appropriate responding processes to the incoming stimuli.

It is important to note that the main emphasis of bottleneck theories is the presence of a single limited capacity processor. Only one stimulus can be processed at any point in time due to a single mechanism through which all incoming stimuli must pass.

Alternatives to the single channel theory of processing were suggested by a number of investigators. Moray (1967) proposed a system in which the capacity of the human processor is not limited by the structure of the processing mechanism, as in the bottleneck theories. Instead, Moray claimed a capacity theory which argues that processing limits are due to the overall capacity of the system as a whole. Every operation is said to draw on an undifferentiated pool of resources. These resources can be divided and used in whatever way is most appropriate to meet the demands placed on the processor. Thus, parallel processing can occur within the system as long as the total demand does not exceed the total capacity of the processor.

Kahneman (1973) provides another model of the processing system. He asserts that neither the single channel nor an undifferentiated capacity model are adequate to fully explain research reported on the subject. Rather, he advocates a model which combines aspects of both. In this model, interference can be explained by competition for the same operation-specific mechanism needed to process two stimuli at once. Interference can also be explained by the combined demands of the two stimuli exceeding the total capacity of the system. Thus, Kahneman includes in his theory both an undifferentiated capacity for the whole system as well as a number of sub-structures for which competition takes place. Furthermore, Kahneman maintains that the total capacity is determined by the demands made upon the system. That is, effort or attention are viewed as operating as a function of the complexity of the task at hand. The task demands a certain degree of arousal independent of the intentions of the processor, but dependent upon the physiological excitation created by the task (Kahneman, 1973).

Norman and Bobrow (1975) expanded on Kahneman's position by introducing the distinction between data-limited and resource-limited processing. According to these authors, interference between two tasks may be due to limited mental resources available to the processor. Diverting resources to a single task will yield an increase in performance only up to a certain point. At this point the limiting factor is the quality of data, and the processing is referred to as being data-limited. This model claims, then, that concurrent performance on tasks which require common resources will show a decrement relative to single task performance.

Other investigators have argued against any inclusion whatsoever of single-channel theory in a model of attention. These theorists (e.g. Allport, Antonis, and Reynolds, 1972; McLeod, 1977; Navon and Gopher, 1979) postulate a multiple resource model of mental processing. In this model, there is no overall capacity containing a number of sub-structures

as in Kahneman's (1973) model. This model posits that different mental operations tap different resource pools, with each pool having its own capacity. The amount of interference between any two tasks depends on the degree to which the two tasks share a common processing mechanism. In this view, the more similar two tasks are to each other, the more interference is expected (Wickens, 1984).

In an effort to clarify the issue of what factors are involved in task similarity, Wickens (1984) proposes a structure of processing which divides our resources into three dimensions. These dimensions are: (1) stages - early vs. late processing. (2) modality - auditory vs. visual encoding. (3) processing codes - spatial vs. verbal. According to this representation, greater interference will occur for two tasks which lie within the same dimension than for tasks which lie in different dimensions.

IV. Measurement Techniques

Measures of cognitive workload are many and varied (Moray, 1982; Williges and Wierwille, 1979; Hicks and Wierwille, 1979; Wierwille and Conner, 1983). O'Donnell and Eggemeier (1986) have proposed three major categories into which workload assessment techniques may be divided. These are: (1) subjective measures, (2) performance-based measures, and (3) physiological measures. Subjective measures require an individual to report (usually by means of a rating scale) his or her subjective assessment of the amount of mental effort demanded by a particular task. Performance-based measures use an individual's ability to perform a single task or concurrent dual tasks as an indication of mental workload. Physiological measures rely on physiological changes within the organism as an indication of workload demands.

O'Donnell and Eggemeier (1986) point out that due to the variety of assessment techniques, one must exercise a good deal of discretion in

choosing the most appropriate method for any particular application. Decisions should be based on practical as well as theoretical considerations such as sensitivity, intrusiveness, and implementation requirements of each technique.

V. SUBJECTIVE MEASURES

Much work has been done in the area of subjective measures of cognitive workload (Moray, 1982). Williges and Wierville (1979) have classified existing subjective techniques into two broad categories - those that use a rating scale in the assessment, and those that rely on a questionnaire or interview. O'Donnell and Eggemeier (1986) have classified subjective scales into the areas of rating scales and psychometric techniques.

Among the rating scale measures is the Cooper-Harper Aircraft Handling Characteristics Scale (1966). This scale was designed for pilot use, but has been modified by several researchers for use in the general population (e.g. Wolfe, 1978; Wierville and Casali, 1983b). Reflective of other rating scales, the Cooper-Harper scale demonstrates a high level of sensitivity to a number of different loads. It also requires minimal practice and implementation requirements. However, the scale rests on the assumption that ease of aircraft handling is directly related to mental workload. Although we may assume a relation between these processes, it may not be the case that this relation is always a direct one (O'Donnell and Eggemeier, 1986). Other problems with rating scales in general include operator adaptivity, subjective confusion between mental and physical workload, and incorrect subjective estimation of the actual workload required (Williges and Wierville, 1979).

An alternative approach to rating scales are interviews and questionnaires. The structure of this method can vary from completely open-ended interviews to highly controlled questionnaire items. These measures are most often used for supplemental data for more objective

techniques, and are rarely used as the only measure of workload (Williges and Wierwille, 1979). The advantage of such techniques lie in the unobtrusiveness and ease with which they may be implemented. However, problems with structuring and quantifying the results of such measures preclude their use as a workload metric in anything more than a corroborative role.

Psychometric techniques, on the other hand, overcome some problems associated with questionnaires by providing a quantitative measure which allows for interval-scaled data. This advantage allows analytic procedures which examine differences in the magnitude of workload between tasks. There are several types of psychometric measures including magnitude estimation, paired comparisons, the method of equal comparisons, and conjoint measurement and scaling (O'Donnell and Eggemeier, 1986).

Although subjective scales have been shown to be sensitive indicators of workload, investigators such as Gartner and Murphy (1976) and Williges and Wierwille (1979) have noted restrictions for these measures. Possible confounding influences include confusion between physical and mental load, subject bias towards what the task "should" require instead of the actual task demand, the relation of subjective report on short term memory, and the possibility that not all processing is open to subjective awareness.

VI. PHYSIOLOGICAL MEASURES

Physiological methods of assessing workload are some of the most widely researched measurement techniques (Wierwille, 1979). O'Donnell (1979) reports that although these measures initially appeared to be good indices of mental effort, many studies failed to find consistent, significant changes that are reflective of concurrent changes in workload. This failure can be attributed, in part, to the implementation requirements of such techniques. Rather than treating physiological measures as a global indication of effort, it was realized that these measures are most

efficacious in respect to specific physiological processes (Hassett, 1978). O'Donnell and Eggemeier (1986) have divided physiological measurement techniques into several groupings. These are: measures of brain function, measures of eye function, measures of cardiac function, and measures of muscle function.

Measures of brain function utilize the electroencephalogram recorded from an individual. The EEG can be monitored in order to distinguish changes in potential which are related to a specific event. This event-related potential (ERP) is then used as the index of workload. Use of ERP's has been discussed by Isreal, Wickens, Chesney, and Donchin (1980). These authors have suggested that use of ERP is indeed a valid measurement technique and may have advantages over other measures including unobtrusiveness and sensitivity to non-cognitive variables such as physical workload.

Investigation of the P300 brainwave has revealed that it is elicited when a subject engages in processing. Although this measure is primarily used with discrete stimuli only, possibilities exist for its use with continuous stimuli. However the technique requires systematic validation. Also, cost and implementation concerns may be inhibitive for such an assessment method.

Measures of eye function are a relatively good tool for assessing mental load. Since humans normally take in much information visually, and due to the relative ease with which the eyes may be observed, measurement of eye functions have been investigated. Current eye functions used to measure cognitive loading include pupillary response, eye point of regard, scanning patterns, eye blinks, and eye movement speed (O'Donnell and Eggemeier, 1986). These techniques, like most other physiological techniques, have the disadvantage of requiring rather elaborate apparatus and do not transfer well outside of the laboratory.

Other physiological measures are those which rely on cardiac and muscle function, by means of electrocardiograms and electromyograms respectively. Use of these measures have shown to yield general, global relationships with mental workload (Kalsbeek, 1973; Stern, 1966). However, there are confounding factors associated with such measures as the exact nature of how each particular measure is taken may vary from one researcher to the next. For example, cardiac measures may vary in their emphasis in timing and volume. These measures may be considered promising in regard to their potential, but lack validity at the present.

VII. PERFORMANCE BASED MEASURES

Measures of mental workload which utilize subject performance on one or more tasks have been used extensively. These measures rely on the assumption of a limited capacity of processing resources. O'Donnell and Eggemeier (1986) have divided these measures into those that make use of primary tasks and those that use secondary tasks.

Primary task measures initially assess the performance of an individual on a task. As task demands increase it is assumed that performance will generally show a degradation, which may be used as an index of workload (Williges and Wierwille, 1979). Primary task measures may use a single aspect or multiple aspects of a task in their assessment. Examples of those that use a single aspect of task performance are measures of error rate or latency of reaction. This technique has had successful implementation by a number of researchers (e.g. Isreal, Wickens, Chesney, and Donchin, 1980; Percival, 1981). Primary task measures which evaluate multiple aspects of a task do so in order to increase their sensitivity by decreasing measurement error or increasing the precision of measurement (O'Donnell and Eggemeier, 1986).

Secondary task measures require that a subject engage in two tasks concurrently. The subject is instructed to give priority to one task, the

primary task, while performing a secondary task. Performance on the secondary task provides a measure of processing demands of the primary task by giving an indication of the spare mental capacity associated with it (the primary task). When a subject performs worse on a concurrent secondary task than on the same task alone, the primary task is considered to require processing resources. Secondary tasks have been extensively employed in mental resource assessment studies and have demonstrated their effectiveness as a diagnostic tool (Kerr, 1973).

A number of secondary tasks have been used with success within this dual task paradigm. Michon (1966) used rhythmic tapping in which the subject is required to maintain a steady rate of finger tapping. Michon proposed that the demands posed by the primary task would disrupt the regularity of the tapping task. Posner and Boies (1971) have used a probe reaction technique in which subjects are required to respond to the presentation of a probe stimulus. This method assumes that as the processing resources for the primary task increases, slower reaction times to the probe will result. Sternberg (1966) proposes a memory search task which is similar to the probe reaction time task. Sternberg's task requires the subject to respond as quickly as possible whether or not a presented probe is a member of a previously memorized set. This method assumes that as more processing resources are demanded by the primary task, slower reaction times to the memory search will result. Yet another secondary task which has been used with success involves tracking. Power (1986) reports using a tracking program in which a subject is required to manually direct a target between a pair of undulating lines. As a concurrent primary task changes in its demands, performance on the tracking task has been shown to change in a reflective manner. That is, the greater the primary task demands, the poorer the tracking.

This dual task paradigm is based on the assumption of a limited capacity within the processing system in which two incoming stimuli requiring processing energy will often compete for available resources. The

question remains, however, as to what the exact nature of the stimuli must be in order for there to be competition.

The literature concerning this issue has demonstrated that concurrent processing of varying stimuli may show interference to varying degrees. However, the processing of multiple stimuli almost always demonstrates a degradation in performance in relation to performance on either task alone. Mowbray (1952) reports that visual and auditory alphanumerics interfere with each other when subjects attempt to process both at the same time. In this study, subjects were required to report missing items in the alphabet or in numerical sequences when presented in one of four possible combinations: visual alphabet, auditory numerals; visual alphabet, visual numerals; auditory alphabet, auditory numerals; auditory alphabet, visual numerals. Sequences were also presented in non-simultaneous conditions. The results indicate that significantly more errors were made in the simultaneous condition than in the non-simultaneous condition.

Brown, Tickner, and Simmonds (1967) examined the effects of concurrent communicating and driving an automobile. Subjects were asked to judge whether they could drive through gaps that were close in size to the width of their car. At the same time, messages presented via a radiophone required the subject to answer true or false to a reasoning problem such as "AB - A follows B". Performance was measured by a correct or incorrect response, as well as the response time. Performance on the driving task was based on the subjects decision to try to clear a gap, speed of completing the driving circuit, and the frequency of foot and steering controls used. Subjects were also tested on their driving and their communicative/reasoning skills alone. The results indicate that subjects performed significantly poorer on both tasks when engaging in them concurrently than when engaging in each alone.

Trumbo, Noble, and Swink (1967) investigated the effects of secondary verbal tasks on tracking performance (primary task). Verbal tasks required subjects to anticipate and respond verbally to a series of numbers presented aurally at three second intervals. A control group which engaged only in the tracking task was also a part of the design. The authors report that those subjects who engaged in both the primary and secondary tasks concurrently showed significantly poorer performance on the tracking task than those subjects who engaged in the primary task alone.

In another study involving tracking a dual-task paradigm, Wright, Holloway, and Aldrich (1974) examined subjects attention to visual and auditory verbal information while tracking. Subjects were required to process verbal information and perform a kinaesthetic tracking task concurrently. The tracking task required that a subject place his left index finger in an apparatus that randomly moved away from and toward a subject over a 15 cm. distance. The subject was to track with his right index finger which was in a similar apparatus. Tracking error was larger while receiving the verbal message, compared to control, for both auditory and visual messages, though the effect was greater for visual messages.

Wickens (1983), in an investigation of the effects of multimodal, concurrent processing reports similar results. Subjects in this study were required to respond either visually or spatially to verbal commands, while performing a manual control task. Greater interference was demonstrated for those subjects who were asked to respond spatially than for those who were to respond verbally. However, time sharing efficiency was disrupted for both conditions.

These studies have been reported here in order to demonstrate the effects of multimodal, concurrent processing of multiple stimuli. Though obviously not an exhaustive survey, these studies are consistent with a great number of other experiments which have examined this issue in that

they report greater interference for processing two stimuli concurrently than for a single stimulus alone. Although it has been demonstrated that timesharing may be poorer if the stimuli arise from the same dimension, the literature is consistent in its findings that stimuli arising from different dimensions should nevertheless show some interference.

VIII. RECOMMENDATIONS

In addressing the need for a measure of cognitive loading during verbal comprehension, this paper has examined some concepts related to the assessment of mental workload. It has been reported that a performance based measure appears to be a valid, easily implemented metric of mental effort. It is argued that the use of a dual task paradigm which employs concurrent tasks of differing dimensions should assess processing load. With this point in mind, it would seem appropriate to measure mental effort for verbal comprehension with a concurrent motor task. As the dual-task paradigm relies on interference between two stimuli, we may conclude that this assessment technique is capable of demonstrating sensitivity to mental effort even if the tasks employed arise from different dimensions.

REFERENCES

- Broadbent, D.E. (1958). Perception and communication. London: Pergmon Press.
- Brown, I.D., Tickner, A.H., & Simmonds, D.C.V. (1969). Interference between concurrent tasks of driving and telephoning. Journal of Applied Psychology, 53, 419-424.
- Cooper, G.E. & Harper, R.P. (1966). The use of pilot rating in the evaluation of aircraft handling qualities. Report No. NASA TN-D-5153. Maffet Field, California: National Aeronautics and Space Administration, Ames Research Center.
- Deutsch, J.A., & Deutsch, D. (1963). Attention: Some theoretical considerations. Psychological Review, 70, 80-90.
- Gartner, W.B. & Murphy, M.R. (1976). Pilot workload and fatigue: a critical survey of concepts and assessment techniques. Report No. NASA-TN-D-8365. National Aeronautics and Space Administration. Washington, D.C.
- Hassett, J. (1978). A primer of psychophysiology. San Francisco: Freeman.
- Hicks, T.G., & Wierwille, W.W. (1979). Comparison of five mental workload assessment procedures in a moving based driving simulator. Human Factors, 21, 129-143.
- Isreal, J., Wickens, C., Chesney, G., & Donchin, E. (1980). The event-related brain potential as an index of display monitoring workload. Human Factors, 22, 211-224.

- James, W. (1890). The principles of psychology. New York: Holt.
- Kahneman, D. (1973). Attention and effort. Englewood Cliffs, N.J.: Prentice Hall.
- Kalsbeek, J.W.H. (1973). Do you believe in sinus arrhythmia? Ergonomics, 15, 99-104.
- Kerr, B. (1973). Processing demands during mental operations. Memory and Cognition, 1, 401-412.
- McLeod, P. (1977) A dual task response modality effect: support for multiprocessor models of attention. Quarterly Journal of Experimental Psychology, 29, 651-657.
- Michon, J.A. (1966). Tapping regularity as a measure of perceptual motor load. Ergonomics, 9, 401-412.
- Moray, N. (1959). Attention in dichotic listening: Affective cues and the influence of instructions. Quarterly Journal of Experimental Psychology, 11, 56-60.
- Moray, N. (1982). Subjective mental workload. Human Factors, 24, 25-40.
- Movbray, G.H. (1952). Simultaneous vision and audition: The detection of elements missing from overlearned sequences. Journal of Experimental Psychology, 44, 292-300.
- O'Donnell, R.D. & Eggemeir, F.T. (1986) Workload assessment methodology. In Boff, K.R., Kaufman, L., & Thomas, J.P. (Eds.) Handbook of Perception and Human Performance, Vol. II, New York: John Wiley & Sons.

Percival, L.C. (1981). Sustained search: number of background characters, target type, and time on watch. Proceedings of the Human Factors Society Twenty-Fifth Annual Meeting, Rochester, N.Y., 283-285.

Posner, M.I. & Boies, S.J. (1971). Components of attention. Psychological Review, 78, 391-408.

Power, M.J. (1986). A technique for measuring processing load during speech production. Journal of Psycholinguistic Research, 15, 371-382.

Stern, R.M. (1966). Performance and physiological arousal during two vigilance tasks varying in single presentation rate. Perceptual and Motor Skills, 23, 691-200.

Sternberg, S. (1966). High speed scanning in human memory. Science, 153, 652-654.

Titchner, E.B. (1908). Lectures on the elementary psychology of feeling and attention. New York: Mcmillan.

Treisman, A.M. (1960). Contextual cues in selective listening. Quarterly Journal of Experimental Psychology, 12, 242-248.

Trumbo, D., Noble, M., & Swink, J. (1967). Secondary task interference in the performance of tracking tasks. Journal of Experimental Psychology, 73, 232-240.

Wickens, C.D. (1984). Processing resources in attention. In R. Parasuraman and R. Davies (Eds.) Varieties of attention, New York: Academic Press.

Wickens, C.D. (1984). Engineering psychology and human performance. Columbus: Merrill Pub. Co..

Wickens, C.D. (1980). The structure of attentional resources. In R. Nickerson (Ed.) Attention and performance VIII, Hillsdale, N.J.: Erlbaum Ass. Inc.

Wierwille, W.W. & Casali, J.G. (1983b). A validated rating scale for global mental workload measurement applications. Proceedings of the Human Factors Society Twenty Seventh Annual Meeting, 1983, 129-133.

Wierwille, W.W. & Connor, S.A. (1983). Evaluation of 20 workload measures using a psychomotor task in a moving-based aircraft simulator. Human Factors, 25, 1-16.

Wierwille, W.W. (1979). Physiological measures of aircrew mental workload. Human Factors, 21, 575-593.

Williges, R.C. & Wierwille, W.W. (1979). Behavioral measures of aircrew mental workload. Human Factors, 21, 549-574.

Wolfe, J.D. (1978). Crew workload assessment: development of a measure of operator workload. (Report No. AFDL-TR-78-165) Wright Patterson Air Force Base, Air Force Flight Dynamics Lab, Dec..

Wright, P., Holloway, C.M., and Aldrich, A.R. (1974). Attending to visual or auditory verbal information while performing other concurrent tasks. Quarterly Journal of Experimental Psychology, 26, 454-463.

1987 USAF-UES FACULTY RESEARCH PROGRAM/
GRADUATE STUDENT SUPPORT PROGRAM

Sponsored by the
AIR FORCE OFFICE OF SCIENTIFIC RESEARCH

Conducted by the
Universal Energy Systems, Inc.

FINAL REPORT

DEVELOPMENT OF A LONG TERM SOLVENT DELIVERY SYSTEM

Prepared by:	Lisa M. Morris
Academic Rank:	M.S. Graduate Student
Department and	Biology Department
University:	University of Dayton
Research Location:	AAMRL/Toxic Hazards Branch Wright-Patterson AFB Dayton, OH 45433
USAF Researcher:	Dr. R. Drawbaugh
Date:	September 29, 1987
Contract No:	F49620-85-C-0013

DEVELOPMENT OF A LONG TERM SOLVENT DELIVERY SYSTEM

by

Lisa M. Morris

ABSTRACT

The basic principles have been established for developing a long term organic solvent delivery system. This system would be useful in studying neurobehavioral toxicity of various organic chemicals. 1,1,1 trichloroethane (TCE) was delivered in vitro from a 0.2 ml reservoir ALCAP (aluminum-calcium-phosphorus oxide) ceramic delivery system. A sustained release of 1,1,1 TCE was attained for 15 days with a release rate of 0.65 mg/hr. A modified 2 ml reservoir ALCAP solvent delivery system had a sustained release of 28.8 mg/hr for four hours. In vivo intraperitoneal implantation of the 2 ml reservoir produced a sustained release of 6.9 mg/hr for 2 days as monitored by blood levels of 1,1,1 TCE. Release declined for the following six days. The data obtained in this investigation suggest that this simple device can be used for long term delivery of organic solvents.

ACKNOWLEDGMENTS

I wish to thank the Air Force Systems command and the Air Force Office of Scientific Research for the sponsorship of this research. I would especially like to thank the AAMRL/Toxic hazards Division for providing the research laboratory and support for this investigation. I also wish to thank Universal Energy Systems for sponsorship of this program.

The University of Dayton Glass Blowing Laboratory deserves special thanks for providing all the glass reservoirs and the modifications needed at a moments notice. Also the University of Dayton Biology Department for providing the ceramics needed for this investigation.

Special thanks goes to S.Sgt. Greg Cason for having the patience to teach me how to use the various gas chromatographs and providing technical assistance, S.Sgt. George Bates and S.Sgt. Todd Facekas for providing catheterized rats needed during this investigation and S.Sgt. Dave Hoover for providing moral support and providing personnel and all the other little things needed during my research. I am indebted to Dr. R. Drawbaugh for providing moral support, encouragment, suggestions for improvement of the device, giving me the opportunity to work at the Toxic Hazards Laboratory and providing facilities and personnel to complete my reserach project.

I. INTRODUCTION:

1,1,1-trichloroethane (TCE) is a widely used solvent for natural and synthetic resins, oils, waxes, tar and alkaloids, cleaning electrical machinery and plastics and is found as a water contaminant. Exposure to this chemical is generally through inhalation or percutaneous absorption in the work environment. Volatilization of 1,1,1 TCE from a disposal site, particularly during drilling or restoration activities, could result in inhalation exposures. In addition, the potential for ground water contamination is high, particularly in sandy soils. Recreational use of these contaminated waters could result in dermal exposures.

The National Institute for Occupational Safety and Health, and the Occupational Safety and Health Administration specify permissible exposure limits for humans to minimize chronic exposure of workers to these chemicals (NIOSH, 1987). These limits are obtained through experience by actual situations where unsafe conditions have occurred and through animal studies.

Acute exposure studies which monitor sensory and motor systems have received considerable attention, however, a lack of knowledge exists on the effects of the solvents after long-term exposure. An animal model of the effects of chronic exposure would lead to more accurate methods for predicting neurotoxicity of toxic chemicals (NIOSH, 1987). Although the patterns of the behaviors observed are often unique to the particular species studied, they are

generally common to all animal species including man (Reiter, 1978). Extrapolation utilizing models can be made to help determine maximum safe levels that can be maintained in the work environment.

A major limitation in performing chronic studies are the devices used for exposure to the chemical. Most studies employ an oral gavage (Melrich, 1987) or inhalation apparatus (Gargas, 1986) which restricts the animals normal movement and behavior patterns or an oral gavage (Melrich, 1987). The solvent delivery device proposed in this study would help to eliminate the need for an inhalation chamber, decrease the amount of experimenter interference, allow accurate dose prediction and allow complete freedom of movement of the animal.

Previous work conducted by Dr. P.K. Bajpai has involved ALCAP ceramics for delivering a variety of substances. ALCAPs can deliver hormones, proteins, and polypeptides (Bajpai, 1985).

II. OBJECTIVES:

a. My project at Toxic Hazards Laboratory was to develop a long term solvent delivery system which could release an organic solvent in a sustained manner for a period of one week. The first phase was designed to obtain a sustained release in vitro.

b. Once a delivery system was decided upon, the second phase involved implanting the device intraperitoneally and monitoring blood levels of the chemical to determine its

pattern of release in vivo.

III. MATERIALS AND METHODS:

A. Chemical

1,1,1 Trichloroethane (99.9% pure) was obtained from the Aldrich Chemical Company (Milwaukee, WI.). Experiments were conducted with a mixture of 5% mineral oil and 1,1,1 Trichloroethane.

B. Fabrication of ALCAP Ceramics

Aluminum-calcium-phosphorus oxide (ALCAP) ceramic capsules were fabricated by calcining a mixture of aluminum oxide, calcium oxide, and phosphorus pentoxide (50:34:16) powders (Fisher Scientific Co., Fairlawn, N.J.) at 1315 C for 12 hours. The calcined material (ALCAP) was ground in a ball mill and sized in a 400 mesh per inch sieve to obtain particles of 1 to 38 microns. One gram of the ceramic particles and .0025 gm polyvinyl alcohol (PVA) were then pressed at a pressure of 5000-7000 pounds on a French pressure cell press (Americal Instrument Co., Silver Spring, MD) into a cylinder shape using a 5/16" die set. The cylinders were then sintered at 1500 C for 36 hours.

C. Glass Tube Inserts

One cm by four mm glass tubes with a reservoir attached to one end were fabricated by the University of Dayton Glass Blowing Laboratory.

1. Two hundred ul Glass Reservoir: One cm by four mm glass tube was inserted inside the ALCAP ceramic with a 200

ul reservoir attached to one end. The reservoir extended beyond the ALCAP giving a total length of 2.54 cm. The glass had an opening of two mm at one end as well as a two mm opening to the reservoir. The front end of the ALCAP and the reservoir end was sealed with Silastic^R Medical Adhesive (Dow Corning, Midland, MI.) and allowed to dry overnight. Two hundred ul of 1,1,1 trichloroethane plus 5% mineral oil were injected by a tuberculin syringe through the silastic adhesive to fill the reservoir.

Various modifications to the 200 ul reservoir were examined. These involved opening the glass tube leading to the reservoir to four mm or opening both ends so the entire tube was four mm.

2. Two ml Glass Reservoir: A four mm by four mm glass tube had a two ml reservoir attached at one end. The two ml reservoir has a removable top with a septum inserted in the center to allow reinjection of fluids into the reservoir. (Total length 5.08 cm.) The four mm end was inserted into the ALCAP and sealed with Silastic Adhesive along with the open end of the ALCAP and allowed to dry overnight.

D. In Vitro Studies

1. Gas Chromatograph Standardization

A Hewlett Packard (HP) 5890 Gas Chromatograph (GC) containing a Flame Ionization Detector (FID) and a 10 ft. 10% SE-30, 80/100 Supplecoport column was standardized in the 10-100 parts per million (PPM) range using a 20 liter respiratory bag. The oven temperature was maintained at

100° C, the injector temperature at 125° C, the detector temperature at 300° C, and the Nitrogen carrier gas was maintained at a flow rate of 25 ml/min. A Hewlett Packard 3393A Integrator and a Hewlett Packard 19405A Sampler/Event Control Module were used in conjunction with the gas chromatograph for analysis of the one ml samples injected into the GC.

2. Analysis of 1,1,1 - Trichloroethane

All ALCAP ceramics used in this phase were pressed at 7000 pounds on the French pressure cell press. In Vitro experiments were conducted by suspending the ALCAP reservoir delivery device (0.2 and 2 ml) by a string inside a 108 ml glass gas injection chamber. The chamber was attached to a reciprotor electromagnetic piston air pump which in turn was connected to the Gas Chromatograph. A constant air flow of 120 ml/min was maintained through the glass chamber by the air pump. The HP Sampler/Event Control Module was programmed to automatically sample one ml of air from the glass chamber. Concentration of 1,1,1 trichloroethane was determined from the standard curve.

E. In Vivo Studies

The ALCAP ceramics used in this phase of the project were pressed at 5000 pound on the French pressure cell press. The rate of release of 1,1,1 trichloroethane into the blood was monitored in rats implanted with a two ml ceramic reservoir containing two ml 1,1,1 trichloroethane and 5% mineral oil.

1. Catherization

Two 320 g Fischer 344 male rats (Charles River, MA.) were anesthetized by a ketamine/rompun mixture (1 ml/kg) for catheterization with a 22 G, 8 inch Deseret Radiopaque cutdown catheter (Deseret Co., Sandy UT.) The catheter tip was passed through the left jugular vein to the right atrium and the sampling end passed under the skin to the back of the neck. A velcro vest was used to protect the sampling port.

2. Intraperitoneal Implantation of Ceramic Reservoir Delivery Device

Four days of recovery from the catheterization were allowed before the delivery device was implanted. The two rats were anesthetized by soaking gauze in a nine liter glass desicator with 35 ml of Pentrane (methoxyflurane, Abott Laboratory, Chicago, IL.) and placing them in the chamber for 10 minutes. The rats remained under the anesthesia for 10 minutes. 1,1,1 trichloroethane plus 5% mineral oil was injected into the reservoir while the rat was becoming anesthetized. A one cm incision was made in the abdomen and the capsule inserted into the peritoneal cavity. The incision was closed with two to three steel wound clips.

3. Gas Chromatograph Standardization

A Hewlett Packard 5700A Gas Chromatograph (GC) containing an Electron Capture Detector (ECD) and a 11 ft. 10% SE-30 Chromasorb W-HP column was standardized with known concentrations of 1,1,1 trichloroethane (1 to 20

ug/ml) in blood. A 100 ul sample of of blood from each standard was placed over one ml of hexane and allowed to equilibrate for one hour. The oven temperature was maintained at 70⁰ C, detector temperature at 250⁰ C and an Argon Methane gas was maintained at a flow rate of 20 ml/min. Aliquots of 100 ul of hexane were injected into the GC port by means of a Hamilton syringe.

4. Blood Analysis Studies

Following implantation, blood samples were taken at 15, 30, 45, 60 minutes and then at one hour intervals for six hours the first day. On the following days blood samples were taken at 25, 26, 27, 28, 70, 72, 73, 99, 100 and 121 hours after implantation. The drawn aliquots of 100 ul of blood were placed over one ml of hexane and allowed to equilibrate for one hour.

IV. RESULTS AND DISCUSSION:

A. Delivery of 1,1,1 Trichloroethane In Vitro

A sustained release of 1,1,1 trichloroethane from the 200 ul reservoir delivery device was maintained for 15 days (Fig 1). The average release was 0.65 mg/hr with a range of 1.08 to 0.43 mg/hr. A constant release was maintained between days 5 and 12. The fluctuations seen prior to and after this time are due to the initial saturation of the ALCAP and the decreasing amount of fluid remaining respectively.

Predicted blood levels by computer modeling found that our levels would be exceeding low. Our values were

predicted to be 3.2 ug/ml, however, a level of 80 ug/ml is necessary to observe behavioral effects in rats.

Modifications of the system were examined to determine if a higher release rate could be obtained. One modification involved opening up the glass insert leading to the reservoir so that the diameter was four mm except for the front end which was maintained at two mm. This resulted in an average release of 6.8 mg/hr for 2 days but the amount of fluid released was steadily declining. A sustained release was not obtained.

The next modification involved opening the entire glass insert providing a diameter of four mm throughout the insert. This system provided a sustained release of 1,1,1 trichloroethane for 24 hours at a rate of 15.5 mg/hr. This was beginning to look very promising but still the release rate was too low to obtain any observable behavioral changes in the animal.

Based on preliminary experiments done by Dr. P.K. Bajpai and Debbie Hollenbach, the release from a plain ALCAP with no glass insert provided a release of 432 mg/hr. However, the rate dropped immediately and within 30 minutes the release was down to 72 mg/hr and dropping steadily. By providing a minimal glass insert of only four mm by four mm attached to a two ml reservoir, it was thought that a high sustained release could be achieved. A similar pattern was obtained as before (Fig 2) except a sustained release was maintained for four hours at a rate of 28.8 mg/hr.

This system provided the best results to obtain

constant release rate in the rat. Since the device would be in the animal for one week, the exposure time of the animal to the chemical would be longer than any other system in use today. Behavioral changes could possibly be observed due to the long exposure.

B. Delivery of 1,1,1 Trichloroethane In Vivo

The blood levels of the rats fluctuated dramatically the first day with an average blood level of 1,1,1 TCE of 8.3 ± 3.6 mg/hr (Table 1). A sustained level was seen on the second day (6.9 ± 0.8 mg/hr). Unfortunately, one of the rats catheters clogged at this time and only one animal was available for blood collection the remainder of the time. Blood samples were not obtained on day 3. The following days showed the rates dropping steadily until a minimum blood level of 2.2 mg/hr was reached on day 6.

Upon removal of the two ml ALCAP ceramic reservoir on the third day from the one rat, 1.5 ml of 1,1,1 trichloroethane was still remaining in the reservoir. Five hundred ul released over three days provides an average release rate of 9.3 mg/hr compared with an observed average release rate of 8.3 mg/hr. The ceramic device removed on day 6 had 1.25 ml of 1,1,1 trichloroethane remaining. Release of 750 ul over 6 days had an average release rate of 7.0 mg/hr. This corresponded well to the actual average release rate of 6.7 ± 3.8 mg/hr.

This data shows that the release rate of 1,1,1 trichloroethane slows down with time and only provides a sustained release rate in the very beginning of

implantation. It was unfortunate that samples could not have been drawn on day three to determine if the rate was maintained or if it started to drop at this point.

V. RECOMMENDATIONS:

Due to the limited amount of time available for work on this device, only the basic ideas and principles were established. Further modifications to the ceramic device will hopefully provide a delivery device for organic solvents used in chronic neurobehavioral toxicity studies.

Recommendations to increase the release rate of the chemicals include: 1) Increase the amount of PVA which would increase the pore sizes; 2) Increase the particle sizes from -400 to 325 or greater. This would also increase the pore sizes; 3) Press the ALCAPs at a lower pressure, from 7000 to 4000; 4) Increase the size of the ALCAP. This would increase the surface to volume ratio providing a greater surface area to release the chemical. Along with these specific recommendations, mathematical modeling of the ALCAP delivery device would be a tremendous asset to help understand modifications implemented and their effects on release. The ultimate test of the delivery device would be to implant it in the animal and monitor the home cage activity of the animal compared with controls.

VI. REFERENCES:

- Bajpai, P.K. ALCAP Ceramics in Drug Delivery. American Chemical Society, Polymer Reprints 1985, vol 26 (2). p. 203.
- Gargas, M.L., M.E. Anderson and H.J. Clewell III. Physiologically based Simulation Approach for Determining Metabolic Constants from Gas Uptake Data. Toxicology and applied Pharmacology, 1986, Vol. 86, pp. 341-352.
- Melnick, R. L., et. al., application of Microencapsulation for Toxicology Studies. II. Toxicity of Microencapsulation Trichloroethylene in fischer 344 Rats. Fundamental and Applied Toxicology, 1986, Vol. 8, pp. 432-442.
- NIOSH. Organic Solvent Neurotoxicity. 1987, U.S. Department of Health and Human Services, Public Health Service, Centers for Disease Control, National Institute for Occupational Safety and Health, Cincinnati, Ohio.
- Reiter, L. (1978). Use of Activity Measures in Behavioral Toxicology. Environmental Health Perspective. Vol. 26, pp. 9-20.

200 μ l CERAMIC RESERVOIR

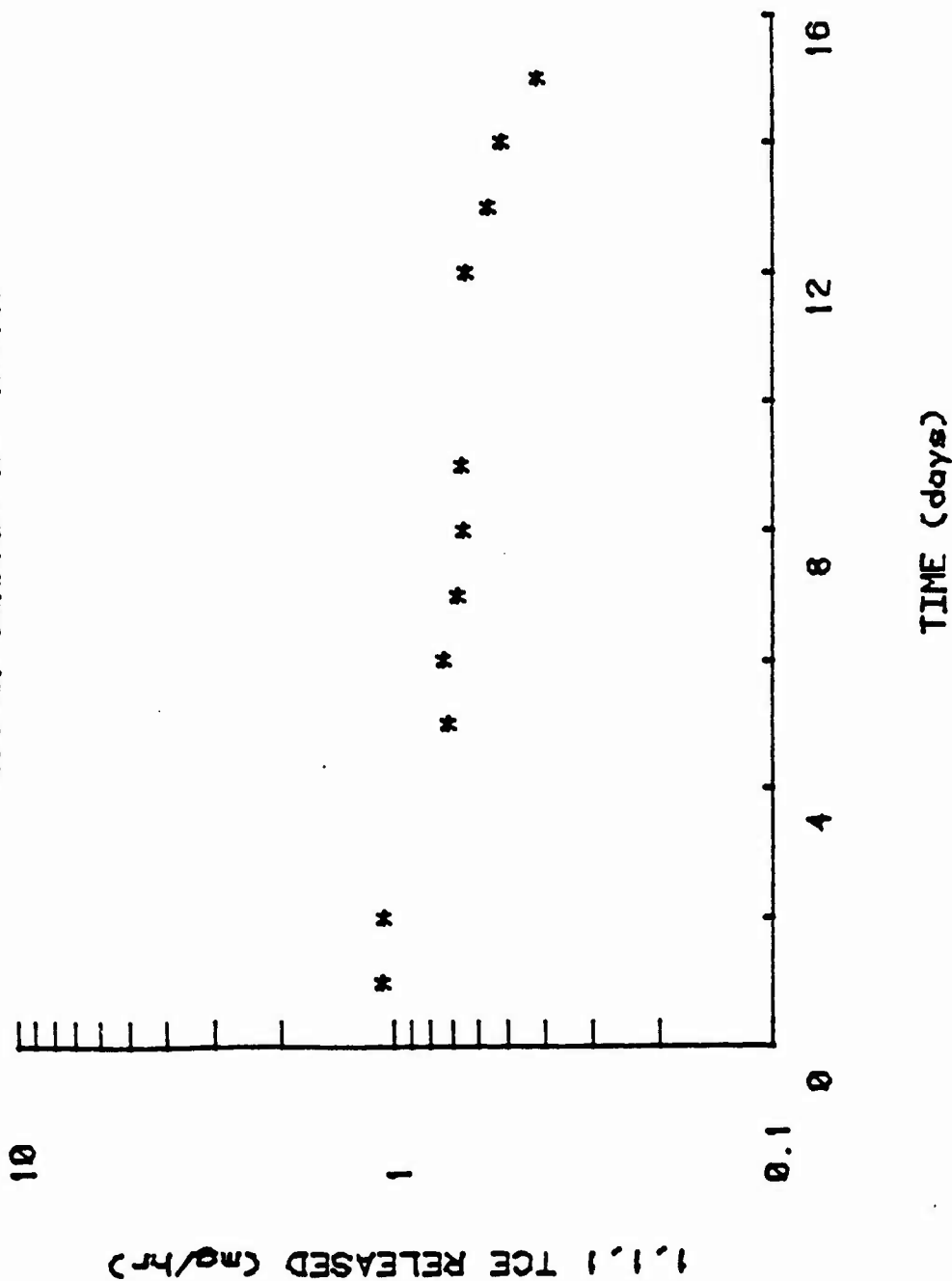


Figure 1. Release of 1,1,1 Trichloroethane for 15 days from the 200 μ l ALCAP ceramic reservoir solvent delivery system containing 200 μ l of 1,1,1 TCE plus 5% mineral oil. A sustained release was attained between days 5 and 12 with an average release rate of 0.7 mg/hr.

TWO ML CERAMIC RESERVOIR

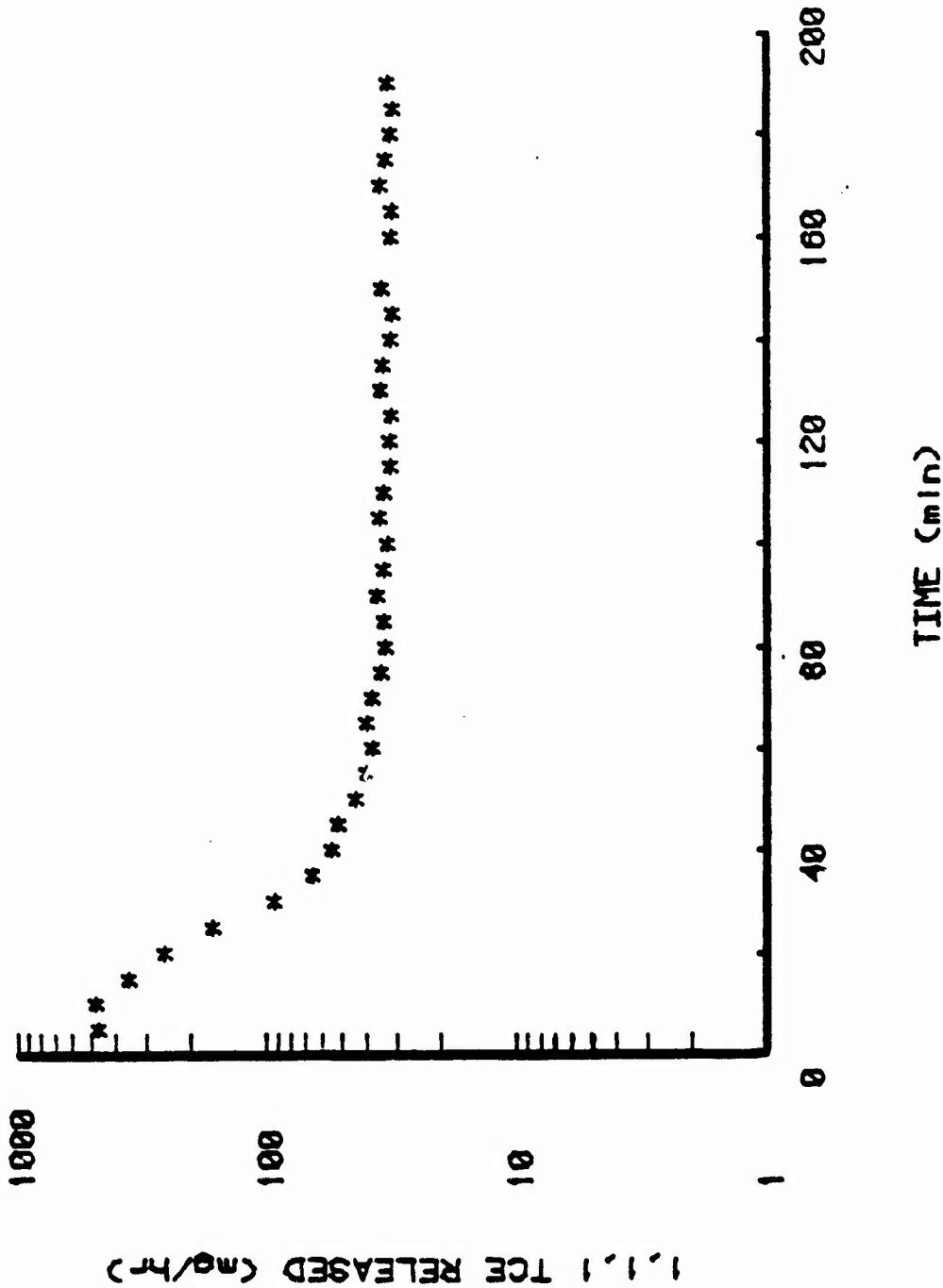


Figure 2. Release of 1,1,1 Trichloroethane for five hours from the 2 ml ALCAP ceramic reservoir solvent delivery system containing 2 ml of 1,1,1 TCE plus 5% mineral oil. A sustained release was obtained after the first hour for a duration of four hours with an average release rate of 33 mg/hr.

Table 1. Amount of 1,1,1 Trichloroethane in the venous blood of two 300 g catheterized Fischer 344 male rats implanted with 2 ml ALCAP ceramic reservoir solvent delivery systems containing 2 ml of TCE plus 5% mineral oil over a six day period.

Time (hrs)	<u>mg/hr</u>		Average
	Rat 1	Rat 2	
0.25	12.66	5.20	8.93
0.50	5.25	2.47	3.86
0.75	2.82	6.13	4.47
1	3.71	3.84	3.77
2	4.31	8.77	6.54
3	4.56	6.34	5.45
4	6.22	7.34	6.78
5	8.36	13.50	10.93
6	12.02	11.60	11.81
25	6.23	5.34	5.78
26	6.06	5.75	5.91
27	6.85	6.09	6.47
28	4.59	5.27	4.93
70	4.12	--	--
72	9.84	--	--
73	2.15	--	--
99	2.31	--	--
100	2.73	--	--
121	1.82	--	--

1987 USAF-UES SUMMER FACULTY RESEARCH PROGRAM

Sponsored by the

AIR FORCE OFFICE OF SCIENTIFIC RESEARCH

Conducted by the

Universal Energy Systems, Inc.

A NEW SENSITIVE FLUOROMETRIC METHOD FOR THE
ANALYSIS OF SUBMICROGRAM QUANTITIES OF CHOLESTEROL

by

Dr. Leonard Price and Conrad Murray

FINAL REPORT

Prepared by Conrad Murray
Academic Rank: Medical Student III
Department and School of Medicine
University: Meharry Medical College, Tennessee
Research Location: USAFSAM/NGI
Brooks AFB
San Antonio, TX 78235-5301
USAF Researcher: Dr. Harvey A. Schwertner
Date: 31 July 1987

REFERENCE DR. PRICE
SFRP FINAL REPORT NUMBER 111

1987 USAF-UES SUMMER FACULTY RESEARCH PROGRAM
GRADUATE STUDENT SUMMER SUPPORT PROGRAM

Sponsored by the
AIR FORCE OFFICE OF SCIENTIFIC RESEARCH

Conducted by the
Universal Energy Systems, Inc.

FINAL REPORT

Prepared by:	Joseph S. Deroucci, Ph.D. Steven J. Naber, M.S.
Academic Rank:	Assistant Professor Graduate Research Assistant
Department and University:	Statistics Department Ohio State University
Research Location:	USAF/OEHL/TSS Brooks AFB San Antonio, TX 78235
USAF Researcher:	Philip Hunter
Date:	20 August 1987
Contract No:	F49620-85-C-0015

REFERENCE DR. VERUCCI
SFRP FINAL REPORT NUMBER 139

1987 USAF-UES SUMMER FACULTY RESEARCH PROGRAM/
GRADUATE STUDENT SUMMER SUPPORT PROGRAM

SPONSORED BY THE
AIR FORCE OFFICE OF SCIENTIFIC RESEARCH

Conducted by the
Universal Energy Systems, Inc.

FINAL REPORT

A Human Factors Evaluation of the Advanced Visual Technology
System (AVTS) Eye Tracking Oculometer

Prepared by: Jerome I. Nadel
Academic Rank: Graduate Student
Department and Psychology Department
University: Kansas State University
Research Location: AFHRL/OT
Williams AFB
AZ, 85240-6457
USAF Researcher: Elizibeth Martin, Ph.D.
Date: 10 August 1987
Contract No: F49620-85-C-0013

A Human Factors Evaluation of the Advanced Visual
Technology System (AVTS) Eye Tracking Oculometer

by

Jerome I. Nadel

ABSTRACT

A human factors evaluation of the Honeywell helmet mounted eye tracking oculometer system was conducted. Experimental tests were directed at identifying the physical and anthropometric factors that lead to both successful and unsuccessful oculometer operability. Pupil size of the user was found to be the most significant factor affecting system performance. Other factors affecting system performance were interpupillary distance (IPD) and helmet fit. It was recommended that the electronic pupillary signal from the systems IR camera be amplified. This, in combination with a lower system pupil threshold, should ensure measurement accuracy for at least 80% of the user population.

Acknowledgement

I wish to thank the Air Force Office of Scientific Research for sponsorship of this excellent research opportunity. I would also like to thank Universal Energy Systems, especially Rodney Darrah and Sue Espy, for their sincerity and concern for all my program related needs.

I am most grateful to Dr. John Uhlarik for his recommendation and instrumental efforts which allowed me to participate in this program. Dr. Harold Warner deserves special mentioning, for he is the individual I worked most closely with over the course of my summer research program. Dr. Warner's commitment to finding solutions and ability to make a working situation extremely pleasurable have made research project very fruitful and fulfilling. Susan Baroff, of General Electric, should also be acknowledged for her efforts with the project. Finally, I would like to thank Dr. Elizibeth Martin, my focal point, for her concern with all aspects of the project.

I. INTRODUCTION:

The Advanced Visual Technology System (AVTS) utilizes a high-resolution area-of-interest (AIO) display surrounded by a lower resolution background. The AVTS employs a combination (or independent operation) of eye and head tracking devices to ensure that the AIO provides the highest resolution at the point of regard. General Electric Corporation, Simulation and Control Systems Department, is the Air Force contracted agent responsible for operations and maintenance of the Honeywell Helmet mounted head and eye tracking systems. This helmet mounted system is similar the eye-control system described by Calhoun, Arbak, and Boff (1984). Presently, the AIO is heavily dependent on the magnetic head tracking device which directs the AIO according to directed head movements.

Because the AVTS was designed to operate with both head and eye tracking capabilities, the Air Force Human Resources Laboratory has requested that research be conducted to determine the cause(s) of the eye-tracking systems poor performance. Such performance was characterized by incorrect positioning of the AIO in in-dome flight simulation. This led to a comprehensive human factors investigation assessing both machine specifications and human limitations that affect the AVTS's oculometer performance.

As a graduate student of Industrial/Organizational psychology I have focused my research efforts towards applied psychological issues, such as the effects of self-esteem on organizational decision-making (thesis research). However, more recently, I have focused my research efforts towards the study of human factors issues. Such efforts, conducted at IBM's Charlotte, N.C. human factors laboratory, include comparisons of graphics vs. text automatic teller machine (ATM) screens, printer function key layouts, and an assessment of color preference for print with multi-color printers. My work with applied human factors experimentation combined with my extensive studies in the fundamentals of psychological experimentation, from design to statistical analysis, have contributed to my assignment at the Air Force Human Resources Laboratory.

II. OBJECTIVES OF THE RESEARCH EFFORT:

As stated previously, the research problem was to first identify the factors relevant to successful oculometer functioning, and perhaps more importantly, to determine feasible solutions to correct these problems. In collaboration with Dr. Harold Warner, University of Dayton Research Institute, a human factors evaluation of the Honeywell oculometer was conducted. The human factors evaluation was conducted (a) to identify the

personnel for whom the oculometer operates either normally or incorrectly, (b) to measure the physical eye and head dimensions of the test personnel, and (c) to analyze the relationship between these measures and the operability of the oculometer.

Unfortunately, unlike most empirical research efforts, the complexity and dynamic nature of the oculometer did not allow for one specific experimental design with individually manipulated variables. The oculometer's operation is based on an infrared reflection from the retina and the cornea which must bypass the incoming IR source to ultimately be picked up by an IR sensitive camera. Once these reflection signals are captured in the camera they must be processed by a host of computer hardware and software to complete the image and insure accurate eye tracking.

This dynamic multi-level processing system made the identification and isolation of specific problem factors extremely difficult. Therefore, a step by step "funnel-type" qualitative approach was taken initially to shorten the list of possible factors. The initial list of manual mode tests contained 37 possible systematic tests. Examples from this manual mode test list included: (1) Eye movement only, with head restrained, (2) head movement with eye movement, (3) eye color, (4) "break-locks", (5) interpupillary distance, (6) infrared viewer to lock on position of IR

beam, (7) vertical vs. horizontal eye movement, (8) calibration & linearization, (9) pupil diameter, and (10) size of tracking envelope for which eye tracking can be maintained.

III. PROCEDURE:

As testing progressed, the previously mentioned funneling of relevant factors became more apparent. The procedures described in this section conform to the sequence in which they were evaluated. The results obtained from each set of tests prescribed a reformulation of the next test series. This building block approach allowed the experimenters to dismiss, or follow up, specific factors depending on their apparent relatedness to oculometer functioning.

a) Initial tests were directed at determining, qualitatively, what factors appeared to effect the eye tracking systems performance. Individuals to be used for testing were screened and categorized by pupil size, interpupillary distance (IPD), eye color, skin tone, and helmet fit. Twelve subjects ran through this procedure which basically consisted of (1) wearing the helmet to determine fit, (2) capturing "lock-on" data, (3) measuring pupil size as viewed on the systems monitor, (4) determining distance of the right eye from the helmet's visor, (5) measuring pupil response as a function of light directed at the eye (by size and

oculometer operability), (6) determining relative position of the corneal reflection on the pupillary reflection, and (7) measuring interpupillary distance. All data were recorded and qualitatively analyzed to determine which factors constituted further investigation.

b) It appeared from the first set of preliminary tests, that although helmet fit appeared more critical for some users than others, a positive helmet fit was needed for both oculometer testing and AVTS "in dome" simulation training. Four designs were proposed to, and discussed with, the General Electric engineers, which included an internal strapping system, a three bladder blood pressure cuff system, thermal lining with position memory, and an internal rigid helmet liner adjusted by a series of hand adjustable screws.

c) The next series of tests were conducted to determine individual differences on oculometer tracking envelopes; the area over which a "lock-on" could be maintained. A "lock-on", indicated by a pupil and corneal reflection enclosed within two vertical and horizontal gates on the systems monitor, defines the eye tracking systems acknowledgement of eye location. All tracking envelopes were calculated in visual angle as measured on a specially designed LED matrix board.

d) The results from previous tests led the experimenter's to pursue, more precisely, the impact of pupil size of the operability of the oculometer. Two subjects (including this experimenter) volunteered to have their right eye dilated with an atropine solution for a within subject comparison of pre- and post-pupil dilation performance with the oculometer. Both pre- and post-dilation experimental sessions were identical; once the helmet was placed on the head, data was collected on pupil size, "lock-on" capabilities, oculometer tracking envelopes, and pupillary response. This full set of procedures was repeated twice for one of the subjects (the experimenter) to determine the reliability of the effect.

e) Once again, based on the findings of the previous tests, additional tests were conducted manipulating the systems software parameters related to pupil size to determine if changing the systems pupil size thresholds and infrared projector intensities could facilitate usability. As part of this test, low light goggles (that pick up IR light sources) were used to determine if the eye was in fact being flooded with IR light. Qualitative inspection suggested that the eye was receiving a strong IR signal from the projector. Therefore, it was felt that the systems inadequacy was coming from its inability to pick-up the reflection coming back from the retina once the light had passed

the pupil. This led to a series of tests specifically manipulating parameters related to pupil threshold.

f) Similar manipulations were conducted with the hardware components of the eye tracking system. Acknowledging the importance of pupil size on the functioning of the oculometer, a pupil video was engaged to monitor the actual pupil image the system was receiving from the camera pick-up. In the systems typical operational mode, the pupil image shown is a composite or processed image that has gone through several computer filters which identify and reconstruct aspects of the pupil signal. If the signal (the IR reflection coming back from the retina) is too weak, the composite image, and its corresponding "lock-on" gates will not appear. However, the pupil video allowed the experimenters to view the pupil signal at below system threshold levels. Pupil sizes and brightness, above and below system threshold, were recorded to assess any systematic effects.

g) The final step in this testing sequence involved a systematic evaluation of the helmet mounted eye tracking system's linearization and calibration procedures. This linearization establishes a correction factor, listed on a computerized look-up table, which adjusts the systems computed eye position according to deviations calculated in linearization.

The linearization task consisted of a subject, with head fixed in a chin rest, fixating on individual LED's on a matrix board while pressing on a trigger which indicated apparent fixation. Through this procedure the computer calculated the fixation deviations for each point, extrapolating for imaginary points not contained on the matrix board. Several tests were conducted, manipulating various software parameters (i.e. normal vs. elliptical modes of operation). At extreme angles of fixation, eye direction is determined from the shape of the eye (Merchant & Morrissette, 1973). For these extreme angles, the elliptical mode of operation should be utilized.

It should be noted that the LED array was initially designed to simulate visual angles on the parabolic surface of the 24' diameter dome. However, the data outputs shown in the Honeywell documentation did not conform to this "off-rectangle" shape. Therefore, several tests were conducted, varying visual vs. projected angles, to determine the configuration that produced the most accurate and reliable results.

IV. RESULTS:

a) The initial series of tests, utilizing data from 12 subjects was perhaps the most valuable because it gave direction for the tests that followed. The results from these tests reliably showed that pupil size had a

significant effect on oculometer operability. The range of the pupil size image, as measured from the systems monitor, ranged from 1.5cm to 3.5cm. Unfortunately, a pupilometer could not be procured to measure actual pupil size. Nevertheless, it was felt that the monitor generated images gave an accurate measurement of the relative differences in pupil size. The operability of the oculometer appeared to be a direct function of pupil size, with consistent "lock-on" above 2.5cm and no "lock-on" below 2.0cm. The size of the pupil also appeared to determine the position of the corneal reflection relative to the pupillary reflection, with the corneal reflection approaching center as pupil size increased. The mean interpupillary distance (IPD) was 69.95mm with a standard deviation of 4.44. This didn't appear to have a significant effect of "lock-on" per se, but it did appear to effect the tracking envelopes (see IV - c). Other physical and anthropometric measures, such as eyes distance from the reflective visor and skin tone and color, did not appear to have any significant effect on performance.

b) Unfortunately, the quantifiable effect of a secure helmet fit on oculometer operability was unobtainable. This was due to the inability of the General Electric engineers to produce the designed helmet systems in the time course of the summer research project. However,

it was observed that the importance of helmet fit was not invariant; it depended on pupil size. For the test subjects with large pupils, obtaining easy "lock-on", there was a large tolerance for helmet slip. Conversely, for subjects with small pupils, proper helmet fit and positioning was critical.

c) The results of the tracking envelope tests indicated that interpupillary distance did have an effect on the symmetry of the envelope. The eye mounted oculometer system has a reflective semi-circular shield over the right eye (the eye the system tracks). Differences in IPD will effect the position of right eye relative to this reflective surface, with larger IPD's positioning the eye toward the right edge of the surface. One factor that affected the size and shape of the tracking envelope was pupil size. However, it also appeared that there was a negative relationship between IPD and the size of the envelope to the right, or the degree of tracking envelope asymmetry.

d) The most conclusive results obtained came from the pre-dilation vs. post-dilation comparison. For both subjects, the pupil dilated at least 1cm ($S_1=1\text{cm}$ gain, $S_2=2\text{cm}$ gain). With both subjects, who were selected for their small baseline pupil size, initial "lock-on" was very difficult to obtain. However, both subjects

obtained excellent "lock-on" in the post-dilation condition. Furthermore, tracking envelopes enlarged on the order of 10-20 degrees visual angle in every direction, and helmet fit became much less critical.

e) As stated previously, software parameters related to pupil size were manipulated to determine if altering the systems pupil threshold could enhance the images coming back from the small pupil. Although several tests were conducted, manipulating several aspects of the programs parameters, no significant differences were found on the systems performance.

f) A more successful approach came from the hardware end of the system. The pupil video allowed the experimenters to view the dynamic changes in pupil size as it went through the threshold range. At the systems subthreshold levels, the composite or processed pupil image and its corresponding gates (indicating "lock-on") do not appear. Examination of the pupil video, comparing sizes and brightness of three subjects with qualitatively different pupil sizes, indicated that although the small pupil may not produce a sufficient signal to obtain "lock-on", the system does acknowledge the image. This is an important finding because it indicates that the weak signal produced from the small pupil's retinal reflection can be amplified

to a sufficient level to obtain "lock-on" with full eye tracking ability.

g) As stated in the procedure section of this report, several tests were conducted to determine the configuration that produced the most accurate and reliable linearization data. Unfortunately, the time constraints associated with the summer research program did not allow for any systematic relationships to be obtained. General Electric plans to continue these efforts, attempting to procure the one test pattern that optimizes the linearization procedure.

V. RECOMMENDATIONS:

Although at least two human factors have been identified that reliably effect the operability of the oculometer, the complexity of the helmet mounted eye tracking system does not lend itself to mending with simple remedies. Furthermore, it should be noted that an interaction of factors (hardware, software, and human user related) could potentially identify a situation that requires a follow-up evaluation of the modified system.

a) The finding with the greatest impact on oculometer operability was the effect of pupil size on "lock-on" and tracking capabilities. When Honeywell designed this head and eye tracking system, an artificial eye

was used (with an artificial pupil of 5mm) to test its performance characteristics. Although a 5mm invariant pupil was used, Honeywell obviously acknowledged the importance of pupil thresholds because hardware mechanisms were allocated for this function; though unfortunately never utilized. Based on the results of this human factors evaluation three specific recommendations related to pupil size are proposed (2 hardware, 1 software).

The test using IR vision goggles to view the IR light envelope on the eye in combination with the pupil video test, showing a pupil image at subthreshold pupil size, indicated that the pupil signal (from the IR camera) needs to be amplified. If amplified, the signal would be strong enough to pass through the filters associated with the composite pupil image and "lock-on" gate programs. (1) It is recommended that a variable amplifier be placed in sequence immediately following the camera's pupil signal. This would allow for subtle changes in magnitude of amplification, depending on the user's pupil size. (2) A second, related recommendation involves a systematic test, varying the systems hardware thresholds to determine the optimal setting for all system users. (3) Once these hardware modifications are completed I recommend a second attempt at systematically manipulating the software

parameters related to pupil threshold (threshold, intensity, chords, etc.).

b) As stated in the results section of this report, the time constraints of this summer research effort did not allow for completion of the linearization testing. General Electric, with the technical help of Honeywell and the Oculometer Research Institute, at Wright Patterson Air Force Base, should continue these efforts. There appears to be a sign problem in the linearization program, such that errors from target are overcompensated in the opposite direction. Once these program problems are corrected a series of linearization tests should be conducted to assess the reliability of the system's data. The final test for the linearization procedure should be "in-dome", with the AOI slaved to the head and eye tracking systems. The errors in linearization would be translated to inappropriate positioning of the AOI; deviations from actual eye position should be monitored and assessed.

c) Before any "in-dome" tests are conducted it is essential that a secure helmet fit is obtained. Presently, General Electric engineers are working on modified designs to produce a universal helmet that will ensure less than a 3mm tolerance slip. This helmet fit issue will become even more critical when the oculometer is at full operational status and prints

are wearing the helmet mounted systems for simulation flying.

d) A last recommendation is derived from the reliable asymmetry of tracking envelopes. As interpupillary distance increased, the asymmetry of the tracking envelope became more apparent; decreasing in size to the right. Presently the reflective surface on the helmet's visor is semi-circular. It was felt that if the reflective surface were extended out to the temporal side of the helmet, creating an elliptical shape, tracking symmetry could be obtained.

REFERENCES

Calhoun, G.L., Arbak, C.J., and Boff, K.R.,
"Eye-Controlled Switching for Crew Station Design,"
Proc. Human Factors Society 28th Annual Meeting, 1984,
258-262.

Merchant, J. and Morrissette, R. "A Remote Oculometer
Permitting Head Movement," Wright-Patterson Air Force
Base, Ohio. 1973, AFAMRL-TR-73-69.

1987 USAF-UES SUMMER FACULTY
RESEARCH PROGRAM/GRADUATE STUDENT
SUMMER SUPPORT PROGRAM

Sponsored by the
AIR FORCE OFFICE OF SCIENTIFIC RESEARCH
Conducted by the
Universal Energy Systems, Inc.

FINAL REPORT
The Effects of Increased Cognitive
Demands on Autonomic Self-regulation: An
Indicator of Parallel Processing in the Brain

Prepared by: Victoria Tepe Nasman

Academic Rank: B.A., M.S., Doctoral student

Department and
University: Department of Psychology
Northwestern University

Research Location: Air Force School of Aerospace Medicine
Brooks Air Force Base
Crew Performance Laboratory

USAF Researcher: Frederick J. Bremner, Ph.D., Visiting Professor

Date: August 21, 1987

Contract No.: F49620-85-C-0013

The Effects of Increased Cognitive
Demands on Autonomic Self-regulation: An
Indicator of Parallel Processing in the Brain

by

Victoria Tepe Nasman

ABSTRACT

A parallel processing scheme is proposed. We tested that scheme through a single-subject experimental design in which subjects performed several tasks. Ongoing electroencephalographic signals were recorded over left and right occipital cortex, and compared between tasks within session. As expected, while performing various meditation and biofeedback tasks, subjects demonstrated characteristic dominant frequencies of 7-13 Hz (alpha). When performing such a task concomitant with another highly associative cognitive task, however, subjects produced results more like those obtained in the performance of the cognitive task alone. These results support the notion that, while engaged in tasks which would require parallel brain processing, processes which would otherwise rely upon serial processing are "uncoupled." We propose a scheme upon which to base this interpretation. Although performance data on the cognitive task have not yet been thoroughly analyzed, our preliminary interpretation of the data is that we have obtained evidence to support a view of cognitive processing in which the flexibility to process either serially or in parallel exists, and in which the type of processing that is invoked will coincide with the demands of the task or tasks being performed.

ACKNOWLEDGMENTS

I would like to thank the Air Force Systems Command and the Air Force Office of Scientific Research for sponsorship. Thanks also to everyone at the School of Aerospace Medicine for creating an environment which is both challenging and motivating.

In particular, I wish to thank Dr. William Storm for his kindness and support; Dr. Fred Bremner for allowing me to work with him again this year; Dr. Douglas Eddy, Neal Takamoto, Gary Bartel, and Lee Shapiro for their support on the project; Sgt. Frank Garcia for his friendship and all he does to help the staff at CPL; Irma Geisberg for her patience; Marsha Jackson for her friendship and transportation services. My second summer working with all of the people at CPL was every bit as enjoyable as my first.

I. Introduction

I have completed three years of the graduate program at Northwestern University (Evanston, IL) in the Department of Psychology's Behavioral Neuroscience Program. My research is in the area of event-related brain potentials (ERPs), and has been focused on the P3 component of the ERP in particular.

The research problem at the School of Aerospace Medicine was an attempt to demonstrate parallel brain processing by requiring subjects to engage in cognitive as well as self-regulatory tasks simultaneously. Inherent frequency (EEG) data were collected as the primary indicator of the effects being tested. Heart-rate self-regulation and cognitive task performance data were also collected.

II. Objectives of the Research Effort

The overall objective of the research is to determine under what conditions human beings can (and cannot) process both cognitive information and biological control information. Our immediate goal was to obtain evidence to support the notion that, in the case where both types of information must be processed simultaneously, reliable and characteristic indicators of co-processing will be apparent in EEG dominant frequency patterns. Reliable patterns of dominant frequency may ultimately be of practical use in the monitoring of aircraft pilots who must engage in self-regulation while at the same time perform highly demanding cognitive activities.

My individual objectives as a participant in the GSSS Program were as follows:

1. This project was begun one year ago (summer 1986). At that time, I was involved in design of the study, instrumentation and set-up, and preliminary data collection. Seven of the 10 total experimental sessions which comprise the data set we present here were run by Dr. Bremner prior to my arrival again this summer. My goal on my arrival here this year was to participate in running the remaining three sessions, to help in the analysis of EEG, ECG, and performance data, and to contribute to the final written report of the study.

2. As a direct result of our findings to date, we decided that one of our objectives should be to design a computer-generated model of parallel brain processing. My goal was to become competent on the software (MicroSaint) used to create the model, to contribute to the refinement and testing of that model, and to contribute to a final written report on the result.

III. Overview

The brain has a slow basic processing cycle time relative to modern computers. To account for this, yet explain its ability to discriminate as quickly as it does, theorists have postulated that the brain somehow engages in parallel processing rather than exclusively in the serial type of processing seen in most modern computers (Hinton, 1985).

The experiment described below is based upon a parallel processing model in which the left cortex, the right cortex, and the hypothalamus/autonomic nervous system (HANS) are taken to be co-processors. The hypothesis is that left cortex and HANS are sometimes coupled and sometimes uncoupled in their processing activities. When coupled, serial processing takes place. When uncoupled, parallel processing predominates. Electroencephalographic dominant frequencies as well as heart-rate biofeedback data and task performance data served as indicators in our attempt to test this scheme.

IV. The Proposed Model

Split-brain experiments have supported the idea that left and right cortex co-process. We assume HANS to be an unconscious co-processor. The left cortex (left co-processor -- LCP) is primarily a conscious processor, and is able to gain control of the HANS (coupling). During biofeedback physiological self-regulatory tasks, such control is necessary. According to this model, then, serial processing is predominant during physiological self-regulation. Where cognitive demands are such that both accurate discriminative performance and fast reaction time are required, however, a more efficient system of parallel processing will become necessary (uncoupling). The HANS is allowed to run in parallel until the LCP is less dedicated to the cognitive problem. We would predict, then, that when subjects are required to perform demanding cognitive and self-regulatory tasks simultaneously, the efficiency of parallel processing will be maintained in

cognitive task performance while uncoupling of the HANS and LCP will lead to a decrease in the ability to self-regulate. Dominant EEG frequencies in this dual task situation should be consistent with those obtained while performing cognitive task alone. Characteristic frequency patterns of the self-regulatory state should dissipate. EEG alpha activity is important as an indicator of attentional processes; demanding cognitive processing should be reflected by a decrease in alpha activity (Ray & Cole, 1985).

V. Method and Experimental Procedure

Subjects. Two right-handed adult male subjects each participated in the experiment over the course of twenty sessions. Each was trained and experienced in the various aspects of each experimental task (meditation, biofeedback, and the Perelli task). Data from the final five sessions were analyzed. Each subject's data was considered to be a separate experiment, in a design similar to Bremner et. al. (1985).

Apparatus. Electrophysiological data-recording and storage methods were standard. The electroencephalogram (EEG) was monitored with Grass Ag-AgCl scalp electrodes over the right and left occipital cortex (O1 and O2), referenced to each ipsilateral mastoid. Electrocardiogram (ECG) monitoring was done with two Con Med pregelled disposable electrodes placed diagonally, one in the right subclavicular space and the other over the left intercostal space between the 10th and 11th rib. This configuration (the CR-5 lead, Simonson, 1971) produces a lead-II-appearing waveform. Subjects were grounded with one pregelled electrode, attached at the back of the neck, approximately vertebral C-3. Electrode impedances were kept below 6 KOhms.

Data Inc. amplifiers (Model 2124) were used. EEG signals were amplified by 30,000, with 3dB filter cutoffs set to pass signals between .5 and 30 Hz. ECG signals were amplified with 3dB filter cutoffs set to pass signals between DC and 30 Hz. Amplification values for ECG signals were determined within-subject, and depended upon each subject's ECG signal strength and the ability of the peak-detector circuit (discussed below) to identify ECG subcomponents. In the case of Subject #1 ("Neal"), signals were amplified by 1000; for Subject #2 ("Douç"), signals were amplified by 2000. EEG and ECG responses were recorded on analog tape (Honeywell 101 analog tape recorder),

and were monitored on an oscilloscope throughout each experimental session.

Biofeedback consisted of filtered ECG signals presented to the subject through a loud speaker (Helmer, 1975). Subjects were tested in an electrically shielded sound-proof Industrial Acoustics Chamber, while seated in a well-padded chair. Instructions were given to the subject through an intercom. The Perelli task was presented on a TV monitor placed 1 meter in front of the subject.

Data reduction and statistical analysis functions were performed in several stages. Conversion of EEG data from analog to digital data (A/D conversion) was performed off-line by a Digital Equipment Corporation PDP 11/34 computer. The digital data were then submitted to Fourier analysis and frequency spectra were generated using SAS. ECG data was analyzed on-line using peak detection software (HIMS) created by Drew (1987), and managed on a Zenith 248 IBM-compatible computer. The HIMS program detected standard ECG subcomponent peaks (P, Q, R, S, T) and determined time duration measurements for heart rate (beats per minute), P-R, Q-R-S, and S-T segments of 100 heartbeats recorded during each task. Mean times and standard deviations were later calculated using the LOTUS 123 (1983) software package (Kapor & Sachs, 1983) on the same computer terminal. Output included descriptive statistics on five consecutive blocks of 20 heartbeats.

Procedure.

Once the subject was instrumented for heart and brain electrophysiological recording, he was seated in the sound-proof chamber, where electrode leads were attached to the amplifiers and recording systems. He then performed the five experimental tasks, each of which lasted a total of two minutes. (Where Perelli task sessions exceeded two minutes, only the first two minutes of recorded data were analyzed.) The order of tasks performed was randomly determined prior to each session. The five tasks were as follows:

Meditation (MEL/R) -- the subject tried to relax and slow his heart rate without any external stimuli (Hyman, 1978).

Perelli (PRL/R) -- the subject performed a complex cognitive task presented to him on a TV monitor (Perelli, 1980). The Perelli task is an adaptive task which involves associative memory load, memory scanning, visual scanning, and

a simple motor response (a right-handed button press). It is computer paced and adaptive to individual subject abilities. Associations are memorized as follows:

- 1.....#
- 2.....*
- 3.....>
- 4.....~
- 5.....[

The computer presents four self-paced trials. An array of the digits is presented, as well as one symbol. The subject must respond by pressing a button he believes to correspond to the correct array digit (see example below, Fig.1a and Fig. 1b).

2 3
 5 >
 1 4

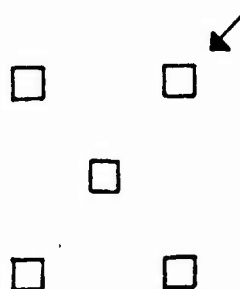


Fig.1a. Example presentation.

Fig. 1b. Button arrangement and correct response (arrow).

The mean reaction time of the four initial trials is used as a beginning presentation rate during the adaptive phase. Trials are presented at successive increments or decrements of 100 milliseconds. Lack of response to two consecutive trials defines the "block" phase of the task. The computer adds 300 milliseconds to the presentation rate at that point to allow the subject to 'catch up' and resume responding. When consecutive blocking occurs within +/- 200 milliseconds, the task terminates. Reaction times are given by the computer as a measure of performance. Three sessions are run.

Biofeedback Slow (BSL/R) -- the subject received audio biofeedback of his ECG responses (described above) and tried to slow his heart rate (Blanchard & Epstein, 1978).

Biofeedback Fast (BFL/R) -- the subject received audio biofeedback of his ECG responses (described above) and tried to increase his heart rate.

Biofeedback Perelli (BPL/R) -- the subject received audio biofeedback of his ECG responses (described above) and tried to slow his heart rate, while at the same time performing the Perelli task.

VI. Results

All experimental sessions were completed. Electroencephalographic data were analyzed and results supported the prediction that, during simultaneous cognitive and self-regulatory task performance, dominant frequencies are characteristic of those generated when subjects perform only the cognitive task. Dominant frequencies obtained during self-regulatory tasks (BSL/R, BFL/R, MEL/R) exhibited clear and consistent frequencies in the range from 8-15 Hz and at intensities which were consistent within session. During performance of the Perelli task alone and the Perelli task with biofeedback, however, subjects demonstrated more widely scattered frequencies which included an increase in 3-7 Hz theta activity; intensities varied widely within session. See Appendix A for examples of frequency spectra which were typical of our findings. During self-regulation tasks, alpha activity was most clear in the right hemisphere. During the Perelli tasks, the scattering of frequencies was most pronounced in the left hemisphere.

Heart rate data has not been thoroughly analyzed as yet. Preliminary analysis, however, indicates that heart rate (as measured by beats-per-minute) did not change remarkably between tasks for Subject #1. Heart rate in this subject remained within 1-2 beats-per-minute between self-regulation tasks (meditation, biofeedback slow) and cognitive tasks (Perelli and Perelli with biofeedback) and were not consistent. Subject #2 demonstrated consistent differences between tasks, however. Self-regulatory tasks (meditation and biofeedback slow) yielded measures which were 4-5 beats-per-minute less than those which were recorded during the cognitive tasks. Hence, while this subject achieved a slowed heart rate during strictly self-regulatory tasks, he was unable to do so when attempting to perform the Perelli task with biofeedback.

Performance data from the Perelli task have not yet been analyzed.

VII. Recommendations

1. If this research is to be extended to an applied setting, we should go on to test aircraft pilots under flight-simulated conditions. Physiological self-regulation and cognitive tasks, then, should be much like those which are encountered by these subjects in flight.

2. Pre-emption of physiological self-regulatory abilities can lead to loss-of-consciousness problems which result from decreased ability to counter the effects of extreme G-forces. The results of our research should be used to contribute to ongoing efforts in the development of tools which will help both to predict and prevent in-flight difficulties.

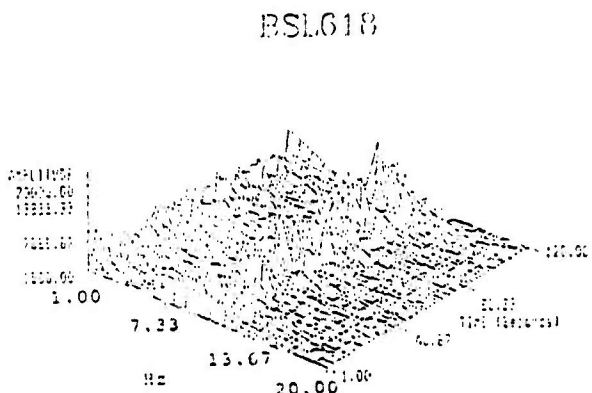
REFERENCES

1. Blanchard, E.B. & Epstein, L.H. (1978). A Biofeedback Primer (3rd ed.). Reading, MA: Addison-Wesley Publishing Company, Inc.
2. Bremner, F.J. & Yost, M. The reliability of the single subject statistics for biofeedback studies. Paper presented at the meeting of the Biofeedback Society of America, Albuquerque, New Mexico, April, 1984.
3. Bremner, F.J., Yost, M. & Zintgraff, C. (1985). A longitudinal study of cardiac component analysis. Behavior Research Methods and Instrumentation, 17(2), 319-322.
4. Drew, G. (1987). Unpublished technical report, School of Aerospace Medicine, Brooks Air Force Base, TX.
5. Eddy, D.R., McKendree, J. McKenzie, R.E. & Bremner, F.J. (1982). Component analysis of ECG by computer. Behavior Research Methods and Instrumentation, 14(2), 290-293.

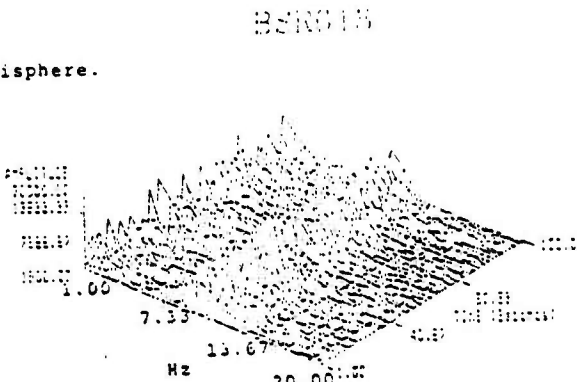
6. Helmer, R.J. (1975). Modular and filter circuitry for EEG biofeedback. Behavior Research Methods & Instrumentation, 7, 15-18.
7. Hinton, G.E. (1985). Learning in parallel networks. Byte, 10, 265-273.
8. Hyman, P.S.(1978). Hemispheric specialization and ideomotor activity. Unpublished Master's thesis, Trinity University, San Antonio, TX.
9. Kapur, M. & Sachs, J. (1983). LOTUS 123 (Computer program). Cambridge, MA: Lotus Development Corporation.
10. Perelli, L. (1979). Effect of fatigue on flying performance. Unpublished doctoral thesis, Catholic University of America, St. Louis, Missouri.
11. Ray, W.J. & Cole, H.W. (1985). EEG alpha activity reflects attentional demands, and beta activity reflects emotional and cognitive processes. Science, 228, 750-752.
12. Simonson, E. (1971). Physiology of Work Capacity and Fatigue. Springfield, IL, Charles C. Thomas.

Appendix A.

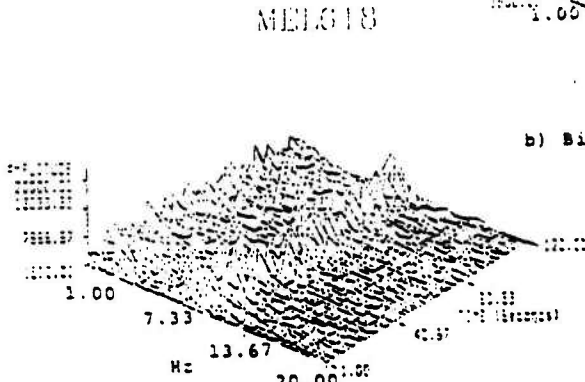
Fig. 2. EEG dominant frequency spectra from Subject #1 during the performance of self-regulatory tasks. Note the presence of 7-13Hz alpha activity in each.



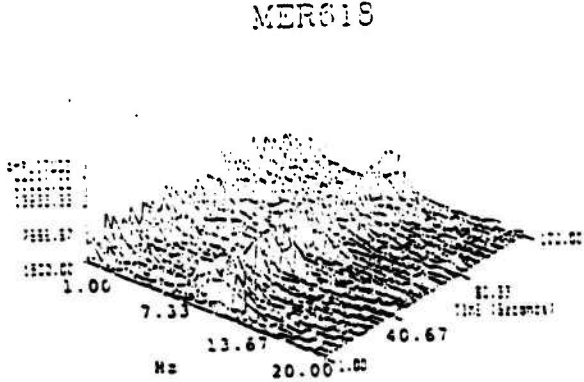
a) Biofeedback slow, left hemisphere.



b) Biofeedback slow, right hemisphere.

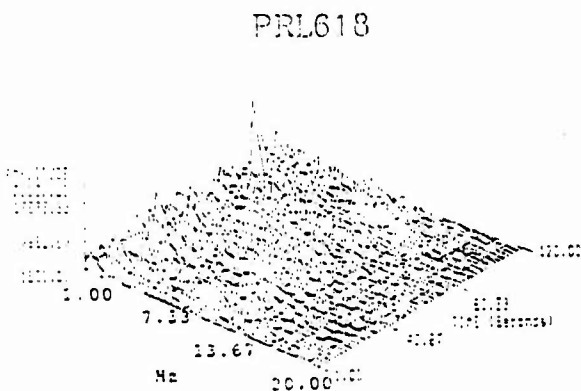


c) Meditation, left hemisphere.

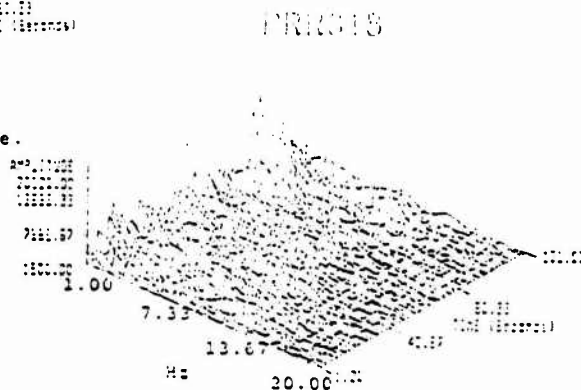


d) Meditation, right hemisphere.

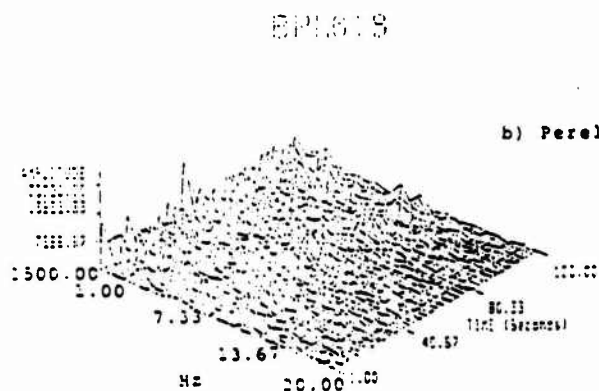
Fig. 3. EEG dominant frequency spectra from Subject #1 during the performance of cognitive tasks. Note that the alpha activity which was previously seen during self-regulatory tasks is no longer present.



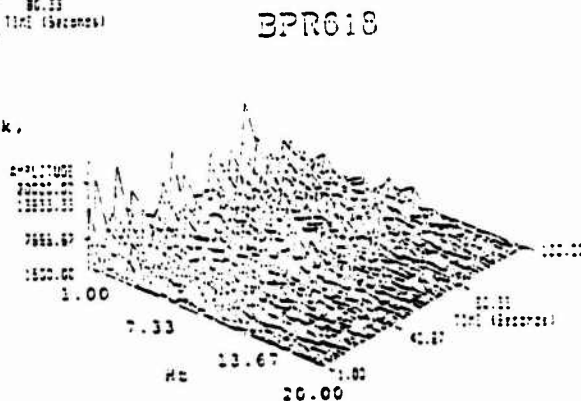
a) Perelli task, left hemisphere.



b) Perelli task, right hemisphere.



c) Biofeedback and Perelli task, left hemisphere.



d) Biofeedback and Perelli task, right hemisphere.

MR. MARK NEUMEIER
FINAL REPORT NUMBER 66
NO REPORT SUBMITTED

1987 USAF-UES SUMMER FACULTY RESEARCH PROGRAM/

GRADUATE STUDENT SUMMER SUPPORT PROGRAM

Sponsored by the
AIR FORCE OFFICE OF SCIENTIFIC RESEARCH

Conducted by the
Universal Energy Systems, Inc.

FINAL REPORT

VAPORIZATION BEHAVIOR OF MULTICOMPONENT FUEL DROPLETS
IN A HOT AIR STREAM

Prepared by: Suresh K. Aggarwal and Khan Nguyen
Academic Rank: Assistant Professor
Department and University: Department of Mechanical Engineering
University of Illinois at Chicago
Research Location: Fuels Division, Aero-Propulsion Laboratory
USAF Researcher: Dr. T.A. Jackson and Dr. M. Roquemore
Date: September 21, 1987
Contract No.: F49620-85-C-0013

REFERENCE DR. AGGARWAL
SFRP FINAL REPORT NUMBER 1

1987 USAF-UES SUMMER FACULTY RESEARCH PROGRAM/
GRADUATE STUDENT SUMMER SUPPORT PROGRAM

Sponsored by the
AIR FORCE OFFICE OF SCIENTIFIC RESEARCH

Conducted by the
Universal Energy Systems, Inc.

FINAL REPORT

Growth Curve and Phototaxis Assays
of Axenic Chlamydomonas reinhardtii 125

Prepared by: Wendy Nguyen
Academic Rank: Graduate Student
Department and Biology Department
University: Trinity University
Research Location: Laser Spectroscopy Clinical Applica-
tions Laboratory
Clinical Sciences Division
School of Aerospace Medicine
Brooks AFB
San Antonio TX 78235
USAF Researchers: Dr. John Taboada
Dr. Rex Moyer
Date: 14 Aug 87
Contract No: F49620-85-C-0013

Growth Curve and Phototaxis Assays
of Axenic Chlamydomonas reinhardtii 125

by
Wendy Nguyen

ABSTRACT

Experimental procedure began with the inoculation of algal cells from a 5-day HSA plate to 5 HS and 5 HSA plates. Two plates, HS and HSA, were sampled every 6-9 hours for 70 hours then at 12 hour interval until 135.5 hours. With each sample, a cell count was done on the ZBI electronic Coulter Counter from which the cells/ml value was calculated. The cells/ml value was then used to construct a growth curve of the C. reinhardtii 125. Percentage motility of the culture was also observed microscopically by the hanging drop technique. The remaining 8 plates of HS and HSA were sampled primarily to determine phototaxis assays on the algal cells for 96 hrs and to observe the effect of the different types of culture medium on phototaxis. Growth Curve of pure C. reinhardtii resembled closely that of the contaminated algae in both HS and HSA media. Experiments showed also that axenic cultures grew better in HSA than HS media. However, phototaxis assays showed that HS grown algal cells were more phototactic than HSA grown cells since after 24 hrs of

ACKNOWLEDGMENTS

I wish to thank the Air Force Systems Command and the Air Force of Scientific Research for the sponsorship of this research. Universal Energy Systems must be mentioned for their help in the directional aspects of this program.

I would especially like to thank three people who made my experience this summer as enjoyable as it was educationally enriching. Many thanks go to Dr. Moyer for providing me with his support, guidance and a truly enjoyable working atmosphere. His concern and help throughout the course of the experiment was greatly appreciated. Working with Dr. Taboada was an enriching experience. His provocative and refreshing ideas about possible future experiments with algae were valuable because they involve experimenting at a physical level an organism that is usually observed from a more biological aspect. I would like also to thank Dr. Bill Schroeder for performing the phototaxis assays on all algal samples. His help on the analysis of the phototactic data played a crucial part toward the completion of this experiment. Finally, my thanks to my mother for accompanying me to the lab in the middle of the night every night during the course of my experiment, her role as my bodyguard made the solitary experimental runs much more bearable.

growth they possessed a higher Δ OD and Δ cells values than those grown in HSA.

I. INTRODUCTION:

Chlamydomonas reinhardtii, a major genera of the Volvocales, is a biflagellated unicellular green algae, 10 - 15 μ m in length and spherical to ovoid in shape. They reproduce vegetatively by cell division and possess a single cup-shaped chloroplast surrounding a single nucleus. An aquatic microorganism, C. reinhardtii has evolved specialized means of regulating its exposure to sunlight by using its flagella and directional light antenna which consists of an eye spot plus associated structures.

C. reinhardtii can be grown on simple defined mineral salts media, either in liquid culture or on agar plates under light. When grown in a liquid medium, the cells retract their flagella before cell division. The protoplast then divides into a number of daughter cells which are released after the enzymatic dissolution of the mother cell wall (Demets et al, 1985). Wild type cells can grow either photoautotrophically, with doubling time of about 5 hours at 25°C when supplied with non-limiting light and CO₂, or heterotrophically in the dark with acetate as a respirable carbon source (doubling time about 15 hours at 25°C). Cell

division of Chlamydomonas can also be readily synchronized with alternating light-dark cycles. Such an experiment was performed by Demets et al. (1985). Chlamydomonas cells can be experimented by standard microbiological techniques.

All photosynthetic organisms have evolved specialized means of regulating their exposure to sunlight. One form this adaptation has taken among the flagellated algae is their phototactic response; the ability to swim toward or away from the source of light. Phototactic algae find the direction or source of light by scanning their environment with an antenna sensitive to light. The light stimulates the antenna of the algae to transmit information to its response mechanism -- the flagella, allowing it to track the light. More data on both the growth and phototactic ability of C. reinhardtii are necessary to fully define and characterize these algae before Phase III of this research program can begin. Phase III involves the testing of drugs for their effect upon phototaxis.

The primary research goal of my UES Summer Graduate Student Research Fellowship this past summer was to conduct a growth curve experiment on axenic cell of Chlamydomonas reinhardtii. The growth curve was compared to a previous growth curve performed on contaminated cultures of C. reinhardtii treated with various concentrations of the antibiotic, gentamycin. My knowledge in the model ZBI

electronic Coulter Counter for cell counts contributed primarily to my assignment of this project.

II. OBJECTIVES OF THE RESEARCH EFFORT:

As a participant in the Summer Graduate Student Research Program working with Dr. Rex Moyer and Dr. John Taboada, my assignment in the algae project was to construct a growth curve and obtain phototaxis assays on pure C. reinhardtii 125. The growth curve of the pure strain 125 was then compared to that of strain 125 contaminated with bacteria. The growth curve experiments on the contaminated algal culture was conducted by Trinity student Dagmar Fertl in Spring, 1987.

III. MATERIALS AND METHODS:

a. Procedures.

C. reinhardtii strain cc-125 was obtained from Dr. Elizabeth Harris, Chlamydomonas Genetics Center, Duke University, Durham, N.C. Experimental procedure began with the inoculation of algal cells from a 5-day HSA plate, incubated at 23°C under light, to 5 HS and HSA plates. 0.5 ml of algal cells was initially harvested from the 5-day

plate and added to 10 separate tubes. Each tube contained 4.5 ml of the following media: 5 tubes of HS and 5 HSA plates. The resulting inocula were mixed gently and then poured onto the appropriate plates. The cultures were incubated at 23°C in a constant light environment. Out of 10 plates, cells from 2 plates, labelled as HS-0 and HSA-0, were removed for a cell count and motility check every 6-9 hours for 70 hours then at 12 hour interval for 135.5 hours. Cells from the remaining 4 HS and 4 HSA plates were harvested for cell counts and phototaxis assays every 24 hours for 4 days. For each motility test, 10 μ l of cells was removed from each culture. The relative percentage of motile cells was determined by the hanging drop microscopy. Finally, to compensate for the liquid loss due to frequent sampling and evaporation, the liquid media of each culture were replaced periodically.

All algal cell counts were done electronically with a model ZBI Coulter Counter in Dr. Moyer's laboratory at Trinity University. Originally 100 μ l of a sample was aseptically removed from the liquid portion of the culture. Then the amount of the sample removed during the course of the experiment decreased to 50 μ l, 25 μ l and 20 μ l in response to the increasing number of cells. The sample was added to 20 ml of Isoton and mixed by gentle inversion. Three counts were taken on the Coulter Counter and then averaged. The averaged count was then used to calculate the

total number of cells/ml of the sample. In addition, each cell count included the identification of the peak channel and the number of cells at each peak. The Coulter channelyzer was also used to generate a cell count for every 5 channels up to 50 channels then per 10 channels up to 99. Fig. 1 illustrates the treatment of the data for each cell count. Finally, a graph of the cell size distribution for each sample was generated from the Coulter Graph Recorder after each cell count. Fig. 4 and 5 show these curves taken during various times in culture for both HS and HSA grown cells.

b. Phototaxis Assay

In addition to the cell count, phototaxis assays were also taken on the HS and HSA cultures every 24 hour. The phototaxis assays included the identification of the Gilford OD of the culture at 500nm, along with the calculation of the ΔOD and of the Δ cells values for each sample. All phototaxis assays were taken on the Gilford Response Recording Spectrophotometer at Trinity University by Dr. Bill Schroeder. Table 3 shows the phototaxis data gathered on both HS and HSA cultures every 24 hours for 96 hours; fig. 6 is an example of time scan curve of an HS culture taken after 24 hours

In a phototaxis assay, the ΔOD was calculated by subtracting the value of the OD_{min} at 500nm from the OD_{max} oc-

Figure 1. Treatment of Data

Cells in HSA-0 were sampled at 0.00 hrs immediately following inoculation of the plate.

HSA-0-1 (0.00 hrs, 100 1/20 ml Isoton, 7/21/87)
 ZBI = 30,369 30,444 32,887 Average = 31,233
 C = 28,296 28,414 31,717

Look on coincidence correction chart. Corrected number is 33,700. Then multiply by dilution factor to calculate the cell/ml of sample.

33,700 cells/0.5 ml of Isoton
* 2
 67,400 cells/ml of Isoton
* 20 ml of Isoton
 1.35*10⁶ cells/0.1 ml
* 10
 1.35*10⁷ cells/ml of sample

2 * 20 * 10 = 400 --> dilution factor
 Dilution factors for 50 1, 25 1 and 20 1 are 800, 1600 and 2000 respectively.

Channel of Peak: 30
 Cell Count at Peak: 516

<u>Channels</u>	<u>Readings</u>
0-5	5,059
6-10	699
11-15	799
16-20	1,110
21-25	2,226
26-30	2,399
31-35	2,450
36-40	2,242
41-45	2,068
46-50	1,937
51-60	3,081
61-70	2,511
71-80	1,942
81-90	1,586
91-99	1,028

Take the percentage of cells in the channels 0-5 which is:
 5,059 / 31,717 * 100 = 16%
 Subtract 16% from 100%, equals 84% of cells w/out subcellular debris.
 Multiply cell count of 1.35 * 10⁷ by 84% to get 1.13 * 10⁷, the # of cells w/out counting the debris in the channels 0-5.

curing at the peak of the curve. The Δ cells value was defined as the total number of cells swimming into or out of the photo-stimulating light. It was calculated as followed:

$$\begin{aligned} \text{cells} &= (\text{cells/beam} * \Delta \text{OD}) / \text{OD} \\ \text{cells/beam} &= \text{cells/ml} * 0.21 \text{cm}^3 \\ &\quad \text{where } 0.21 \text{cm}^3 = \text{volume of the beam} \\ \text{cells} &= (\text{cells/ml} * 0.21 * \Delta \text{OD}) / \text{OD} \end{aligned}$$

IV. Results and Discussion

a. Growth Curve Comparisons

Fig.2 illustrated the growth curve of C. reinhardtii in cultures HS-0 and HSA-0 as they were sampled over 135.5 hours. Tables 1-3 record the principle features of the growth curves of the cultures. The shape of the axenic HS-0 and HSA-0 curves resembled those of the contaminated cultures. Both noncontaminated HS-0 and HSA-0 growth curves matched closely with the contaminated HS-0 and HSA-0 curves in which no gentamycin was added. The maximum cell numbers of both cultures peaked at approximately the same time with the axenic HS-0 at 94.25 hours and contaminated HS-0 at 90.0 hours. Similarly, the maximum cell numbers of the contaminated HSA culture peaked at 40.7 hours as compared to that of the axenic HSA-0 culture which peaked at 36.75 hours. The longer growth period of pure algal cultures before they reached maximum cell number was due to the presence of the lag phase in these growth curves. Since an

older inoculum (5-day) was used in the experiment, the cultures had to go through the lag phase thus requiring more time to prepare for cell division during the log phase.

Experiments with both contaminated and noncontaminated cultures showed that HSA cultures reached the maximum cell numbers in a shorter growth period than HS cultures. This observation indicated that algal cells whether contaminated or pure grew better in HSA than HS media. In addition, the shorter generation of HSA cultures showed that the cells grown in this media doubled at a faster rate than those grown in HS media. Finally, it was observed that the log phase of axenic HS algal culture (79.25 hours) was longer than that of the contaminated HS culture (55 hours); but, the log phase of the axenic HSA culture (24 hours) was shorter than that of the contaminated culture (39.20 hours).

Cell Size Distribution Curves

Fig.4 and 5 showed tracings of the cell size distribution curves of HS-0 and HSA-0 cultures as they were sampled over 135.5 hours. These curves showed that in both samples as the time in culture increased so did the width of the curves and the peak channel of each sample. In culture HS-0, the peak channel of the samples increased from 13 at 0.00 hours to 39 at 135.5 hours. Similarly, HSA culture showed an even greater increase in the peak channels than HS culture, from 30 at 0.00 hours to 87 at 135.5 hours.

The width of the peak channel generally represented the heterogeneity of the cell size distribution of each sample. The increasing channel peak of the curves showed that although the cell size was initially small (1x) after inoculation they became gradually bigger (2x) as they prepared to divide over a period of time. The cell count in the peaks increased as the time in culture increased because of the increasing number of dividing 4x cells which had settled at the bottom of the culture while preparing to divide. This pattern of cell size distribution curve also occurred in the contaminated culture.

Motility

Table 1 lists the relative motility of the cells over the 135.5 hours of culture. As the cell number in the culture gradually increased, the relative percentage of motility of all cultures both in HS and HSA media decreased to 0. Both HS-0 and HSA-0 cultures initially showed approximately a 60% motility in which the cells moved rapidly in a circular pattern. It was observed that at approximately every 12 hour interval the HS and HSA cell motility percentage either increased or decreased. This periodically alternate motility percentage value was dependent on the amount of cells that became static as they lose their flagella in preparation for cell division. After 40 hours of growth, HSA-0 cells became sluggish in movement due

to their rapid cell division which resulted in the dense area of growth observed in the hanging drop sample of the culture. Cell clumping of HSA cells also appeared to inhibit cell movement. In contrast, HS-0 cells at this time continued to move energetically and no clumping of cells was observed. The absence of acetate in this media seemed to inhibit the rapid cell division seen in HSA media thus allowing for more rapid cell movement and no cell clumping.

b. Phototaxis

Analysis of the phototaxis assays of HS and HSA cultures showed that HS algal cells were more phototactic than HSA algal cells although cells in both culture exhibited a high phototactic response. Table 3 showed that the OD of HS culture over the 96 hour growth period peaked earlier and possessed a higher value Δ OD after 24 hours than HSA cells. Furthermore, when HS cells were sampled after 24 hours of growth, the Δ cells of HS was the greatest value obtained during the entire run of this experiment. Thus, the experiment indicated that even though algal cells grew better in HSA they were not as phototactic as HS cells.

Phototaxis, according to Stavis and Hirschberg, varies with the age of the culture and is maximum during balanced growth. Since the HS algal cells were more phototactic than HSA cells, the HS media most probably contained nutrients that provide the algae with a medium in which they could

have a balanced growth thus enhancing their phototaxis. The phototaxis values of algal cells were observed to have decreased as the cultures grew older. Also, similar to Stavis and Hirschberg's experiment, the phototaxis values of the cells in HS and HSA media were very high during rapid growth period and decreased gradually as growth slowed. The experiment showed that the ΔOD and Δ cells value of both HS and HSA cells peaked after 24-48 hour of rapid growth and then gradually decreased after 48 hours.

Table 1. Algal Cell Counts and Cell Size Distribution of *C. reinhardtii* 125 at Various Times During the Growth Period.

HS-0

<u>Time in Culture (Hours)</u>	<u>Cell/ml * 10⁷</u>	<u>Cell/ml - Debris * 10⁷</u>	<u>Channel of Peak</u>	<u>Number of Cells in Peak</u>	<u>Relative Motility (%)</u>
0.00	1.51	1.40	13	1,311	60
9.25	1.70	1.51	25	245	--
15.00	1.65	1.53	23	537	60
22.50	1.86	1.73	17	449	70
32.25	2.85	2.65	25	293	--
40.00	2.74	2.52	17	396	30
46.50	5.16	4.90	15	727	50
56.75	3.94	3.70	21 & 23	425	80
64.50	3.30	3.10	22	348	50
70.00	4.80	4.51	23	471	60
82.00	5.40	5.08	27	484	30
94.25	7.52	7.22	21	785	5
105.75	5.68	5.57	27	407	10
119.00	5.40	5.08	26	364	5
135.50	4.80	4.18	39	258	0

HSA-0

<u>Time in Culture (Hours)</u>	<u>Cell/ml * 10⁷</u>	<u>Cell/ml - Debris * 10⁷</u>	<u>Channel of Peak</u>	<u>Number of Cells in Peak</u>	<u>Relative Motility (%)</u>
0.00	1.35	1.13	30	516	60
9.25	0.833	0.725	25	110	--
15.00	0.904	0.777	32	155	60
22.50	1.91	1.78	31	433	90
32.25	4.26	4.05	31	519	--
40.00	7.08	6.80	29	726	40
46.50	5.8	5.51	27	622	50
56.75	10.8	10.40	19	957	50
64.50	8.18	7.77	29	686	80
70.00	8.04	7.40	31	647	10
82.00	10.6	9.86	25	728	30
94.25	9.54	8.68	35	597	5
105.75	9.32	8.67	44	548	30
119.00	9.02	8.39	47	501	0
135.50	8.76	7.62	87	460	0

Table 2. Characteristics of Chlamydomonas reinhardtii Growth

<u>Culture</u>	<u>Max. # of cells/ml * 10⁷</u>	<u>Time in Culture (Hrs)</u>	<u>Log Phase (Hrs)</u>	<u>Generation Time (Hrs)</u>
HS-0	7.22	94.25	15.0-94.25	34.25
HSA-0	10.4	56.75	22.5-46.5	12.00
HS-3	3.29	72.00	48.0-72.0	24.0
HSA-3	4.70	72.00	24.0-72.0	24.0

Table 3. Phototaxis Assays of Noncontaminated C. reinhardtii 125 at every 24-hr during the 4 day Growth Period

HS

<u>Time in Culture (Hrs)</u>	<u>cells/ml * 10⁷</u>	<u>ΔOD₆₈₀</u>	<u>Gil OD₆₈₀</u>	<u>Δcells * 10⁶</u>
24	1.81	+0.6660	1.030	1.18
48	1.98	+0.5590	1.0045	0.580
78	3.58	+0.2810	0.8536	0.550
96	2.90	+0.1981	0.9653	0.312

HSA

<u>Time in Culture (Hrs)</u>	<u>cells/ml * 10⁷</u>	<u>ΔOD₆₈₀</u>	<u>Gil OD₆₈₀</u>	<u>Δcells * 10⁶</u>
24	1.97	+0.6181	1.004	0.8481
48	3.67	+0.7199	0.9540	0.963
78	5.05	+0.4348	0.7628	0.637
96	4.49	+0.3234	0.9790	0.519

Fig. 2. Growth Curve of Pure Greenhardia 125 in Simplus
 HS-O and HSA-O

Time in culture (Hrs.) vs. Cells/ml $\times 10^7$

Cells/ml $\times 10^7$

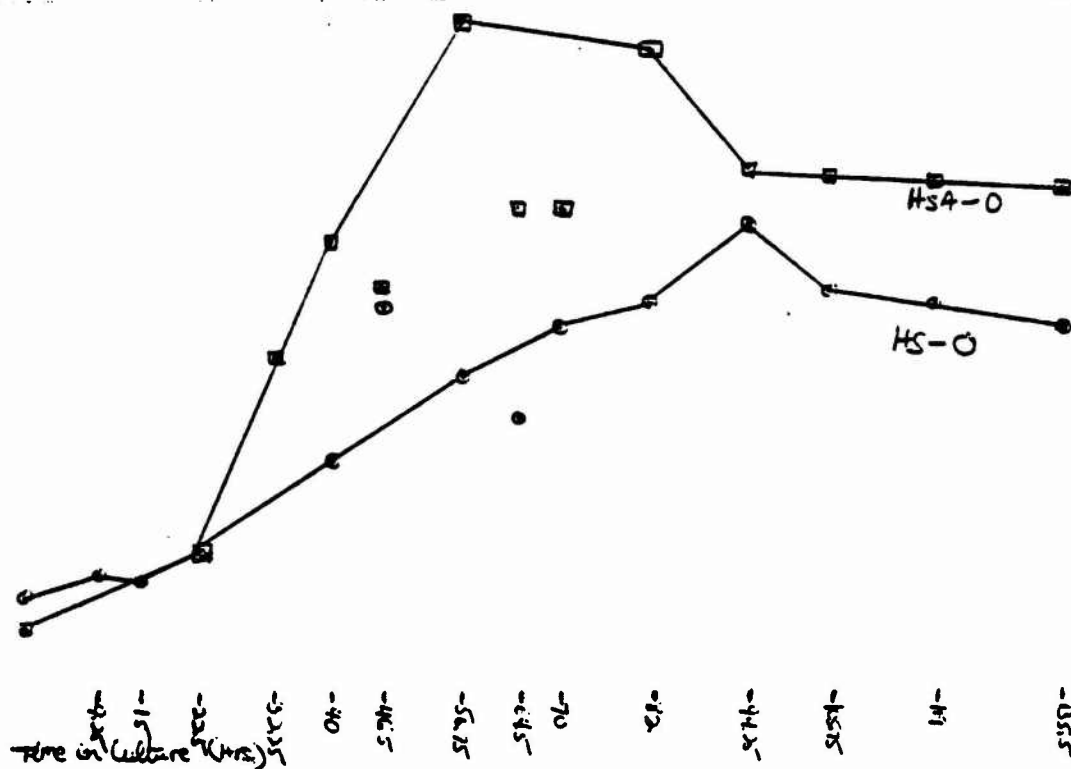


Fig. 4. Cell size Distribution Curve of *C. reinhardtii* in MS-0

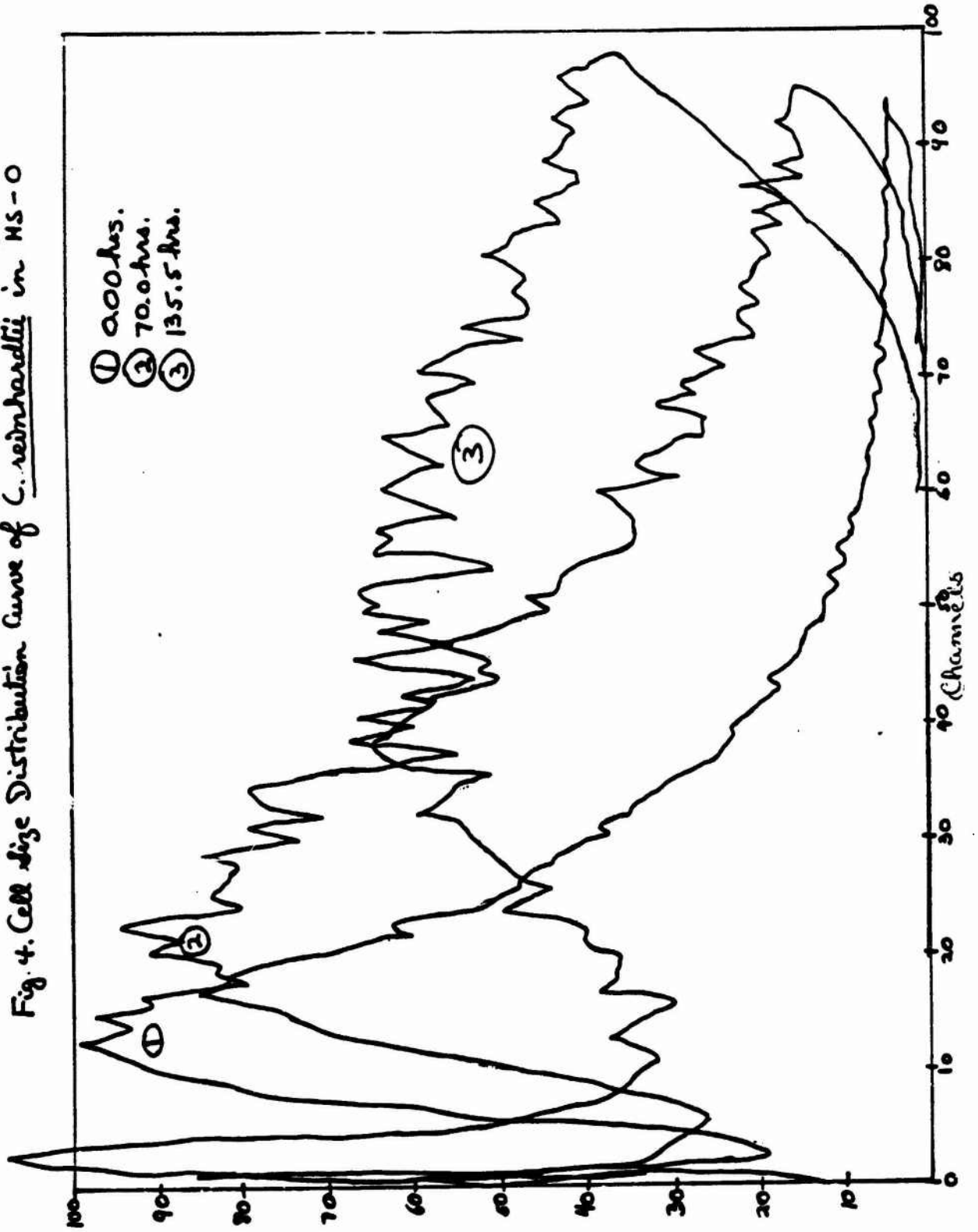


Fig. 5. Cell Size Distribution Curve of *C. reinhardtii* in HSA-O

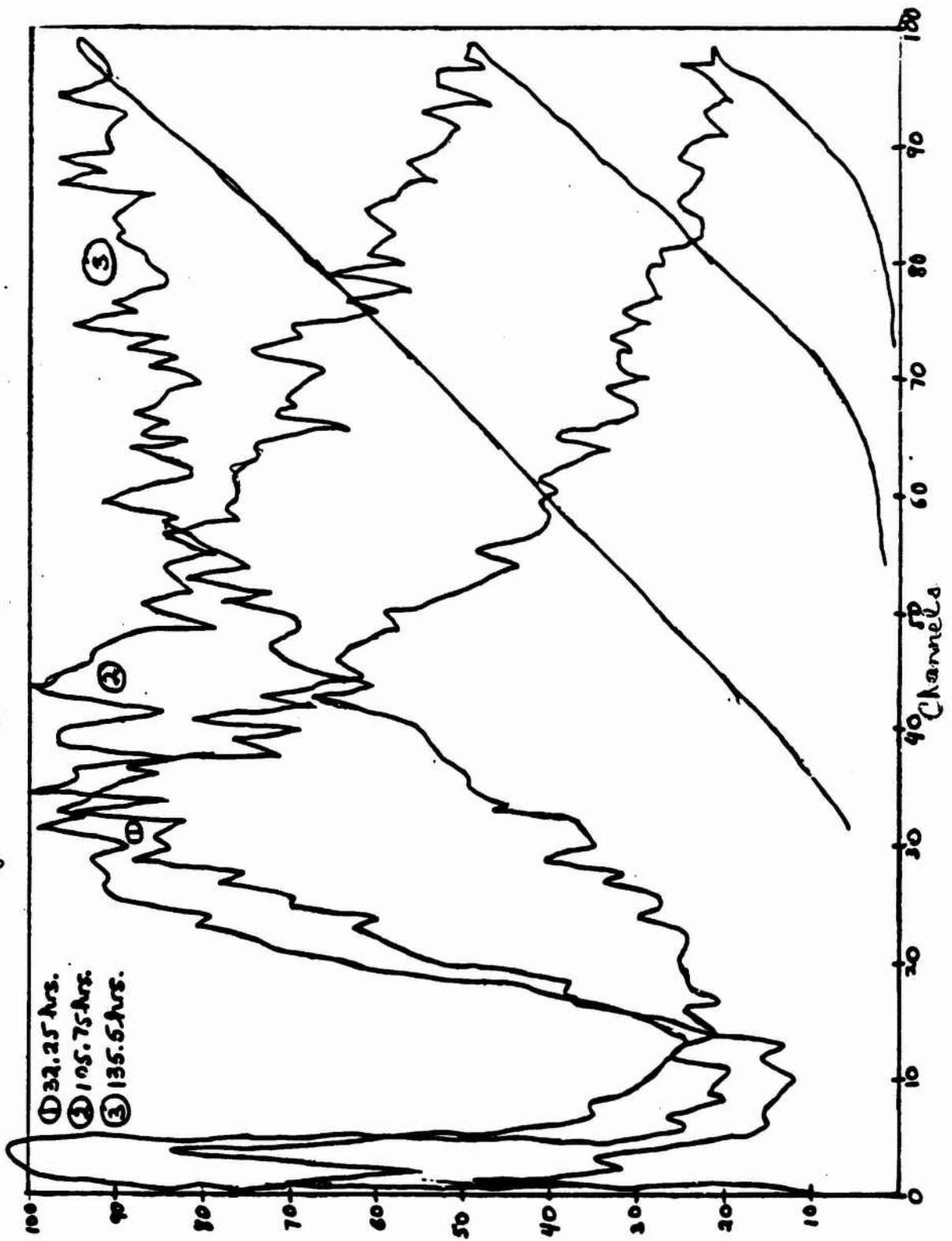
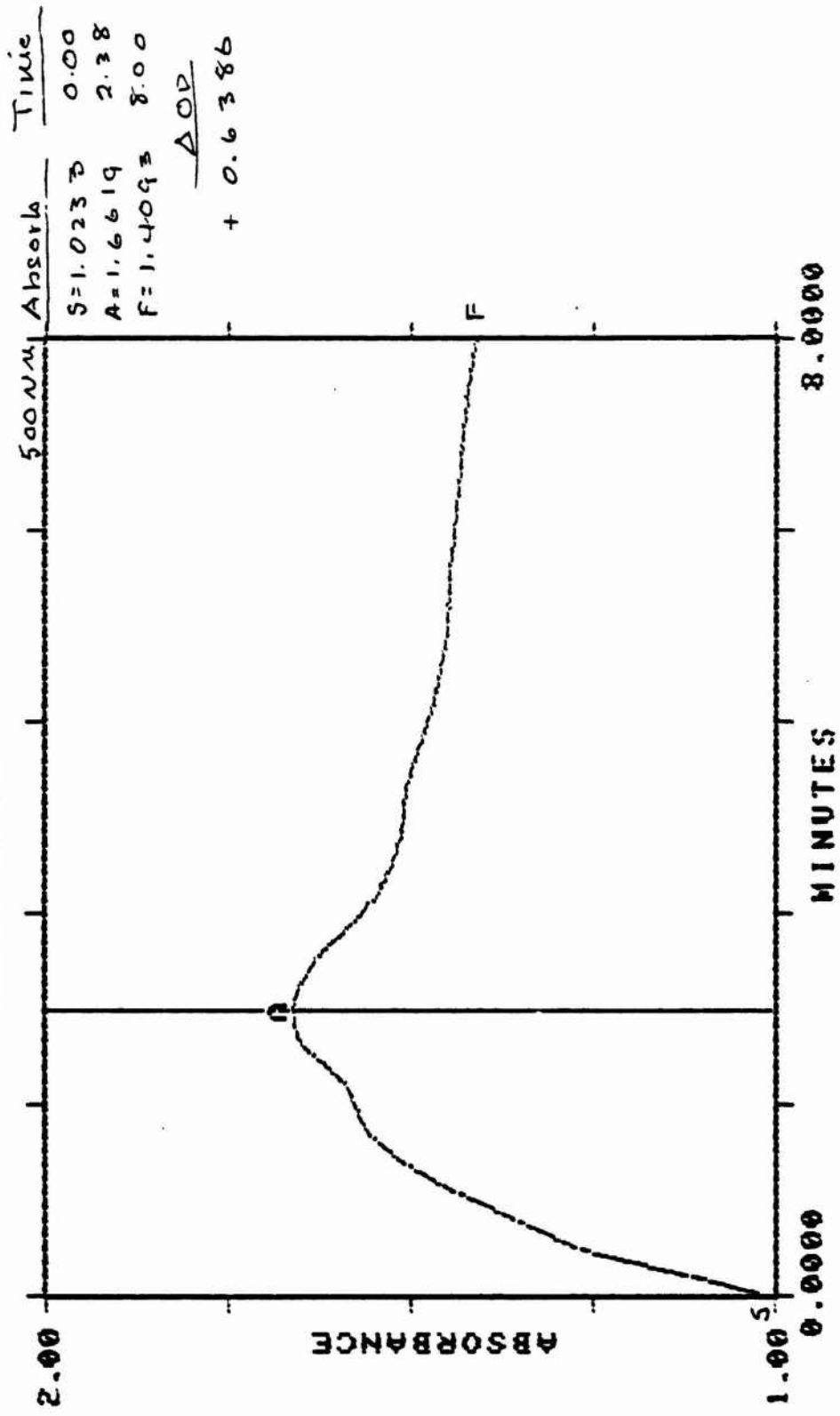


Fig. 6 - Time Scan Curve of HS at 24 Hrs.
 TIME SCAN IN LIGHT
 HS REF

ANALYSIS = 1741(1250)

SAMPLE = Adc MSP



RECOMMENDATIONS

To further study the characteristics of C. reinhardtii, other experiments on algal growth are being considered. These projects involved the application of a circadian light-dark regime and/or plant hormones on the algae to test those effects on their growth.

Chlamydomonas is a microorganism that undergoes both mitotic and meiotic division to develop into phototactic gametes. Since both of these growth processes involves multiple steps in which the cells expressed different phenotypes, it is desirable to have all cells being tested to be in the same stage of development. One means of synchronizing the growth of Chlamydomonas is to apply a circadian light-dark regime to a culture of algal cells. Demets, et al. observed that when C. eugametos was grown under a regime of 16 hr light/ 8 hr dark, in a static culture only, the cell number doubled daily during the exponential phase of growth. Thus, similar experiments can be performed by observing the cell division of algae when they are being synchronized under a circadian regime in both static and shaken cultures.

In addition to studying algal growth in a circadian rhythm, growth can also be observed by testing various plant hormones on algal cells. Initial experiments have begun in which a few plant hormones such as giberellic acid, indole-

3-acetic acid, kinetin, etc. were added to a plate of algal cells. Results showed that certain plant hormones at a specific concentration did inhibit or enhance algal growth. Since very few effort of research have been made in this area, the possibilities for experimental research in plant hormones and algal cells are infinite.

REFERENCES

- Demets, R., Tomson, A. M., Ran, E. T., Sigon, C. A. M. et al., "Synchronization of the cell Division Cycle of Chlamydomonas eugametos," Journal of General Microbiology, vol.131, 1985, pp. 2919 - 2924.
- Nultsch, Wilhelm, Throm, Gunter, "Effect of External Factors on Phototaxis of Chlamydomonas reinhardtii: Light," Archives of Microbiology, vol. 133, 1975, pp. 175-179.
- Stavis, Robert L., Hirschberg, Rona, "Phototaxis in Chlamydomonas reinhardtii," The Journal of Cell Biology, vol. 59, 1973, pp.367-377.

1987 USAF-UES SUMMER FACULTY RESEARCH PROGRAM/
GRADUATE STUDENT SUMMER SUPPORT PROGRAM

Sponsored by the
AIR FORCE OFFICE OF SCIENTIFIC RESEARCH

Conducted by the
Universal Energy Systems, Inc.

FINAL REPORT

MICROESOTROPIA PATIENTS PERFORM WELL AS MILITARY JET PILOTS

Prepared by: Bernadette P. T. Njoku
Academic Rank: Junior(3rd year)
Department and University: School of Medicine
Meharry Medical College
Research Location: Aerospace Vision Laboratory
Ophthalmology Branch
Clinical Sciences Division
School of Aerospace Medicine
Brooks AFB, Texas
USAF Researcher: Maj. Lawrence Tychsen
Date: September 12, 1987
Contract No: F49620-85-C-0013

MICROESOTROPIA PATIENTS PERFORM WELL AS MILITARY JET PILOTS

by

Bernadette P. T. Njoku

ABSTRACT

A computer listing of all patients examined at Brooks AFB with the diagnosis of microesotropia (sometimes referred to as microstrabismus, monofixation syndrome) is obtained. Key terms, especially used to determine patients not clearly defined as microesotropics include: a) failed depth perception, b) anisometropia, c) esotropia/esophoria, d) strabismus, e) microexotropia, f) hyperopia/hypermotropia, g) suppression/amblyopia, h) monofixation syndrome, i) diplopia (not monocular), j) heterotropia/strabismus and k) failed red lens test. (Not until 1980 were the physicians at Brooks AFB alerted to keep specific records of microesotropia patients.) The patients' charts, mainly pilots and navigators, are studied and specific information is gathered, then transferred to individual 'microstrabismus data sheets'. From this, six straightforward graphs are constructed: 1) Refraction Spherical Equivalent vs Patient #, 2) Refraction Cylinder Astigmatism vs Patient #, 3) Verhoeff (no. passed/8) vs Patient #, 4) Howard-Dolman vs Patient #, 5) Alignment vs Patient # and 6) Stereo Arc Sec vs Patient #. These data and graphs allow primarily for at-a-glance obtaining of quantitated information and comparisons from patient to patient; and thus, subsequent in-depth judgement and theories to be made by Maj. Dr. L. Tyghsen and Col. Dr. Thomas Trodici.

Acknowledgements

Universal Energy Systems, Inc. deserves all the credit for granting me my first experience in research(Summer 1986) and for having me return the following summer. As a novice, I have obtained invaluable skills in aspects ranging from basic to complex paperwork necessary just to initiate research, then the actual workings of a project, to the final conclusions, theories and projections(publications, continuations, etc.).

The hospitality of every staff member with whom I came in contact for the past two summers at Brooks AFB has made my experience most rewarding. I would like to thank the whole Ophthalmology Department for their support, encouragement, and most of all personal concern: Col. Tredici, Col. Dennis, Lt. Col. Miller, Maj. Tychsen, Maj. Carlsen, Maj. Woessner, Dr. Brice Hartman, Dr. Wolfe, Dr. Taboada, Dr. Yates, Dr. Peters, Mrs. Frances Williams, Ms. Donna Norton, Ms. Olivia Lewis-Thomas, the Clinical Records staff, and others I should mention(but there are so many). I especially thank Dr. Tychsen for his enthusiasm and desire to make headway with this project, Col. Tredici for providing the initial proposal and study at Brooks AFB, and both their ability in helping me understand the necessity of this project.

I. Introduction

As a medical student, I have been and will be introduced to many clinical conditions indirectly, through reading material, and directly, through patient contact. The field of ophthalmology is one which has proven to be interesting and progressive, especially noting the constant, innovative research developed at Brooks AFB. Since last year's assignment of collecting and compiling data on central serous retinopathy patients, I have realized that there are many other eye pathologies beyond my scope of knowledge. For this reason, returning this past summer further enhanced my education, particularly in the area of microstrabismus. By posing as a subject, I was also introduced to other eye diseases through projects lead by various other physicians and technicians.

The Department of Ophthalmology at Brooks AFB is concerned chiefly with eye pathologies and the resulting effects on flying personnel. Since with microstrabismus where the misalignment of the eye(s) is cosmetically inapparent, it is necessary to determine whether this condition affects flying status, or whether these patients acquire some sort of accommodation such that flying ability is adequate.

II. Objectives of the Research Effort

"Microstrabismus is a cosmetically inapparent misalignment of the eyes causing mildly defective perception of depth using binocular cues (stereopsis). The cause of the condition is unknown, but available data suggest a developmental abnormality of the visual cortex."⁵ Previously, a study was accomplished by Epstein and Tredici (1973) consisting of approximately 10-15 chart reviews of Air Force flyers. After the diagnosis of microstrabismus, these patients were seen "in close follow-up in order to assess the stability of their condition."^{2,4} As done with the previous study, I was to obtain a computer list of all cases seen at USAFSAM (199 patients are used for this study) and compile data -- specific test values used in making the diagnosis. By completing this, we should have at hand information concerning:

1. standard demographic data
2. ophthalmic performance: visual acuity best corrected, cycloplegic refraction, stereopsis, alignment, funduscopy, diagnosis and other eye abnormalities, and
3. flying performance: waiver recommended? waiver granted?

III.

Microesotropia, or microstrabismus, is a condition of unknown etiology in which patients have straight, or almost straight (cosmetically inapparent), eyes. Common clinical features include:^{1,3,5}

1. Amblyopia -- Monocularly measured, patients show reduced visual acuity not correctable by refractive means, and not attributable to obvious structural or pathological ocular anomalies. "There is a history of hyperopia and/or anisometropia, requiring correction with spectacles during pre-school years."⁵

2. Defective stereopsis -- The majority of patients have gross stereopsis, with exception of patients with congenital esotropia.

3. Inability to bifixate, or monofixation -- In monofixation, one eye fixates and there is a small tropia of the other eye with suppression of its fovea. The inability to bifixate is based on a scotoma (an area of depressed vision within the visual field, surrounded by an area of less depressed or of normal vision) in the visual field of the non-fixating eye during binocular vision.

4. Suppression -- Suppression is seen in the fovea of the deviating eye. An absolute macular scotoma is present under binocular viewing and disappears with monocular viewing. According to Jampolsky, suppression explains the solving of the diplopia caused by the minimal deviation.

5. Anisometropia -- These patients show different refractive error in each eye which produces the effect of having one eye out of focus and images of different size in each eye. If the error is great, either alternating vision or monocular preference occurs.

Specific clinical tests for microesotropia consist of tests for stereopsis, or depth perception, and tests for alignment. Stereopsis tests include the VTA-ND, Howard-Dolman and A/O Vectograph, which examine at distance, the Verhoeff and Titmus, which examine at near, the Red Lens, Bagolini, and Worth 4 Dot. These tests quantitate stereopsis in values ranging from 15 - 3000 arc seconds. Alignment tests include the Single and Alternate Cover Tests and the Four Diopter Base-Out. These tests measure phorias, tendencies of the visual axis of one eye to deviate when the other eye is covered and fusion is prevented(definition), and tropias, deviations of the visual axis of one eye when the other eye is fixing(definition). A small tropia of up to 6 - 8 diopters is expected.

Surgical, or motor, treatment is usually not necessary, except in rare cases with horizontal deviation greater than or equal to 20 diopters. The primary objective is to teach the patient to bifixate instead of monofixate, or rather, to become aware simultaneously of similar images on each macula.¹

The major goal of this aspect of the microstrabismus study is to record patient data in hopes of finding valid similarities and differences to make comparisons and thus create further hypotheses and theories attributable to the disease. So far, we have one of the largest, if not the largest, patient logs since the discovery of microstrabismus(199 patients). Also of chief concern is the flying performance of these pilot-patients. Formerly, all trained pilots seen at USAFSAH were granted a waiver to continue flying. Undergraduate pilot trainees were denied waiver, and were instead trained as navigators.⁵

At the conclusion, six graphs are constructed which allow for at-a-glance obtaining of quantitated information and comparisons from patient to patient, right eye to left eye. These are:

- 1) Refraction Spherical Equivalent vs Patient #
- 2) Refraction Cylinder Astigmatism vs Patient #
- 3) Verhoeff(no. passes/8) vs Patient #
- 4) Howard-Dolman vs Patient #
- 5) Alignment vs Patient #, and
- 6) Stereo Arc Sec(lowest value) vs Patient #.

IV. Recommendations

Future work will be completed by Dr. L. Tychsen. My function was to serve as a data collector, and perhaps provide suggestions. As stated in the protocol, lack of objective evidence that fine stereopsis is a critical factor in flying performance is a question of concern. Also, follow-up would make an interesting study, that is, a comparison of stereopsis and alignment from past to present per patient per examination. Much more work is proposed for the microstrabismus study. Through the enthusiasm of Dr. Tychsen and the background and aid of Col. Tredici, this will be a well-accomplished, innovative research endeavor.

REFERENCES

Duane, Thomas D. Clinical Ophthalmology, "Monofixation Syndrome," Ch. 14.

Epstein, David L. and Tredici, Thomas J., "Microtropia (Monofixation Syndrome) in Flying Personnell." American Journal of Ophthalmology, November, 1973, Vol. 76, pp. 832-841.

Harley, Robison D. Pediatric Ophthalmology, Chs. 5-7, 23.

Tredici, Lucia, O'Connor, Patrick and Tredici, Thomas J., "Natural History of Monofixation Syndrome," p. 15.

Tychsen, Lawrence, "Microstrabismus Study Group Protocol."

1987 USAF-UES SUMMER FACULTY RESEARCH PROGRAM/

GRADUATE STUDENT SUMMER SUPPORT PROGRAM

Sponsored by the

AIR FORCE OFFICE OF SCIENTIFIC RESEARCH

Conducted by the

Universal Energy Systems, Inc.

FINAL REPORT

DETERMINATION OF LUMPED-MASS THERMAL PROPERTIES ASSOCIATED

WITH AUTOCLAVE CURING OF GRAPHITE/EPOXY COMPOSITES

Prepared by: Charles W. Norfleet
Academic Rank: Bachelor of Science
Department and: Civil Engineering and Mechanics
University: Southern Illinois University at Carbondale
Research Location: AFWAL/MLBC
Wright-Patterson AFB, OH 45433
USAF Researcher: Frances L. Abrams
Date: 18 September 1987
Contract No: F49620-85-C-0013

Determination of Lumped-Mass Thermal Properties Associated
With Autoclave Curing of Graphite/Epoxy Composites

by

Charles W. Norfleet

ABSTRACT

Determination of the parameters affecting the thermal response of a graphite/epoxy composite was performed. A governing equation was developed for the process based on lumped-mass heat transfer principles. Numerical values of the thermal properties included in the energy balance equation were determined by a Newton-Raphson root solving method. The results of this method indicated that the bagging material surrounding the laminate during the cure process had significant thermal mass which created a slow response during the initial heating of the laminate. This observation led to the development of energy balance equations for both the bagging material and the laminate.

Acknowledgments

I wish to acknowledge the Air Force Systems Command and the Air Force Office of Scientific Research for sponsorship of this research. Further acknowledgments go to Universal Energy Systems for their administrative assistance and for providing the opportunity for me to participate in the Graduate Student Summer Support Program.

My experience at the Materials Laboratory was very rewarding and made a tremendous influence on my thesis research. In singling out those individuals to whom special attention is noteworthy, the first should be my graduate advisor, Dr. Bruce DeVantier, for his constant guidance and allowing me to accompany him to take part in this program. I also wish to thank Bill Lee for lending his modeling expertise in helping me with my research. Additional thanks goes to Frances Abrams for her insights and encouragement, not to mention providing shelter and guard dogs, to make this summer a truly unforgettable experience.

I. INTRODUCTION

Graphite/epoxy composite materials have traditionally been cured by imposing a conservative autoclave heating schedule as suggested by the manufacturer of the prepreg material from which the laminate is composed (1). Recent advances in micro-computer technology and software has enabled the in-situ monitoring and control of the process parameters and cure conditions associated with the fabrication of composite materials, thus being able to save considerable time in this aspect of constructing materials made from graphite/epoxy laminates.

The Structural Materials Branch of the Non-Metallic Materials Division at Wright-Patterson Air Force Base has developed expert systems software capable of controlling and optimizing the curing process of graphite/epoxy composites (2,3). The expert systems software monitors the temperatures of the top and middle of the laminate as well as the autoclave air temperature. The air pressure in the autoclave and viscosity of the epoxy are also measured to more fully recognize the process state of the cure cycle. The software contains a knowledge base consisting of rules which have been established through experimentation and analysis of the curing process. These rules use the sensor data to monitor the progress of the curing laminate. Commands are then sent to the autoclave controller to maintain a successful cure by varying the temperature and pressure of the autoclave.

In order to continue to refine and improve on the knowledge base without the expense and time consumption of actual fabrication experiments, computer models which accurately predict the transient conditions of the composite are desired. Use of these models permit repetition of certain cure conditions while varying the knowledge base

pertinent to the process state being studied. Testing the rules in this fashion would allow for a more complete analysis of the effects on the cure of laminates composed of a diverse range of thicknesses, shapes, and prepreg materials.

In addition to preliminary testing of the expert systems software, computer models would also be helpful in predicting and verifying the data being acquired during the cure process. Predicting ahead of the present process state would enable process control based on the past, present and the predicted future cure conditions of the laminate. Verification of the sensor data would permit the expert system to ignore seemingly erroneous sensor data and possibly replace it with data predicted by the model should the sensor fail completely.

Because the expert systems can monitor the cure process without previous information dealing with the thermal characteristics of the laminate and bagging material or about the cure kinetics of the epoxy resin, simultaneous use of computer models would necessitate the ability to extract these properties based on the thermal response of the composite to the initial heating of the laminate. A further requirement would be that the data determined from the model be calculated at least as fast as the sensor data is acquired.

My graduate research in process modeling of composite materials contributed to the development of a computer program which applied the theory of lumped-mass heat transfer to the prediction of the temperature history of a graphite/epoxy composite. The primary assumption in applying this principle is that the temperature gradients through the body are small enough to assume a uniform temperature distribution throughout the body (4). This concept lends itself nicely to modeling

the temperature history of the composite, since a uniform temperature is desired to promote a uniformly cured composite (5). The results of the lumped-mass model proved to be in very good agreement with a one-dimensional model developed by Loos and Springer (6). This simpler model enabled the extraction of the thermal time constant and calculated the transient laminate temperatures quickly. It was this research work and involvement with the lumped-mass model which contributed to my assignment at the Materials Laboratory at Wright-Patterson Air Force Base.

II. OBJECTIVES

In curing graphite/epoxy composites, the cure is an Arrhenius function dependent on the laminate temperature. Therefore to be able to control the cure of the epoxy resin in the laminate means that one must be able to control the temperature of the laminate by altering the autoclave air temperature. The speed of the temperature response of the laminate is due to the thermal characteristics of the laminate and its environment.

My assignment was to determine what factors affected the net response of the laminate temperature. Once these factors were recognized, a lumped-mass heat transfer equation expressing the energy balance of the process was to be established. The coefficients in the equation would represent the thermal masses having a significant effect on the process. The values of these coefficients were to be determined from the sensor data recorded from various fabrication experiments. The correct form of the governing equation would result in constant values of the coefficients during the process when no heat generation from the curing epoxy was occurring.

III. DEVELOPMENT

In developing the lumped-mass energy equation, it was assumed the the conductivity of the bagging material and the heat transfer coefficient of the autoclave air were incorporated into an effective heat transfer coefficient h_{eff} . This resulted in the governing equation

$$mc \frac{dT_L}{dt} = Ah_{eff}(T_A - T_L) + \dot{q} \quad (1)$$

where m is the mass of the composite, c is the specific heat, A is the surface area, T_A is the autoclave air temperature, T_L is the laminate temperature, and \dot{q} is the heat generation rate of the curing epoxy.

During the initial heating and also during the final cooling of the laminate, heat generation by the epoxy was considered to be negligible and its respective term was dropped from equation (1). This permitted an exact solution for the laminate temperature to be determined from the governing equation. In deriving this solution an expression for the autoclave air temperature was assumed to be

$$T_A = T_0 + \beta t \quad (2)$$

where T_0 is the initial autoclave temperature, β is the autoclave temperature rate, and t is the time. This expression implied that the autoclave temperature would follow a linear path through all of the data points in any heating or cooling cycle. Inclusion of equation (2) yielded equation (3) for the exact solution of the laminate temperature history

$$T_L = T_0 + \beta \{ t + \tau [\exp(-t/\tau) - 1] \} \quad (3)$$

where the thermal time constant, τ , was given by

$$\tau = \frac{mc}{Ah_{eff}} \quad (4)$$

Evaluation of the time constant from the sensor data was attempted by two common numerical techniques, a least squares fit and the Newton-Raphson root solving method.

A. Least squares method

The least squares method was employed by reducing the expressions for the first and second derivatives of equation (3) into the form of linear regressions, equations (5) and (6), respectively.

$$\text{Ln} \left(1 - \frac{1}{\beta} \frac{dT_L}{dt} \right) = - \frac{1}{\tau} t \quad (5)$$

$$\text{Ln} \left(\frac{d^2 T_L}{dt^2} \right) = - \frac{1}{\tau} t + \text{Ln} \left(\frac{\beta}{\tau} \right) \quad (6)$$

In both equations the time constant was the negative inverse of the slope of the line generated. Determination of the time constant by the least squares method with respect to equation (5) was deemed unsatisfactory because the autoclave temperature rate was not constant as described in equation (2). Instead, its magnitude decreased slowly over the time intervals used for this method. With regards to using the second derivative in equation (6), this method also produced undesirable results. In this case the fault lie in the method used in the expert systems software for calculating the value of the second derivative. This method permitted an error of the same order of magnitude as the second derivative.

B. Newton-Raphson method

To accommodate for calculation of the time constant by the Newton-Raphson method the expression for the autoclave temperature was modified to assume a piece-wise linear path from one data point to the next,

$$T_{A_i} = T_{A_{i-1}} + \beta_i \Delta t \quad (7)$$

where Δt is the time step between the data points, β_i is the temperature rate for the time interval, and T_{A_i} and $T_{A_{i-1}}$ are the autoclave temperatures at the present and previous data points, respectively. This resulted in an exact solution of the form

$$T_{L_i} = T_{A_i} - \beta_i \tau + (T_{L_{i-1}} - T_{A_{i-1}} + \beta_i \tau) \exp(-t/\tau) \quad (8)$$

This equation allowed the value of the time constant to be calculated at each data collection point. The results from using this method as shown in Figure 1 indicated that the bagging material surrounding the laminate during the curing process had a significant thermal mass. This material acted as an insulating blanket and greatly contributed to the response time of the laminate temperature. This effect was most noticeable during the initial heating of the laminate as shown in Figure 1. However, as the epoxy bled into the bagging material, the insulating effect decreased. This signified that the overall thermal properties of the laminate and bagging material changed during the process due to the mass transport of the epoxy. To account for the thermal characteristics of the bagging material, energy balance equations were written for both

the bagging material and the laminate, equations (9) and (10), respectively.

$$(mc)_B \frac{dT_B}{dt} = hA(T_A - T_B) - U(T_B - T_L) \quad (9)$$

$$(mc)_L \frac{dT_L}{dt} = U(T_B - T_L) + \dot{q} \quad (10)$$

where the subscripts B and L pertain to the properties and temperatures of the bagging and laminate, respectively. The bagging material consisted of the items illustrated in Figure 2. However the bagging material represented in Loos and Springer (5) consisted of only the bleeder plies of which the thermal mass was determined to be negligible.

IV. CONCLUSION

Verification of these equations will continue in the form of a Master's thesis by this investigator. Preliminary studies have indicated that equation (10) could be used to determine the difference between the top and mid laminate temperatures by replacing T_B and T_L with the top and mid laminate temperatures, respectively. The ability to predict the bagging material temperature with equation (9) appears to require additional investigation into the existence of large temperature gradients through the bagging material.

V. RECOMMENDATIONS

Because of the significance the bagging material has on the thermal response of the composite, it is this investigators suggestion that the temperature at the top of the bagging material be monitored along with

the data already being recorded. Although it would not have a direct impact on the detection of exothermic reactions, it would be of considerable help in modeling the process. Specifically, knowing the temperature at this location would permit the estimation of the energy being added into the bagging material by the expression

$$q'' = h (T_A - T_S) \quad (11)$$

where q'' is the heat flux per unit area, h is the convection heat transfer coefficient, and T_S is the surface temperature of the bagging. For the model discussed in this report the surface temperature would allow for an average temperature of the bagging to be calculated and used in equation (9).

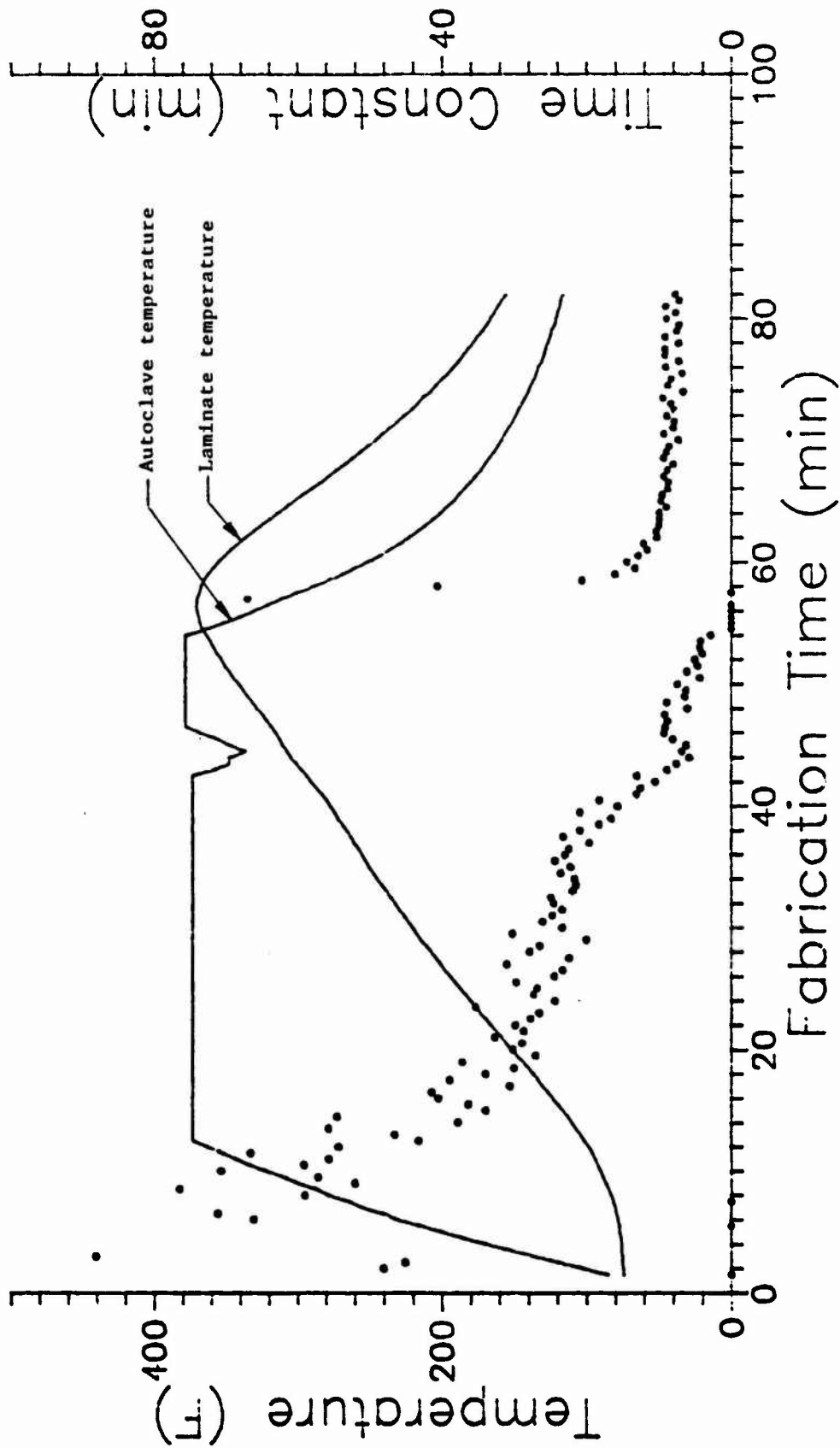


Figure 1. Time constant variation during autoclave curing

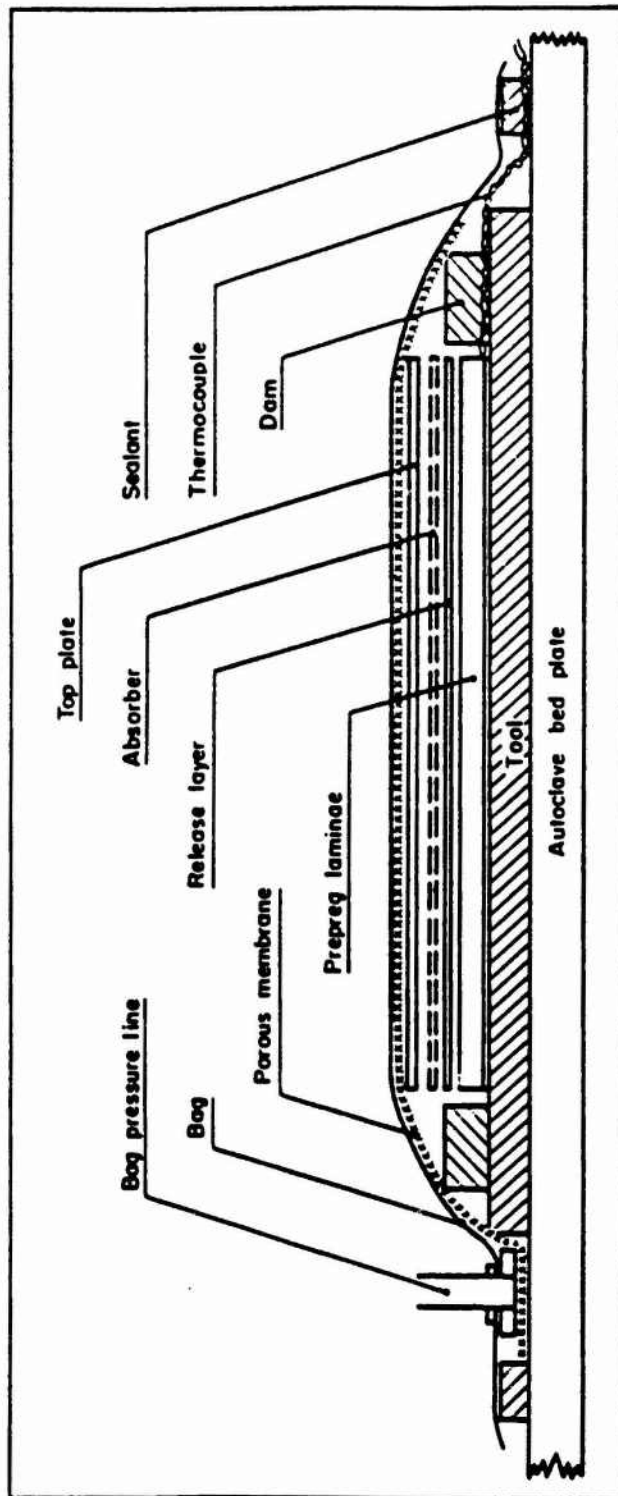


Figure 2. Autoclave curing bagging layup

REFERENCES

1. Dave, R., Kardos, J. L., and Dudukovic, M. P., "Process Modeling of Thermosetting Matrix Composites: A Guide for Autoclave Cure Cycle Selection", Proceedings of the First Conference on Composite Materials of American Society for Composites, Dayton, OH, 7-9 October 1986, pp 137-153.
2. Qualitative Process Automation for Autoclave Curing of Composites, AFWAL-TR-87-4083, 15 May 1987.
3. Lee, C. W., "Composite Cure Process Control by Expert Systems, Proceedings of the First Conference on Composite Materials of American Society for Composites, Dayton, OH, 7-9 October 1986, pp 187-196.
4. White, F. M., Heat Transfer, Reading, Massachusetts, Addison-Wesley Publishing Company, 1984.
5. Springer, G. S., "Modeling the Cure Process of Composites", SAMPE Journal, September 1986, pp 22-27.
6. Loos, A. C., Springer, G. S., Curing of Graphite/Epoxy Composites, AFWAL-TR-83-4040, March 1983.

1987 USAF-UES SUMMER FACULTY RESEARCH PROGRAM/
GRADUATE STUDENT SUMMER SUPPORT PROGRAM

Sponsored by the
AIR FORCE OFFICE OF SCIENTIFIC RESEARCH

Conducted by the
Universal Energy Systems, Inc.

FINAL REPORT

EQUITABLE SAFETY STOCKS FOR USAF
CONSUMABLE ITEMS

Prepared by: Douglas E. Phillipott
Academic Rank: Graduate Student
Department and Management Department
University: Auburn University
Research Location: Logistics Management Center
Gunter AFS
Montgomery, AL 36114
USAF Researcher: Captain Wes Roberts
Date: September 30, 1987
Contract No: F49620-85-C-0013

EQUITABLE SAFETY STOCKS FOR USAF

CONSUMABLE ITEMS

by

Douglas E. Phillipott

ABSTRACT

Current safety stock policy of the United States Air Force provides for different levels of absolute protection from backorders for different consumable items. In a group of items considered to be equally important to mission capability, current policies lead to different amounts of absolute safety stock protection for different items. The purpose of this research was to introduce equitable safety stock protection for consumables in a given mission impact code (MIC) category.

Research findings indicate that by adopting the equity policy proposed, annual backorders can be decreased by 3.7% with a corresponding increase of 2.9% in inventory investment. In addition, the equity policy offers the opportunity to optimize inventory dollars and reduce inventory investment in less critical items.

ACKNOWLEDGEMENTS

I would like to thank the Air Force Systems Command and the Air Force Office of Scientific Research for sponsorship of this research. In addition, I wish to express my gratitude to the people at the Logistics Management Center for their help and support.

Several people were instrumental in the success of this research. Mr. Chuck Miller and Mr. Nick Godbey provided me with invaluable help with the various computer programs. Mr. Wayne Faulkner and LTC George Orr offered their technical expertise. Captain Wes Roberts provided me with support, understanding and encouragement. I am particularly indebted to Ms. Gale Jarnagin who helped me every step of the way.

I. INTRODUCTION

The United States Air Force (USAF) uses safety stocks (or safety levels) as protection against stockouts due to variations in demand during order and ship time (or leadtime). The specific inventory and safety stock equations cited here are given in Part Two, Volume II of Air Force Manual (AFM) 67-1, and are the basis for all subsequent references to current USAF practices.

The USAF uses the simple Wilsonian equation for determining the economic order quantity (EOQ). Current USAF policy sets order costs at \$5.20 (for non-local purchases) and holding costs at 15%. Also, the USAF defines the daily demand rate (DDR) as annual demand divided by the 365 days per year. With these stipulations, the Wilsonian EOQ equation becomes:

$$EOQ = 8.3 \sqrt{\frac{365(DDR)P}{P}} \quad (1)$$

The USAF currently uses a two-factor model to calculate safety stock for consumable items. The first factor is an estimate of the leadtime variance and is based upon both the variability of demand and the variability of the leadtime period. The second factor is called a C-factor and is simply the number of standard deviations of leadtime demand which the safety stock is expected to cover. The statements given in AFM 67-1 regarding stock-outs (or backorders) for different C-factors imply that leadtime demand is expected to be approximately normally distributed. For example, a safety stock equivalent to two standard deviations is expected to

yield three percent of inventory cycles in which stock-outs are expected to occur. The safety level quantity (SLQ) is given by:

$$SLQ = C \sqrt{O\&ST(VOD) + DDR^{**2} (VOO)} \quad (2)$$

where:

O&ST = order and ship time (leadtime)
 VOD = variance of demand during O&ST
 VOO = variance of O&ST

Current USAF policy limits C-factors to one standard deviation for items with urgency justification codes (UJC) of C; items with UJCs of B are assigned C-factors of 1.5; items with UJCs of A are assigned C-factors of 2.

The variance of demand during O&ST is calculated by the equation:

$$VOD = \{[\sum CRD^{**2}][(\sum CRD)^{**2}/n]\}/n \quad (3)$$

where:

CRD = cumulative recurring demand
 n = number of days elapsed since first demand

The variance of O&ST is calculated by equation (4):

$$VOO = [\sum FI(MI^{**2}) - (\sum FI(MI))^{**2}/N]/N \quad (4)$$

where:

FI = number of receipts reflected in each segment of the routing identifier record, frequency distribution table

MI = midpoint, in days, of each segment of the routing identifier record, frequency distribution table

N = number of receipts

Hadley and Whitin (1963) state that the number of

expected backorders per cycle can be approximated by :

$$E(Bo)c = \int_r^{\infty} (x - r)f(x)dx \quad (5)$$

where:

$E(Bo)c$ = expected number of backorders per cycle
 r = reorder point
 x = demand rate
 $f(x)$ = probability that the demand will occur

The number of expected annual backorders is obtained simply by multiplying equation (5) by the number of reorder periods per year.

$$RDR = \frac{D}{Q} \quad (6)$$

where:

RDR = Number reorder periods per year
D = annual demand
Q = EOQ value

Given equation 6, the number of expected annual backorders can be expressed as in equation 7:

$$E(Bo)a = RDR \int_r^{\infty} (x - r)f(x)dx \quad (7)$$

where:

$E(Bo)a$ = number of expected annual backorders

II. Objectives of the Research Effort

The current USAF safety stock policy for consumables considers only the expected number of backorders per reorder period (or cycle) and neglects the number of reorder periods per year. The net effect of neglecting the number of annual backorders is to provide greater absolute safety stock protection for less expensive items.

Consider a set of consumable items that have identical inventory data except for price. The following data were taken from AFM 67-1, Part Two, Volume II:

D = 6.055 units
 DDR = 0.0166 units
 VOD = 2.594 units
 SLQ = 8.815 units
 VOO = 38 days
 VOD = 30 days

Using these data, Table 1 shows that when items have identical inventory data except for price, less expensive items receive greater absolute safety stock protection.

Table 1

The Effect of Unit Price on Absolute Annual Backorder Protection

Unit Price	Integer EOQ	Annual Number Reorder Periods	Annual Number Expected Backorders	Annual SS Holding \$
\$ 1	20	0.30	0.05	\$ 1.35
6	8	0.73	0.12	8.10
10	6	0.94	0.15	13.50
100	2	2.97	0.47	135.00
1000	1	9.31	1.49	1350.00

The results given above show the impact of the current USAF policies upon expected annual backorders. Under current policy, expected backorders per cycle is identical for all items; however, less expensive items receive greater annual absolute safety stock protection. The inventory data for each item is identical, except for price, which was varied to show the effect upon annual backorders. The results given above suggest that when items have identical inventory data

except for price, then annual backorder protection declines by one-third given a ten fold increase in price.

The implications of these findings are better appreciated when consideration is given to items identified as high mission impact items. Such items are defined by the USAF using Mission Impact Codes (MICs). The MICs identify consumable items deemed critical to the successful accomplishment of a mission. Given two items with identical MICs, the current USAF policy would expensive item. This conclusion holds despite the fact that USAF policy provides for increased safety stock protection per cycle for mission critical items.

This inequity in safety stock protection for items identified as being equally important to mission capability is the main concern of this study. The purpose of this research is to provide equitable safety stock coverage for consumables identified as high mission impact items. The equity to be introduced is an equivalent number of annual expected backorders for each item in a given category. The three basic research questions to be answered by this study are:

1. Does equity in the number of annual expected backorders increase the unit fill rate?
2. What is the impact of the proposed changes on safety stock investment?
3. Does equity provide for a reduction in the number of backorders per year?

III. METHODOLOGY

Population and Data Selection

The population studied in this research was limited to the database maintained by the Air Force Logistics Management Center (AFLMC) at Gunter AFS, AL. The AFLMC receives data directly from the respective bases on a consistent basis. The AFLMC database is considered to be representative of the USAF Standard Base Supply System (SBSS).

Foremost in the selection of data for this study was the selection of a suitable base for analysis. Of the 12 bases for which data is maintained, several are overseas bases. Data for overseas bases, as well as for larger continental United States (CONUS) bases, contain much data not directly associated with mission accomplishment. Data for such bases may contain item information associated with direct support of personnel. For example, the data for these bases might include clothing, toiletries and the like. In addition, these bases maintain several weapons systems which makes tracing a particular item to its parent weapons system particularly difficult. For these reasons, overseas and larger CONUS bases were excluded from consideration for study. Two bases which are relatively "clean" of the type of data mentioned above are England AFB and Minot AFB. Because of the ease of access to data for Minot AFB, it was chosen for study.

Of the number of consumables contained in the Minot AFB item record, only those identified as having mission impact

codes (MIC) of one and stockage priority codes (SPC) of one were selected for study. The reason for this stratification was that items having MICs of one are considered to be most critical to mission capability. In addition, items bearing an SPC of one may indicate a problem in the current stockage policy for that item. The September 1986 item record for Minot AFB was searched by computer for items meeting the above criteria. The result of computer search was approximately 1,200 items. From this population, a random sample of 31 items was chosen for analysis. The time frame for the study was from September 1986 through March 1987.

Model Development

For the purposes of this study, the economic order quantity (EOQ) formulation and associated variables currently used by the USAF was accepted (reference Equation 1). In addition, the safety level quantity (SLQ) formulation was accepted. However, only the variables associated with demand and order and shiptime in the SLQ equation were accepted (reference Equation 2). The variables under the radical are those concerning demand and O&ST and were accepted. The C-factor, which represents the number of demands the SLQ is expected to cover, was varied from current USAF practice.

With the above stipulations, the experimental model was designed to provide equitable safety stock coverage for each item in the 31 item sample of MIC 1, SPC 1 consumables. To introduce equity, the expected number of annual backorders for each item was given an identical value. The value of

zero expected annual backorders was assigned to each item in the sample because it best reflected the considerable impact of these items on mission capability.

The relation given by Buchan and Koenigsberg (1963) was used to approximate the expected number of annual backorders:

$$E(Bo) = RDR * Pb \quad (8)$$

where:

$E(Bo)$ = expected number of annual backorders
RDR = number of reorder periods per year
 P_b = probability (as a %) of a backorder

The RDR value is a characteristic of a particular item and is dependent on the annual demand and the EOQ value for the item (see Equation 6). The previous stipulations concerning accepted values required that RDR be a fixed value for each item. Therefore, in order to force equation 8 to zero for each item, P_b was varied. Given that P_b is simply the complement of the probability of filling an order, we can write:

$$P_b = (1 - P_f) \quad (9)$$

where:

P_f = probability (as a %) of filling an order

As mentioned earlier, AFM 67-1 implies that demand can be expected to be normally distributed. If we assume that demand is approximately normally distributed, then P_f values can be obtained from standard normal distribution tables (provided that standard deviation values are given). Recalling that the C-factor is merely the standard deviation of demands, if we assume a C-factor then P_f values can be

obtained from the normal distribution tables. Further P_b values can then be obtained by the simple relation given by equation 9.

This relation between C-factor, P_f and P_b was used to drive the model and force the expected number of annual backorders to zero for each item. The process was an item-by-item iterative procedure that was performed until the value of zero backorders was obtained. Before the iterative process began, RDR values for each item were calculated using equation 6. The iteration began by assuming a value for the C-factor, obtaining the corresponding P_f value and calculating P_b (Alternatively, P_b values can be obtained directly from the tables). Finally, the expected number of annual backorders was calculated using equation 8. If the obtained value was not zero, the iterative procedure was repeated using a different C-factor until a value of zero was reached. With the proper C-factor values necessary to achieve zero annual backorders obtained, the remaining task was to answer the three research questions given earlier. These questions were answered by simulating the operation of the USAF supply system using the System to Analyze and Simulate Base Supply (SASBS).

The SASBS is a computer routine written in the Simscript programming language and contains some 3,000 lines of code. The purpose of the SASBS is to simulate actual operation of the USAF Supply System (SBSS). The model has been validated as accurately representing the operation of the SBSS. The

SASBS was used in this study because it provided the unique opportunity to make policy changes in current USAF practices and immediately observe the results.

The simulation of the SBSS under the proposed equity was achieved by inputting the obtained C-factors necessary for zero backorders to the SASBS. Also, a simulation was made using the same 31 item sample under current USAF practices. The current USAF policies are those presented earlier in this paper. The latter simulation could then be used as a baseline for comparing the performance of the proposed equity policy with the performance of current USAF practice. The performance measure in both cases was the three criteria mentioned previously.

IV. RESULTS AND ANALYSIS

Results of Simulations

In addition to the baseline and zero backorder simulations, a third simulation was made using a value 0.5 annual backorders for all items. The SASBS simulated the operation of the USAF Supply System for a period of 12 months in all three simulations. As mentioned previously the three criteria used to evaluate the effectiveness of each policy were unit fill rate, actual number of annual backorders and dollar investment in inventory. Table 2 presents the results of the simulations for the three runs.

Table 2
Results of Simulations

<u>Performance Criterion</u>	<u>Baseline</u>	<u>Equity (E(Bo) = 0)</u>	<u>Equity (E(Bo) = 0.5)</u>
Unit fill rate	89.08%	89.15%	89.04%
Dollars in inventory	\$7038	\$7243	\$6623
Number of Backorders			
UJC A	68	67	74
UJC B	5	5	5
UJC C	34	31	34
TOTAL	107	103	113

The results presented in the table above represent the cumulative results of the 12 month simulation. The only difference in the input to the SASBS for each simulation was the value of the C-factor for each item. The baseline simulation assigned C-factors based on the current USAF policies; the equity simulations assigned C-factors to each item based on the computer iterative procedures described earlier. In examining the results in Table 2 it should be remembered that all the items in the sample are MIC 1 items. That is, all the items have the potential of grounding a mission regardless of the UJC value. Table 3 presents a comparison of the equity simulations relative to the baseline simulation.

Table 3
Comparison of Equity Simulations
Relative to Baseline

<u>Performance Criterion</u>	Equity (<u>E(Bo) = 0</u>)	Equity (<u>E(Bo) = 0.5</u>)
Increase in Unit fill rate	0.07%	-0.04%
Increase in Dollars in inventory	2.9%	-5.9%
Decrease in Number of Backorders		
UJC A	1.5%	-8.8%
UJC B	----	----
UJC C	8.8%	----
TOTAL	3.7%	-5.6%

Analysis of Results - Zero Backorder Model

The results presented in Table 3 show that a 3.7% reduction in total annual backorders can be achieved by adapting the equity policy presented in this paper. The corresponding increase in inventory investment is 2.9%. The table also shows that a modest increase in unit fill rate can be obtained.

The reduction in annual backorders using the zero backorder equity model was an expected outcome. As a result of current USAF stockage policy, less protection is offered for more expensive items having a larger number of annual reorder periods. The proposed equity policy provides for equitable safety stock protection by equating the expected number of annual backorders for all items in a given MIC class. By providing equal protection for all items, a reduction in the total number of backorders is achieved. As a result of the equity, the percentage of demands covered by

the safety stocks for items having high RDR values is increased. At the same time, coverage for items having extremely low RDR values decreased.

The implication of these findings is that current USAF stockage policy is investing too much money in inventories for items with low RDR values. Similarly, current policy is investing too little in inventories for items with high RDR values. By assigning the lowest C-factors necessary to achieve equity for each item, the equity policy can be viewed as an optimization policy. The proposed policy allows more monies to be invested in items with higher RDR values while at the same time reducing the unnecessary over-investment in items with lower RDR values. However, the optimal assignment of dollars in inventory did not result in an even trade-off of over-investment dollars for under-investment dollars. An additional \$205 was necessary to achieve equity. In a sense, this increase in inventory investment "buys" a decrease of 4 annual backorders. However, the reduction in the number of backorders is more important than it may first appear. The net effect of reducing annual backorders is to increase mission capability. In a real sense, by decreasing backorders by 4, the equity policy provides for an equal increase in units available for missions. A further appreciation for the proposed equity policy can be realized by comparing the additional \$205 necessary to the purchase price of 4 additional mission capable units. Under current USAF policy, the purchase of these units would be necessary

to obtain the same number of mission capable units. The ultimate result of the equity policy is to increase operational readiness through more efficient stockage policy. This outcome is consistent with the recommendation of the General Accounting Office (1981).

Analysis of Results - 0.5 Backorder Model

The results presented in Table 3 show that as compared to the baseline simulation, the unit fill rate falls by 0.04% and the number of backorders increased by 5.6%. These results are not unrealistic. By increasing the number of expected annual backorders from zero to 0.5, the number of actual backorders is expected to increase. However, what is potentially important is the decrease in inventory investment of 5.9%.

It was mentioned previously that because of the importance of the MIC 1 items to mission capability, the number of expected annual backorders was set to zero. It appears, then, that because this model increases the number of expected annual backorders, it is inappropriate for the sample of MIC 1 items. However, the model may be of potential benefit in setting stockage policy for the MIC 3 and MIC 4 items. Because these items are less critical to mission accomplishment, a greater number of backorders can be tolerated.

Given a specified number of expected annual backorders, the equity policy appears to have the potential to significantly reduce the dollars invested in inventory. The data in Table 6 shows that if 113 actual annual backorders

could be tolerated, then inventory investment could be decreased by 5.9%. While this number of backorders may not be acceptable for MIC 1 items, it may be entirely acceptable for MIC 3 or MIC 4 items. Thus, by specifying a higher number of expected annual backorders, the equity policy appears to offer the potential of cost savings over current USAF stockage policy.

V. Conclusions and Recommendations

This study has shown that for the selected sample of consumable items, the actual number of annual backorders can be reduced by adopting the described equity policy. The proposed equity policy differs from current USAF stockage policy in that it considers the number of reorder cycles per year in determining the number of expected annual backorders. The current USAF stockage policy, by considering only the expected number of backorders per reorder cycle, results in different levels of absolute safety stock protection for different items.

The proposed equity policy can benefit the USAF in three areas. By setting the expected number of annual backorders to zero for each item in the sample, the proposed policy achieved equity in backorder protection for all items. The results indicate that the proposed equity policy offers a 3.7% reduction in annual backorders with a corresponding increase in inventory investment of 2.9%. Since the items sampled are high mission-impact items, this decrease in

backorders can be viewed as 3.7% increase in combat capability.

Additionally, the proposed equity policy leads to optimal use of inventory investment dollars. By assigning the smallest C-factor necessary to achieve the desired number of annual backorders, the policy prevents over-investment in items having a small number of annual reorder periods. These saved dollars can then be invested in providing the additionally backorder protection needed for items having a large number of annual reorder periods.

Thirdly, the proposed equity policy can be used for lower mission-impact items to realize substantial savings in inventory investment. The savings arise from specifying the largest number of annual backorders that can be tolerated for a group of items. This then results in reduced C-factors, safety levels and inventory investment.

While this study has achieved favorable results, it is the recommendation of the author that further study be undertaken. Specifically, it should be determined on a larger scale that the increased inventory investment required for higher mission-impact items is justified by the reduced number of backorders. Additionally, further study is needed to determine the maximum number of allowable annual backorders for each class of items. Finally, research should be initiated to separate high mission-impact items for aircraft from those for other systems. Additional study is necessary in order to distinguish those parts related to combat aircraft from those related to other systems.

REFERENCES

Blazer, Douglas J. Major et al., "EOQ Item Mission Impact Analysis", Air Force Logistics Management Center Report, October 1984.

Buchan, Joseph and Koenigsberg, Ernest, Scientific Inventory Management, Englewood Cliffs, NJ, Prentice Hall, Inc., 1963.

Hadley, G. and Whitin, T.M., Analysis of Inventory Systems, Englewood Cliffs, NJ, Prentice Hall Inc., 1963.

United States Air Force, Air Force Manual 67-1, Volume II, Part Two, December 1984.

United States General Accounting Office, "Logistics Managers Need to Consider Operational Readiness in Setting Safety Level Stocks", Report to the Secretary of Defense, August 1981.

1987 USAF-UES SUMMER FACULTY RESEARCH PROGRAM/
GRADUATE STUDENT SUMMER SUPPORT PROGRAM

Sponsored by the
AIR FORCE OFFICE OF SCIENTIFIC RESEARCH

Conducted by the
Universal Energy Systems, Inc.

FINAL REPORT

Investigation of Expert System Design Approaches
for Electronic Design Environments

Prepared by : Susan A. Poppens
Academic Rank: Graduate Student
Department and Computer Science Department
University: University of Missouri-Rolla
Research Location: ESMC/DVEP
Patrick AFB, Florida 32925
USAF Researcher: Ray Laudermilch
Date: 6 Aug 87
Contract Number: F49620-85-C-0013

Investigation of Expert System Design Approaches
for Electronic Design Environments

by

Susan A. Poppens

ABSTRACT

The intent of this project is to investigate various schemes that are available for the design effort of electronic systems. The information is to be incorporated into a knowledge base to determine approaches for a particular design. Various design methodologies are to be investigated for their appropriateness and application in the aforesaid design environment.

The second phase is to focus the knowledge base gathered in the design effort for electronic design. This knowledge base is to be incorporated into a rule based expert system which can be utilized by the design engineer in the design/development of functional specifications.

ACKNOWLEDGMENTS

I would like to express my appreciation to the Air Force Eastern Space and Missile Center and to the Air Force Office of Scientific Research for sponsorship of this research. Thanks must also be given to Universal Energy Systems for their commendable job in the administration of this program.

This opportunity proved to be a learning but nevertheless enjoyable experience because of the support given by those I worked with. Dr Zobrist's help and guidance throughout the summer was very much appreciated for the summer would not have been as successful without it. Mr Ray Laudermilch provided support and still allowed the freedom necessary for working. Lt Randy Pettit and Gene Hickey aided in providing a very enjoyable working atmosphere. I'd like to thank Capt Bill Ramey and Barbara Willis for their aid and their concern. The help of Latrice Weaver, Joyce Cercle, Sharon Bothwell, and Peggy Norman surely alleviated some of the busy work. A special thanks is also given for all of those who by being themselves made the summer more enjoyable.

I. INTRODUCTION:

An expert system is a tool which could be implemented in the structuring of code in the actual code design. In the structuring of code, the characteristics of an expert system seem to indicate that an expert system is indeed capable of efficiently performing code structuring.

An application of this could be very useful in an area where governmental projects are common. The range systems control of the Eastern Space and Missile Center employ many government employees who create and monitor code. Often, especially in the testing of unproven code, an ease of error finding is appreciated. If the code were to be originally structured in a uniform manner, perhaps error recovery and code modification would be easier.

My interests lie in the area of Software Engineering, especially in the applications of CASE, computer aided software engineering. I intend to further research the applications of expert systems and artificial intelligence in this area.

II. OBJECTIVES OF THE RESEARCH EFFORT:

Traditionally software has been viewed as being static. But recently this view has been changed. Software is quite the opposite. It is an evolutionary process and undergoes continuous change in order to cope with its everchanging environment (Belady and Leavenworth 1980). This constant change increases the program's entropy (unstructuredness) unless something is done to reduce it (Van Horn 1980). The answer could be found in an expert system. One of its responsibilities would be to retain the structuredness of programs. Thus maintaining modifiability and allowing programmers more ease and less effort during program maintenance.

My objective was to see if through the use of an expert system, perhaps an unstructured already written program could be run through a variety of tests: checking precompiler syntax, conformance to standards, etc. The expert system would then give advice on the correction or reformation of the program.

This is done through a variety of rules incorporated into a knowledge base of an expert system. This system asks the name of the file which is to be checked, runs a variety of tests on it, and determines if the program is sound structurally and syntactically. If it is not, then it reports what the trouble is and then gives a recommendation on how to correct the problem.

A variety of research has been done in code structuring by some major software developers. But these mainly deal with aiding the actual writing of the code and the design of it. I plan to use a reverse engineering approach which would take a rough finished product and clean it up so as to conform to standards. All of this would be accomplished through the implementation of an expert system.

III.

The expert system originally chosen to use was called Personal Consultant Easy, a Texas Instruments product. Easy is part of the Personal Consultant family consisting of Easy, a mini expert system, and two versions of Personal Consultant Plus, a full scale expert system. This series is written in a derivation of Lisp, namely Scheme. After working with Easy, the requirements of this project proved Easy to be too limited. So Personal Consultant Plus became the system used to carry on with the project.

a. Maintenance is more easily performed on the specification of a language rather than the implementation resulting from that specification (Goldberg 1986). So it is necessary to create some sort of knowledge base which takes the implementation (i.e. program) and using the knowledge base rules generates a specification tree which is the structure where all the necessary information is stored. Then tests can be run on this tree more efficiently because it has many of the unimportant and unnecessary details pruned away leaving only the information needed for the tests.

This demands that one decide just what information is critical and needs to be kept and what can be discarded. This vital information is stored at the lowest possible level meaning below this level the information is utilized and the above levels have no need for it. An expert system has an inherent tree-like structure which naturally suggests that it would be able to perform the actual syntax checking through the use of this internal structure. It could walk through the language's specification tree, checking the syntax as it goes, by progressing through different frames of the expert system.

Structure of the program should also conform to standards. A structured program tends to be easier to modify and understand. Some of the key requirements that a structured program should uphold are

modularity: keeping the tasks of a program within certain modules and having one function done in an independent module.

coupling: separate unrelated tasks are done within separate unrelated modules.

localization: all variables are kept as localized as possible. Global variables are kept at a minimum.

In order to accomplish each of these requirements, some sort of internal database or knowledge base needs to be kept on all the variables and modules. Then as the system goes through the tests on

the program, it would interact with this knowledge base and would be able to give recommendations when necessary.

One example of when a recommendation would be required is when a goto is used in the code. The system would then run some tests on what use the goto has in order to ascertain whether this goto could be replaced with another control structure (Peterson, Kasimi, and Tokura 1973). Then the system would then tell the user how the restructuring of the program could be accomplished.

b. The aim of using the expert system was based on the hope that its internal structure would naturally handle all that was needed. The tree-like specification could be utilized through use of the frame characteristic in the Personal Consultant Plus expert system. Each non-terminal in the specification could correspond with a separate frame of the system. Thus the knowledge needed for each frame could be stored in its own frame parameters and variables. A lexical analyser was written in PASCAL which takes a source program input and returns one by one each of the tokens. Then the system depending where it was in the program would be expecting a certain token from this program, i.e. expecting an identifier name after the word function in the declaration part of the source program. I used a very simple pseudo PASCAL specification to work with (figure A-1) for my source language.

When I tried to have the system check a sample program written from this specification, I encountered some trouble. The first problem

```

[program] : [block],PERIOD;
[block] : [declist],[stmtlist];
[declist] : [decl],[declist]|#;
[decl] : FUNCTION,IDENT,left_paren,[parmlist],right_paren,
        semicolon,[block],RETURN,IDENT,END;
[parmlist] : IDENT,[mparms];
[mparms] : (comma,IDENT,[mparms]|#);
[stmtlist] : [stmt],[mstmt];
[mstmt] : semicolon,[stmt],[mstmt]|#;
[stmt] : [asstmt]|[ifstmt]|[whilestmt]|[instmt]|[outstmt];
[ifstmt] : IF,[cond],THEN,[stmtlist],END;
[whilestmt] : WHILE,[cond],DO,[stmtlist],END;
[instmt] : INPUT,left_paren,[inarglist],right_paren;
[inarglist] : IDENT,[minargs];
[minargs] : comma,IDENT,[minargs]|#;
[outstmt] : OUTPUT,left_paren,[outarglist],right_paren;
[outarglist] : [outarg],[moutargs];
[moutargs] : comma,[outarg],[moutargs]|#;
[outarg] : (ident|intgr|char);
[asstmt] : [leftside], assign, [expr];
[leftside] : IDENT;
[cond] : [expr] , equal, [expr];
[expr] : [term],[plus],[term]*;
[term] : [fact],[asterisk],[fact]*;
[fact] : IDENT,(left_paren,[fnarglist],right_paren|#)|
        left_paren,[expr],right_paren| INTGR ;
[fnarglist] : [expr],[mfnargs];
[mfnargs] : (comma,[expr],[mfnargs]|#);

```

FIGURE A-1. The specification of the simple language used to test out the expert system.

arose from the reading of the tokens from the file. A DOS-Call was required in order to run the lexical analyser. The read-from-file predicate of the system is not capable of consecutively reading from a file. It opens the file, reads from the top, and then closes the file. So I modified the lexical analyser to handle that problem. It would delete the corresponding word from the source file with each call so that the top of the file was the virtual pointer. But the continual DOS-Calls really delay the program since you have to travel from one environment to another. So some way to retrieve the tokens from the source program without changing the environments needs to be found.

One idea that was tried to see if it might be a possible answer was using DBASE III to store the information and working with that. But this involved the timely changing environments also.

Another problem encountered was the way the rules are fired by the system. A rule is not tried more than once in any instantiation of the frame to which they belong. This makes recursive calls of frames impossible. I tried to get around this trying to implement the meta-rules to some extent. This did not work. Then I tried to see if it was possible if I could write a lisp function to do what I wanted. It was at this point that the summer came to an end just as I was trying to acquire a feeling for lisp. In summary, the system will work if no looping is required and it is very slow due to the constant environment changes.

IV. RECOMMENDATIONS

a. The expert system developed this summer is not going to be implementable due to the problems encountered with structure and characteristics of the expert system. If a system could be made so that all the reading could be done within the system's environment and the system was capable of the actual storing of the information needed, within the internal superstructure of the system, then I believe the system could be made to help keep the code structured. As it ended up, I found that although an expert system seems to be a logical choice with this project, the Personal Consultant Plus proved to be too cumbersome for the actual implementation.

b. If the system could be developed so that the problems confronted this summer are overcome, then the real goal of the project could possibly be carried out. Even then a separate system would have to be built, or at least rules written, to handle the variety of languages most commonly used today: pascal, fortran, C, etc.. Each of these would require a little different environment although all would use the same basic logic.

c. Another idea would be to implement the system to rewrite the code, documenting it according to the government's standards. This could be very useful as many contractors today do not meet these standards. Much time is spent simply documenting code when this tedious job could be done by a computer since it is such a repetitious exercise.

REFERENCES

Belady, L.A. and B. Leavenworth. Program Modifiability. Software Engineering, edited by Herbert Froman and Philip M. Lewis II, 1980, pp. 25 - 36.

Goldberg, Allen T.. Knowledge-Based Programming: A Survey of Program Design and Construction Techniques. IEEE Trans. of Software Engineering, 1986, Vol. SE-12, No. 7, pp. 753.

Myers, Glenford J.. Composite / Structured Design. 1978, pp. 13 - 29.

Peterson, W.W., T. Kasimi, and N. Tokura. On Capabilities of While, Repeat, and Exit Statements. Communications of ACM, Aug 1973, Vol. 16, No. 8, pp. 503 - 513.

Van Horn, Earl C., Software Must Evolve. Software Engineering, edited by Herbert Froman and Philip M. Lewis II, 1980, pp. 209 - 223.

1987 USAF-JES SUMMER FACULTY RESEARCH PROGRAM

GRADUATE STUDENT SUMMER SUPPORT PROGRAM

Sponsored by the
AIR FORCE OFFICE OF SCIENTIFIC RESEARCH

Conducted by the
Universal Energy Systems, Inc.

FINAL REPORT

THERMAL STABILITY CHARACTERISTICS OF A NONFLAMMABLE CHLOROTRIFLUORETHYLENE

CTFE BASE STOCK FLUID

Prepared by:	Vijay K. Gupta	and	Mark Prazak
Academic Rank:	Professor of Chemistry		Graduate Student
Department and	Chemistry Department		Chemistry Department
University:	Central State University		Wright State University
	Wilberforce, Ohio 45384		Dayton, Ohio 45435
Research Location:	Materials Laboratory (AFWAL/MLBT)		
	Wright Patterson Air Force Base		
	Dayton, Ohio 45433		
USAF Researcher:	Mr. Carl E. Snyder Jr.		
Date:	September 4, 1987		
Contract No.:	F49620-85-C-0013		

Thermal Stability Characteristics of A Nonflammable Chlorotrifluoroethylene
CTFE Base Stock Fluid

by

Vijay K. Gupta and Mark Prazak

ABSTRACT

Thermal stability characteristics of a nonflammable chlorotrifluoroethylene CTFE base stock fluid MLO 86-7 have been investigated as function of time and temperature via micro-thermal stability tests. It has been found that this fluid is a complex mixture of chlorofluorocarbon compounds. The fluid was found thermally stable when stressed for 22 hours at 246.1°C or below, but when stressed at temperatures above 246.1°C, degradation was observed, and the extent of degradation increased with the increase in stress temperature. The fluid degraded severely when stressed at 315.6°C for 22 hours. When the fluid was also stressed at 176.7°C for 260 hours, some degradation of the fluid was observed as indicated by change in acid number. The increase in acidity of the fluid caused by thermal degradation process might be producing corrosive products that may be harmful to system components.

ACKNOWLEDGEMENTS

The authors would like to thank the Air Force Systems Command and Universal Energy Systems Inc. for providing an opportunity to work as Summer Research Participants at Materials Laboratory, Wright Patterson Air Force Base, Dayton, Ohio 45433-6533. Thanks are also due to Nonstructural Materials Branch of the Materials Laboratory for their hospitality and excellent working conditions. The authors are thankful to Mr. Lee D. Smithson of the Analytical Services Branch, and Dr. Jeff Workman and Dr. Chi Yu of the Technical Services Inc. for providing gas chromatographic/mass spectrometric (GC/MS) analysis. Thanks to all the members of the Nonstructural Materials Branch and University of Dayton Research Institute lubricants group for their technical assistance. Finally, the authors would like to thank Mr. Carl E. Snyder Jr. and Ms. Lois J. Gschwender for suggesting this area of research and for their collaboration and helpful suggestions.

Thermal Stability Characteristics of A Nonflammable Chlorotrifluoroethylene
CTFE Base Stock Fluid

INTRODUCTION

The extreme hazards associated with the flammability characteristics of the one-time standard aerospace hydraulic fluid, MIL-H-5606 are well known. The MIL-H-5606 hydraulic fluid is a naphthenic mineral-oil-base stock product with a Cleveland Open Cup flash point of 93°C to 107°C. The hazard generated by the flammability of the fluid is greatly increased by the high pressure (2.07×10^7 pascals) required for hydraulic system operation and also by the vulnerability of the hydraulic lines widely distributed throughout the aircraft. As a result, a need was identified by the Air Force for a fire-resistant direct replacement for MIL-H-5606. A synthetic hydrocarbon-based fluid MIL-H-83282 was developed and was found completely compatible with MIL-H-5606 hydraulic fluid systems and associated materials (1). All physical properties were equivalent or superior to those of MIL-H-5606 except low temperature viscosity: MIL-H-83282 had a kinematic viscosity of 3000 centistokes (cSt) at -46°C compared to an equivalent value for MIL-H-5606 at -54°C. All fire-resistance properties of MIL-H-83282 were superior than those of MIL-H-5606 with the exception of hot manifold ignition temperature which was found to be somewhat lower than that of MIL-H-5606. These two deficiencies resulted in an Air Force decision not to adopt MIL-H-83282 as a total fleet replacement fluid for MIL-H-5606.

In 1975, the Air Force Materials Laboratory at Wright Patterson Air Force Base began a program to develop a nonflammable hydraulic system, without the

constraints of compatibility with existing hydrocarbon systems (2-6). In the initial stages of the program (4), many fluid classes such as: phosphate esters; alkyl aromatics and alpha-olefin-based synthetic hydrocarbons; silicones; chlorophenyl substituted (Nadraul MS-5 and MS-6); cyclic ethers; alkyl amines; fluorinated phosphonates; fluoroalkylethers, chlorofluorocarbon polymers; perfluoropolyalkylethers; and perfluoroalkylether triazines, were considered as nonflammable candidates. Only those fluids were considered which were known as fire-resistant or were received after an industry survey to companies known to have experience in fire resistant fluids. The essential properties for a candidate fluid to be considered as serious non-flammable candidates were: heat of combustion more than 5,000 BTU/lb.; auto ignition temperature greater than 1300°F; hot manifold ignition temperature both stream and spray in excess of 1700°F; and atomized spray open flame (fluid may ignite, but flame must self-extinguish when ignition source is removed). Of all the above fluid classes, four fluid chemical classes that had acceptable flammability and physical property characteristics were: chlorofluorocarbon (CTFE), fluoroalkylether (FAE), linear perfluoroalkylether with minor branching, and perfluoroalkylether triazine. The thermal stability characteristics of a commercially available chlorotrifluorethylene oligomer (CTFE base stock fluid MLO 86-7) as a function of time and temperature are reported.

OBJECTIVES

The objectives of the summer program were to understand the thermal stability characteristics of the nonflammable CTFE base stock fluid (MLO 86-7) as a function of time and temperature. The results from this program were

expected to develop the suitable experimental conditions for conducting thermal stability studies on CTFE based pure and well-defined model compounds.

RESULTS AND DISCUSSION

The viscosity of a fluid can be expressed as a function of temperature by the equation given below:

$$1/\phi = \eta = A \exp E_{\text{vis}}/RT$$

where ϕ is the fluidity

η is the viscosity

A is the pre-exponential factor

and E_{vis} is the activation energy for viscous flow, the energy barrier that must be overcome before the elementary flow process can occur.

The above equation in the logarithmic form can be written as

$$\log_{10} \eta = \log_{10} A + E_{\text{vis}}/2.303 RT$$

Figure 1 represents the plot of $\log_{10} \eta$ as a function of $1/T$. From the viscosity data E_{vis} has been computed and the value is 22.15 KJ/mole. The fluid MLO 86-7 has the desired viscosity in the temperature range -54°C to 98.9°C and exhibits linear relationship within the limited temperature range.

The composition of the fluid MLO 86-7 was determined by GC/MS analysis, and the results are given in table 1. Specific GC conditions are given in

table 2. The sample chromatogram of the fluid MLO 86-7 is given in figure 2 (A). From the data in table 1, it appears that the CTFE base stock fluid is a mixture of several components. There were other components present in small amounts which were not identified that is why the total concentration is about 97%. Four major components $C_6F_9Cl_5$, $C_7F_{11}Cl_5$, $C_7F_{10}Cl_6$, and $C_8F_{12}Cl_6$ constitute about 94.5% of the fluid.

The thermal stability of the CTFE base stock fluid was determined using the following procedure. Thermal stability test bombs were made of 304 stainless steel tubing with 316 stainless steel Swagelok end caps. The bombs were 20 cm (8") long X 6 mm (0.25") outside diameter (unless otherwise specified). The bombs were cleaned with a suitable solvent (usually naphtha) and dried in an oven at 100°C for one hour. Approximately 2.0 cc of the test fluid was added to the partially assembled bomb (one Swagelok end fitting attached), and 99.9% pure nitrogen was bubbled through the fluid for 5 minutes to remove the air. The bomb was then quickly capped with the top Swagelok fitting and the whole assembly weighed to the nearest mg. The bomb was then placed in an oven at specified temperature (controlled within 2°C) for the specified time. The bomb was then removed, allowed to cool to ambient temperature, and then re-weighed. If the weight of the assembly changed more than 0.1 g, the test was considered invalid and rerun. The bomb was then opened and the liquid sample was transferred to a glass vial and analyzed using capillary column gas chromatography, acid no. measurements (using ASTM D664 method), and then viscosity measurement at 37.8°C.

The thermal stability data of MLO 86-7 stressed for 22 hours at different temperatures is given in table 3. The data in table 3 shows the concentration

of the unstressed fluid remaining after heating the sample for 22 hours at a specified temperature. These concentrations represent the amount of a specific component determined by gas chromatographic analysis using area percentage of the peak as percent concentration. The total concentration, the concentration of four major components, the viscosities at 37.8°C, and acid numbers are given in the table. In order to determine the catalytic effect of the metal surface on thermal degradation of MLO 86-7, the fluid was placed in the sealed glass tube and the tube was placed in the bomb and then the fluid was stressed at 287.8°C for 22 hours and the data for that test given in table 3 indicates there may be some catalytic effect of the metal surface. From the data it appears that the fluid was thermally stable when stressed for 22 hours in the temperature range of 176.7°C to 246.1°C. When the stress temperature exceeded 246.1°C, the changes in concentration, viscosity, and acid number were observed, and when the fluid was stressed at 315.6°C the fluid was severely decomposed and the viscosity of the stressed fluid could not be determined due to the particles present in the fluid. Thus thermal stability tests were not performed above 287.8°C. The thermal degradation data of MLO 86-7 stressed at 176.7°C as a function of time from 0 to 260 hours given in table 4 indicated no change in concentration and viscosity but increase in acid number was observed. Sample chromatograms of MLO 86-7 stressed under conditions as indicated in the diagram are given in figure 2 (B, C, and D).

The concentration of stressed fluid as a function of stress temperature is plotted in figure 3. The data points at 25.0°C represent the concentration of the component in the unstressed fluid. From the plots, it appears that the fluid MLO 86-7 and its components $C_6F_9Cl_5$, $C_7F_{10}Cl_6$, and $C_8F_{12}Cl_4$ did undergo decomposition as the stress temperature exceeded 246.1°C, but the component

$C_7F_{11}Cl_5$ did not show any noticeable degradation until the stress temperature exceeded $301.7^{\circ}C$. Thus it may be concluded that the fraction $C_7F_{11}Cl_5$ in the base stock fluid MLO 86-7 is slightly more stable than the other fractions. The acid numbers of MLO 86-7 as a function of stress temperature plotted in figure 4 indicate increasing acidity of the fluid as the stress temperature is increased, but when the stress temperature exceeded $285.0^{\circ}C$ the increase in acidity was exponential. The viscosities of MLO 86-7 as a function of stress temperature plotted in figure 5 indicate decreasing viscosity of the fluid as the stress temperature is increased. The plot in figure 6 shows the acid numbers of fluid MLO 86-7 when stressed at $176.7^{\circ}C$ as a function of time.

Using gas chromatography coupled with mass spectrometry, the degradation components present in the gas and liquid phase of fluid MLO 86-7 stressed at $287.8^{\circ}C$ for 22 hours were identified and the data is given in table 5. Carbon dioxide and low-molecular weight chlorofluorocarbon compounds were found as the degradation products along with the chlorofluorocarbon compounds originally present in the base stock fluid.

In order to determine chemical changes occurring during the degradation process the infrared spectra of unstressed and stressed fluid were recorded and no differences were observed in the two spectra. The acidity of the fluid may be due to dissolved CO_2 gas in the stressed fluid and or due to the formation of acids like HF and HCl. When the bombs were opened, the vapor that escaped was pungent smelling and showed a positive test for the presence of HCl vapors when a glass rod dipped in NH_4OH was held above the opening of the bomb. In addition the liquid phase of the stressed sample also showed a positive test with silver nitrate solution indicating the presence of chlorine

in the ionic form. The presence of fluoride ion was checked using fluoride ion-selective electrode, and the fluoride ion was absent both in the stressed and unstressed CTFE base stock fluid (MLO 86-7). Based on this observation and higher bond strength for C-F bond (552 kJ/mole) than C-Cl bond (397 ± 29 kJ/mole) one may conclude that HF is less likely to form than HCl as the fluid is stressed. The hydrogen required for the formation of acid may have come from the moisture absorbed in the fluid itself or the moisture absorbed during the test procedure. The Karl Fischer determination indicated that the fluid contained 3-5 ppm water.

CONCLUSIONS

Based upon the results presented in the previous section, the following conclusions are derived.

1. The CTFE base stock fluid MLO 86-7 is a complex mixture of chlorofluorocarbon compounds.
2. The experimental fluid was found thermally stable when stressed at 246.1°C or below for 22 hours, and the extent of degradation increased as the stress temperature was raised above 246.1°C , the degradation was severe when the fluid was stressed at 315.6°C for 22 hours.
3. The active metal surface of the bomb may have some catalytic effect on the degradation of the fluid, and needs further investigation.
4. When the fluid was stressed at 176.7°C for time periods 0 to 260 hours,

some degradation was observed as indicated by increase in the acid number, but it was not as severe as when the fluid was stressed at 287.8°C for 22 hours.

5. The increase in acidity of the fluid during thermal degradation may be forming undesirable corrosive products harmful to system components.

RECOMMENDATIONS

In order to gain good understanding of the structure-property relationships in CTFE base stock fluids, the experiments should be performed on pure well defined chlorofluorocarbon model compounds. The catalytic effect of the active metal surface on thermal degradation of chlorofluorocarbon compounds needs further investigation. The use of techniques such as differential scanning calorimetry and thermogravimetric analysis along with thermal stability studies can be helpful.

REFERENCES

1. Snyder, C.E. Jr., Krawetz, A.A., and Tovrog, T., "Determination of the Flammability Characteristics of Aerospace Hydraulic Fluids", Lubr. Eng., 37, 705-714, 1981.
2. Snyder, C.E. Jr., and Gschwendler, L.J., "Development of Nonflammable Hydraulic Fluid for Aerospace Applications Over a -54°C to 135°C Temperature Range", Lubr. Eng., 36, 458-465, 1980.

3. Snyder, C.E. Jr., Gschwender, L.J., and Campbell, W.B., "Development and Mechanical Evaluation of Nonflammable Aerospace -54°C to 135°C Hydraulic Fluids", Lubr. Eng., 38, 41-51, 1982.

4. Snyder, C.E. Jr., Gandee, G.W., Gschwender, L.J., Graham, T.L. Jr., Berner, W.E., and Campbell, W.B., "Nonflammable Aircraft Hydraulic Fluid Systems Development", SAE Technical Paper Series #821566; 1982.

5. Snyder, C.E. Jr., and Gschwender, L.J., "Nonflammable Hydraulic Fluid Systems Development for Aerospace", J. Syn. Lubr., 188-200, 1984.

6. Snyder, C.E. Jr., and Gschwender, L.J., "Fluoropolymers in Fluid and Lubricant Applications", Ind. Eng. Chem. Prod. Res. Dev., 22, 383-386, 1983.

Table 1. Composition of MLO 86-7 (CTFE Base Stock Fluid) Determined by GC/MS Analysis.

Component	Concentration (%)	Retention Time (min.)
$C_5F_7Cl_5$	0.363	2.45
$C_6F_9Cl_5$	39.068	3.00-3.35
$C_7F_{11}Cl_5$	13.489	3.95-4.10
$C_8F_{12}Cl_4$	1.064	4.80-5.00
$C_7F_{10}Cl_6$	11.102	6.80-7.00
$C_8F_{12}Cl_6$	31.065	7.60-8.00
Unidentified	0.932	8.45-8.65
Total ^a =	97.083	

^a There were other components present in small amounts which were not identified.

Table 2. Gas Chromatographic Conditions.

Model: Hewlett-Packard 5710A

Detector: FID

Column: Fused Silica Capillary Column

Length: 12 meters

Diameter: 0.22 mm

Liquid Phase: Methyl Silicone Carbowax Deactivated

Carrier Gas: 1 ml/min He

Auxiliary Gas: 40 ml/min

Chart Speed: 10 cm/hr.

Attenuation: 10 x 32

Temperatures:

Injector: 300°C

Detector: 350°C

Column: 70°C to 270°C

Program Rate: 8°C/min

Initial Hold: 2 min

Final Hold: 32 min

Sample Size: 1 Microliter

Table 3. Thermal Degradation Data of MLO 86-7 (CIFE Base Stock Fluid) Stressed at Different Temperatures for 22 Hours.

Temperature (°C)	Viscosity (cSt at 37.8°C)	Acid No. (mg KOH/g)	Total*	Concentration of Components (%)				
				C ₆ F ₉ Cl ₅	C ₇ F ₁₀ Cl ₆	C ₇ F ₁₁ Cl ₅	C ₈ F ₁₂ Cl ₆	C ₈ F ₁₂ Cl ₆
Unstressed	2.932	0.023	97.083	38.749	11.117	13.474	31.080	
176.7	2.857	0.010	97.228	39.032	11.152	13.544	31.169	
190.6	2.947	0.035	96.742	38.472	11.254	13.372	31.316	
204.4	2.952	0.134	96.984	38.508	11.159	13.448	31.332	
218.3	2.954	0.050	97.291	38.983	11.126	13.522	31.284	
232.2	2.938	0.000	96.489	38.486	10.990	13.785	30.842	
246.1	2.926	0.196	98.140	39.928	11.045	14.046	30.898	
260.0	2.884	0.258	95.942	38.584	10.671	13.872	30.425	
273.9	2.770	0.213	94.645	38.145	10.321	13.764	29.826	
287.8	2.660	0.906	92.773	37.593	9.910	13.511	29.086	
301.7	2.651	0.822	90.934	36.724	9.620	13.071	28.698	
315.6	ND	0.614	85.106	34.811	8.384	12.728	26.022	
287.8**	2.789	0.444	94.677	38.115	10.584	13.331	30.132	

ND Viscosity could not be determined as the sample contained particles.

* Includes all major components identified by GC/MS analysis.

** The fluid was sealed in the glass tube and the tube was placed in the bomb.

Table 4. Thermal Degradation Data of MLO 86-7 (CTFE Base Stock Fluid) Stressed at 176.7°C as a Function of Time.

Time (Hours)	Acid No. (mg KOH/g)	Viscosity (cSt at 37.8°C)	Concentration (%)
0	0.023	2.932	97.083
22	0.010	2.857	97.228
90	0.400	2.935	97.102
140	0.641	2.954	97.162
260	1.044	2.936	97.314

Table 5. GC/MS Analysis of MLO 86-7 (CTFE Base Stock Fluid) Stressed at 287.8°C for 22 Hours.

Component	Concentration (%)		Retention Time (min.)
	Unstressed	Stressed	
CO ₂		g	
CFC1 ₃		g	
C ₂ F ₃ Cl		g	
C ₂ F ₃ Cl ₃		g	
C ₃ F ₅ Cl		g	
C ₂ F ₃ Cl ₃		1.316	0.48-0.50
C ₄ F ₆ Cl ₂			
C ₃ F ₄ Cl ₄			
C ₄ F ₆ Cl ₂		0.986	0.60-0.70
C ₇ F ₁₀ Cl ₂			
C ₄ F ₆ Cl ₄		1.074	0.80
C ₅ F ₇ Cl ₅	0.363	0.676	2.45
C ₆ F ₉ Cl ₅	39.068	37.593	3.00-3.45
C ₇ F ₁₁ Cl ₅	13.489	13.511	3.95-4.10
C ₈ F ₁₂ Cl ₄	1.058	1.064	4.80-5.00
C ₇ F ₁₀ Cl ₆	11.102	9.918	6.80-7.00
C ₈ F ₁₂ Cl ₆	31.065	29.086	7.60-8.00
Unidentified	0.932	0.922	8.45-8.65

g Found in the gas phase of the stressed fluid.

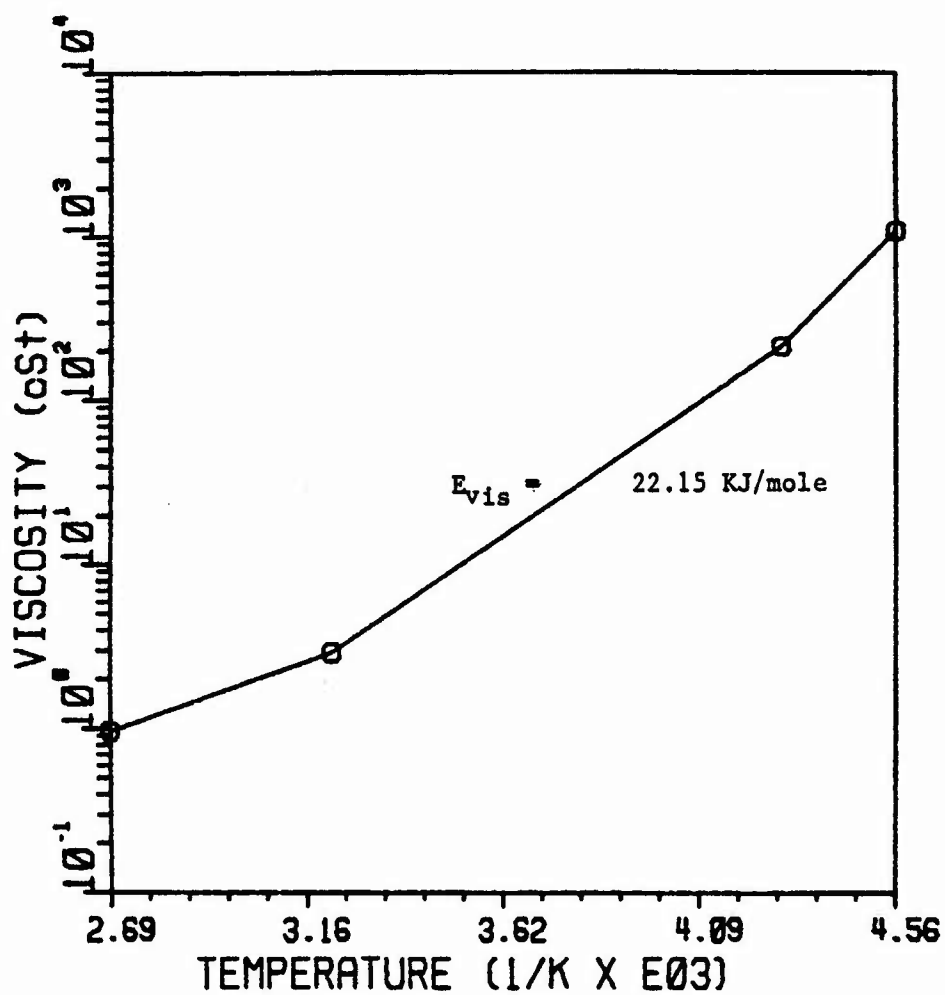


Fig. 1. Viscosity of MLO 86-7 (CTFE Base Stock Fluid) as a Function of Temperature.

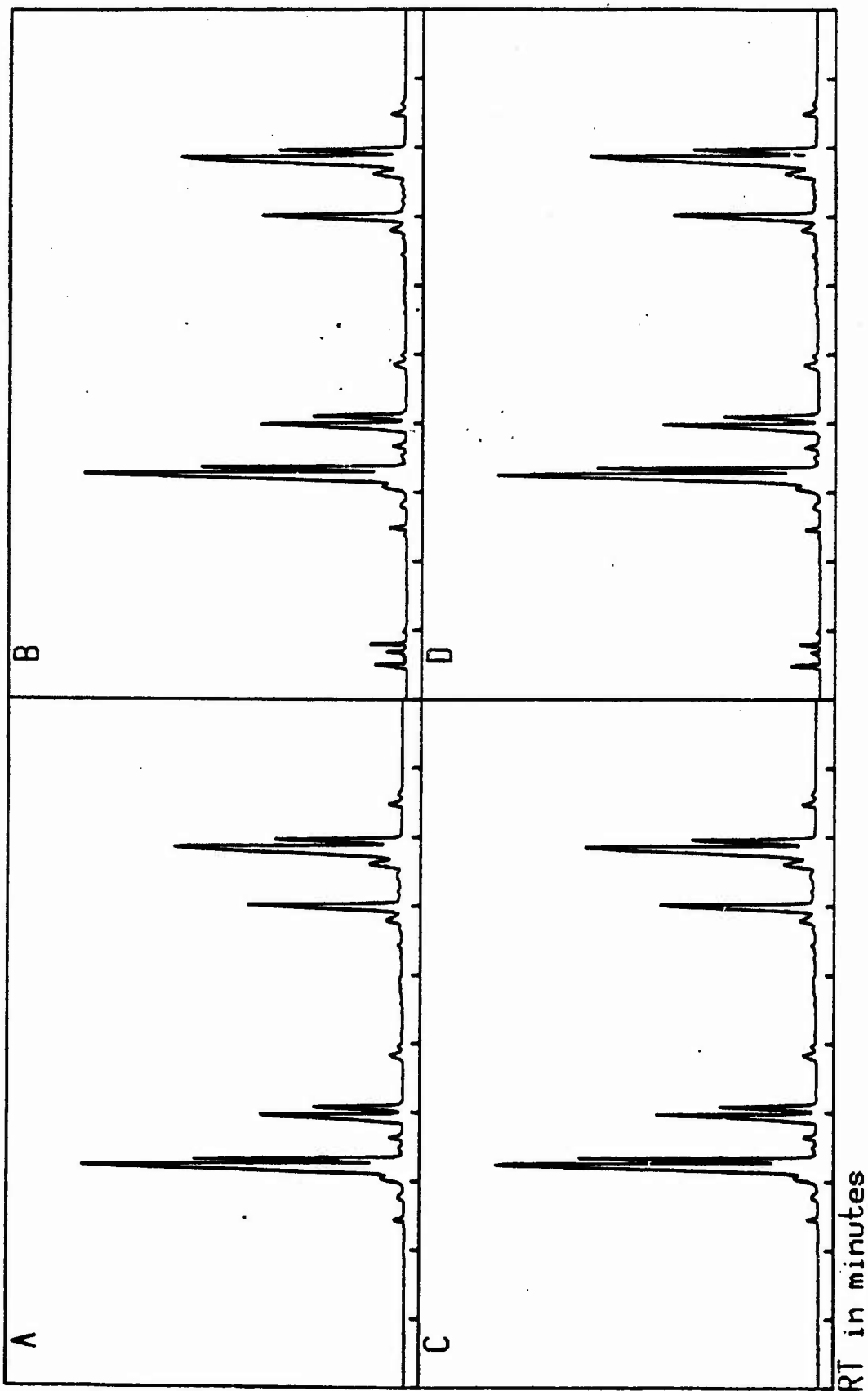


Fig. 2. Sample Chromatograms of MLO 86-7 (CTFE Base Stock Fluid).

A: CTFE Unstressed B: CTFE Stressed at 287.8°C for 22 Hours C: CTFE Stressed at 176.7°C for 260 Hours
 D: CTFE Stressed at 287.8°C for 22 Hours, Fluid Contained in a Sealed Glass Tube.

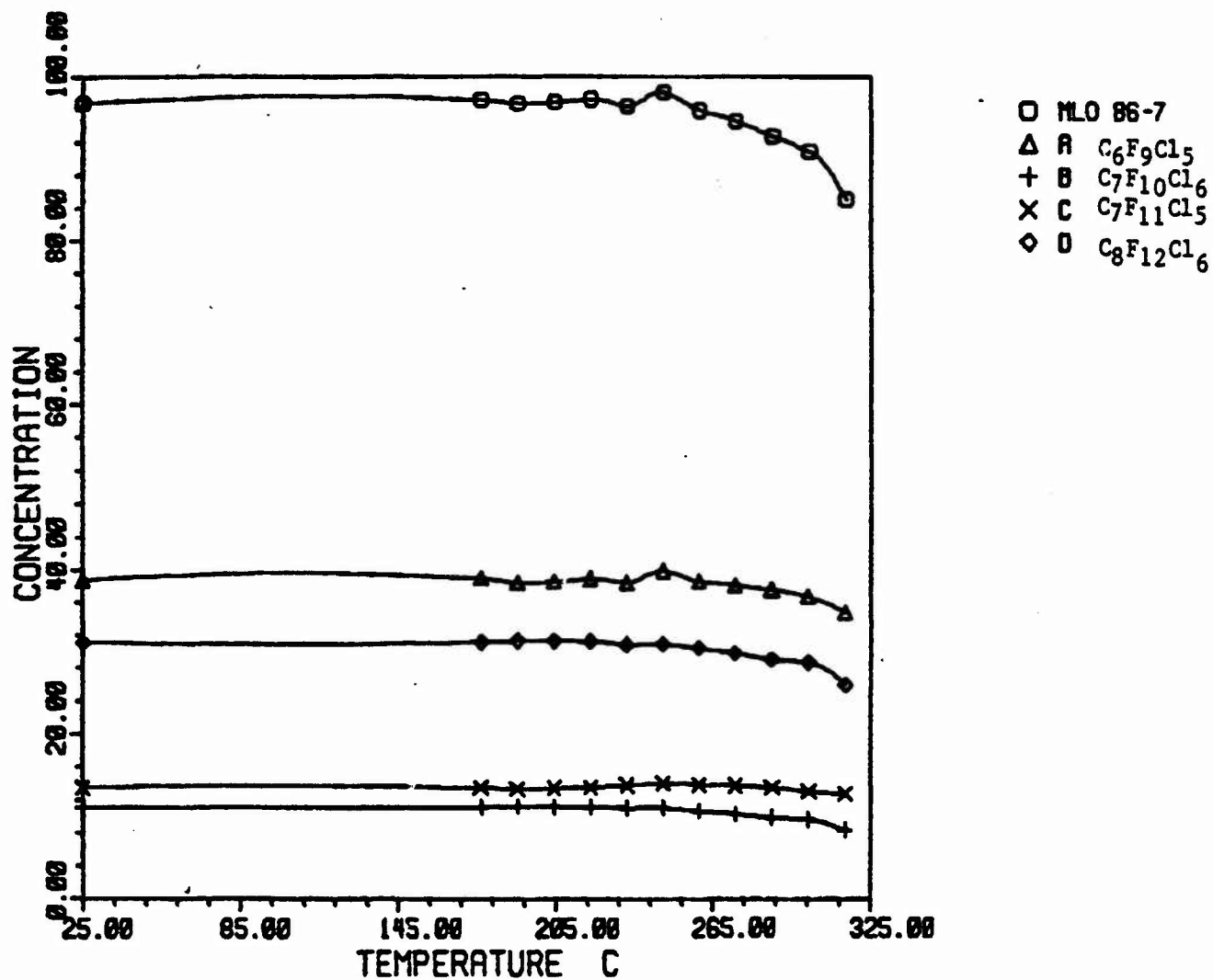


Fig. 3. Concentration of MLO 86-7 (CTFE Base Stock Fluid) and its Components Stressed at Different Temperatures for 22 Hours.

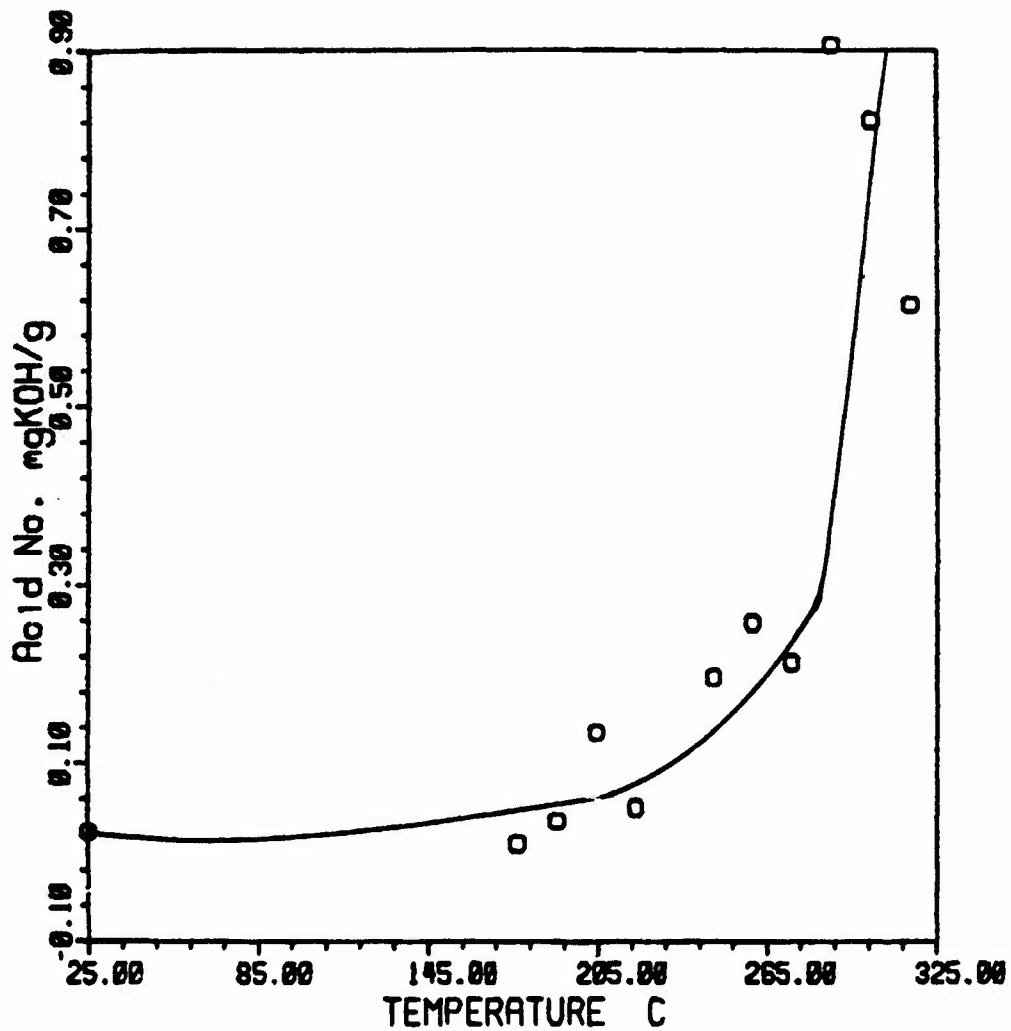


Fig. 4. Acid Numbers of MLO 86-7 (CTFE Base Stock Fluid) Stressed at Different Temperatures for 22 Hours.

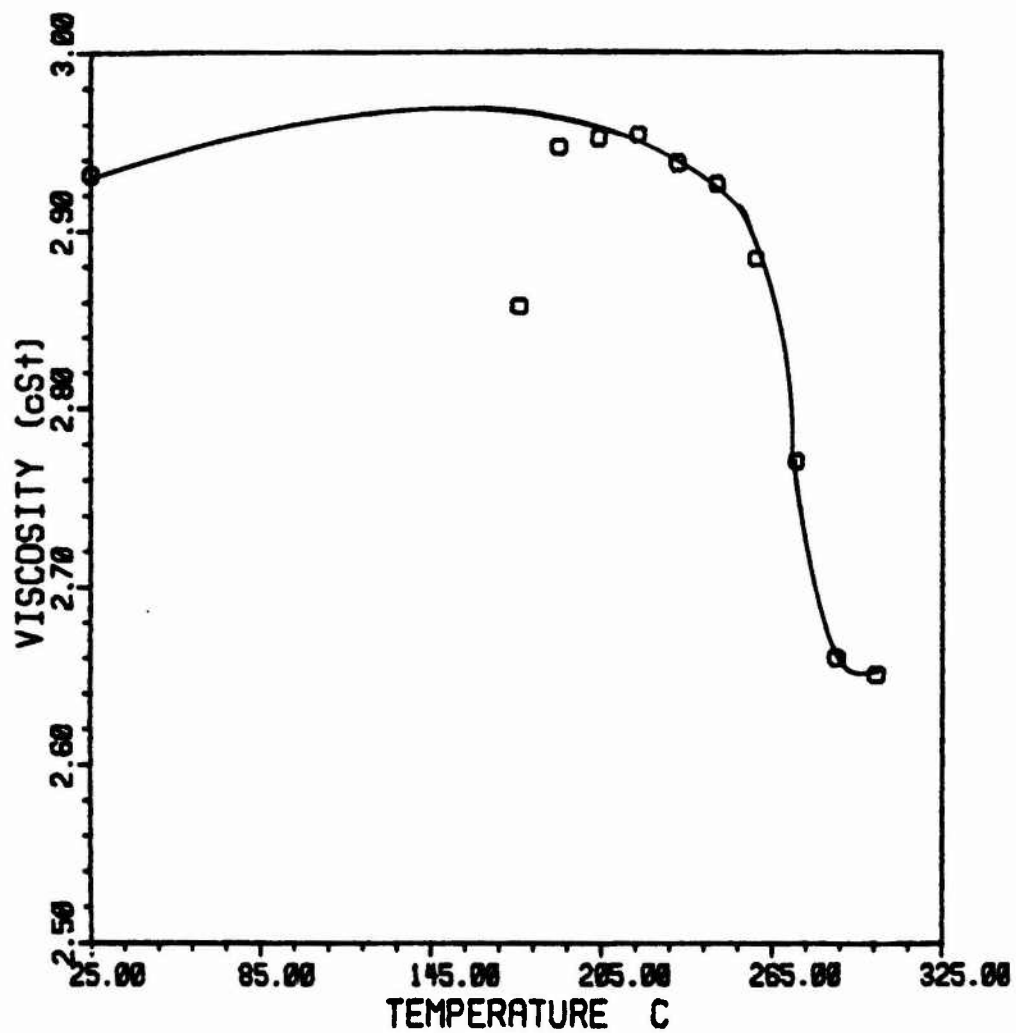


Fig. 5. Viscosity Data Determined at 37.8°C of MLO 86-7. (CTFE Base Stock Fluid) Stressed at Different Temperatures for 22 Hours.

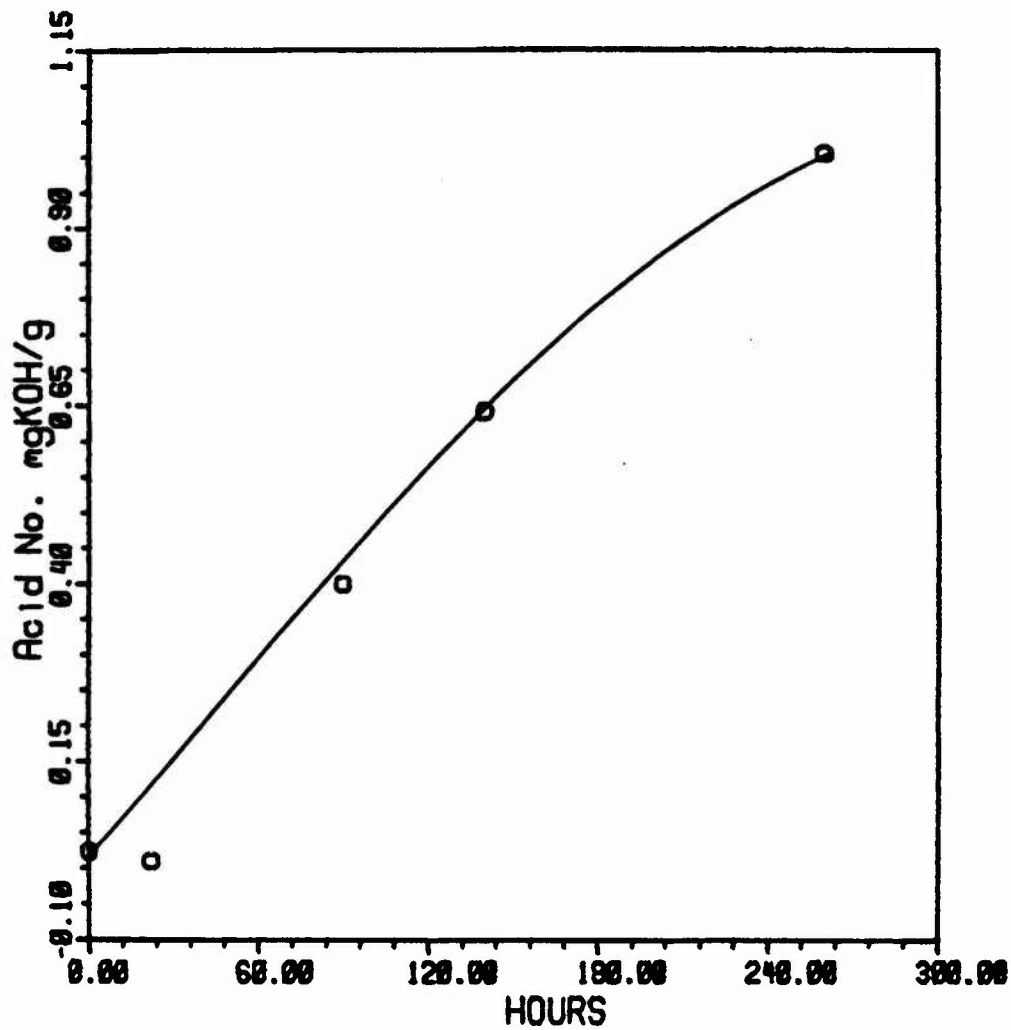


Fig. 6. Acid Numbers of MLO 86-7 (CTFE Base Stock Fluid) Stressed at 176.7°C as a Function of Time.

1987 USAF-UES SUMMER FACULTY RESEARCH PROGRAM/
GRADUATE STUDENT SUMMER SUPPORT PROGRAM

Sponsored by the
AIR FORCE OFFICE OF SCIENTIFIC RESEARCH

Conducted by the
Universal Energy Systems, Inc.

FINAL REPORT

CONTROL AND USE OF UNSTEADY FLOWS: INSECT USE OF VARIOUS
WING KINEMATICS AND RELATED PRESSURE MEASUREMENTS USING A
PITCHING AIRFOIL

Prepared by: Mark Andre Reavis
Academic Rank: Graduate Student (M.S.)
Department and University: Aerospace Department, University of
Colorado, Boulder
Research Location: Frank J. Seiler Research Laboratory,
United States Air Force Academy,
Colorado Springs, Colorado
USAF Researcher: Dr. Michael Robinson
Date: September 22, 1987
Contract No: f49620-85-C-0013

CONTROL AND USE OF UNSTEADY FLOWS: INSECT USE OF VARIOUS WING KINEMATICS AND RELATED PRESSURE MEASUREMENTS USING A PITCHING AIRFOIL

by

Mark Andre Reavis

ABSTRACT

Based on a detailed analysis of insect flight kinematics, pressure measurements were made from a NACA 0015 airfoil undergoing a constant pitch motion carried to high angles of attack. Previous work revealed the important contribution that high pitch rates and high angles of attack play in dragonfly flight kinematics. Changes in the initial angle of attack, pitch displacement angle, pitch amplitude and non-dimensional pitch rate altered the integrated values of C_l and C_d in a reproducible and predictable manner. Pitching profiles were varied to provide different initial conditions for vorticity accumulation: 1) starting at 0 degrees and pitching at constant rates to different maximum angles, 2) varying alpha initial and pitching to an alpha final of 60 degrees, and 3) varying alpha initial but holding the displacement angle constant. All of the above tests were conducted at alpha plus values of 0.1 and 0.5. These results suggest that dynamic pitch motions of an airfoil can enhance lift even if the pitch motion is initiated beyond normal static stall angles. Also, an optimal maximum pitch angle exists which enhances the unsteady lift potential while minimizing drag.

ACKNOWLEDGEMENTS

I would like to thank the following organizations for there personal and administrative assistance to me during the completion of this program: Frank J. Seiler Research Laboratory, Universal Energy Systems, Air Force Systems Command, and the Air Force Office of Scientific Research.

I would also like to thank Major John Walker, Chris Kedzie, and Eric Stephens for their assistance with the computers, experimental set up and discussion of the overall project. But most of all, I would like to thank Dr. Mike Robinson for his support, assistance and constructive input on my project with the United States Air Force.

I. INTRODUCTION:

Exerting control over an unsteady separated flow field is not yet fully understood. Yet continuing research, such as air pulse injection and sinusoidal oscillation, has shown reasonable control over such flow fields. Combining the promise of controllability with research showing the enhanced lift capabilities of unsteady aerodynamics suggests that application of this science may be very beneficial to the aircraft industry. These benefits could appear in as increased payloads, aiding short takeoff and landing vehicles, hovercraft, and enhanced low-speed flight regime maneuverability. Therefore, additional information concerning what types of wing motions or what types of forcing functions would create higher lift or control over an unsteady flow field would be very beneficial.

The Air Force has also recognized the potential of utilizing unsteady separated flow fields. A broad spectrum of experiments have been conducted at several universities in conjunction with Air Force sponsored projects and at Frank J. Seiler Research Laboratory located at the United States Air Force Academy. These investigations have examined a wide range of forced unsteady flow phenomena effects ranging from high amplitude pitching motions to interaction of a sinusoidal oscillating airfoil and a stationary swept forward wing.

This authors research interests have paralleled those of the United States Air Force^{4,5,6}. Experiments have been conducted in the three separate areas including discrete air pulse injections from the leading edge of a sinusoidally oscillating airfoil, unsteady separated flow effects on a air inlet, and the effects of dragonfly wing kinematics upon the aerodynamic forces produced. These research interests prompted the continuing research activity at Frank J. Seiler Research Laboratory this summer.

II. OBJECTIVES:

One area of research conducted at the University of Colorado Aerospace Department, deals with understanding what wing kinematics the dragonfly elicits to significantly increase its aerodynamic forces. Simultaneous collection of flow visualization and force balance data have provided some insight into this problem. Wing kinematics are changed by the dragonfly to produce large scale unsteady flow field structures and enhance the aerodynamic force generation. Although force balance data provides information on the overall force generation, it cannot provide any assessment of the pressure fluctuations that the wings experience during varying wing kinematics. Therefore, collecting pressure data on various wing motions can provide some insight into what wing motions are beneficial for enhanced lift.

The wing kinematics which appear to change the

aerodynamic force production include: wing stroke amplitude, maximum angle of attack, pitch rate, phase relationship and stroke plane angle. Since the dragonfly has very thin wings, its wings also experience much flexure and twisting through each wing stroke cycle. The initial experimental objectives were designed to investigate the effects kinematic perturbations would have upon an unsteady separated flow field using a 2-D pitching wing to simulate portions of the dragonfly wing kinematics.

Due to time constraints and the complication of setting up completely new hardware for the proposed experiments, this research effort focused upon variations in pitch rate and pitch amplitude. The airfoil was pitched about its 1/4 chord point. Pitching profiles were varied to provide different initial conditions for vorticity accumulation by: 1) starting at 0 degrees and pitching at constant rates to different maximum angles, 2) varying initial alpha and pitching to an alpha final of 60 degrees, and 3) varying alpha initial but holding the displacement angle constant. All of the above tests were conducted at a non-dimensional pitch rate (alpha plus) of 0.1 and 0.5. Alpha plus equals the pitch rate (rad/sec) times the chord length divided by the freestream velocity.

III. Methods

Simultaneous force balance measurements and flow

visualization photographs were collected from tethered dragonflies. A smoke wire and a 16mm Locam II high speed movie camera were used to visualize the flow and provide photographic documentation. An Oscillograph-Record Camera continuously monitored the changes in aerodynamic forces measured from a three degree of freedom strain guage force balance. A stroboscopic flash unit, triggered by the high speed movie camera, illuminated the flow and simultaneously marked the photographs position on the Oscillograph-Record Camera. This allowed the flow visualization pictures to be correlated to the force balance data.

Two-dimensional simutations of the dragonfly wing kinematics were conducted using a NACA 0015 airfoil in the 2' x 3' low speed wind tunnel at the United States Air Force Academy. A 6" chord airfoil with a 2' span was mounted to end plates, such as to model a 2-D flow. The airfoil had 15 pressure ports evenly distributed over the chord length at a span position of 1'. The airfoil was pitched by a microprocessor controlled high-power driver coupled with a DC micro-stepping motor. Two hundred descrete measurements were made by each pressure port during each pitch motion. The average pressure value was then computed for each pressure port from ten pitch motions.

IV. RESULTS:

As previously mentioned, changes in many of the wing kinematics of the dragonfly can alter the overall resulting

aerodynamic forces. Two such motions include the rate at which the wings pitch and the maximum angle of attack that the wings achieve. The effects that these two parameters have upon the lift force of the dragonfly are shown in Figure 1. The maximum lift achieved during each wing beat cycle is plotted versus the pitch rate and maximum angle of attack for both the fore and aft wings. The y-axis is either in degrees per second for the pitch rate or in degrees for the maximum angle of attack and the x-axis is in grams. These graphs show that the lift increases as either the maximum angle of attack or the pitch rate increases for either wing.

Data point A shows the influence that the aft wings maximum angle of attack has on overall lift production. All of the other parameters shown, maximum angle of attack fore wing and pitch rates for both wings, indicate that with their high values the lift force should be substantially higher than it is for point A. But the small maximum angle of attack that the aft wing achieves, 38 degrees, is not of high enough amplitude to substantially increase the lift force (graph lower right corner figure I). Thus, the maximum angle of attack of the aft wing is the dominant factor of the four parameters shown that forced data point A to have a lower lift value. Another important fact to note is that for significant changes in the lift force only small changes in the aft wings pitch rate and angle of attack are necessary (column II), whereas large changes are required

for the same parameters of the fore wing (column I). The line through these data points was not put there to suggest the trend is linear, it is there to show the increase in maximum lift for each parameter. Finally, it should be noted that these dragonflies, *Aeschna palmatta* species, show here that they can create lift of 5 to 6 times their bodyweight (bodyweight averages about 0.6 grams).

The strong interdependence of wing kinematics on the resulting forces suggested a series of 2-D experiments to help understand the pressure fluctuations the wing experiences during high amplitude pitching motions and high pitch rates.

Figure II shows how the coefficients of lift and drag are affected by changing the pitch rate, pitch amplitude, and the angle of attack. Although 3-D plots of the pressure coefficient varying over the chord with time are not available (the 3-D plotting routine at the Air Force Academy is not yet up and running), the unsteady lift and drag coefficients from the integrated pressure measurements plotted versus time are shown. 3-D pressure plots will be available and included when this data is submitted for publication. In figure II, the maximum lift coefficient (left column) and maximum drag coefficient (right column) obtained during the pitch motion are plotted for the different test conditions. Results from the three kinematic motions are plotted by rows: row I is the final angle of attack achieved during the pitch motion starting from 0 degree alpha, row II is the initial starting angle of attack

pitching to 60 degrees, and row III is the initial starting angle of attack and pitching through a constant delta alpha of 30 degrees.

Graph I of Figure II (C_{lmax} versus a pitch of 0 degrees to an independent alpha final) shows two alpha plus pitch rates, 0.1 and 0.5. This graph shows that as alpha final increases C_{lmax} rapidly increases until about an alpha final of 45 degrees. At that time both pitch rates appear to start converging to some asymptote, thus increasing alpha final past 45 degrees only modestly increases the C_{lmax} . In this case the asymptotes are located approximately at a C_{lmax} of 2.5 and 3.9 for an alpha plus of 0.1 and 0.5, respectively. When the alpha final is below the static stall angle of the airfoil the C_{lmax} seems to be independent of pitch rate. An alpha plus of 0.1 and 0.5 gave values of 0.95 and 0.87, respectively, for an alpha final of 10 degrees. Once the alpha final exceeds 20 degrees an alpha plus of 0.5 enhances the C_{lmax} much more dramatically than an alpha plus of 0.1.

Graph II, which shows C_{dmax} versus a pitch of 0 degrees to a varying alpha final, contains two important points. The first two data points representing alpha finals of 10, and 20 degrees, show similar values for both pitch rates, 0.1 and 0.5. This may suggest that the C_{dmax} is independent of pitch rate up to airfoil static stall angle. The trends for different pitch rates diverge from each other after an alpha final of 30 degrees is exceeded. Both test yield

trends that appear to yield increasing values of C_{dmax} beyond the alpha final of 60 degrees. When considering the previous statement and the fact that both pitch rates appear to have some asymptote for C_{lmax} , there may be some optimal alpha final that achieves an enhanced C_{lmax} while not substantially increasing the C_{dmax} . From the graphs shown, such an optimal alpha appears to be somewhere between an alpha final of 30 to 50 degrees.

Graph III (C_{lmax} versus a pitch from some initial angle of attack to 60 degrees) again shows that the alpha plus of 0.5 enhances the C_{lmax} in comparison to an alpha plus of 0.1. For an alpha plus of 0.1 the C_{lmax} does not substantially increase until the airfoils angle of attack dips beneath static stall angle, while an alpha plus of 0.5 does produce a noticeable increase in C_{lmax} even though the airfoil starts beyond the static stall angle. This may be because the higher pitch rate has the necessary energy to organize the vorticity that is available at the leading edge of the airfoil, which still has some attached flow. Both pitch rates again appear to be headed toward some asymptote as alpha initial goes to zero degrees. This graph again shows that increasing the delta alpha past 45 degrees does not substantially increase the C_{lmax} of the airfoil. And finally, even though increasing the pitch rate affected the C_{lmax} when the airfoil began from a stalled angle, the most effective pitch motions occurred when the airfoil began its pitch below the static stall angle.

Comparing the C_{dmax} versus a pitch from some initial

angle of attack to 60 degrees (graph IV) shows that the C_{dmax} is almost directly proportional to C_{lmax} for an alpha plus of 0.1. As with C_{lmax} , there is almost no change in C_{dmax} as alpha initial decreases from 30 to 15 degrees. Then, the C_{dmax} quickly increases as the alpha initial goes beneath the airfoil static stall angle. For an alpha plus of 0.5 the C_{dmax} increases almost linearly.

Graphs V and VI show the effects of a constant delta alpha while changes occur in alpha initial. Both C_{lmax} and C_{dmax} are given. With an alpha plus of 0.5, the C_{lmax} graph show a very similar structure to that of the same alpha plus in graph III. The major differences is that in graph III the C_{lmax} 's are larger. This is consistent with graph I that indicates the larger pitch amplitudes should have larger C_{lmax} 's. The alpha plus of 0.1 does not show the same similarity between graphs III and V. It does show again that as alpha initial dips below the static stall angle of the airfoil, C_{lmax} increases.

Graph VI makes two important points. An initial alpha of 0 degrees yeilds the lowest C_{dmax} . And, a local maxima appears for C_{dmax} somewhere around the static stall angle. Therefore, when the delta alpha remains constant, starting the pitching motion from 0 degrees gives the maximum C_{l1} while maintaining a minimum C_d , and as the alpha initial increases toward the static stall angle the C_d increases with a reduction in C_{l1} .

Figure III shows alpha and the coefficients of lift and

drag verses non-dimensional time (sec.*velocity/chord). A ramp motion from 0 to 60 degrees was used at a non-dimensional pitch rate of 0.5. The Fig. shows that the C_l starts increasing as soon as the airfoil begins to pitch, while the drag is delayed a small amount of time. The C_l and C_d then climb at an almost identical rate, a rate that is faster than the maximum pitch rate of the airfoil. The C_l achieves its maximum of 3.6 at the time when the airfoil first begins to slow down (approximately 41 degrees), while the C_d reaches its maximum of 3.4 once the airfoils motion is almost completed (approximately 56 degrees). After the maximums are reached each coefficient of lift and drag rapidly decrease to values below 1.0 and 2.0, respectively.

Figure IV has the same parameters as Figure III except that the non-dimensional pitch rate is changed to 0.1. The C_l starts to increase as soon as the wing begins the pitching motion. The C_l increases to a maximum of 2.5 at alpha equals 30 degrees, then it quickly drops off to a value of about 1.3. In this case the rate at which the C_l climbs is much faster than the pitch rate of the airfoil, but is slower than the alpha plus 0.5. The increase of the C_d is again delayed until after the wing motion starts, it then increases rapidly until a local maxima of 1.7 is achieved, which is shortly after the C_l is reached. This time the C_d does not drop off but continues to climb to a value near 2.0. This is a value similar to that the C_d attained when the alpha plus equaled 0.5.

V. DISCUSSION

The pressure measurement methods implemented in this study provided an excellent means for studying the coefficients of lift, drag, and pressure over a pitching airfoil. This study shows that there is a specific parameter space related to optimal pitching that both maximizes the lift and minimizes the drag of an NACA 0015 airfoil. For non-dimensional pitch rates of 0.1 and 0.5, the desired angles of attack appear to be between 30 and 50 degrees. Beyond 50 degrees the coefficient of lift increases slowly, while the coefficient of drag increases rapidly. Starting the pitching motion from 0 degrees seems to be the most advantageous. This is best shown when pitch amplitude remains constant, graphs V and VI figure II. The coefficients of drag remain minimal while the coefficient of lift is maximized. Another important finding of these studies is that the pitch rate can influence the coefficient of lift even if the airfoil begins a pitch motion from stalled angles of attack. A non-dimensional pitch rate of 0.5 showed increased coefficients of lift in comparison to a pitch rate of 0.1.

VI. RECOMMENDATIONS:

After analyzing the data from this experiment, there are three additional areas in which experiments are

recommended. The first of these recommendations would be to continue evaluating lift, drag and pressure data using different and extended parameters. Such an extended investigate would reveal whether an alpha plus of 0.7 and 1.0 would follow the trends that 0.1 and 0.5 show in graph I figure II. These recommended test would also show whether the C_{dmax} 's of an alpha plus of 0.7 and 1.0 remain similar to those for an alpha plus of 0.1 and 0.5 when the wing pitches from 0-10, and 0-20 degrees (graph II figure II). The effects of allowing the initial angle of attack to start at negative values should be evaluated for the coefficients of lift, drag, and pressure. And, we should obtain additional data points for C_{dmax} verses an independent initial angle of attack with a constant delta alpha. Here, the parameter of critical interest is the starting initial angle of attack, especially angles around the static stall angles of the airfoil. These parameters should be evaluated using flow visualization and hot wire anemometry measurements that are correlated to the pressure measurements discussed herein.

Finally, other critical kinematic parameters exhibited by the dragonfly should be subjected to similar evaluations. Taken together, the synthesis of the results of such studies should reveal how we can both control the generation of unsteady flows and maximize the subsequent use of them.

REFERENCES

1. Walker, J.M., Helin, H.E., and Chou, D., "Unsteady Surface Pressure Measurements on a Pitching Airfoil," AIAA Paper No. 85-0532, Boulder, Colorado, Mar. 1985.
2. Walker, J.M., Helin, H.E., and Strickland, J.H., "Experimental Investigation of an Airfoil Undergoing Large Amplitude Pitching Motions," AIAA Paper No. 85-0039, Reno, Nevada, Jan. 1985.
3. Helin, H.E., Robinson, M.C., and Luttges, M.W., "Visualization of Dynamic Stall Controlled By Large Amplitude Interrupted Pitching Motions," AIAA Paper 86-2281, Williamsburg, VA, Proceedings AIAA CP868, Aug. 1986, pp. 456-471.
4. Robinson, M.C. and Luttges, M.W., "Vortices Produced by Air Pulse Injection from the Surface of an Oscillating Airfoil," AIAA Paper No. 86-0118, Reno, Nevada, Jan. 1986.
5. Reavis, M.A. and Luttges, M.W., "Aerodynamic Forces Produced by a Dragonfly," AIAA Paper, Reno, Nevada, Jan. 1988.
6. Reavis, M.A., "Effects of Unsteady Separated Flow on an Air Inlet," AIAA Region V Student Paper Conference, Ames, Iowa, April 1986.

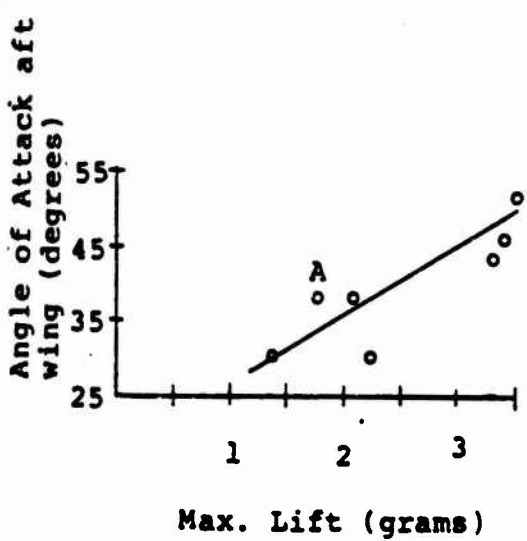
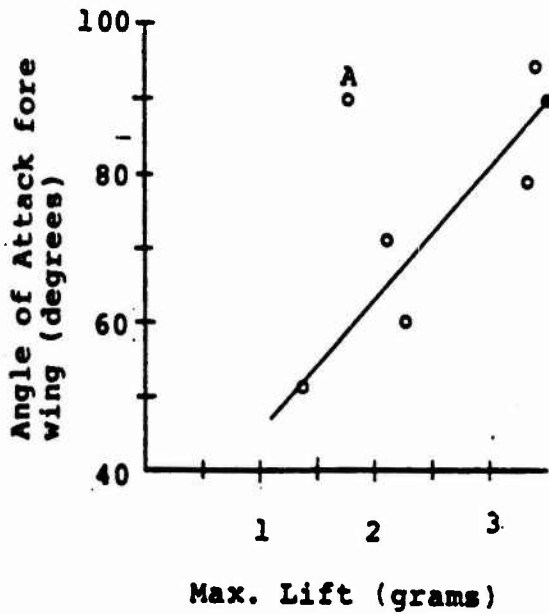
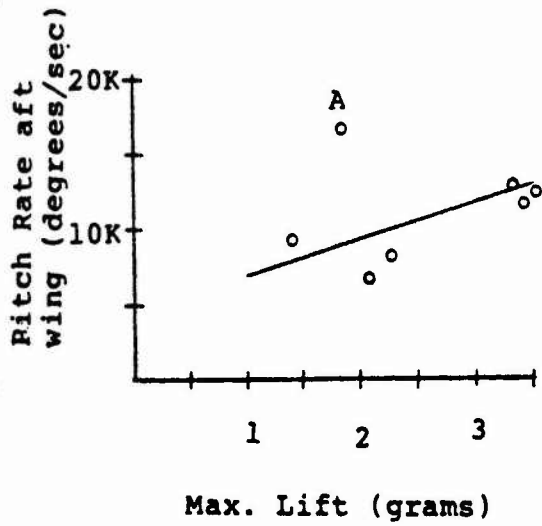
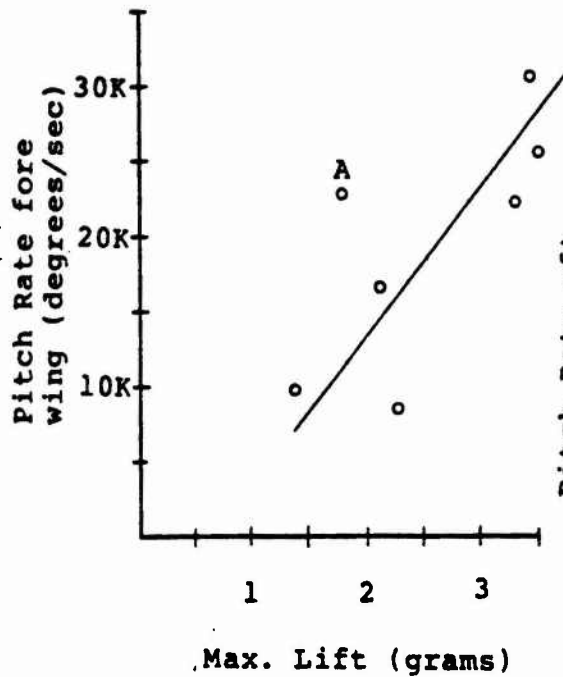


Figure I - Compares the maximum lift of a dragonfly verses the wing pitch rate and the wing maximum angle of attack for both the fore and aft wings.

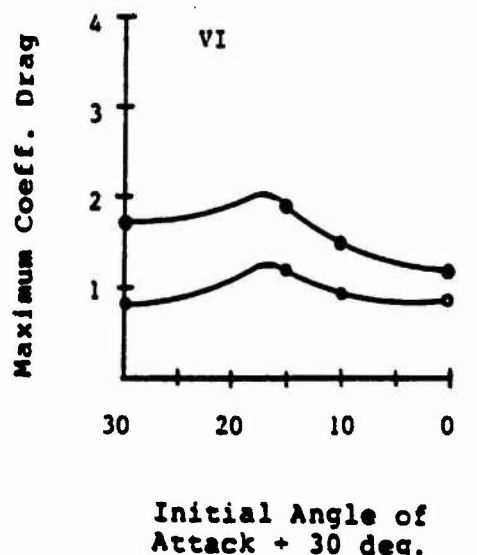
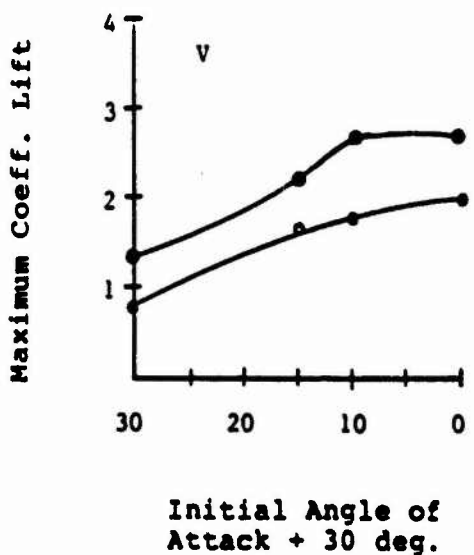
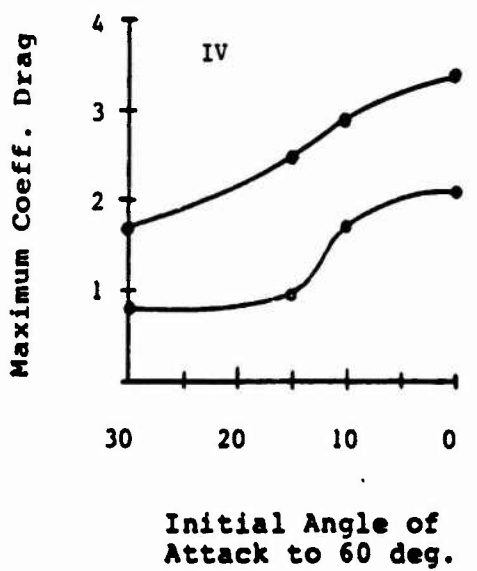
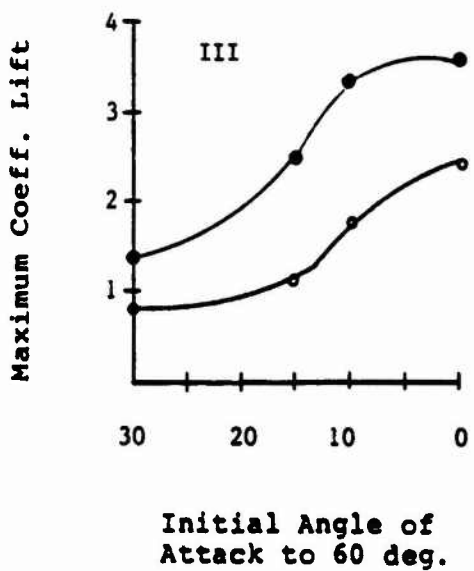
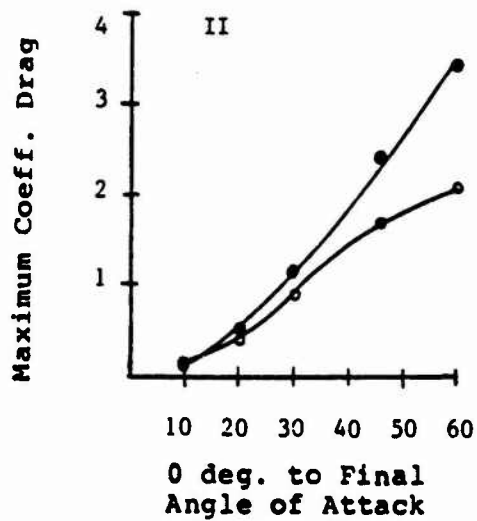
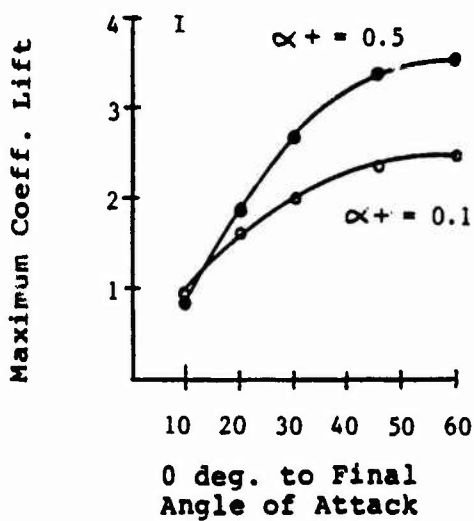


Figure II - Shows two different non-dimensional pitch rates, 0.5 and 0.1, and the effect that changing the initial or final angle of attack has upon the C_{lmax} and C_{dmax} of a NACA 0015 airfoil.

AL+ = 0.5 0-60

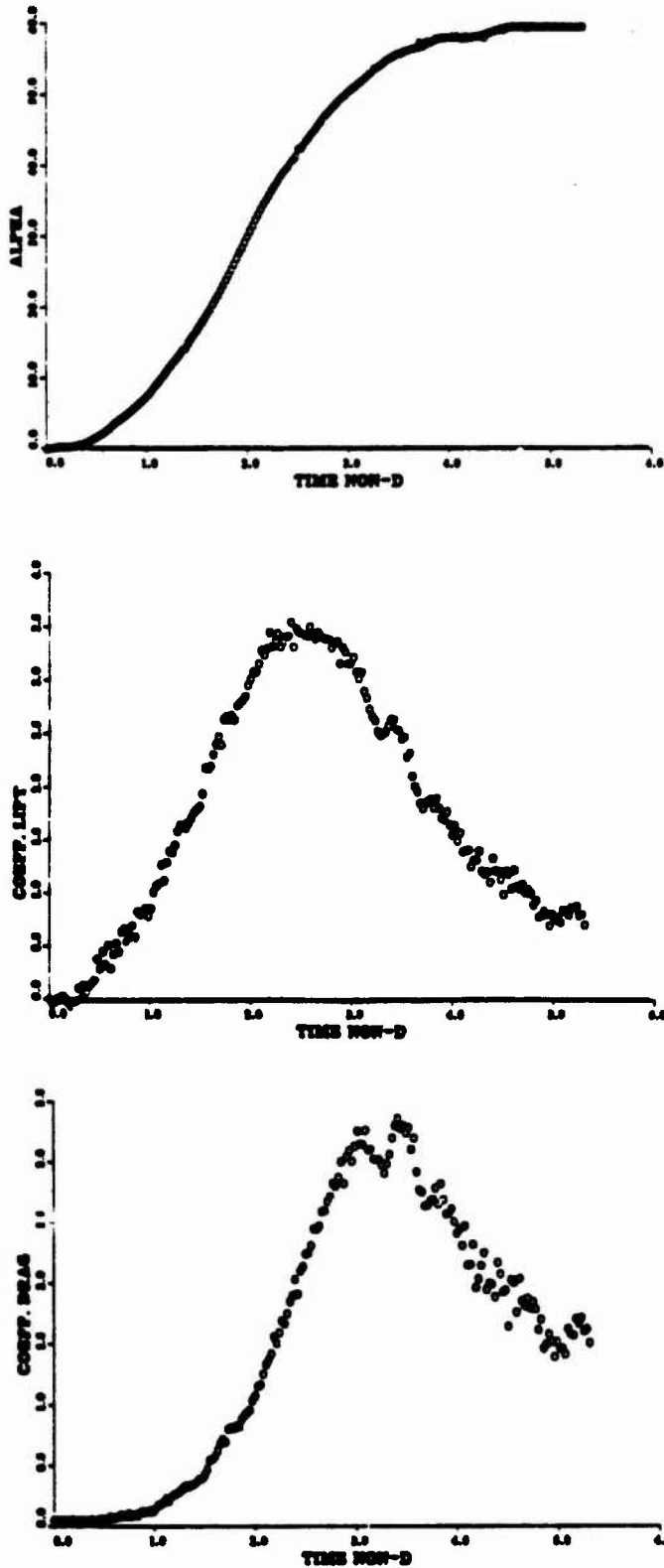


Figure III - Comparing non-dimensional time verse angle of attack and coefficients of lift and drag at a non-dimensional pitch rate of 0.5. The pitch is from 0 to 60 degrees.

AL+ = 0.1 0-60

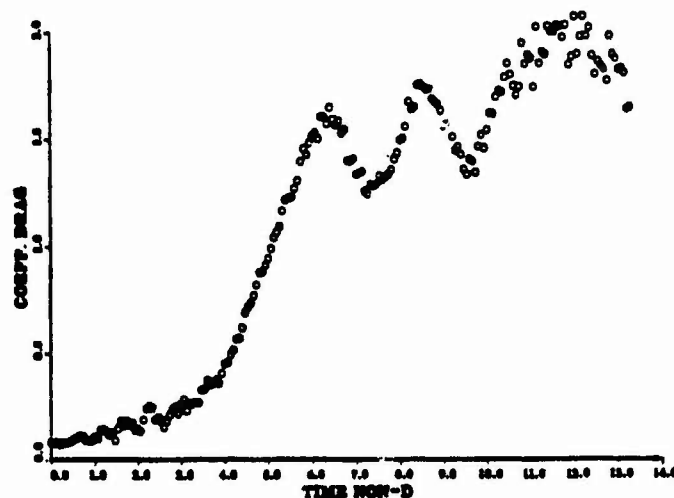
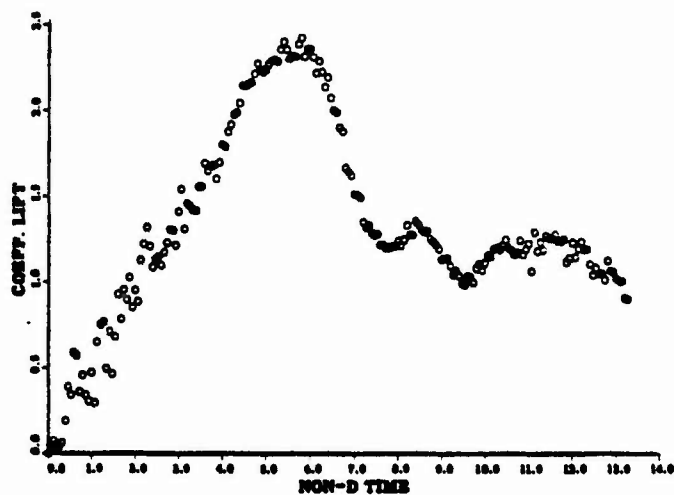
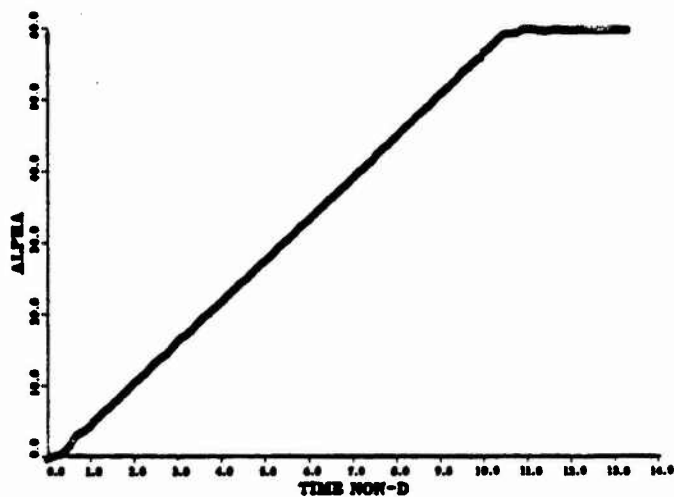


Figure IV - Comparing non-dimensional time verse angle of attack and coefficients of lift and drag at a non-dimensional pitch rate of 0.1. The pitch is from 0 to 60 degrees.

1987 USAF-UES SUMMER FACULTY RESEARCH PROGRAM/
GRADUATE STUDENT SUMMER SUPPORT PROGRAM

Sponsored by the
AIR FORCE OFFICE OF SCIENTIFIC RESEARCH

Conducted by the
Universal Energy System, Inc.

FINAL REPORT
AIRCRAFT REFUELING DEMONSTRATOR
USING A MICROBOT ALPHA II ROBOT

Prepared by: Bryan P. Riddiford
Academic Rank: Graduate Student
Department and: Electrical Engineering
University: The University of Dayton
Research location: AFWAL/FIEMB, WPAFB, Dayton, OH 45433
USAF Researcher: Capt. A. D. Davis
Date: Aug 21, 1987
Contract No.: F49620-85-C-0015

AIRCRAFT REFUELING DEMONSTRATOR

USING A MICROBOT ALPHA II ROBOT

by

Bryan P. Riddiford

ABSTRACT

A demonstration was set up using a Microbot Alpha II robot to study the feasibility of robotic ground-based aircraft refueling for use in chemically and biologically hazardous environments. An overhead gantry with the robot hanging beneath was designed to provide the easiest access to the aircraft midair refueling port. A 1/12 scale model of an F-16 was underneath and acted as the receiving aircraft. The midair refueling port was used so little or no modification was needed to accommodate existing aircraft. The robot was controlled by a Zenith-100 computer.

Acknowledgements

I wish to thank the Air Force Systems Command and the Air Force Office of Scientific Research for sponsorship of this research, and Universal Energy Systems for handling all the administrative aspects of this program.

It was a pleasure to work with Capt. Davis. I would like to thank Vergil King for helping me set up the robot in the beginning. The technicians and designers of the Systems Research Labs were also a great help.

I. Introduction

Today aircraft turnaround is a time consuming and manpower intensive process. In a CB environment the turnaround time is, at the minimum, doubled. By placing robots and automated machinery in the CB environment and protecting the operators in a clean room, the risks to humans is reduced and the turnaround time is not compromised. The use of the midair refueling port enables current production aircraft to be automatically refueled with little or no modification.

The Special Projects group at Wright Patterson AFB work on a number of experimental projects. They specialize in air cushion technology and power augmented wing-in-ground effects. Robotics is a new addition.

My interests have been in the electrical aspects of robotics. I have studied the Mitsubishi robot in my undergraduate work, and I have worked with the Adaptive Suspension Vehicle (ASV) project at the Ohio State University. The ASV is an experimental six legged walking vehicle funded by DARPA. I was involved in the electrical documentation and I wrote the operating system for a new onboard memory.

II. Objectives of the Research Effort:

I first had to apply classroom knowledge to the Microbot robot and become acquainted with its functions. The Alpha II is an excellent general purpose robot to learn robotic functions, because it is not damaged by trying to move the robot past its physical stops. The links are driven by electric stepper motors connected to cables and pulleys which are designed to slip under too much force (i.e. when the physical stops are hit, or about 8lbs.). The robot system also contains a teach control pendant to help teach the robots capabilities.

A general control program was written in BASIC, using the Zenith-100 computer and Zenith MS-DOS. The robot is controlled by specifying the location of the end effector in cartesian coordinates or by specifying the joint angles directly. It is also capable of storing the robots movements and recalling the movements sequentially.

The main objective is to design a demonstration platform to test and demonstrate the automatic aircraft refueling. We decided an overhead gantry built to hold the robot over the aircraft, and within reach of the refueling port, would be best. With the refueling being done over the plane, other operators or robots would be free to move around and under the plane. The gantry

could easily be built into the european aircraft bomb shelters, which are especially vulnerable to the Soviet CB attacks. Or the gantry could be a self standing system under which the aircraft taxies. The self standing gantry could be used in undeveloped areas. A new end effector or nand was designed to telescope into the midair refueling port. Sensors will need to be incorporated into the system to locate the refueling port.

III.

The first weeks were spent learning about the robot functions and capabilities and programming the robot using the teach control. I was unable to control the robot from the zenith using IBM MS-DOS and a gemini board as originally planned. I tried the Zenith MS-DOS which worked with a configuration of 9600 baud, 1 stop bit, 8 bit word, no parity, and DTR negative handshaking. Once the communication was completed I could start programming.

I computed the kinematics for the alpha II using the Deavit-Hartenburg notation (figure 1). For the program, however, I used a modified version of the kinematic equations given in the manual to compensate for the singularities and to increase the speed. The joint angles are defined in figure 2.

The kinematic equations (joint angles to cartesian coordinates), as given in the manual, are repeated here for reference.

H = 215.9mm base to shoulder height
L = 177.8mm Shoulder to elbow and elbow to wrist length
LL = 114.8mm Wrist to fingertip length
PI = 3.14159
C = 180 / PI

Pitch = $-0.5 \cdot (T4 + T5)$	1
Roll = $0.5 \cdot (T5 - T4)$	2
X = $[L \cdot \cos(T2 / C) + L \cdot \cos(T3 / C) + LL \cdot \cos(\text{Pitch} / C)] \cdot \cos(T1 / C)$	3
Y = $[L \cdot \cos(T2 / C) + L \cdot \cos(T3 / C) + LL \cdot \cos(\text{Pitch} / C)] \cdot \sin(T1 / C)$	4
Z = $H + L \cdot \sin(T2 / C) + L \cdot \sin(T3 / C) + LL \cdot \sin(\text{Pitch} / C)$	5

The inverse kinematics (cartesian coordinates to joint angles) are as follows. The first singularity occurs when $X=0$. In this case $T1$ (see figure 1 for definitions of the following variables) will be either 90 or -90 degrees depending on the sign of Y . The equation for $T1$ when $X=0$ is

$$T1 = \text{sgn}(Y) \cdot 90 \quad 6$$

When $X \neq 0$

$$T1 = \text{atn}(Y / X) \cdot C \quad 7$$

But by using equation 7 the quadrant is lost. A better solution is to check the quadrant and adjust equation 7 if needed. If $X < 0$ and $Y \leq 0$ (third quadrant) then

$$T1 = \text{atn}(Y / X) \cdot C - 180 \quad 8$$

If, however, $X < 0$ but $Y > 0$ then

$$T1 = \text{atn}(Y / X) \cdot C + 180 \quad 9$$

The angles $T4$ & $T5$ are with respect to the cartesian frame.

$$T4 = -\text{Pitch} - \text{Roll} \quad 10$$

$$T5 = -\text{Pitch} + \text{Roll} \quad 11$$

The height of the end effector from the shoulder level is

$$Z0 = Z - LL \cdot \sin(\text{Pitch} / C) - H \quad 12$$

The radius of the end effector from the base in the XY plane is

$$R0 = \text{sqr}(Y^2 + X^2) - LL \cdot \cos(\text{Pitch} / C) \quad 13$$

The second singularity occurs when solving for $T2$ & $T3$. The solution is identical to that for equation 7.

$$\alpha = \begin{cases} \text{sgn}(Z_0) \cdot 90 & \text{for } R_0 = 0 & 14 \\ \text{atn}(Z_0 / R_0) \cdot C & \text{for } R_0 > 0 & 15 \\ \text{atn}(Z_0 / R_0) \cdot C - 180 & \text{for } R_0 < 0, Z_0 > 0 & 16 \\ \text{atn}(Z_0 / R_0) \cdot C + 180 & \text{for } R_0 < 0, Z_0 < 0 & 17 \end{cases}$$

$$\beta = \text{atn} \left[\text{sqr} \left(\frac{4 \cdot L^2}{R_0^2 + Z_0^2} \right) - 1 \right] \cdot C \quad 18$$

Once alpha and beta are computed T2 & T3 may be computed directly

$$T_2 = \alpha + \beta \quad 19$$

$$T_3 = \alpha - \beta \quad 20$$

With the kinematic equations (variables T1, T2, T3, T4, T5, X, Y, Z, Pitch, Roll) available to the program a number of errors can be checked. The program checks for errors after the kinematic computations and before moving the robot. In this way the robot will not be allowed to move to an illegal position. The following is a list of possible errors.

Hand-body interference	Wrist-body interference
Hand-base interference	Wrist-base interference
Hand-slide interference	Wrist-slide interference
Reach out of range	Shoulder out of range
Elbow out of range	Pitch out of range
Roll out of range	Base out of range
Reach out of range for shoulder and elbow	

The next objective was to set up the robot as if it were in a shelter hanging from a gantry. I designed the gantry to be 7' X 7' X 6' high. The gantry enables the robot base full motion in the XY plane and can be raised or lowered 4 feet in the Z direction to accept different scale models. See figure 3. For the refueling demo the robot was set at 3'6". This height allows the robot access to the refueling port on the F-16 scale model. The end effector can be positioned anywhere within the gantry

boundaries by first using the XY platform for coarse movements and then using the XYZ capabilities of the robot itself for fine adjustments. By using the midair refueling port the robot hardware, software and sensory system are simplified because the refueling port accepts alignment errors of up to 30 degrees about the center line of the nozzle.

I designed a new telescoping end effector (figure 4). The end effector is a model of a fuel nozzle similar to the end of a midair refueling nozzle. SRL is currently refining the design.

IV. Recommendations

The robot control program can be enhanced by expanding the menu and adding new functions such as a delay until a switch is closed function. A function key could be made to toggle between two or more menus. The program could be compiled using a BASIC compiler and the I/O could be interrupt driven instead of being polled. Both of these changes would increase the speed which would allow more time for sensory computations.

The robot is currently controlled by an open loop. To increase the capabilities and finish the project a closed loop controller must be added. Each joint must have position feedback and the ability to detect cable slippage and motor stall. The feedback is necessary to safely move around an airplane refueling port. On a life size unit velocity feedback would also need to be included because of the large mass and inertia of the robot arm.

In addition to the joint feedback the robot will need feedback from its surroundings and some way of aligning with the refuel port. A simple ultrasonic sensor for collision avoidance cannot be used within an airport environment because of the noise. A more complex vision system (pattern recognition) used in conjunction with proximity sensors (retro-reflective) would work well. The sensors and the camera would be connected to the

nozzle at the end of the robot arm. The camera would be used by the operator as a monitor and possibly by the control system for pattern recognition to find the refueling port. One proximity sensor would be used for distance measurement, and another for the final fine alignment of the nozzle and the fuel port.

For a total refueling system (figure 5) a supervisory computer could control separate modules such as 1. the robot refuel arm controller, 2. the refueling controller to control fuel pumping, 3. the operator control panel to give the operator manual control in an emergency, and 4. the safety system for collision avoidance and possibly fire protection.

$${}^0T_E = \begin{bmatrix} r_{11} & r_{12} & r_{13} & p_x \\ r_{21} & r_{22} & r_{23} & p_y \\ r_{31} & r_{32} & r_{33} & p_z \\ 0 & 0 & 0 & 1 \end{bmatrix}$$

$$\begin{aligned} r_{11} &= -c_{123} \cdot s_4 - s_{123} \cdot c_4 \\ r_{12} &= c_{123} \cdot c_4 \cdot c_5 - s_{123} \cdot s_4 \cdot s_5 \\ r_{13} &= -c_{123} \cdot c_4 \cdot c_5 + s_{123} \cdot s_4 \cdot s_5 \end{aligned}$$

$$\begin{aligned} r_{21} &= s_{12-3} \cdot s_4 - c_{12-3} \cdot c_4 \\ r_{22} &= -s_{12-3} \cdot c_4 \cdot s_5 - c_{12-3} \cdot s_4 \cdot s_5 \\ r_{23} &= s_{12-3} \cdot c_4 \cdot c_5 + c_{12-3} \cdot s_4 \cdot s_5 \end{aligned}$$

$$\begin{aligned} r_{31} &= 0 \\ r_{32} &= c_5 \\ r_{33} &= s_5 \end{aligned}$$

$$\begin{aligned} p_x &= -c_{123} \cdot s_4 \cdot LL - s_{123} \cdot c_4 \cdot LL + L \cdot (c_{123} + c_{12}) \\ p_y &= s_{12-3} \cdot s_4 \cdot LL - c_{12-3} \cdot c_4 \cdot LL + L \cdot (-s_{12-3} + s_{12}) \\ p_z &= 0 \end{aligned}$$

Figure 1: Denavit-Hartenburg Kinematics for Alpha II

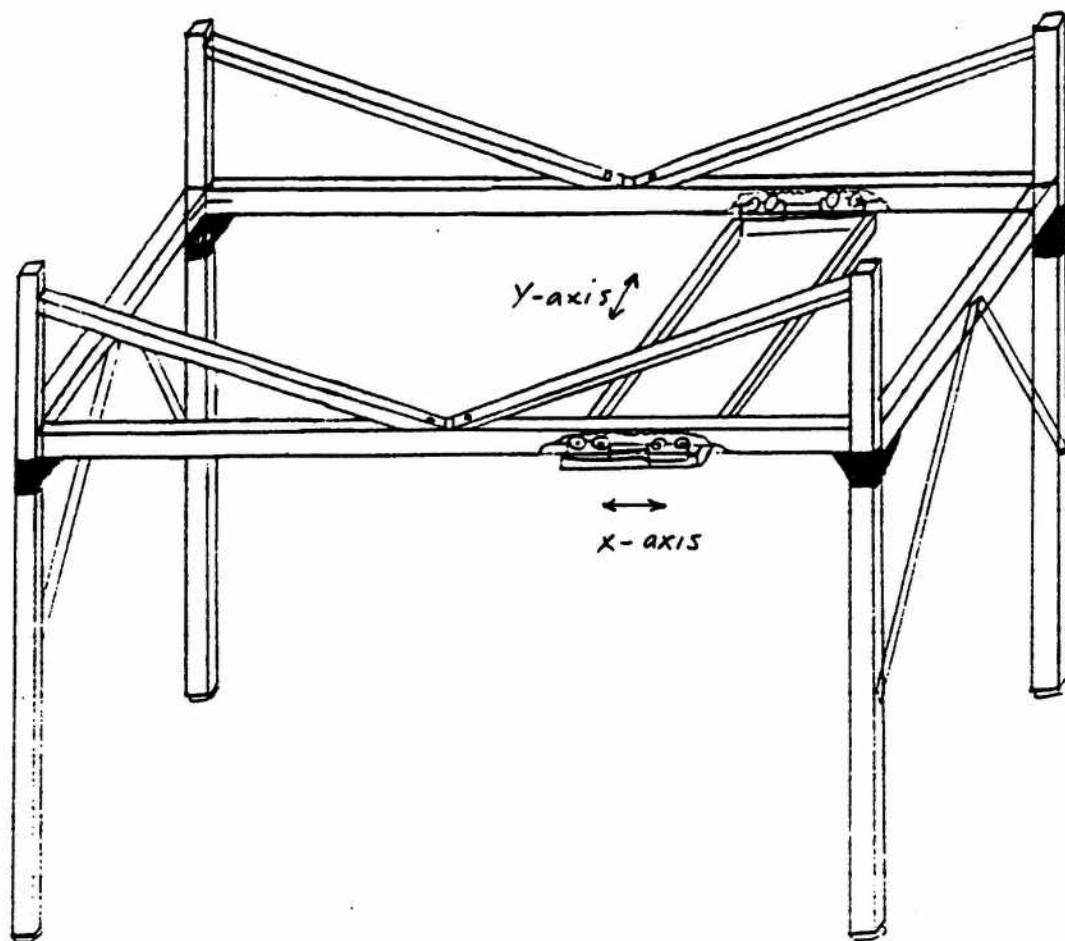


FIGURE 3: GANTRY ASSEMBLY
7ft x 7ft x 6ft high

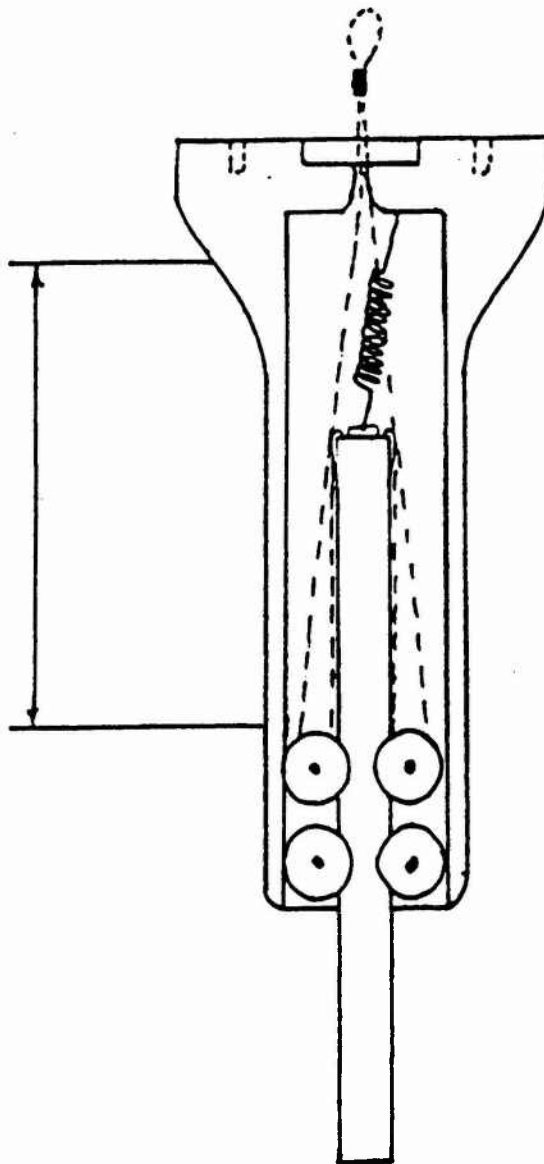


FIGURE 4: ROBOT TELESCOPING END EFFECTOR
MODEL FUEL PROBE

REFERENCES

Craig, J. J., Introduction to Robotics. Mechanics & Control., Reading, Mass., Addison-Wesley. 1986.

"Task II Report on Concept Development for Robotic Aircraft Turnaround," Battelle Research Inst., Columbus, Ohio, May 1987, pp. 11-14, 26-32. (to be published)

Schultz, Edwin R., "Robotic Refueling System for Tactical and Strategic Aircraft," Invention No. 16766.

1987 USAF-UES SUMMER FACULTY RESEARCH PROGRAM/
GRADUATE STUDENT SUMMER SUPPORT PROGRAM

Sponsored by the
AIR FORCE OFFICE OF SCIENTIFIC RESEARCH

Conducted by the
Universal Energy Systems, Inc.

FINAL REPORT

Influence of Moving Visual Environment on Saccadic Eye
Movements and Fixation

Prepared by: Keith A. Riese, M.S.E.E.
Academic Rank: Assistant Professor
Department and Electrical Engineering
University: University of Nebraska
Research Location: USAFSAM/NGFVL
Brooks AFB, TX 78235-5301
USAF Researcher: Dr. Edward J. Engelken

Date: 12 August 87
Contract No: F49620-85-C-0013

Influence of Moving Visual Environment on Saccadic Eye
Movements and Fixation

by

Keith A. Riese

ABSTRACT

Saccade parameters of amplitude, peak velocity, duration, and latency were compared for a stationary visual background environment versus a moving visual background environment to determine environmental effects. For visual stimuli, latency differences were significant ($p < 0.005$) while all other parameter variations were not. Mean saccade latency for a stationary visual background was 161.7 msec while for a moving visual background the mean latency was 175.3 msec. Saccades made in the same direction as the moving background showed minor variation as compared with those made in the opposite direction. No significant differences in saccade parameters were found when audio stimuli were used. Also, no parameter significance was found between target fixation and pseudo-target fixation.

Acknowledgements

I wish to thank the Air Force Systems Command and the Air Force Office of Scientific Research for sponsorship of this research. I also thank Universal Energy Systems for their administrative support of this program.

My experience was most rewarding due to the influence of many people, especially those in the Flight Vestibular Laboratory of the Clinical Sciences Division. Dr. James W. Wolfe and Dr. Edward J. Engelken provided me with support, encouragement, guidance, and a superb working atmosphere. The help of Sgt Virginia LaVan-Olsen, Sgt John Frey, and Sgt Gary Muniz was much appreciated. The computer expertise of Kenneth Stevens and statistical expertise of William Jackson were most valuable. The cooperation of all the participants made this study truly enjoyable.

I. INTRODUCTION

Characteristics of oculomotor function have been investigated in recent years. Many of these characteristics have been useful in developing oculomotor function criteria for pilots. These characteristics have also been useful in understanding, detecting, and treating pathological disorders of the oculomotor system.

Specific investigations have been made in the generation and execution of saccadic eye movements. Normal parameter values of eye position, saccade latency, peak saccade velocity, and saccade duration have been established by various eye movement measurement techniques. Additional peripheral factors affecting saccade generation and execution have not been given serious study. These include the affects of single and/or multisensory stimuli in a moving visual background. There is a need to establish normal parameter levels of oculomotor function under these conditions.

My research interest has centered in two areas: the oculomotor system's interaction with other senses, and the affect of pathological disorders on the function of the oculomotor system. My work in these areas has involved

comparing the oculomotor function of stuttering subjects with normal subjects and preliminary studies using audio, visual, and audio-visual stimuli.

The Flight Medicine Vestibular Laboratory of the Clinical Sciences Division of the USAF School of Aerospace Medicine at Brooks Air Force Base is particularly suited to eye movement studies dealing with the senses. Special facilities have been developed to measure eye movements involving visual and/or audio stimuli with computers used for data collection and analysis. The resulting information on saccadic eye movements from studies in this lab are useful in pilot evaluation and pathological determination.

II. OBJECTIVES OF THE RESEARCH EFFORT:

There is presently no clear evidence on how consistently the oculomotor system functions in a moving background visual environment versus a stationary background environment. It seems reasonable to assume that differing visual backgrounds have varying affects on the oculomotor system. Thus it is desirable to determine quantitatively the effect of saccadic eye movement parameters due to a moving visual background environment as well as the directional effect on these movements due to directional moving background environments.

An additional goal of this effort was to determine the oculomotor response during the latent period of a saccade. It would seem likely that the oculomotor response while fixating on a target is different from the response while pseudo-fixating on a spot where no target is but has just moved from (the latency period before a succeeding saccade begins).

My assignment as a participant in the 1987 Graduate Student Summer Support Program (GSSSP) was to determine what the significant differences in saccadic eye movements are as a function of background visual environment. Specific questions to be addressed were: What is the affect on saccadic eye movement parameters due to a moving visual background? Does the direction of background movement alter the directional oculomotor response in generating saccades? What differences, if any, appear in the parameters between fixation and pseudo-fixation? Answers to these questions will help determine oculomotor function under these varying conditions.

III.

a. The approach taken to reach the goals of this study was to record saccade eye movement data, generate oculomotor

parameter values from the eye movement data, and analyze these values to determine significance. Conclusions and recommendations would then be made on the results.

The physical apparatus for measuring and analyzing eye movements and eye movement data already existed in this lab. These included an anechoic chamber with visual and audio stimulus capacity, and infrared limbus-sensing recording spectacles with associated circuitry. Included were computers with programs for data collection and analysis.

Visual targets were provided by an array of nine green light-emitting diodes (LEDs) placed along an arc of two meters radius. The LEDs were positioned at angles of 0, 5, 10, 15, and 20 degrees either side of the center in the horizontal plane. Extinguished LEDs were not visible to the subject.

Audio targets were provided by nine loudspeakers located immediately behind the LEDs. The audio sound was a 1-kHz to 2-kHz band of noise of medium intensity. The speakers were not visible to the subjects.

An optokinetic nystagmus (OKN) drum was used to provide a moving visual background and was installed above the subject

chair. The OKN drum provided vertical stripes to all surfaces of the room. The stripes could arbitrarily be stationary, rotating clockwise, or rotating counter-clockwise. The light intensity was set at a subdued level: high enough to have a significant conscious affect on the subject but low enough so as to not overpower the visibility of the targets. Dark stripes measured 1/2 degree in width and white stripes measured 2 degrees in width on the target arc. A drum speed of 10 degrees/second provided optimum background movement. Slower speeds could easily be ignored by the subject while faster speeds would produce retinal slip, negating the moving background's affect.

Nine subjects, ages 19-44, participated in the study. None had any history of audio or vestibular problems and all but two (20/70 and 20/450) had normal eyesight. None were on prescription drugs. The subjects were each to sit for six runs of data collection with appropriate rest between runs as desired. A short calibration procedure preceded each run. Three of the runs consisted of the subject looking at a series of 80 visual target movements each. The other three runs required the subject to look at a series of 80 audio target movements each. For each type of target, one run had stationary stripes, one run had clockwise moving stripes, and one run had counter-clockwise moving stripes.

All runs were conducted in a random sequence.

Target motion appeared instantaneous to the subjects. Visual target motion was created by extinguishing the currently illuminated LED and simultaneously illuminating the LED at the new target position. Audio target movement was realized by simultaneously switching the noise source from one loudspeaker to another.

Target presentation and data collection were accomplished with the aid of a Digital Equipment Corporation PDP-11/34 computer. A digital I/O buffer controlled the target presentation apparatus. Eye movement data were recorded by the computer through an A/D converter sampling at a 1000 samples/second rate. Programming was done in FORTRAN except for MACRO control of the A/D, real-time clock, and digital I/O buffer. Subject raw data were stored in computer disk files. An array processor with a PDP-11/24 was used to calculate eye movement parameters of saccade amplitude, saccade duration, peak saccade velocity, and saccade latency from the raw data files. A separate program was developed to align the final fixation data of one saccade with the pseudo-fixation latent period data of the next saccade. All of this parameter data were statistically analyzed by SAS, a standard computer statistical analysis program.

b. Results of the four oculomotor parameters tested were achieved by visual and statistical methods. Main sequence plots for visual analysis were made by plotting parameter values for each saccade. These plots, with 80 data points on each plot, were difficult to evaluate for significance. Plots were also made for averages over groups of saccades including standard deviations. Latency differences were apparent on these plots.

Statistical significance of parameter variations were determined on the computer using the SAS statistical program. The three saccade parameters of peak velocity, saccade amplitude, and final position) showed little change for either audio or visual stimuli pertaining to stationary versus moving visual background environments. There were also no directional affects, such as when saccades were made in a direction the same as the direction of the moving background compared with those made in the opposite direction.

The only saccadic parameter of significance was saccade latency. With visual stimuli saccade latency was longer for a moving visual background than for a stationary one. The mean latency for a stationary background was 161.7 msec while for a moving background the mean latency was 175.3

msec ($p < 0.005$). No directionally sensitive significance was found relating background movement to saccade direction.

Audio stimuli produced no significant change in saccadic latency in any case. Latency did tend to be slightly longer for saccades in the same direction as the direction of background movement, but was not statistically significant. There was no significant difference in the saccade latency for still versus moving background for audio stimuli.

IV.

a. Using the same physical apparatus discussed previously, parameter data were collected for the last period of fixation on a target and compared with the first 80 msec of the latency before the next saccade. Average velocity and RMS values of position and velocity were determined for saccades to each of the nine target positions and then analyzed.

b. Target fixation parameter values showed no detectable differences from pseudo-fixation values. The results indicate the oculomotor system during pseudo-fixation has not had time to realize a target no longer exists to fixate on. Also, total attention of the oculomotor system may be taken up in the process of generating the next saccade,

making intervention during the latent period "unnecessary."

V. RECOMMENDATIONS

a. There is a significant effect on saccade latency due to the type of visual background present. Pilot function criteria needs to take this into account. A "normal" value for this latency difference should be determined as a test standard. Ophthalmologists should be aware of this difference for pathological uses.

b. Continuing research on saccade latency in a moving visual background environment is indicated. This would help determine where the oculomotor system is being affected by the moving background. Using an OKN drum, certain parts of the stripe pattern could be projected (and other parts blocked out) which would help determine retinal involvement in the changed saccade latency. Foveal versus peripheral retinal involvement would be indicated by blocking foveal or peripheral regions of the drum and measuring saccade latency. Blocking the right or left half of the drum would indicate a hemi-field effect, if present. A more exhaustive study with a larger population of subjects would indicate a "normal" latency difference. It is recommended a further summer effort and/or mini-grant should be appointed to give

this complete and detailed attention. A joint appointment of both university professor and graduate student is suggested.

c. The fixation versus pseudo-fixation results do not indicate further study. The time periods of less than 100 ms for each condition are very short and little oculomotor function dealing with fixation variation appears to be occurring.

REFERENCES

1. Arnoult, M. D., "Localization of Sound During Rotation of the Visual Environment," American Journal of Psychology, 1952, Vol. 65, pp. 48-58.
2. Boghen, D., B. T. Troost, R. B. Daroff, L. F. L. F. Dell'Osso, and J. Z. Birkett, "Velocity Characteristics of Normal Human Saccades," Investigative Ophthalmology, 1974, Vol. 13, No. 8, pp. 619-623.
3. Engelken, Edward J., Influence of Visual and Auditory Stimuli on Saccadic Eye Movements, University of Texas, Austin, Tx, May 1987.
4. Kapoula, Z. A., D. A. Robinson, and T. C. Hain, "Motion of the Eye Immediately After a Saccade," Experimental Brain Research, 1986, Vol. 61, pp. 386-394.
5. Mastroianni, George R., "The Influence of Eye Movements and Illumination on Auditory Localization," Perception and Psychophysics, 1982, Vol. 31, No. 6, pp. 581-584.
6. Robinson, D. A., "Control of Eye Movements," Handbook of Physiology, 1981, Section 1, Vol. 2, Part 2, American Physiological Society, pp. 1275-1320.
7. Stream, Richard W., E. T. Whitson, and V. Honrubia, "Visual Tracking of Auditory Stimuli," Journal of Auditory Research, 1980, Vol. 20, pp. 223-243.

8. Thurlow, W. R., and T. P. Kerr, "Effect of a Moving Visual Environment on Localization of Sound," American Journal of Psychology, 1970, Vol. 83, pp. 112-118.
9. Traccis, S., L. A. Abel, and L. F. Dell'Osso, "Audio-Ocular Response: Saccadic Programming," Aviation, Space, and Environmental Medicine, 1984, Vol. 55, pp. 735-739.
10. Zahn, J. R., L. A. Abel, and L. F. Dell'Osso, "Audio-Ocular Response Characteristics," Sensory Processes, 1978, Vol. 2, pp. 32-37.
11. Zahn, J. R., L. A. Abel, L. F. Dell'Osso, and R. B. Daroff, "The Audioocular Response: Intersensory Delay," Sensory Processes, 1979, Vol. 3, pp. 60-65.
12. Zambarbieri, D., R. Schmid, G. Magenes, and C. Prablanc, "Saccadic Responses Evoked by Presentation of Visual and Auditory Targets," Experimental Brain Research, 1982, Vol. 47, pp 417-427.

1987 USAF-UES FACULTY RESEARCH PROGRAM/
GRADUATE STUDENT SUMMER SUPPORT PROGRAM

Sponsored by the
AIR FORCE OFFICE OF SCIENTIFIC RESEARCH

Conducted by the
Universal Energy Systems, Inc.

FINAL REPORT

Thermal Stress and its Effects on Fine Motor

Skill and Decoding Tasks

Prepared by: M. Carolyn Robinson
Academic Rank: Graduate Student
Department and Health, Physical Education, and Recreation
University: The University of Alabama
Research Location: School of Aerospace Medicine
Chemical Defense Branch
Brooks AFB
San Antonio, TX 78235
USAF Researcher: S. H. Constable, Ph.D.
Date Prepared: September, 1987
Contract No: F49620-85-C-0013

Thermal Stress and Its Effects on Fine
Motor Skill and Decoding Tasks

by

M. Carolyn Robinson

Abstract

The current thermal research being done on the Chemical Defense Ensemble (CDE) has focused on work productivity as measured by the amount of time a subject is engaged in gross motor movement. To help determine if thermal stress has an effect on fine motor and cognitive skills, two tasks were utilized to measure any change in these skills. The fine motor skill task was a hand-eye steadiness task; the cognitive task was a decoding task. An examination of the data indicated that under the thermal stress induced by a work-rest protocol resulting in a cyclic body core temperature (T_{re}), 1) there appears to be a trend between T_{re} and fine motor performance; 2) there does not appear to be a trend between T_{re} and decoding performance.

An examination of the data from this study indicates that personnel experiencing a cyclic variation in T_{re} may preserve cognitive functioning, but may suffer a decrement of steadiness performance. The results of the decoding task may be an indication that the task utilized is not sensitive to T_{re} .

Acknowledgements

I wish to thank both the Air Force Office of Scientific Research and Universal Energy Systems for the opportunity to participate in this research effort.

The following individuals helped to make my experience an enriching and rewarding one, professionally and personally. Thank you all.

Phillip A. Bishop, Ed.D.

Stefan H. Constable, Ph.D.

John Garza

Sally Nunneley, M.D.

Tai Chen

William Storm, Ph.D.

Cadet Bruce Brady

Suzanne Enlow

Ann Miksch

Liz Staves

Tom Wells, Ph.D.

Roxanne Constable

All the chamber technicians and crew who helped to insure the safety of our subjects, and finally,

All of my subjects, each of whom has willingly made a contribution to our country by participating in this study.

I. INTRODUCTION

Recent emphasis has been placed on research concerning the military's chemical defense ensemble (CDE). When the CDE is worn while engaging in physical activity, the wearer's body core temperature (T_{re}) increases dramatically, relative to the environmental temperature. This aspect of CDE usage has been recognized and ways to minimize this increase are being tested. Because of the temperature increments experienced, the wearers participate in a work-rest cycle causing a cyclic variation in T_{re} .

While the ground crews wear the CDE, they are required to perform specific tasks, some highly skilled requiring concentration and manual dexterity. A test procedure including the measurement of two psychomotor skills was indicated.

Because my undergraduate minor is psychology with an interest in the cognitive process, this aspect of the CDE testing was of particular interest and concern to me.

My graduate study is in the field of Health Education with work in exercise physiology and psychology. The blending of these two disciplines has helped to equip me to work within this particular framework.

II. Objectives of the Research Effort

Prior thermal stress research has focused primarily on body temperature (rectal and/or skin) and heart rate. Thermal stress has generally been induced by gross muscle activity (work) and/or environmentally induced. In military and industrial settings the use of protective clothing (CDE) while engaging in physical labor exacerbates the thermal stress response resulting in the need for a rest period to allow the body to cool. The resultant work-rest cycle causes a cyclical increment/decrement in heart rate, skin temperature, and T_{re} . When external supplemental cooling is provided the cyclic amplitude in T_{re} is increased.

The purpose of this study was to examine subjects' fine motor and cognitive responses in relation to cyclic variation of T_{re} as a result of concomitant work and environmentally induced thermal stress when tested in a work-rest protocol which included microenvironmental cooling during the rest cycle.

III. The Study

The subjects were composed of volunteers, three military (all males) and two civilians (1 male, 1 female). The male civilian was a participant on three separate occasions, making a total of 7 experimental observations. Subjects were heterogeneous concerning age, acclimatization state, and physical activity and fitness levels.

Each subject participated in two training sessions consisting of three trials of both a fine motor task and a cognitive task in order to reduce the influence of the learning curve. The training scores of both tasks were posted on record sheets (Appendix A). A baseline score was established immediately prior to the experimental situation. Experimental scores were posted on separate record sheets (Appendix B). During both training sessions subjects wore the CDE jacket, M-17 mask and hood, and rubber gloves with cotton glove liners. The baseline data were collected while the subject wore the full CDE gear which also included CDE pants, standard issue fatigues, a heart monitor, rectal probe, four skin thermistors, and a microenvironmental cooling system beneath the CDE jacket (total clo = 2.55 and im/clo = .280). They also wore their own athletic shoes; the standard rubber boot covers were eliminated for safety purposes.

A microenvironmental liquid cooling system was used with three subjects. Four subjects were cooled by an air system. The liquid cooling system consisted of a close-fitting ILC Dover liquid cooling vest which covered about .5 square meters of the upper body. The vest included approximately 48 meters of tygon tubing with quick release, self-sealing connectors. An electrically powered cooling system supplied liquid coolant to the vest at a rate of .8 liters of coolant per minute at 10-15 degrees C. A coolant of 95% water, 5% propylene glycol was used.

The microenvironmental air-cooled system was composed of a mesh vest through which air flowed from an inlet hose and was distributed over the upper torso (90%) and face (10%). A separate mask adapted for the air cooling system was used. Mean air temperature to the vest was maintained 15-20°C.

Heart rate, skin temperature, and T_{re} were monitored and recorded each 30 seconds on a PDP-11 computer by means of a system custom-developed by John Garza (OAO Corp.). Gross motor movement (work) was accomplished by having the subject walk on a motorized treadmill at 3 mph, 3% or 6% grade depending upon fitness level (35-40% of VO_2^{max}). The subject worked in a thermal chamber under one of the following conditions.

28°C, working 45 minutes followed by a 15 minute rest period during which the subject was tested and cooled.

38°C, working 30 minutes followed by a 30 minute rest period during which the subject was tested and cooled.

At the beginning of the rest cycle the subject was escorted to a chair and was immediately tested with a fine motor performance task and a cognitive task. These were repeated prior to the resumption of the work cycle.

III. Method

a. The fine motor task was a hand-eye coordination steadiness task which lasted for a 60-second period. During this time the subject held a wand (approximately 17.5 cm long) which was inserted

through a hole (approximately 1 cm in diameter) located in a metal plate. Each time the wand touched the side of the hole, a buzzer sounded and the length of touching time was recorded. At the end of the 60 second period the total touching time was recorded, rounded to the nearest tenth of a second.

Cognitive function was measured by a decoding task which was a modification of the Wechsler (1955) digit symbol substitution test. The 90 second test required subjects to identify a digit (1-9) which had been paired with one of nine letters randomly assigned. These randomly assigned number-letter combinations appeared on the NEC computer LED screen. Beneath the nine pairings one letter appeared, requiring the subject to identify as quickly as possible the number which was paired with it in the row above. When selection was made, another letter was presented. The computer recorded the number of correct responses, attempted responses, and response time.

III. Results

b. A review of the literature concerning hyperthermal stress and human performance yields no definitive evidence of a causal relationship. Chiles (1957) found no effect upon performance under high environmental temperature; Fine & Kobrick (1985) found no decrement of performance during hyperthermia; and Sharma (1983) and Bell (1978) in separate studies found that performance on certain tasks declined while performance on other tasks was not negatively affected.

An examination of Figure 1 reveals a strong association between Tre and steadiness. As body temperature increased, so did the amount of touching time. As body temperature decreased, less touching time was noted.

The cognitive function (decoding) test is much less clear in its results (Fig. 2). An inverse relationship between Tre and number of correct responses (Fig. 2) was expected, i.e., an increase of Tre would result in a decrease of correct responses; a decrease of Tre would result in an increase of correct responses. Instead, there appears to be no obvious trend; an increase in Tre resulted in both increases and decreases of correct responses. Because of the small sample size available and the small effect size anticipated, no statistical tests were performed.

IV. Recommendations

The tasks which ground crews are required to perform while wearing the CDE are varied. They range from simple to complex, both physical and cognitive tasks, many of which require intense concentration and dexterity. Because of the differing results of various studies, it seems that the prudent course of action is to investigate the effects of thermal stress upon the performance of specific tasks which are required of the ground crew. It is very possible that the varying results obtained in this and other studies are task-specific, i.e., the results cannot be generalized from one task to another one.

Another possible explanation of the results of this and other studies may lie in the fact that most studies are conducted with a small number of subjects. Individual variation may weight the results unduly, obscuring the meaning of any relationship which may exist. A larger sample size is needed to detect significance small effects.

Because most studies have been conducted in the laboratory using tasks which are far removed from those engaged in by the ground crew while performing their jobs, it is recommended that thermal studies in the field under "normal" environmental temperatures with tasks which are performed by the ground crew on a regular basis be conducted. These studies should simulate actual work conditions, including war time, when tasks will be performed on a more continuous basis for a long duration. Assessments regarding error rates under these conditions would be valuable.

References

1. Allan, J. R. and T. M. Gibson, "Separation of the Effects of Raised Skin and Core Temperature on Performance of a Pursuit Rotor Task," Aviation, Space, and Environmental Medicine. July 1979, 678-682.
2. Bell, Paul A., "Effects of Noise and Heat Stress on Primary and Subsidiary Task Performance," Human Factors. (1978) 20(6), 749-752.
3. Chiles, W. D., "Effects of Elevated Temperatures on Performance of a Complex Mental Task," Ergonomics. (1979) 2:89-96.
4. Fine, B. J. and J. L. Kobrick, "Assessment of the Effects of Heat and NBC Protective Clothing on Performance of Critical Military Tasks," Health and Performance Division, U. S. Army Research Institute of Environmental Medicine, Natick, Massachusetts 01760, Technical Report No. T11/85; June 1985.
5. Sharma, V. M., G. Pichan, and M. R. Panwar, "Differential Effects of Hot-Human and Hot-Dry Environments on Mental Functions," International Archives of Occupational and Environmental Health. (1983) 52:315-327.
6. Wechsler, D. Manual for the Wechsler Adult Intelligence scale, New York: Psychological Corp., 1955.

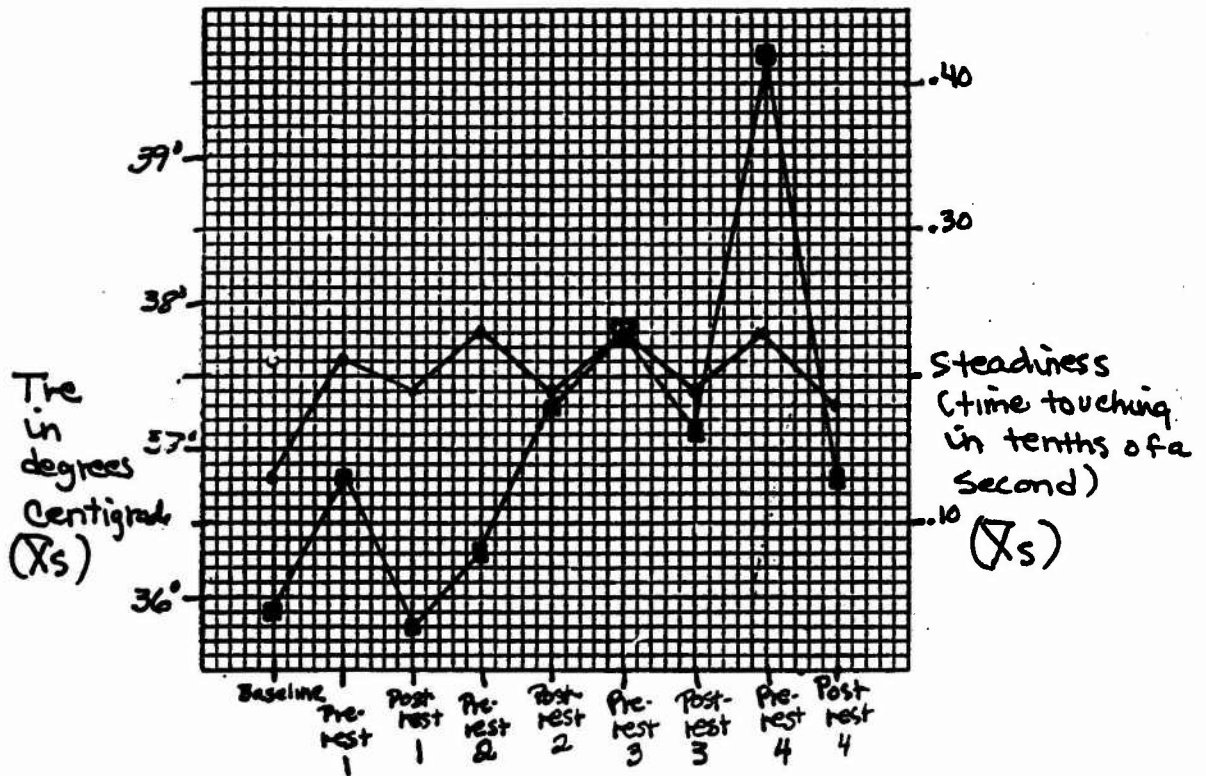


Fig. 1. Tre vs. Steadiness Task (fine motor skill) plotted throughout the experiment. Steadiness conforms closely to the pattern which Tre follows.

●— Tre (Xs)
 ■— Steadiness (Xs)

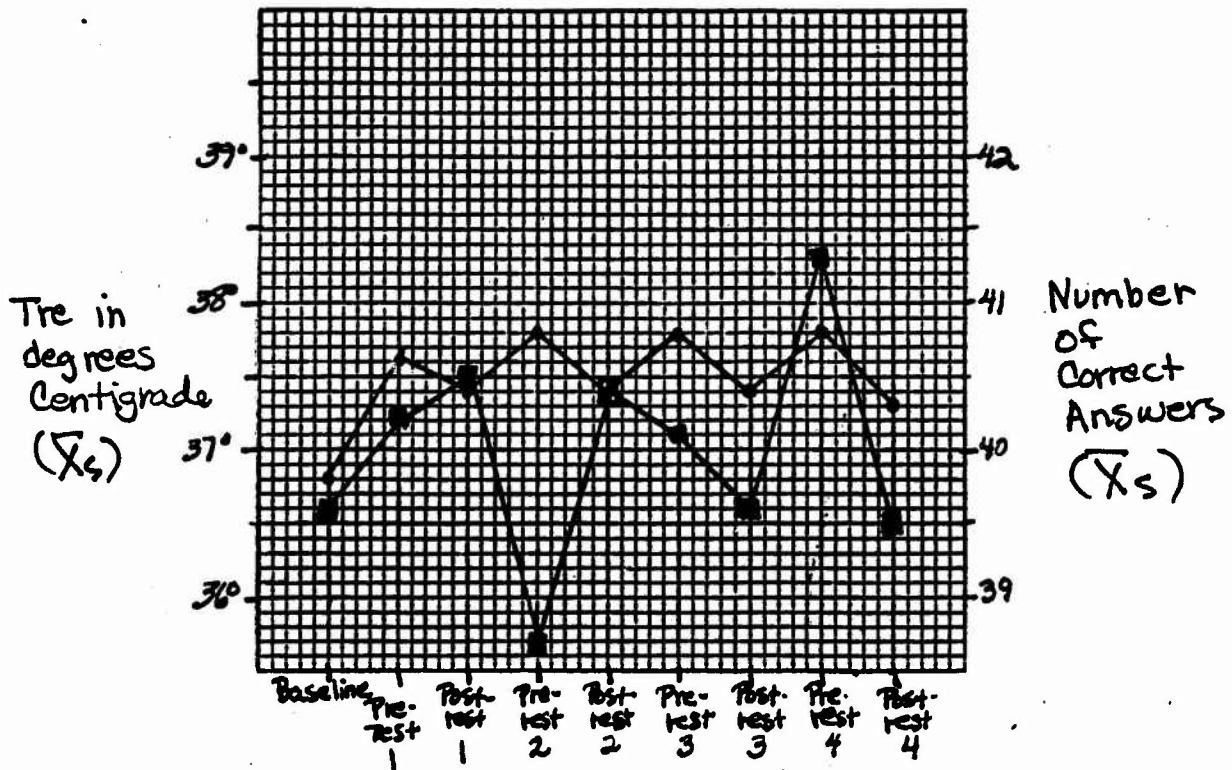


Fig. 2. Tpe vs. Decoding Task (Cognitive Skill), plotted throughout the experiment. Decoding scores do not necessarily conform to the pattern which Tpe follows.

—■— Tpe (Xs)
 —●— Number of correct answers (Xs)

Appendix A

SUBJECT:

DATE: _____

CONDITION: TRAINING

	STEADINESS	CODE SUBSTITUTION
1)		
2)		
3)		
1)		
2)		
3)		
	TIME TOUCHING (SECS)	# CORRECT, # ATTEMPTED, #PRESENTED; X, S.D.

Appendix B

SUBJECT:

DATE: _____

CONDITION:

STEADINESS

CODE SUBSTITUTION

BASELINE:

time _____ core temp _____ _____

REST PERIOD #1:

time _____ core temp _____ _____

time _____ core temp _____ _____

REST PERIOD #2:

time _____ core temp _____ _____

time _____ core temp _____ _____

REST PERIOD #3:

time _____ core temp _____ _____

time _____ core temp _____ _____

REST PERIOD #4:

time _____ core temp _____ _____

time _____ core temp _____ _____

REST PERIOD #5:

time _____ core temp _____ _____

time _____ core temp _____ _____

REST PERIOD #6:

time _____ core temp _____ _____

time _____ core temp _____ _____

1987 USAF-UES SUMMER FACULTY RESEARCH PROGRAM/
GRADUATE STUDENT SUMMER SUPPORT PROGRAM

Sponsored by the
AIR FORCE OF SCIENTIFIC RESEARCH

Conducted by the
Universal Energy Systems, Inc.

FINAL REPORT

DESIGN OF A MECHANISM TO CONTROL WIND TUNNEL TURBULENCE

Prepared by: Filiberto Santiago
Academic Rank: Master Degree Candidate
Department: Mechanical Engineering
University: University of Puerto Rico, Mayaguez Campus
Research Location: Arnold Engineering Development Center/
 Arnold AFS, DOTR
USAF Researcher: Daryl Sinclair/CALSPAN'S Technology
 Applications Section
Date: September 20, 1987
Contract No. F49620-85-D-0013

Copy available to DTIC does not
permit fully legible reproduction

DESIGN OF A MECHANISM TO CONTROL WIND TUNNEL TURBULENCE

by

Filiberto Santiago

ABSTRACT

My appointment period for the 1967 U.S.A.F. Graduate Student Support Program was from 6/1/67 to 8/7/67. I worked as Research Assistant to Dr. Marco A. Egoavil and under the supervision of Mr. Daryl Sinclair/CALSPAN'S Technology Applications Section. The following report covers my assignment for the ten week period.

The research investigation was performed in the Arnold D.F.G. Acoustic Research Wind Tunnel. An extensive literature survey was done during the first weeks covering the fundamental aspects of the "TURBULENCE" phenomena. Turbulence of the air stream is generally recognized as a variable of considerable importance in many aerodynamics phenomena, specially those observed in wind tunnels.

In the Acoustic Research Wind Tunnel turbulence was generated in the stilling chamber using two devices. First a grid 20.5 in. by 20.5 in. with 1/2 in. diameter rods. This grid was used in two ways, one the grid by itself and the other the grid with small legs attached to the horizontal center line and to the vertical center line. Second a manifold with fourteen jets producing a flow of air perpendicular to the main stream flow in the wind tunnel.

The turbulence level of the tunnel with the grid is approximately 3%. The goal was to get at least 20% or more of turbulence and according to some of the experimental runs it is possible to get up to 27.4% which is very encouraging by the use of jets.

Nomenclature

Item	Description	Units
P ₀	Total or Stagnation Pressure	psia
T ₀	Total or Stagnation Temperature	R
P _s	Static Pressure	psia
M	Mach Number	none
s.c.	Stilling Chamber	none
T _s	Static Temperature	R
U	Velocity	ft/s
E _{nl}	Non-linear dc Output	volts
E _{rms}	Root Mean Square Output	volts
Turb.	Turbulence	%
Jets no.	Number of Jets	none
P _{man}	Manifold Pressure	psia
m	Mass Flow	lb/s
m _{jet}	Jets Mass Flow Over s.c. Mass Flow	%

Copy available to DTIC does not permit fully legible reproduction

I. Introduction

I began to study Mechanical Engineering in 1979 at the University of Puerto Rico. In 1982 I was accepted to work under the Cooperative Education Program for N.A.S.A./Wallops Flight Facility in Virginia. Here I worked in the Mechanical Systems Section for a year in two separate periods; seven months in 1983 and five months in 1984. This experience gave me the opportunity to work in N.A.S.A.'s sounding rocket program. I learned different techniques for the redesign of mechanical devices in payloads, computer programming and professional drafting skills. In May of 1985 I finished my B.S.M.E. and that summer I worked for ALCOA (Aluminum Company of America) in Pittsburgh, Pennsylvania. Here I worked in the Equipment Division at the R & D facility. My project was to verify a Finite Element Mathematical Model of a forging simulation process with laboratory experimental tests (part of the Near Net Shape Technology). I developed and became familiar with skills in the design of experiments, how to make a presentation, computer skills and the ability to work with many people and technicians from other divisions. For ALCOA I worked two summers and I attend during regular semesters to graduate school at the University of Puerto Rico. For the summer of 1987 I was accepted to work for the Air Force Office of Scientific Research Program under the DOTR (Directory of Technology and Research) division. The project objective is to develop a technique to control wing tunnel turbulence. This is an thesis research project and is the subject that I am currently analyzing. I started this project of Turbulence Generation in January of 1987. I decided to apply to

I. Introduction

I began to study Mechanical Engineering in 1977 at the University of Puerto Rico. In 1981 I was accepted to work under the Cooperative Education Program for M.S.B. (Mallory Flight Facility) in Virginia. Here I worked in the Mechanical Systems Section for a year in two separate periods; seven months in 1983 and five months in 1984. This experience gave me the opportunity to work in M.S.B.'s sounding rocket program. I learned different techniques for the redesign of mechanical devices in order to improve performance, and process cost, drafting abilities. In May of 1985 I finished a B.S.M.E. and thereafter I worked for ALCOA (Aluminum Company of America) in Pittsburgh, Pennsylvania. Here I worked in the Equipment Division at the R & D facility. My project was to verify a Finite Element Mathematical Model of a forging simulation process with laboratory experimental tests (part of the Near Net Shape Technology). I developed and became familiar with skills in the design of experiments, how to make a presentation, computer skills and the ability to work with very particular formulations from other divisions. For ALCOA I was part of the design and I started to do regular assignments to graduate students at the University of Puerto Rico. For the summer of 1987 I was a research assistant for the Air Force Office of Scientific Research. My work was under the DOTS (Directorate of Technology and Systems) program. The project objective was to develop a simulation model for the design of a turbine. This was a highly technical project and as the project progressed I started to do more and more work. I started to work as a Technical Representative in January of 1987. I decided to work as

the program because; my thesis research advisor suggested me to do so, it is real research, I found it challenging and it will allow me to fulfill the requirements of an M.S.M.E. I applied to work at Arnold Engineering Development Center in Tullahoma, Tennessee because there primary work is in Wind Tunnel Testing. This result proved to be a good match of job and person.

II. Objectives of the Research Effort

The objective of this research effort is to develop a device to generate variable "Turbulence Levels" on air streams in wind tunnel testing. Researchers at A.E.D.C. want to study the effect of the turbulence level on experimental data. The device should allow researchers to perform experiments where having Mach and Reynolds Numbers fixed the level of turbulence could be increased independently. At the present time there is control over the Mach and Reynolds Numbers but not precisely over turbulence.

The final design will be used for testing a Transonic Technology (TST) Wing in the 4T Wind Tunnel. This specific test is a joint venture of the Air Force, N.A.S.A., and the Government of West Germany. Initially the preliminary goal was to test the use of jets to generate turbulence. But after the literature survey the idea of using a grid to increase turbulence level was added during the course of the research effort. The use of a grid is an economical alternative and after a telephone conversation with Mr. Norman Meese who is Coordinator of Wind Tunnel Testing at the National Bureau of Standards in Gaithersburg Md. the idea of using square tags in the grid became part of the actual experimental setup.

During my 1987 S.F.R.P. important data were collected. Turbulence was generated by jets, grid and grid with tags. More research needs to be done in the jets and grid with tags techniques. This will continue with funding from the Mini Grant Program.

III. Test Apparatus

3a. Acoustic Research Tunnel

The experimental testing was performed in the Acoustic Research Tunnel (A.R.T.). The Acoustic Research Tunnel is an in-draft tunnel with constant stagnation pressure (atmospheric) and very low level of generated turbulence.

The stilling chamber is square in cross-section and is composed of a number of flanged sections. This segmentation of the stilling chamber allows easy installation of grids, honeycombs, screens and jets in multiple arrangements. The stilling chamber section is 20.5 in. by 20.5 in. The test section is 6 in. by 6 in. and has a surrounding plenum chamber. The tunnel pressure ratio and plenum chamber pressure is controlled by valves in the exhaust line. Mach numbers normally obtainable extend to up to 1.10. A sketch of A.R.T. is presented in (fig.1).

3b. Test Items

The items were tested in the tunnel stilling chamber. The first item is a grid 20.5 in. by 20.5 in. with 1/2 in. diameter rods (see drawing 102). This grid was used in two ways, one the grid by itself and the other the grid with small tags attached to the horizontal center line and to the vertical center line. The second item is a manifold with fourteen jets producing a flow of air perpendicular to the main stream flow in the wind tunnel (see drawing 101).

3c. Hot Wire Sensor

The hot wire sensor used in this program was a DISA R Fiber-film probe. The wire has a Nickel film coating ($0.5 \mu\text{m}$) deposited on $70 \mu\text{m}$ diameter quartz fiber. The overall length

is 3 mm. , and the sensitive film length is 1.25 mm. The wire has a temperature resistance of 6.86 ohms (at 20 C), and a temperature coefficient of 0.47%/ C. The cold resistance setup value was 7.44 ohms at room temperature. The probe was a single-sensor wire type and measured fluctuations in velocity, primarily axial velocity. The hot wire was operated in the "constant temperature" mode to minimize the high frequency attenuation of the system.

3d. Traversing Mechanism

The traversing mechanism was a commercial unit manufactured by DISA R Electronics. The traversing rod is a tube with a gear rack milled on one side and driven by a small stepping motor. The stepping motor is powered from a DISA R Type 52B01 sweep drive unit which drives the traversing rod, and indicates its position. The traversing rod was approximately 17.3 in. long which permitted a traverse of 13.5 in. The drive motor and traverse rod is shown in (fig.2). The sweep drive unit has a D.C. voltage output which was used as the X input (probe position) on an X - Y recorder which plotted turbulence level versus probe position. The traversing rod with the probe installed traveled a range of 11 in. Distance zero 3 in. above the floor of the tunnel stilling chamber and highest at 14 in. above the floor of the tunnel stilling chamber. The strut was installed with the down stream end of the strut at an axial station approximately 26.5 in. down stream of the turbulence generator. The traverse reveals if there is any turbulence difference accross the stilling chamber section.

3e. Instrumentation

The hot wire system was operated in the "constant temperature"

mode which is described by the simplified circuitry shown in (fig.3). The hot wire is in one leg of a bridge circuit whose signal output is fed to an amplifier. The output of the amplifier provides the power to the bridge and the electrical signal whose D.C. component represents the mean velocity and whose A.C. component represents the fluctuating velocity component (i.e., the turbulence). One side of the bridge is called the active side because its resistance is 1/20th the resistance of the inactive side. Thus virtually all of the current from the amplifier output goes through the active legs of the bridge. The bridge is always operating in a "balanced" condition. This is accomplished by allowing the voltage across the bridge (amplifier output) to vary in a manner such that the hot wire resistance is kept constant by the varying current through it. Since the resistance of the wire is a monotonically varying function of the temperature, the temperature of the wire is thus held constant. The operating temperature of the wire is set by selecting the overheat resistance. The cable resistance is balanced in the bridge circuit by the cable compensating resistance in the inactive side. Since the bridge is always operated in a balanced condition:

$$\frac{R_1}{R_2} = \frac{R_c + R_w}{R_{cc} + R_o}$$

Since R_1 , R_2 , R_c and R_{cc} are fixed, R_w (and the wire temperature) can be selected by setting R_o . The D.C. voltage from the amplifier can be fed to a linearizer that transforms a curved relationship between amplifier output voltage and velocity to a linear relationship.

The hot wire was powered and read out on a DISA R type 55 MID CTA standard bridge unit. The linearizer was a TSI Systems Inc. R Signal Linearizer model 1072. The D.C. output voltages from the standard bridge unit and the linearizer were read on Fluke R model 600A digital voltmeter. The A.C. voltage output from the standard bridge unit was read on a Thermo System Inc. R model 1076 true rms. voltmeter. This rms meter had a D.C. output voltage that was representative at the direct rms voltage reading on the face of the instrument. This output voltage was connected to the "Y" function of an X - Y recorder. Using the output voltage of the DISA sweep drive as the "X" input from the recorder, a plot of turbulence versus traverse position was obtained as the traverse was being performed.

Power spectral density measurements at the turbulence were made using a Hewlett Packard Structural Dynamics Analyzer model 5423A, a Hewlett Packard Digital Filter model 54470B, and a Hewlett Packard model 9872B plotter. This instrumentation system could plot the power spectral density in nearly real time.

IV. Test Description

The experimental test is to generate turbulence in the stilling chamber using the grid, grid with tags, and jets. Each configuration was tested, at a minimum of seven different stilling chamber velocities to provide sufficient data for hot wire calibration. A calibration was performed on each test day for three days.

The turbulence of the tunnel in an empty condition was found to be about 3%. This is due to the fact that a honeycomb 4 in. long with hexagonal cells of .180 in. in diameter approximately was installed at the tunnel entrance at the present time.

4a. Stilling Chamber Velocity Measurements

The average stilling chamber velocity V_{sc} , was obtained from the Mach number M_{sc} , which was determined by measuring the total pressure $P(t)$, the differential pressure between total and static in the stilling chamber $DP_{s.c.}$, the total temperature $T(t)$ and then since the flow is subsonic from the isentropic relations for one-dimensional steady flow of a perfect gas (ref.18).

4b. Hot Wire Calibration and Measurements

For each configuration tested the hot wire outputs (both D.C. and R.M.S.) were recorded at several different velocities. A linear equation relating the non-linearized hot wire D.C. amplifier output to the stilling chamber velocity was used to provide an in place calibration of the hot wire. The slope of the calibration equation was then used as the sensitivity of the hot wire to velocity changes or turbulence. The turbulence was determined by dividing the R.M.S. output of the hot wire by the slope of the D.C. output voltage versus velocity in the stilling chamber curve. The equation used is known as the King's Equation

(ref.1).

$$E_{dc}^2 = A + B (\text{Vel.})^2$$

Using the least square method the values at A and B are found. Then solving the equation to find an instantaneous fluctuation relation of voltage and velocity

Deriving partially, $2E dE = .5BU^{-.5} dU$

Simplifying the relation;

$$\frac{dE}{E} = \frac{dU}{U} \frac{(E^2 - A)}{4E^2}$$

Where;

$$dE = V_{rms.}$$

$$dU = \text{Vel.}_{rms.}$$

$$E = V_{dc.}$$

$$U = \text{Vel.}$$

$$\frac{E'}{E_{dc.}} = \frac{(E^2 - A)}{4E^2} \frac{U'}{U} \quad \text{Instantaneous Relation}$$

Squaring;

$$\left(\frac{E'}{E_{dc.}} \right)^2 = \frac{(E^2 - A)^2}{16E^4} \left(\frac{U'}{U} \right)^2$$

Time average-mean square;

$$E'_{rms} = \left(\frac{1}{T2-T1} \int_{T1}^{T2} E'(t)^2 dt \right)^{.5}$$

$$\left(\frac{1}{T2-T1} \int_{T1}^{T2} \frac{1}{E_{dc.}^2} E'^2 dt \right)^{.5} = \left(\frac{(E - A)^2}{16E^4} \frac{1}{T2-T1} \int_{T1}^{T2} U'^2 dt \right)^{.5}$$

V. Results and Discussion

A sample of the data, of August 6 (Run# 8-11) generating turbulence with jets only, from a traverse of the hot wire probe is presented in (fig.4), where the rms component of the probe voltage is plotted versus probe position. The data shows the condition of having Mach and Reynolds number constant while the manifold pressure is being varied. As can be seen there is a big difference in the turbulence level between Run no. 8 with 23.4% and Run no. 12 with 4.04%. From the traverse it seems that the rms voltage is fairly constant over most of the traverse.

Power spectral density (PSD) plots were taken at fixed points. A sample is illustrated in (fig.5). All PSD's show that most of the turbulence power is concentrated at the lowest frequencies (below 400Hz.). Comparing Run no. 24 and 29 of August 4, generating turbulence with a grid and jets, having almost exact flow conditions in the tunnel but 6 jets in Run 24 and 3 jets in Run 29, the jet nozzle is choked and the manifold pressures are 5,233 and 8,833 psfa. The PSD's have peak values of 21.3mV compared to 16.7mV, indicates that more jets with less manifold pressure contribute to increase turbulence.

For the tunnel test of August 5 (Run#1 to 16) using a grid with tags the level of turbulence starting from the lowest flow speed up to the highest tunnel flow speed were 12.2% to 5.35%. Comparing this with a turbulence baseline of 3% indicates that the tags improve the turbulence level. This condition was having the grid with tags at a fixed distance. It could be interesting to see the effect of changing the grid position with respect to the probe to observe the effect. From my literature survey I consider that if

the grid is moved closer to the probe at a certain position the turbulence percentage will be higher.

In the appendix the data for each test day is included with stilling chamber calculations. From the graphical results, graph 1 is a sample calibration curve of the data of August 4, to apply King's Law and the least square method to estimate the turbulence level. The correlation value is 0.995 which is good for the estimation of turbulence. Graph 2 illustrates the point where the jets are choked and the turbulence value reaches the highest level at the condition having the Mach number for the stilling chamber constant. Graph 3 shows the condition of having the manifold pressure constant and the effect of reducing the turbulence level as the velocity of the flow in the stilling chamber is increased. In graph 4 for the same tunnel setting different Mach number values are held constant and it is seen how as the jets mass flow is increased, the turbulence level increases.

Also as the Mach number is higher, to increase turbulence more jets mass flow is needed. In graph 5 with Mach constant the higher the jets pressure; the higher the turbulence level. Graph 6 shows the difference in tunnel settings where the condition of grid with tags has good turbulence percentages. Graph 7 shows the effect of having jets but at constant jet pressure and main stream velocity increasing. Graph 8 shows that as the mass ratio is increased; the turbulence percentage increases.

VI. Recommendations

The use of only a grid to generate turbulence seem to make very little effect according to the data of test August 4 (Run#1 to 14). This condition of tunnel setting should be analyzed changing the grid distance from the probe to see how the turbulence changes. According to (refs.2,9,12 and 17) if the grid is moved closer to the probe the turbulence level should be higher. If this is considered for the 4T wind tunnel the grid bar size should be bigger proportionally compared to the grid bar size used in the A.R.T. The use of jets proved to be effective for turbulence generation. It was observed that at a certain manifold pressure where the jet was considered to be choked the turbulence percent could be as high as seven times the turbulence baseline value of 3%. There should be more jet testing to analyze the use of more than six jets and having a higher supply pressure available for the manifold. For this test the highest value for supply pressure was 90 psig. Using jets to generate turbulence has the disadvantage of incurring in high project costs. Because besides of the cost for power for running the tunnel it will be necessary to spend a lot of money in power for putting air thru jets in the 4T wind tunnel. The uncertainty here is if the mass flow ratios observed in the A.R.T. for high turbulence percentages apply in 4T. Running the tunnel at high stilling chamber velocities made the turbulence percentages decrease. I suggest a test having higher supply pressure available to see how is the mass flow ratio because this is to be applied in 4T and the region of air flow will be transonic.

Regarding the use of a grid with tags high turbulence percentages were obtained. The tags were attached with a tight holder it could be interesting to see if the holder is made in a way that the tag can oscillate more. This could produce higher turbulence levels. The condition of having Mach and Reynolds numbers constant and varying the turbulence levels with jets provides the most appropriate approach in terms of what the main objective is. Making tests with higher supply pressure available is one of the things I will consider if the Mini Grant program provides funding for more testing.

VII. Acknowledgements

I wish to thank the Air Force Systems Command and the Air Force Office of Scientific Research for the sponsorship of this program. I also thank Universal Energy Systems for their concern, proper coordination, encourage and help to me in all administrative and directional aspects of this program.

I will also like to express my deep gratitude to the A.E.D.C. librarians and they are: The Technical Librarians; Della Burch, Brenda Warren, Effie Boyd, and Gay Goethert (Supervisor). The Library Clerks; Linda Adams, Linda Love, and Lib Fry. Their dedication, efficiency and concern was my inspiration. I thank Wallace Luchuk and Hubert Black (Test Engineering and Operations Branch) for their help in all technical aspects of the test. My special thanks to Daryl Sinclair (Project Engineer, Technology Applications) for being a guiding light, for his help, patience, and interest in every phase of this project that truly served as a source of stimulation.

Also thanks to the technicians from the Instrumentation Branch (R.M.West and R.L.Meyer) and from the Installation and Maintenance Branch (E.C.Keele and A.D.Currey) for making the test possible. Finally, but not least important I thank Marshall Kingery for his constant help in all technical and personnel matters during to my ten weeks work period.

Taking the root mean square;

$$\frac{E'_{rms.}}{E_{dc.}} = \frac{(E_{dc.}^2 - A)}{4E^2} = \frac{U'_{rms.}}{U}$$

This is the relation used to estimate turbulence.

The R.M.S. output of the hot wire was also recorded on an X - Y recorder as a function of probe position. Power Spectral Density (PSD) plots were made from the hot wire R.M.S. outputs. The power spectral density plot shows the distributions of the turbulence intensity.

VIII. References:

1. King, L.V. : Philosophical Transactions of the Royal Society, London, 214A, 373 (1914).
2. Dryden, H.L., and Kuethe, A.M. : Effect of turbulence in Wind Tunnel Measurements. N.A.C.A., Technical Report No. 342, 1929.
3. Dryden, H.L., and Kuethe, A.M. : The Measurements of Flunctuation of Air Speed by the Hot Wire Anemometer. N.A.C.A., Technical Report No. 320, 1929.
4. Dryden, H.L. and Heald, R.H. : Investigation of Turbulence in Wind Tunnels by a Study of the Flow About Cylinders. N.A.C.A., Technical Report No. 231, 1926.
5. Dryden, H.L. : Reduction of Turbulence in Wind Tunnels. N.A.C.A., Technical Report No. 392, 1931.
6. Dryden, H.L. : Turbulence, Companion and Reynolds Number. Journal of Aeronautical Sciences, Vol. 1 No. 2, April 1934, p. 67.
7. Dryden, H.L., Schubauer, G.B., Mock, W.C., Jr., and Skramstad, H.K. : Measurements of Intensity and Scale of Wind Tunnel Turbulence and their Relation to the Critical Reynolds Number of Spheres. N.A.C.A., Technical Report No. 581, 1936.
8. Dryden, H.L., and Schubauer, G.B. : The Use of Damping Screens for the Reduction of Wind Tunnel Turbulence. Journal of Aeronautical Sciences, April 1947, p. 221.
9. Baines, W.D., and Peterson E.G. : An Investigation of Flow Through Screens. Transactions of the A.S.M.E., 73, July 1951, p. 467.

10. Townsend, A.A.: The Passage of Turbulence Through Wire Gauges. Quart. Journal of Mech. and Applied Math., Vol. IV, Pt.3 (1951), p. 308.
11. Uberoi, M.S. : Effect of Wind Tunnel Contraction on Free-Stream Turbulence. Journal of Aero. Sci. 23, pp. 754-764, University of Michigan, 1956.
12. Grant, H.L. & Nisbet, I.C.T. (1957) : The Inhomogeneity of Grid Turbulence. J. Fluid Mech. 2, p. 263.
13. Comte-Bellot, G. and Corrsin, S. : The Use of a Constriction to Improve the Isotropy of Grid Generated Turbulence. J. Fluid Mech. (1966), Vol. 25, Part 4, pp. 657-682.
14. Uberoi, M.S. & Wallis, S. (1966) : Small Axisymmetric Contraction of Grid Generated Turbulence. J. Fluid Mech. 24, p. 539.
15. Evans, R.L. : Free Stream Turbulence Effects on the Turbulent Boundary Layer. A.R.C., C.P. No. 1282, 1974, London.
16. Hinze, J.O. : Turbulence. Second Edition, Copyright 1975, by Mc Graw-Hill, Inc.
17. Nakamura, Y. and Ohya, Y. : The Effects of Turbulence on the Mean Flow Past Square Rods. J. Fluid Mech. 24, p. 539.
18. John, James E.A. : Gas Dynamics, Second Edition, Copyright 1984, by Allyn and Bacon, Inc.

Appendix

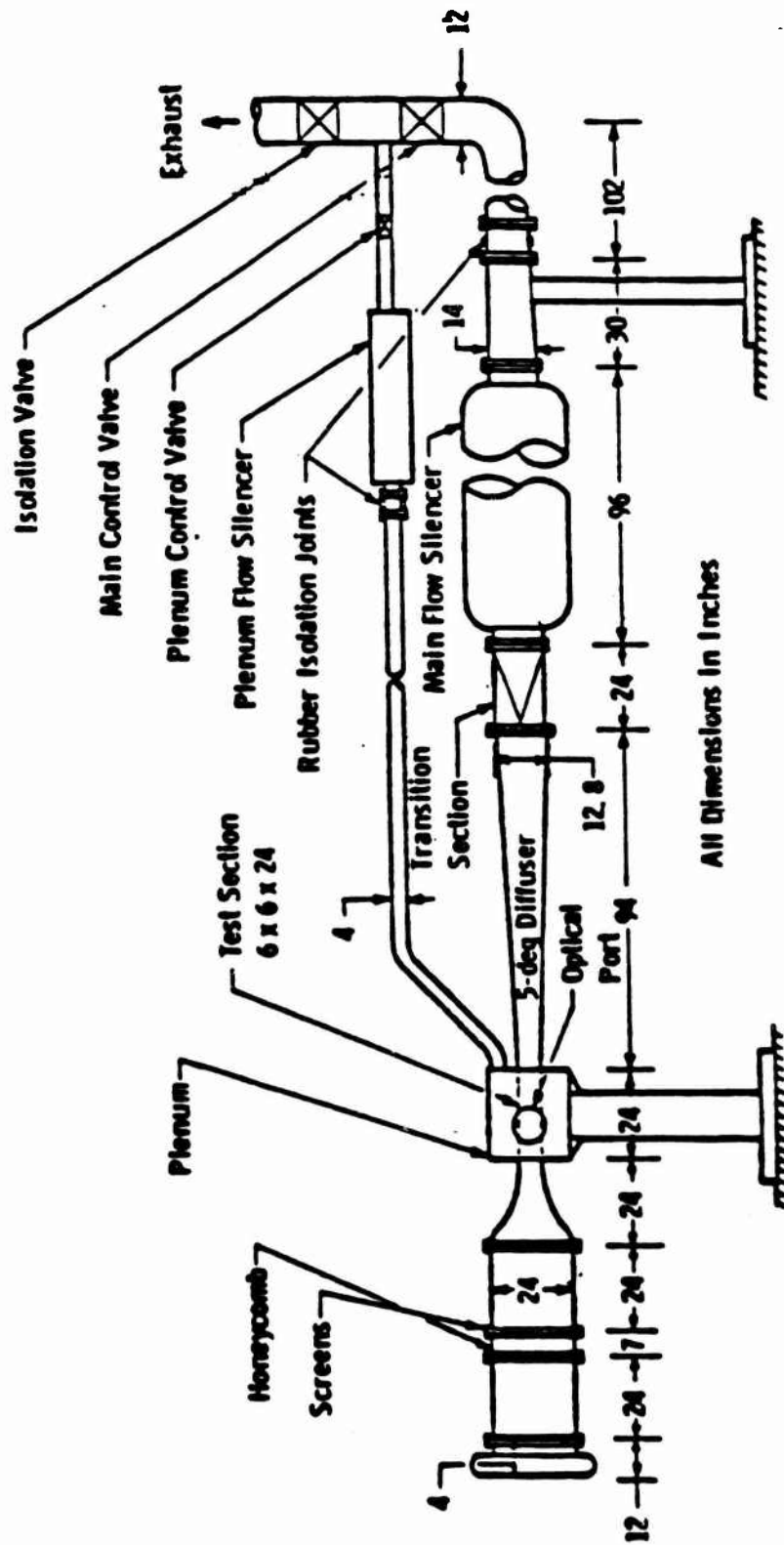
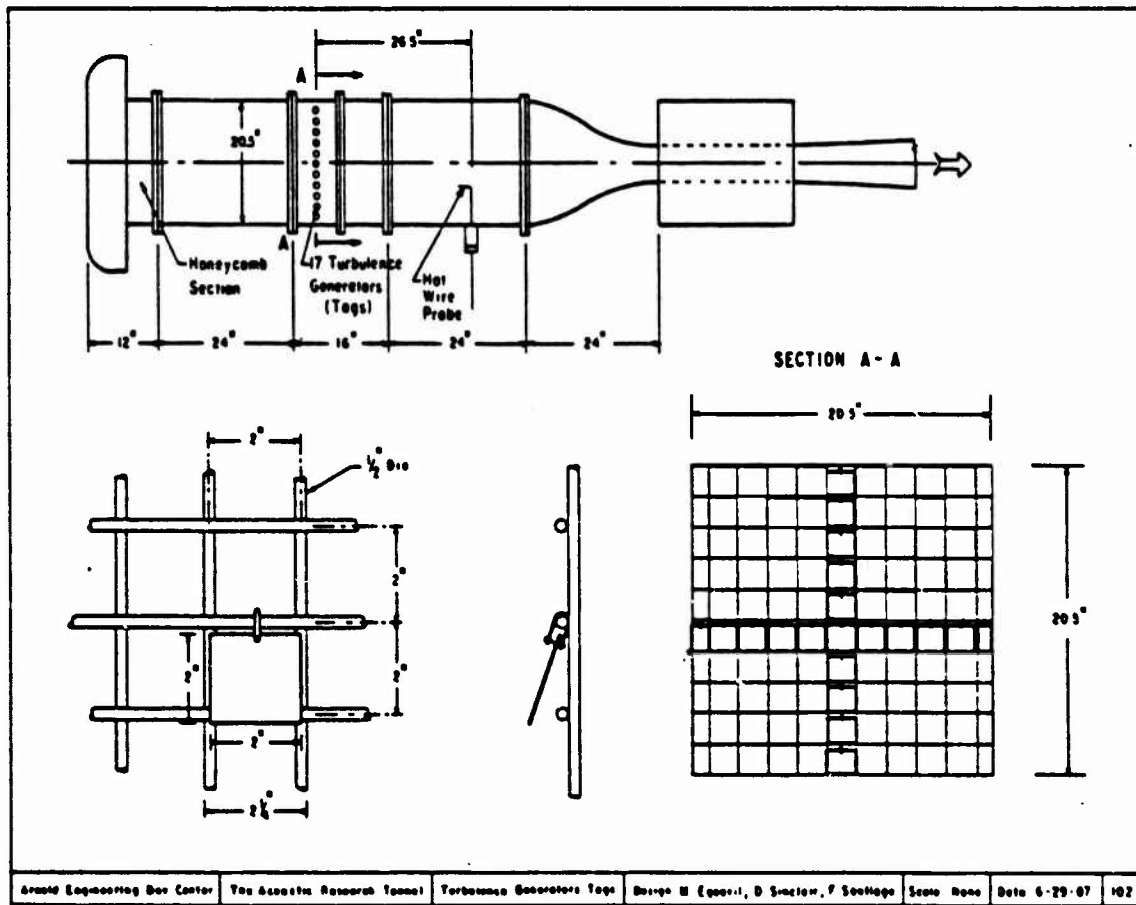
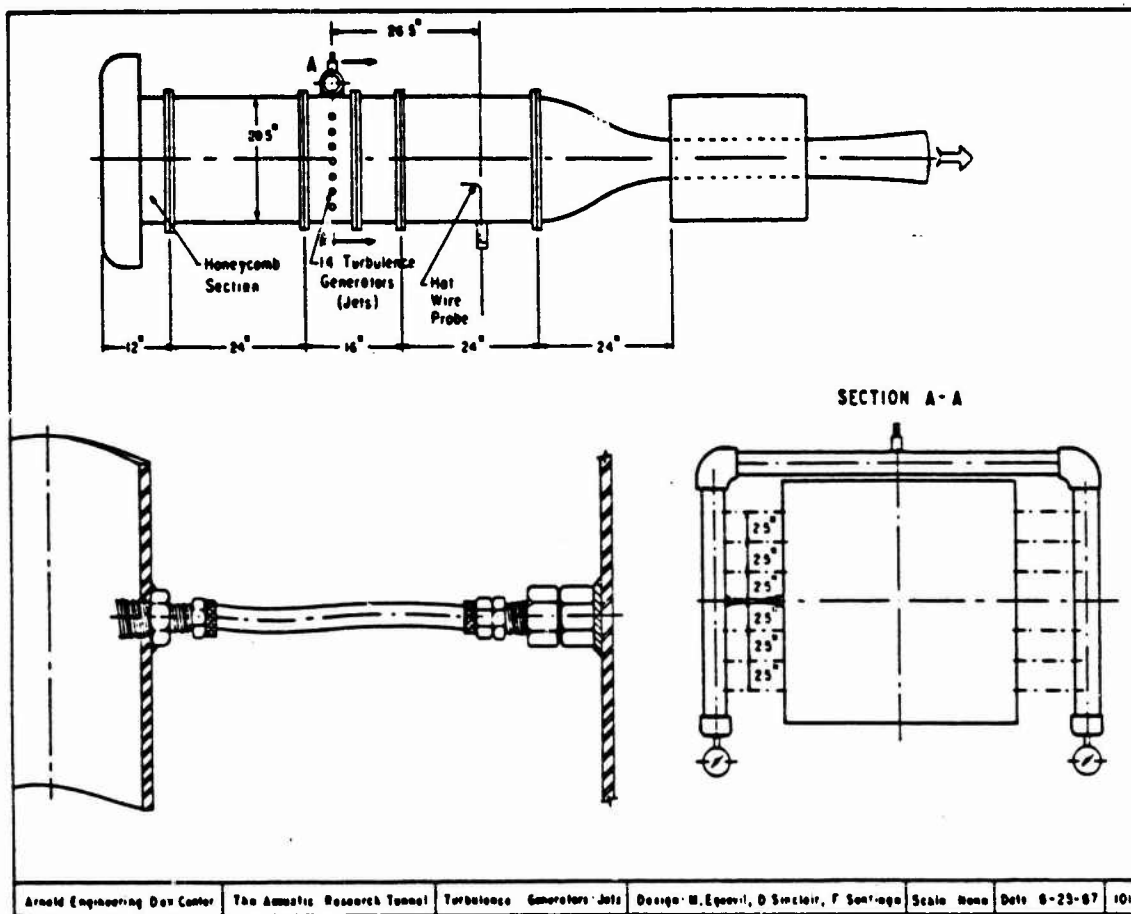


FIGURE 1. THE ACCOUSTIC RESEARCH TUNNEL



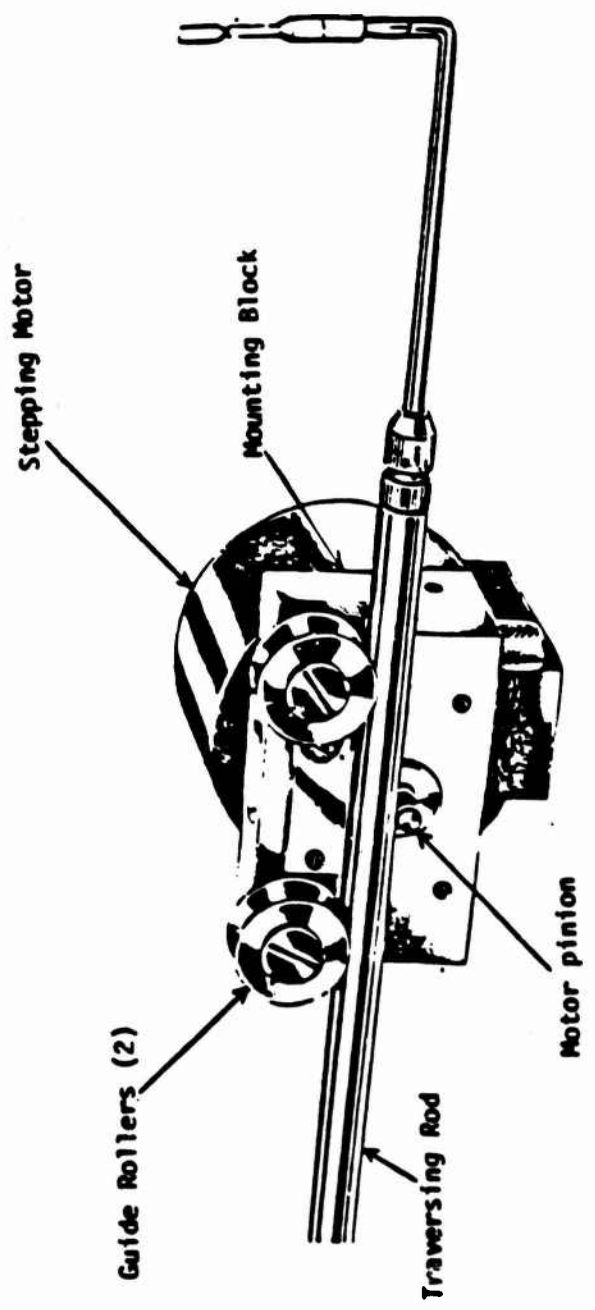


Figure 2. Hot Wire Probe Traverse Mechanism

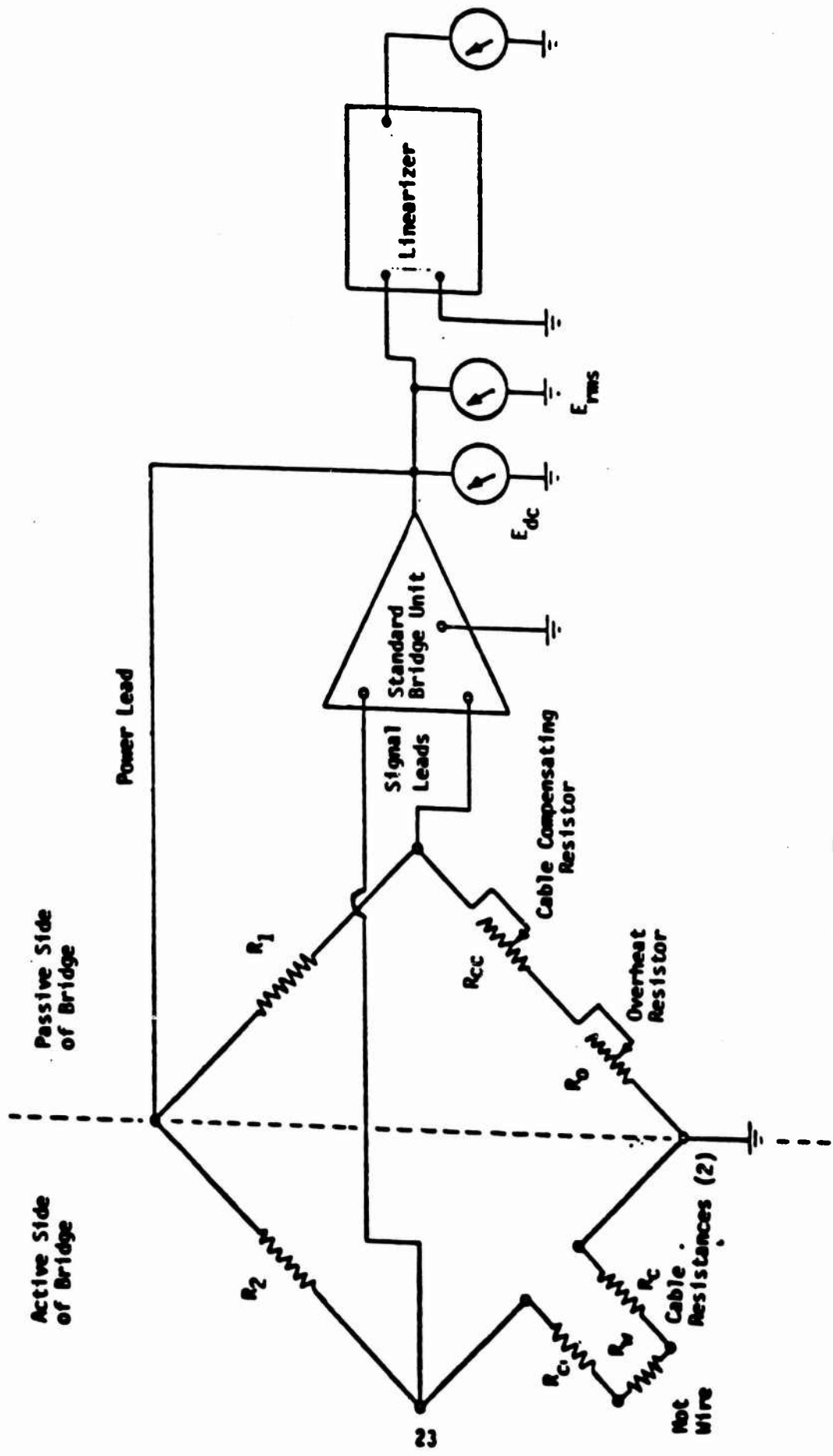


Figure 3. Hot Wire Probe Circuitry

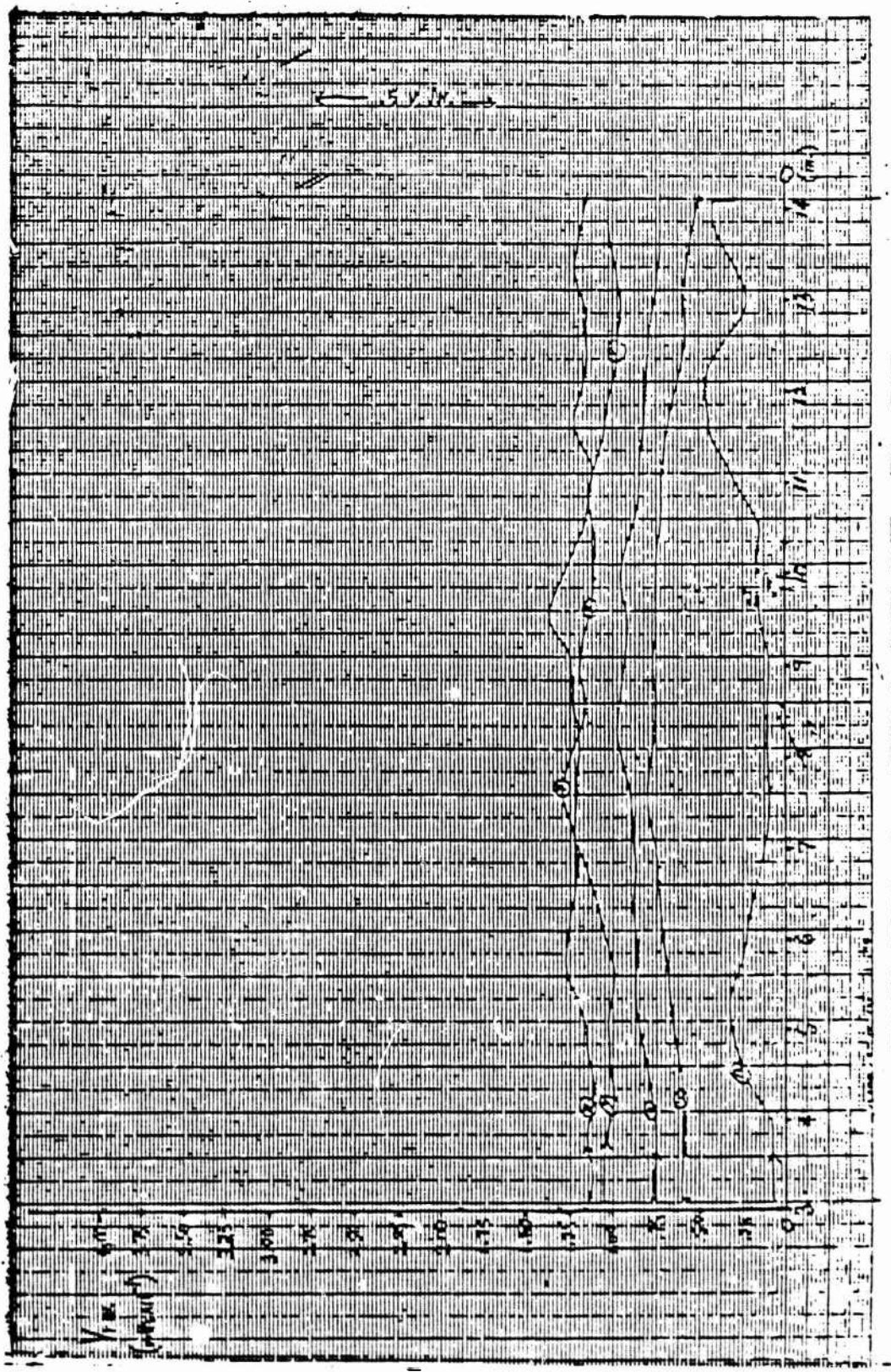


FIGURE 4. TRAVERSE PLOT
 V_{RMS} VS. VERTICAL DISTANCE

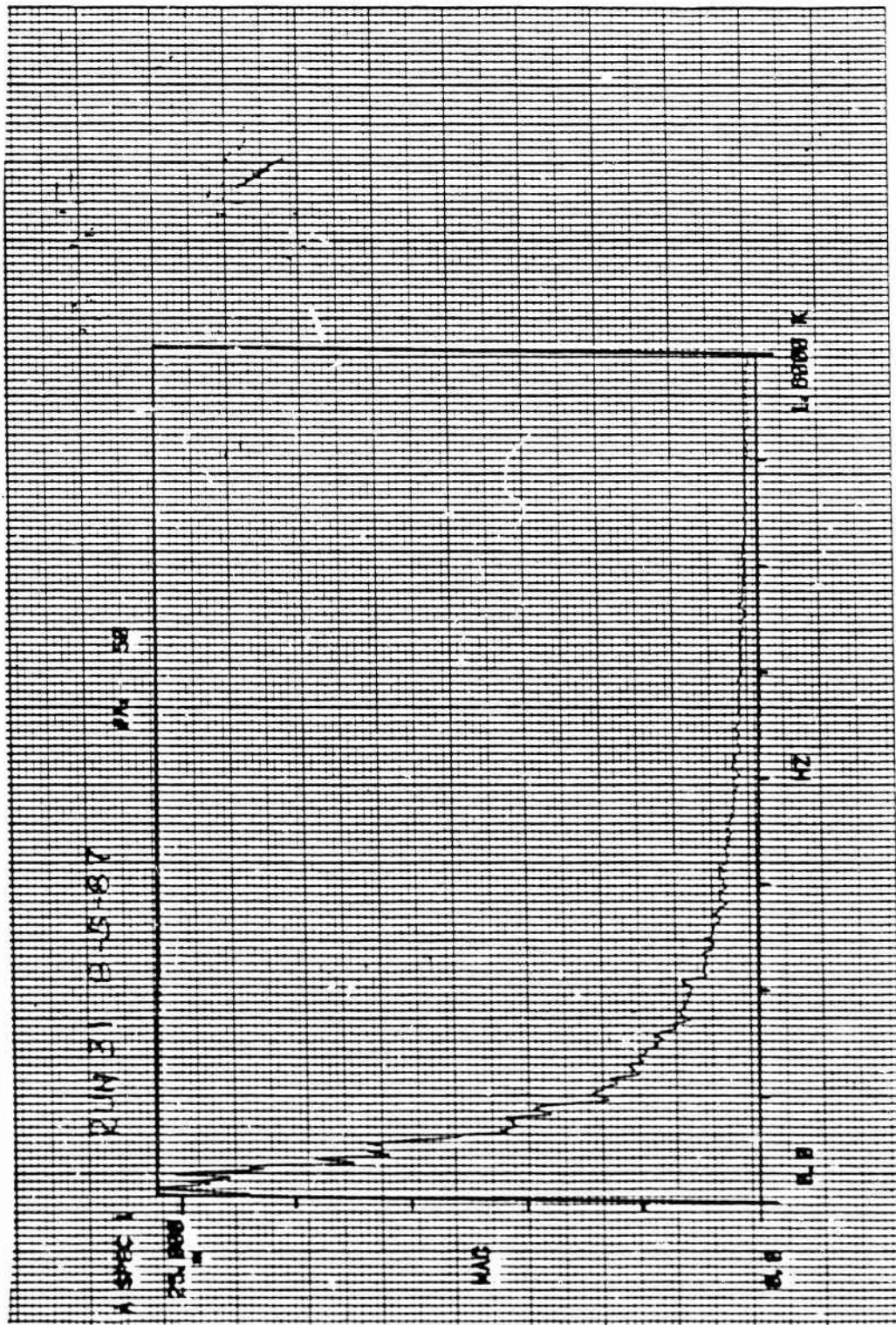


FIGURE 5. POWER SPECTRAL DENSITY
 PLOT TURBULENCE VS. FREQUENCY

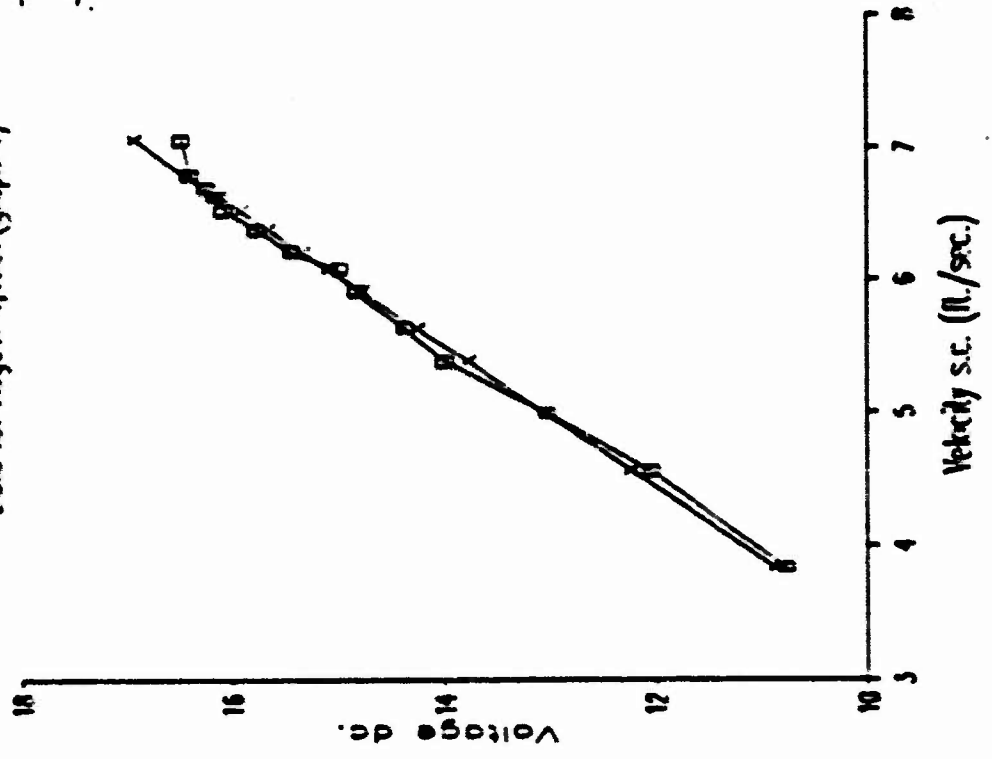
Run#	Run#-17	Grid T(t) R	Only	Ms.c.	August 4 Test				Run#18-26 Grid & Jets						
	F(t) def.		Pis/psfa. s.c.		T(s) R s.c.	U(ft/s) s.c.	Ecc volts	Erms volts	Turb. (%)	Jets no.	Pres. psfa.	M mach of jets	a (lb/s) of jets	z (lb/s) of jets	r ratio s.c. jets/s.c.
1	2033	547	2032.766	.013	546.982	14.720	3.280	.017	3.198	0	0	.000	.000	2.990	0
2	2032	547	2031.532	.018	546.964	20.625	3.470	.018	2.998	0	0	.000	.000	4.228	0
3	2032	546	2031.324	.022	545.948	25.006	3.610	.019	2.866	0	0	.000	.000	5.025	0
4	2033	546	2032.090	.025	545.930	25.006	3.740	.019	2.792	0	0	.000	.000	5.701	0
5	2031	547	2030.906	.028	546.916	31.813	3.790	.021	2.960	0	0	.000	.000	6.457	0
6	2032	548	2030.674	.031	547.898	35.090	3.850	.022	2.980	0	0	.000	.000	7.108	0
7	2030	548	2028.519	.032	547.856	37.115	3.870	.021	2.922	0	0	.000	.000	7.510	0
8	2029	548	2027.389	.034	547.876	38.720	3.930	.023	3.108	0	0	.000	.000	7.831	0
9	2029	549	2027.207	.036	548.861	40.885	3.970	.024	3.097	0	0	.000	.000	8.253	0
10	2028	549	2026.051	.037	548.849	42.638	4.010	.024	3.100	0	0	.000	.000	8.602	0
11	2028	549	2025.921	.038	548.839	44.038	4.020	.025	3.152	0	0	.000	.000	8.854	0
12	2027	550	2024.843	.039	549.833	44.908	4.030	.024	3.075	0	0	.000	.000	9.036	0
13	2027	550	2024.713	.040	549.823	46.242	4.050	.024	3.052	0	0	.000	.000	9.306	0
14	2026	549	2023.635	.041	548.817	46.993	4.060	.023	2.964	0	0	.000	.000	9.469	0
15	2029	549	2027.493	.033	548.883	37.483	3.890	.022	2.930	0	0	.000	.000	7.567	0
16	2033	550	2032.454	.020	549.958	22.548	3.240	.018	3.337	0	0	.000	.000	4.555	0
17	2029	549	2027.493	.033	548.883	37.483	3.680	.022	2.929	0	0	.000	.000	7.567	0
18	2025	551	2022.661	.041	550.818	46.831	4.050	.025	3.128	0	0	.000	.000	9.398	0
19	2026	552	2023.921	.038	551.836	44.180	3.990	.023	2.994	0	0	.000	.000	8.855	0
20	2026	552	2024.337	.034	551.870	39.512	3.990	.024	3.125	6	4875	1.000	.056	7.921	.7123368
23	2033	544	2032.766	.013	543.982	14.679	3.320	.016	3.157	0	0	.000	.000	2.998	0
24	2033	542	2032.392	.021	541.954	23.629	3.260	.114	21.339	6	5233	1.000	.061	4.843	1.262576
25	2033	542	2032.387	.021	541.953	23.730	3.300	.117	21.365	6	3933	1.000	.046	4.864	.9448926
26	2033	543	2032.631	.016	542.972	18.424	3.360	.047	6.351	6	2783	.685	.029	3.770	.7796389
27	2033	542	2032.532	.018	541.964	20.725	3.380	.081	14.107	6	3193	.830	.036	4.248	.8551972
28	2033	539	2032.766	.013	538.982	14.612	3.380	.017	2.943	0	0	.000	.000	3.012	0
29	2033	539	2032.480	.019	538.961	21.784	3.290	.091	16.719	3	8833	1.000	.052	4.490	1.152603
30	2033	539	2032.579	.017	538.968	19.606	3.400	.066	11.381	3	3023	.775	.017	4.041	.4175860

Run#	P(t)ipsf.	T(t) R	P(s)ipsfa. s.c.	ns.c.	T(s) R s.c.	U(ft/s) s.c.	Edc volts	Eros volts	Turb. (%)	Jets no.	Psan. psfa.	P each of jets	of jets of s.c.	of jets of s.c.	ratio % jets/s.c.
1	2031	548	2030.792	.012	547.984	13.897	3.260	.070	12.198	0	0	.000	.000	2.815	0
2	2030	544	2029.532	.018	543.964	20.778	3.420	.070	11.120	0	0	.000	.000	4.287	0
3	2030	544	2029.220	.023	543.940	26.825	3.510	.071	10.836	0	0	.000	.000	5.470	0
4	2029	544	2027.908	.028	547.916	31.750	3.600	.068	9.994	0	0	.000	.000	6.470	0
5	2029	544	2027.700	.030	547.900	34.642	3.650	.066	9.472	0	0	.000	.000	7.058	0
6	2028	544	2025.947	.038	543.843	43.562	3.730	.058	9.440	0	0	.000	.000	8.668	0
7	2028	546	2026.259	.035	545.866	40.189	3.820	.065	8.694	0	0	.000	.000	8.137	0
8	2027	547	2025.129	.036	546.856	41.710	3.860	.064	8.267	0	0	.000	.000	8.441	0
9	2027	547	2024.975	.038	546.844	43.415	3.900	.059	7.557	0	0	.000	.000	8.756	0
10	2026	546	2023.845	.039	547.833	44.837	3.990	.046	6.604	0	0	.000	.000	9.052	0
11	2026	547	2023.661	.041	546.819	46.649	4.020	.048	5.925	0	0	.000	.000	9.404	0
12	2025	547	2022.505	.042	546.807	48.191	4.050	.044	5.372	0	0	.000	.000	9.741	0
13	2025	547	2022.349	.043	546.795	45.676	4.070	.043	5.151	0	0	.000	.000	10.040	0
14	2025	549	2022.277	.044	548.791	50.253	4.070	.044	5.345	0	0	.000	.000	10.120	0
15	2027	547	2023.181	.036	546.860	41.126	3.820	.065	8.681	0	0	.000	.000	8.323	0
16	2031	547	2030.662	.015	546.974	17.701	3.200	.070	12.605	0	0	.000	.000	3.592	0
17	2030	548	2029.870	.010	547.990	10.988	3.260	.116	20.185	6	5085	1.000	.001	2.225	2.759764
18	2028	544	2027.532	.018	543.964	20.786	3.690	.073	10.307	6	4587	1.000	.058	4.225	1.372491
19	2027	546	2026.142	.025	545.934	28.206	3.790	.035	4.779	6	4823	1.000	.056	5.723	.9534441
20	2026	545	2024.830	.029	548.909	33.038	3.890	.030	3.878	6	5033	1.000	.058	6.651	.8773075
21	2025	549	2023.519	.032	548.985	37.195	3.950	.028	3.573	6	5253	1.000	.061	7.494	.8138460
22	2030	548	2029.644	.010	547.988	12.037	3.210	.118	21.150	6	5073	1.000	.029	2.407	2.419027
23	2030	549	2029.844	.010	548.988	12.048	3.210	.119	21.509	6	4973	1.000	.028	2.425	2.304584
24	2030	549	2029.844	.010	548.988	12.048	3.210	.103	16.444	6	3573	.956	.041	2.425	1.697798
25	2030	549	2029.844	.010	548.988	12.048	3.210	.072	10.072	6	3013	.773	.033	2.425	1.367691
26	2030	546	2029.844	.010	547.986	12.037	3.270	.034	5.925	6	2613	.612	.026	2.427	1.060574
27	2027	548	2026.402	.021	547.954	23.590	3.600	.020	2.946	6	2613	.614	.026	4.769	.5431676
28	2027	548	2026.402	.021	547.954	23.590	3.600	.020	2.946	6	2973	.761	.023	4.766	.6857474
29	2027	548	2026.402	.021	547.954	23.590	3.620	.029	4.139	6	3623	.950	.042	4.768	.6611262
30	2027	548	2026.402	.021	547.954	23.590	3.620	.044	6.390	6	4173	1.000	.048	4.768	1.017047
31	2027	548	2026.402	.021	547.954	23.590	3.650	.061	8.684	6	4753	1.000	.055	4.768	1.158405

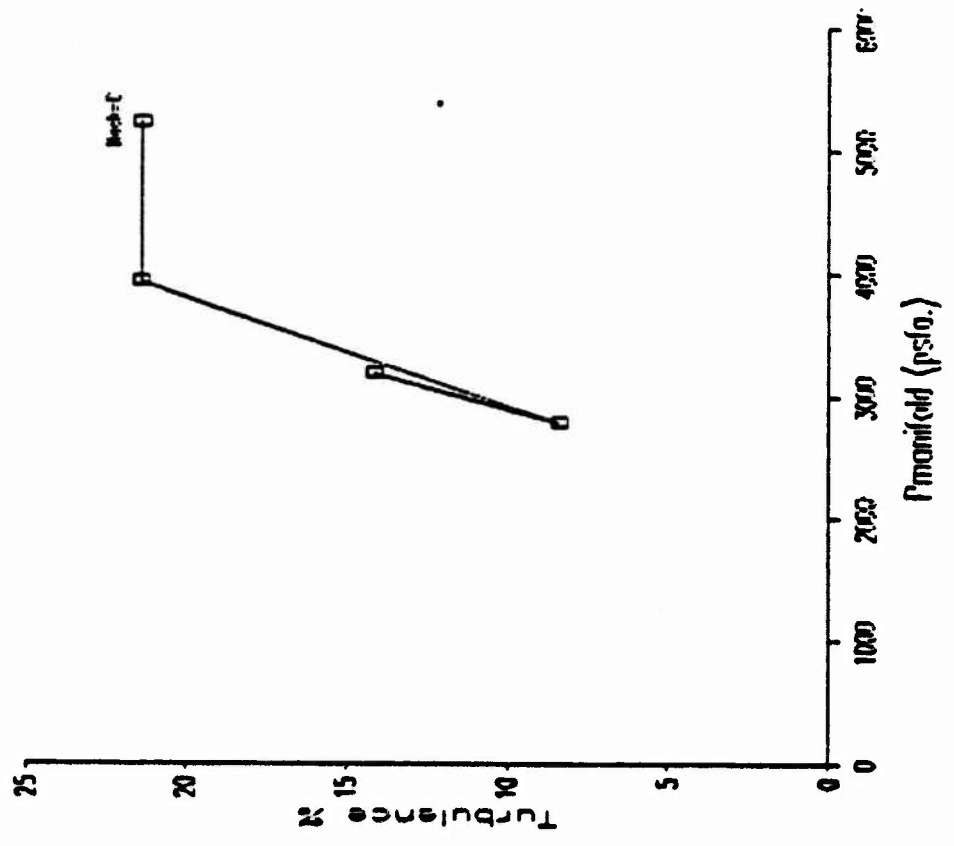
Run#	P(t)ipsf.	Empty T(t) R	Tunnel P(s)ipsfa. s.c.	ns.c.	August 6 T(s) R s.c.	Test U(ft/s) s.c.	Edc volts	Eros volts	Turb. (%)	Jets no.	Psan. psfa.	Run#-19 M each of jets	Jets Only e(ft/s)(m)(lb/s)(ratio % of jets of s.c. jets/s.c.	ratio % jets/s.c.	
1	2038	541	2037.766	.013	540.982	14.621	3.390	.015	2.774	0	0	.000	.000	3.010	0
2	2036	541	2035.376	.021	540.953	23.890	3.670	.017	2.681	0	0	.000	.000	4.917	0
3	2035	542	2033.966	.027	541.921	30.881	3.840	.018	2.612	0	0	.000	.000	6.333	0
4	2035	544	2033.623	.031	543.895	33.613	3.920	.019	2.658	0	0	.000	.000	7.277	0
5	2034	543	2032.233	.035	542.865	40.317	4.010	.020	2.691	0	0	.000	.000	8.246	0
6	2034	543	2031.947	.038	542.843	43.457	4.090	.012	1.563	0	0	.000	.000	8.890	0
7	2037	543	2030.817	.039	542.833	44.823	4.140	.014	1.786	0	0	.000	.000	9.194	0
8	2037	544	2036.844	.010	543.988	11.972	3.270	.117	22.424	6	5035	1.000	.029	2.450	2.407726
9	2037	542	2036.844	.010	541.988	11.950	3.300	.102	20.003	6	3723	.977	.044	2.425	1.778297
10	2037	542	2036.844	.010	541.988	11.950	3.400	.079	14.518	6	3183	.826	.036	2.425	1.475883
11	2037	544	2036.844	.010	543.988	11.972	3.390	.056	10.336	6	2943	.745	.032	2.450	1.314820
12	2037	542	2036.792	.012	542.984	12.813	3.330	.021	4.077	0	0	.000	.000	2.822	0
13	2036	543	2035.774	.021	542.952	23.973	3.650	.021	3.246	0	0	.000	.000	4.904	0
14	2036	544	2035.584	.017	543.966	19.561	3.720	.061	9.278	6	4858	1.000	.027	4.001	1.425031
15	2036	544	2035.584	.017	543.968	19.561	3.670	.041	6.465	6	4158	1.000	.048	4.001	1.212264
16	2036	544	2035.584	.017	543.968	19.561	3.700	.053	8.230	6	4328	1.000	.053	4.001	1.322992
17	2035	545	2032.617	.039	544.833	44.883	3.800	.050	7.793	0	0	1.000	.000	9.122	0
18	2035	545	2032.617	.039	544.833	44.883	3.830	.036	4.373	6	4798	1.000	.026	9.122	.610421
19	2035	545	2032.617	.039	544.833	44.883	3.810	.000	.000	0	0	.000	.000	9.122	0

Data and Least Squares Fit
 (Data for August 4, 1987 (graph 1))

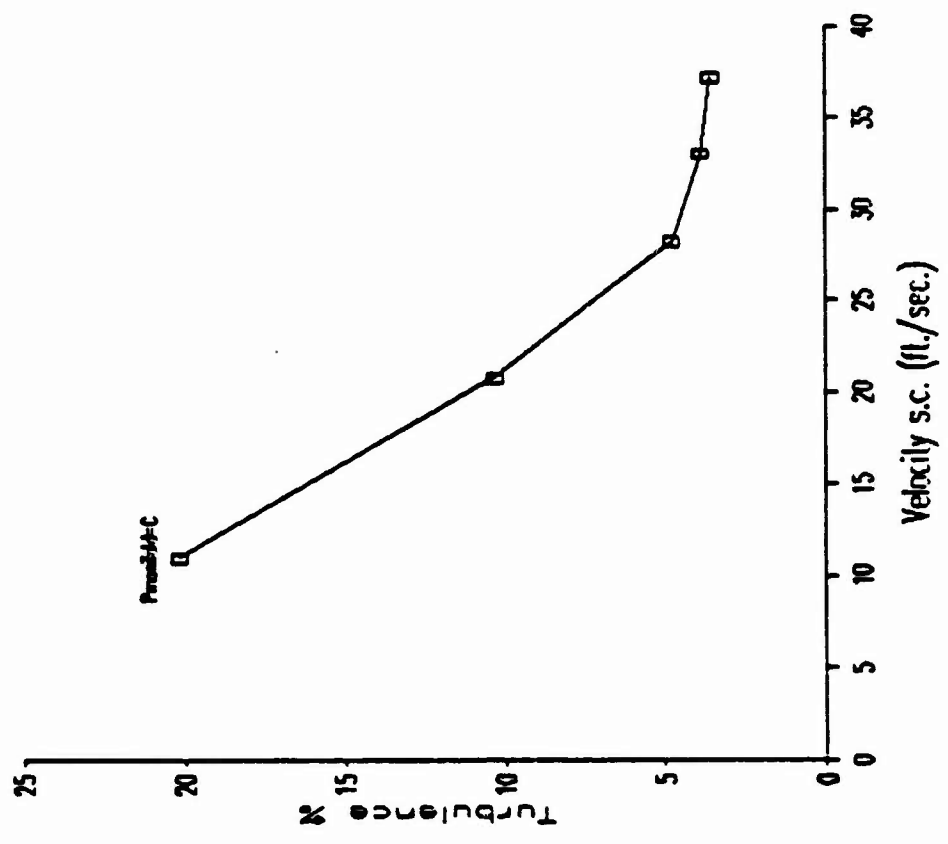
—○— OMA
 —+— Regre.



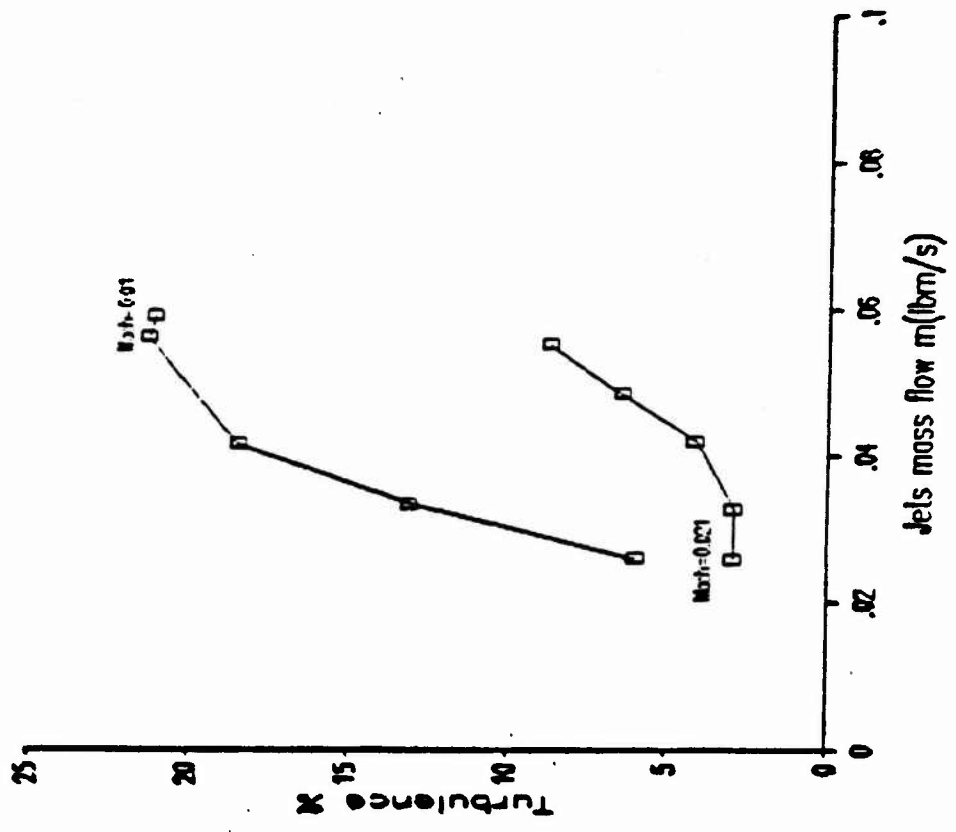
August 4 Grid & Jets
 Run# 24-27 (graph 2)



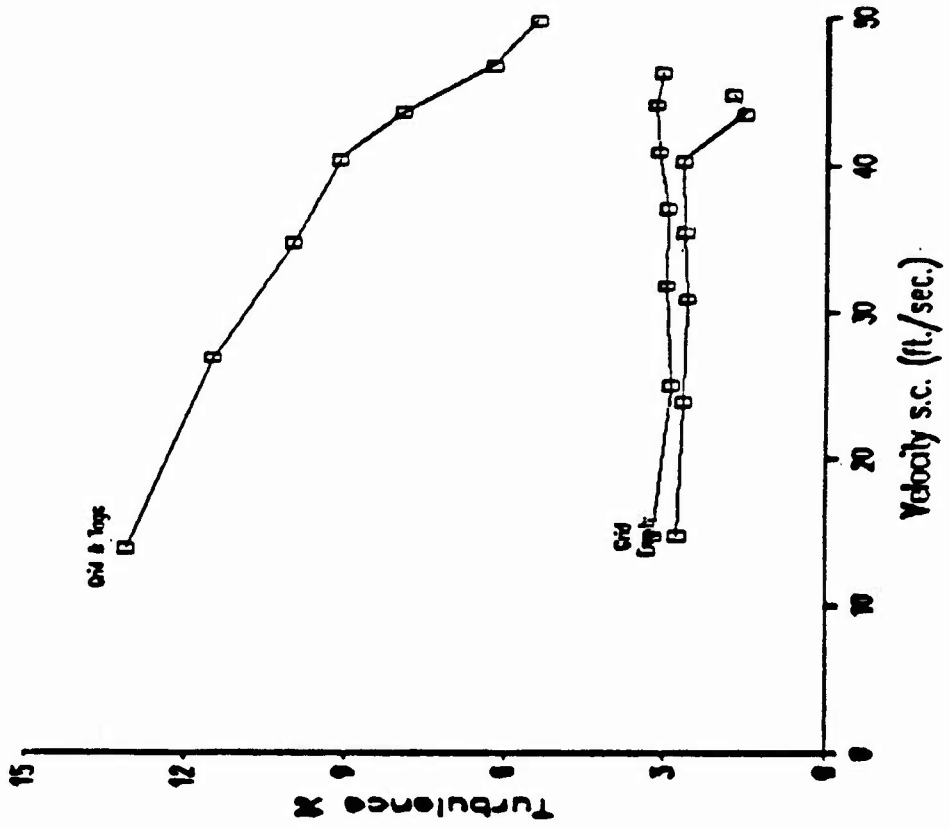
August 5 Grid & Jets only
Run# 17-21(graph 3)



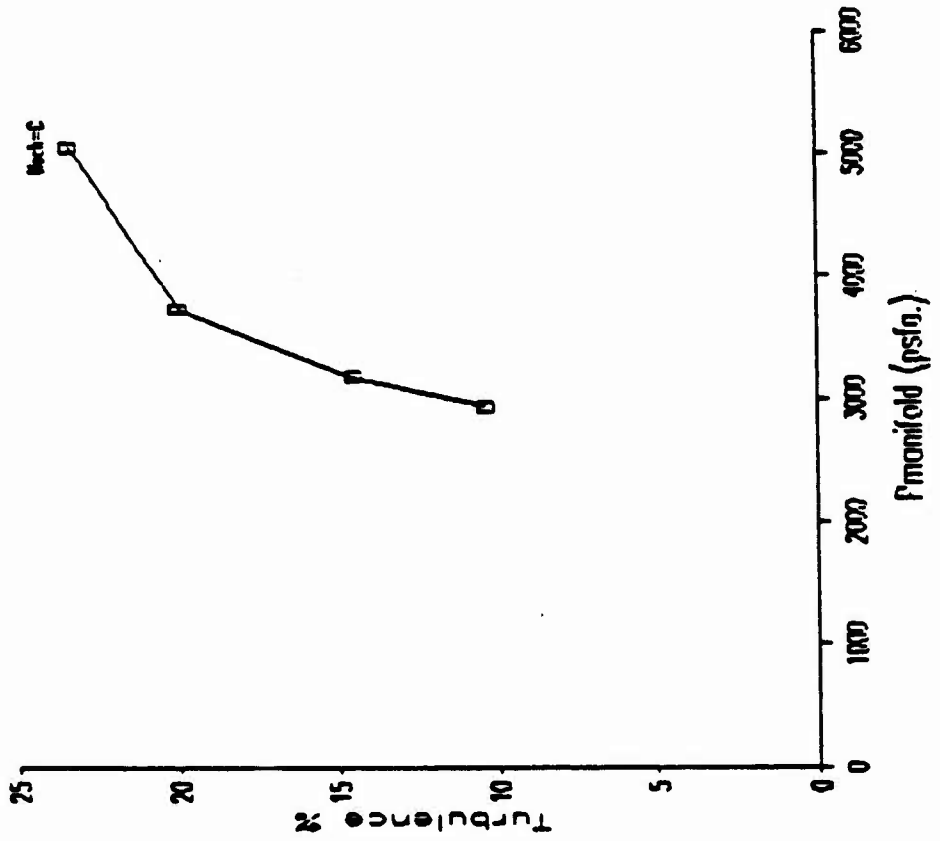
August 5 use of Grid & Jets
Run# 22-26,27-31(graph 4)



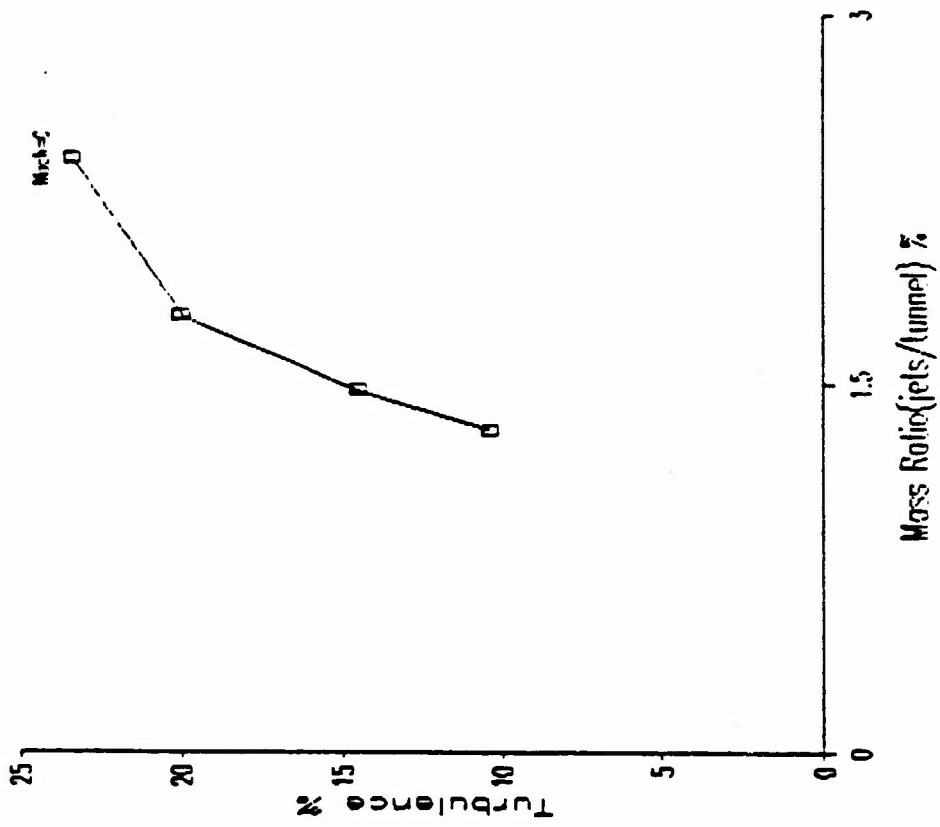
August 4, 5 & 6 Comparison of
Tunnel Settings (graph 6)



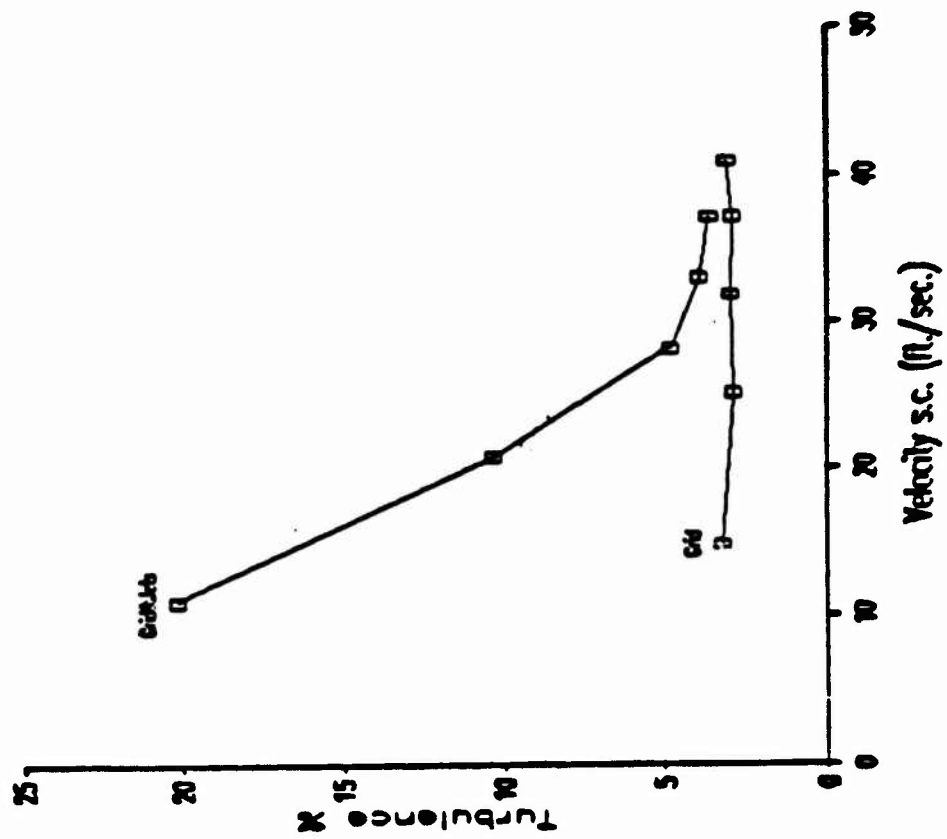
August 6 use of Jets only
Run # B-11 (graph 5)



August 6 use of jets only
 Run#8-11 (graph 8)



August 4 & 5 Comparison of
 Tunnel Settings (graph 7)



1987 USAF-UES SUMMER FACULTY RESEARCH PROGRAM/
GRADUATE STUDENT SUMMER SUPPORT PROGRAM

Sponsored by the
AIR FORCE OFFICE OF SCIENTIFIC RESEARCH

Conducted by the
Universal Energy Systems, Inc.

FINAL REPORT

LOW VELOCITY IMPACT OF GRAPHITE/EPOXY PLATES

Prepared by: William E. Wolfe, Ph.D. and Gregory A. Schoeppner
Academic Rank: Associate Professor
Department and University: Civil Engineering Department
The Ohio State University
Research Location: AFWAL/FIBCA
Wright Patterson AFB
OH 45433
USAF Researcher: Dr. R. S. Sandhu
Date: 30 Sep 87
Contract No: F49620-85-C-0013

REFERENCE DR. WOLFE
SFRP FINAL REPORT NUMBER 154

1987 USAF-UES SUMMER FACULTY RESEARCH PROGRAM/
GRADUATE STUDENT SUMMER SUPPORT PROGRAM

Sponsored by the
AIR FORCE OFFICE OF SCIENTIFIC RESEARCH

Conducted by the
Universal Energy Systems, Inc.

FINAL REPORT

EXPERIMENTAL RESEARCH OF COMBUSTION SYSTEMS

Prepared by:	James P. Seaba
Academic Rank:	MSME
Department and University:	Mechanical Engineering University of Iowa
Research Location:	Aeropropulsion Lab AFWAL/POSF Combustion Group
USAF Researcher:	W. M. Roquemore
Date:	August 15, 1987
Contract No:	F49620-85-C-0013

Experimental Combustion Techniques

by

James P. Seaba

ABSTRACT

Several small experiments regarding different combustion phenomena were explored. A new diagnostic tool known as the phase doppler anemometer was used in a spray environment. It measures droplet size and velocity. Diffusion flame work was completed from last summers work. Other experiments include a multiple jet flame, and multicomponent evaporation of a droplet.

ACKNOWLEDGEMENTS

I would like to thank the Air Force Office of Scientific Research for sponsorship of this program. Universal Energy Systems was very helpful to me with respect to administrative and social aspects of this program.

The combustion group was extremely helpful to me. Special recognition goes to Cindy Obringer, Jeff Stuttrude, and Curtis Reeves. Also, I greatly appreciated Mel Roqemore and Tom Jackson for their insights and guidance. The Systems Reseach Lab (SRL) was very informative and highly educational in their demonstrations and experimental procedures. Special thanks to Larry Goss, Gary Switzer, and Ben Sarka all of whom work and play for SRL.

I. Introduction

Presently, I am enrolled in the PhD program in Mechanical Engineering at the University of Iowa. My primary field of study consists of combusting and noncombusting sprays. My PhD thesis will be centered in this area.

Last summer I participated in GSSSP for the first time working with L.D. Chen (advisor) and W.M. Roquemore (USAF). I worked on jet diffusion flame flow visualizations and digitized several sequences of this phenomena.

This summer I pursued several areas of interest. First, the jet diffusion flame work was completed. Second, my interests were focused on the phase doppler anemometer which is a new diagnostic tool for sprays. The last phase of this summers research was to perform experiments relating to possible thesis topics.

• II. Objectives of Research Effort

The jet diffusion flame work was completed. This consisted of verification of large scale structure phenomena from digitized data and to observe and run a new device that automatically digitizes films. This system was developed by L.P. Goss (SRL).

A new diagnostic technique for sprays was developed by W.D. Bachelo of Aerometrics. The phase doppler anemometer measures size and velocity of droplets ranging in size from 7 to 200 microns. My objective was to learn the theory and experimental procedure of the phase doppler.

An experiment was developed to verify the theory of a multicomponent fuel droplet in a noncombusting spray environment. Once the initial model (1-D) was verified by the experiment, an updated version (2-D) was to be applied. This experimental setup could possibly be used for visualizing drop-turbulent interactions.

The most important objective of the summer of 1987 was to determine my PhD thesis topic. A couple of preliminary experiments were setup and run regarding drop-turbulent interaction, and instability problems.

III. Diffusion Flame

The final work relating to the diffusion flame research consisted of organizing pictures illustrating the periodic large scale structure phenomena. Thousands of photographs were taken as well as several rolls of film, each illustrating different or related diffusion flame phenomena.

L. P. Goss set up a digitizing device which scans a frame of film using a linear array of 500 with a 12 bit microprocessor for the intensity levels. This data was stored on the modcomp system. One of the purposes of this procedure is to compare the digitized data with the hand held digitizing from the previous summer. No comparisons have been made at this time due to time constraints and priorities of work load.

IV. Phase Doppler

An important objective was fulfilled this summer concerning experiments using the phase doppler anemometer. This new diagnostic technique combines fringe patterns produced by droplets and geometric optics theory to determine the size and velocity of the droplet. The objective was to learn the theory behind the device and determine if it can be used in combusting and noncombusting sprays.

Work involving the phase doppler was underway when I arrived in mid May. I helped with data reduction with colleagues Terry Blitzer (SPU) and Cindy Gringer (USAF) and observed the experimental procedures. The

experiment consisted of velocity and size measurements of a known spray field relative to LDA measurements. The purpose of this particular experiment was to determine the validity of the phase doppler. The theory of the device is presented in several papers (Bachalo W. D., and Houser M. J., 1984).

The data is in good agreement with the LDA measurements except for a few velocity profiles further down stream of the nozzle. The plane of discrepancy was located at approximately 10 nozzle diameters downstream. This discrepancy was also discovered independantly by Bachalo. No size comparisions can be made due to the lack of base line data.

V. Multicomponent Droplet Experiment

A multicomponent droplet experiment was designed by Tom Jackson (USAF), W.M. Roquemore (USAF), S. Aggarwal (Univ. of Illinois-Chicago), and myself. The purpose of the experiment is to verify the theoretical prediction of S. Aggarwal (Aggarwal S., 1987). The theoretical prediction is a Lagrangian-Eulerian approach in one dimension with molecular diffusivity as the main property in determining the evaporation rate of the droplet. The components of the droplet was limited to two fuels, with significantly different boiling points of each component.

The experimental set up consisted of a rectangular pyrex channel connected to a converging section to create a flat velocity profile in the channel. A droplet generator was positioned in the center of the volume at the entrance of the pyrex channel. Heating coils were placed in the test apparatus up stream of the channel and converging section to heat the

ambient air. Due to time constraints the test stand was not operational at the end of my fellowship.

Once the test stand is operational, the velocity and temperature gradients can be determined. The phase doppler will be utilized in this experiment with size and velocity information used to help verify the theory. To fully analyze the theory, species concentrations will be required at the surface of the droplet. A possible solution to this situation is the use of laser induced fluorescence on the fuels. Fuels having this characteristic are not common but do exist.

VI. Pre-PhD Thesis

Experimental work involving Droplet-Turbulent interaction is an important topic in today's combustion society. To observe this interaction a constant and controllable eddy environment must be created and visualized. A multijet flowfield was constructed to simulate a constant eddy environment. This was accomplished by having seven tubes supported by three thin disks at various axial locations with the first disc flat relative to the tube ends. This arrangement failed to create such an environment in both cold flow and combustor situations. It did have a significant impact on other types of combustion phenomena.

The multiple diffusion flames with the central jet as air has promise for a stable, cool flame at various flow conditions. The vertical laser sheet revealed the azimuthal interactions of the outer and inner structures. The azimuthal instability was first visualized by L. C. Chen (Univ. of Iowa)

VII. Recommendations

The multijet flow visualization has potential for future work. The flame demonstrates high stability at all flow conditions. The flame characteristics may be changed by controlling the central jet when the central jet consists of air. Colleague W.M. Roguemoore and Advisor L. D. Chen showed interest in pursuing this idea.

The test apparatus used in the multicomponent experiment shows promise for possible drop-turbulent interaction experiments. The turbulence can be created by grids and the droplets provided by the existing droplet generator. Visualizing the flow field remains the major problem in conducting this experiment.

REFERENCES

1. Bachalo, W.D., M.J. Houser. Phase/Doppler spray analyser for simultaneous measurements of drop size and velocity distributions. Optical Engineering, 1984, Vol.23, No. 5, pp. 583-590.
2. Aggarwal S.K., Modeling of a dilute vaporizing multicomponent fuel spray. Int. J. Heat Mass Transfer, 1987, To be presented.

**1987 USAF-UES SUMMER FACULTY RESEARCH PROGRAM/
GRADUATE STUDENT SUMMER SUPPORT PROGRAM**

**Sponsored by the
AIR FORCE OFFICE OF SCIENTIFIC RESEARCH**

**Conducted by the
Universal Energy Systems, Inc.**

FINAL REPORT

**THE INTEGRATION OF DECISION SUPPORT PROBLEMS
INTO FEATURE MODELING BASED DESIGN**

Prepared by:	Jon A. Shupe
Academic Rank:	Ph.D Candidate
Department:	Mechanical Engineering
University:	University of Houston
Research Location:	AFWAL/MLTC Wright-Patterson AFB Ohio 45433
USAF Researcher:	Major Steven LeClair
Date:	27 July 1987
Contract No:	F49620-85-C-0013

THE INTEGRATION OF DECISION SUPPORT PROBLEMS
INTO FEATURE MODELING BASED DESIGN

by
Jon A. Shupe

ABSTRACT

This report is an effort to consolidate and report about components of the design environment. In this report, design is discussed as being composed of decisions of various types and activities. These types and activities are set forth and described. Further, Feature Modeling as posed by the Materials Lab is discussed, as well as the relationship of decision making to Feature Modeling. Finally, it is posed that an appropriate and useful design environment will utilize a balance of knowledge based techniques and numerical decisionmaking algorithms, such as the Decision Support Problem technique for solving design problems. Several scenarios where this blend would be useful are discussed.

ACKNOWLEDGEMENTS

I wish to thank the Air Force Systems Command and the Air Force Office of Scientific Research for sponsorship of this research. The encouragement, guidance and help of Major Steven LeClair clearly added to every aspect of this research project.

I INTRODUCTION

Decision making in engineering design has been more of an art than a science, with a great deal of emphasis placed on decisions made on the basis of expertise and engineering intuition. Since World War II, there have been two areas of research that have had a bearing on decision making, namely Operations Research and Artificial Intelligence. Among other things, researchers in Operations Research have invented methods to allow a person to make optimal improvements, better choices, and better plans. These methods have generally been implemented on computers, since they require large amounts of numeric processing. One of the biggest, most successful applications¹ for Artificial Intelligence has been the development of expert systems, whereby the heuristic, intuitive, "rule-of-thumb" knowledge of an expert can be captured and then employed by others to assist in making decisions in the domain of the expert.

The Materials Laboratory of the Wright Aeronautical Laboratories at Wright-Patterson Air Force Base is particularly interested in the integration of design and manufacturing and what methods could be used to achieve this end. This report examines some of the possibilities of combining these areas of research into a useful design environment.

My research interests lie in the areas of partitioning and planning the design process. I am examining methods by which a model of a design artifact can be partitioned into submodels for synthesis. Important in this partitioning is the links and interfaces to be maintained amongst the submodels. Also, I am very interested in the types of decisions in design and creating a planner for the sequencing of design decisions.

II OBJECTIVES

Among the issues to be covered in this report are:

- Decision making in general, and the types of decisions encountered in design
- Feature Modeling as the Materials Lab has posed it.
- The useful balance between heuristic decision making and numerical decision making.
- Scenarios for decision making in a Feature Modeling Environment.
 - Intelligent material selection
 - Intelligent selection of input to features
 - optimal modification to features

¹Many Artificial Intelligence Researchers would maintain that if something can be applied it is no longer AI research, or today's AI research is tomorrow's algorithm. However, as designers and engineers, we are not as interested in the cutting edge of AI research so much as the application of any research that is useful to decision making and design.

III DECISIONS IN DESIGN

An engineer/designer performs two types of activities: symbol processing and decision making. Decisions made in the design of engineering systems are based on information from different disciplines. However, it is often the case that the computer-based tools that are presently used to support decisions are disciplined-based and analysis-oriented. Decisions are improved by repeated analysis; an inefficient approach that has been used successfully in the past when there were sufficient resources to allow it. Since analysis is disciplined-based, the interaction between disciplines cannot be taken into account without the use of synthesis.

Decision Making Activities

In addition to looking at the different words related to "decide", one can look at words that represent decision making activities. [1]

Intuition - insight, Rule-of-thumb;

Compare - bracket, collate, contrast;

Evaluate - estimate, appraise, assess; judge; rate;

Rank - class, classify; evaluate; grade, rate, order, sort;

Select - choose, cull, elect; prefer, opt for, optate; pick, mark, take;

Guess - decide under uncertainty;

Optimize - improve, modify for best results.

From these words, one can see certain patterns emerge in terms of mechanisms or activities useful to decision making.

Characteristics of Decisions

Real-world practical decisions are characterized by the following descriptive sentences:

- Decisions involve information that comes from different sources and disciplines.
- Decisions are governed by multiple measures of merit or performance.
- The measures of merit may not be of equal importance to the final decision and may conflict with each other.
- All of the information for making an adequate decision may not be available.
- Some of the information may be hard (based on scientific principles), some may be soft (based on the perceptive judgement of the designer) and some may be partially-soft (empirical in nature).
- The problem for which the decision is being made is open-ended.

These characteristics are shown in Figure 1. This figure is a visual demonstration of the decision characteristics to fix the principles in the mind. These characteristics will guide the thinking in the next section as the discussion moves from words about decisions to actual decision methods.

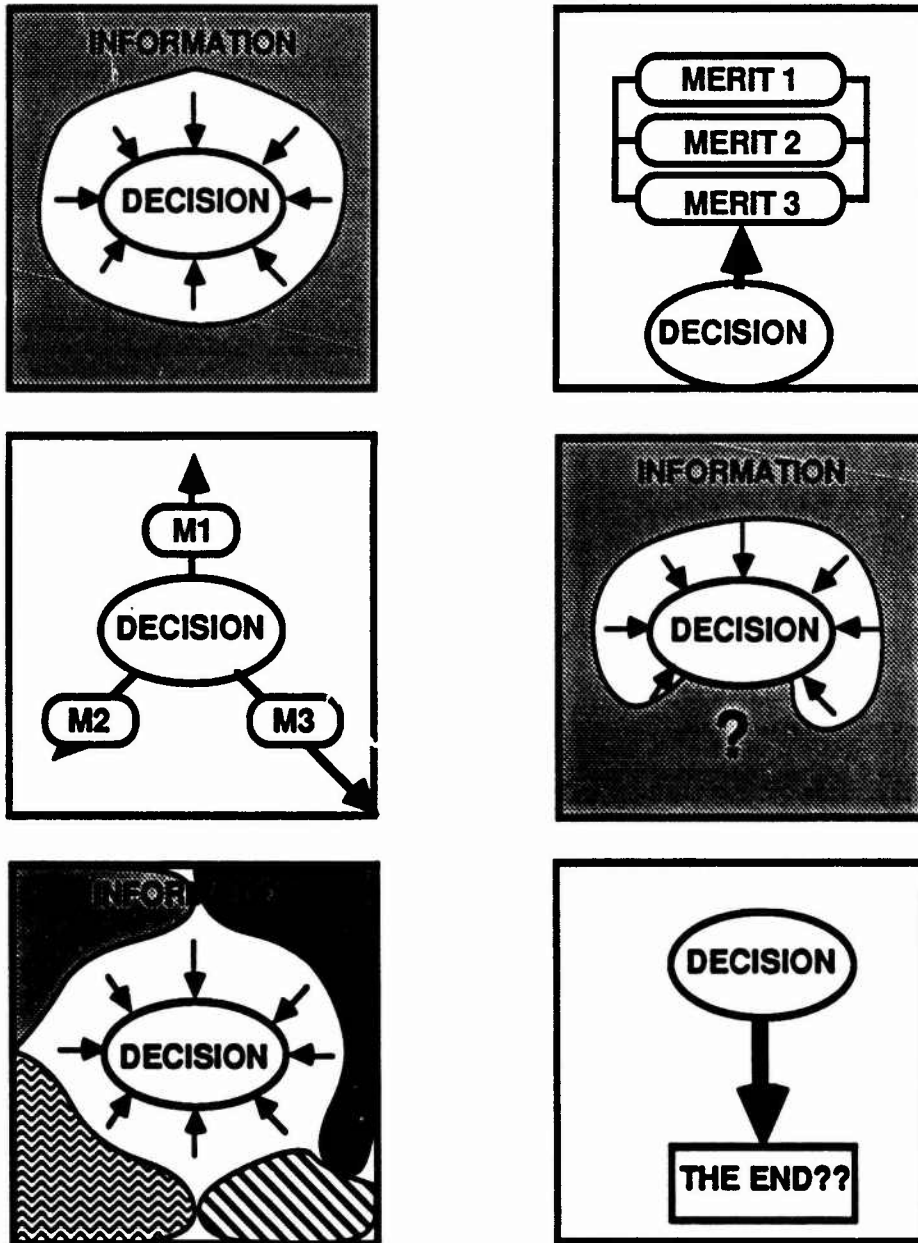


FIGURE 1 – DECISION CHARACTERISTICS

Separability and Order of Decisions

In addition to the characteristics of decisions listed above, it is desirable to define the relation of one decision to other decisions being made in the design environment. Among other things, it would be useful to determine the classes of decisions, not only in terms of types of decisions, but classes of decisions according to their separability and concurrency. It has been observed that it is useful to characterize the structure of the decisions in relation to each other by the following statements. Please refer to Figure 2.

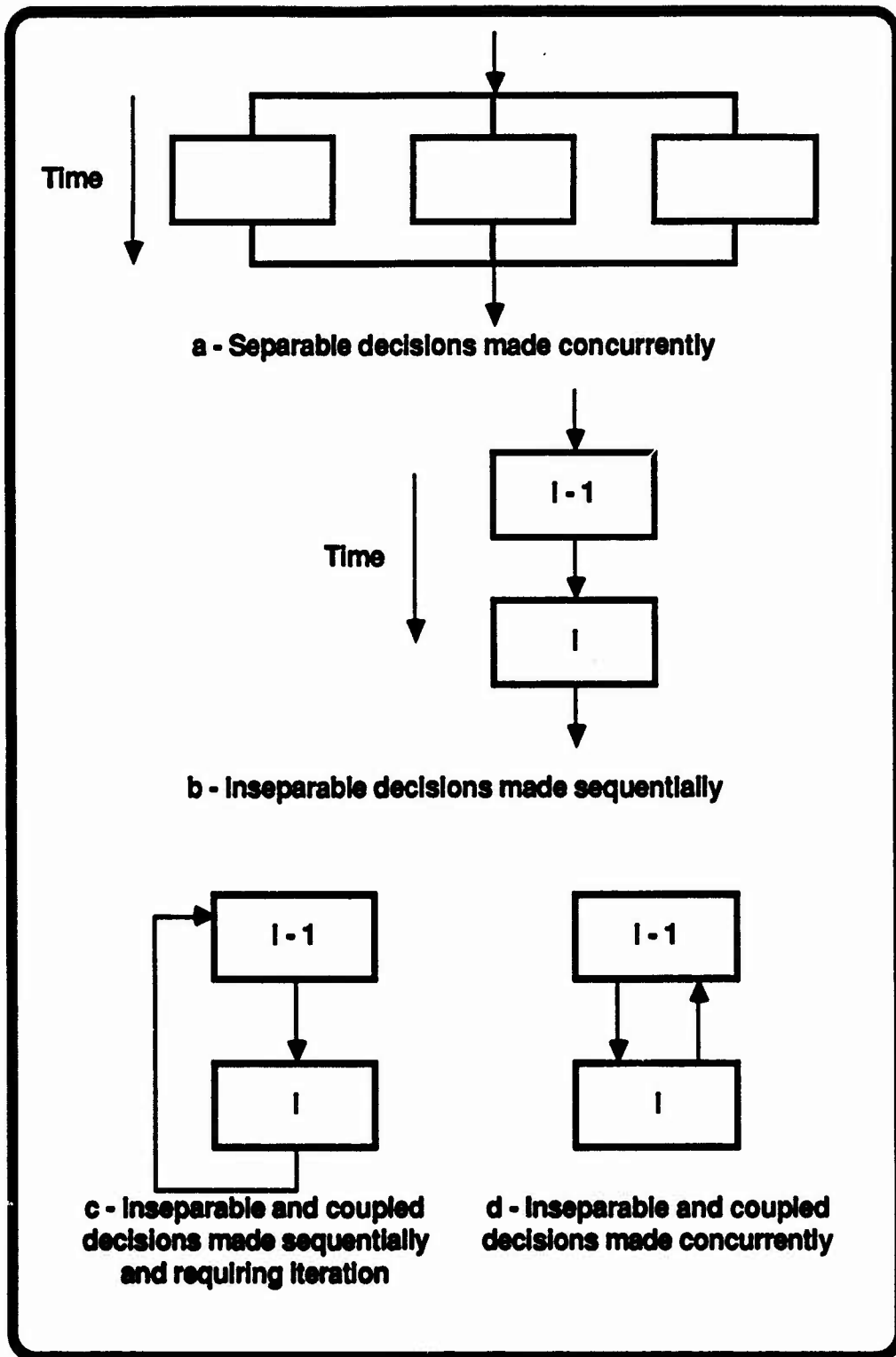


FIGURE 2 - DECISION INTERACTIONS

The previous description gives an idea of the relationships of decisions. There is a need to go further and order the decisions in relation to the artifact being designed. One must consider the relationship of decisions with in the hierarchy of the model of the artifact and its subsystems.

Assuming such a hierarchy exists, one then defines the plan for the decisions. In this decision plan:

- interaction between decisions to be made at the various levels of subsystems exists. This interaction may go one way or both ways.
- interaction between decisions to be made at the same subsystem level also exists. This interaction can also go one way or both ways.

Types of Decision Support Problems

Now that there is some idea of the characteristics of decisions and the recognition of the fact that there needs to be a plan of decisions, it is a good time to discuss the types of decision support problems that exist. The relationships between decision activities and decision support problem blocks are shown in Figure 3.

The DSP blocks are defined as follows.

- **Classification**
The selection of the top-of-the-heap concepts for further development
- **Selection**
The indication of a preference based on multiple attributes for one amongst several feasible alternatives.
- **Compromise (optimization)**
The improvement of an alternative through modification
- **Conditional**
Decisions in which the risk and uncertainty of the outcome are taken into account
- **Heuristic**
Decisions which are made on the basis of a knowledge base of expert facts and rules of thumb.
- **Coupled**
Decisions in which both selection and compromise occur.
- **Hierarchical**
High level decisions, between levels of decisions, which involve decision interaction, selection and compromise.
- **Heterarchical**
High level decisions, between decisions within a level, which involve decision interaction, selection and compromise.

DECISION MAKING ACTIVITIES

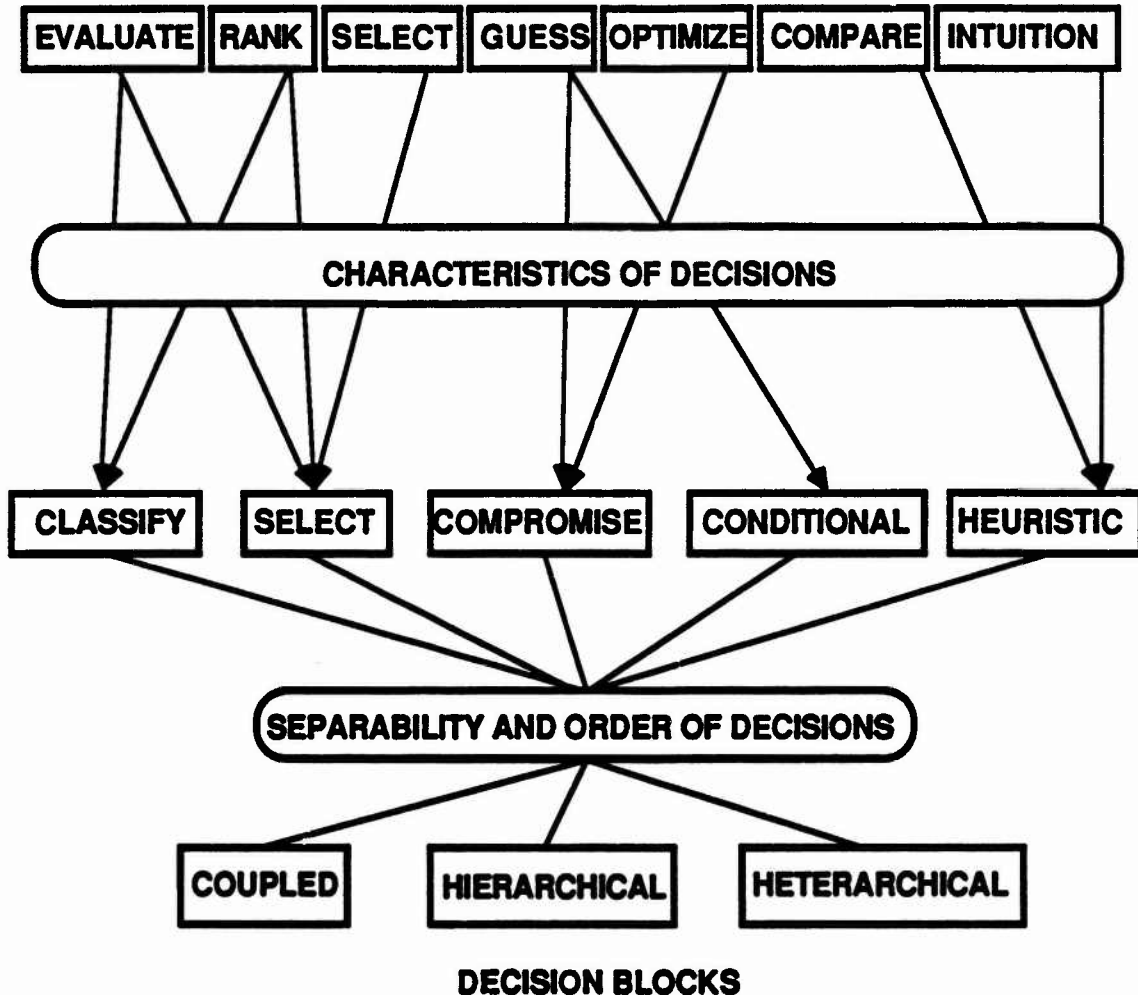


FIGURE 3 -- DECISIONS: FROM ACTIVITIES TO DSP BLOCKS

A classification DSP allows a designer to classify or group preliminary concepts based on criteria important to the design. A selection DSP is used to choose an alternative from several. The choice is made based on ratings given to multiple attributes and their relative importance. A compromise DSP improves an alternative, by changing design variables optimally, to find a superior solution. This involves the compromise between meeting stated constraints and reaching desired goals. The coupled, hierarchical and heterarchical DSPs involve the combined solution of multiple selection and compromise decision support problems simultaneously. Decisions in which risk and uncertainty of the outcome are taken into account are facilitated through the solution of conditional support problems. Decisions that are based on insight and rules-of-thumb captured from experts are heuristic in nature.

In Figure 3, these decision support problems are shown as generic decision building blocks. These building blocks can be fitted together to form the decision plan for the design of an artifact. Items such as time, organization, economics and so forth, affect the decision plan and the order of

the decisions within it. Referring to Figure 4, one sees the types of knowledge necessary to build a plan. This includes the knowledge of how the model of the artifact is partitioned for design. This would be the minimum information needed. Next, is the knowledge represented by the features of the artifact and the knowledge represented by the qualitative and quantitative models of production, quality and inspection. Finally, knowledge of the organization and temporal knowledge are useful to insure the decision plan takes advantage of the resources of the company.

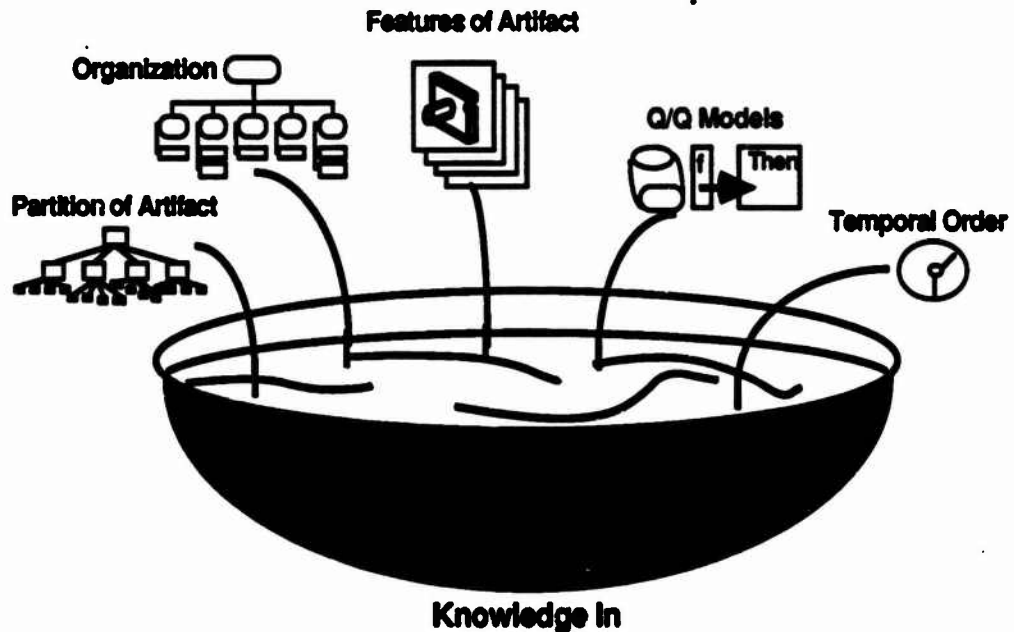
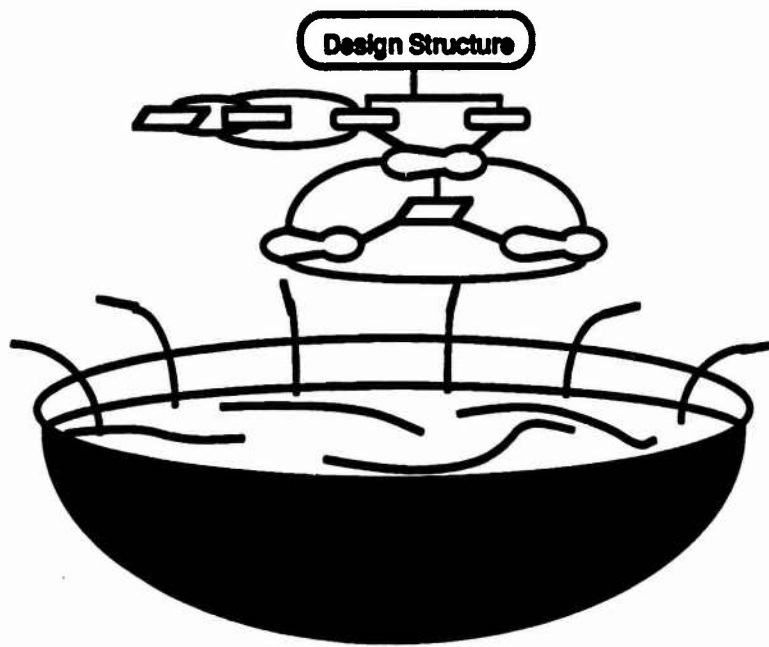


FIGURE 4 -- PLANNING DECISIONS: A WITCHES BREW

In Figure 5, a depiction is made of the output desired of such a decision planning procedure. The procedure should deliver a structure or hierarchy of the decision blocks and the links between the blocks. This structure is shown in more detail in Figure 6. Here a structure is depicted for the preliminary design of the artifact shown. Materials and manufacturing processes are to be selected. In addition, there is a coupling between the structure compromise (optimization) and analysis and the selection of the material. Further, there are heuristic decisions to be made about the producibility, etc. of the artifact as designed. This information is provided for redesign and cost optimization.

The development of an executive system that is capable of the process depicted in Figures 4-6 is very desirable. However, just how would one develop such a system for planning, ordering or structuring the decision hierarchy. There are several examples of knowledge based systems that plan, for example, MOLGEN, a planning system for genetic laboratory experiments. On the other hand, in the area of Operations Research, many methods have been developed for planning actions. These methods generally involve the use of an optimization package to find the



Structure Out

FIGURE 5 - PLANNING DECISIONS: DESIRED OUTPUT

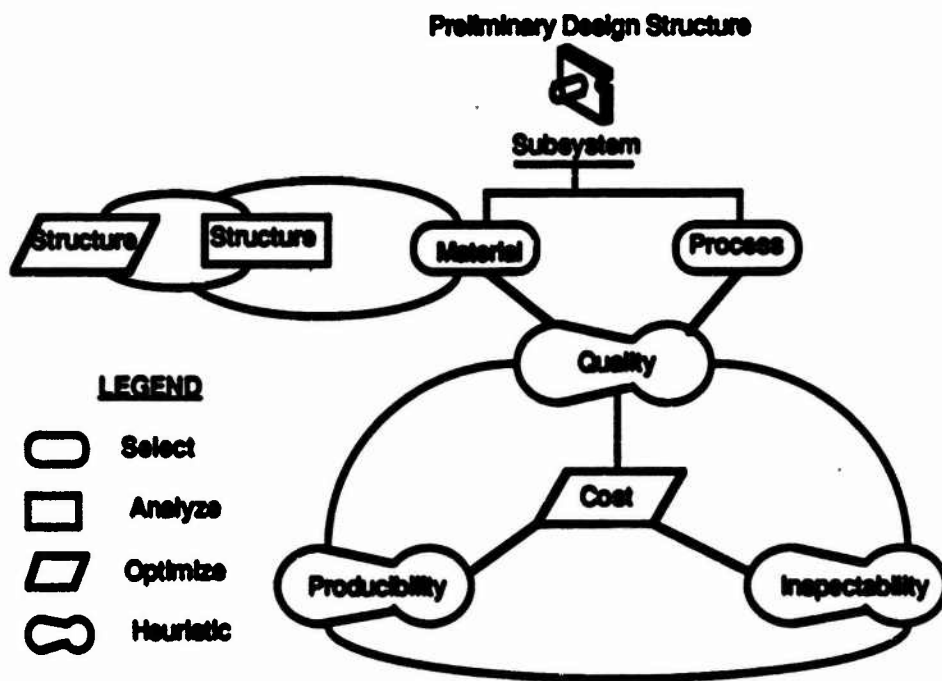


FIGURE 6 - PLANNING DECISIONS: A SAMPLE PLAN

sequence of actions that result in minimum time, minimum cost, maximum profit, etc. Experience indicates that probably no single method will suffice for creating the executive system. Rather, a synthesis of methods from both fields is necessary. The wide variety of knowledge input to the executive system is seen in Figure 4. There are many AI techniques that would be useful for representing and handling this knowledge. The optimization and other decision making

techniques would allow the executive system to pare away any excess in the sequence of decisions. Additionally, these methods could prove useful in conflict resolution. Often, if the conflict resolution is performed in a pairwise fashion, looping will result. This has been dealt with in the DSP techniques developed by Mistree, et al [8], particularly in the selection DSP.

IV BLEND OF DECISION MAKING TECHNIQUES IN DESIGN/MANUFACTURING

Decision making in the environment of design/manufacturing is necessary and useful, of that there is no doubt. However, the particular blend of the different types of decisions is the question. With the increase in popularity and application of knowledge based systems such as expert systems, there has been a move away from other forms of decisionmaking (optimization, conditional decisions, etc.). In some cases, knowledge based systems have been designed to do activities already performed by numerical algorithms [2, 3]. Which way is best is open to argument. In this section, methods for representing information about design artifacts is discussed. A proposal is made for a balance of knowledge based techniques and numerical algorithms for solving design problems. Several scenarios where this blend would be useful are discussed.

Feature Modeling: Representing Knowledge for Design and Manufacture

Feature modeling [4,5] is called for by the design-manufacturing sequence. In particular, feature modeling is the data structure that is needed to support the information needs of the following design and manufacturing functions:

- a user-friendly interface, including graphics output, for the designer;
- production of engineering drawings;
- selection of materials and manufacturing processes;
- evaluation for manufacturability as early in the design process as possible;
- analysis for functionality and cost, including finite element analysis when needed;
- process design, including die or mold design when needed;
- process planning and control;
- development of expert systems:
 - to guide, control, or advise on any of the above functions, or
 - to perform redesign based on results of analysis or manufacturability evaluation.

Presently, the databases of current CAD systems contain geometric description only in terms of points, lines, and faces; they do not provide information needed for the functions listed above. That the essential requirement of a suitable CIM data base is that it contain "high-level" knowledge or more abstract knowledge about the geometry of the design.

Design with features is being examined as a possibility for developing a higher-level CIM data

base. A feature is a geometric form or entity:

- whose presence or dimensions are relevant to one or more CIM functions (as listed above);
- whose availability to a designer as a primitive facilitates the design process.

Further, there are four types of features:

- **Primitive features**
 - Wall-like
 - Intersections
 - Projections
 - Depressions
- **Macrofeatures**
 - Generic Shape
 - Processing
- **Assembly features**
 - insert
 - Receptacle
- **Tooling features**
 - Gates
 - Runners

The information required by the various activities of design and manufacturing determine the features to be made available to the designer in that domain.

An important advantage of designing with features cited by Dixon and the Materials Lab is that, in a given domain, the design process itself can be facilitated when those geometric features most useful in the domain are readily available to the designer as primitives and when the design language provides effective and concise commands for combining such primitives into composite structures. There is still much to learn about the design representation data structures actually needed. In discussions with Lieutenants Wright and Madden, a new requirement for the representation of design/manufacturing knowledge via frames was described. The representation should not be a representation of geometry, that then provides information for the determination of manufacturability, etc. Rather, the representation should be more general, one that would then provide information for the determination of geometry, manufacturability and so forth. A possible representation is shown in Figure 7 [5].

Feature modeling will be used to provide a comprehensive data structure for computer aided design. However, other methods must be used to supply the design environment with decision making capability, since feature modeling is a knowledge representation scheme and has no inherent decision making capability.

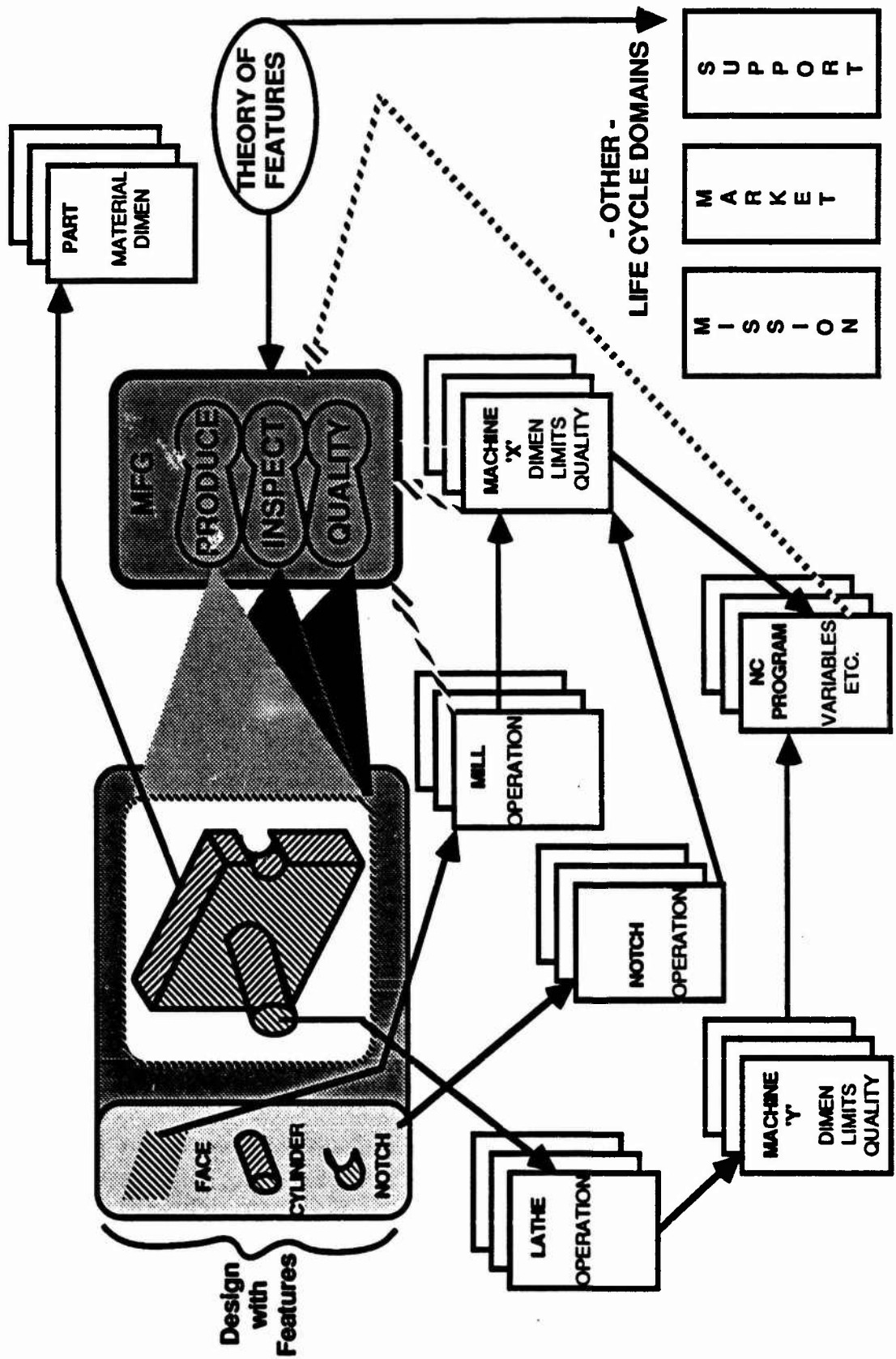


FIGURE 7 - FEATURE MODELING: DESIGN FOR MANUFACTURE

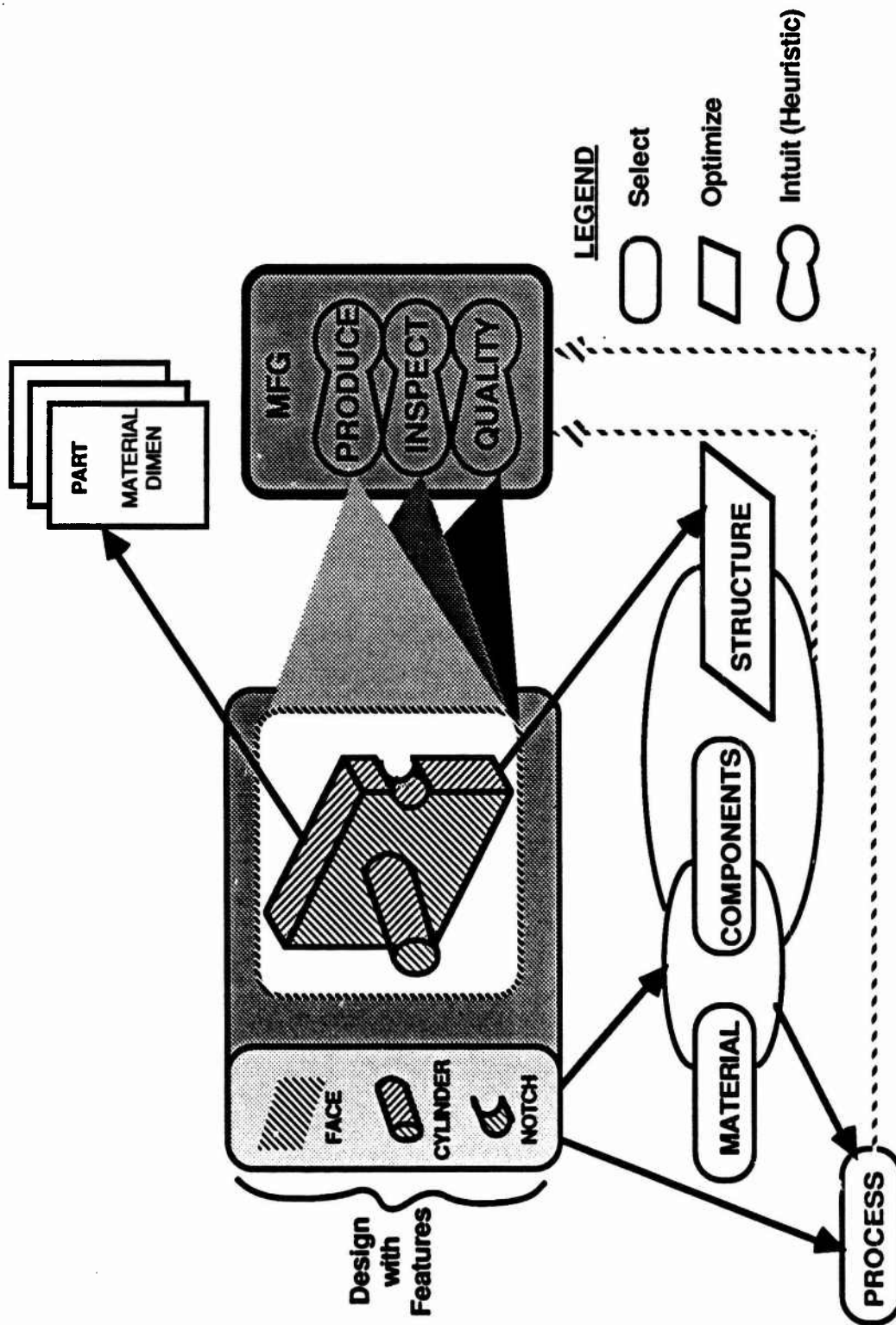


FIGURE 8 -- INTEGRATION OF FEATURE MODELING AND DSP TECHNIQUES

Feature modeling and decision making

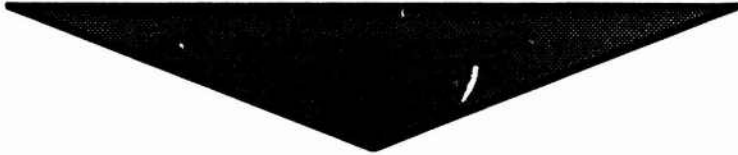
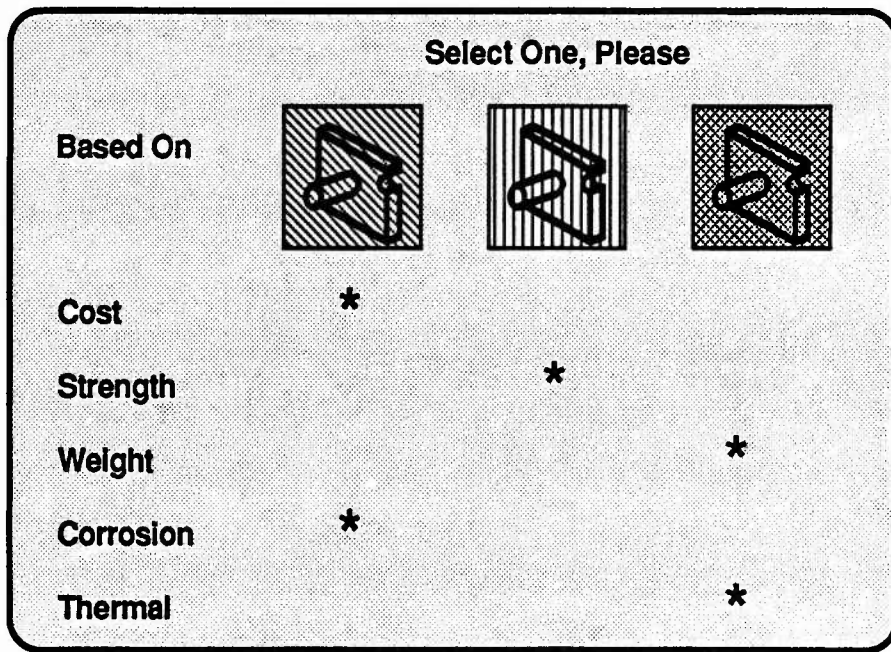
One decision that must be made about the features is the whether or not a feature meets manufacturability constraints, as shown in Figure 8. This will most probably be done via heuristics

operating on knowledge about the available manufacturing technology. Another decision to be made about features is that of which Macrofeatures with which the designer will begin. Selection of the "higher-level" features will then drive the selection of the primitive features. The selections of the features can be done with the selection DSP mentioned previously. A third decision to be dealt with is the modification of features or the artifact as a whole. Some modifications are required by the difference in what a designer specifies in terms of machining and what is actually available. Other times, the modification requires the change in a number of variables simultaneously to meet one or more specified goals, such as reduced weight, or maximum strength. This would be most appropriately handled by an optimization technique, such as the compromise DSP developed by Mistree, et al [8]. Examples of the selection and compromise DSPs follow.

Scenario: Material Selection

The need here is to select an appropriate material for an artifact (see Figure 9). It is possible that 'material' would be considered as a feature. Selection of the material would then lead to definition of related primitive features, as well as containing such physical information as yield strength, ultimate strength, density and so forth. A front end could be written to gather information about the environment for which the artifact is intended. This information could then be applied to cull out unsuitable alternatives. Heuristics could then be applied to determine the relative importance of the attributes for the remaining alternatives. The following is a simple formulation of a material selection decision for N materials. Notice that there would probably need to be more attributes to provide a comprehensive model.

GIVEN	The Alternatives:
	N materials
IDENTIFY	The Attributes:
	Economic factors
	Technical factors
	strength
	weight
	corrosion resistance
	fatigue resistance
	creep
	thermal properties
	Relative Importance
	Determined via heuristics
RANK	Alternatives based on resulting merit function values



Material Feature

FIGURE 9 – MATERIAL FEATURE SELECTION

Scenario: Multiple Feature Selection of a Turbine Blade

This is an example of the design of an artifact based on the selection of features and their combination. This problem would be done upstream from the layout of the parts. However, this selection would assist the designer (or even provide the designer) with the needed features for design.

- | | |
|-----------------|--|
| GIVEN | <ul style="list-style-type: none"> Alternatives <li style="padding-left: 20px;">Material alternatives <li style="padding-left: 20px;">Production alternatives <li style="padding-left: 20px;">Fastening alternatives |
| IDENTIFY | <ul style="list-style-type: none"> Attributes <li style="padding-left: 20px;">Material attributes |

Production attributes
 Fastening attributes
 RANK The alternatives according to merit function values
 PICK The best combination

The result of this would be indicate certain features. For example, if a nickel-chromium, cast blade with a fir tree root is chosen, then those features are provided with which the designer will work.

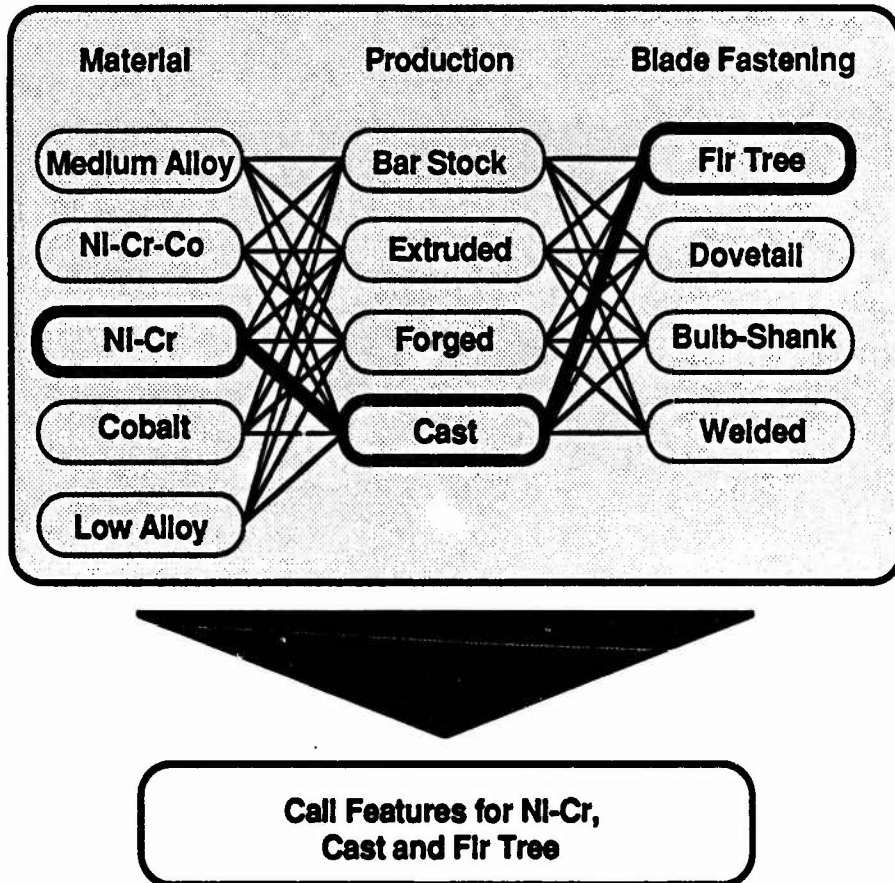


FIGURE 10 - MULTIPLE SELECTION FOR A TURBINE BLADE

Scenario: Compromise Problem for Primitive Mechanical Artifact (component)

This is a generic example for the optimization of an artifact. This involves the compromise between meeting stated constraints and reaching desired goals. Shown are typical mechanical considerations, plus economic considerations. Notice that some manufacturing constraints can be included. This would reduce the need to reapply heuristics to the features that are modified by the optimization, although the heuristics and numerical constraints could be used together for a double check. Further, heuristics specific to decision making could be applied to allow ease of input by the user and ease of interpretation of the results.

- GIVEN:**
- Material Constants
 - Load Conditions
 - Standards
 - Production and Maintenance databases
- FIND:**
- Dimensions of artifact
 - Dimensions of laminates for composites
 - Selection of material
- SUBJECT TO:**
- System Constraints
 - Strength
 - Fatigue
 - Displacement
 - Expansion
 - Creep
 - Wear
 - Tolerances and fit
 - Standards
 - System Goals
 - Minimum Weight
 - Minimum Cost
 - Maximize Strength
 - Bounds
- MINIMIZE:**
- Deviation from specified goals

V RECOMMENDATIONS

This report outlined some ideas about design and decision making. It further called for a blend between heuristic, knowledge based techniques with DSP techniques in an appropriate balance. No one is sure what the exact balance should be; however, several scenarios were presented showing such a blend.

The next step is to further structure the design/manufacture environment and to build a sample system that uses feature modeling representation and decision support problems for selection of features, conflict resolution and optimization. The types of decisions for the sample system must be determined and then specific scenarios can be developed, instead of the general ones presented here. The Materials Laboratory is moving ahead on a system that uses feature modeling. It is hoped that this report will assist them in integrating decision making capabilities.

REFERENCES

- [1] Webster's Dictionary and Webster's Thesaurus
- [2] Dixon, J.R., A. Howe, P.R. Cohen and M.K. Simmons, "Dominic: Progress Towards Domain Independence in Design by Iterative Redesign", Proceedings of the ASME Computers in Engineering Conference, Chicago, IL, July 20-24, 1986.
- [3] Nicklaus, D., S. Tong, and D. Russo, "Engineous, A Knowledge Directed Computer Aided Design Shell", Proceedings of the Third IEEE Conference on Artificial Intelligence Applications, February 22-28, 1987.
- [4] Dixon, John R, Eugene C. Libardi, Jr, Steve C. Luby, Mohan Vaghul and Melvin K. Simmons, "Expert systems for Mechanical Design: Examples of Symbolic Representations of Design Geometries", Engineering with Computers, 2, 1-10 (1987)
- [5] LeClair, Steven, "Briefing Slides on Feature Modeling", Personal Notes, 1987.
- [6] Tomiyama, T. and P.J.W. ten Hagen, "The Concept of Intelligent Integrated Interactive CAD Systems", Report CS-R8717, Computer Science/Department of Interactive Systems, Centre for Mathematics and Computer Science, Amsterdam, The Netherlands, April, 1987.
- [7] Stefik, Mark, "Planning and Met-Planning (MOLGEN: Part 2)", Artificial Intelligence, Volume 16, Number 2, 1981.
- [8] Mistree, Farrokh, Harsharandan Karandikar and Jon A. Shupe, Design By Decision Making, Springer-Verlag, (in production), 1988.

1987 USAF-UES SUMMER FACULTY RESEARCH PROGRAM/
GRADUATE STUDENT SUMMER SUPPORT PROGRAM

Sponsored by the
AIR FORCE OFFICE OF SCIENTIFIC RESEARCH

Conducted by the
Universal Energy Systems, Inc.

FINAL REPORT

OPTIMAL CONTROL OF THE WING ROCK PHENOMENON

Prepared by: Christopher D. Sierra
Academic Rank: Bachelor of Science
Department and University: Department Of Mechanical Engineering
The University Of Iowa
Research Location: Flight Dynamics Lab, Flight Controls Division, Control Dynamics
Branch and Control Analysis Group
USAF Researcher: Dr. Siva Banda
Date: 30 July 1987
Contract No: F49620-85-C-0013

OPTIMAL CONTROL OF THE WING ROCK PHENOMENON

by

Christopher D. Sierra

ABSTRACT

The nonlinear phenomenon of the wing rock of a slender delta wing about the mid-span axis was chosen for study. Time histories of the roll angle and the roll angle velocity were obtained and used to verify the results of the phase plane analysis of Nayfeh, Elzbeda and Mook. A simulation of the pilot changing the angle of attack of the wing was implemented in order to observe the effect the maneuver had on the behavior of the uncontrolled system. The time history of the build-up of wing rock was developed. The need for a method of controlling this phenomenon was observed. A control was then obtained using optimum systems control. The optimal control was also found for the system experiencing an "unexpected" pulse. The time histories of the roll angle for both cases were obtained.

Professor Patten's Sub-Optimal Control Algorithm was also used to obtain a control for this wing rock phenomenon. These results were presented so that a comparison between the two optimal control techniques could then be made.

ACKNOWLEDGEMENTS

I would like to thank the Air Force Systems Command and the Air Force Office of Scientific Research for their sponsorship of this research. The staff of Universal Energy Systems, Inc. must also be cited for all the assistance they provided. They cheerfully provided answers to any questions I had concerning the administrative aspects of the program. They were also able to help me find suitable living arrangements during my stay in Dayton, Ohio. For this I am truly grateful.

I also wish to acknowledge the help and support of all the people in the Flight Dynamics Lab. The members of the Control Analysis Group were especially friendly and helpful. The work environment which Dr. Siva Banda created as the head of the Control Analysis Group made my research effort rewarding and less difficult than it might otherwise have been.

I. INTRODUCTION

My principle research interest is in the control of dynamic systems. In particular my interest is in the use of optimal control techniques to achieve the control solution.

My interest and familiarity with the work of professor Patten, in addition to the course work I have completed to date led to my assignment with the Control Analysis Group of the Flight Dynamics Laboratory. It is hoped that continued work under the guidance of Professor Patten will result in the further development and implementation of his Sub-Optimal Feedback Control Algorithm (1).

II. OBJECTIVE OF THE RESEARCH EFFORT

The objective of my research effort as a participant in the 1987 Graduate Student Summer Support Program was to aid professor Patten in the implementation of his Sub-Optimal Control Algorithm.

The use of optimal control is limited because of the numerical and computational problems which typically occur when using the standard solution methodology. This method relies on the use of the variational calculus to change the optimum control problem to a two-point boundary value problem. It is in the solution of this two-point boundary value problem where the previously mentioned problems occur. The solution of the two point boundary value problem usually requires the use of an iterative algorithm. The large number of iterations and the computational time associated with each iteration prohibits the use of optimal control on line in real time and allows this optimal control process to yield only an open-loop control.

The wing rock of a slender delta wing was selected for analysis as it's effects on aircraft are of particular interest to the Air Force. Wing rock describes the rolling, oscillatory motion an airplane experiences when operating at a high angle of attack while simultaneously operating at a low subsonic Mach number (2). The angle of attack is the relative angle between the leading edge of the wing and the direction opposite that of the airflow. The onset angle is the lowest angle of attack for which this rolling motion develops spontaneously.

Wing rock causes a reduction in an aircraft's ability to track a target and it's overall tactical effectiveness. Safety during flight is also affected by the phenomenon of wing rock. Typically the

oscillations occur just before stall and can be a major factor limiting both maneuverability and landing speed. The study of the wing rock phenomenon is worthwhile as the result of further study will surely increase the flight envelope of future aircraft.

My assigned objectives were to duplicate the dynamics of the equation of motion which resulted from the work of Nayfeh, Elzbeda and Mook (3), to then simulate an aircraft maneuver and study the effect of the maneuver on the uncontrolled system and finally to study the effects of the same maneuver simulation on the optimally controlled system.

The control for this system was developed using the method of Open-Loop Optimal Control. These "optimal" results were then compared with those which resulted from the implementation of professor Paten's Sub-Optimal Control Algorithm.

III. THE DYNAMICS OF THE EQUATION OF MOTION

a. A result of the work of Nayfeh, Elzbeda and Mook (3), was an equation of motion for the subsonic wing rock phenomenon for slender delta wings,

$$\ddot{\phi} = -\omega^2 \phi + \mu_1 \dot{\phi} + b_1 \phi^3 + \mu_2 \phi^2 \dot{\phi} + b_2 \phi \dot{\phi}^2 \quad (1)$$

where ϕ was defined as the roll angle. The coefficients of the equation of motion were defined in table 1. They then used this equation to generate two phase planes for fixed angles of attack. These phase planes were represented in figures 1 and 2.

The work of Levin and Katz (4) demonstrated that the onset angle for a slender delta wing was at approximately 20 degrees. The phase plane for a 15 degree angle of attack showed the existence of one stable equilibrium point. Other possible trajectories may exist for phase planes generated from a nonlinear equation. For example horizontal parallel lines located above and below the presented equilibrium point region would be examples of other possible trajectories.

The phase plane for 25 degrees exhibited trajectories which either converged to a stable limit cycle or diverged. This divergence would cause uncontrolled continuous revolutions of the delta wing about its mid-span axis.

Phase planes do not explicitly show the behavior of the system as a function of time. Time histories

of the roll angle and the roll angle velocity will result from the solution of the equation of motion. The coefficients of the equation of motion were then calculated at 15 and 25 degrees from values found in table 1. The second-order differential equation of motion was represented as a system of two first-order differential equations.

$$\dot{\phi} = \dot{x}_1 = x_2 \quad (2)$$

$$\ddot{\phi} = \dot{x}_2 = -\omega^2 x_1 + a_1 x_2 + b_1 x_1^3 + a_2 x_1^2 x_2 + b_2 x_1 x_2^2 \quad (3)$$

An approximation to the solution of this system of differential equations was found using a variable order Adams-Predictor method or Gears method. Appropriate initial conditions were chosen from the phase planes.

b. The time histories of the dynamic behavior of the system were presented in figures 3 and 4. The angle of attack and the chosen initial conditions were denoted on each figure. The behavior of the system represented in these figures were in general agreement with the characteristics observed from the phase planes.

Initial conditions were chosen from the phase plane for a 15 degree angle of attack. They were all chosen from the region near the equilibrium point and appeared to converge to this point. This was of course in agreement with the phase plane for a 15 degree angle of attack.

A number of initial conditions were chosen from the phase plane for a 25 degree angle of attack. Convergence to the limit cycle for initial conditions chosen from inside the limit cycle did converge to the limit cycle. It was noted that there was a change of phase and that the periods did not appear to be constant.

It was also observed that divergence did occur for initial conditions chosen from the region of the phase plane outside the limit cycle.

IV. MANUEVER SIMULATION AND THE UNCONTROLLED SYSTEM

a. The dynamic behavior for the system at two constant angles of attack was observed in the results of the previous section. The phase planes and time histories of the roll angle exhibited the dynamic behavior of the system at angles of attack of 15 and 25 degrees. The constant angles of attack used in the above analysis were chosen because they were either above or below the onset angle. Angles of attack less than the onset angle caused the equation of motion to exhibit stable characteristics.

nonlinear, the probability was high that these values of the roll angle and the angular velocity of the roll angle caused the solution to diverge to large values of the roll angle.

Variable-step integration, fixed-step integration and integrators for use with stiff equations were all used in an attempt to show that this divergence was due to computational error and not the true behavior of the system. All of these integration schemes used on the equation of motion indicated that the roll angle was diverging to angles greater than those found on the limit cycle. This would indicate that the aircraft was experiencing uncontrolled continuous revolutions of the delta wing about it's mid-span axis.

Other functions for the angle of attack were tried. The general shapes of these functions remained unchanged except that the time the angle of attack was kept at 25 degrees was increased. This was done to allow the unstable system dynamics to develop fully to the limit cycle. The results were the same; The roll angle had gone beyond the angles which made up the limit cycle.

The phase plane for a 15 degree angle of attack implied that if an angle of attack of 15 degrees could be reached at a time when the absolute value of the roll angle velocity was less than 0.02 then convergence would occur. Convergence then in general was not possible. This indicated that some sort of outside input would be need to control these wing oscillations.

V. MANUEVER SIMULATION AND THE CONTROLLED SYSTEM

a. The development of the optimal control for a nonlinear system of equations was similar to the approach used for linear systems (5). A nonlinear system of equations with known initial conditions will typically have the following form.

$$\begin{aligned}\dot{\hat{x}} &= \hat{F}(\hat{x}, t) + \hat{B}(x, t) \hat{U} \\ \hat{x}(t_0) &= \hat{x}_0\end{aligned}\quad (4)$$

A convex index of performance was chosen as the cost function.

$$J = \int_{t_0}^{t_f} \{ \|\hat{x}\|_q^2 + \|\hat{U}\|_r^2 \} dt = \int_{t_0}^{t_f} C dt \quad (5)$$

The objective of the optimal control approach was to minimize the cost function constrained by the system of nonlinear differential equations. This constrained problem was reformulated as unconstrained by using a set of time dependent Lagrange multipliers (λ). The Lagrange multipliers may also be referred to as the costate variables.

Angles of attack greater than the onset angle caused the equation of motion to exhibit unstable characteristics. The stability and characteristics of the equation of motion depended upon the angle of attack used in calculating the equation's coefficients.

The phase plane analysis implied that if the angle of attack was greater than the onset angle the wing rock experienced by the aircraft was either approaching the limit cycle or had already converged to the limit cycle. Was it possible for the pilot to stop the wing oscillations by simply reducing the angle of attack below the onset angle? The answer to this was not apparent by simply utilizing the two constant angle phase planes.

A function of time for the angle of attack was needed to simulate the actions a pilot might undertake while engaged in the tracking of a target or the evasion of a pursuer. A possible scenario was for the pilot to increase the angle of attack from below the onset angle to a higher "unstable" angle of attack. At this angle of attack the pilot should have noticed the build-up of wing rock. Instinctively he would have attempted to reduce the angle of attack to a "stable" value below the onset angle. The function developed was presented graphically in figure 5. To insure continuous derivatives of this function, a function of the cosine was used to add "smoothness" to the corners during the ramped portions of this angle of attack function.

A Predictor-Corrector algorithm was again used for approximating the solution to the differential equation of motion. The known initial conditions allowed a forward integration with time. Recall that the angle of attack was constructed as a function of time. The appropriate angle of attack for a particular time was obtained from the angle of attack function. The coefficients of the equation of motion could be calculated from the values presented in table 1. The values were available for four angles of attack. Each of the columns making up this table consists of four data points. These four data points were then "fitted" with a third-order polynomial. The resulting polynomials were functions of the angle of attack. The coefficients were then calculated from these polynomials for the indicated angle of attack and then substituted appropriately into the equation of motion. The predictor-corrector method of solution was an iterative process and the approximations of the solution were then calculated at this time until the specified error tolerance was satisfied.

b. The method outlined above was used to generate time histories of the roll angle and the roll angle velocity. The results of this analysis were presented in figure 6. The initial value of the roll angle was 0.0 and the initial value of the roll angle velocity was 0.03.

The time history of the roll angle does not exhibit the characteristics intuitively expected from the phase planes. During the ramps the onset angle was crossed thus changing the characteristics of the equation of motion. It was noted that because of this change in characteristics a transition from stable to unstable or vice versa occurred during the ramped portions of the angle of attack function.

The amplitude of the first excursion of the roll angle was larger than that of the second. This was expected as the angle of attack was initially set at 15 degrees and the equation should exhibit stable characteristics. The characteristics of the equation should have remained stable until the onset angle was reached. The onset angle was reached at approximately 0.75 seconds. Though the second excursion occurred after 0.75 seconds the unstable dynamics did not have enough time to fully develop. Because the unstable dynamics had not fully developed, the time history of the roll angle gave the appearance of stability after the actual stability had ceased.

The angle of attack reached 25 degrees at 1.0 seconds and was held there until 4.0 seconds. The behavior of this portion of the plot during this period of time was also not unexpected. The transitions during the ramps had increased the time the equation was unstable by approximately 0.5 seconds. Half of this additional time was before the 25 degree plateau was reached while the remaining time occurred after the plateau. The unstable dynamics of the system were indeed apparent as the magnitude of the roll angle increased with each oscillation.

At approximately 4.25 seconds the equation of motion should have once again started to exhibit stable characteristics. The magnitude of the roll angle should have decreased. However this did not occur.

The coefficients of the equation of motion at 4.5 seconds corresponded to those found at an angle of attack of 15 degrees. The phase plane for this angle of attack showed only the stable equilibrium position and trajectories which led to this position. Mentioned previously was the probable existence of other trajectories. Though other stable equilibrium positions were apparently not possible (3), divergent trajectories were not ruled out and probably did exist.

The value of the roll angle and the value of the roll angle velocity at 4.5 seconds were both approximately 0.042. The value of the roll angle velocity placed it on a trajectory not near the known trajectories which converged to the equilibrium position. As the equation of motion was

This reformulation process also required the use of the Hamiltonian. The Hamiltonian was a scalar quantity defined by

$$H = H(\hat{x}, \hat{\lambda}, \hat{u}, t) = C + \hat{\lambda}^T \{ \hat{F} + \tilde{B} \hat{u} \} \quad (6)$$

where it should be noted that the Hamiltonian was not a function of \hat{x} .

The reformulated cost function then incorporated the use of the original cost function, the Hamiltonian and the set of time dependent Lagrange multipliers. This unconstrained formulation of the index of performance rewritten in terms of the Hamiltonian and the set of time dependent Lagrange multipliers was

$$J = \int_{t_0}^{t_f} \{ H - \hat{\lambda}^T \dot{\hat{x}} \} dt \quad (7)$$

The minimization of the index of performance required the use of the variational calculus which resulted in the following set of Euler Necessary Conditions.

$$\hat{\sigma} = \hat{\lambda} + H_{,\hat{x}} \quad (8)$$

$$\hat{\sigma} = -\dot{\hat{x}} + H_{,\hat{\lambda}} \quad (9)$$

$$\hat{\sigma} = H_{,\hat{u}} \quad (10)$$

The state and costate equations derived from the above may then be represented in the following form.

$$\begin{bmatrix} \dot{\hat{x}} \\ \dot{\hat{\lambda}} \end{bmatrix} = \begin{bmatrix} H_{,\hat{\lambda}} \\ H_{,\hat{x}} \end{bmatrix} \quad \begin{array}{l} \hat{x}(t_0) = \hat{x}_0 \\ \hat{\lambda}(t_f) = \hat{\lambda}_f \end{array} \quad (11)$$

The above Two-Point Boundary Value Problem was solved using a multiple shooting method. At each "shot" the initial value problem was solved using a Runge-Kutta differential equation solver. Newton's method was used to solve the resulting system of nonlinear equations simultaneously.

To apply the open-loop optimal control method outlined above, the equation of motion must appear in the form of equation (4). The control u must explicitly appear in the equation of motion.

$$\ddot{\phi} = -\omega^2 \phi + \mu_1 \dot{\phi} + b_1 \phi^3 + \mu_2 \phi^2 \dot{\phi} + b_2 \phi \dot{\phi}^2 + u \quad (12)$$

A system of two first-order differential equations was obtained from the single second-order differential equation of motion.

$$\dot{\phi} = \dot{x}_1 = x_2 \quad (13)$$

$$\dot{\phi} = \dot{x}_2 = -\omega^2 x_1 + \mu_1 x_2 + b_1 x_1^3 + \mu_2 x_1^2 x_2 + b_2 x_1 x_2^2 + u \quad (14)$$

The method of obtaining the optimal control for a system experiencing wing rock was developed above. The same simulation of the pilot changing the angle of attack was used. The initial conditions were the same as those chosen for the uncontrolled system. These were chosen because

the unstable nature of the system for these initial conditions had already been demonstrated.

b. The results of this analysis were presented in figure 7. The optimal control had attenuated the roll angle to zero in approximately 3 seconds. All energy in the system appeared to have been nearly dissipated. The ability of the optimal control to achieve such a good result in such a short time provided the incentive to continue the use of the optimal control method to control the phenomenon of wing rock.

VI. THE OPTIMALLY CONTROLLED SYSTEM AND AN UNEXPECTED PULSE

a. The behavior of the controlled system while acted upon by an unexpected disturbance was also of interest. The open-loop optimal control was again used to control the system. The initial conditions were identical to those used previously. The entire problem was identical to the previous case except that a pulse acted upon the system. The pulse was used to simulate turbulence, taking a "hit" from enemy fire or any number of other similar phenomenon. The duration of the pulse was 0.1 seconds. The strength of the pulse was 0.005.

The optimal control method yielded the optimal control for the system experiencing the situation described above. However, the manner in which the two-point boundary value problem was solved produced a control which "anticipated" having to control the pulse. The resulting control acted upon the system to control the pulse even before the pulse occurs. A proper control should have reacted to the pulse as it occurred.

Finding the control for this type of problem was essentially a three step process. The first step was to find the control for the system not acted upon by the pulse. This was simply the result of the last section. The second step was to rerun the simulations used to obtain the control. The simulation was started at 3 seconds to coincide with the start of the pulse. The initial conditions of this simulation were all equal to zero. This was justified because by this time the dynamics of the system which had resulted from the initial conditions had been sufficiently reduced. The third step was to form a composite of the controls found in the previous two steps. The control found in the first step was valid for time greater than or equal to 3 seconds. The complete optimal control was then formed using these two valid controls.

The corresponding time history of the roll angle was also found in this manner.

b. The results of this process were presented in figure 8 and figure 9. The plot of roll angle versus time demonstrated the disturbance rejection capacity of the open-loop optimal control method.

VII. COMPARISON WITH RESULTS OBTAINED USING THE SUB-OPTIMAL CONTROL ALGORITHM

a. The open-loop optimal control method used in finding the optimal control for this system demonstrated the inherent problems of this approach. This control certainly could not be developed "on line" in "real time".

The work of professor Patten has resulted in the development of a sub-optimal control algorithm. The advantage of using Patten's control method was that it could be implemented in a feedback loop in "real time". This close-loop sub-optimal control algorithm was outlined in professor Patten's Summer Faculty Research Final Report. This method was used by him to also develop the control for the system undergoing the pulse disturbance.

b. The results of professor Patten's analysis was represented in figure 10 and figure 11. A comparison could then be made between the results obtained using the open-loop optimal control and the results obtained using his method. The time histories of roll angle had similar characteristics. The attenuation of the system motion using the technique of Patten was faster than that of the open-loop optimal control. The magnitude of the initial excursions of the roll angle were less than those observed in figure 8. The system in figure 10 appears to be almost overdamped.

A comparison between the results presented in figures 9 and 11 verified that a larger control effort was used by the sub-optimal control to achieve this "better" attenuation of the system motion.

VIII. RECOMMENDATIONS

a. A suggestion for follow-on research would be a series of wind tunnel tests. The model used in obtaining the equation of motion could be appropriately modified so as to provide the necessary torque to be used in countering the wing rock. This counter torque would then be used to implement the control solutions obtained. This testing would be conducted to verify that the optimal controls developed do in fact provide proper system response and control of the phenomenon of wing rock.

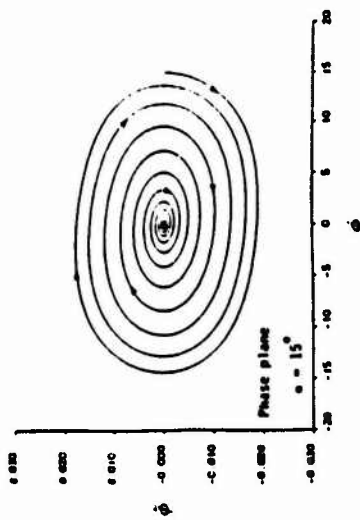


FIG. 1 Phase Plane $\alpha = 15^\circ$

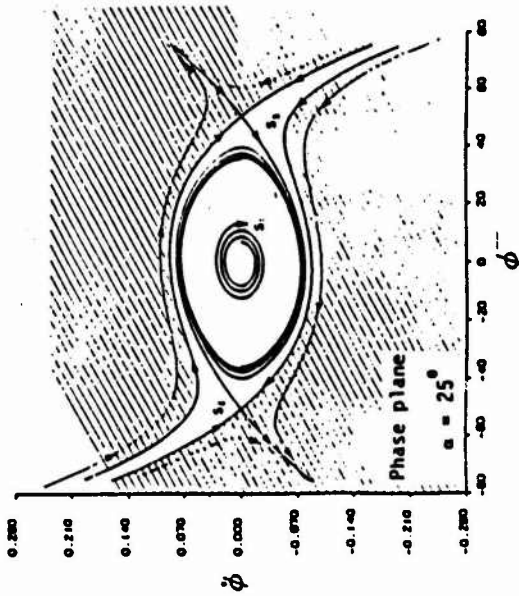


FIG. 2 Phase Plane $\alpha = 25^\circ$

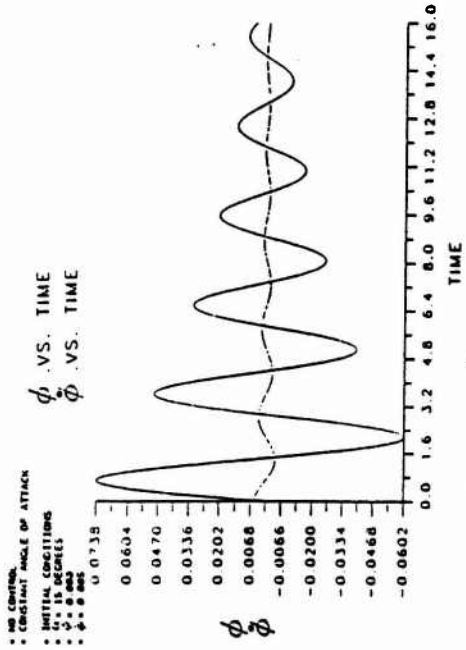


FIG. 3 ϕ and $\dot{\phi}$ vs time

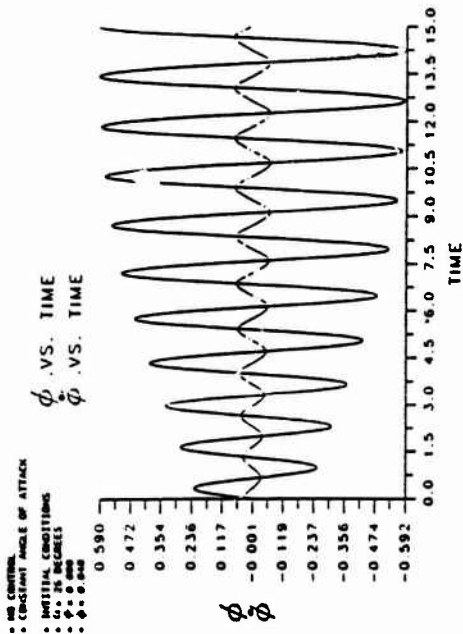


FIG. 4 ϕ and $\dot{\phi}$ vs time

a	a_1	a_2	a_3	a_4	a_5
15	-0.01026	-0.02117	-0.14181	0.99735	-0.83478
21.5	-0.04207	0.01455	0.04714	-0.18533	0.24234
22.5	-0.04681	0.01996	0.05671	-0.22691	0.59065
25	-0.05686	0.03254	0.07334	-0.3597	1.4681

$$\ddot{\phi} + \omega \dot{\phi} = u_1 \dot{\phi} + b_1 \phi^3 + u_2 \dot{\phi}^2 + b_2 \phi^2$$

where

$$\omega^2 = -C_1 a_1$$

$$u_1 = C_1 a_2 - C_2 \quad C_1 = 0.354$$

$$b_1 = C_1 a_3$$

$$u_2 = C_1 a_4 \quad C_2 = 0.001$$

$$b_2 = C_1 a_5$$

TABLE 1 Values For Coefficients of EOM

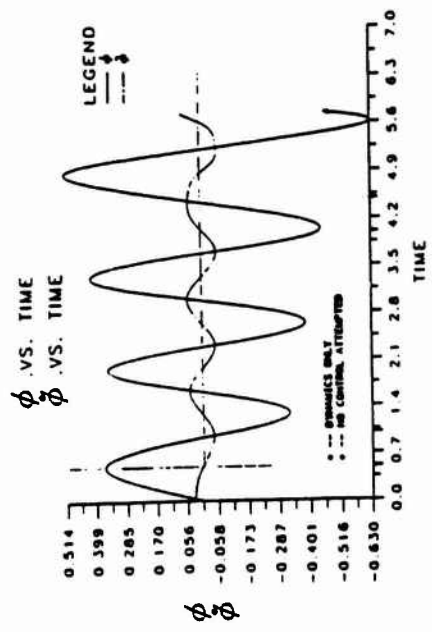


FIG. 6 ϕ and $\dot{\phi}$ vs time

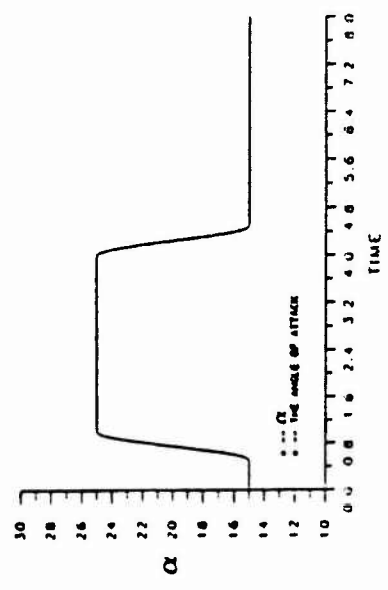


FIG. 5 α vs time

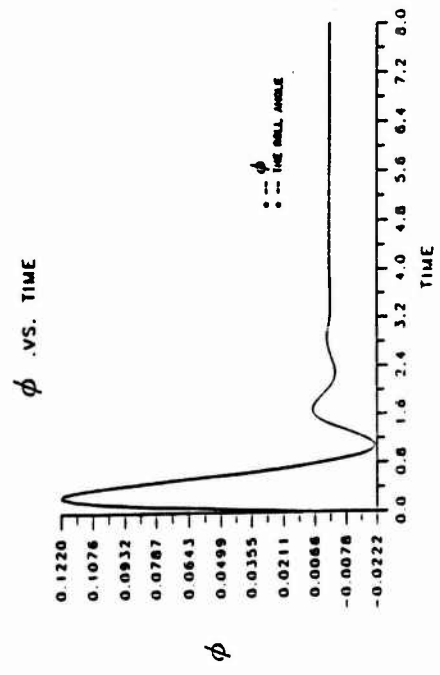


FIG. 7 ϕ vs time

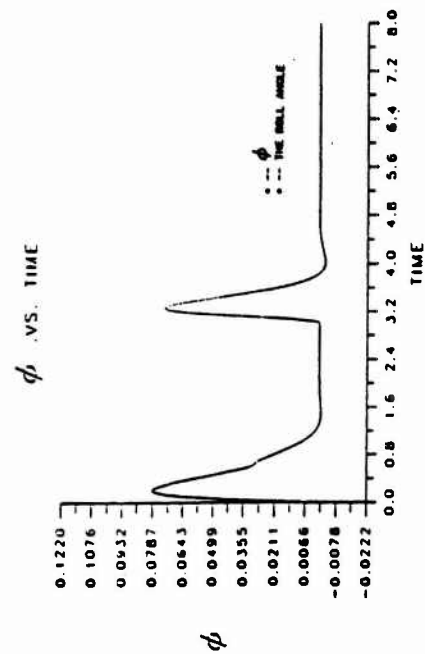


FIG. 10 ϕ VS TIME

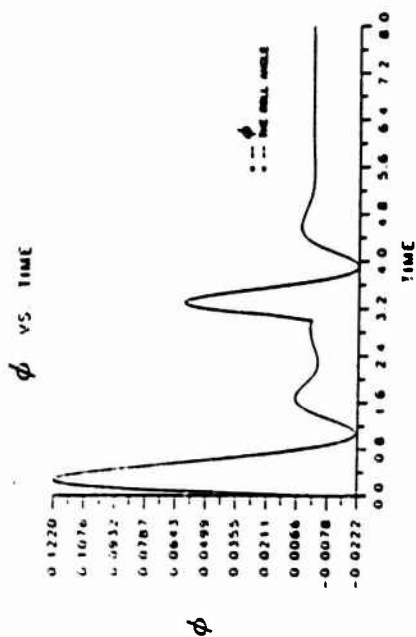


FIG. 8 ϕ VS TIME

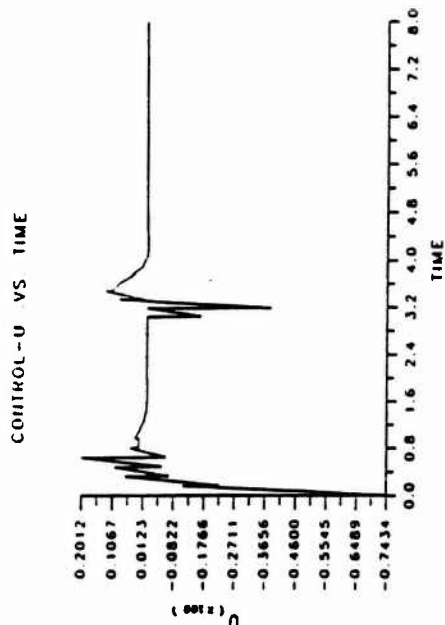


FIG. 11 U VS TIME

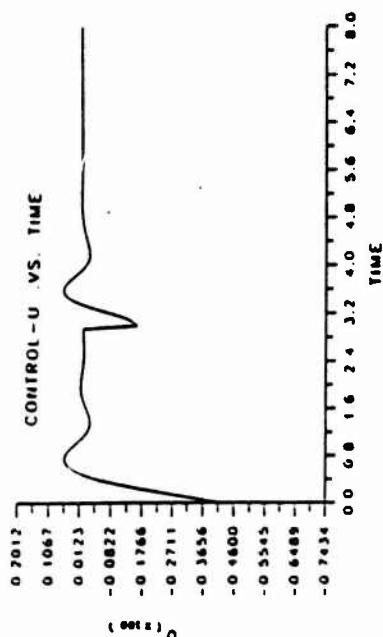


FIG. 9 U VS TIME

1987 USAF UES SUMMER FACULTY RESEARCH PROGRAM/
GRADUATE STUDENT SUMMER SUPPORT PROGRAM

Sponsored by the
AIR FORCE OFFICE OF SCIENTIFIC RESEARCH

Conducted by the
Universal Energy Systems, Inc.

FINAL REPORT
CALIBRATION AND DATA REDUCTION TECHNIQUES FOR
THE AFGL INFRARED ARRAY SPECTROMETER

Prepared by:	Gregory Sloan
Academic Rank:	Graduate Student
Department and University:	Department of Physics and Astronomy University of Wyoming
Research Location:	Air Force Geophysics Laboratory, Optical Physics Division, Infrared Branch
USAF Researcher:	Paul LeVan
Date:	8 August, 1987
Contract No:	F49620-85-C-0013

CALIBRATION AND DATA REDUCTION TECHNIQUES FOR
THE AFGL INFRARED ARRAY SPECTROMETER

by

Gregory Sloan

ABSTRACT

AFGL's Infrared Array Spectrometer has now taken data at the Wyoming Infrared Observatory on three occasions. This data has been used to calibrate the array and to test data reduction schemes. I present here the results of this effort: a calibration and data reduction algorithm for future use with the instrument.

Acknowledgements

I would like to express my gratitude to Universal Energy Systems, who provided me with the opportunity to conduct this research, and to Air Force Systems Command and the Air Force Office of Strategic Research for the funding which made it possible. In addition two individuals at the Air Force Geophysics Lab, Optical Physics Division, helped me greatly. The designer of GLADYS, Paul LeVan, proved to be a pleasure to work with. His support (and patience) were invaluable. The director of the Infrared Branch, Stephan Price should also be mentioned for his leadership and his encouragement.

I. Introduction

In the past infrared spectroscopy suffered from a lack of mosaic detector arrays sensitive to wavelengths beyond about 1 micron (μ). While optical spectra could be recorded at all wavelengths simultaneously on a photographic plate or a CCD, infrared spectra required the use of a single detector or several individual detectors. Low resolution ground-based spectroscopy has been based for the most part on circular variable filter (CVF) wheels. To use these, the spectroscopist must rotate the filter over a period of time, recording the flux from the object as the transmitted wavelength changes. The Infrared Astronomical Satellite (IRAS) used a different technique: the Low Resolution Spectrometer (LRS) was based on a prism spectrometer with a single detector. As the observed object was tracked across the aperture of the instrument, the wavelength of the light incident on a detector changed (Wildeman et al, 1983).

Both methods suffer from the same defect: all wavelengths in the spectrum cannot be recorded simultaneously. This limitation results in less efficient use of telescope time. In addition, for the case of ground-based observations, any changes in the atmospheric transmission during a wavelength scan will introduce noise in the spectrum and possibly distort its shape.

Recent technological advances have made possible the construction of detector arrays sensitive to wavelengths out to 30 microns. They hold great promise for infrared spectroscopy. One such array, a 58x62 Si:Ga array constructed by the Santa Barbara Research Corporation in California, is the heart of a prism slit spectrometer constructed under the supervision of Paul LeVan at the Air Force Geophysics Laboratory. This instrument has been used on three observing runs at the 2.3 m telescope at the Wyoming Infrared Observatory (WIRO). Here, I report on the progress made during the summer of 1987 to calibrate the instrument and to set up data reduction software for it, primarily using data collected in the most recent runs, in February and April, 1987.

II. The Instrument

The following section for the most part only highlights information presented by LeVan and Tandy (1987). As mentioned, the Geophysics

Laboratory Array Detector Spectrometer (affectionally known as GLADYS) is built around a 58x62 Si:Ga detector chip. The active area of the chip is only 4.35x4.65 mm in size, with a pixel spacing of 75 microns. Two 12-bit analog-to-digital converters (ADC's) digitize the output from each pixel on the detector, each ADC handling 1798 of the 3596 addresses.

Reading the chip has not proven to be a simple task. At the moment, the LSB in each ADC flickers, resulting in a resolution of $1:2^{12}$, or 1 part in 4096. Additionally, only one of the ADC's was operating properly during the two observing runs made so far. Pixel addresses read by the two chips are interleaved in the spectral direction on the detector, so this problem reduces the spectral sampling by a factor of two. Because the spectrum is slightly oversampled, this decreases the spectral resolution by a factor between one and two. When both ADC's are functioning, the spectral resolution ($\lambda/\Delta\lambda$) runs from 58.3 at 8.5 μ to 100 at 14 μ .

The array resides in a liquid He Dewar, designed as a down-looker (i.e., the beam enters the Dewar from the bottom). The spectrographic optics are built around a NaCl prism. Theoretically, these optics are designed for a spectral range of 8 to 14 μ across the chip, but edge effects raise the lower limit to roughly 8.5 μ . The Dewar window is BaF1, which has a rapidly deteriorating transmission beyond 12 μ ; thus the upper spectral limit is only about 12.5 μ . This window will eventually be replaced with a ZnSe material, which should extend the upper limit to about 13.5 μ .

The WIRO 2.3 meter telescope has an f-ratio of 27, giving a plate scale at the Cassegrain focus of 3.27"/mm. The spectrographic slit width of 1 mm therefore corresponds to 3.27" on the sky. The Dewar optics re-image the f-ratio down to 7.5, giving a plate scale of 0.88" per pixel.

The ADC's read the array pixel by pixel, with each pixel taking about 3 μ sec to be read. To scan the entire array thus takes about 5 msec. The array is repeatedly scanned while the secondary mirror on the telescope chops between the source and a blank sky position with a frequency of 2-5 Hz (usually 3). Data from the two chop positions collect in separate memory blocks. After 60 individual scans (this number can be changed) the data from one chop position is subtracted from the other and the resulting information stored as a file on the PDP 11 at the observatory. Such a

file, or picture, will be referred to as a frame. The background level has now been removed, but due to gradients in both the sky and the the telescope optics, the frame will still contain a background residual.

The signal/noise ratio in the spectra is not background limited; rather, the noise is presently dominated by the instrument itself. Likely sources are the ADC's and the clocking system. As a result, the noise is independent of the signal and thus the signal/noise ratio is proportional to the signal. This fact is exploited in the weighting procedure used to combine spectra discussed below.

III. Calibration

First, the instrument must be calibrated. This is done by obtaining a high signal to noise frame of an object whose spectrum was also taken by the LRS. The simplest approach is to treat each row on the array as a separate spectrum and compare the fluxes to obtain multiplicative correction factors for each pixel. Such a factor would contain corrections for pixel response as a function of wavelength, sensitivity from pixel to pixel, atmospheric absorption, and instrumental transmission.

There are, however, some complications. To match the LRS with the observed spectrum, one must know the wavelength corresponding to each pixel. Unfortunately, the uncertainty in the present calibration is still a significant fraction of a micron. Observations of planetary nebulae and objects with similarly narrow spectral lines should resolve this problem.

Another complication is the large number of spikes contained in the data; roughly 5-10% of the pixels in any frame contain signals well above their neighbors. These pixels must be identified and their signals ignored. This is done by passing the data through two complementary filters. The first identifies a spike as a pixel whose value is both above the background residual and three times or greater than its neighbors. The second filter resembles a median filter; it examines the pixels in groups of three, identifying the middle point as a spike when its value falls above or below both of its neighbors by a large (adjustable) number.

One would then expect each row to correspond to a spectrum, but this

unfortunately is not the case. The problem lies in a slight misalignment between the axis of the prism and its optics and the axis of the array; they are off by roughly $.85^\circ$. The resulting spectrum therefore does not fall along a row, but at a slight cant: the spectrum moves closer to the top of the array at longer wavelengths. This shift can have a significant effect on the appearance of a spectrum. For example, if one considers a row above the peak spectrum, as one moves to higher wavelengths, one is moving into the peak spectrum; the effect will be a "redder" spectrum. The opposite is true below the peak spectrum; spectra there will take on a "bluish" nature.

To correct for this, the calibration program determines what the array should look like, given the slope of the spectrum, its actual position on the array, and the behavior of its seeing disk as a function of wavelength. These parameters are easily determined from the spectrum in question. The algorithm is as follows:

1. For each column, find the row with the peak signal. Using this datum, and the signal from the two adjacent rows, a gaussian curve can be fitted, giving the fractional peak row, y_m (where the peak signal actually should lie), the peak signal at this position, s_m , and the spread σ of the gaussian.
2. Because these data are somewhat noisy (due in large part to responsivity variations from pixel to pixel), a least squares fit is used to fit a line to the fractional peak row position across the columns. Given a misalignment angle of $.85^\circ$, the slope is $-.015$ (in pixel units). Since only 31 of the 62 pixels are used at the moment, the slope among the usable pixels becomes $-.030$. This value is clamped and the y intercept (y_0 , the intercept in the zeroth column) solved for. Then,

$$y_m'(\lambda) = mj + y_0; \quad m = -.030, \quad j = \text{pixel column number.} \quad (1)$$

Note that $j=j(\lambda)$, where $j(\lambda)$ is determined in the wavelength calibration mentioned above. Additionally, the behavior of the gaussian spread as a function of wavelength is also fitted to a line. While this certainly is not the case, except in purely diffraction-limited observations, a linear relation is quite adequate given the nature of the data.

$$\sigma(\lambda) = m_\sigma j + \sigma_0; \quad m_\sigma \approx .011 \quad (2)$$

3. These parameters are then used to lay down the assumed spectrum across several rows, finding the expected signal value for each pixel.

$$S(y, \lambda) = f(\lambda) \exp[-(y - y_m'(\lambda))^2 / 2\sigma(\lambda)^2], \quad (3)$$

where $y_m'(\lambda)$ and $\sigma(\lambda)$ are given above and $f(\lambda)$ is related to the LRS spectrum $F(\lambda)$ by the equation

$$f(\lambda) = \frac{F(\lambda)}{\sqrt{2\pi} \sigma(\lambda)}. \quad (4)$$

This equation follows from the assumption that the spatial profile of a point source fits a gaussian spread. One cannot just use $F(\lambda)$ as the initial spectrum, since the IRAS beam width integrated over the entire gaussian profile. One must instead solve for $f(\lambda)$, the peak amplitude of the gaussian.

The calibration object used so far has been the extremely bright infrared source IRC+10216, observed in February, 1987. Figure 1 gives the LRS spectrum for the object, while Figure 2 shows the calibration block for one of the frames. The effects of the misalignment are clearly illustrated. Row 2 has a noticeable bulge in the mid-wavelength region and a slower drop-off toward longer wavelengths than the rows below the peak spectrum (4 and 5). Figure 3 presents actual data, corrected only for atmospheric and instrumental transmission. While the data is a little noisy, the trends match those of Figure 2.

Now the calibration block can be compared to the array data pixel by pixel to give multiplicative correction factors. These correction factors are normalized on a row-by-row basis and averaged together to obtain an average correction spectrum, which is divided out of the correction array. Thus, each correction coefficient in the array is on the order of one. The average spectral correction includes atmospheric and instrumental absorption as well as the average wavelength dependent response function of the detectors. This spectral correction is presented in Figure 4. The two major features are the ozone corrections around 9-10 μ (pixels 4-7) which compensate for ozone absorption, and the rise in the correction factors at longer wavelengths to compensate for decreasing instrumental

and atmospheric transmission in this part of the spectrum.

The correction array now contains only information on the relative responses among the pixels in a given row. By taking spectra of the night sky, one can determine how the pixel response varies from one row to the next. The results indicate that row 1 and rows 47-58 behave poorly. The behavior of rows 1 and 58 results from edge effects, but rows 47-57 indicate a more serious problem, possibly in the indium connections between the detector and the readout array. Of the remaining good rows, all except rows 2 and 3 on the top of the array and rows 42 and 46 on the bottom have virtually identical responses. So the correction array can be used to flat-field the data pretty much as is.

The correction array should not change over time, as the pixel responses should remain constant. At present, only rows 2-17 have been calibrated. During future observing runs, data will be obtained to calibrate the rest of the array.

The average spectral correction, on the other hand, will change with time due to variations in atmospheric ozone and water vapor content. In the future, a list of standard objects will be selected so that the average spectral correction can be measured repeatedly during an observing run to determine its behavior both with time and airmass.

IV. Data Reduction

A typical observation of an object consists of 10 to 40 frames, which the the data reduction software can co-add into one frame along with estimated uncertainty. The general procedure is to reject spikes on a frame-by-frame basis and then co-add. The spike rejection technique has already been described above.

Next the background residual can be removed from the frame. This residual can be taken from separate frames, but usually it is calculated by averaging the blank sky rows in the same frame. The software allows the user to determine which rows contain background data and which contain source data. The benefit of this "self-subtraction" method is that the uncertainty in the background will usually be much less than the uncertainty in the spectra themselves, since the background is based on

the same number of frames as the spectra and is a combination of many more rows. However, if there are gradients in the background sky across the frame or if very faint objects are lurking in supposedly blank rows, this method can be dangerous.

The program then corrects the signal spectrum by flat-fielding it and multiplying the average spectral correction back in to correct for atmospheric and instrumental transmission.

The next step is to correct for the misalignment between the optics and the array. A subroutine handles this as follows:

1. It locates the (fractional) peak row in the middle column of the array and calculates the position of the old array points in a new coordinate system rotated about this point by an angle of -85° .
2. Signal values in the new array are then determined by averaging together all old data points in a circular neighborhood around the new position:

$$S'_{ij} = \frac{\sum w_k S_{i,j,k}}{\sum w_k}, \quad (5)$$

where w_k is the inverse of the distance between the old and new data points. If the distance is zero, then the new signal is taken to be the old signal. If the distance is more than 1.6 pixels, then the weight is taken to be zero. Note that in all equations in this paper, the subscript i refers to the row number on the array (spatial position), while the subscript j refers to the column number (spectral position).

The effect of this rotation is to significantly smooth the data. This effect could be increased or reduced somewhat by enlarging or decreasing the cut-off distance of 1.6 pixels. One can also change the dependence of the weights upon r .

The resulting frame now can be examined row-by-row to study the spatial nature of the source object's spectrum. Any range of rows can also be summed together to simulate a wider beam, using a technique based loosely on that presented by Robertson (1986). In this sum the rows are weighted by the square of their signal in a given wavelength range (i.e. by the square of their signal to noise ratio)

$$S_{sum, j} = A \frac{\sum w_i S_{i,j}}{\sum w_i}; \quad w_i = \sum S_{i,j}^2, \quad (6)$$

$$A = N \frac{\langle w \rangle_{all}}{\langle w \rangle_{def}}; \quad N = \text{total number of summed rows,}$$

where $\langle w \rangle_{all}$ is the average over all rows, and $\langle w \rangle_{def}$ is the average of those rows with a defined signal in a given column. The factor A is necessary to conserve flux and to account for those pixels with missing values.

V. Estimating the Uncertainty

The uncertainty of the mean from a set of co-added frames is, for each pixel,

$$\sigma_{i,j} = \left[\frac{\sum (S_{i,j,k} - \langle S_{i,j} \rangle)^2}{N_{i,j}(N_{i,j}-1)} \right]^{1/2} = \left[\frac{\sum S_{i,j,k}^2 - N_{i,j} \langle S_{i,j} \rangle^2}{N_{i,j}(N_{i,j}-1)} \right]^{1/2}. \quad (7)$$

The index k, summed over in the numerator, represents the individual frames. When several rows are combined to produce one background spectrum, the uncertainty can be expressed by the analogous expression,

$$\sigma'_j = \left[\frac{\sum S'_{j,k}^2 - M_j \langle S'_j \rangle^2}{M_j(M_j-1)} \right]^{1/2}, \quad (8)$$

where

$$M_j = \sum N_{i,j}, \quad (8a)$$

$$\langle S'_j \rangle = \frac{\sum N_{i,j} \langle S_{i,j} \rangle}{\sum N_{i,j}}, \quad (8b)$$

$$\sum_k S'_{j,k}^2 = \sum_i \left(\sum_k S_{i,j,k}^2 \right), \quad (8c)$$

$$\sum_k S_{i,j,k}^2 = (N_{i,j}-1)\sigma_{i,j}^2 + N_{i,j} \langle S_{i,j} \rangle^2. \quad (8d)$$

After this uncertainty is determined, all uncertainties resulting from algebraic operations are simply taken to be the rss (root sum square: the square root of the sum of the squares).

VI. Some Results and Plans for the Future

The April observing run included observations of the following objects: μ Cep, α Ori, and NML Cyg. These objects, as well as IRC+10216, are extended post-main sequence stars and are all very bright in the infrared. The spectra obtained are presented in Figures 5-9. It should be noted that the spectra here have been examined primarily to study the instrument, not the objects themselves. Comparison with LRS and CVF spectra indicate that GLADYS is behaving well.

An examination of the spectra from α Orionis and NML Cygni demonstrates that GLADYS can detect changes in spectral shapes with distance from the star (Figures 7 and 9). While the signal/noise ratio is not really strong enough to draw any conclusions about the objects themselves, the possibilities for future observations with longer integration times look very promising.

Future software will focus on the analysis of spectra such as these. Fitting a blackbody curve to the spectra would allow the absorption and emission line widths to be calculated, a necessary step before the data can be thoroughly studied. In addition, methods of improving the signal to noise by different integration and co-adding strategies will be examined.

The instrument shows great potential, although it is far from perfect at this stage. Hopefully, it can be turned on more extended and fainter objects such as galaxies and star formation regions. I am truly excited about the possibilities and am looking forward to future work with GLADYS.

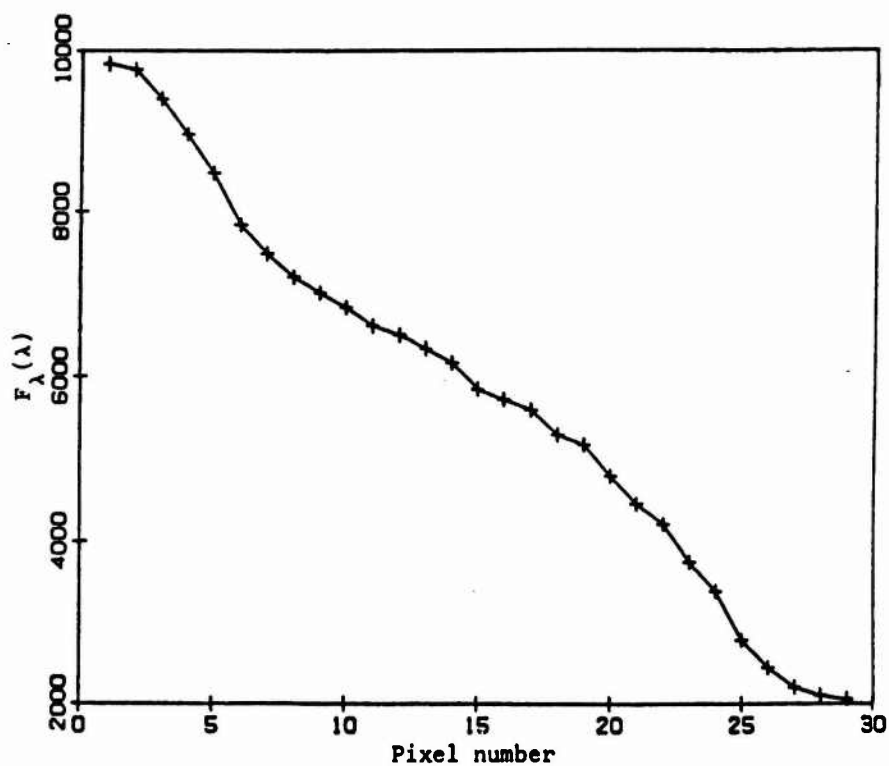
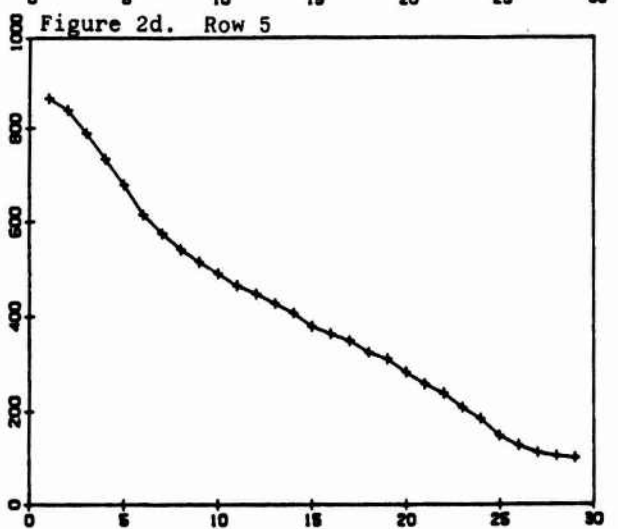
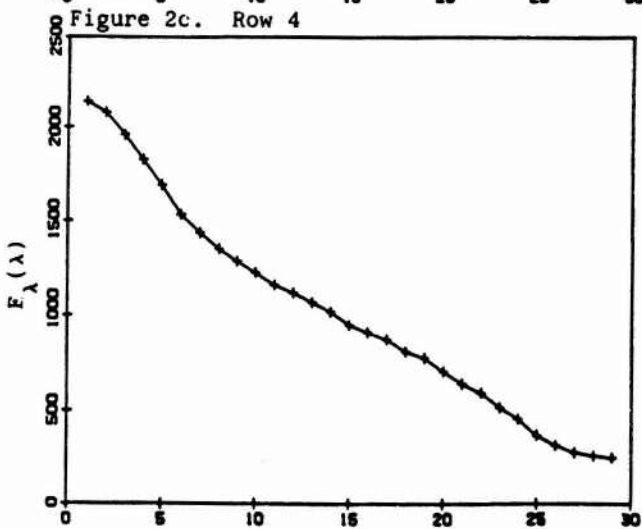
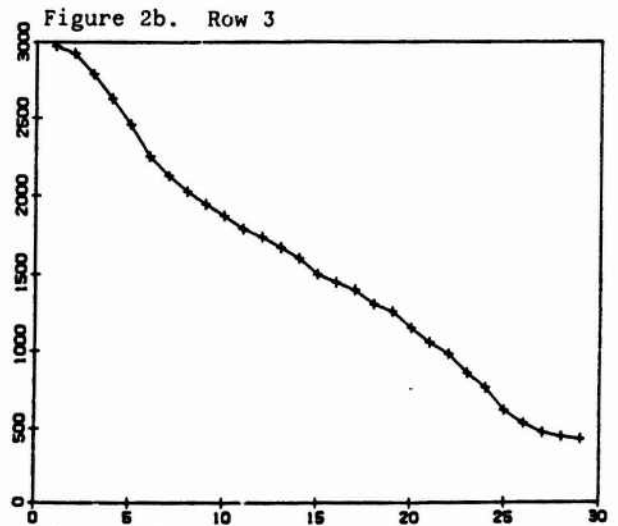
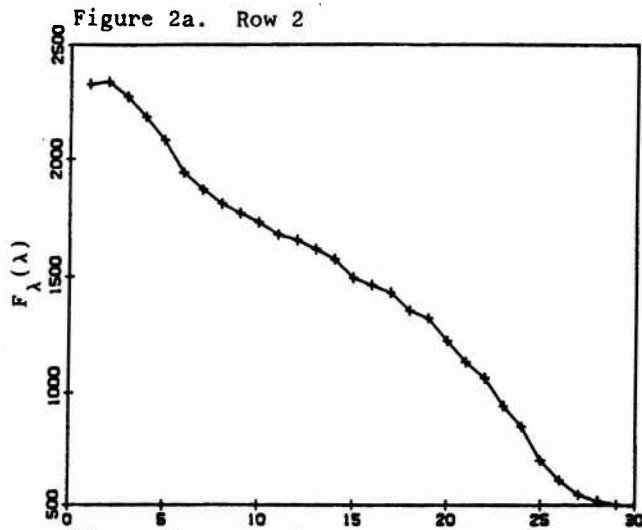


Figure 1. LRS data for IRC+10216. The vertical axis is $F_{\lambda}(\lambda)$, in arbitrary units scaled to match the signal counts from GLADYS.



Pixel number

Pixel number

Figure 2. Calibration block for IRC+10216. For one of the frames taken in February, the position of the spectrum has been determined and the behavior of its spatial spread $\sigma(\lambda)$ calculated. This information has been used to determine what the spectrum should look like across several rows of the array. Again, the vertical axis is in arbitrary units. Note how row 2 (Figure 2a.) is bowed upward in the central region, while rows 3, 4, and 5 show progressively steeper slopes. This behavior results from the misalignment in the optics, as discussed in section III.

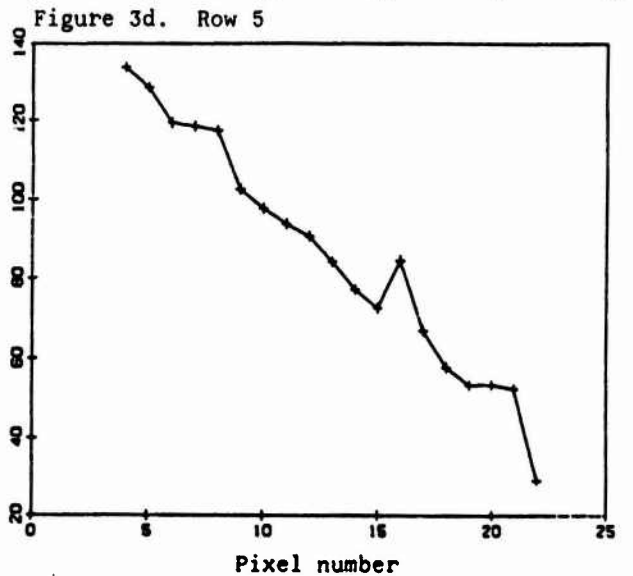
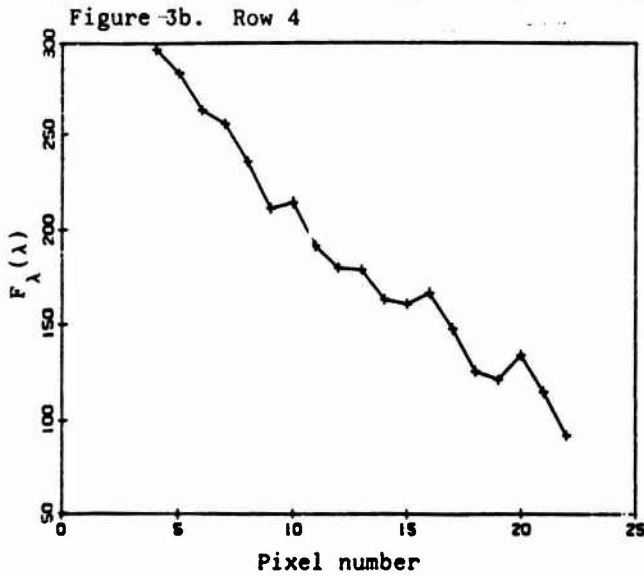
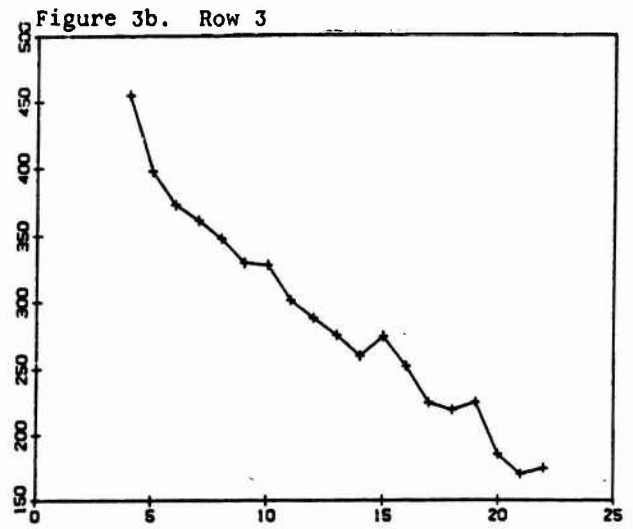


Figure 3. Actual spectrum for IRC+10216, corrected for atmospheric and instrumental transmission. By comparing this block of data with that in Figure 2, the calibration program can determine the array of corrections necessary to flat-field the instrument. Note that the spectra behave from row to row just as predicted in Figure 2. The vertical axis is in arbitrary units, which should differ from those in Figure 2 only by a scale factor.

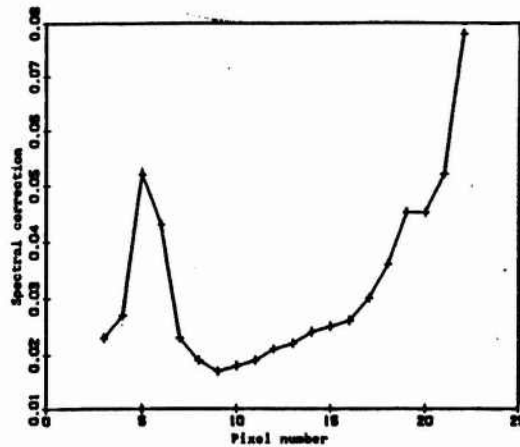


Figure 4. Average spectral correction. Note the peak at 9-10 μ (pixels 4-7), which corrects for atmospheric absorption at these wavelengths, and the rising corrections at longer wavelengths, compensating for the deterioration in instrumental and atmospheric transmission in this spectral region.

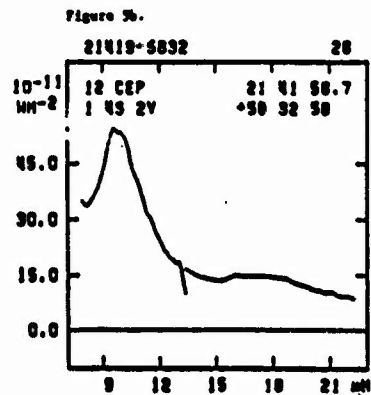
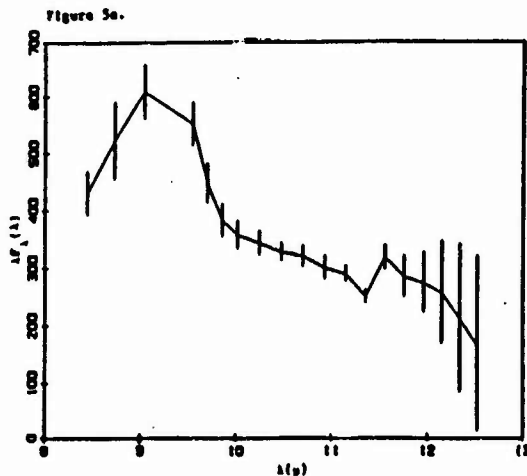


Figure 5. μ Cephei. The left graph illustrates the spectrum obtained by GLADYS after 20 co-adds. For all these plots, note that the vertical axis is $\lambda F_{\lambda}(\lambda)$ (multiplied by the wavelength in units of 10 μ). Error bars are the relative uncertainty in the mean. An examination of the right-hand spectrum, from the LRS (IRAS Science Team, 1986), shows that the two are comparable.

Figure 6a.

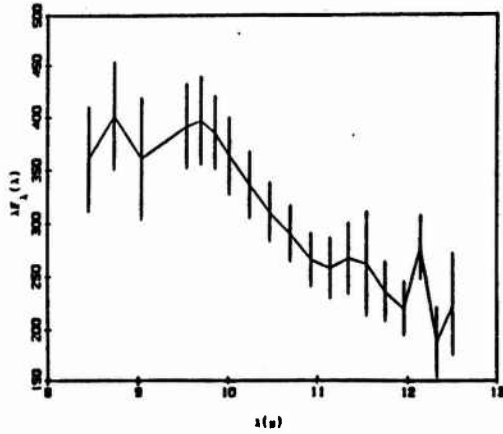


Figure 6b.

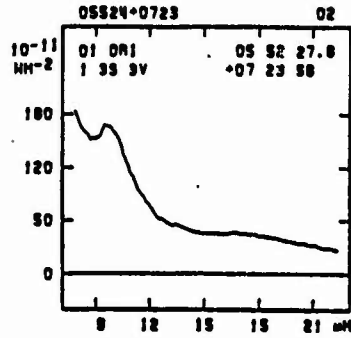


Figure 6. α Orionis. The left graph is taken from 60 co-adds on GLADYS. The larger error bars reflect the fact that the frames were taken at the telescope in groups of ten, rather than in one large group; this method serves to increase the apparent noise in a given pixel.

Figure 7a. Row 16

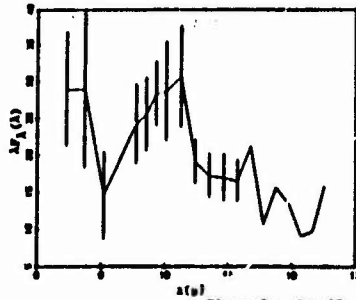


Figure 7b. Row 17

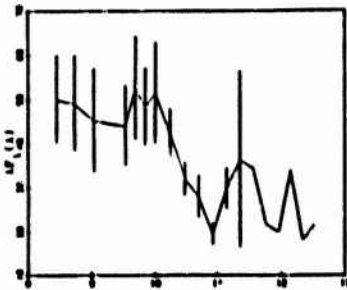


Figure 7c. Row 18

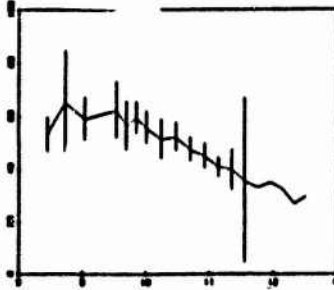


Figure 7d. Row 19

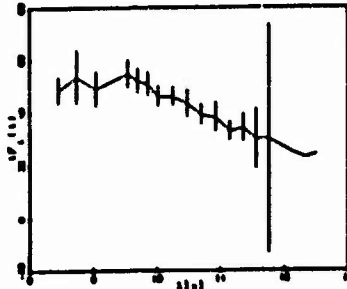


Figure 7e. Row 20

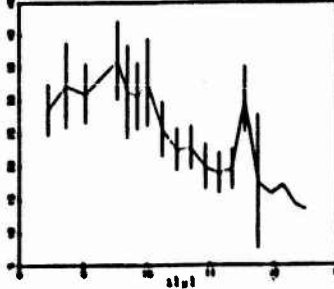


Figure 7. Spatial extent of the α Ori spectra. The data is from one group of ten co-adds. Note that the missing error bars beyond 11.5 μ imply uncertainties greater than 150%. The brightest spectrum lies on row 18 (Fig. 7c). Two features dominate these spectra. First, the uncertainty decreases rapidly as one looks away from the peak row. Second, there appears to be emission between 9 and 10 μ in rows 16 and 20. Unfortunately, ten co-adds is not sufficient to reduce the uncertainty to the point that any definite statements can be made. If the emission is real, it would be from dust nearly 2 arc-seconds away from Betelgeuse.

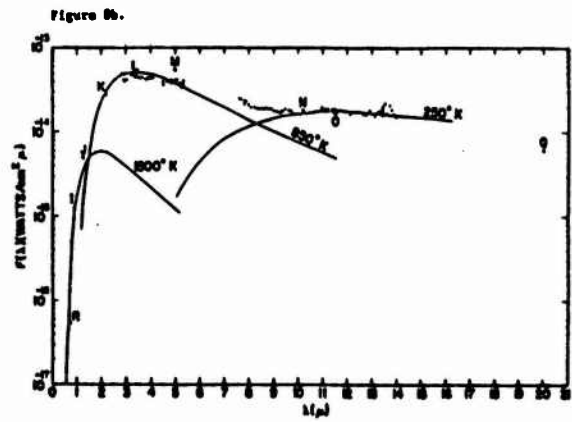
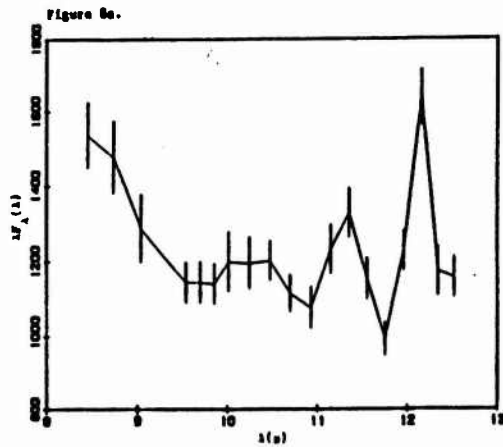


Figure 8. NML Cygni. The left plot is from 30 co-adds on GLADYS. The right plot is from Stein et al (1969). Unfortunately, no LRS spectrum exists; the Cygnus region is probably too crowded for the coarse LRS beam. The feature at 12.15μ is not real, it is due to a spurious pixel (see Figure 9).

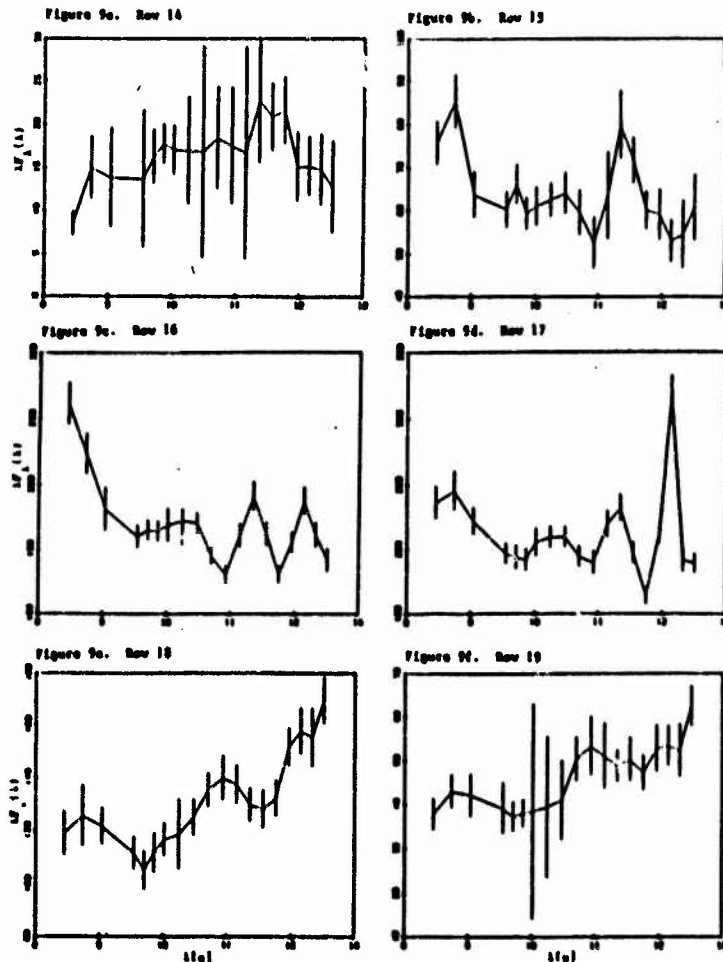


Figure 9. Spatial extent of the NML Cygni spectra. Row 14 (Fig. 9a) demonstrates just how noisy the spectra can get away from the peak row (17, Fig. 9d). Nonetheless, the increase in emission away from the peak row is evident in these spectra, especially in rows 18 and 19. Two lines stand out, one at 11.3μ , the other at roughly 12.2 . The strong feature at 12.15μ in row 17 does not appear to be real; it actually results from a very sensitive pixel (a look at the α Ori spectra shows that this same pixel is over-responsive there as well). Future calibration should correct this problem.

1987 USAF-UES SUMMER FACULTY RESEARCH PROGRAM/
GRADUATE STUDENT SUMMER SUPPORT PROGRAM

Sponsored by the
AIR FORCE OFFICE OF SCIENTIFIC RESEARCH

Conducted by the
Universal Energy Systems, Inc.

FINAL REPORT

Prepared by: Elisabeth Smela
Academic Rank: Graduate Student
Department and University: Electrical Engineering Department
University of Pennsylvania
Research Location: AFWAL/MLPO
Wright-Patterson AFB
Dayton, OH 45433
USAF Researcher: Dr. Ohmer
Date: August 7, 1987
Contract No: F49620-85-C-0013

Thermal conductivity of isotopically pure semiconductors, superlattices, semiconductor alloys, and semiconductors as a function of temperature; control of the segregation coefficient in LEC crystal growth; and photo-Hall measurements of GaAs.

by

Elisabeth Smela

ABSTRACT

A table of isotopes was prepared. Literature searches on the effects of isotopes on thermal conductivity, the thermal conductivity of superlattices, the control of the segregation coefficient in LEC crystal growth, and on the relationship between In doping of GaAs and both CRSS and thermal conductivity were completed. Computer programs were written to evaluate the phonon mean free path and the thermal conductivity as a function of alloy composition. Finally, photo-Hall effect measurements were done on several GaAs samples.

ACKNOWLEDGMENTS

I wish to thank the Air Force Systems Command, Air Force Office of Scientific Research, for their sponsorship.

I would especially like to express my appreciation to all the people at MLPO this summer for providing such a wonderful atmosphere in which to work. The kindness, enthusiasm, and good humor they never failed to display made these 10 weeks very rewarding. Bill Mitchell, Laura Rea, Capt. Peisert, Gladys Higgins, Ray Linville, and Nils Fernilius deserve special mention for their time and concern. I would also like to thank Debbie at UES for all her assistance.

I. INTRODUCTION

I am a graduate student in electrical engineering studying solid state physics; my undergraduate degree was in physics. I am particularly interested in sensors, and my master's thesis research was on a fiber optic chemical sensor. Therefore I was interested in the nonlinear optics work that was listed as a research area here, and in the infrared detector work.

It so happened that the nonlinear optics lab was only just being established, and I thus had the opportunity to work with materials, specifically GaAs, instead. AFWAL/MLPO does mainly materials characterization work, as well as some theoretical modelling. This provided a valuable exposure to materials preparation and characterization that I would not otherwise have received. I was also able to learn about the exciting new area of superlattices, of which I had only just heard for the first time four months ago.

II. OBJECTIVES OF THE RESEARCH EFFORT

The research goals and objectives included:

- 1) Preparation of a table of information about the isotopes of the semiconducting elements.
- 2) Evaluation of the phonon mean free path and the thermal conductivity in semiconductors as a function of alloy composition.

- 3) Library investigation of the effect of isotopes on thermal conductivity.
- 4) Literature search on the thermal conductivity of superlattices.
- 5) Literature search on the possibility of controlling the segregation coefficient in LEC crystal growth.
- 6) Literature search on the relationship between In concentration, CRSS, and thermal conductivity.
- 7) Laboratory experience with both photo-Hall effect measurements and SIMS.

III. ISOTOPE TABLE

The table of isotopes I prepared is a Lotus123 spreadsheet. The elements are ordered by column, and within that group, by row. Columns 2-6 in the periodic table are included. The information contained in the table includes: the isotopes, the lattice constant, the atomic number, the number of neutrons in the isotope, the isotopic relative abundance in nature, the atomic weight of the isotope, the average atomic weight of the element (both as listed, L, and as calculated from numbers in the table, C), the difference between the isotope weight and the average weight, the weight variation, and the phonon mean free path due to isotope scattering.

IV. PHONON MEAN FREE PATH

SUMMARY

I have written a short Basic program to calculate the component of the mean free path due to mass variations on one of the lattice sites. It can be applied to alloys, where A and B are two different elements, or it can be applied to the same element with two isotopes. The "X", in increments specified by the user, goes from either 0 to 100%, exclusive, or in a range alternatively specified. After calculating the mean free path, gamma, for each value of X, the program plots the resulting curve.

USING THE PROGRAM

The program is entitled "ABC.BAS", and is run in ZBASIC on the Z100's. The Okidata 83A can print the plot from a screen dump.

After loading "a:abc.bas", tell the program to "run". It will ask you to "enter name" and "enter weight" three times. The names and weights should be entered in the order A,B,C. For example, an alloy of $Ga(x)In(1-x)As$ or a compound of GaAs taking into account isotope variation:

	Case 1: Alloy	Case 2: Isotopes
Enter Name	Ga	Ga69
Enter Weight	69.72	68.9257
Enter Name	In	Ga71
Enter Weight	114.82	70.9249
Enter Name	As	As
Enter Weight	74.92	74.9216

The program next asks for the lattice constants for AC and BC compounds:

Enter AC Lattice		
Constant	5.65	5.65
Enter BC Lattice		

Constant 6.06 5.65

The increment must now be entered. The smallest increment that the program will be able to handle is .1% of the range.

Enter Increment .1 .01

The program asks if you want lines connecting the points on the graph, which is answered either "y" or "n". Then it wants to know if there are any remarks, which can be answered with a return if you don't wish any additional comments printed on the plot, or with a note like the date or "full range", etc. It next inquires whether you want to change the range, which is again answered with "y" or "n". If the answer is "y", then it asks for the beginning and end of the range.

	Case 1: Alloy	Case 2: Isotopes
Change range?	n	y
Enter beginning of range		0
Enter end of range		10

The program then calculates gamma for the x values specified and produces a plot on the screen. The plot can be printed by doing a screen dump, which means pressing the F12 key. The program is then over. To run it again, say "run".

ABOUT THE PROGRAM

<u>Line #</u>	<u>Purpose</u>
10-50	Comments
60	Arrays begin with element # 1
70	Dimensioning arrays
72	Setting default range from 0 to 100%
90-166	Entering information
170	Determining N, the number of points to be calculated
190	Starting loop to calculate variables at each N; variables at each value of N are put in an array
200	The average atomic weight is calculated

210 The difference in atomic weights is calculated, using
 the compound weights (ex: InAs and GaAs weights)
 215 The average lattice constant is calculated
 220 Gamma is calculated
 200-220 A linear interpolation is used, the beginning of the
 range is accounted for
 260-310 The maximum and minimum values of gamma calculated are
 found
 330 The vertical axis increment for the plot is set to 1/10
 of the difference between the minimum and maximum
 values of gamma
 360 The screen is cleared
 370 The screen is set to accept graphics instructions
 380 A box is drawn which will be the border of the plot
 390-440 Axis tick marks and labels are placed on the plot
 400 Vertical tick marks are made on the horizontal axis
 410 The horizontal axis is marked with x values
 420 Horizontal tick marks are made on the vertical axis
 430 The vertical axis is marked with gamma values
 460-480 The points are plotted
 465 The horizontal position (x coord) is found
 470 The vertical position (y coord) is found
 472 A circle is drawn around the x,y coordinates
 473 The circle is filled in so that it is solid
 475 If lines connecting the points were desired, they are
 drawn
 500-570 The plot is labelled
 575 The screen is readied for characters from the terminal
 577 The cursor is placed on the bottom of the screen so
 that it doesn't interfere with the plot when it prints "Ok"

ABOUT THE CALCULATIONS

The equations used were taken from Ziman's Electrons and Phonons, Chapter 8.6, Isotopes and other point imperfections. The phonon mean free path is calculated assuming, among other things, that the isotopes or imperfections are the only cause of phonon scattering, that the collisions are elastic, that the solid is isotropic, and that the isotopes (or imperfections) are randomly distributed.

As the isotopic variation goes to zero, the mean free path becomes infinity. When estimating the thermal conductivity this means that phonon scattering from isotopes is no longer

significant. Other scattering mechanisms act to reduce the thermal conductivity and as the mean free path gets longer they begin to play the limiting role. This program could be expanded to include these other mechanisms at a future time.

V. THERMAL CONDUCTIVITY OF ALLOYS

GENERAL

The name of this program is "quadrat.bas". It calculates the thermal resistivity as a function of Indium content in $\text{In}(x)\text{Ga}(1-x)\text{As}$ using the relationship:

$$W(x) = xB(\text{InAs}) + (1-x)B(\text{GaAs}) + x(1-x)C(\text{InGa})$$

The formula and the constants were taken from the following articles by Adachi:

Lattice thermal resistivity of III-V compound alloys

S. Adachi

J. Appl. Phys., 54, 4 (1983), 1844

GaAs, AlAs, and AlGaAs: Material parameters for use in research and device applications.

S. Adachi

J. Appl. Phys., 58, 3 (1985), R1

The thermal resistivity of InAs, the $B(\text{InAs})$, is 3.70 deg cm/W, and that of GaAs, $B(\text{GaAs})$, is 2.27 deg cm/W. The alloy-disorder bowing constant $C(\text{InGa})$ was determined by Adachi to be 72 deg cm/W by fitting published experimental data. No information is needed from the user -- the program just prints the thermal resistivities and conductivities for $.0001 < x < .9$ for $\text{In}(x)\text{Ga}(1-x)\text{As}$, although if figures for other alloys were required the program could be modified.

ABOUT THE PROGRAM

<u>Line #</u>	<u>Purpose</u>
10-45	Comments
50	Set array element numbers to begin at 0
60	Dimension arrays
70-90	Set constants for In(x)Ga(1-x)As
101-103	Print table headings
110-167	Calculate thermal resistivity and conductivity, and print
112	Vary x between .0001 and .9
113	Calculate resistivity
114-135	Print x, resistivity, conductivity

PLOT

The calculated values (dashes) were plotted on a log scale alongside our experimental (circles) and the literature (squares) values. Because the value for C(InGa) had been fitted to the literature data, it is not surprising that the calculated curve agrees in that range (x = .1 to .9). The calculated values are too high at the lower concentrations.

VI. ISOTOPE EFFECT ON THERMAL CONDUCTIVITY

I found two articles in the literature on this subject and summarized the relevant points so that others will be able to determine immediately whether the article is of interest or importance to them. I am enclosing the summaries of these two articles an example :

Isotopic and other types of thermal resistance in Germanium
 T.H. Geballe and G.W. Hull
 Physical Review, 110 (1958), 773

In Ge, the increase in thermal conductivity with decreasing temperature above Θ_D was not exponential, even in perfect crystals, as was predicted by Peierls. This was thought to be due to isotope scattering since Ge is a mixture of 5 isotopes. These investigators compared crystals of "normal" Ge (with

isotope proportions 20.52, 27.43, 7.76, 36.54, and 7.76) with an "enriched" Ge crystal (0.691, 1.135, 1.56, 95.80, and 0.818). The material was of very high purity. The thermal conductivity below 5 K of the enriched Ge was limited by boundary scattering, as predicted by theory, which gives a T^2 dependence. The normal Ge sample showed a T^4 dependence, which was attributed to isotope scattering. The ratio of the normal and enriched Ge thermal conductivities agreed well with theory. The theoretical results indicate that when boundary and isotopic scattering are most significant, isotopic scattering can be observed at temperatures as low as 1/10 of the peak thermal conductivity temperature.

Although the thermal conductivity was expected to increase to 15 times the value in normal Ge near the peak thermal conductivity, it increased by only 3 times. This is apparently due to Umklapp scattering that can take place in Ge and Si even below $\Theta_D/10$. This scattering is not expected to take place in diamond at low temperatures. At high temperatures the thermal resistance difference is 0.15 cm·deg/W.

Isotope scattering of dispersive phonons in Ge

S. Tamura

Physical Review B, 27, 2 (1983), 858

Isotopic scattering of acoustic phonons in Ge was investigated theoretically using the Born-von Karman lattice dynamics model. The interatomic forces were the same for each isotope, and they assumed that the isotopes were randomly distributed. They found no spatial anisotropy or polarization dependence of the scattering rate, which does depend on frequency. The relaxation time depends on ω^2 for low frequencies, with a stronger dependence at higher frequencies.

VII. THERMAL CONDUCTIVITY OF SUPERLATTICES

The following papers were unearthed and summarized:

Thermal conductivity of superlattices

S.Y. Ren and J.D. Dow

Physical Review B, 25, 6 (1982), 3750.

Effects of mini-Umklapp processes on heat transport in superlattices

S.Y. Ren and J.D. Dow

Solid State Communications, 41, 3 (1982), 211

Acoustic phonon transmission in superlattices

M.J. Kelly

J. Phys. C: Solid State Physics, 18 (1985), 5963

Selective transmission of high-frequency phonons by a superlattice: the "dielectric" phonon filter

V. Narayanamurti, H.L. Stormer, M.A. Chin, A.C. Gossard, and W. Wiegmann

Physical Review Letters, 43, 27 (1979), 2012

The fifth international conference on phonon scattering in condensed matter

A.C. Anderson, J.P. Wolfe, and H.J. Maris

Comments Cond. Mat. Phys., 13, 3 (1987), 169

Folded acoustic and quantized optic phonons in (GaAl)As superlattices

C. Colvaró, T.A. Gant, M.V. Klein, R. Merlin, R. Fischer, H. Morkoc, A.C. Gossard

Physical Review B, 31, 4 (1985), 2080

Phonons in semiconductor superlattices

M.V. Klein

IEEE Journal of Quantum Electronics, QE-22, 9 (1986), 1760

Interface vibrational modes in GaAs-AlAs superlattices

A.K. Sood, J. Menendez, M. Cardona, and K. Ploog

Physical Review Letters, 54, 19 (1985), 2115

Vibrations in superlattices; application to GaAs-AlAs systems

J. Sapriel, B. Djafari-Rouhani, and L. Dobrzynski

Surface Science, 126, (1983), 197

Resonance Raman scattering by confined LO and TO phonons in GaAs-AlAs superlattices

A.K. Sood, J. Menendez, M. Cardona, and K. Ploog

Physical Review Letters, 54, 19 (1985), 2111

Superlattice effects on confined phonons

E. Molinari, A. Fasolino, K. Kunc

Physical Review Letters, 56, 16 (1986), 1751

Calculated longitudinal superlattice and interface phonons of InAs/GaSb superlattices

A. Fasolino, E. Molinari, and J.C. Mann

Superlattices and Microstructures, 3, 2 (1987), 117

Confined longitudinal and transverse phonons in GaAs/AlAs superlattices

E. Molinari, A. Fasolino, and K. Kunc

Superlattices and Microstructures, 2, 4 (1986), 397

Dispersion of folded phonons in Si/Si Ge superlattices

H. Brugger, H. Reiner, G. Abstreiter, G. Jorke, H.J. Herzog, and

E. Kasper
Superlattices and Microstructures, 2, 5 (1986), 451

Resonant Raman scattering in In Ga As/InP(100) quantum wells
J.A.C. Bland, W. Hayes, M.S. Skolnick, D.J. Mowbray, and S.J. Bass
Superlattices and Microstructures, 3, 1 (1987), 83

Theory of phonon dispersion relations in semiconductor
superlattices

S. Yip and Y. Chang
Physical Review B, 30, 12 (1984), 7037

ADDITIONAL PAPERS BY NARAYANAMURTI

Observation of velocity bunching of near-zone-edge phonons in
semiconductors: an intense, tunable phonon source near 10 A

P. Hu, V. Narayanamurti, and M.A. Chin
Physical Review Letters, 46, 3 (1981), 192

Direct observation of phonons generated during nonradiative
capture in GaAs p-n junctions

V. Narayanamurti, R.A. Logan, and M.A. Chin
Physical Review Letters, 40, 1 (1978), 63

Direct determination of symmetry of Cr ions in semi-insulating
GaAs substrates through anisotropic ballistic-phonon
propagation and attenuation

V. Narayanamurti, M.A. Chin, and R.A. Logan
Appl. Phys. Lett., 33, 6 (1978), 481

Anisotropic phonon generation in GaAs epilayers and pn junctions

V. Narayanamurti, R.A. Logan, M.A. Chin, and M. Lax
Solid State Electronics, 21 (1978), 1295

Phonon optics in semiconductors: phonon generation and electron-
phonon scattering in n-GaAs epilayers: I. Theory

M. Lax and V. Narayanamurti
Physical Review B, 24, 8 (1981), 4692

Most of the work in this area has been done by Narayanamurti et. al. The experimental results and the theoretical predictions are exactly opposite -- theory predicts increased conductivity at wavelengths corresponding to the superlattice period, whereas experiments show stopbands. This may be due to either poor

material interfaces or not taking into account key factors in the theory.

There are several models of phonon transmission in superlattices, each applicable in a particular regime. No comprehensive theory has been formulated.

VIII. CONTROL OF SEGREGATION COEFFICIENT

The segregation coefficient has been controlled by the application of a magnetic field, passing a current through the growth interface, crystal orientation, and growth rate. The papers include:

MAGNETIC FIELD

Effect of axial magnetic field on gallium segregation in Czochralski silicon crystal growth

T.T. Braggins, H.M. Hobgood, and R.N. Thomas
supported by Dept. of Navy

The effect of strong magnetic field on homogeneity in LEC GaAs single crystal

T. Kimura, T. Katsumata, M. Nakajima, and T. Fukuda
Journal of Crystal Growth, 79 (1986), 264

ELECTRIC FIELD

Liquid-phase electroepitaxy: Dopant segregation

J. Lagowski, L. Jastrzebski, and H.C. Gatos
J. Appl. Phys. 51, 1 (1980), 364

Electric current controlled growth and doping modulation in GaAs liquid phase epitaxy

D.J. Lawrence and L.F. Eastman
Journal of Crystal Growth, 30 (1975), 267

Current-controlled growth, segregation and amphoteric behavior of Si in GaAs from Si-doped solutions

L. Jastrzebski and H.C. Gatos
Journal of Crystal Growth, 42 (1977), 309

OTHER

Growth rate dependence of the interface distribution coefficient in the system Ge-Ga

C.A. Wang, J.R. Carruthers, and A.F. Witt
Journal of Crystal Growth, 60 (1982), 144

Interface field effects on solute redistribution during crystallization

W.A. Tiller and K. Ahn
Journal of Crystal Growth, 49 (1980), 483

Orientation dependent variation in antimony segregation coefficient near the silicon (111) plane: an explanation using lateral microscopic growth L & G concepts

R.A. Frederick and G.A. Rozgonyi
Journal of Crystal Growth, 70 (1984), 335

Growth of copolymer chains and mixed crystals -- trial-and-error statistics

A.A. Chernov
Soviet Physics Uspekhi, 13, 1 (1970), 101

Nondestructive measurement of indium content in semi-insulating GaAs substrates and ingots

D. Kirillov, M. Vichr, and R.A. Powell
Appl. Phys. Lett. 50, 5 (1987), 262

IX. PHOTO-HALL EFFECT MEASUREMENTS OF GAAS SAMPLES

Samples from GaAs wafers were cut into the Van der Pauw cross shape, etched, and contacted electrically. They were then connected with the leads of the sample holder of a dour equipped with a glass window. The sample was cooled to liquid nitrogen temperatures, 77 K, under vacuum. Light of sub-bandgap energy, 1.1 micrometers, shone on the sample to induce photoquenching while the current, voltage, and temperature were monitored by computer for 1/2 to 1 hour. Data was taken in 8 configurations for each sample. Between runs the sample was heated to 130-150 K to tnermally recover it.

The photoquenching takes place because the electrons in the

deep defect level EL2^o are photoexcited into the metastable state EL2*, where they can no longer participate in conduction. Photoquenching results in the number of carriers decreasing with time as the light shines on the sample, which can be measured with the Hall effect.

Several samples were characterized. The process improved over the weeks as modifications were made. These included modifying computer programs to automate the data analysis and adding an extra heater to warm the sample.

X. OTHER

As the file containing the papers on In doping of GaAs was misplaced, no summaries or conclusions were possible. The literature search printout is in hand, however, so the papers can always be copied and collected again.

No actual laboratory work with SIMS (secondary ion mass spectrometry) was done due to lack of time. I did read about SIMS and other characterization techniques, however, and was able to observe the process and get a flavor for what was involved. In addition, I learned about the various vacuum systems -- how they operate and when each is used to best advantage.

XI. RECOMMENDATIONS

SUPERLATTICES

Phonon filter

More information about the phonon filter on which Narayanamurti et. al. have been working should be acquired. Perhaps Bell Laboratories has some internal papers or one of the authors can be contacted. The proceedings of the Fifth International Conference on Phonon Scattering in Condensed Matter (see below) should be located. W. Eisenmenger may be in the Bell Labs group or it may be independent work; in either case it would be interesting to see in more detail what has been done. Finally, M.J. Kelly referred to enhanced thermal conductivity seen in a wafer bounded on one side by a superlattice, and which is listed as a private communication. This should be pursued.

The patent that M.A. Chin applied for (# 4349796, 1982) has been ordered and will arrive for Dr. Ohmer at MLPO.

Isotope superlattice

It would be interesting to build an isotopic superlattice, perhaps using Ge70 and Ge76. The interfaces would need to be good quality. Different layer sizes could be made and the thermal conductivity tested. Because only the masses in the layers are changing, it would be straightforward to calculate the theoretical values and compare those with experiment.

Papers still needed

I strongly recommend that MLPO get Superlattices and Microstructures, especially Volume 1. None of the local

libraries have the first volume, and most of the interesting papers seem to be in it. Wright State University has Volume 2 and forward; the few issues that Building 22 got were removed.

The library has the following book on order:

Zucker, Proceedings of the 17th International Conference on the Physics of Semiconductors, 6-10 August 1984, San Francisco

in which the article by Shah, Pinczuk, Stormer, Gossard, and Wiegmann, pp 345-8, may be useful.

I have ordered these articles through interlibrary loan for Dr. Ohmer:

Narayanamurti, J. Phys. Colloq. (France), 45, C5, 157

Sapriel, J. Phys. Colloq. (France), 45, C5, 139

I was unable to obtain the following articles which may or may not be of interest:

Springer Series in Solid State Sciences, Vol. 68, "Phonon Scattering in Condensed Matter", eds. A.C. Anderson and J.P. Wolfe, article by W. Eisenmenger.

Zucker, Proceedings of the Yamada Conference XII on Modulated Semiconductor Structures (2nd International Conference), 9-13 September 1985, Kyoto, Japan.

Kobayashi, Superlattices and Microstructures, 1, 6, 471

Colvard, Superlattices and Microstructures, 1, 1, 81

Hu, Phys. Rev. Lett., 46, 3, 192

Bochkov, Sov. Phys. Semicond., 77, 4, 456

Syrkin, Sov. J. Low Temp. Phys., 8, 7, 381

Lax, Phys. Rev. B, 22 (1980), 4876

Also, have Lax and Narayanamurti come out with another article since 1981 in Phys. Rev. B, part II: Experimental?

SEGREGATION COEFFICIENT

According to Lagowski et. al., electric current control of the segregation coefficient has not been successful in LEC crystal growth because of convection instabilities and Joule heating. However, there were no references given for this statement. The authors should be contacted to get the experimental data or a reference.

The following papers were not available in Building 22 and may have some useful information:

L. Jastrzebski, J. Electrochem. Soc., 125, 1140

M. Kumagawa, J. Electrochem. Soc., 120, 583

W.G. Pfann, Electron. Control., 2 (1957), 597

1987 USAF-UES SUMMER FACULTY RESEARCH PROGRAM
GRADUATE STUDENT SUMMER SUPPORT PROGRAM

Sponsored by the
AIR FORCE OFFICE OF SCIENTIFIC RESEARCH

Conducted by the
Universal Energy Systems, Inc.

FINAL REPORT

Prepared by: Rita Rex Smith
Academic Rank: Graduate Student
Department and: Mechanical Engineering
University: University of New Mexico
Research Location: USAFWL/ARBL
Kirtland AFB, NM 87117-6008
USAF Researcher: Dr. Bruce S. Masson

Date: 30 Sep 1987
Contract No: F49620-85-C-0013

PREDICTING OPTICAL DEGRADATION OF A LASER BEAM
THROUGH A TURBULENT SHEAR LAYER

by

Rita Rex Smith

ABSTRACT

The degradation in optical quality of a coherent laser beam passing through a turbulent shear layer has been predicted by relating the phase error of the coherent beam to the time-mean index-of-refraction profile across the shear layer. The prediction of the optical degradation is, therefore, dependent on the accuracy of the model used to analyze the turbulent shear layer. The turbulence model in the ALFA shear layer code was investigated. A code was developed to calculate the index-of-refraction profile, phase error, and Strehl ratio using the results of the turbulence analysis from ALFA and plot the significant turbulence parameters.

The above method employs a mixing-length assumption. A better approach would be to predict optical degradation by relating the phase error to index-of-refraction fluctuations, eliminating the need to make a mixing-length assumption. The scalar fluctuation equation in the ALFA code and a perturbation of the Gladstone-Dale relation were examined for this purpose.

Acknowledgements

I wish to thank the Air Force Weapons Lab and the Air Force Office of Scientific Research for sponsorship of this research. Universal Energy Systems must be mentioned for their concern and help to me in all administrative and directional aspects of this program.

The summer fellowship position provided me with a very rewarding work experience. I would especially like to thank Dr. C. Randall Truman for recommending me for the summer fellowship position and for his support in conducting this research. I am also very grateful to Dr. Bruce S. Masson for his technical support and encouragement. The support of Capt. Steve Rinaldi, Capt. Nan Founds, Capt. Marty Trout, Capt. Rich Charles, Lt. Craig Woolhiser, Capt. Paul Sydney, and Mr. Brian Kennedy, provided me with a truly enjoyable atmosphere and work experience.

I. INTRODUCTION:

In high power density laser systems a high speed gas jet (commonly called an aerodynamic window) is passed across the front of the lasing cavity to allow the laser beam to exit the cavity while maintaining low cavity pressure. As the gas of the jet passes across the front of the cavity, two turbulent shear layers (or mixing layers) are formed: one between the gas jet and the atmosphere, and one between the gas jet and the cavity gas. These turbulent shear layers act to degrade the optical quality of the laser beam and limit the intensity to which the beam can be focused in the far field. The Air Force Weapons Laboratory at Kirtland Air Force Base is currently conducting research into aero-optic interactions between high energy laser beams and turbulent flow fields. A measure of the optical degradation is the Strehl ratio which has been related to the random phase error by

$$R_s = \exp(-\overline{\psi^2}) \quad (1)$$

A simple "turbulence model" has related the mean-square optical phase error to the index-of-refraction fluctuations across the turbulent mixing layer. The Air Force Weapons Lab is working to develop an improved model to better predict the index-of-refraction fluctuations and optical degradation in the turbulent field.

My research interests are in the study of turbulence and turbulence modeling. My Master's degree course work has been concentrated in the

areas of computational fluid dynamics, viscous flow, and boundary layer theory. These courses and my previous work experience in mathematical modeling provided the needed background to understand the turbulence models and methods used to predict turbulent shear layers and led to my assignment at the Air Force Weapons Laboratory.

II. OBJECTIVES OF THE RESEARCH EFFORT:

An expression relating the mean-square optical phase error and the index-of-refraction fluctuations across the shear layer was developed by Sutton (1969). Problems arise in obtaining index-of-refraction fluctuations either experimentally or computationally. Bogdanoff (1984) modified Sutton's expression to obtain an approximate relation between the mean-square optical phase error and the gradient of the time-mean index of refraction across the mixing layer using a mixing length assumption. Baxter's (1987) predictions of beam degradation through a turbulent shear layer using Bogdanoff's model showed the right trend of the phase errors for the different gases, but the magnitude of the phase errors was wrong. This was probably because of the use of an inappropriate length scale. The objectives of my research as a participant in the 1987 Graduate Student Summer Support Program were:

- (1) to evaluate the turbulence model in the ALFA shear layer code (Theones, 1979) used by Baxter (1987) and to determine the type of flows used to calibrate the empirical constants in the model;

(2) to run test cases using the ALFA shear layer code with standard (Imperial College) constants, rather than those presently in the code, and to check the effect of these changes upon the results;

(3) to investigate the use of a model that predicts index-of-refraction fluctuations directly (rather than time-mean index of refraction); and to determine the theoretical basis for the scalar fluctuation equation in the ALFA shear layer code and the feasibility of using this equation to model index-of-refraction fluctuations in the mixing layer.

III. EVALUATION OF THE TURBULENCE MODEL IN ALFA:

a. The turbulence model in ALFA was found to be the standard two-equation $k-\epsilon$ model given by Jones and Launder (1971) but with different empirical constants. For two-dimensional plane flow, the $k-\epsilon$ transport equations become:

k -equation:

$$\rho u \frac{\partial k}{\partial x} + \rho v \frac{\partial k}{\partial y} - \frac{\partial}{\partial y} \left[\frac{\mu_L + \mu_T}{\sigma_k} \frac{\partial k}{\partial y} \right] + C_{1k} \mu_T \left(\frac{\partial u}{\partial y} \right)^2 - C_{2k} \rho k \quad (2)$$

ϵ -equation:

$$\rho u \frac{\partial \epsilon}{\partial x} + \rho v \frac{\partial \epsilon}{\partial y} - \frac{\partial}{\partial y} \left[\frac{\mu_T}{\sigma_\epsilon} \frac{\partial \epsilon}{\partial y} \right] + C_{1\epsilon} \frac{\epsilon}{k} \mu_T \left(\frac{\partial u}{\partial y} \right)^2 - C_{2\epsilon} \rho \frac{\epsilon^2}{k} \quad (3)$$

The two-equation model is used to determine turbulent eddy viscosity

in the momentum equation by

$$\mu_t = C'_\mu \rho k^{1/2} l \quad (4)$$

where k is turbulent kinetic energy and l is the length scale. At high Reynolds numbers, ϵ , the turbulent dissipation is assumed proportional to $k^{3/2}/l$ and the turbulent viscosity can be written as

$$\mu_t = C_\mu \rho k^2 / \epsilon \quad (5)$$

b. The empirical constants used in ALFA are the same as those used by Launder et. al. (1972) with the exception of C_{1k} and C_{2k} . These are the constants in the production and dissipation terms, respectively, of the turbulent kinetic energy transport equation as shown in Table 1. Mikitarian and McDanal (1975) used this same two-equation $k-\epsilon$ turbulence model to analyze mixing layers in laser cavity flows. Starting with the constants given by Launder et. al. (1972), Mikitarian and McDanal found it necessary to reduce the constants C_{1k} and C_{2k} in the production and dissipation terms, respectively, of the turbulent kinetic energy transport equation in order to obtain reasonable agreement with experimental data. This is apparently the source of the values of these constants currently in ALFA.

IV. ALFA TEST CASES:

a. The ALFA shear layer code was used to analyze the turbulent mixing

layer between an aerodynamic window gas jet and the atmosphere. Several test cases were run using the nitrogen gas to check the effect of varying the empirical constants in the $k-\epsilon$ equations. Table 2 shows the values of the empirical constants used for each run. The first run, NITRO0 matched the nitrogen case predicted by Baxter with 33 points across the shear layer. The value of $C_{2\epsilon} = 1.98$ used in the NITRO0 run is believed to be a typographical error in the ALFA input data. Four runs were made varying the constants C_{1k} , C_{2k} and $C_{2\epsilon}$. NITRO3 was run to determine the influence of the initial velocity fluctuation level on the turbulence. Finally, since the results of some of the above runs showed problems in the density and species concentration profiles, one case was run with a refined grid (74 points) across the shear layer.

To facilitate checking the results and plotting the data, program STRIPES (STrehl Ratio Integral Phase Error) was written to read the output file from ALFA, calculate the time-mean index-of-refraction profile, shear layer width, optical phase error, and Strehl ratio, and set up the input for a plotting routine.

b. The shear layer width, optical phase error, and the Strehl ratio were calculated for each case using program STRIPES and are shown in Table 3. All calculations were made at an x-location 16 cm. downstream. The use of the STRIPES code automated the calculations and plotting of the shear layer parameters. This allowed changes in the turbulence model to be studied more easily.

The results from NITRO0 agreed with those from Baxter's (1987) work and were used as a basis for comparison with the other runs. The four runs made to check the effect of the constants in the turbulent kinetic energy equation were made with the value of $C_{2\epsilon} = 1.92$ given by Launder et. al. (1972). For the cases of $C_{2\epsilon} = 1.98$ and $C_{2\epsilon} = 1.92$ (NITRO0 and NITRO10), the velocity and density profiles are nearly the same. The Strehl ratio changes by about four percent as shown in Table 3.

Figures 1-3 show the velocity, density, and index of refraction profiles for NITRO10 and NITRO11 runs. From Table 3 it can be seen that varying the values of C_{1k} and C_{2k} individually changes the turbulent kinetic energy balance and resulted in a significant effect on the density and velocity profiles and hence on the optical phase error. When both constants were changed in the same direction by about the same amount, the overall balance of the turbulent kinetic energy didn't change very much. In this case the changes in the constants between runs NITRO10 and NITRO11 had little effect on the density and velocity profiles and on the Strehl ratio calculation. The same is true for the change in constants between runs NITRO0 and NITRO1.

The NITRO3 case was run with an initial velocity fluctuation $= .0001$ compared to an initial fluctuation $= .01$ used in NITRO0 and by Baxter (1987). For the run with the higher initial velocity fluctuation, the

shear layer developed faster than for the run with the lower initial velocity fluctuation but differences downstream were small.

In several of the above runs, the results showed what appeared to be a numerical instability propagating downstream which produced unrealistic values in the density profile. This happens right at the grid points which correspond to the initial interface between the two gases. The ALFA code uses first-order differences in the conservation-of-mass equation. Because of this, a large change in density between the two adjacent points sets up large gradients in density and normal velocity. This tends to produce oscillations in the density profile near the start. This is typical of boundary layer solutions using a parabolic marching technique. An attempt to correct the problem by refining the grid across the shear layer did not work. It is believed that smoothing the initial profiles will correct the situation and will have minimal effect on the profiles downstream. Figure 4 shows the density profiles at 16 cm. downstream for both grids.

V. MODELING OF INDEX-OF-REFRACTION FLUCTUATIONS DIRECTLY:

a. The mean-square phase error is related to index-of-refraction fluctuations in the mixing layer by the following relation (Sutton, 1969).

$$\overline{\psi^2} = 2k^2 \int \langle (n')^2 \rangle \Lambda dy \quad (6)$$

Using a mixing-length assumption, the mean-square optical phase error has also been related to the time-mean index-of-refraction (Bogdanoff, 1984) across the shear layer as follows.

$$\overline{\psi^2} = 2k^2 \int \frac{\ell_n^3}{a} \left(\frac{dn}{dy} \right)^2 dy \quad (7)$$

Both Baxter's (1987) work and the calculations made in this work using program STRIPES used the mixing-length assumption. If the index-of-refraction fluctuations could be predicted, the use of equation (6) would be preferable over equation (7) since it would avoid using a mixing-length approximation.

The time-mean index of refraction is currently being calculated based on time-mean density profiles (obtainable from ALFA) using the Gladstone-Dale (Liepmann and Roshko, 1957) relation

$$n = 1 + \beta_m \frac{\rho}{\rho_{ref}} \quad (8)$$

ALFA also contains a transport equation for the fluctuation of a scalar quantity. The equation, given below, has the same form as the transport equations for turbulent kinetic energy and dissipation (Launder and Spalding, 1972).

$$\rho u \frac{\partial g}{\partial x} + \rho v \frac{\partial g}{\partial y} - \frac{\partial}{\partial y} \left[\frac{\mu_L + \mu_t}{\sigma_g} \frac{\partial g}{\partial y} \right] + C_{1g} \mu_t \left(\frac{\partial \bar{f}}{\partial y} \right)^2 - C_{2g} \frac{\rho g \epsilon}{k} \quad (9)$$

In the above equation, \bar{f} represents a mean quantity and $g = \overline{(f')^2}$ represents the mean square of the fluctuating component. In the past, this equation has been used to model fluctuations of temperature and species concentrations (Wilson, 1973).

The equation is currently set up in ALFA to calculate velocity fluctuation, temperature fluctuation, and the concentration fluctuation of the one of the chemical species. An attempt was made to relate the index-of-refraction fluctuation to the fluctuation of velocity, temperature, and/or species concentration since these quantities are already calculated by ALFA.

b. In order to relate the index-of-refraction fluctuation to fluctuations obtained from ALFA, the Gladstone-Dale relation was formulated in two (equivalent) ways: (1) in terms of density and mass fractions of the chemical species, and (2) in terms of molar concentrations of the chemical species. Taking a perturbation of either of these equations gives index-of-refraction fluctuations as a function of the fluctuations of the other quantities. However, in both cases, terms appear containing cross products of the fluctuations which are not available and are not easily modeled.

An alternative approach to obtaining index-of-refraction fluctuations would be to model index-of-refraction fluctuations directly using the scalar fluctuation transport equation in ALFA. The values of the constants C_{1g} and C_{2g} in the scalar fluctuation transport equation

that are currently in ALFA have been used for rocket plume flow (Wilson, 1973). In order to use the equation to model index-of-refraction fluctuations in the shear-layer flow described, the constants will need to be optimized to fit experimental data.

VI. RECOMMENDATIONS:

- (1) The two-equation $k-\epsilon$ turbulence model in ALFA is a widely used model. The use of $C_{1k} = .7$ and $C_{2k} = .5$ was recommended specifically for lasing cavity flows by Mikitarian and McDanal (1975). The values of $C_{1k} = C_{2k} = 1.0$ (Launder et. al., 1972) are recommended for a wider range of flows including the mixing layer studied herein.
- (2) The oscillations in density profiles needs further investigation. It is suggested that the density and species concentration profiles be smoothed upstream and the results checked as the solution marches downstream. This is expected to eliminate oscillations in the density profile due to initial starting conditions.
- (3) The scalar fluctuation transport equation in ALFA has been used to model fluctuations of temperature and species concentration. It is suggested that this equation be used to model index-of-refraction fluctuations directly to obtain better predictions of phase errors.

Table 1: Turbulence Model Empirical Constants

Empirical Constant	ALFA	Lauder et al. (1972)
C	0.09	0.09
σ_k^μ	1.0	1.0
C_k^k	0.7	1.0
C_{1k}	0.5	1.0
C_{2k}	1.30	1.30
σ_ϵ	1.43	1.43
$C_{1\epsilon}$	1.92	1.92
$C_{2\epsilon}$		

Table 2: ALFA Test Cases

	C_{1k}	C_{2k}	$C_{2\epsilon}$	Number of Grid Points	Initial Velocity Fluctuation
NITRO0	.7	.5	1.98	33	.01
NITRO1	1.0	1.0	1.98	33	.01
NITRO3	.7	.5	1.98	33	.0001
NITRO5	.7	.5	1.98	74	.01
NITRO10	.7	.5	1.92	33	.01
NITRO11	1.0	1.0	1.92	33	.01
NITRO12	.7	1.0	1.92	33	.01
NITRO13	1.0	.5	1.92	33	.01

For all cases shown: $C = .09$, $\sigma_k = 1.0$, $\sigma_\epsilon = 1.30$,
 $C_{1\epsilon} = 1.43$, $C_{1g} = 3.5$, $C_{2g} = 0.17^k$

Table 3: Optical Degradation Parameters

	L_{95n} (cm)	Mean Squared Phase Error	Strehl Ratio
NITRO0 *	2.873	1.186	.305
NITRO1	2.752	1.208	.299
NITRO3	1.924	1.122	.325
NITRO5	3.245	1.227	.293
NITRO10	2.693	1.168	.316
NITRO11	2.552	1.191	.304
NITRO12	.352	1.029	.357
NITRO13 *	3.097	.600	.549

* Indicates runs for which the density profile had to be smoothed before calculating the results.

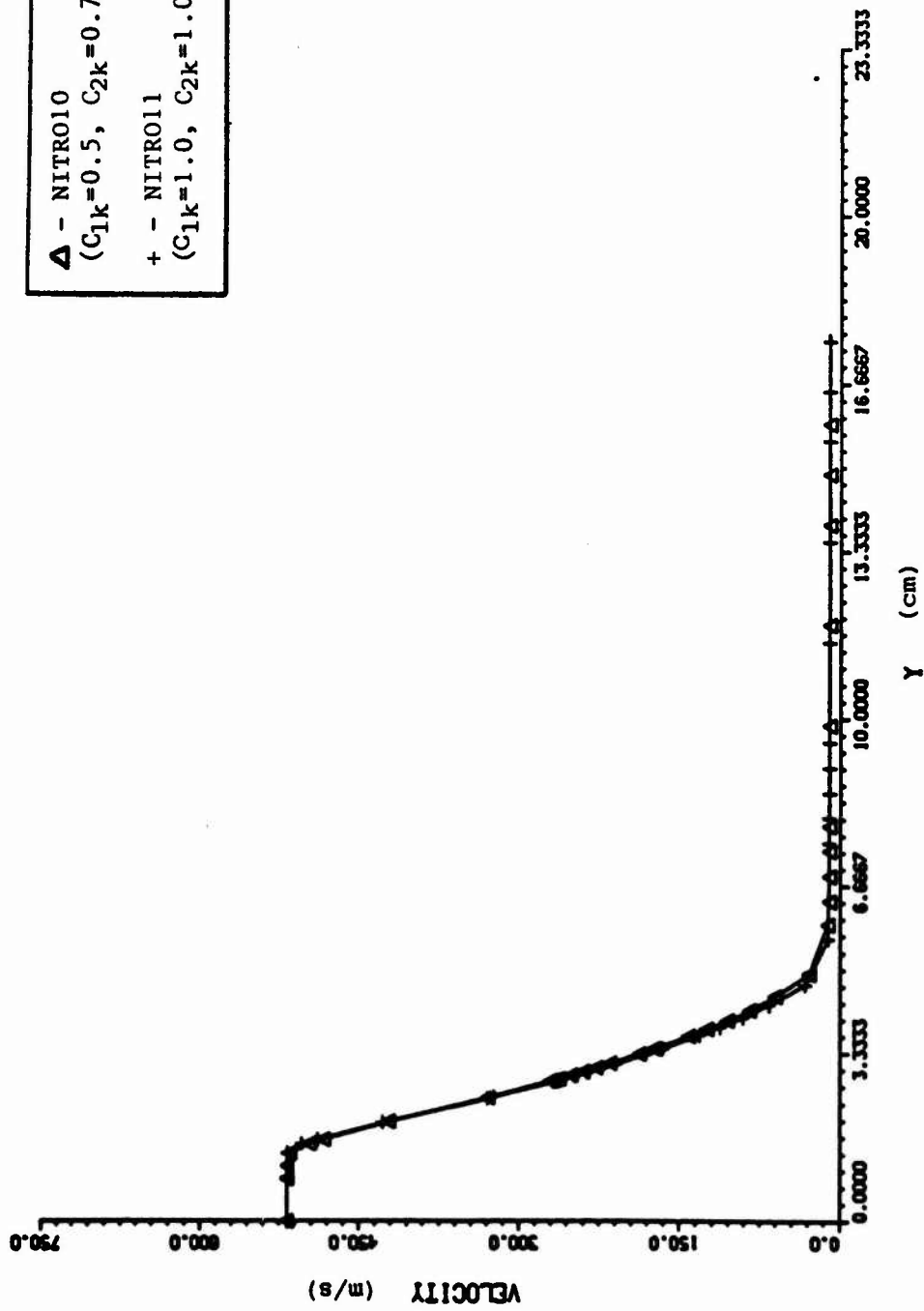


Figure 1: Velocity Profiles at 16 cm. Downstream
 Showing Effects of Changing C_{1k} and C_{2k}

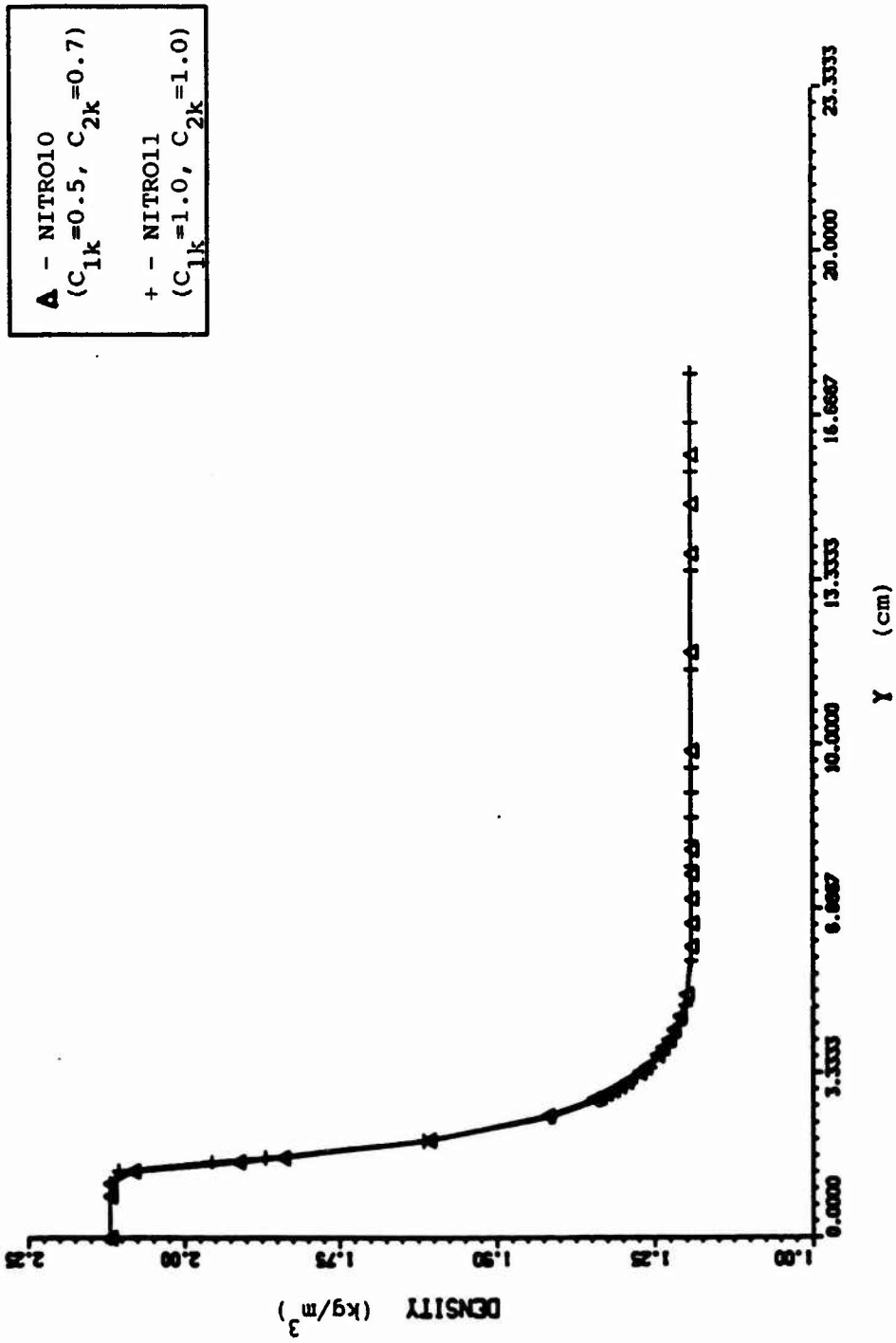


Figure 2: Density Profiles at 16 cm. Downstream
 Showing Effects of Changing C_{1k} and C_{2k}

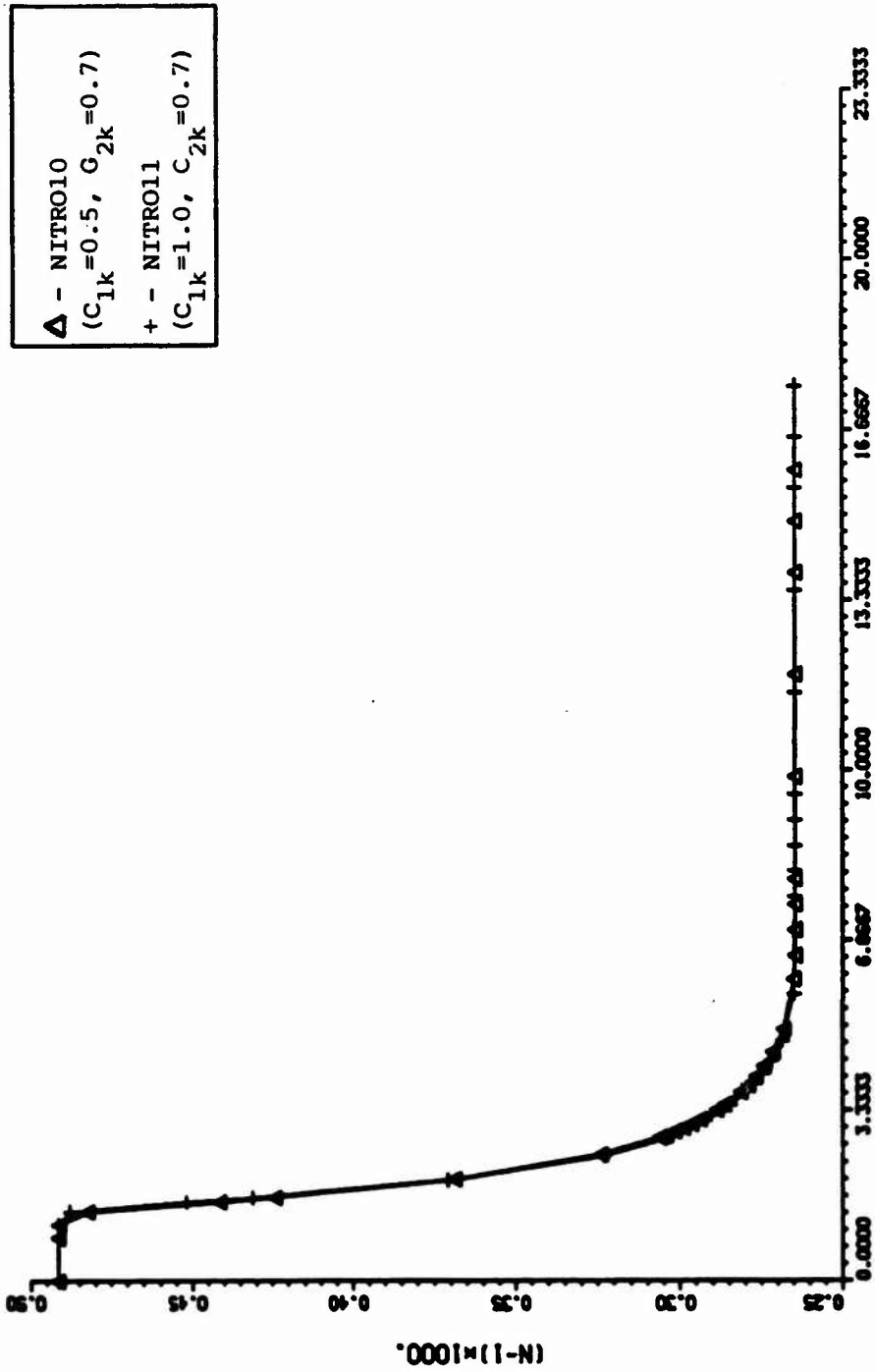


Figure 3: Index-of-Refraction Profiles at 16 cm. Downstream
 Showing Effects of Changing C_{1k} and C_{2k}

▲ - NITROO
 (33 grid pts.)
 + - NITRO5
 (74 grid pts.)

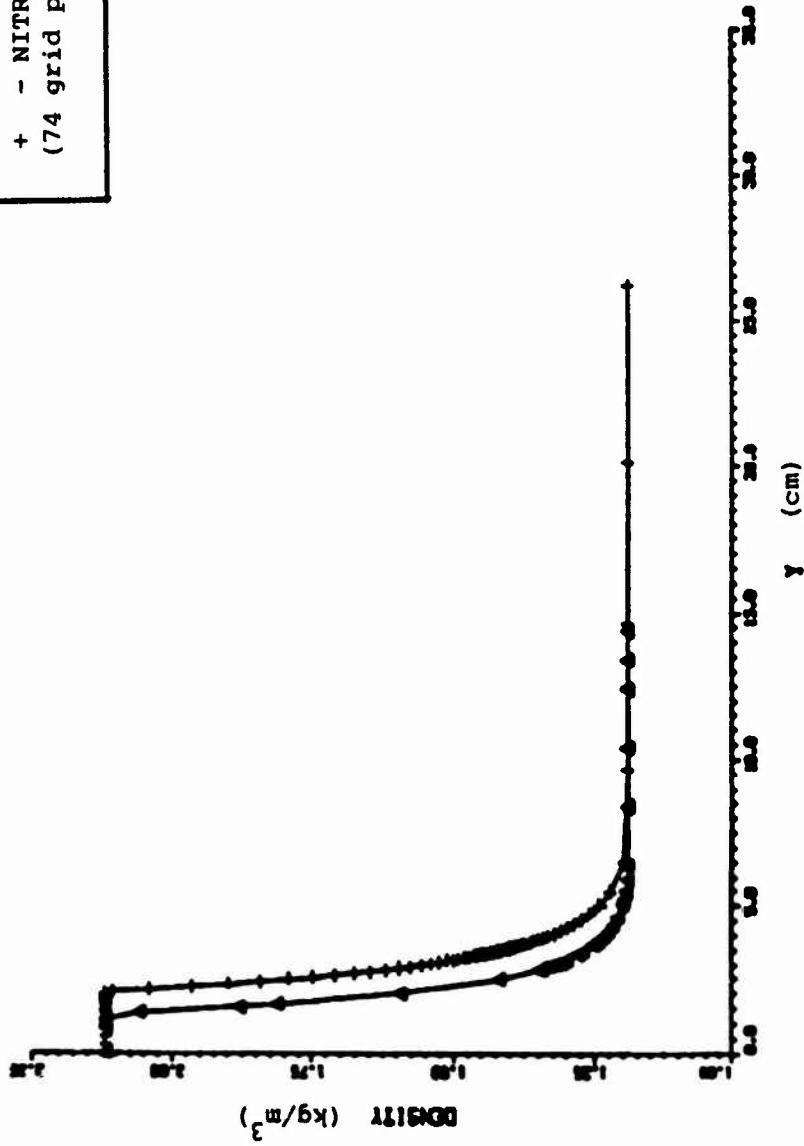


Figure 4: Density Profiles at 16 cm. Downstream
 Showing Effect of Transverse Grid Spacing

REFERENCES

- Baxter, M.R., "Predicting the Optical Quality of Supersonic Shear Layers," Master's Project Report, Department of Mechanical Engineering, University of New Mexico, 1987.
- Bogdanoff, D.W., "The Optical Quality of Shear Layers: Prediction and Improvement Thereof," AIAA J., Vol. 22, No. 1, 1984, pp. 58-64.
- Jones, W.P. and Launder, B.E., "The Prediction of Laminarization with a Two-Equation Model of Turbulence," Int. J. Heat Mass Transfer, Vol. 15, 1971, pp. 301-314.
- Launder, B.E., Morse, A., Rodi, W. and Spalding, D.B., "The Prediction of Free Shear Flows - A Comparison of the Performance of Six Turbulence Models," NASA Langley Free Turbulent Shear Flows. Vol. 1. Conference Proceedings, NASA SP 321, 1972, pp. 361-426.
- Launder, B.E. and Spalding, D.B., Mathematical Models of Turbulence, Academic Press, Inc., New York, 1972, pp. 126, 127.
- Liepmann, H.W. and Roshko, A., Elements of Gas Dynamics, John Wiley & Sons, Inc., New York, 1957, p. 154.
- Mikitarian, R.R. and McDanal, A.J., "Analytical and Experimental Correlation of the HF Chemical Laser Flow Data," AIAA Paper 75-39, 1975.

Sutton, G.W. "Effect of Turbulent Fluctuations in an Optically Active Fluid Medium," AIAA J., Vol. 7, No. 9, 1969, pp. 1737-1743.

Theones, J., Hendricks, W.L., Kurzuis, S.C., and Wang, F.C., "Advanced Laser Flow Analysis (ALFA) Theory and User's Guide," AFWL/TR-78-19, 1979.

Wilson, A.S., "The Modeling of Chemically Reacting Turbulent Plumes," presented at the 7th JANAF Plume Technology Meeting, Redstone Arsenal, Alabama, 1973.

1986 USAF-UES SUMMER FACULTY RESEARCH PROGRAM/

GRADUATE STUDENT SUMMER SUPPORT PROGRAM

Sponsored by the

AIR FORCE OFFICE OF SCIENTIFIC RESEARCH

Conducted by the

Universal Energy Systems, Inc.

FINAL REPORT

EXPERIMENTAL TESTING OF IMAGING CORRELOGRAPHY

Prepared by:

Jerome Knopp

Associate Professor

and

Brian E. Spielbusch

Graduate Student

Department and

Department of Electrical and Computer Engineering

University:

University of Missouri - Columbia

Research Location:

Air Force Weapons Laboratory

Kirtland AFB, NM 87117-6008

Group ARBB

USAF Researcher:

Captain Paul S. Idell

Date:

19 August 1987

Contract No:

F49620-85-C-0013

REFERENCE DR. KNOPP
SFRP FINAL REPORT NUMBER 80

**1987 USAF-UES SUMMER FACULTY RESEARCH PROGRAM/
GRADUATE STUDENT SUPPORT PROGRAM**

Sponsored by the
AIR FORCE OFFICE OF SCIENTIFIC RESEARCH
Conducted by the
Universal Energy Systems, Inc.

FINAL REPORT

**AN ASPECT GRAPH-BASED CONTROL STRATEGY FOR 3-D OBJECT
RECOGNITION**

Prepared by: Louise Stark

Academic Rank: Graduate Student

**Department and
University:** Department of Computer Science and Engineering
University of South Florida, Tampa, Florida

Research Location: RADC/COES Griffiss AFB
Rome, New York 13441

USAF Researcher: Jacob Scherer

Date: July 10, 1987

Contract No: F49620-85-C-0013

**AN ASPECT GRAPH-BASED CONTROL STRATEGY FOR 3-D OBJECT
RECOGNITION**

by
Louise Stark

ABSTRACT

Several researchers have described methodologies for three-dimensional object recognition which use nonlinear optimization as a control strategy for matching features of a three-dimensional object model to features found in an image. An acknowledged problem with this type of system is how to efficiently choose a set of starting parameter estimates so as to avoid recognition errors due to local minima. This paper presents a new methodology for applying nonlinear optimization in three-dimensional object recognition. Our method enumerates a complete set of relevant starting points for each object model by choosing one starting point for each viewing cell defined by the aspect graph of the object. Constrained nonlinear optimization is used to find a minimum within each viewing cell. Examples are given to illustrate how recognition errors can occur due to local minimum found from poor starting parameter estimates, and how the methodology based on the aspect graph object models eliminates this problem.

ACKNOWLEDGMENTS

I would like to thank the Air Force Systems Command and Air Force Office of Scientific Research for the opportunity to participate in the Graduate Student Summer Support Program. I feel that the program has been a very beneficial experience for me. The personnel at Universal Energy Systems have been very accommodating and prompt in all administrative aspects of the program.

A special acknowledgment must go to the people at RADDC/COES for their helpfulness and kindness. All involved made me feel welcome and right at home. The working atmosphere was friendly and relaxed. The help and guidance provided by Jake Scherer was greatly appreciated. The support, encouragement and patience of Dr. Kevin Bowyer throughout this project made all of this work enjoyable and rewarding.

I. INTRODUCTION

Computer vision research has been extensive in the broad field of Artificial Intelligence. My research in the area of computer vision deals mainly with the development of an intelligent vision system to be used in three-dimensional object recognition.

One of the key components of an intelligent vision system is the prior knowledge it holds about the objects in the environment. In computer vision, this knowledge, which will hold some unique information on each object, constitutes a model-base which can be searched for a match with the object found in an input image. Given a single arbitrary two-dimensional perspective image, the three-dimensional object recognition process is expected to be capable of identifying objects and estimating their location and orientation parameters. The ability to interpret an image depends critically upon the model-base. Determining what knowledge is needed for object representation, how that knowledge should be represented and how it can efficiently be applied in the search technique is the essence of the object recognition problem.

Object representation techniques can be divided into two categories, view-dependent and view-independent [1,4]. Some earlier systems used view-dependent representation comprised of libraries containing a fixed number of views. The limitations of this approach should be apparent due to the fact that the accuracy of the recognized orientation parameters is limited by the number of precomputed views. Since, in the general case, the object may appear in any orientation, the model should be able to be viewed from any viewpoint. This leads to the view-independent or model-oriented approach, in which a three-dimensional model of an object is stored, and two-dimensional projections are created dynamically. The sequence of projections created is controlled by a nonlinear optimization algorithm.

The standard paradigm for approaching the three-dimensional object recognition problem appears in Figure 1. The process begins with input from the environment; for example, a digitized two-dimensional image of a three-dimensional object. Features are extracted from the image and passed on to be used in a matching process. Possible features include Fourier descriptors [15,16], silhouettes [3,14], or feature points [11]. On the first iteration the feature extraction and matching module processes the input image and sends a summary of the actual image feature information to the recognition control strategy module. This information is utilized as an "index" into the model-base. If the actual image features have certain attributes that do not exist in the list of attributes of a certain object, that object can be bypassed in the search strategy. The attributes used in the comparison

will be specific to the feature extraction process chosen.

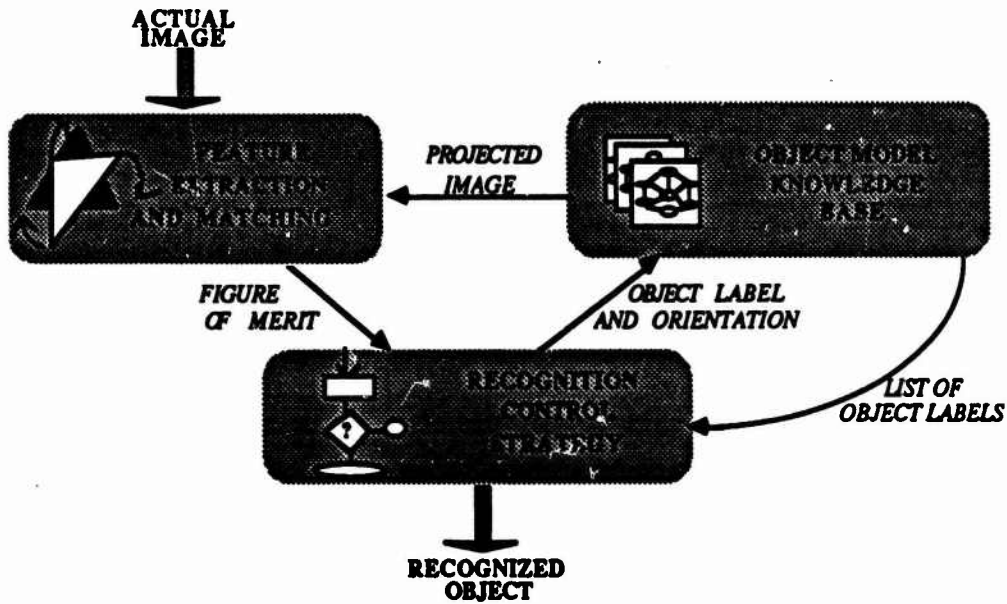


Figure 1 Three stages of object recognition process

The recognition control strategy initiates the recognition process by producing an object label and initial orientation estimates. The object label is generated from a list of objects which are held in the object model-base. The object model knowledge base holds enough information on each object to produce the requested projection of the specified object. It will be shown later in this paper that knowledge of the geometry of each object can be used to formulate an "intelligent" control strategy and also to greatly simplify the process of generating hidden surface projections.

The projected image is passed to the feature extraction and matching module. A figure of merit is produced from the feature match. The recognition control strategy utilizes the figure of merit to produce either the same object label with new orientation or a new object label and orientation. The recognition control strategy maintains a record of "best match" object label and orientation.

The three stage process is repeated, matching the new projected image with the actual image and producing a new figure of merit on each iteration. The control strategy terminates the process when the "best match" is found, at which time the identification of the recognized object and its orientation are output.

II. OBJECTIVES OF THE RESEARCH EFFORT

Referring to the general solution structure of the object recognition problem (Figure 1), we

are currently concentrating our efforts on developing the object model knowledge base and the recognition control strategy. The aspect graph object model allows us to construct an intelligent methodology for applying nonlinear optimization in the recognition control strategy. Experiments described in this paper illustrate the importance of the viewing cell concept in choosing starting points and avoiding recognition errors due to local minima. We currently use a very simple feature extraction and matching module which we plan to update with a more powerful technique.

III. BACKGROUND

Some examples of three-dimensional object recognition systems that use nonlinear optimization to control the matching process are found in [11,14,16]. Points of differentiation between these systems include the particular optimization algorithm used, the structure of the model-base, and the method of choosing initial parameter estimates.

An iterative silhouette matching scheme was proposed by Hemami et al. [11]. A single greyscale original image is input to the system. A model-base is used which is capable of generating a three-dimensional wire-frame model of each object. The three-dimensional model is projected, using a perspective transformation, to a two-dimensional image. "The silhouette is derived from the outline of the image by erasing the internal detail" [11]. The original and projected images are matched based on the comparison of a sequence of points along the boundaries. Initial estimates of translational parameters are made from the first and second moments and the size of the observed object. The initial rotational parameters are generated by a uniform random search which is "used to rule out local minima" [11]. No reference is given as to the precision of the uniform random search executed. An error function is defined as the sum of squares of the misalignment between feature points extracted from the silhouettes of the original and projected images. Gauss-Newton or Newton-Raphson iteration is used to minimize the error function. Tests for identity and orientation were run using three concave objects. Each object matched with its corresponding model-base object by choosing the object with the minimum error function. However, it was found that the method "requires substantial numerical computation, since many local minima exist" [11].

Watson and Shapiro [16] describe a method of matching two-dimensional projections of unique three-dimensional space curves of three-dimensional objects to two-dimensional perspective views of the object. Periodic cubic splines were used to approximate the two-dimensional curves. The matching process uses the Levenberg-Marquardt algorithm to minimize the error between Fourier descriptors of closed curves. Starting points were

chosen at random for each test. If the test gave a correct match the program was terminated. "If the program reported a failure due to converging on a local minimum, a new starting point was randomly chosen, and the process was repeated" [16]. Tests were run using the unique characteristic edge curves of five different chairs. A perspective view was projected for each curve moved from its standard position. Matching of the two-dimensional curve against all five given space curves was simply a minimization problem that searched for the parameters of rigid motion with the least error. Results of the tests were dependent upon the object tested. Instances of incorrect identification were thought to be due to "converging to a local minimum, but not recognizing the fact" [16].

The ACRONYM system, developed at Stanford University, uses a model-base to construct a three-dimensional model of the object in any orientation, which is then projected to a two-dimensional image plane. The mismatch of the original and projected images is found using "the perpendicular distance of each endpoint of the model line from the corresponding line in the image" [14]. Newton-Raphson iteration is used in ACRONYM. This method approximates the first derivative of each error term with respect to each of the six orientation parameters. Lowe points out that the best results were obtained when the derivatives were fairly independent of one another, and were smooth enough over the error range for good convergence [14]. Lowe also points out that the choice of initial starting parameters is one of the most difficult problems in the recognition process. Initial parameter estimates for ACRONYM were chosen from a set of quasi-invariant features from the model, which are features "observable over a wide range of orientations and viewing conditions" [14].

Two interrelated problems acknowledged by each of the systems mentioned above are 1) choice of starting points and 2) knowing when a global minimum is found. Our system uses the viewing cells defined by the aspect graph of an object in order to solve these problems. The aspect graph summarizes a complete partition of space around the object according to its geometry. It will be pointed out later that a major advantage of combining the nonlinear optimization control strategy of damped least squares with the aspect graph model-base is the ease with which a set of relevant initial starting parameters can be intelligently chosen.

IV. OVERVIEW OF THE OBJECT RECOGNITION ALGORITHM

The recognition control module of our system uses a damped least squares algorithm. The control strategy is to minimize the scalar mismatch of features in the original image with those of the image of the model projected at the current parameter values. We use damped

least squares because it has been claimed that, even for complex problems, "starting estimates of the parameters may be very rough indeed," and the damped least squares method will still converge quickly [6].

The object model knowledge base of our system uses an aspect graph representation. The aspect graph concept was introduced by Koenderink and van Doorn, who described a graph structure which they called the "visual potential" of an object [12]. Each node of the graph represents a different "aspect" of the object. The aspect is defined by a specific collection of visible faces and edges, along with a definition of the cell of space from which that collection of faces and edges is visible. Nodes of the graph are connected by arcs that represent a transition from one viewable aspect to another. "Thus a visual potential represents in a concise way any visual experience an observer can obtain by looking at the object when traversing any orbit through space" [12].

Several researchers have proposed object representations based on multiple views obtained by partitioning the surface of the viewing sphere. Fekete and Davis proposed the "property sphere" concept [8]. They subdivide the sphere into 320 "trixels" in a "quasi-uniform" manner and compute the silhouette of an object as it would be seen from each view. Korn and Dyer introduce a model-base consisting of three-dimensional multiview models, which are represented by a finite set of viewer-centered descriptions [13]. Viewpoints are selected from the surface of a view sphere which has been tessellated into a set number of bins. Bins are joined into regions by grouping feature equivalent adjacent views from the sphere surface.

Castore and Crawford discuss the use of aspect graphs for solid modeling and robotic vision [2,5]. They indicate that algorithms have been developed and implemented for 2.5-dimensional convex objects. Reference is given that the algorithm "is based on methods developed by Goad" [5]. Goad defines the set of positions on the unit sphere from which a given feature is visible as the "visibility locus" of that feature [9,10]. The loci of viewing positions are found by tessellating the surface of a set radius viewing sphere into quasi-uniform patches. Two restrictions of this method are 1) "the distance of the object be known exactly in advance," and 2) that the "resolution of this representation is bounded by the maximum diameter of a patch" [10]. It is important to point out that all of these object representations are based on patches of surface area on a sphere centered about an object, and not on cells of three-dimensional space.

Our system uses a true aspect graph in the sense of [12], rather than an approximation via a tessellated viewing sphere. Each node of the graph contains 1) a definition of visible

faces, and 2) a definition of a cell of space. The information obtained from the aspect graph will enhance our recognition process over others reviewed here in the related problem areas of initial parameter estimation and recognition errors due to local minima. The information in the aspect graph also helps to eliminate much of the work in hidden surface projection problems.

The algorithm we use to construct aspect graphs is currently restricted to planar-face, convex, 3-D objects. Thus the object shapes depicted in later examples are very simple. The same concepts illustrated here should still be valid for non-convex objects of arbitrary shape, but original construction of the aspect graph will be more difficult.

A. Feature Extraction and Matching

The complete edge structure of the object is examined to select a list of relevant internal and external feature points. Several distinct types of feature points are distinguished. Edges of the object are chain coded and ordered by their length relative to the boundary curve. Within each chain coded edge, the selected feature points are distinguished by type and by distance from the starting point in the chain. The set of chain codes for the projected image is processed against that for the actual image to obtain a list of corresponding feature points. A minimum number of feature points (at least three) must match to show a correspondence between the actual image and the projected image.

B. Recognition Control Strategy

Given an observed image, known as the original image, the objective is to identify the object appearing in the image and find the orientation and translation of the object. Due to the nonlinearity of the problem, the method developed here for finding the parameters of translation and orientation uses the method of damped least squares. Damped least squares is desirable due to the fact that it has been found to converge in a reasonable time frame and is successfully used in automatic optical design programs which can have over thirty parameters [7]. The damping factor helps to control the oscillation due to the nonlinearity of the problem, and thus assists in the convergence to a solution.

1. Damped Least Squares

A very broad view of the problem is simply to start at some initial guess of the parameter values and to iterate, changing the parameters until a match is found. The parameters of an object are defined here as three rotational parameters (R_x , R_y , R_z) and three translational

parameters (X, Y, Z). These six parameters make up the parameter vector P. The sum of squares term E will be the merit function, or criterion function, defined as:

$$E = \sum f_i^2$$

where f_i is the scalar mismatch between points of the original image and the image projected at the current parameter values. The objective is to minimize the merit function and therefore minimize the error between points. The parameters that can vary in order to minimize E are the six rotational and translational parameters in P. E can be minimized by setting the partial derivatives of E with respect to each of the parameters equal to zero. One of the problems in this application is that the objective function can be highly nonlinear, causing oscillation around the minimum. The oscillation can be thought of as "overshooting" the solution point. To avoid oscillation we are limiting the ΔP values by use of a damping factor λ to try to keep the steps small enough to ensure they are in a linear range.

The initial choice of λ seems to be arbitrary. We start with a damping factor $\lambda=1$ for the first iteration. If the merit function decreases, then λ is decreased on the next iteration. A decrease in E denotes a closer approximation of the solution. As long as the merit function continues to decrease, λ should also be decreased. It should be noted that when $\lambda=0$ and E decreases, the amount of nonlinearity is "small". Therefore, the damping factor is a modification that is added when the amount of nonlinearity is "large".

If E increases after an iteration, then we increase λ , return to the last set of data in which E decreased and calculate a new change in parameters. A point can be reached when the changes in parameter values are so small there is essentially no change in E. If E continues to show an increase after increasing λ a set maximum number of times, then the process is terminated. At this point the magnitude of the damping factor is restraining the step size enough to keep the change in merit function zero. The parameters used for the last decrease in E are reported as the best estimate of the object's parameters. Sample output results for the matching process of a cube are shown in Table 1. The actual image parameters, the initial estimated parameters and the parameter values for each iteration are shown. The error function E and the damping factor λ are also listed to illustrate how the damping factor changes as the change in parameters becomes more linear.

There seem to be two major interrelated problems encountered by systems which use nonlinear optimization as a recognition control methodology. The first problem is that of choosing initial parameter estimates. One possibility is to perform a uniform random

search (as in [11]), which does not guarantee that all of the "best" estimates have been tried. Another possibility is to generate a new starting point at random if the algorithm seems to hit a local minimum [16]. One other possibility is to choose "quasi-uniform" viewpoints (as in [14]). These viewpoints are object specific yet not exactly chosen according to the object's geometry. The viewpoints seem to have been visually extracted by the user instead of generated automatically. The optimal solution to the problem of choosing starting parameter estimates would be to automatically pick out all relevant starting points based on fundamentally different views of the object, without duplicating or overlapping search areas, yet still ensuring all possibilities are covered. By having a starting point for each fundamentally different view, we can be assured of finding a global minimum. By having no "extra" starting points, a substantial amount of unnecessary computation can be avoided.

The second problem involves encountering local minima, which can cause errors in recognition (as in [16]). This problem is clearly related to the first. Incorrect choice of initial estimates can result in convergence on a local minimum and hence incorrect identification of the object. This problem is illustrated in the simple example depicted in Figure 3. Initial parameter estimates and final parameter estimates (after damped least squares convergence) are listed. The original image view is a side of a rectangular block, rotated 5 degrees about the Z axis (line of sight), shown as actual image view. Orientation parameter estimates are made for different objects in the model-base, which include the rectangular block and a cube. Due to improper arbitrary initial estimates of parameters it can be shown that the cube will match the original image better than an invalid view of the actual object (as shown by the lower error function E for the cube, view #1), thus an incorrect identification is made.

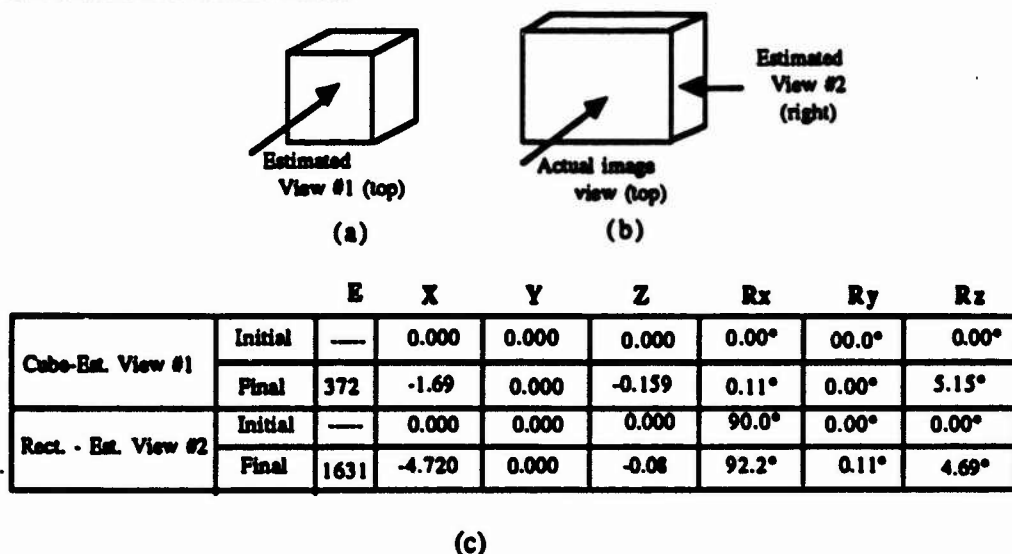


Figure 3 Illustration of incorrect choice of initial parameter estimates.

(a) Model-base Cube (b) Model-base Rectangular Block (c) Matching process output

The important distinguishing property of our methodology is that the aspect graph object model directly reflects the unique individual geometry of the object. Systems that use random search for initial viewpoints are not utilizing the information available in the object's geometry. Prior knowledge of the geometry of the objects in the model-base helps to define the viewspace for each object. A definite advantage can be gained from this information, which is drawn directly from the aspect graph.

C. Exploiting the Aspect Graph Object Model

Imagine subdividing space around an object into cells. These cells would group all possible viewpoints into regions from which the object appears essentially the same. The viewing cell concept summarizes all possible viewpoints and subdivides the viewing space around an object into a finite number of areas, represented by the nodes of the aspect graph (Figure 4b). Cells are bounded by extensions of the object's planar faces. Each node of the aspect graph is attributed with a list of planes, lines and points of intersection which define the viewing cell of space for that node. The planes are the sides, lines are edges and points of intersection are corner points of the viewing cell.

1. Viewing Cell Bounds Checking

Nodes of the aspect graph are associated with faces of the object which are visible from within the viewing cell defined for that node. Each node has a unique set of visible faces. A face of the object is visible if the viewpoint is "outside" the plane of that face. Outside is defined as the side of the plane opposite that of the origin of the model coordinate system. The origin is always placed inside the object model. More precisely, if the viewpoint is outside the plane and directed toward the origin then the plane containing the face is between the viewpoint and origin and is therefore visible.

To determine if a viewpoint is inside or outside of a specific plane, the planar equation is evaluated using the point. If the point lies inside the plane (the face is not visible) the planar equation will evaluate to a negative value. If the point lies outside the plane (the face is visible) the planar equation will evaluate to a positive value. If the point lies on the plane (lies on the boundary of two viewing cells) the planar equation evaluates to zero. A point that lies on the boundary is considered to be a part of both viewing cells.

To determine in which viewing cell a specific viewpoint lies, all planar equations of the object must be evaluated using the viewpoint. The positive and negative values obtained

by evaluating the planar equations can be translated into which faces of the object are visible from that viewpoint.

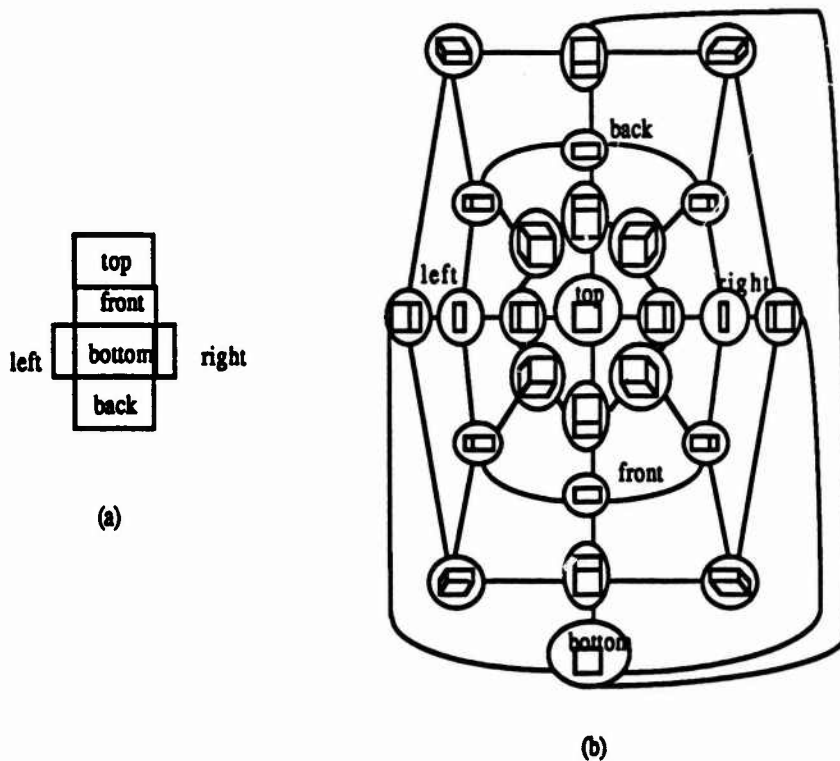


Figure 4 (a) Faces which make up rectangular block (b) Illustration of its aspect graph

Each node of the aspect graph is attributed with a definition of visible faces. It can therefore be calculated as to which cell(s) a viewpoint is associated. This process is used as "bounds checking" to constrain the nonlinear convergence process.

2. Viewing Cell and Selection of Starting Parameter Estimates

If the approximate viewing distance is known, as is the case in many robotics applications, it is easy to envision an object placed in the center of a transparent sphere whose radius is equal to the approximate viewing distance. The viewpoint can be placed anywhere on the sphere and directed toward the object. Using the bounding information of the viewing cell it is easy to envision a "patch" defined on the surface of the sphere for each aspect in the graph. Figure 5a denotes the projection of the bounds for three nodes of the aspect graph in Figure 4. The surface area patch is defined by the intersection of the bounds of a nodes cell and the sphere surface. The entire surface of the sphere is parcellated in a like manner. The center of mass of each surface area patch can be calculated. By directing viewpoints from each center of mass point to the origin of the sphere a set of initial parameter estimates can be defined for the object.

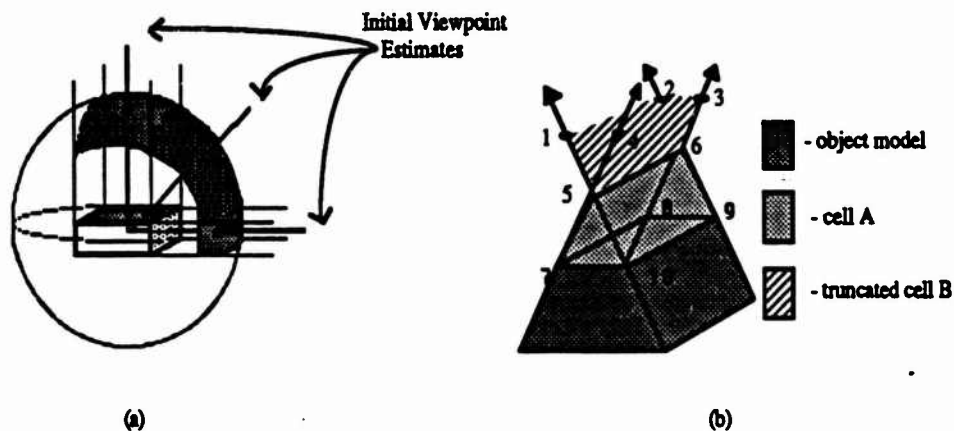


Figure 5 (a) Initial viewpoint estimates for object of known viewing distance. Surface patches formed by projecting "bounds" of three nodes of Figure 4. (b) Example of finite (cell A) and infinite (cell B) viewing cells. Complete set of initial parameter estimates are calculated for all cells of object.

Since the viewing distance is not always known, the fixed radius sphere is not general enough for normal object recognition conditions. The complexity of the object must also be considered. For the simple rectangular block, as the viewing distance changes, all nodes of the aspect graph project a "patch" on the surface of the sphere which change proportionally. This is not true for more complex objects. For some objects, as the viewing distance changes, some viewing cells can end and others begin (see Truncated Wedge in Figure 5b). A more general set of initial parameter estimates can be calculated for each object by inspecting all viewing cells around the object. It is important to enumerate a "complete" set of starting parameters so that identification and/or orientation errors do not occur, as in the example depicted in Figure 3. It is also important to enumerate an "efficient" set of starting parameters so that overlapping search areas are not investigated. We feel that a complete and efficient set of initial parameter estimates would be directly related to the nodes of the aspect graphs in the object model knowledge base.

A starting viewpoint estimate can be chosen for each node of the aspect graphs stored in the object model knowledge base. Features can be extracted for each initial parameter estimate and stored as an attribute with its specific node. Calculation of a representative starting point for a node of the graph is dependent upon the description of the cell of space defined for that node. There are two types of cells defined; 1) finite and 2) infinite.

Finite cells are closed regions formed by the intersection of the extension of the planar faces of the object model, (e.g. cell A in Figure 5b). Infinite cells are cells that form regions of infinite extent (e.g. cell B in Figure 5b). Both finite and infinite cells are defined by a list of planes, lines and points of intersection held as attributes in the aspect graph. Initial viewpoint calculation for a finite cell is a simple process of averaging the

points of intersection associated with that cell. These are essentially the corner points that define the boundary of that cell. For example, points 5, 6, 7, 8, 9 and 10 would be averaged for the finite cell A (Figure 5b). Finding the average point ensures a representative point that lies inside the cell.

Initial viewpoint calculation for infinite cells requires the estimation of a possible maximum or typical viewing distance. Since a representative viewpoint is all that is necessary to place the initial estimate inside the viewing cell, the maximum viewing distance chosen does not place a limitation on the possibility of converging to parameters outside the maximum distance chosen. The estimated maximum is only used to allow the definition of a finite cell using the infinite cell boundary information.

Infinite cells are defined as any region that has a line (edge) which has only one boundary "corner point" for that cell and extends outward from that point infinitely. The line equations of the cell bounds are stored in coefficient form (a,b,c), where:

$$X = at + X_0$$

$$Y = bt + Y_0$$

$$Z = ct + Z_0$$

The values for point (X_0, Y_0, Z_0) can be substituted by the single corner point associated with the "infinite" edge. To calculate temporary boundary points for infinite boundary edges, a maximum distance D is estimated. A distance measure equation can be written:

$$(at + X_0)^2 + (bt + Y_0)^2 + (ct + Z_0)^2 = D^2$$

A value must be found for the temporary boundary points which are part of the specified cell boundary. Temporary points are verified as belonging to a specified cell by the process of bounds checking.

For infinite cell B, temporary points must be found on the infinite edges to create a closed region (points 1,2,3 and 4 in Figure 5b). Once an infinite cell has been "closed" by calculating temporary boundary points, the representative initial starting point for that cell can be calculated. This is accomplished in the same way as with true finite regions, by calculating the average representative point for the cell. By repeating this process for all cells, a more general and complete set of initial parameter estimates can be established.

A merit function E is calculated for projections produced from the orientation parameters of the representative viewpoint of each node on the graph. The iterative damped least squares process is used to converge on the "best match" parameters. The viewing "bounds" are used in the iterative matching process to insure that the new parameters

chosen are still within the specified viewing space. If the new parameters chosen fall outside the bounds of the current aspect, the damping factor can be increased and the process repeated. This action, which will decrease the size of the step taken, can be repeated until the new parameters fall inside the present aspect. This bounding constraint also insures a single local minimum for each aspect. By checking all nodes of the aspect graphs in the object knowledge base it can be seen that the incorrect identification encountered in Figure 3 will now be resolved.

Each node of the aspect graph contains feature attributes which could include the number of feature points and their types. Certain nodes of the aspect graph can be eliminated in a preliminary comparison of types and number of feature points extracted from the original image. Results for the test run using the actual image viewpoint shown in Figure 3, rotated about the Z axis 5 degrees are listed in Table 2. Initial parameter estimates, final parameter estimates after convergence and E are listed for each. The actual image parameters are : $(X=0, Y=0, Z=0, R_x=0^\circ, R_y=0^\circ, R_z=5^\circ)$. To consolidate the data, and due to the symmetry of the object, the results are only shown for three unique nodes of the rectangle's aspect graph and one node of the cube's.

V. RECOMMENDATIONS

It has been shown that use of knowledge of the specific geometry of individual objects can improve the recognition control methodology. This information is naturally incorporated into an attributed aspect graph of the object. Using this form of object model, an intelligent methodology can be developed for applying nonlinear optimization in the control of the recognition process.

By choosing a representative viewpoint for each node of the attributed aspect graph, initial parameter estimates can be made which assure that the entire search area of the entire object will be covered, without omitting any possible aspect and without using more starting estimates than necessary. Using damped least squares and the bounding constraints, the optimization process converges to the single local minimum of each cell without overlapping search areas. The minimum cell error is chosen as the minimum error for that object. The model-base object with the minimum error overall is chosen as the object in question. While we have no direct mathematical proof that this must always converge to the global minimum, we feel it has compelling intuitive appeal. Having this extra information in the model-base should result in reduced search time and improved accuracy when compared to systems which use uniform search or have no structured method of choosing starting parameter estimates. We are proceeding to design experiments with more complex objects.

	E	λ	X	Y	Z	Rx	Ry	Rz
Actual Parameters			0.000	0.000	0.000	0.00°	60.0°	0.00°
Estimated Parameters	(408)	1	0.000	0.000	0.000	0.00°	45.0°	0.00°
Iteration #1	234	16	0.002	-0.029	0.006	0.35°	60.8°	-5.61°
Iteration #2	63	8	0.002	-0.021	0.006	0.45°	57.8°	-2.34°
Iteration #3	51	4	0.002	-0.021	0.006	0.45°	60.4°	-2.29°
Iteration #4	48	512	0.002	-0.021	0.006	0.45°	60.1°	-2.00°
Iteration #5	42	2048	0.002	-0.021	0.006	0.35°	59.6°	-1.89°
Iteration #6 (final)	20	1024	0.002	-0.040	0.006	0.23°	60.4°	-1.77°

Table 1 Sample output to illustrate the effect of the damping factor λ

	Rectangle (top)		Rectangle (back)		Rectangle (right)		Cube	
	Initial	Final	Initial	Final	Initial	Final	Initial	Final
X	0.000	0.025	0.000	0.000	0.000	-4.27	0.000	-1.69
Y	0.000	0.016	0.000	0.000	0.000	0.00	0.000	0.00
Z	0.000	0.002	0.000	0.000	0.000	-0.08	0.000	-0.16
Rx	0.00°	0.02°	0.00°	2.86°	90.0°	92.18°	0.00°	0.11°
Ry	0.00°	-0.17°	90.00°	87.0°	0.00°	0.11°	0.00°	0.00°
Rz	0.00°	5.04°	0.00°	0.04°	0.00°	4.69°	0.00°	5.15°
E	252	7	610	379	1770	1631	572	372

Table 2 Sample output for identification and orientation test found in Figure 3 rotated about the z axis 5 degrees. Correct identification is made.

REFERENCES

1. Besl, P.J. and Jain, R.C. "Three-Dimensional Object Recognition," ACM Computing Surveys 17, 1 (March 1985), pp. 75-145.
2. Castore, G. and Crawford, C.G. "From Solid Model to Robot Vision," Proceedings of the 1984 IEEE International Conference on Robotics, (1984), pp. 90-92.
3. Chakravarty, I. and Freeman, H. "Characteristic Views as a Basis of Three-Dimensional Object Recognition," SPIE Volume 36: Robot Vision, (1982), pp. 37-45.
4. Chin, R.T. and Dyer, C.R. "Model-Based Recognition in Robot Vision," ACM Computing Surveys 18 (1), (March 1986), pp. 67-108.
5. Crawford, C.G. "Aspect Graphs and Robot Vision," Proceedings of the 1985 IEEE International Conference on Computer Vision and Pattern Recognition, (1985), pp.382-384.
6. Fanning and Taylor "An Application of Photogrammetry to the Problem of Store Separation," Mathematical Services Branch, Eglin Air Force Base, Florida (June 1972).
7. Feder, Donald P. "Automatic Optical Design," Applied Optics 2, 12 (December 1963), pp. 1209-1226.
8. Fekete, G. and Davis, L.S. "Property Sheres: A New Representation for 3-D Object Recognition," Proceedings of the IEEE Workshop on Computer Vision: Representation and Control, (1984), pp.192-201.
9. Goad, C. "Automatic Construction of Special Purpose Programs for Hidden Surface Elimination," Computer Graphics 16 (3), (July 1982), pp. 167-178.
10. Goad, C. "Special Purpose Automatic Programming for 3-D Model-Based Vision," Proceedings of the 1983 DARPA Image Understanding Workshop, (1984), pp. 94-104.
11. Hemami, H, Weimer, F.C., and Advani, J.G. "Identification of Three-Dimensional Objects by Sequential Image Matching," Proceedings of IEEE Conference on Computer

Graphics, Pattern Recognition, and Data Structures (1975), pp. 273-278.

12. Koenderink, J.J. and van Doorn, A.J. "The Internal Representation of Solid Shape with Respect to Vision," Biological Cybernetics 32, (1979), pp. 211-216.

13. Korn, M.R. and Dyer, C.R. "3-D Multiview Object Representations for Model-Based Object Recognition," Pattern Recognition 20 (1), (1987), pp. 91-103.

14. Lowe, David G., "Solving For the Parameters Of Object Models From Image Descriptions," Proceedings : Image Understanding Workshop, April, 1980, pp. 121-127.

15. Richard, C.W. and Hemami, H. "Identification of Three Dimensional Objects Using Fourier Descriptors of the Boundary Curve," IEEE Transactions on Systems, Man, and Cybernetics 4, 4 (July 1974), pp. 371-378.

16. Watson, L.T. and Shapiro, L.G. "Identification of Space Curves from Two-Dimensional Perspective Views," IEEE Transactions on Pattern Analysis and Machine Intelligence 4, 5 (September 1982), pp. 469-475.

1987 USAF-UES SUMMER FACULTY RESEARCH PROGRAM/

GRADUATE STUDENT SUMMER SUPPORT PROGRAM

**Sponsored by the
AIR FORCE OFFICE OF SCIENTIFIC RESEARCH**

**Conducted by the
Universal Energy Systems, Inc.**

FINAL REPORT

LINEAR PROGRAMMING FOR AIR FORCE DECISION AIDING

Prepared by: Steven J. Steinsaltz
Academic Rank: Graduate Student
Department and Department of Mathematical Sciences
University: The Johns Hopkins University

**Research Location: RADC/COAD
Griffiss AFB
Rome, NY 13441**

USAF Researcher: Joseph Carozzoni
Date: 18 Aug 87
Contract No.: F49620-85-C-0013

LINEAR PROGRAMMING FOR AIR FORCE DECISION AIDING

by

Steven J. Steinsaltz

ABSTRACT

The program "Enemy Sortie Capability Measurement Aid" was examined to determine what was required of a linear program solver so that it could replace the commercial package being used. A program was written in PASCAL, using the upper bound form of the revised simplex method, and various problems with memory had to be overcome. The completed program took 23 minutes to solve, compared to three minutes for the commercial package. The program was rewritten in C, and when debugged ran in ten minutes. This was improved upon by changing the program so that, instead of using the revised simplex method, which saves memory (a problem not faced in C), the regular simplex method was used. This improved the running time to seven minutes, within the bounds desired.

Acknowledgements

I wish to thank the Air Force Systems Command and the Air Force Office of Scientific Research for sponsorship of this reasearch.

I would also like to thank the Rome Air Development Center and all the people in the Decision Aids Branch. Joe Carozzoni helped me familiarize myself with a computer and two languages with which I had never before worked, and also kept my nose to the grindstone. Tim Trueheart put up with my constantly being in his office using his terminal, and often thinking out loud, with good humor. Yale Smith's help in obtaining answers to my questions about ESCMA was greatly appreciated.

I. INTRODUCTION:

"Enemy Sortie Capability Measurement Aid" is a program which determines, based on such data as weather and intelligence on manpower and equipment, the optimal use of aircraft by the enemy in a battle. Much of the Aid is taken up with such things as determining which airbases are being considered and what the possible targets are. However, in order to determine an optimal allocation, a linear program based on the data must be solved.

Because the authors of the program had no experience with linear programming, they did not work on this part, but instead purchased a commercial linear program solving package called LP83, from Sunset Software. This package does its job well, but it has a major drawback. Each time a copy of the Aid is given to someone, another copy of LP83 must be purchased at a cost of approximately one thousand dollars. It is therefore in the best interests of the government to have their own linear program solver, even at the cost of somewhat increased running time, as long as such increase is within a reasonable limit.

My research interests have been in the area of operations research, and I have had much experience with linear programming. Although my computer programming experience had been limited, it was assumed that I could learn this quickly.

II. OBJECTIVES OF THE RESEARCH EFFORT:

Because the LP83 package costs almost one thousand dollars a copy, a non-licensed program would be of great use to the government. My assignment as a participant in the 1987 Graduate Student Summer Support Program was to write such a program, based on my experience with linear programming, which would be reasonably efficient with respect to running time.

III. INITIAL RESEARCH:

a. The initial efforts spent on the project were directed towards determining just what was required by "Enemy Sortie Capability Measurement Aid" (ESOMA) of a linear program solver. The package being used, LP83, includes in the output file such things as names of variables and names of constraints, which are not needed, and sensitivity analysis, which is not used. So, these things could be ignored in the output delivered by my program.

b. The next thing that had to be done was to decide what solution method would be used by the program. As I am most familiar with the simplex method, this was the method chosen. The upper bound version of the simplex method would be used, as it is much more efficient when variables have upper bounds. Because it was expected that memory might be a problem, and in the mistaken assumption that it would be faster, it was decided to use the revised form of the simplex method.

c. The LP83 package was run to determine how long it takes, and therefore what would be expected of my program. LP83 took approximately three minutes to run.

IV. CODING IN PASCAL:

a. Because ESCMA is written in PASCAL, and because it is an easy language to work with, it was decided to write the program in PASCAL. Microsoft PASCAL was used. The simplex algorithm was broken down into procedures so that the program could be made modular. When it was written, a compilation was attempted, but failed, as the program exceeded the limit set by the compiler of 64K of memory.

b. In order to avoid this memory limitation, a different compiler, called TURBOPASCAL, was used. It has a feature called BIGARRAY, which allows arrays of larger than 64K in a special format, at the cost of increase in access time. The program was converted to TURBOPASCAL and debugged and succeeded in solving the problem before it. Unfortunately, it took 25 minutes to do so, more than eight times as long as LP83.

c. In the hope that it would be faster, the original program, in Microsoft PASCAL, was re-examined. The computer being used allows a "RAM disk" to be used, where files can be stored in memory as if they were on a disk, without the access time required from a disk. This method did cut down the running time, but only to 23 minutes, still too slow.

V. CODING IN C:

a. Because a program written in PASCAL would not be fast enough, it was decided to translate the program into C. This is a faster language, although it is also more difficult to learn and implement. When the translation was completed and debugging accomplished, the program ran in 10 minutes, a great improvement and little more than three times the time taken by LP83. The compiler used, Microsoft C, has a "huge memory module" option, which allows up to one megabyte of RAM to be used, avoiding the memory problems faced in PASCAL.

b. The reason for the large amount of time taken by the program was the large number of arithmetical operations necessary. This number could be reduced by using the regular form of the simplex method instead of the revised form. This could be done because there were no memory problems to worry about. When this change was accomplished, the program ran in seven minutes, barely twice the time used by LP83 and within the limit set. A listing of this final version of the program is attached to this report.

VI. RECOMMENDATIONS:

a. The time needed to optimize the linear program could be reduced by incorporating the program directly into the data structure of the Aid. This would eliminate the time needed to read in a data file from the disk, as well as eliminating the time needed by the Aid to save the input file to disk. Because of all the modifications needed in the program, I did not

have time to do this, and in any case, this would be better done by someone with more experience with computers than I have.

b. There must be some reason, which I have been unable to determine, why the LP83, which is a generalized linear programming solver which must work for any linear program, runs twice as fast as a program written specifically for this problem, on the same machine. It might be worth investigating LP83's method of solving linear programs and incorporating these findings into a program.

VII. Program Listing:

```
/* This program solves a linear program for the Enemy Sortie Capability
Measurement Aid. It uses the upper bound method of linear program,
as all non-slack variables have upper bounds. The initial problem is
max c'x s.t. Ax<=b, x>=0. Slack variables are added to make the
problem max c'x s.t. [A:I][x]=0, x>=0, s>=0. The slack variables
are the initial basic [s] feasible solution.
The constants defined below may need to be increased.
Maxfield is the maximum number of airfields in ESCMA (currently 10).
Nocraft is the number of kinds of aircraft available (now 5).
Nomiss is the number of kinds of mission available (now 4).
Norow is the maximum number of constraints. This will always be no
greater than (6*maxfield)+2*(maxfield*nocraft)+nomiss and will
often be fewer.
Nocol is the maximum number of variables. This will always be no
greater than maxfield*nocraft*nomiss and will often be fewer.
Matsiz is norow+nocol.
The constants which are identical to another except for a missing
third letter (e.g. masiz) or reversed first two letters (oncol)
are one more than their neighbor, for dimensioning purposes.
Maxbnd is a number larger than the value any slack variable can take
on. It suffices to make it larger than any number in the
right-hand side vector.
Changer is a scaling factor used to prevent overflow. Some of the
constraints involve a lot of large numbers, so they are scaled
down during pivoting and scaled back up when completed. */
```

```
#include "stdio.h"
typedef char BOOLEAN;
#define value(i) dummy=ina[i]-'0'
#define TRUE 1
#define FALSE 0
#define abs(x) ((x)<0) ? -(x) : (x)
#define loop(v,s,e) for ((v) = (s); (v) <= (e); (v)++)
#define maxfield 10
#define mafield 11
#define oncraft 6
#define nocraft 5
#define nomiss 4
#define onmiss 5
#define norow 123
#define onrow 124
#define oncol 94
#define nocol 93
#define masiz 216
#define matsiz 215
#define maxbnd 9999999.0
#define changer 10000.0
```

In max c'x s.t. [A:I][x]=b, c is cost[], and redcost[] is used during pivoting for [s] changing. [A:I] is a[][]. The basic part of x is kept in act[], which is initialized to ba rhs. Plusmin[] tells whether a variable is at its upper or lower bound. Nonbas[] tells whether a variable is nonbasic or not. Currbas[] tells which variable is where in the basis. Nofield

```

is the actual number of fields used (may be < maxfield).*/

int  outs[4],c,i,count,cocol,index,outdex,miss,nofield=0,nopivot=0;
int  flag1,flag2,flag3;
float  bnd[oncol],result[oncol],cost[masiz],act[onrow],valu,amt,dummy
;
float  rhs[onrow],col[onrow],fin[onrow],obj[3],redcost[masiz];
int  plusmin[oncol],currbas[onrow],field,craft,field1=0,craft1=0,con;
int  nonbas[masiz],inbas[masiz],jrow,jcol,fake[3][7],helper,where;
char  line[38];
FILE  *fp,*sp;
BOOLEAN  yup[maxfield][oncraft],yes[onrow],uhuh[maxfield][oncraft][onmiss
];
int  dumy;
static float  a[onrow][masiz];

/*  This function takes a real number which is in string form, and
converts it to a real number.*/

convertno()
{
valu=0.0;
flag1=1;
flag2=0;
amt=10.0;
loop(c,23,32)
{
if (line[c]=='-')
{
flag2=1;
i++;
line[c]=' ';
break;
}
}
while (i<=35)
{
if (line[i]=='.')
{
flag1=0;
line[i]=' ';
}
while (line[i]==' ')
i++;
if (flag1)
{
valu*=10.0;
value(i);
valu+=dummy;
}
else
{
value(i);
valu+=dummy/amt;
}
}
}

```

```

        amt*=10.0;
    }
    i++;
}
if (flag2)
    valu=-valu;
}

```

/* The following two functions read in data from the input file ES.MPS. The file is a text file, so conversion from string to number is necessary. The file is examined to find the value of nofield, and then the data is read in. The numbers fake[][] are necessary because in different parts of the file, information is given in different orders. This procedure is broken into two functions because, as a single function, it is too large to be optimized by the processor.*/

```

getldata()
{
    fake[1][1]=1;
    fake[1][2]=6;
    fake[1][3]=4;
    fake[1][4]=5;
    fake[1][5]=2;
    fake[1][6]=3;
    fake[2][1]=1;
    fake[2][2]=6;
    fake[2][3]=3;
    fake[2][4]=4;
    fake[2][5]=5;
    fake[2][6]=2;
    loop(field,1,maxfield)
    {
        loop(craft,1,nocraft)
        {
            loop(miss,1,nomiss)
            {
                uhuh[field][craft][miss]=FALSE;
                yup[field][craft]=FALSE;
            }
        }
    }
    fp=fopen("es.mps","r");
    fgets(line,38,fp);
    while (line[1]!='L')
        fgets(line,38,fp);
    while (line[1]=='L')
    {
        fgets(line,38,fp);
        if (line[5]=='E')
            nofield++;
    }
    fgets(line,38,fp);
    cocoi=0;
    where=6*nofield+2;
    while (line[14]!='M')

```

```

{
    value(5);
    field=10*(dummy-1);
    value(6);
    field+=dummy;
    value(7);
    craft=dummy;
    value(8);
    miss=dummy;
    yup[field][craft]=TRUE;
    uhuh[field][craft][miss]=TRUE;
    i=23;
    convertno();
    cocol++;
    cost[cocol]=valu;
    fgets(line,38,fp);
}
jrow=6*nofield-1;
jcol=0;
loop(field,1,nofield)
{
    loop(craft,1,nocraft)
    {
        loop(miss,1,nomiss)
        {
            if (uhuh[field][craft][miss])
            {
                jcol++;
                if ((craft1=craft) || (field1=field))
                    jrow++;
                field1=field;
                craft1=craft;
                loop(con,1,8)
                {
                    i=23;
                    convertno();
                    if ((con==3) || (con==5))
                        valu*=(1.0/changer);
                    if (con<7)
                        a[6*(field-1)+fake[1][con]][jcol]=valu;
                    else
                        a[jrow+con-7][jcol]=valu;
                    fgets(line,38,fp);
                }
            }
        }
    }
}
jrow++;
loop(con,1,nomiss)
{
    jrow++;
    rhs[jrow]=0.0;
    loop(jcol,1,cocol)

```

```

        {
            i=23;
            convertno();
            a[jrow][jcol]=valu;
            fgets(l line,38,fp);
        }
    }
}
get2data()
{
    count=jrow;
    loop(field,0,nofield-1)
    {
        loop(con,1,6)
        {
            fgets(l line,38,fp);
            l=23;
            convertno();
            if ((con==4) || (con==6))
            {
                valu*=(1.0/changer);
                yes[6*field+fake[2][con]]=TRUE;
            }
            rhs[6*field+fake[2][con]]=valu;
        }
        loop(craft,1,nocraft)
        {
            if (yup[field+1][craft])
            {
                fgets(l line,38,fp);
                l=23;
                convertno();
                rhs[where]=valu;
                where+=2;
            }
        }
    }
    where=6*nofield+1;
    loop(field,1,nofield)
    {
        loop(craft,1,nocraft)
        {
            if (yup[field][craft])
            {
                fgets(l line,38,fp);
                l=23;
                convertno();
                rhs[where]=valu;
                where+=2;
            }
        }
    }
    fgets(l line,38,fp);
    loop(jcol,1,cocol)

```

```

    {
        fgets(line,38,fp);
        i=23;
        convertno();
        bnd[jcol]=valu;
    }
    fclose(fp);
}

/* This function initializes the various matrices and vectors.
The part of a corresponding to slack variables is set equal
to the identity matrix.*/

initialize()
{
    loop(jrow,1,count)
        a[jrow][jrow+cocol]=1.0;
    loop(jrow,1,cocol)
    {
        plusmin[jrow]=1;
        nonbas[jrow]=1;
    }
    loop(jrow,1,count)
    {
        act[jrow]=rhs[jrow];
        cost[jrow+cocol]=0;
        currbas[jrow]=cocol+jrow;
        nonbas[jrow+cocol]=0;
    }
    act[0]=0.0;
}

/* This function decides which nonbasic variable will be
operated on during this pivot */

entervar()
{
    valu=0.0;
    loop(jcol,1,count+cocol)
    {
        if (redcost[jcol]<valu)
        {
            valu=redcost[jcol];
            index=jcol;
        }
    }
}

/* This function is used in leavevar()*/

poscheck()

```

```

{
    valu=act[jrow]/col[jrow];
    if (valu<amt)
    {
        amt=valu;
        flag1=1;
        flag2=0;
        outdex=jrow;
    }
}

/* This function is used in leavevar()*/

negcheck()
{
    valu=(act[jrow]-bnd[currbas[jrow]])/col[jrow];
    if (valu<amt)
    {
        amt=valu;
        flag1=1;
        flag2=1;
        outdex=jrow;
    }
}

/* This function decides which variable, if any, will leave the
basis. If the entering variable is not a slack, than it examines
its upper bound. Then, it goes through the basis, seeing if any
of the basic variables should leave, or if, instead, the nonbasic
variable in question should merely be sent to its opposite bound.
To decide whether a variable should leave, poscheck() and
negcheck() are used.*/

leavevar()
{
    loop(1,1,count)
        col[1]=a[1][index];
    if (index<=cocol)
    {
        amt=bnd[index];
        flag1=0;
        flag2=1;
    }
    else
        amt=maxbnd;
    outdex=0;
    loop(jrow,1,count)
    {
        if (col[jrow]>0.000001)
            poscheck();
        else if ((col[jrow]<-0.000001) && (currbas[jrow]<=cocol))

```

```

        negcheck();
    }
    outs[3]=outs[2];
    outs[2]=outs[1];
    outs[1]=outs[0];
    outs[0]=outdex;
}

/* This function is used to send a variable to its opposite bound.
   The same procedure is used whether the variable in question is
   basic or nonbasic, but if it is basic, certain quantities are
   known to be zero, so it is not necessary to consider them.*/

```

bndswitch(coi j)

```

int coi j;

{
    if (nonbas[coi j])
    {
        loop(i,1,count)
        {
            act[i]-=bnd[coi j]*coi[i];
            a[i][coi j]*=-1;
        }
        redcost[coi j]*=-1;
        act[0]+=redcost[coi j]*bnd[coi j];
    }
    else
    {
        act[outdex]-=bnd[coi j];
        a[outdex][coi j]=-1;
    }
    plusmin[coi j]*=-1;
}

```

```

/* This function does the actual pivoting. It divides the row
   belonging to the leaving variable, by the corresponding entry
   in the column belonging to the entering variable. Then, it
   changes all the other rows so as to make the rest of the
   entering column all zeroes*/

```

```

dopivot()
{
    act[outdex]/=coi[outdex];
    loop(i,1,count+cocoi)
        a[outdex][i]/=coi[outdex];
    loop(i,1,count)
    {
        if (ii=outdex)
        {
            loop(jcol,1,count+cocoi)
                a[i][jcol]-=coi[i]*a[outdex][jcol];
            act[i]-=coi[i]*act[outdex];
        }
    }
}

```

```

)
act[0]-=redcost[index]*act[outdex];
amt=redcost[index];
loop(i,1,count+cocoi)
    redcost[i]-=amt*a[outdex][i];
nonbas[currbas[outdex]]=1;
currbas[outdex]=index;
nonbas[index]=0;
obj[2]=obj[1];
obj[1]=obj[0];
obj[0]=act[0];
}

/* This function decides which of the preceding two functions
needs to be used*/
pivot()
{
    if (flag1 && flag2)
    {
        jrow=currbas[outdex];
        bndswitch(jrow);
        dopivot();
    }
    else if (flag1 && (flag2-1))
        dopivot();
    else
    {
        jrow=index;
        bndswitch(jrow);
    }
}

/* This function decides whether the current solution is optimal.
it does so by checking if there are any negative reduced costs.
If there is one, it sets a flag to tell the main function to
go through another pivot*/

checkopt()
{
    flag3=0;
    loop(1,1,count+cocoi)
    {
        if (redcost[i]<0)
        {
            flag3=1;
            break;
        }
    }
}

/* This function checks whether there is degeneracy. if there is, it
makes a change in the value of a variable to end the cycling.
Because high precision is not required, it is not necessary to
be too careful about this perturbation.*/

```

```

checkdeg()
{
    if ((abs(obj[1]-obj[2])<0.0001) && (abs(obj[0]-obj[1])<0.0001))
    {
        i=1;
        flag2=1;
        while (flag2 && (i<=count))
        {
            if (act[i]<0.0001)
            {
                act[i]=0.001;
                flag2=0;
            }
            i++;
        }
    }
}

/* This function tells the program where in the basis each basic
variable is. In effect, it finds the inverse of currbas[] */

findbas()
{
    loop(i,1,count)
        inbas[currbas[i]]=i;
}

/* This function finds the values of the nonslack variable in the
optimal solution */

results()
{
    loop(jcol,1,cocol)
    {
        valu=(nonbas[jcol]) ? 0.0 : act[inbas[jcol]];
        if (plusln[jcol]-1)
        {
            valu*=-1;
            valu+=bnd[jcol];
        }
        result[jcol]=valu;
    }
}

/* This function finds the final activity levels of the constraints.
It does this by taking the original right-hand side value, and
subtracting the final value of the corresponding slack variable.
*/
final()
{
    loop(i,1,count)
    {

```

```

        if (nonbas[i+cocoi]-1)
            col[i]=rhs[i]-act[inbas[1+cocoi]];
        else
            col[i]=rhs[i];
        if (yes[i])
        {
            col[i]*=changer;
            rhs[i]*=changer;
        }
    }
}

/* This function is used by writefile() to write certain lines in
a special format.*/

writeit(colj)

int colj;

{
    if (col[colj]<1000000.0)
    {
        if (rhs[colj]<1000000.0)
            fprintf(sp,"\"          \",%11.4f,%11.4f\n",col[colj],rhs[colj]);
        else
            fprintf(sp,"\"          \",%11.4f,%11.3f\n",col[colj],rhs[colj]);
    }
    else
        fprintf(sp,"\"          \",%11.3f,%11.3f\n",col[colj],rhs[colj]);
    heiper++;
}

/* This function writes the output file TEST.DAT. Certain features
of the output file from LP83, such as variable and constraint
names and sensitivity analysis, are not used by ESCMA, and so are
not included in this file.*/

writefile()
{
    results();
    final();
    heiper=1;
    sp=fopen("test.dat","w");
    fprintf(sp,"\"ESCMA\"\n");
    fprintf(sp,"%4d,%4d,%11.4f\n",count,cocoi,obj[0]);
    i=1;
    loop(jrow,1,cocoi)
        fprintf(sp,"\"X
\",%11.4f,%11.4f\n",result[jrow],cost[jrow]);
    loop(field,1,nofield)
    {
        loop(i,1,6)
            writeit(heiper);
    }
}

```


REFERENCES

Cooper, D. and M. Clancy, Oh! Pascal, W.W.Norton & Company, Inc. (New York, 1982)

Hunt, W.J., The C Toolbox, Addison-Wesley Publishing Company, Inc. (Reading, Massachusetts; 1985)

Miller, L.H. and A.E. Quilici, Programming in C, John Wiley & Sons, Inc. (New York, 1986)

1987 USAF-UES SUMMER FACULTY RESEARCH PROGRAM/
GRADUATE STUDENT SUMMER SUPPORT PROGRAM

Sponsored by the
AIR FORCE OFFICE OF SCIENTIFIC RESEARCH

Conducted by the
Universal Energy Systems, Inc.

FINAL REPORT

Creating Aspect Graphs for Use in Object Recognition

Prepared by:	John H Stewman
Academic Rank:	Graduate Student
Department and University:	Computer Science and Engineering University of South Florida
Research Location:	RADC/COES Griffis AFB Rome, NY 13441
USAF Researcher:	Jake Sherer
Date:	8 July 87
Contract Number:	F49620-85-C-0013

Creating Aspect Graphs for Use in Object Recognition

by

John H. Stewman

ABSTRACT

This paper is concerned with the creation of aspect graphs for use as object models in a 3-D object recognition system. A method is presented which directly creates the aspect graph of a convex planar-face object from its boundary surface representation. The aspect graph created by this process is an undirected graph. Each node in the graph has attributes describing one aspect of the object and the cell of space from which that aspect can be viewed. Each arc in the graph indicates an adjacency between two aspects and is attributed with the plane separating the two associated cells. This representation is consistent with that originally proposed in [Koen79]. There are two significant differences between this approach and others of which I am aware. First, determination of the structure of the aspect graph is done in a direct manner based on the geometry of the object. The resulting aspect and cell descriptions are exact rather than approximate. Second, the cell associated with each aspect is a true 3-D volume of space rather than a surface patch on a viewing sphere.

ACKNOWLEDGEMENTS

I wish to thank the Air Force Systems Command and the Air Force Office of Scientific Research for sponsorship of this research. Universal Energy Systems was efficient and helpful, providing administrative and directional support.

At RADC/COES, Lou Hobel was most helpful in arranging for me to have a quiet workspace and access to department computer facilities. Jake Sherer kept me informed of special opportunities, such as chances to meet visiting reserchers in my field and a chance to take a short course in Natural Languages. John Crowter and Mike McHale provided invaluable assistance during my first several weeks. They helped me learn how to use the VMS operating system and helped me locate supplies and facilities.

I. INTRODUCTION

The object representations used in 3-D object recognition systems can generally be classified as either viewpoint-dependent, or viewpoint-independent [Besl85, Chin86]. A viewpoint-dependent representation maintains some representative set of 2-D projections of an object; for example, the set of views obtained from the faces of a polyhedral approximation of a unit sphere centered about the object. A viewpoint-independent representation maintains an exact model of the 3-D geometry of an object; for example, a boundary surface representation.

The aspect graph representation combines an exact 3-D model of an object with a set of generic views. Each generic view is associated with a cell of space from which it can be seen. Thus the aspect graph is, in a sense, a hybrid representation which combines the completeness of a viewpoint-independent representation with the simplicity of a viewpoint-dependent representation. As such, it is potentially a very powerful representation for use in 3-D object recognition.

I have been working with the aspect graph concept for over a year. The importance of object recognition to the field of Artificial Intelligence was, no doubt, one of the reasons I was asked to continue this research at RADC.

II. OBJECTIVES OF THE RESEARCH EFFORT

The objective of my summer research was to continue the development of a process for creating aspect graphs of objects from their boundary surface representations. I have concentrated on a simple class of objects initially, with the

hope of expanding the process to include more complicated objects at a later date.

III. The Aspect Graph Concept

The aspect graph concept was first proposed by Koenderink and van Doorn as a possible mechanism involved in human vision [Koen79]. They described a graph structure which they called the "visual potential" of an object. Each node of the graph represents a different "aspect" of the object. An aspect is a specific collection of visible faces and edges. Each aspect is associated with a cell of space from which that collection of faces and edges is visible. Nodes are connected by arcs which represent "visual events." A visual event represents a transition of an observer from one cell to another, thus changing the aspect of the object being viewed. "Thus the visual potential represents in a concise way any visual experience an observer can obtain by looking at the object when traversing any orbit through space" [Koen79]. Figure 1 illustrates the aspect graph concept for a simple object, the same one used as an example in [Koen79].

Many efforts related to object recognition have used aspect graphs or similar structures. Chakravarty and Freeman [Chack82], Castore and Crawford [Cast84, Craw85], Goad [Goad82, Goad84], Fekete and Davis [Feke84], Herbert and Kanade [Herb85], Korn and Dyer [Korn87], Callahan and Weiss [Call85], Scott [Scot84], and Kim, Jain and Volz [Kim85] are representative of the researchers working in this area. None of these teams has implemented a true aspect graph in the sense of Koenderink and van Doorn [Koen79]. Only the "characteristic view" representation [Chak82] is based on volumes of viewing space ("vantage point domains") rather

than surface areas of a viewing sphere. Most of the other approaches are based on quasi-uniform tessellation of a viewing sphere [Cast84, Goad84, Feke84, Herb85, Korn87]. A few researchers have discussed, but, apparently, have not implemented, representations based on partitioning a viewing sphere according to singularities in the visual mapping [Scot84, Call85].

The importance of using a representation based on volumes of viewing space is illustrated in a simple way by the aspect graph in Figure 2. One of the nodes of this aspect graph has an associated viewing cell with finite extent. A viewing sphere of a given radius can have an area corresponding to the finite cell or an area corresponding to the infinite cell above it, but not both. Thus, a representation based on volumes of viewing space is clearly more complete and general.

IV. Aspect Graphs for Convex Planar-Face Objects

My algorithm for aspect graph creation operates in five stages. The first stage uses the definitions of the planar faces of the object to create a "parcellation graph" which completely describes the parcellation of space surrounding the object into viewing cells. The second stage uses the parcellation graph to create an "evaluation matrix." The evaluation matrix contains values which describe the relationship of each point of intersection in the parcellation to all of the planes which contain faces of the object. The third stage uses the evaluation matrix to construct identification numbers for plausible aspect graph nodes and identify points on the boundary of the cell corresponding to each node. The fourth stage extracts each cell boundary description from the parcellation graph and

prunes it of redundant or "dangling" boundary features. Also, during this stage, plausible cells that do not actually enclose a volume of viewing space are eliminated. The last stage generates an explicit aspect graph structure.

V. Boundary Surface Description

The input assumed by the algorithm is a standard boundary surface representation of a convex planar-face object. The boundary is specified by a collection of faces, each face is specified by a planar polygon, and each polygon is specified by an ordered list of its vertices. The vertices around the edge of a face are specified in counter-clockwise order as seen from outside the object. This allows easy calculation of an outward-directed normal. The origin of the model coordinate system is assumed to lie inside the model. This allows easy and unambiguous reference to the "inside" and "outside" of each plane which contains a face of the object. The boundary surface description of the example object in Figure 2 is depicted in Figure 3.

VI. Parcellation Graph

The creation of the parcellation graph is done in two steps. Across the top level of the parcellation graph is a node for each plane which contains a face of the object. I will refer to these planes as the bounding planes of the object. The first step is to test all pairs of these planes for lines of intersection. The equations for two planes which intersect are linked to the equation for their line of intersection. Thus, across the middle level of the parcellation graph is a node for every line of intersection between planes at the top level. The second step is to test all pairs of lines found in the first step for points of

intersection. The equations for intersecting lines are linked to the coordinates for their point of intersection. A node for each point of intersection appears across the bottom level of the parcellation graph. The linked set of plane equations, line equations, and point coordinates constitutes the parcellation graph. The parcellation graph for our example object appears in Figure 4.

Note that the parcellation graph of an object contains all of the lines and points resulting from intersections of the planes which bound the object. The points and lines that are part of the object boundary are generally only a subset of those contained in the parcellation graph. The parcellation graph contains additional points and lines whenever there is a viewing cell which has finite extent.

VII. Evaluation Matrix (Identifying Plausible Cells)

Nodes of an aspect graph, and so their corresponding cells of space, are identified using N -bit numbers. Each bit corresponds to one of the N bounding planes of the object. A bit value of 1 indicates that the interior of the viewing cell lies to the outside of the corresponding plane, and a value of 0 indicates that the interior of the cell lies to the inside of the corresponding plane. This numbering scheme allows for the specification of any of the 2^N possible combinations of relationships to the N planes. Note, however, that for a given set of N planes, fixed in 3-D space, there will always be less than 2^N real cells. The numbering system would allow for such an object, but it cannot actually be realized. It is impossible, for example, to conceive of a cell simultaneously outside of all of the N planes bounding an object (i.e., one from which all faces of the object could be viewed). The first task, then, is to

determine which of the 2^N different kinds of cells really exist for a given object. Once it is known which cells exist, the explicit structure of the aspect graph can be determined.

A cell identification number specifying a set of relationships to the N planes bounding the object is considered valid if at least one point, lying in the interior of the cell, satisfies the specified relationships. In other words, a valid cell actually exists (i.e., actually encloses some volume of the viewing space).

All cells, even those of infinite extent, have at least one of the points listed in the bottom level of the parcellation graph as a part of their cell boundary. In essence, this means that every cell must have at least one corner. Since the parcellation graph summarizes the complete parcellation of space about the object, it contains all of the cell boundary corner points.

In order for this set of test points to be used for cell validation, each cell boundary has to be treated, in essence, as part of its interior. Now a value of 1 in a bit of the cell identification number will mean that cell points lie to the outside of, or on, the corresponding plane. Likewise, a value of 0 will mean that the cell points lie to the inside of, or on, the corresponding plane. Using these "relaxed" relationships it is possible to identify plausible cell identification numbers using the N planes bounding the object and the set of points from the bottom level of the parcellation graph. We define a "plausible" cell as one which has at least one point from the parcellation graph on its cell boundary.

Two related problems result from this approach. The first is that plausible cells may be identified in this stage of the process which do not correspond to valid cells. The difference is that valid cells must enclose some actual volume of viewing space. The only requirement for a cell to be plausible is that it have some identifiable boundary. If the boundary encloses nothing, then the plausible cell is actually invalid. The second problem is that cell boundaries having redundant or "dangling" pieces may result, even for those cells that are truly valid. The solutions to both problems are related and will be addressed in the next section of this paper.

The evaluation matrix is created to allow more efficient determination of plausible cell identification numbers. It has one column for each plane listed across the top level of the parcellation graph and one row for each point listed across the bottom level. The value of each entry in the evaluation matrix is determined by solving the plane equation indicated by the column with the point coordinates indicated by the row. The resulting value will be negative if the point lies to the "inside" of the plane, zero if the point lies on the plane, or positive if the point lies to the "outside" of the plane. Thus the evaluation matrix indicates the relationship of each point in the parcellation to each of the planes. The evaluation matrix for our example object appears in Figure 5.

The evaluation matrix is recursively examined to construct plausible node identification numbers. At each stage, the procedure takes a set of rows of the evaluation matrix as its input, examines a column of the matrix to split the input into two possibly overlapping subsets, and then recursively processes each subset. The algorithm continues

until all columns have been processed, at which point all plausible node identification numbers have been enumerated.

Specifically, at the first stage of the recursive algorithm, the input is the set of all rows in the evaluation matrix. Rows with a non-negative entry in the first column are grouped together as indicating plausible cell identification numbers with a 1 in the first bit position. All such cell identification numbers indicate cells located to the outside of the plane corresponding to the first bit position. Similarly, rows with a non-positive entry in the first column are grouped together as indicating plausible cell identification numbers with a 0 in the first bit position. All cell identification numbers of this kind indicate cells located to the inside of the plane corresponding to the first bit position. This same procedure is applied recursively to each of the two subsets of rows in the evaluation matrix, splitting each subset based on the values in the second column of each row. The recursive calls continue, similarly, to a maximum depth of N calls. During any call, one of the subsets created by the splitting process may be empty. This indicates that no plausible cell identification number has the previously established pattern of bit values along with the particular value in the bit position being examined. When an Nth level call is made, those row subsets that survive the last split indicate boundary points of plausible cells. The cell identification numbers are formed by concatenating the bit values used to split the row subsets at each level of the recursive process. The pattern of the processing of the evaluation matrix for our example object is illustrated in Figure 6.

As a result of processing the evaluation matrix, a list of plausible cell (node) identification numbers is obtained. A

set of rows survive the N-stage splitting process for each plausible identification number. The points corresponding to the rows of such a set can be used to locate a subgraph of the parcellation graph which defines the cell's boundary. This is accomplished by identifying the subgraph comprised of all points indicated by the row indicators, all lines linked to those points, and all planes linked to those lines.

VIII. Pruning Invalid Cell Boundaries

At this point, for a certain class of objects (including the example object), the algorithm has effectively identified the nodes of the aspect graph, along with the points, lines, and vertices defining the boundary of each node's viewing cell. This, however, is not the case for any arbitrarily formed convex planar-face object.

Since cell boundaries are treated as part of cell interiors, each corner point has to be considered as a validating part of every potential cell which could have that point on its boundary. The result is that there will be 2^M plausible cells identified for every point in the parcellation having M planes passing through it.

Figure 7 depicts an example object for which the processing of the evaluation matrix identifies, as plausible, two invalid cells in addition to the set of valid cells. The top point of this four-sided pyramid represents the intersection of four planes. The evaluation matrix processing identifies sixteen plausible cells of space as having this point on their boundary. However, only fourteen of these are valid cells.

Whenever there are overdetermined points on the boundary of a cell (i.e., those with more than 3 planes passing through them), there also exists a problem with redundant or dangling lines and planes being identified as parts of its cell boundary. There is no need to include these "extra" boundary features in a node's cell boundary attribute, so it is highly desirable to prune them from the subgraph that initially describes the cell boundary. The solution to this problem, fortunately, also helps us to eliminate invalid cells from the set of plausible cells.

Invalid cells are degenerate in the sense that they do not enclose a volume of space which satisfies the relationships specified by their plausible cell identification number. Another way of saying this is that they can be viewed as cells that have boundaries completely comprised of dangling lines and planes. Thus, a process for eliminating dangling lines and planes will also reduce the boundaries of invalid cells sufficiently for them to be identified and discarded.

The elimination of invalid cells and dangling lines proceeds as follows. For each plausible node identification number, extract a copy of the subgraph of the parcellation graph located by the points associated with the identification number. For each overdetermined point in this subgraph, check each of the lines linked to it to see if the line dangles. A dangling line touches the cell boundary at only one point. This check is performed by testing two points, each of which lies a small distance away from the point in the parcellation graph, but in opposite directions along the line. If neither new point satisfies the relaxed planar relationships specified by the cell identification number, then the line touches the cell boundary at only one point. In this case, the line dangles, so the line and its links to

planes above it can be pruned away. When a plane has less than two lines linked to it, then it touches the cell boundary along only one edge. In this case, the plane dangles, and can be pruned away. When all overdetermined points have been checked, either the subgraph has less than three planes left, indicating an invalid cell, or the subgraph represents the exact boundary of a valid cell.

IX. Creation of an Explicit Aspect Graph Structure

Creation of an explicit graph structure is now a relatively simple task. The following steps are performed for each valid identification number.

First, allocate a node and attribute it with the identification number and the cell boundary description. The identification number is a link to the definitions of the visible faces. The positions of the 1 values in the identification number indicate the object faces which are visible as part of the aspect associated with the node. The cell boundary description was determined explicitly in the preceding process.

Next, two nodes are considered to be adjacent if their identification numbers differ in only a single bit position, so, for each node, individually invert each bit of its identification number, and check to see if this results in some other valid identification number. If it does, then create a link between the two nodes to indicate their adjacency in the aspect graph. The link is attributed by the bit position in which the two identification numbers differ, representing the plane crossed in moving from one cell to the other.

X. RECOMMENDATIONS

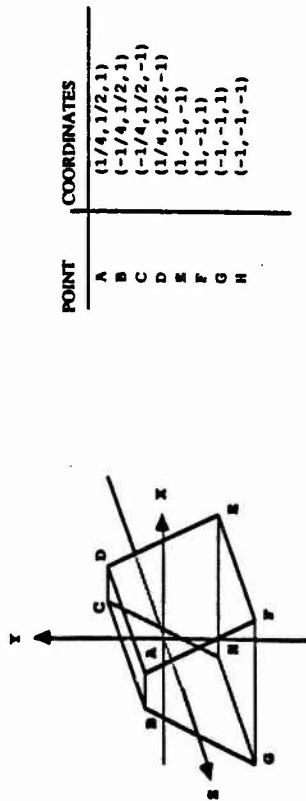
I have presented a method for creating the aspect graph of a convex planar-face object from its boundary surface description. The process is accomplished in five stages and involves the creation and use of two major data structures. The parcellation graph describes the complete parcellation of the viewing space about the specified object and includes, as subgraphs, the boundary descriptions of all individual cells. The evaluation matrix is useful in identifying plausible cells. The cell boundary of every plausible cell is extracted from the parcellation graph and is pruned of dangling line and planes. Cells that are found to have boundaries actually enclosing some volume of the viewing space, along with their associated aspects, become attributes of the nodes of the aspect graph. The fact that aspect graphs can be produced for this limited class of objects is encouraging, but much more work is needed before aspect graphs of reasonably complex objects can be created.

I plan to continue this research effort by (1) implementing an object modeling system which uses this aspect graph creation algorithm, (2) investigating upper and lower bounds on the node complexity of aspect graphs, (3) developing and implementing algorithms for determining the "equivalent" nodes of an aspect graph, (4) developing a method of attaching relative probabilities to the nodes of an aspect graph (using the ideas of [Kend87]), and (5) extending this aspect graph creation algorithm to handle non-convex objects.

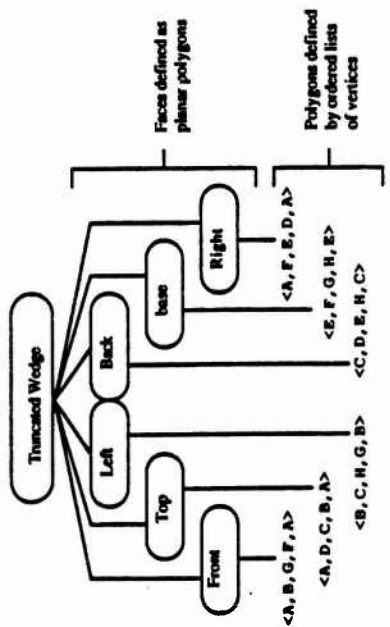
REFERENCES

- Besl85 Besl, P.J. and Jain, R.C. Three-Dimensional Object Recognition, ACM Computing Surveys, 17(1), 75-145, (March 1985).
- Call85 Callahan, J. and Weiss, R. A Model for Describing Surface Shape, IEEE International Conference on Computer Vision and Pattern Recognition, 240-245, (1985).
- Cast84 Castore, G. and Crawford, C.G. From Solid Model to Robot Vision, IEEE International Conference on Robotics, 90-92, (1984).
- Chak79 Chakravarty, I. A Generalized Line and Junction Labelling Scheme With Applications to Scene Analysis, IEEE Trans. PAMI 1 (2), 202-205, (April, 1979).
- Chak82 Chakravarty, I. and Freeman, H. Characteristic Views As a Basis of Three-Dimensional Object Recognition, SPIE Volume 36: Robot Vision, 37-45, (1982).
- Chin86 Chin, R.T, and Dyer, C.R. Model-Based Recognition in Robot Vision, ACM Computing Surveys 18 (1), 67-108, (March, 1986).
- Craw85 Crawford, C.G. Aspect Graphs and Robot Vision, IEEE International Conference on Computer Vision and Pattern Recognition, 382-384, (1985).
- Fek84 Fekete, G. and Davis, L.S. Property Spheres: A New Representation for 3-D Object Recognition, IEEE Workshop on Computer Vision: Representation and Control, 192-201, (1984).
- Goad82 Goad, C. Automatic Construction of Special Purpose Programs for Hidden Surface Elimination, Computer Graphics 16 (3), 167-178 (July, 1982).
- Goad84 Goad, C. Special Purpose Automatic Programming for 3-D Model-Based Vision, 1983 ARPA Image Understanding Workshop, 94-104, (1984).
- Herb85 Herbert, M. and Kanade, T. The 3D-Profile Method for Object Recognition, IEEE International Conference on Computer Vision and Pattern Recognition, 458-463 (1985).

- Kend87 Kender, J.R. and Freudenstein, D.G. What Is A "Degenerate" View?, ARPA 1985 Image Understanding Workshop, 589-598, (1987).
- Kim85 Kim, H., Jain, R.C., and Volz, R.A. Object Recognition Using Multiple Views, IEEE International Conference on Computer Vision and Pattern Recognition, 28-33, (1985).
- Koen79 Koenderink, J.J and van Doorn, A.J. The Internal Representation of Solid Shape with Respect to Vision, Biological Cybernetics 32, 211-216, (1979).
- Korn87 Korn, M.R. and Dyer, C.R. 3-D Multiview Object Representations for Model-Based Object Recognition, Pattern Recognition 20 (1), 91-103, (1987).
- Scot84 Scott, R. Graphics and Prediction from Models, 1984 ARPA Image Understanding Workshop, SAIC-84/1726, 98-106, (1984).



(a) Truncated wedge and coordinates of its corner points



(b) Faces and Points used in Object Definition

Figure 3 -- Boundary Surface Description for a Truncated Wedge

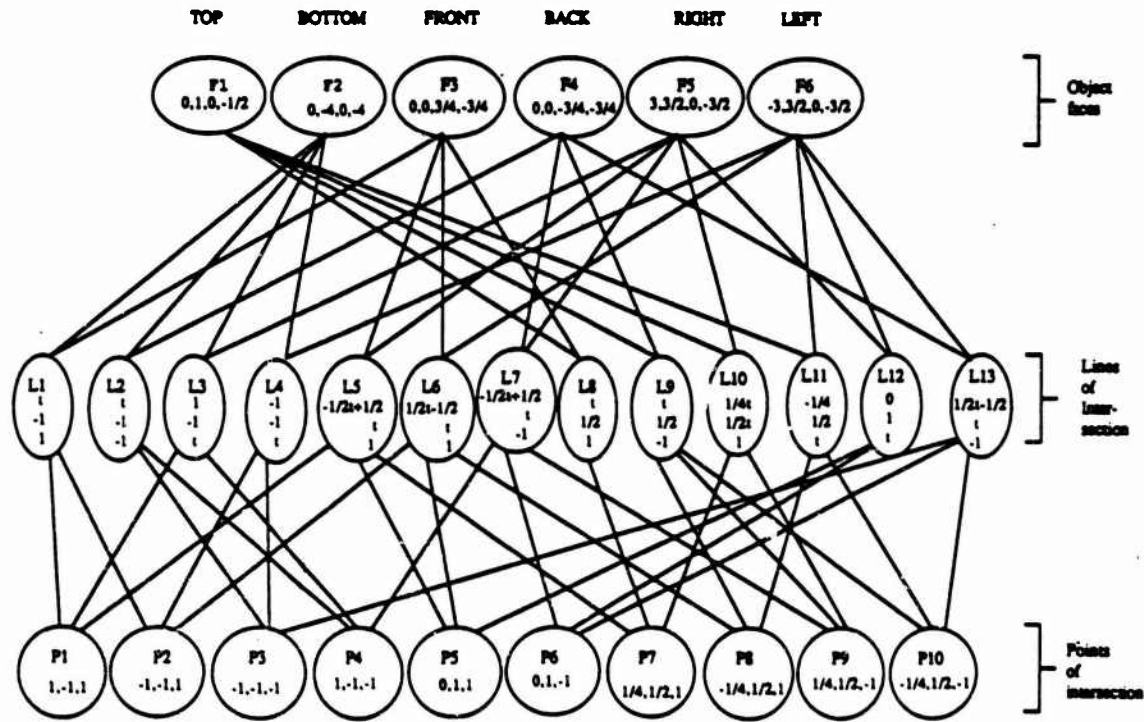
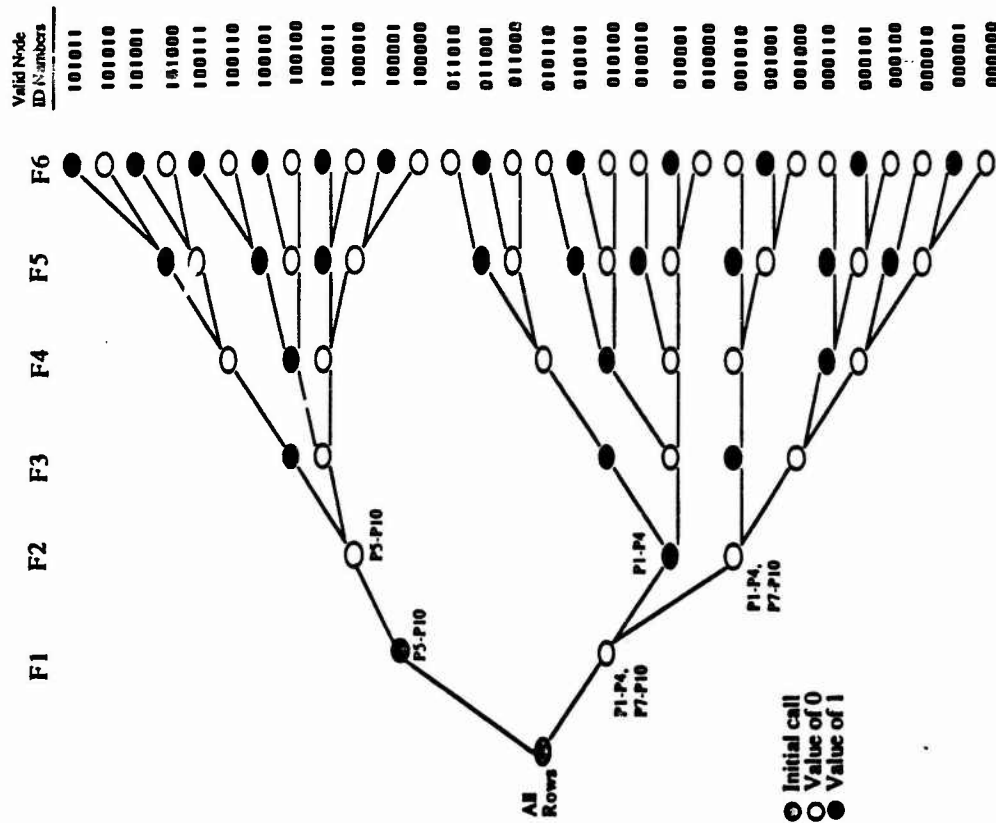


Figure 4 -- Parcellation Graph for the Wedge in Fig.3.

Planes Listed Across Top Level of Parcelation Graph

	P1	P2	P3	P4	P5	P6
P1	-1.5	0	0	-1.5	0	-6
P2	-1.5	0	0	-1.5	-6	0
P3	-1.5	0	-1.5	0	-6	0
P4	-1.5	0	-1.5	0	0	-6
P5	0.5	-6	0	-1.5	0	0
P6	0.5	-6	-1.5	0	0	0
P7	0	-6	0	-1.5	0	-1.5
P8	0	-6	0	-1.5	-1.5	0
P9	0	-6	-1.5	0	0	-1.5
P10	0	-6	-1.5	0	-1.5	0

Points Listed Across Bottom Level of Parcelation Graph



Valid Node ID Numbers

- 101011
- 101010
- 101001
- 101000
- 100111
- 100110
- 100101
- 100100
- 100011
- 100010
- 100001
- 100000
- 011010
- 011001
- 011000
- 010110
- 010101
- 010100
- 010010
- 010001
- 010000
- 001010
- 001001
- 001000
- 000110
- 000101
- 000100
- 000010
- 000001
- 000000

Figure 5 -- Evaluation Matrix for the Wedge in Fig.3.

Figure 6 -- Construction of Plausible Cell Identification Numbers

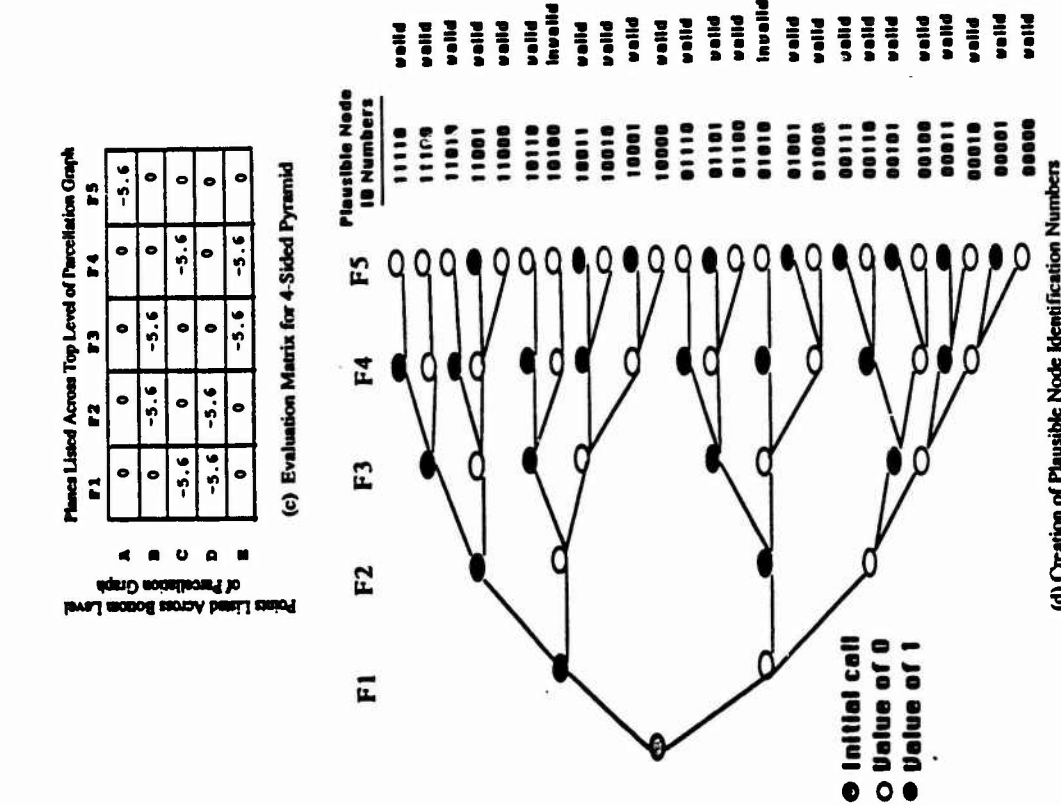


Figure 7 -- Example of an Object for which Plausible Cells are not all Valid Cells

1985 USAF-UES SUMMER FACULTY RESEARCH PROGRAM/
GRADUATE STUDENT SUMMER SUPPORT PROGRAM

Sponsored by the
AIR FORCE OFFICE OF SCIENTIFIC RESEARCH

Conducted by the
UNIVERSAL ENERGY SYSTEMS, INC.

FINAL REPORT

Analysis of Emission Features in IRAS LRS Spectra

Prepared by: Tod Strohmayr
Academic rank: Master of arts
Department and Physics and Astronomy
University: University of Rochester
Research Location: Air Force Geophysics Laboratory
 Optical Physics Division
 Infrared Branch
USAF Researcher: Stephan Price
Date: August 4, 1987
Contract Number: F4962-85-C-00

Analysis of Emission Features in IRAS LRS Spectra

by

Tod Strohmayer

ABSTRACT

I have done a study of IRAS low resolution spectra (LRS) of variable M stars. Specifically I have looked at the 1n class of LRS spectra in order to study the various types of emission features seen in these spectra. Although classified by the IRAS science team as "featureless" spectra I find that approximately 30% of the spectra have emission features in the 9 to 15 micron region. The average excess emission above the local continuum is about 7% and ranges from as low as 2% to as high as 20%. Emission due to silicates at about 10 and 18 microns is seen as well as emission due to silicon carbide at 11.6 microns. A large number of objects show a broad feature between 9 and 15 microns usually centered between 11 and 12 microns. It is not clear yet whether the feature is due to carbon rich or oxygen rich dust, and may possibly be evidence for evolution from spectral type M to C.

In order to facilitate this study I have written and modified computer programs which allow the user to graphically analyze the LRS data. I have implemented programming that allows the user to fit the local continuum using two models. The first allows the user to co-add 2 blackbody distributions, each normalized to a different region of the spectrum, to obtain the continuum. The second employs a simple dust shell model to estimate the continuum. Another program calculates color corrections to the IRAS broad band fluxes.

ACKNOWLEDGMENTS

I wish to express my appreciation to Irene Little-Marenin, my advisor for this 10 week research effort, without whom I would not have had this opportunity. I would also like to acknowledge the work of Len Marcotte, of AFGL, who initial set up the data files containing the LRS spectra. The availability of these files made it possible for me to concentrate on the actual analysis of data rather than the details of data management. I also acknowledge the work of Charles Wilton, University of Wyoming, who began this work along with Irene Little-Marenin a few years ago. Some of the programs I developed were modifications to some already existing code written by Mr. Wilton.

Perhaps most importantly I wish to express my appreciation to the Air Force Systems Command and the Air Force Office of Scientific Research, and specifically to the people of the Air Force Geophysics Laboratory, notably the people of the Optical Physics Division/Infrared Branch and its director Stephan Price, as well as Paul Levan. Without them I would not have had the opportunity to conduct this research.

I. INTRODUCTION

The Infrared Astronomical Satellite (IRAS) conducted an all sky survey in the infrared region of the spectrum. The satellite obtained both photometric and spectroscopic data. The spectroscopic data consists of approximately 5000 low resolution spectra of point sources having fluxes greater than 10 Jy at 12 and 25 microns. The spectra were measured from 7.7 to 22.6 microns, and overlap in the region from 11 to 13.4 microns. Many of the spectra show emission features due to circumstellar dust shells and are therefore ideally suited to the study of evolved M stars.

Currently at AFGL we have roughly 1200 LRS spectra of stars which are catalogued in the General Catalog of Variable Stars (GCVS). This large amount of data affords us an excellent opportunity to study the structure and composition of circumstellar dust shells, as variability in the visible is often a result of absorption by dust around the star, which then gives rise to infrared excess.

II. OBJECTIVES

My major objectives during this 10 week research effort have been, the development of new software to allow graphic analysis of the LRS spectra, the development of a program to compute color corrections to the IRAS broad band fluxes, and the use of the software to make a preliminary study of the 1n class of LRS spectra. The programs written during the course of this 10 week research effort are meant to assist the research of Dr. Irene Little-Marenin. This research is concerned with the study of long period variables, such as Mira stars, in an attempt to understand better the evolution of these stars. Of principal interest is

the evolution from spectral class M to class S and possibly to carbon stars, as this process is not well understood at present.

III. SOFTWARE DEVELOPMENT:

In order to accurately measure emission profiles from the LRS spectra it is important to reliably obtain a fit to the continuum emission from a given source. When analyzing the spectra of stars with circumstellar dust a principal source of continuum emission is the stellar photosphere. In many LRS spectra a single temperature thermal distribution fits the continuum accurately. However in many spectra this is not the case, and generally the failure is to underestimate the emission in the 7.7 to 9 micron region. This effect is almost certainly due to photospheric emission in sources whose dust shells are optically thin at these wavelengths. Therefore the next step toward improving the estimate of the continuum was to create a simple two temperature model to fit the continuum.

Two programs were developed to do the task discussed above. The first, designated MAXADD (in honor of Mr. Planck), allows the user to match two thermal distributions at different wavelength positions on the LRS spectra. The two distributions are then co-added and the sum matched to a designated position on the LRS spectrum. Typically this allows the user to fit the shorter wavelength photospheric emission as well as the cooler dust contribution. The other program, designated MODSHEL, is a bit more sophisticated and employs a simple dust shell model to fit the continuum. The model employs three parameters, the stellar effective temperature or 'core' temperature, the dust shell temperature, and the ratio of the stellar radius to the dust shell radius. The star and its dust shell are assumed to be optically thick thermal emitters, the emission is then simply calculated using equation 1, and the distribution is matched to

$$S_{\lambda} = B_{\lambda}(T_s) + r^2 B_{\lambda}(T_d)$$

E 0 1

a designated wavelength of the LRS spectrum. This simple model serves to fit the majority of spectra that I have analyzed remarkably well. In fact according to N. Epchtein (Valinhos-ESO survey) this model fits the near and far infrared emission of most objects reliably.

It is clear that the emission from a dust shell can be modelled reliably by a spherical shell model that integrates the transfer equation through the shell, see Rowan-Robinson (1982,1983). It is also clear that the relatively simple two temperature model allows a good approximation over this wavelength range to the formidable task of integrating the equation of transfer through a spherical shell. The model therefore allows a simple, reliable means to obtain the continuum emission.

The programs developed plot the observed LRS spectrum, the model spectrum, and the excess emission (observed-continuum). The programs also calculates the excess emission ratio with respect to the local continuum, and allow the user to compare flux values and obtain flux ratios at specific wavelegths. Fig. 1 shows a comparison between the fit obtained using each model on two different sources.

Another program developed that employs the 3 parameter shell model is MODNORM. This program allows the user to plot normalized emission profiles. The program also allows the normalized spectra to be over-plotted to test for uniformity among certain features and to obtain averages of many emission profiles. Fig. 3 and Fig. 4 contain spectra obtained with MODNORM.

IV. COLOR CORRECTION PROGRAM:

The IRAS satellite obtained an enormous amount of photometric data. The data is in the form of broad-band fluxes measured at 12, 25, 60, and

100 microns. The detectors aboard the space craft, and the optics as well, have different sensitivities as a function of wavelength. These factors conspire to produce a system responsivity that varies over the wavelength band of interest. The survey fluxes are calculated assuming that the input energy distribution is constant in the flux per logarithmic frequency interval. The upshot is that the quoted survey fluxes must be color corrected according to the actual energy distribution of the source. Given an energy distribution over the wavelength band in question the color correction coefficient can be uniquely determined. The goal then is to determine the actual energy distribution of the object in the band of interest.

The program developed uses the quoted IRAS fluxes to calculate a color temperature for the bands of interest. The color temperature then defines an energy distribution of the source in that band, and uniquely determines the color correction coefficient. The program uses the coefficients calculated for blackbody distributions from the IRAS explanatory catalog. The program will calculate the corresponding color temperature for any of the six possible flux ratios, and give the corrected flux.

V. A SURVEY OF \ln LRS SPECTRA:

The LRS spectra obtained by IRAS have been broken up into 10 different classifications. The various groupings depend on the presence or absence of certain spectral features, such as 10 micron silicate emission. The \ln classification denotes spectra that are 'featureless', meaning they show no emission features. The numeral 'n' is equal to twice the absolute value of the spectral index between 8 and 13 microns. Thus normal K stars show only photospheric emission and have 'n' equal to 8. Another class

that I examined are the 2n class of spectra. These spectra show 10 micron silicate emission. The 21 and 22 groups were examined in order to make comparisons with the 1n sample, as the 21 and 22 groups show the weakest 10 micron features. As mentioned previously we currently have a database of approximately 1200 spectra of variable M stars. Of this group a sample of about 500 1n spectra were examined. The sample includes stars of spectral types M, S, and C. The variability types include Mira variables, semi-regular variables and irregular variables.

Each spectrum in the sample was examined and a best fit to the continuum established. This was done using the two programs described previously, as well as a third program which fits a single planck function to the LRS spectrum. Many of the 1n spectra have a rather low signal to noise ratio, therefore each spectrum had to pass a visual inspection if it was to be classified as showing an emission feature. Having carried out this procedure the spectra revealing emission features were classified into 3 types of 10 micron excesses. Table 1 gives a numerical breakdown of the sample (note: where the totals in a given column do not add up the missing spectra were those showing carbon star features).

The three types of excesses seen in the sample were categorized according to the flux ratios at three wavelengths, 10, 11.2, and 13 microns. The reasoning behind this stems from the fact that many of the 21 and 22 LRS spectra show a prominent 3 component feature with the components peaking around 10, 11, and 13 micron. This would allow us to determine whether the features are identical in the two groups, or if they had different carriers. Type 1 spectra are those spectra with a flux ratio at 10 and 11 microns (ie 10/11) greater than 1, but with a 13/10 ratio of

less than .2. Type 2 spectra have a 10/11 ratio again close to 1, but the 13/10 ratio is between .2 and .7. Finally the type 3 spectra have a 10/11 ratio less than 1, and a 13/10 ratio greater than .7. There does not seem to be a strict separation between the three types rather the values of the flux ratios are roughly continuous through the sample. Fig. 2 shows typical examples of type 1 and type 2 excesses, and Fig. 3c shows three examples of the type 3 feature. The 21 and 22 LRS spectra also show the same types of features, but the type 3 feature appears only in a few sources, and this may be due to the somewhat arbitrary cutoff between spectra of type 2 and 3. Fig. 3a,b show examples of the type 2 and type 1 spectra in the 21 and 22 LRS sample.

We also observe other emission features in the 1n sample. A dozen sources show 11.5 micron emission due to silicon carbide, as well as a feature at about 8.7 microns which is well known in C stars. All of these sources are catalogued as carbon stars. Also of interest is a narrow feature observed at about 8 microns. This feature is presumably due to molecular SiO, but its existence could be questioned due to detector edge effects. The excess emission above the local continuum ranges from as low as 2% to as high as 13% in this feature. Fig. 3d shows several examples of sources with the carbon star features at 8.7, and 11.6 microns.

VI. THE 1n SURVEY: DISCUSSION

The standard signature of oxygen rich dust is the 10 and 18 micron emission feature. The sources with spectra of type 1 would appear to be of this type. The Spectra of type 2 and 3 would appear to be another matter however. One hypothesis put forward by M. S. Vardya (1986) is that the features are due to structurally and compositionally different forms of

silicates. It is not yet possible to verify this hypothesis with existing laboratory data. Vardya's conclusions are based on several assumptions, one of which being that there is a cutoff in spectra which show 10 micron silicate emission according to the fractional rise time (light curve asymmetry, 'f' factor) of the variable star in question. In order to test this assumption I have plotted the fractional rise time versus the excess emission ratio between 9 and 11 microns for 53 long period variables in the sample for which 'f' values were available. The data is presented in Fig. 7a. The claim made by Vardya is that stars with 'f' values greater than .43 show little or no 10 micron silicate emission. A look at the graph would seem to indicate that there is a tendency for variables with higher 'f' values to have a weaker excess emission but a distinct cutoff is not immediately evident. The importance of this cutoff value in 'f' is related to the belief that the strength of the shock wave which drives the stellar outflow is related to the 'f' value. If this is correct the cutoff in 'f' for 10 micron emission essentially reflects a temperature difference which allows different species of silicate dust to condense out of the flow at different values of 'f'. Variables with 'f' greater than the cutoff allow the type 3 component to condense out, but not the type 1 component. Although this process would explain the appearance of the feature, at present it is still speculative and more data is needed to verify the hypothesis.

A further aspect of the survey was to examine S star spectra to see if there are any distinctive features between 8 and 23 microns which could be used to easily identify these spectral types. Of the S stars in The sample most show excesses of type 2 and 3 but there does seem to be a tendency for the peak normally seen at about 10 microns to be shifted

toward slightly longer wavelengths. Fig. 5c shows a plot of the average spectrum for the highest signal to noise S star spectra. When compared with the type 2 excess average feature the shift is just noticeable. A possible explanation is that we are beginning to see a contribution from carbon rich dust in these stars. In fact by taking 'standard' silicate and SiC features and co-adding them in various percentages one can produce much of the structure of the S star feature (Little-Marenin, Emission features in IRAS LRS spectra of MS, S and SC stars).

Vardya (1986) reported the detection of the 8 micron line of molecular SiO in Mira variables. We observe the line in many of the In spectra, and give an average profile of the line from some of the strongest sources (see Fig. 5b). The excess emission over the local continuum ranges from as low as 2% to as high as 13%. The average peak falls just longward of 8 microns, and gives strong support to the identification of this feature with SiO.

The most interesting feature remains the type 3 excess seen in many of the In spectra. No identification of the carrier has yet to be made, but speculation is always possible. A soon to be published study by R. Papoular (1987) and associates reports on a statistical analysis of the In LRS sample. They produce an average feature with their technique almost identical to the type 3 excess that I have generated. The French group claims that the feature is due to SiC. Although the peak emission is at about 11.5 microns, about right for SiC, the overall feature shape is quite different from the SiC feature observed in carbon star spectra. The feature also seems to resemble the type 2 excess in shape more than the SiC feature seen in carbon stars. There seems to be evidence for an identification both with oxygen rich and carbon rich material. I have plotted the flux ratios at 10

and 11.2 microns versus the flux ratios at 13 and 10 microns for 86 of the brightest sources in the sample, this includes excesses of all types. The results are plotted in Fig. 7b. There is definitely a correlation between the ratios. Whether this correlation is significant is not known at this time, and more study is necessary.

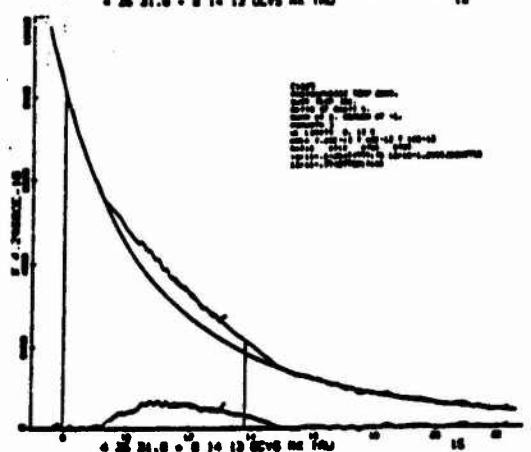
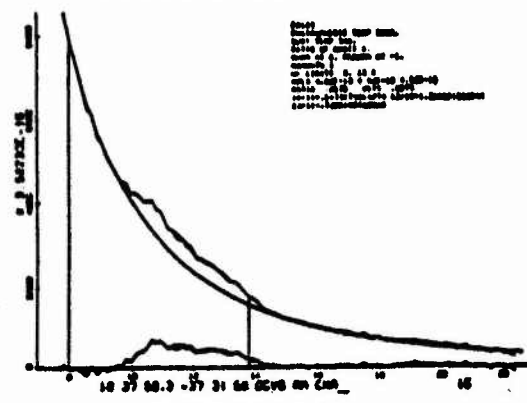
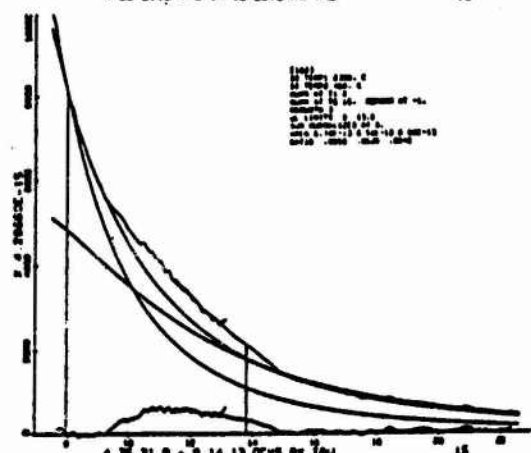
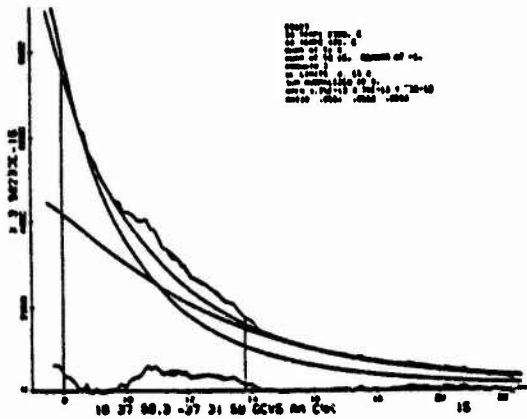
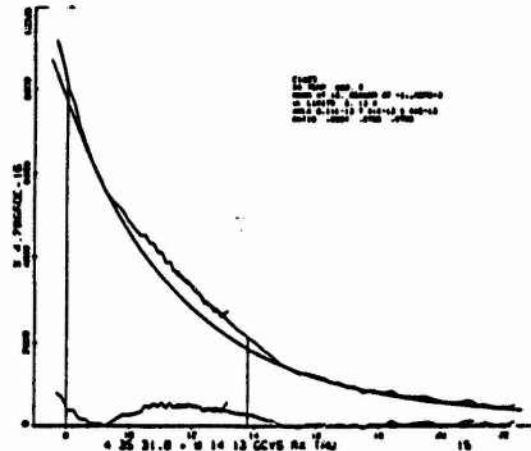
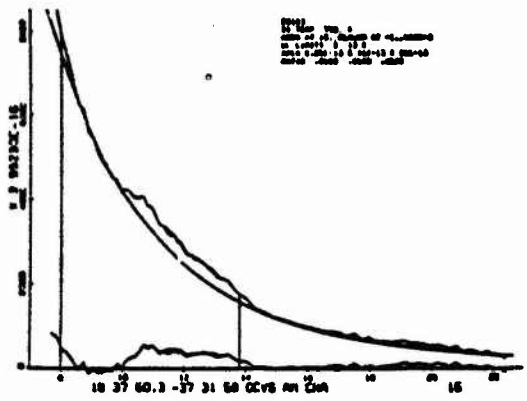
VII. RECOMMENDATIONS:

There is still work to be done in modelling the continuum emission in these types of sources. Perhaps the next sophistication to be made is the development of a program to actually integrate the transfer equation through a spherical shell. This would be a substantial task, but nevertheless it would be worthwhile. Perhaps a less intensive approach could be taken to modify the simple model used up till now by including effects such as varying the optical depth, and including grain properties. This could most likely be done with much less pain than a full-blown radiative transfer treatment. With the main aim of present research being the study of emission features it is important to have a good estimate of the continuum, but it should be noted that to a large extent the shapes of features are fairly constant as long as the continuum is estimated reasonably. This insight is possible given the number of spectra that have been examined in this manner.

Continued work with the LRS database is needed, as well as new data, to unravel the nature of the features seen in these spectra. Of keen interest would be the continued study of MS, SC, and C stars in order to get a better knowledge of the stellar evolutionary processes involved.

References

1. Vardya, M. S., de Jong, T., and Willems, F. J., 'IRAS Low Resolution Spectrograph Observation of Silicate and Molecular SiO Emission in Mira Variables. *Astrophysical Journal*, 304:L29-L32, 1986 May 1.
2. Little-Marenin, I. R., and Wilton, C., 'An analysis of IRAS low dispersion spectra of carbon and M stars,' Proc. of the Fourth Cambridge Workshop on Late-type Stars, Stellar Systems and the Sun, Santa Fe, New Mexico. 10/15/86.
3. Epchtein, N., etal 'Valinhos-ESO Survey,' A. J. 1987, to be published
4. Rowan-Robinson, M., and Harris, S., 'Radiative Transfer in dust clouds-II, Circumstellar dust shells around early M giants and supergiants,' *MNRAS*. 200, 197, 1982.
5. Baron, Y., de Muizon, M., Papoular, R., Pegourie, B., 'An analysis of the emission feataurew of the IRAS Low Resolution Spectra of C-stars,' *Astronomy and Astrophysics*, Dec. 1986.
6. Beichman, C. A., and the Joint IRAS Science Working Group (JISWG). 'IRAS Catalogs and Atlases Explanatory Supplement,' and 'Atlas of Low Resolution Spectra.'
7. Willems, F. J., 'Infrared Studies of Asymptotic Giant Branch Stars,' 1987, Doctoral Thesis.
8. Kukarin, B. V., etal, 'General Catalog of Variable Stars,' 3rd edition 1969, Astronomical Council of the Academy of Sciences in the USSR.



Wave length in microns

Fig. 1 Sample plots of two different sources using the three continuum fitting routines used in the survey. From top to bottom the plots are from the following routines; PLANCK, MAXADD, MODSHEL.

LRS Class	Spectra in Sample	Spectra with low S/N	No 10 μ m Excess	Type 1 10 μ m Excess	Type 2 10 μ m Excess	Type 3 10 μ m Excess
12	1	1	1	0	0	0
13	13	4	0	0	3	6
14	87	34	11	4	16	22
15	190	42	72	3	16	44
16	136	24	58	3	14	36
17	78	10	53	0	3	2
18	45	8	34	0	0	2
19	4	2	2	0	0	0
Totals	544	125	231	10	51	112

21	21	2	0	3	15	2
22	73	6	0	19	40	2
Totals	94	8	0	22	55	4

Table 1: Some numerical data on the 1n survey as described in the text. Also tabulated are the results from the survey of 21 and 22 spectra.

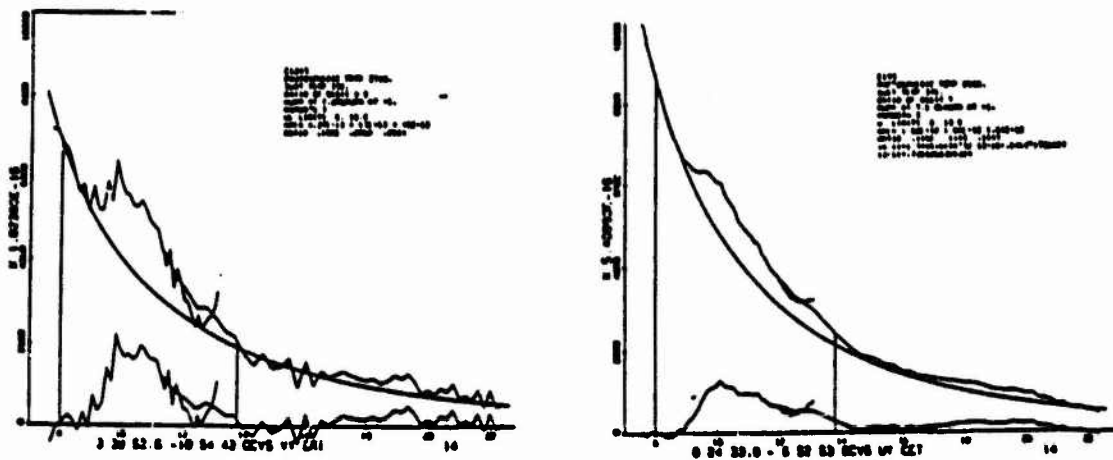


Fig. 2: Examples of sources displaying the type 1 and type 2 emission excesses.

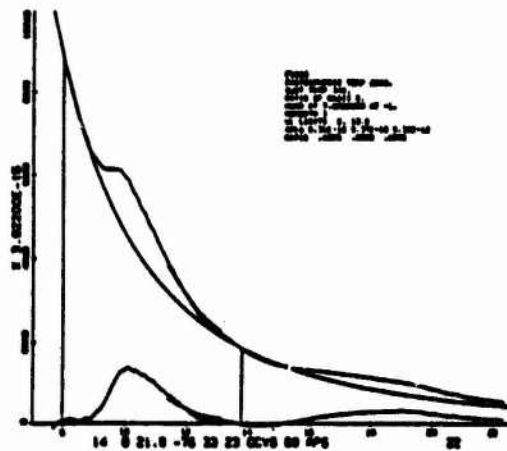
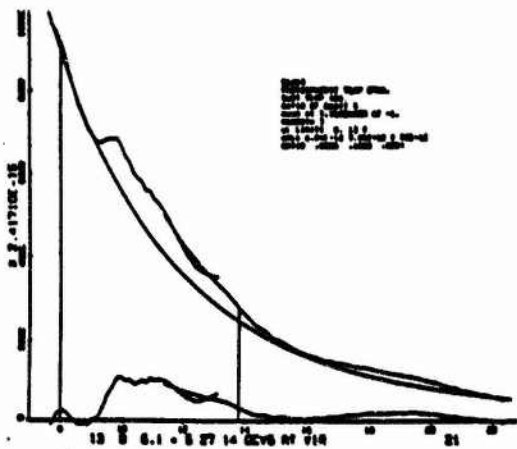
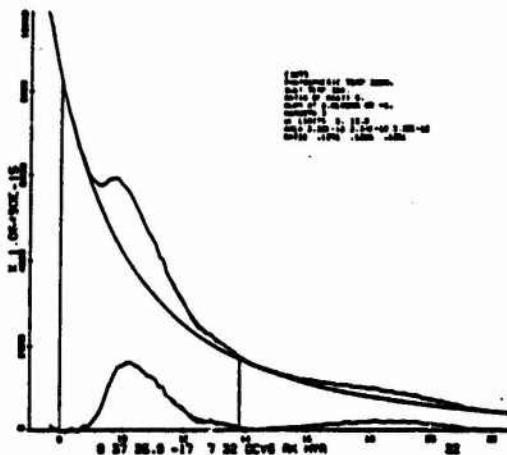
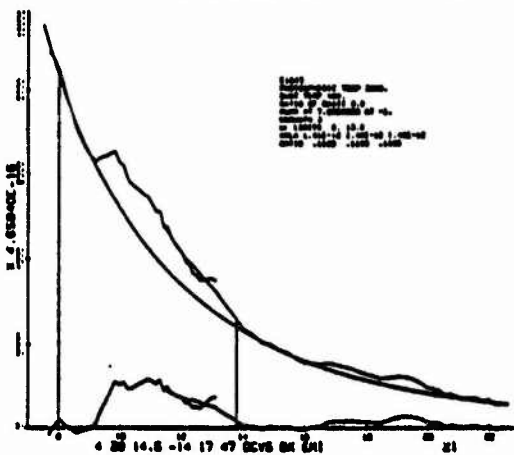
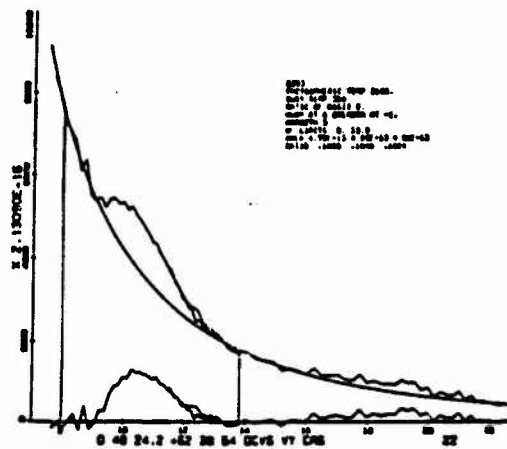
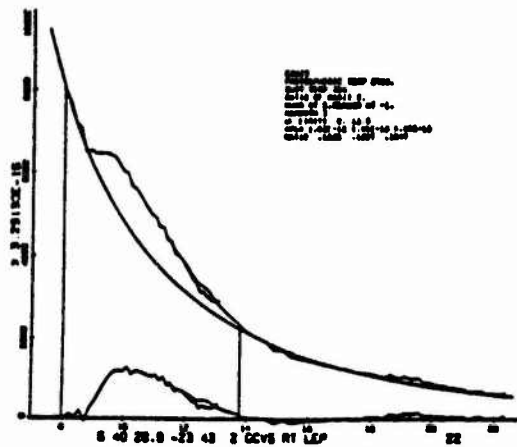


Fig 30

Fig 36

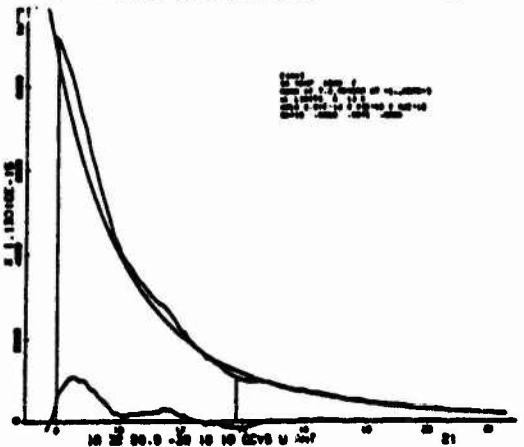
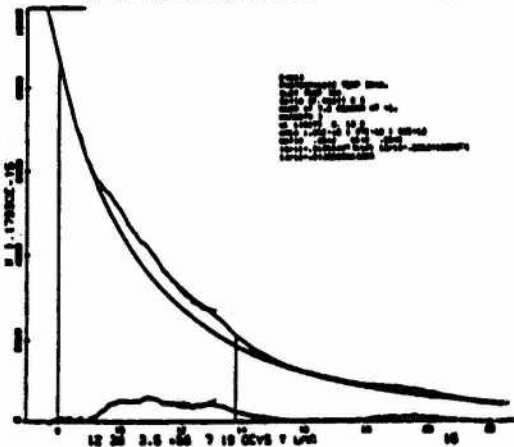
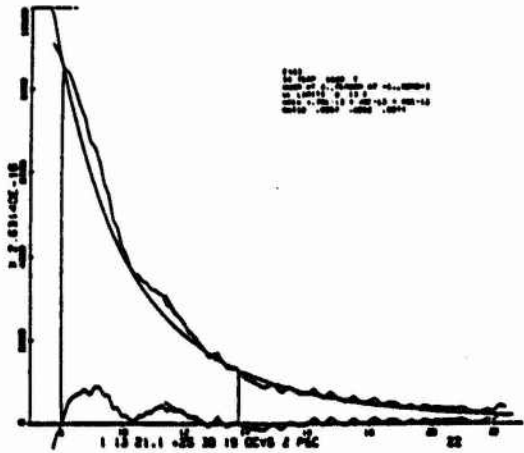
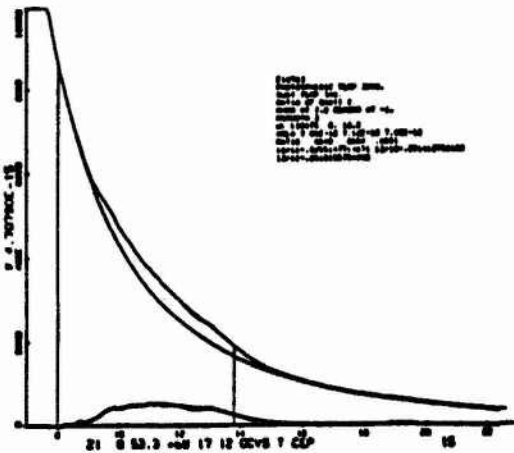
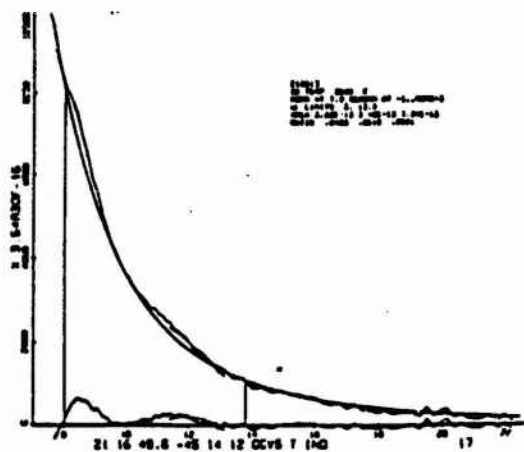
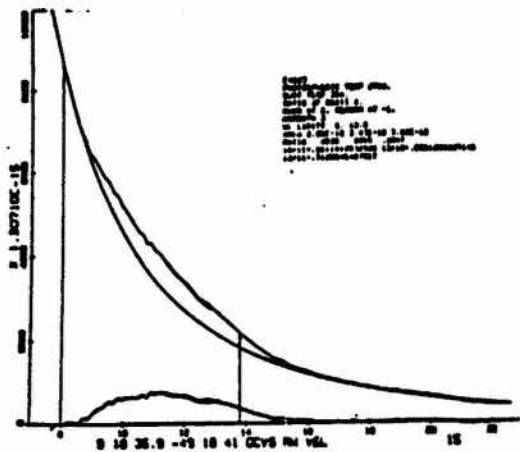


Fig. 3a

Fig. 3b

Fig. 3a,b,c, a: Sample sources exhibiting the type 2 excess emission.
 b: Sample sources exhibiting the type 1 excess emission.
 c: Sample sources exhibiting the type 3 excess emission.
 d: sample sources exhibiting the 11.6 micron and 8.5 micron carbon star features.

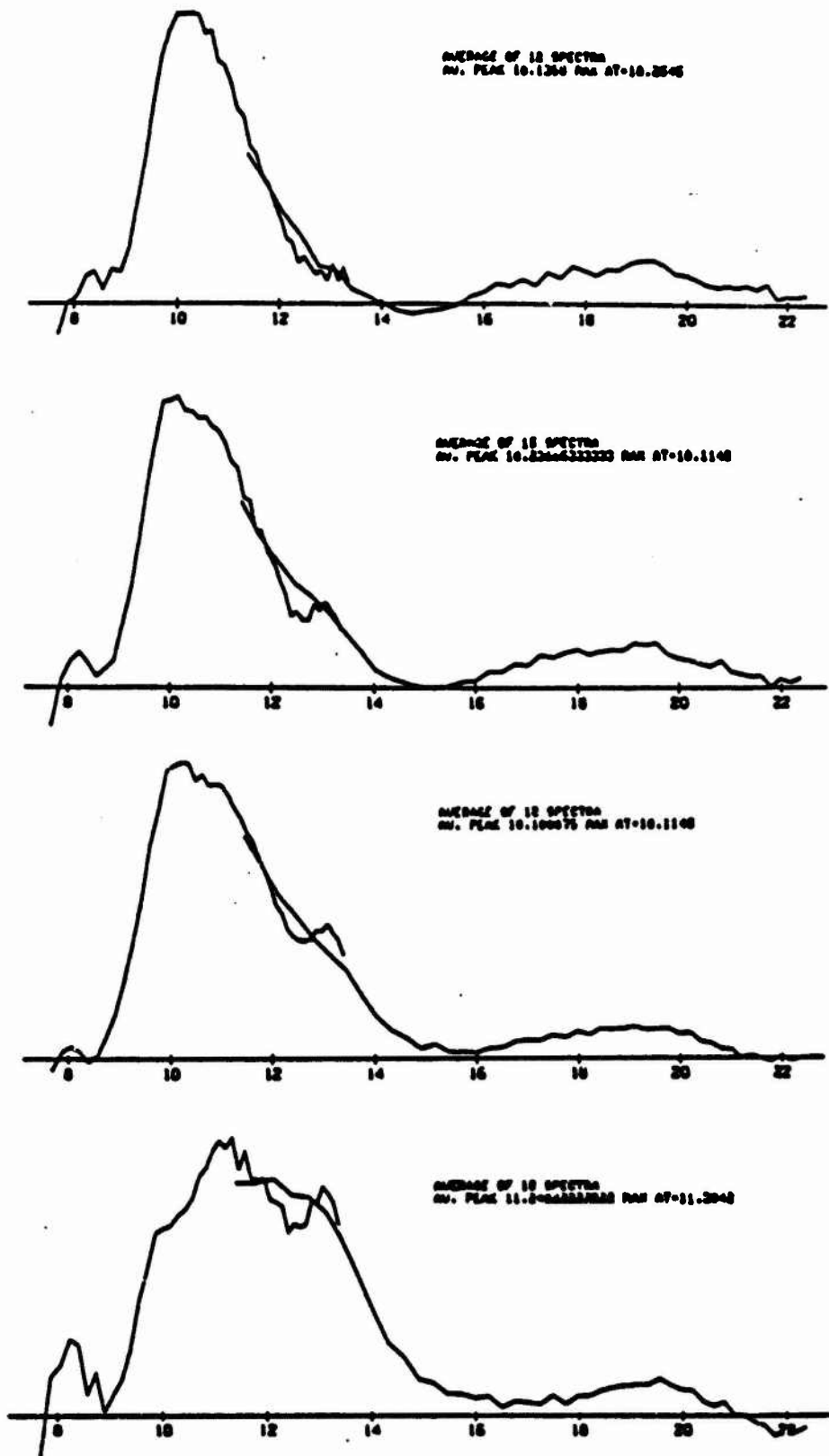


Fig. 4 Average spectra of sources showing the change in profile of the emission excess from type 1 (top) to type 3 (bottom). (wavelength in microns).

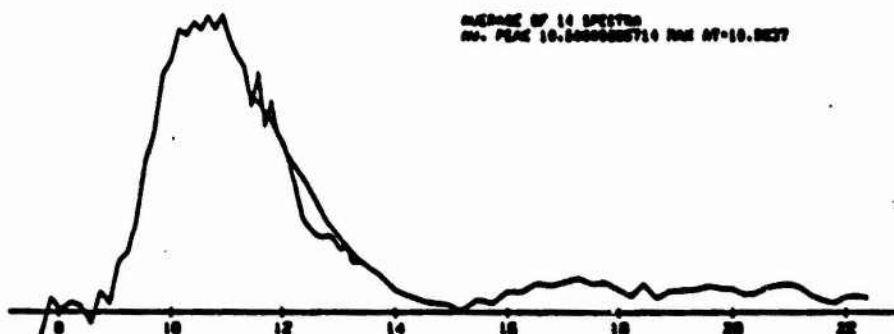
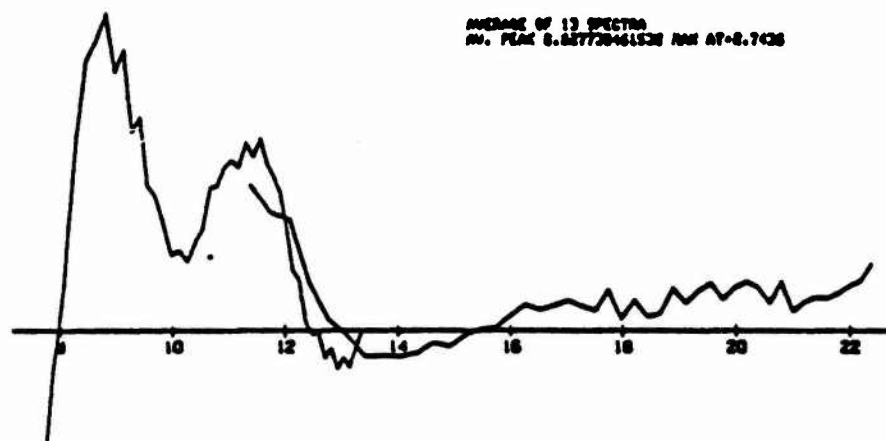


Fig. 5 Average spectra of, from top to bottom; highest signal to noise carbon stars, spectra exhibiting the 8 micron feature presumably due to molecular SiO and the highest signal to noise S stars.

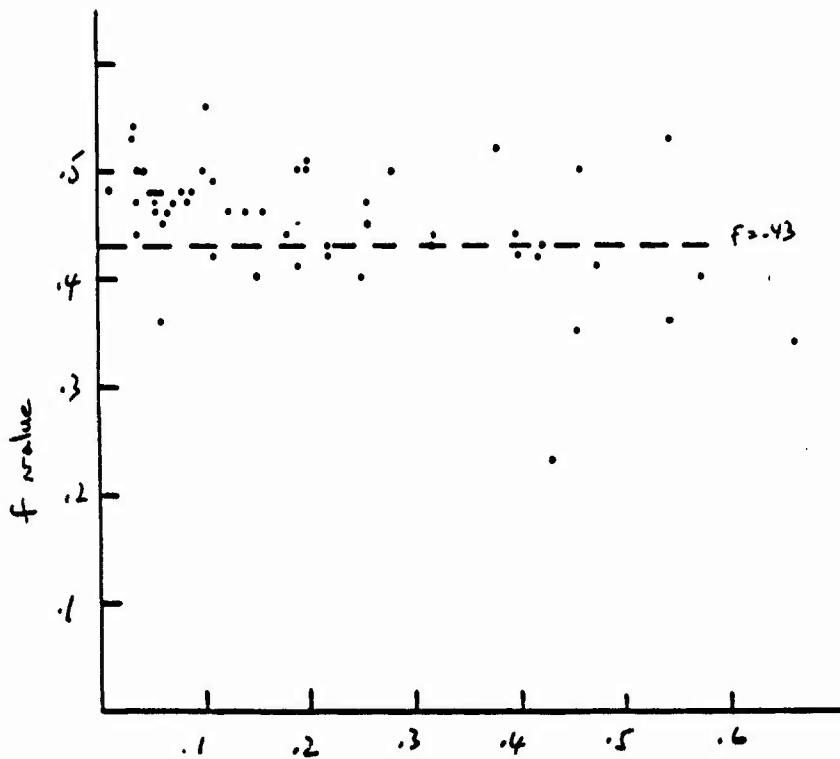


Fig. 7a Plot of light curve asymmetry factor ("f" value) versus excess emission above the local continuum between 9 and 11 micron (an indication of the strength in the 10 micron feature).

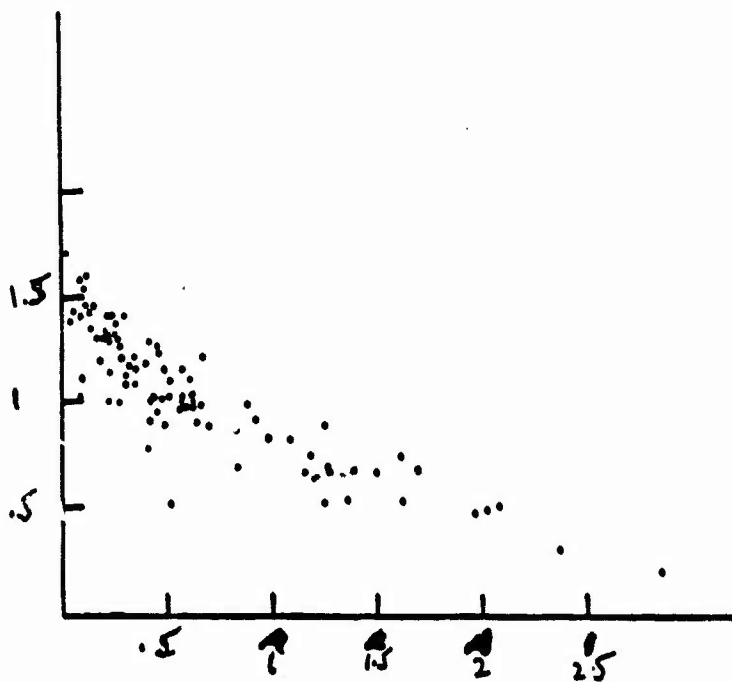


Fig. 7b Plot of flux ratio at 10 and 11 microns (10/11) versus flux ratio at 13 and 10 microns (13/10).

1987 USAF-UES SUMMER FACULTY RESEARCH PROGRAM/
GRADUATE STUDENT SUMMER SUPPORT PROGRAM

Sponsored by the
AIR FORCE OFFICE OF SCIENTIFIC RESEARCH

Conducted by the
Universal Energy Systems, Inc.

FINAL REPORT

CENTRIFUGE MODELING OF PROJECTILE PENETRATION
IN DRY, GRANULAR SOIL

Prepared by: Teresa Taylor
Academic Rank: Graduate student
Department and Department of Civil and
Environmental Engineering
University: Washington State University
Research Location: USAFESC/RDCO
Tyndall AFB, FL 32403-6001
USAF Researcher: Lt. Steven Kuennen
Date: 14 Sept 87
Contract No.: F49620-85-C-0013

Centrifuge Modeling of Projectile Penetration
in Dry, Granular Soil

by

Teresa Taylor

ABSTRACT

Centrifuge tests designed to investigate projectile penetration depths in dry, granular soils were performed. A major objective of the tests was to determine the need for centrifuge testing to achieve similitude between model and prototype for this phenomenon. Penetration testing was accomplished using a pistol with interchangeable barrels to fire spherical projectiles of brass, aluminum, nylon and polyvinyl chloride at vertical impact angles into dry Ottawa Flintshot sand prepared at an average density of 17.54 kN/m³. The sand samples were formed using a special large-scale sand rainer constructed specifically to produce 0.46 m diameter, uniform density samples for centrifuge testing. The modeling-of-models technique used in the centrifuge tests, along with results from complementary 1-g tests also performed, confirmed the need for centrifuge testing to investigate penetration depths in cohesionless soils.

ACKNOWLEDGEMENTS

Thanks are extended to the Air Force Systems Command, the Air Force Office of Scientific Research and the Air Force Engineering and Services Center for sponsorship of this research.

Project technical monitors Paul Rosengren and Lt. Steven Kuennen must be thanked for their assistance with organizational and logistical details, as well as for their ideas and support.

Thanks are also extended to the many employees of the Air Force Engineering Services Center who made significant contributions to this research, not only by their direct help, but by their friendliness and interest. It was a rewarding experience and a genuine pleasure working with them. A very special thank you must be given to William Naylor, whose labors in a variety of capacities including those of centrifuge operator and general technician, were greatly appreciated. His help was indispensable and contributed largely to the success of this research.

Dr. Richard Fragaszy, supervising professor, must also be thanked for his support and encouragement, as well as his many technical contributions.

I. INTRODUCTION:

One of the difficulties involved in developing methods of predicting penetration depths is the lack of good data. Most approaches to penetration research have involved either empirical equations based on large-scale experiments, solutions to standard equations of motion evaluated experimentally through an instrumented projectile, or predictions based on simplified constitutive equations for the target material (Young, 1967; Colp, 1968; Thigpen, 1974; True, 1974; Forrestal et al., 1984). Where the target material is a soil, these methods of depth prediction are typically constrained by very general, qualitative soil descriptions which are not directly related to standard engineering properties or classifications. Performing a large number of tests on samples with known properties could help refine a number of penetration prediction methods.

Full scale field tests are very expensive; consequently, the range of data that may be generated practically by such tests is limited. Further, full scale tests are conducted on in situ soil, the description and classification of which is often uncertain and very general in nature.

In contrast to full scale tests, comparatively large numbers of tests can be performed in a laboratory environment, on soil samples with known engineering properties and

classifications (within realistic limits). However, directly applying typical 1-g laboratory results to field conditions may not be appropriate for granular soils, in view of the strong relationship between confining pressure and soil strength. The alternative laboratory technique of centrifuge testing allows duplication of stress levels between model and prototype, unlike typical 1-g laboratory testing. At the same time, centrifuge testing shares some of the benefits of 1-g laboratory testing in terms of economics and sample quantification capabilities. A major question addressed in this research was the validity of using centrifuge testing instead of standard 1-g laboratory testing to model the penetration phenomenon in granular soils.

The Air Force Engineering Services Center (AFESC) is interested in developing their centrifuge facility to support research appropriate to centrifuge testing, in many areas of military interest including projectile penetration and protection of buried structures. My educational background in geotechnical engineering and ongoing research in centrifuge modeling contributed to my assignment to the Air Force Engineering Services Center.

II. OBJECTIVES OF THE RESEARCH EFFORT:

The main objective of the research effort was to determine if centrifuge modeling was a viable and necessary technique for modeling projectile penetration in dry granular soils. To satisfy this main objective, several secondary objectives were addressed.

The first of these secondary objectives was to develop a method for creating reproducible sand samples at a known density. This would allow direct comparison of penetration depths obtained in different tests, as well as document actual penetration depths for a soil with known engineering properties, that could readily be classified by standard soil classification systems.

Second, the actual centrifuge tests required the design of a projectile delivery system that can successfully fire projectiles at desired velocities into a rotating sand target at a vertical angle of impact. To adequately assess the centrifuge modeling technique, this delivery system must be capable of firing projectiles of different sizes and masses.

Third, to help determine the validity of using centrifuge modeling to investigate projectile penetration, it was important to conduct a number of tests in a 1-g environment

to compare with identical centrifuge tests. If significant differences between 1-g and elevated g tests were observed for the same projectiles at the same velocities, then gravity dependence and the need for centrifuge modeling would be demonstrated.

Finally, performing centrifuge tests of the same prototype event (i.e. same prototype mass, projectile velocity and soil density) at different g-levels, could further establish the validity of centrifuge testing for investigation of penetration depth, provided the same prototype penetration depth was obtained for the same prototype event. This testing technique, termed modeling-of-models, can also be used to determine a range of test validity over which boundary conditions have no significant effect on test results (Cheney and Fragaszy, 1984).

III. SAMPLE PREPARATION:

A circular aluminum sample bucket, constructed of 0.0127 m thick aluminum, was used in all tests. The bucket was 0.46 m in diameter and 0.45 m deep, allowing a large range of sample depths to be accommodated.

A 2.2 m high circular sand rainer was constructed to prepare the test samples, using the technique of pluviation. This

rainer was a scaled version of that designed by Eid (1987), who demonstrated that this design could produce very uniform and reproducible samples over a wide range of relative densities. To test the validity of Eid's results using the sand rainer constructed for this research effort, 20 initial tests were conducted at two different relative densities using Ottawa Flintshot and Sawing sands. During these tests, modifications were made to the rainer, and assessments of equipment leveling requirements and other preparation techniques were made. Sample depths ranged between 0.07 m and 0.3 m. Some samples were prepared by pluviating an entire sample through the rainer at one time. Other samples were prepared by pluviating small layers individually through the rainer, incrementally building the sample up to the final desired height. This approach enabled densities to be calculated for individual layers as well as for entire samples. Density values calculated in this manner were virtually identical for all tests, indicating uniform density with depth.

Also of importance in preparation of samples for testing was the ability to create a level sample surface. This was of particular significance in the centrifuge tests, especially for those tests where shallow penetration depths were anticipated. It was determined that very level surfaces could be achieved by this method if great care was exercised

in equipment set-up, particularly in leveling of the sample bucket and component parts of the sand rainer.

Following the initial tests, a total of 40 actual test samples, used for both 1-g and centrifuge tests, were prepared with the sand rainer. The samples had an average density of 17.54 kN/m^3 , with less than one percent variation from this value between samples.

Based on the excellent results obtained in both the initial tests and in preparation of the actual test samples, this method appears extremely useful for preparation of large samples of dry, cohesionless soils.

IV. DELIVERY SYSTEM DESIGN:

A Thompson Contender bull barrel pistol with interchangeable barrels was used for the centrifuge tests. This pistol was chosen because of the need to accommodate a variety of projectile sizes as well as to provide greater flexibility for future research. The two standard caliber barrels (30/30 Winchester and 44 Magnum) used in these tests were modified by shortening and smoothboring to remove the riffling. These modifications were made to lessen the effects of projectile spin, and to allow projectiles

manufactured from relatively hard materials to be safely fired.

Design of a suitable delivery system was complicated by the configuration of the AFESC centrifuge. This centrifuge, which has a maximum payload of 2.22 kN and maximum acceleration of 100 g's, does not have suitable space for mounting a pistol directly on the rotor hub. As a consequence, the pistol had to be mounted some distance along the rotor arm, thus subjecting it to elevated g levels. This in turn required considerable flexibility in the gun mounting location to enable vertical impact in the center of the centrifuge bucket to be achieved at different g-levels and different projectile velocities. To obtain this flexibility, the pistol was attached to a wheeled swivel plate assembly which allowed the pistol barrel to be rotated up to 30 degrees. The plate assembly itself rode on a system of rack gears which permitted movement in both the radial direction along the rotor arm platform, and perpendicular to this direction. Using a computer program to solve the equations of motion for the projectile, it was possible to properly position the pistol to achieve vertical projectile impact in the center of the sample bucket.

Spherical projectiles were manufactured of nylon, polyvinyl chloride (PVC), aluminum and brass. A small seating collar was machined around each sphere to allow the projectiles to

be loaded in standard brass cartridge cases. A commercial smokeless pistol powder and appropriate primers were used in conjunction with standard reloading equipment and procedures. The desired test velocity of approximately 300 m/second was obtained at powder charges ranging between 1.6 to 7.0 grains (approximately 0.1 to 0.45 gm). To improve the reproducibility of velocities at these very small charges, polyester fiber fill was used as a spacer between the powder and the projectile. Required amounts of powder and fill for each caliber and projectile type were determined in a series of over 200 velocity tests. Results of these tests indicated that velocities could generally be duplicated within approximately 6 to 10 m/second.

V. PENETRATION TESTS:

Both 1-g and centrifuge tests were performed on samples of Ottawa Flintshot sand. 1-g tests were conducted at measured velocities ranging between approximately 153 m/second and 313 m/second. Centrifuge tests were conducted at an estimated velocity of approximately 305 m/second. Table 1 presents the actual penetration depths obtained for both sets of tests.

Table 1. Actual Penetration Depths in Ottawa Flintshot Sand

Type	Caliber	Mass (g)	G Level	Velocity (m/sec)	Final Depth (m)	Soil Density (kN/m ³)
Nylon	30	.299	1	224 ¹	.0246	17.64
PVC	30	.570	1	229 ¹	.0197	17.53
PVC	30	.570	44	305 ²	.0126	17.54
Aluminum	30	.732	1	240 ¹	.0317	17.54
Nylon	44	.804	1	153 ¹	.0220	17.53
Nylon	44	.804	34	305 ²	.0150	17.54
Nylon	44	.804	50	305 ²	.0149	17.54
Nylon	44	.804	50	305 ²	.0157	17.57
PVC	44	.940	1	158 ¹	.0244	17.53
PVC	44	.940	47	305 ²	.0163	17.54
Aluminum	44	1.992	1	287 ¹	.0465	17.43
Aluminum	44	1.992	1	310 ¹	.0490	17.57
Brass	30	2.214	46	305 ²	.0650	17.46
Brass	30	2.214	46	305 ²	.0635	17.53
Brass	30	2.214	53	305 ²	.0594	17.57
Brass	30	2.214	53	305 ²	.0602	17.51
Brass	44	6.036	1	309 ¹	.1126	17.59
Brass	44	6.036	1	313 ¹	.1125	17.59
Brass	44	6.036	33	305 ²	.0777	17.54
Brass	44	6.036	38	305 ²	.0823	17.51
Brass	44	6.036	41	305 ²	.0838	17.57

¹ Measured velocity

² Estimated velocity

As can be seen in Table 1, significant differences in actual penetration depths were obtained at different g-levels for the same projectiles. These differences clearly demonstrate that g-level is an important consideration in assessing penetration phenomena in granular soils.

Table 1 also illustrates that very good test reproducibility was obtained. This can be seen by directly comparing results from identical tests, for example results from the

two 1-g tests performed with 44 caliber brass projectiles, or results from the tests at 46 g and 53 g performed with 30 caliber brass projectiles.

Figure 1 presents the predicted prototype final penetration depths, based on centrifuge tests at different g-levels, for different prototype masses. As can be seen in this figure, test results were very good. Prototype penetration depths obtained at different g-levels for the same prototype mass and velocity were virtually identical. These results also demonstrated the importance of gravity scaling penetration depths in cohesionless soils.

VI. RECOMMENDATIONS:

The results of this research confirm the need for duplication of stress levels in granular soils to adequately model the phenomenon of projectile penetration, and also demonstrate the validity of using the centrifuge modeling technique for this purpose. The delivery system designed for this research was shown to be successful in firing projectiles at known velocities to impact a target at a given angle and location. This, or a similar system, can easily be used for additional work in this area. The sand rainer constructed for sample preparation was shown to produce very uniform, level samples; the design is

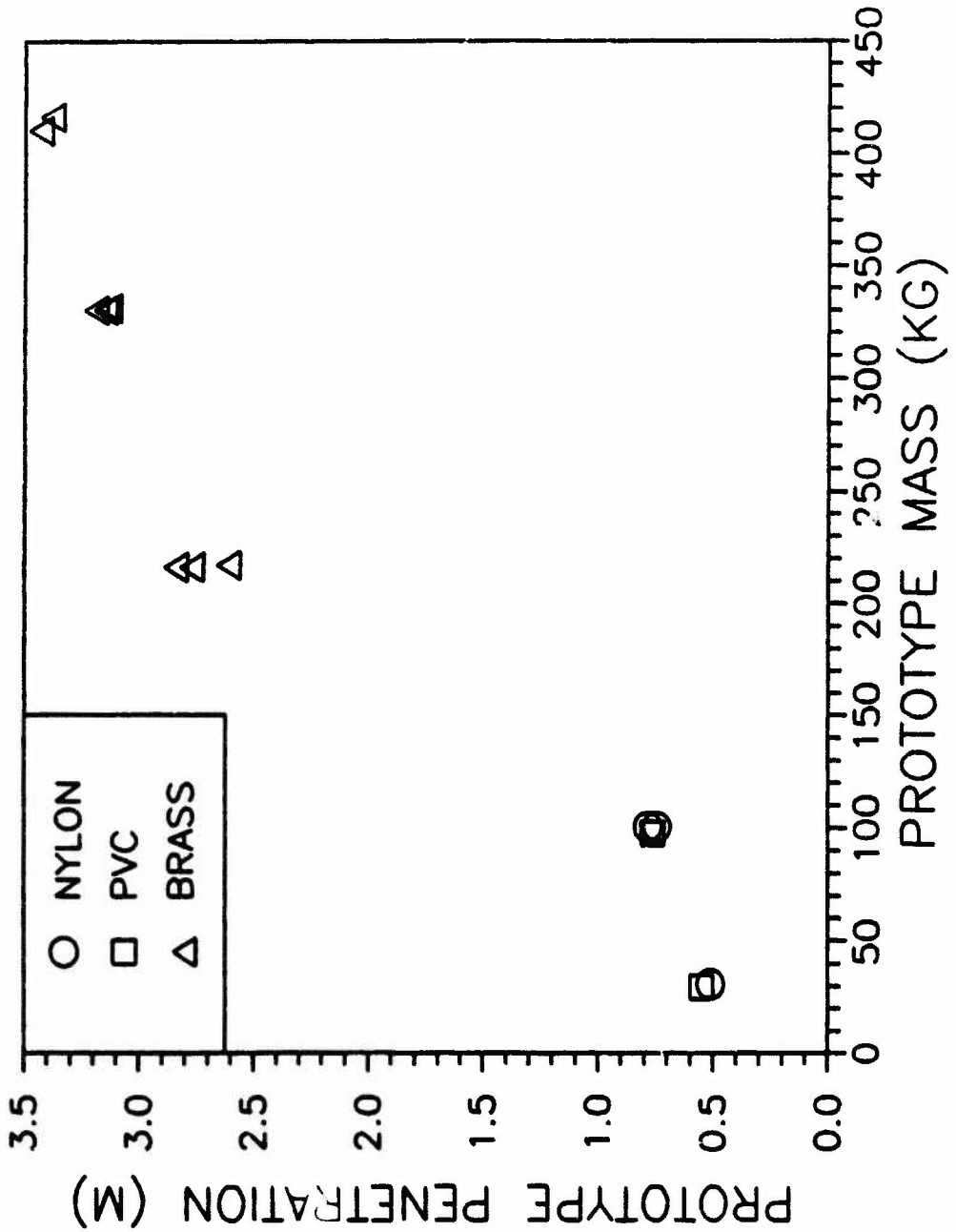


Figure 1. Prototype penetration depths for different prototype masses.

recommended for preparing large samples of dry, cohesionless soils of uniform density.

The work presented herein is being continued as part of an ongoing research project sponsored by AFESC. The initial modeling-of-models centrifuge tests will be expanded by testing projectiles of two additional calibers and of additional material types. This will contribute to better definition of the range of validity for these tests. Additional centrifuge tests, along with corresponding 1-g tests, will also be conducted at different projectile velocities and impact angles. After completion of tests on dry sand, a number of similar tests on saturated sand will be performed. Both penetration depth and pore pressure response due to projectile impact will be measured in these tests.

REFERENCES

Cheney, J. A. and R. J. Fragaszy, "The Centrifuge as a Research Tool," Geotechnical Testing Journal, 1984, Vol. 7, No. 4, pp. 182-187.

Colp, J. L., "Terradynamics: A Study of Projectile Penetration of Natural Earth Materials," Sandia Laboratories Report No. SC-DR-68-215, 1968, 61 pp.

Eid, W. K., "Scaling Effect in Cone Penetration Testing in Sand," Ph.D. Thesis, Virginia Polytechnic Institute and State University, Blacksburg, Virginia, March, 1987, 244 pp.

Forrestal, M. J., Lee, L. M., Jenrette, B. D. and R. E. Setchell, "Gas-gun Experiments Determine Forces on Penetrators into Geological Targets," Journal of Applied Mechanics, 1984, Vol. 51, pp. 602-607.

Thigpen, L., "Projectile Penetration of Elastic-Plastic Earth Media," Journal of the Geotechnical Engineering Division, ASCE, 1974, Vol. 100, No. GT3, pp. 279-294.

True, D. G., "Rapid Penetration into Seafloor Soils," Proc. Sixth Offshore Technology Conference, Houston, Texas, May 1974, pp. 607-618.

**1987 USAF-UES SUMMER FACULTY RESEARCH PROGRAM /
GRADUATE STUDENT SUMMER SUPPORT PROGRAM**

**Sponsored by the
AIR FORCE OFFICE OF SCIENTIFIC RESEARCH**

**Conducted by the
Universal Energy Systems, Inc.**

FINAL REPORT

Optical Interconnections for Digital Image Coding

Prepared by:	Tien N. Tran
Academic Rank:	Graduate student
Department and University :	Electrical and Computer Engineer Department University of Cincinnati
Research Location:	Rome Air Development Center, Griffin Air Force Base, Rome, NY
Date:	September 16, 1987
Contract No.:	F49620-85-C-0013

Optical Interconnections for Digital Image Coding

by

Tien N. Tran

ABSTRACT

To achieve very compression rate, Digital Image Coding algorithms are becoming more complicated than ever. Combining this with high speed nature of image processing, transmission, parallel and pipeline processing have to be involved with the help of multiple processing units type architecture. Because of the large number of cells or chips involved, communications between cells or chips pose many problems. Optical interconnections seems to offer a hope for a solution.

ACKNOWLEDGMENTS

The author sincerely appreciates the Air Force Systems Command and the Air Force Office of Scientific Research for giving him the opportunity to acquire new knowledge. Most of all, he also would like to thank everyone at Rome Air Development Center, Griffin Air Force Base for the warm welcome and a wonderful summer.

I. INTRODUCTION

Digital Image Processing, by nature, is a computational intensive process. Most image processing and coding techniques or algorithms require the power of supercomputers and make real-time processing impractical with general purpose computers. Special purpose hardware implementing these algorithms usually employ architectures that allow massive parallel processing; these hardware with their multiple processing elements, however, are limited by the interconnections possible between processing elements. As the size of devices getting smaller and more elements can be implemented on the same chip, the interconnection problems and associated costs increase significantly. On the other hand there are recognized advantages of optical systems that may make it possible to get a very high throughput when processing multi-dimension data. In the foreseeable future, most computation tasks will still be done with electronic hardware; however, we cannot afford to overlook the advantages of optical interconnections, especially the global interconnection property.

II. OBJECTIVES:

Traditionally, less computationally complex image coding techniques are favored over more complex ones. With VLSI technology combining with special architectures (systolic array for example) a different view has to be taken: a computationally complex algorithm with a superior performance as compared to that of a less complex algorithm may be preferred if the architecture for its implementation

happens to be modular and can easily mapped into simple VLSI design. With these architectures, high processing speed or throughput rate can be achieved with massive parallel and pipelining. Stated differently, the resulting VLSI chip will consist of a multitude of basic cells connecting together. As devices can be made smaller (scaling), the complexity of the cells can be increased along with the number of cells that can be squeezed into a single chip. The number of of interconnections required also increases with the number of cells along additional problems of scaling like interfering, electromigration, etc. Thus at chip level there is a disparity between the number of interconnections that can be realized and the number required.

In this project, we look at one particular coding algorithm that fits the description of computationally complex yet highly modular structured; that algorithm is Vector Quantization. With its modular structure VQ can be implemented using parallel type architecture; this project involves an investigation on the possibility of using optical interconnections to ease the communication problem associated with its electronically implementation.

III. VECTOR QUANTIZATION and its implementation:

Generally, VQ involves decomposing signals into vector blocks and quantizing each vector to the nearest neighbor vector in an optimal code book [1]. Thereafter, the codevector's index in the code book is used to identify the original vector. VQ makes use of four interrelated properties of vector parameters: linear dependency (correlation), non-linear dependency, shape of the probability density function and

vector dimensionality to remove redundancy that is present in any signal. Hence, VQ results in a better compression ratio than scalar quantizations which normally make use of only the linear dependency and the probability shape.

A common distortion measure for the nearest neighbor vector selection is the minimum squared error criteria. If $\hat{X} = [X_j]$, $j = 0$ to $M - 1$ be one block of signals, $\hat{C} = [C_{ij}]$, $j = 0$ to $M - 1$ and $i = 0$ to $N - 1$ be codebook consisting of N code vectors of size M , then the distortion error D_i with i th code vector is given by:

$$D_i = \sum_{j=0}^{M-1} (C_{ij} - X_j)^2 ; i = 0 \text{ to } N - 1 \quad (1)$$

For good quality coding at reasonable bit rates, vector size M and codebook size N have to be quite large which also increases the amount of computations significantly besides requiring large memory. All these factors prohibit real-time implementation.

Fortunately, it can be noted that in calculating (1), we go through repeated process of subtraction, squaring and addition, for each code vector and data vector. Hence, they can be mapped on to a systolic architecture that can be implemented with considerable ease in VLSI technology [2]. Some of the important properties of systolic architecture are:

- 1 . The array can be implemented with only a few types of simple cells.
- 2 . The data and control flow of the array is simple and regular, so that the

cells can be connected by a network with local and regular interconnections; long distance or irregular communication is not needed.

- 3 . The array uses extensive pipelining and multiprocessing. Typically, several data streams move at constant velocities over fixed paths in the network, and interact where they meet. In this fashion, a large proportion of the processors in the array are kept active, so that the array can sustain high rate of computational flow.
- 4 . The array makes use of each input data item a number of times. As a result high computational throughput can be achieved without requiring high bandwidth between the array and the host.

The architecture of VQ is shown in Figure 1 and the operation of the VQ encoder is illustrated in Figure 2. From Figure 1, it can be noted that the VQ encoder uses only two types of cells and the number of cells needed are $M.N$ and N respectively. There are only local connections among the cells making the design simpler. Also from Figure 2, we can see that after some initial delay or latency, the VQ encoder will produce an address of a code vector for a given data vector in a time equal to the delay in a basic cell which can be considerably small. By increasing the size of the data vector M , we increase the available time for encoding. Hence an implementation using simple serial architecture should be possible [3].

From the initial work, we have two options for the operational nature of the cells: parallel (multiplication and addition) or serial operation. Unless we are

using waffersize chip, however, an array of VQ chips is needed for VQ encoder. For example, we can put 32x32 basic cells on a normal size silicon chip using 3 micron technology; for a 256-vector size codebook with 8x8 size vector, the number of cells needed is in the order of 16k cells. Even for a chip with only 32x32 cells and employing serial type operation we need 128 I/O pins; time multiplexing just will not do with this kind of operation speed. Furthermore, to avoid global clock, handshaking communication between cell is needed; this also increases the number of pins required. In addition to this, is the problem of codebook updating or replacement. The new codebook values have to be transferred serially from the border cells to their assigned cells, a very slow process. Individual cell control program codes also have to be transferred the same way.

In this project we propose a two parts solution to these problems.

The first part involves giving the border cells with input need light detectors and those with output need light sources. An holographic routing element will direct light from sources to corresponding receivers which may be located on adjacent chips (figure 3). If locating a light source on the chip complicates the design (heat dissipation), light modulators can be used with off-chip light source.

The next part involves equipping every cell with light detector. With the help of programmable holographic routing element, such as a reflective spatial light modulator, control intructions can be broadcasted, codebook updating can be done in shorter time, and with global clock broadcasted intercells handshaking may not

needed.

IV. RECOMMENDATIONS:

While the above mentioned chip is designed for Vector Quantization encoding, individual cell doing simple calculations and data transfer, the concept can be expanded to make the cells more sophisticated. In this way the chip can perform other functions, be it some image processing or image coding algorithms, besides Vector Quantizing. With optical interchip connections, a multiple chip system can achieve a very high throughput rate.

As individual cell becoming more complicated, more chip area, the ratio of light source (or modulator) plus receiver area and cell area decreases. Thus we we can afford to equip every cell with source and detector; this will allow even greater flexibility in the chip usage and operation.

V. REFERENCES

- [1] R. GRAY, "Vector Quantization," *IEEE ASSP Magazine* April 1984, pp 4-29
- [2] H. T. KUNG, "Why Systolic Architecture," *IEEE Computer*, pp. 37-46 January 1982
- [3] P. A. RAMAMOORTHY, T. TRAN, "A Systolic Architecture for Real-Time Composite Video Image Coding," *IEEE Military Communications Conference* October 1986

DATA VECTOR d_1, d_2, \dots, d_m CODEBOOK $C_{ij}, n \times m, e_1, \dots, e_m, C_{ij} - d_j, i=1$ to n

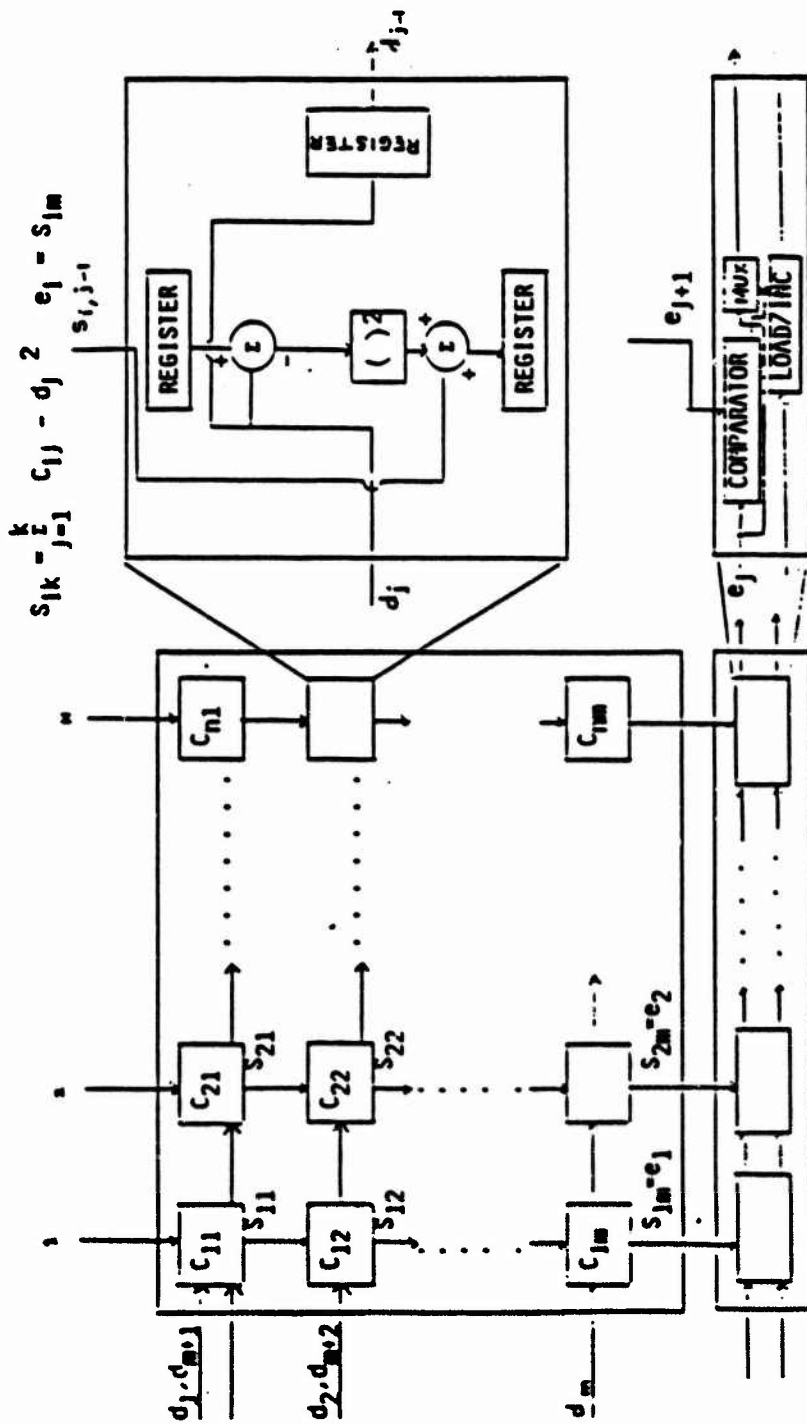
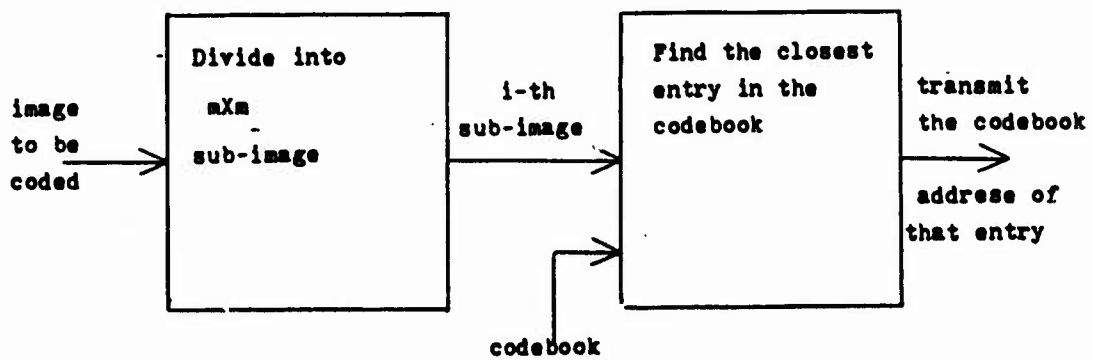


Figure 1: VQ Systolic Architecture implementation block diagram



1b- Image encoding using vector quantization

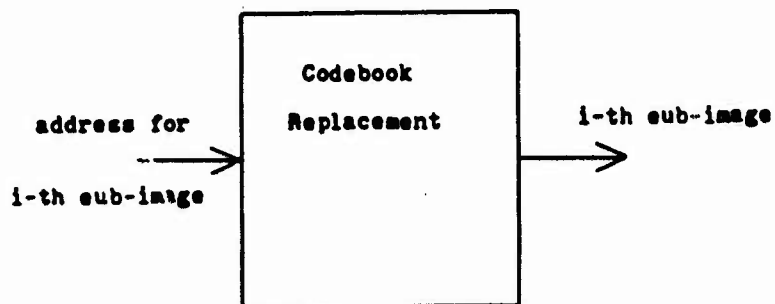


Figure 2: VQ encoder

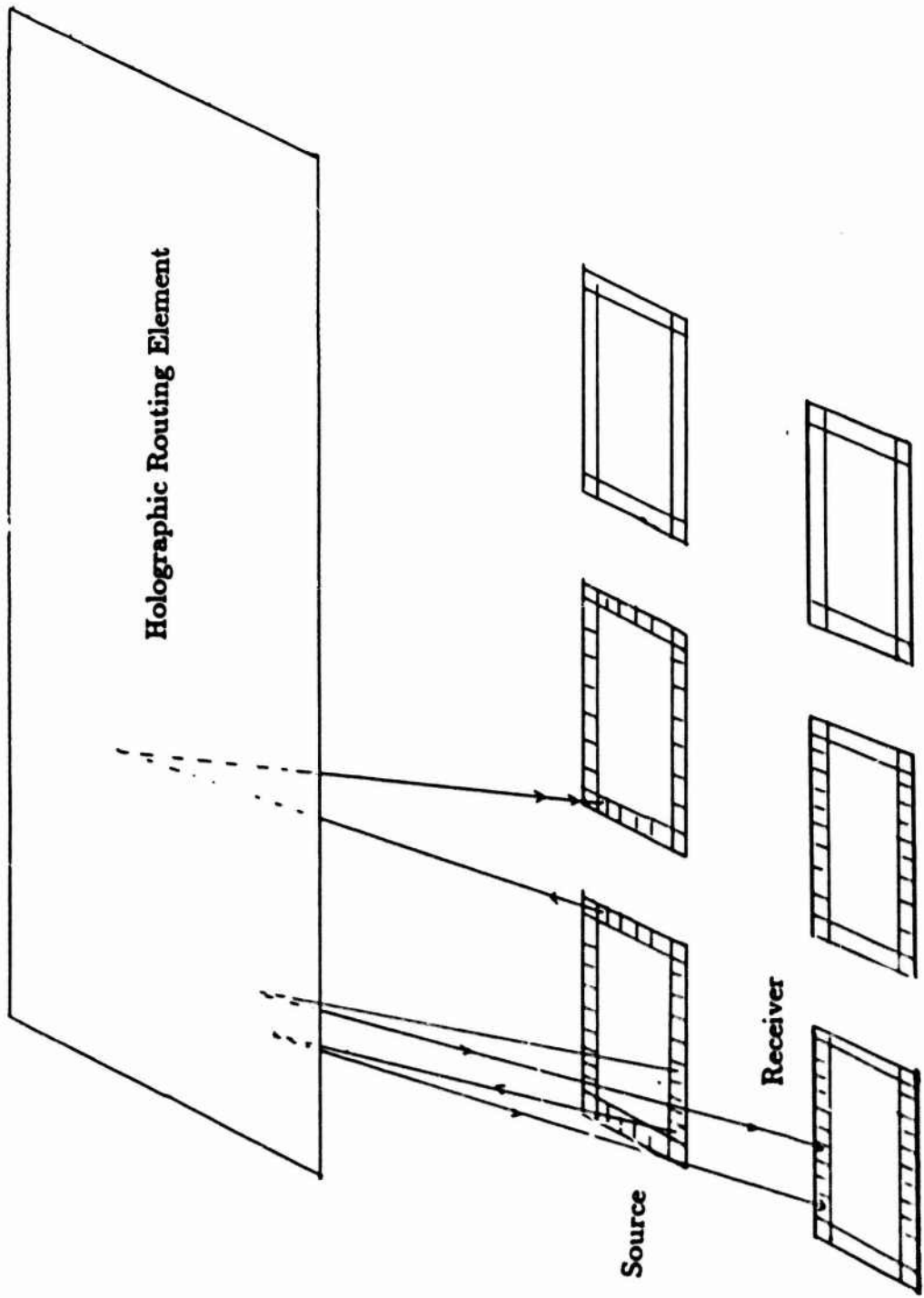


Figure 3: Proposed interconnection for VQ chip array

1987 USAF-UES SUMMER FACULTY RESEARCH PROGRAM/
GRADUATE STUDENT SUMMER SUPPORT PROGRAM

Sponsored by the
AIR FORCE OFFICE OF SCIENTIFIC RESEARCH

Conducted by the
Universal Energy Systems, Inc.

FINAL REPORT

AN INVESTIGATION OF PERFORMANCE IMPROVEMENT
IN KNOWLEDGE-BASED CONTROL SYSTEMS

Prepared by: John M. Usher
Academic Rank: Ph.D. Candidate
Department and Engineering Sciences
University: Louisiana State University
Research Location: USAF/AFWAL-MLTC
Wright-Patterson AFB
Dayton, OH 45433-6533
USAF Researcher: Major Steven R. LeClair
Date: August 7, 1987
Contract No: F49620-85-C-0013

AN INVESTIGATION OF PERFORMANCE IMPROVEMENT
IN KNOWLEDGE-BASED CONTROL SYSTEMS

by

John M. Usher

ABSTRACT

The use of knowledge-based systems in real-time process control is a relatively new application. Even though there is much interest in this area, developers and users are reluctant to utilize the full potential that the knowledge-based system can offer. This restraint is due to the problem of resolving conflicts in the control actions prescribed by the system. In most cases, a human operator is made an integral part of the control system by requiring him to select the action to implement from among the alternatives offered by the system. This paper proposes a new method for resolution of conflicts which uses deterministic process knowledge in addition to heuristics and statistics. It is hoped that such a system will encourage removal of the operator and use of the system in a fully automatic mode of operation. To further enhance the system an idea is presented for the incorporation of a learning system to allow for on-line automatic editing of the process knowledge contained in the knowledge-base. This configuration results in a coupled system which uses dynamic deterministic and heuristic knowledge to resolve process conflicts which arise.

ACKNOWLEDGMENTS

I thank the Air Force Systems Command and the Air Force Office of Scientific Research for sponsoring my work. In addition, I appreciate the aid of Universal Energy Systems for their administrative help. I would also like to thank the Materials Laboratory for providing the facilities in which to perform this effort and Major Steve LeClair for his concern and guidance of my work.

I. INTRODUCTION:

The Manufacturing Group of the Materials Laboratory at Wright-Patterson Air Force Base has been working on the development of a real-time knowledge-based system for process control. The use of knowledge-based systems for real-time process control is relatively new and has required the development of such a system from the scratch. The developed system is termed the Qualitative Process Automation (QPA) system and has proved successful in its use for control of an autoclave for the lamination process. (For further details on the QPA system the reader is referred to reference [1].)

Since this is a new area there are several issues that require further investigation. One such area is the realization of performance improvement in the system through the employment of deterministic process knowledge to complement the heuristic knowledge currently used. This deterministic knowledge will be used to enhance the current method of process conflict resolution. Also of importance is the investigation of the capability for the system to learn new process knowledge by means of scientific discovery.

My research interests have been in the area of adaptive techniques for process control (i.e. inferential, model-reference, etc.). I have been interested in the design of a

new controller which utilizes both experienced-based knowledge found in knowledge-based system with deterministic knowledge employed in adaptive control systems. It is my work in this new area that contributed to my assignment to the project discussed above.

II. OBJECTIVES OF THE RESEARCH EFFORT:

The main objective in this study was to realize a means for improving the performance of the QPA control system by determining a more effective manner for resolving the command conflicts which occur.

The proposed method to be used for enhancing conflict resolution requires that deterministic process knowledge be used in cooperation with the knowledge-based control system. There is currently no knowledge-based control system which allows for the capability to use deterministic process knowledge in the system. The deterministic knowledge required is present in the form of process model equations and thereby, requires traditional computing techniques for performing the necessary calculations. Therefore, my second objective was to propose a design for a system which incorporates numerical computing into the knowledge-based program currently used for the Qualitative Process Automation (QPA) system.

The heuristics which identify the process conflicts are static, but the process models are dynamic (in the sense that they use current sensed process variables values in their calculations); therefore, it would be beneficial to develop a learning component to allow the system to learn new knowledge about the process and edit the heuristics in the knowledge-base. A specification for such a learning system that can be incorporated into the QPA program was the third objective of this study.

III.

a. The problem in using a knowledge-based system for process control is in the requirement of the system to select among the final control alternatives offered by the heuristics. These alternatives represent possible control actions to be implemented for controlling the process. For the case of the QPA system, the alternatives represent adjustments to the controller set-point used to drive the process. The selection of the proper alternative action is important, because a poor choice can cause reduced process operating efficiency and possibly result in process instability.

The problem of conflict resolution is not constrained to control applications alone, but exists for all uses of

knowledge-based systems. Several techniques are available for resolving these conflicts. One method uses arbitrary selection of an alternative (e.g. based on order of appearance). This method does not use any process knowledge and should only be employed when the outcome of each possible alternative is approximately equivalent and non-threatening. Another technique uses process knowledge in the form of meta-rules which reason about the conflicting alternatives to determine the proper selection. This technique is useful as long as the conflicts can be resolved using only heuristic knowledge and the knowledge is available. A third method utilizes probability information, in the form of certainty values (weighting) for each alternative, to guide selection. This technique's weakness rest in the method used to determine certainty values (weights) for each of the alternatives.

Each of these methods are currently being used in a variety of systems and can also be applied to the knowledge-based control system. Using these methods does not guarantee that the alternative selected is the best choice. The problem of selecting the correct alternative can't be eliminated entirely, but the number of times a poor choice is made, can be reduced.

b. A conflict resolution system is proposed which will complement meta-level knowledge with the use of deterministic knowledge of the process obtained from the results of numerical computations on process model equations. The proposed system, as shown in Figure 1, utilizes three main components, the comparator, the process model, and the response evaluator, to perform its duties.

The purpose of the comparator is to use deterministic knowledge to evaluate the alternatives of a conflict and eliminate any alternatives when there is reason to believe the process conditions triggering an alternative do not exist. The remaining alternative actions are then used by the process model to generate predicted response data for each alternative in the conflict. The resulting data is then used by the response evaluator to select the one alternative to be issued to the controller.

IV.

a. A search of the literature revealed that of the real-time knowledge-based control systems in development or use, none possess the ability to perform numerical computation using process model equations [1,2,3,4]. To provide such a capability will require the combination of numerical computing with symbolic computing to form a coupled system

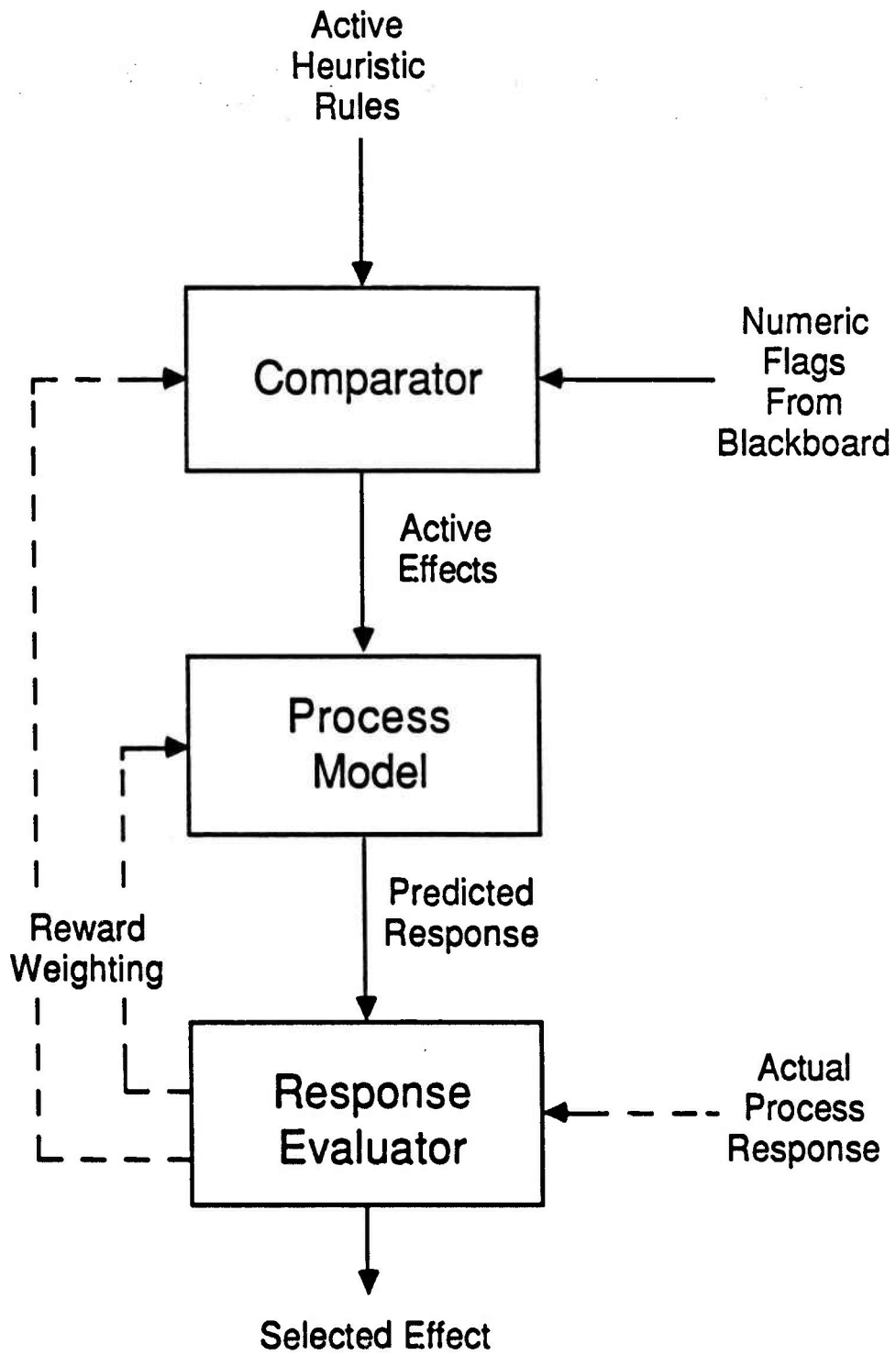


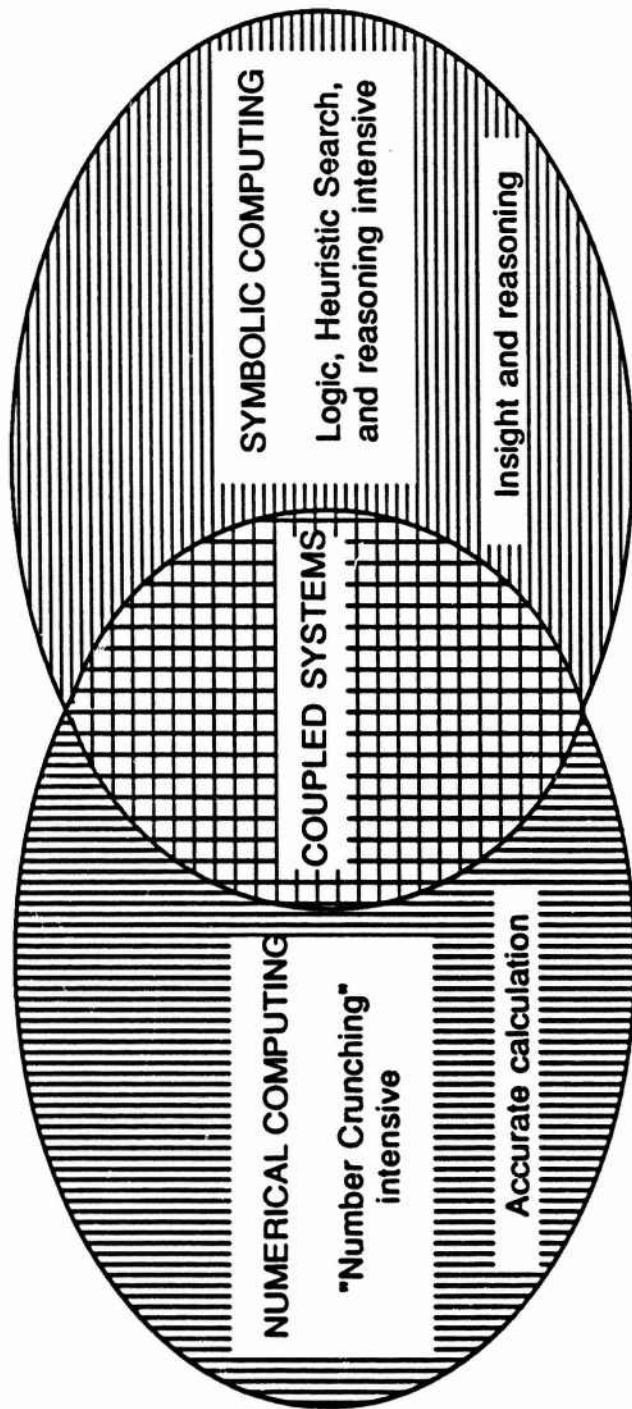
Figure 1: Conflict Resolution System.

(see Figure 2). Even though many of the current knowledge-based systems use some numeric processing they are not necessarily a coupled system. To be considered a true coupled system, the "system must have some knowledge of the numeric processes embedded within them and must reason about the application or results of these numeric processes" [5].

b. A design for the proposed coupled system is shown in the block diagram of Figure 3. This system will involve a shallow level of coupling whereby the symbolic component will have a limited knowledge of the numeric components (i.e. process equations) of the system. The architecture of the system involves the use of multiple processors with intercommunication achieved through a blackboard. The numeric component will reside in either a separate processor or remain resident among the same processor as the blackboard. The numeric results will be processed by the conflict resolution system as a part of the Thinker program. The architectural details will be determined when actual implementation is performed.

V.

a. There currently exists an abundance of literature on machine learning. There are many different methods in which



Numerical Computing

- Data processing & reduction
- Simulation & quantitative models
- Statistics and probability
- Numerical Algorithms

Application: algorithmically tractable problems

Symbolic Computing

- Data interpretation
- Cognitive & qualitative models
- Search and heuristics
- Non-deterministic solution strategies,

Application: problems intractable algorithmically

Figure 2: Computing Techniques [5].

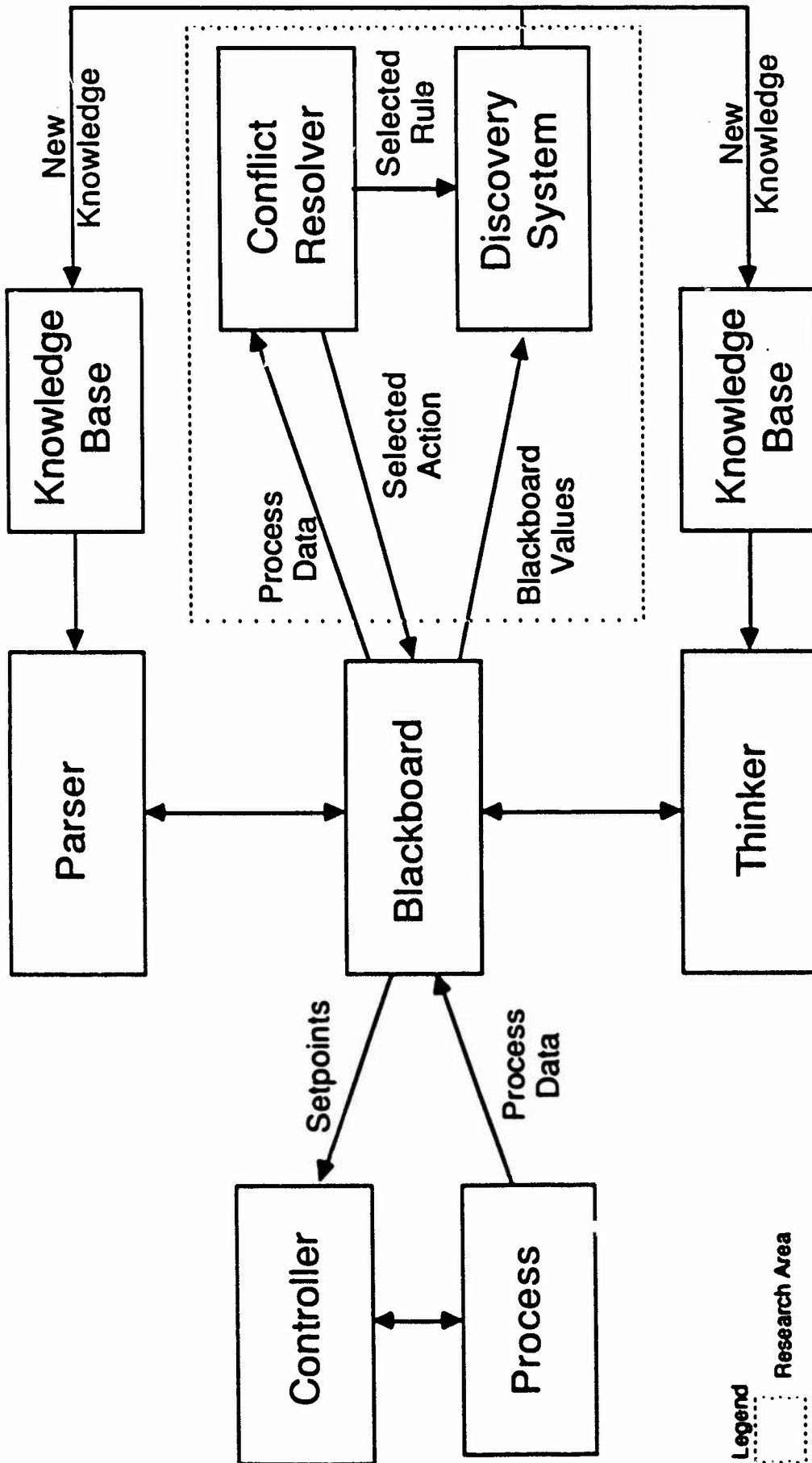


Figure 3: Block Diagram of Proposed Coupled system.

to implement learning into AI-based programs. The methods and types pertinent to the QPA system were identified.

b. The approach for learning to be applied to the QPA program falls under the primary learning research area identified by Carbonell, et. al. [6] as "task-oriented". Carbonell, et. al. defines a "task-oriented" approach as "the development and analysis of learning systems to improve performance in a predetermined set of tasks" [6]. The type of learning system to be employed is termed a discovery system and is concerned with the acquisition of new facts and theories through observation and experimentation.

The degree of interaction of the discovery system can be view as passive, in that it does not provide any control over the process of concern, but merely observes data which results from normal process operation. If it is necessary, the deterministic knowledge could be used by the discovery system to obtain needed information about the process (predictions only) without disturbing the actual process. The representation of knowledge by the discovery system will be in the form of production rules. This system will utilize some or all of the following operations for acquiring and refining the production rules contained in the knowledge-base, these operations are [6]:

- creation
- construction of a new rule,

- generalization - elimination or relaxing of the conditions of a rule,
- specialization - addition of conditions to a rule,
- composition - combination of rules with identical conditions.

It has not been decided where the discovery program will reside in the overall system architecture. Either it will be implemented using a separate processor or become part of the thinker system. This decision will require further investigation of the software design of the knowledge-based system, EXPERT-5 [7].

VI. RECOMMENDATIONS:

b. The idea and design of a coupled system opens up a new avenue for the application of knowledge-based systems in engineering and both the production and manufacturing environment. The application of such coupled systems is not limited to process control, but is useful in any engineering domain where deterministic knowledge can enhance the heuristic knowledge, or existing numerical-based programs can be augmented by symbolic computing. The actual implementation and details of the system proposed in this paper will be the work of my doctoral dissertation.

c. The design proposed here is based only on an initial short-term view of the problem. It is believed that as this research effort matures there will be a number of changes in the design and implementation. In addition, the details of the discovery system can not be determined until further study of the process is completed.

REFERENCES

1. LeClair, S. R., "Sensor Fusion: The Application of Artificial Intelligence Technology to Process Control," Proc. of 1986 Rochester Forth Conf., Univ. of Rochester, Rochester, N.Y., 11-14 June 1986, pp. 15-22.
2. Raulefs, P. and P. W. Thorndyke, "An Architecture For Heuristic Control of Real-Time Processes," to be published.
3. Kraus, T. W., "EXACT -- An Expert System: From Concept to Commercialization," Proc. of ISA/85, 1985, pp. 553-559.
4. Moore, R. L., Hawkinson, L. B., Knickerbocker, C. G., and L. M. Churchman, "A Real-Time Expert System For Process Control," Proc. of the First Conf. on AI Applications, 1984, pp. 569-576.
5. Kitzmiller, C. T., Kowalik, J. S., "Coupling Symbolic and Numeric Computing in Knowledge-Based Systems," AI Magazine, Summer, 1987, pp. 85-90.
6. Carbonell, J., et. al., Machine Learning: An Artificial Intelligence Approach, Palo Alto, CA, Tioga Publishing Co., 1983.

7. Park, Jack, "Toward the Development of a Real-Time Expert System," Proc. of 1986 Rochester Forth Conf., Univ. of Rochester, Rochester, N.Y., 1-14 June 1986, pp. 23-44.

1987 USAF-UES SUMMER FACULTY RESEARCH PROGRAM/
GRADUATE STUDENT SUMMER SUPPORT PROGRAM

Sponsored by the
AIR FORCE OFFICE OF SCIENTIFIC RESEARCH

Conducted by the
Universal Energy Systems, Inc.

FINAL REPORT

COMPUTER MODELING FOR SURFACE PROPERTIES OF CARBON FIBERS

Prepared by: Pretta L. VanDible
Academic Rank: Instructor
Department and University: Department of Chemical Engineering
Prairie View A & M University
Research Location: AFAL/MKBN
Edwards AFB
Edwards AFB, CA 93523-5000
USAF Researcher: Ismail K. Ismail
Date: 20 Sept 87
Contract No: F49620-85-C-0013

Computer Modeling for Surface Properties of Carbon Fibers

by

Pretta L. VanDible

ABSTRACT

Defining the structure of carbonaceous materials required extensive computer solutions of several mathematical models. Pressure vs volume experimental data was displayed graphically to observe the shape of the curve. The external surface area as well as the internal surface areas of macropores and mesopores was defined by the BET method. The solutions of the Dubinin-Polanyi and Dubinin-Astakhov equations gave the micropore surface area. The estimation of the shape of the pores was determined by solving a series of mathematical equations. The numerical solutions yielded average pore radius, Kelvin radius, adsorbed volume and surface area of the pore walls.

II. OBJECTIVES OF THE RESEARCH EFFORT

Determining the surface structure of carbon fibers requires both the solution of several mathematical models and the graphical representation of those solutions. Experimental data obtained by adsorption and desorption techniques can be used for numerical (and graphical) analysis. The computed data can then characterize the physical features of the materials. The task was too tedious to perform by calculator and the necessity to view graphs of computed data also complicated the procedure. It was essential that the arithmetic and graphical operations be combined to facilitate a smooth transfer of data from one function to another.

As a summer fellow, I was assigned the project of developing a computer model that would give a profile of the surface structure of carbon fibers. The computer program would estimate the surface areas of the materials using various mathematical models. The program would also utilize graphics software to plot raw data and calculated data sets. Finally, the model would determine volume, surface area and average radius of pores present in carbon fibers using existing mathematical models.

III.

a. Physical adsorption occurs when the surface of a material attracts the molecules of a gas. The van der Waals attraction is relatively weak, and the quantity of gas adsorbed increases with decreasing temperature. Adsorption measurements at low temperature can be used to calculate surface area and pore distribution of the material. The amount of gas adsorbed can be removed without varying temperature, and the desorption measurements are also applicable in surface structure calculations.

Three factors influence the volume of gas adsorbed per unit mass of carbon fiber. Inert gases are used so that the surface structure of the material is unaffected. Low temperatures are necessary in order to maximize the amount of gas adsorbed and prevent chemisorption. The equilibrium pressure is expressed in terms of relative pressure. Relative pressure is the ratio of equilibrium pressure to the saturation pressure of the adsorbing gas. Several adsorption measurements can be performed at constant temperature and varying pressures. If the volume adsorbed per unit mass is plotted against relative pressure, the graph is referred to as an adsorption isotherm.

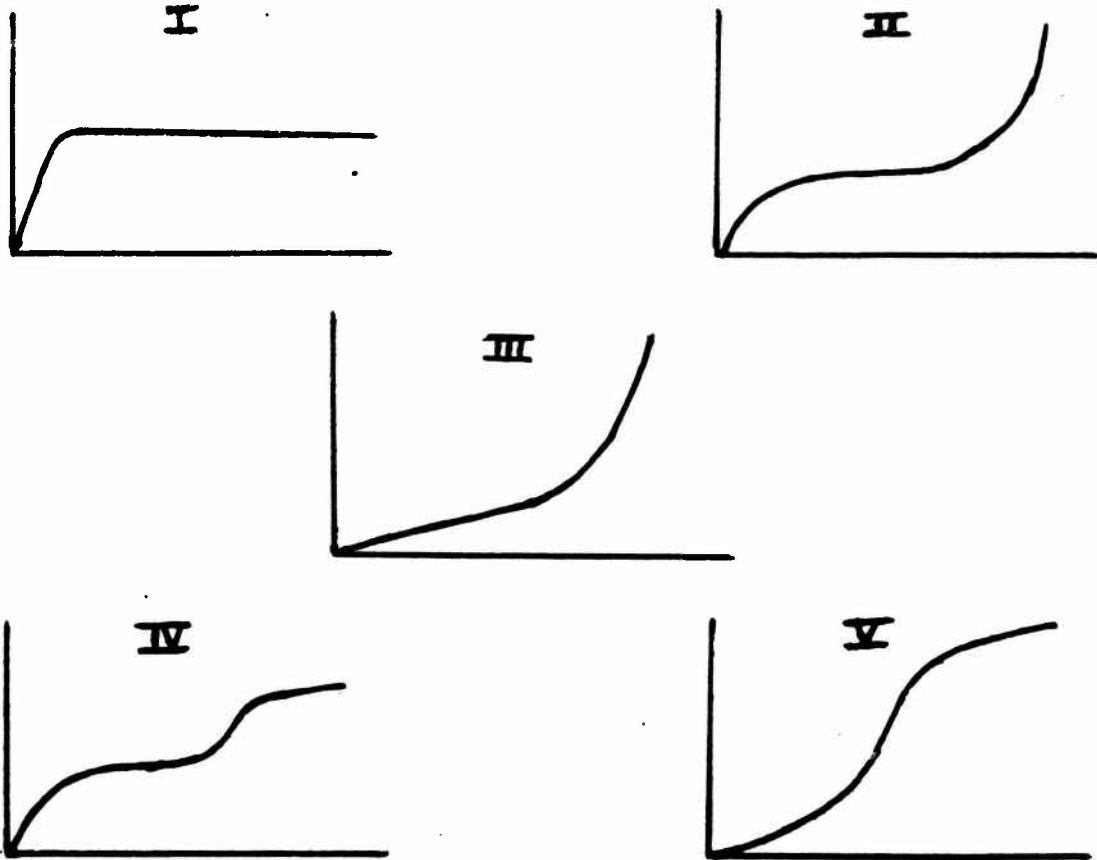
I. INTRODUCTION:

Gas adsorption is a powerful technique which can be utilized to investigate the structure of carbonaceous materials. Physical adsorption, known as Van der Waals adsorption, occurs when there is a weak attraction between molecules of a gas and the surface of a solid. The amount of gas adsorbed increases with decreasing temperature and low temperatures are ideal for adsorption measurements. Surface area and pore characteristics may be converted from the experimental data obtained through the application of this analytical technique.

Pores are classified by size and type. Micropores, less than 2 nm width, mesopores with a range of 2-50 nm and macropores having a width greater than 50 nm are all present in the surface structure. The internal surface area and volume of the pores must be determined in order to better define the structure of the carbon fiber. Non-reactive gases are instrumental in gathering raw data for the calculation of pore characteristics.

The extensive number of equations necessary in determining the physical aspects of the surface of carbon fibers required numerical solutions by computer. My background in fortran programming along with my interest in heterogeneous catalysis provided a suitable foundation for this research challenge. My knowledge of mathematical applications, chemical principles of catalysis and fortran computations analysis resulted in my assignment to the project.

There are five basic types of adsorption isotherm curves.



Type I isotherms are representative of gas adsorption for solids with microporous structures. The layer thickness of the gas is greater than one molecular diameter and the surface area cannot be mathematically determined. Types III and V depict solids that adsorb molecules more readily as adsorption proceeds. A continual increase in adsorption exceeds the monolayer thickness and the surface area for these solids is difficult to calculate. Both Type II and IV isotherms are graphs for solids when adsorption is carried out at low temperature with inert gases.

An isotherm resembling the Type II curve is a result of adsorption on a nonporous solid. Porous materials with varying pore diameters have adsorption curves resembling the Type IV isotherm. Carbon fibers have adsorption isotherms similar to Type II or Type IV curves.

b. The program is designed to read a filename given by the user, access the designated file and read the data set from the file. It was necessary to graph by computer method the experimental data of volume adsorbed V_a versus relative pressure P/P_o so that the plot could be observed. The type of isotherm can be determined by inspection. Any points not contributing to a smooth curve should be deleted.

IV.

a. Brunauer, Emmett and Teller developed an equation to determine the external surface area of a material based on monolayer thickness. Relative pressure P/P_o and volume adsorbed V_a are related by the BET equation

$$\frac{P}{V_a(P_o - P)} = \frac{1}{V_m C} + \frac{C-1}{V_m C} \left(\frac{P}{P_o} \right) \quad (1)$$

where V_m is the volume of gas adsorbed when a monolayer of

gas molecules cover the surface of the solid and C is a constant. The slope $C-1/V_m C$ and the intercept $1/V_m C$ can be determined from the linear portion of the graph and the values of C and V_m can be calculated. The inert gas nitrogen at an absolute temperature of 77 K is used in gathering experimental data for the BET solution. The mesopore area, with an aperture width of 2-50 nm, and the macropore area, diameter greater than 50 nm, are also defined using this equation. Krypton at liquid nitrogen temperature is useful in collecting data for the BET solution also.

The area of the micropores, less than 2 nm width, must also be obtained to complete the analysis of the total surface area of the carbon fiber. Carbon dioxide gas is utilized in the determination of micropore area. Dubinin and Polanyi reduces CO_2 experimental data according to the equation

$$\ln V_a = \ln V_o - (BT / \epsilon^2) [\ln P_o/P]^2 \quad (2)$$

where the monolayer capacity V_o is derived using the intercept from the plot of V_a versus P_o/P on a natural logarithmic scale. The coefficient ϵ describes the affinity of CO_2 relative to nitrogen, B is a constant and T is the absolute temperature of the gas.

The surface area of the micropores is determined by the equation

$$S = \frac{V_0(6.023 \times 10^{23}) \sigma}{22414 \text{ cc/g-mol}} \quad (3)$$

where σ is the molecular area of CO₂.

Dubinin and Astakhov can reduce the same pressure volume data but with slightly different assumptions. The D-A equation

$$\ln V_a = \ln V_0 - \left[\frac{RT}{E} \right]^n [\ln(P_0/P)]^n \quad (4)$$

uses the gas constant R to determine the characteristic free energy E in the slope $(RT/E)^n$. The value of the exponent n can be determined by iterative method. The micropore area is calculated by solving the equation previously mentioned.

b. The calculations for the BET area equation are written as functions for the program and each relative pressure is tested against the 0.3 constant to determine the points along the linear portion of the curve. The raw data set is tested to distinguish between nitrogen and carbon dioxide data sets. The Dubinin-Polanyi equation can be used with both sets of data but the Dubinin-Astakhov

equation is restricted to CO data. Linear regression² is written as a subroutine to allow access by all three equations for least squares analysis. Graphs for data obtained using each equation are displayed for the user's benefit.

V.

a. The internal surface area of pores does not adequately describe the pore structure. Other characteristics must be evaluated so that the total surface of the carbon material will be well defined. When a carbon fiber is porous, adsorbed molecular layers can be several diameters thick. For cylindrical pores, the fluid layer thickness is a function of relative pressure. Halsey and Wheeler, DeBoer, Harkins and Jura, Cranston, Inkley, Kankare and Jantti as well as Ismail have developed thickness equations based on experimental data. Either the Halsey Wheeler equation

$$t = 3.54 \left[\frac{-5}{\ln(P/P_0)} \right]^{0.33} A \quad (5)$$

the DeBoer, Harkins and Jura equation;

$$t = \left[\frac{13.99}{0.034 - \log(P/P_0)} \right]^{0.5} A \quad (6)$$

or the Cranston, Inkley, Kankare and Jantti equation

$$t = 6.1 - 2.47 [\ln (P_0/P)] A \quad (7)$$

can be used to calculate thickness for each relative pressure. The pore radius and the Kelvin radius describe the internal surface of the pore for any given relative pressure.

Both r_p and r_k are related by the equation

$$r_p = r_k + t \quad \text{expressed in } A \quad (8)$$

where Kelvin radius r_k is defined by the equation

$$r_k = \frac{-2 \gamma V_1 \cos \theta}{RT \ln (P_0/P)} \quad (9)$$

with γ defined as surface tension, V_1 is the molar volume of the gas, θ is the contact angle (assumed zero), R is the gas constant and T is the absolute temperature.

For liquid nitrogen at 77 K, the r_k equation reduces to

$$r_p = 0.415 / \ln(P_0/P) \quad (10)$$

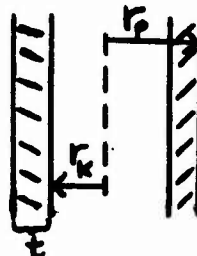
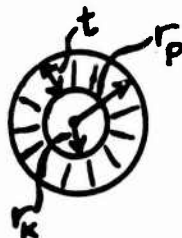
The molar volume of gas can be calculated using the equation

$$V_1 = \frac{34.6 V_a}{22.4 \times 10^3} = 1.54 \times 10^{-3} V_a \quad (11)$$

The actual pore volume V_p is defined by the relation

$$V_p = \frac{r_p^3}{r_k^3} \left[V_1 - (\Delta t \sum S) (10^{-4}) \right] \text{ cc} \quad (12)$$

where r_p and r_k represent the average pore radius and average Kelvin radius, Δt is the change in film depth, V_1 is the change in adsorbed liquid volume and $\sum S$ is the summation of the surface area of the pore walls.



The surface area of the pore walls, S , is calculated from the pore volume by the equation

$$S = \frac{2 V_p}{r_p} \times 10^4 \quad (13)$$

with the units of V_p in cc and r_p in Angstroms.

Slit shaped pores are analyzed using the desorption branch of the isotherm. In the pores, vapor and liquid is in

equilibrium and the Kelvin equation relates the radius of curvature τ of the surface of the liquid to its vapor pressure.

The radius of curvature for a liquid constricted between walls is given by

$$\tau = \frac{2\bar{V} \gamma \cos \theta}{RT \ln(P_0/P)} \quad (14)$$

For liquid nitrogen at 77 k, the molar volume \bar{V} is $34.68 \text{ cm}^3 \text{ mol}^{-1}$, angle θ is again zero and surface tension

$\gamma = 8.72 \times 10^{-3} \text{ Nm}^{-1}$. Substituting these values simplifies to

$$\tau = \frac{0.405}{\log(P_0/P)} \text{ nm} \quad (15)$$

It is assumed that the general adsorption isotherm relating t and P/P_0 is independent of diameter. This mathematical relationship is

$$\log(P_0/P) = 0.1399/t^2 - 0.034 \quad (16)$$

Taking into account that

$$\tau = d - 2t \quad (17)$$

is true when the Kelvin equation is applied, the pore

diameter d can be evaluated. The pore volume V_k is determined in a stepwise manner according to the equation

$$\Delta V_k = \frac{dk}{d - 2t_k - t_{k-1}} \left[\Delta X_k - (t_{k+1} - t_{k-1}) \sum_i A_i \right] \quad (18)$$

with ΔX_k as volume of desorbed liquid and $\sum_i A_i$ as the summation of the surface area of the pore for the i 'th step. The surface area is calculated by

$$\Delta V_k = d \Delta A_k / 2 \quad (19)$$

Cumulative values of V_k and A_k are obtained by successively subtracting ΔV_k and ΔA_k from total pore volume and total pore area, respectively.

b. The extensive number of equations given for thickness, cylindrical pore type and slit pore type required that each set of equations be grouped in a subroutine. The program following these comments is a complete computer code of the project.

NOTE: All computer code that designates plotting is preceded by the letter C.

VI. RECOMMENDATIONS:

a. Only two models for pore characteristics could be programmed. Models which examine other pore shapes need to be added to the computer code.

b. The graphics portion of the code can be expanded to include other pictorial details such as titles, scales and numerical values of data points. A graphics software package with greater flexibility is recommended.

c. With the limited capabilities of a PC, the program should be installed on a main frame and accessed by modem.

REFERENCES

1. Brunauer, S., Demming, L.S., Demming, W.E., and Teller, E., "On the Theory of van der Waals' Adsorption of Gases," J. Am. Chem. Soc. 62, 1940, pp. 1723-32.
2. Brunauer, S., Emmett, P.H., and Teller, E., "Adsorption of Gases in Multimolecular Layers," J. Am. Chem. Soc. 60, 1938, pp.309-319.
3. Cranston, R.W. and Inkley, F.A., "The Determination of Pore Structures from Nitrogen Adsorption Isotherms," Advances in Catalysis and Related Subjects Vol. 9, 1957.
4. Dollimore, D. and Heal, G.R. "Pore-Size Distribution in Typical Adsorbent Systems," J. Colloid & Interface Sci. 33, 1970, pp.508-19.
5. Halsey, G. "Physical Adsorption on Non-Uniform Surfaces," J. Chem. Phys. 16, 1948, pp.931-937.
6. Hanna, K.M., Odler, I., Brunauer, S., Hagymassy, J. and Bodor, E.E. "Pore Structure Analysis by Oxygen Adsorption I. t-Curves and Methods of Analysis," J. Colloid & Interface Sci. 45, 1973, pp.27-37.

7. Harkins, W.D. and Jura, G. "A Vapor Adsorption Method for the Determination of the Area of a Solid Without the Assumption of a Molecular Area, and the Areas Occupied by Nitrogen, and other Molecules on the Surface of a Solid," J. Am. Chem. Soc. 66, 1944, pp. 1366-1373.
8. Jelinek, Z.K. "Particle Size Analysis," New York, Halsted Press, 1970.
9. Kankare, J. and Jantti, O. "The Determination of Pore Structure from Physical Adsorption Isotherms Part II. Digital Computer Program," Soumen Kemistilehti_B 40, 1969, pp.51-53.

```

PROGRAM ISOTHERM
CHARACTER*64 FNAME,PNAME
CHARACTER*15 EQN,SLOPEQ
INTRINSIC ALOG,ABS
DIMENSION X(100),Y(100),VA(100),XI(100),T(100),XX(100),VAV(100)
DIMENSION RK(100),RP(100),ARK(100),ARP(100),AVA(100),DT(100),
* DVL(100),SUR(100),DTSUR(100)
DOUBLE PRECISION DELTAV(100),DELA(100),SUMA(100),SAVP(100),
* ADD(100),DVG(100),SUMVK(100),RADIUS(100)
DIMENSION MRSUM(100),TH(100),MXRAW(100),MYRAW(100),MX2RAW(100),
* MY2RAW(100),MXBET(100),MYBET(100),XIL(100),VAL(100),MXIL(100),
* MVAL(100),MXIL2(100),MVAL2(100),XIG(100),MXIG(100),MVALG(100)
DIMENSION VAL3(100),XIL3(100),XIL2(100),VAL2(100),MARP(100),
* MSUM(100),RARP(100),RSUM(100),MRP(100)
SAVE /X/,/XX/,/VAV/
WRITE(*,900)
900 FORMAT(' FILENAME PLEASE - ',\ )
READ(*,910)FNAME
910 FORMAT(A10)
OPEN(1,FILE=FNAME,STATUS='OLD')
OPEN(5,FILE=' ',STATUS='NEW')
READ(1,*)
READ(1,*)K,N
DO 9 I=1,N
9 READ(1,*)X(I),VA(I)
C WRITE(*,183)
C 183 FORMAT(' FOR THE RAW DATA PLOT ')
C CALL PLOTPREP(X,VA,N,MXRAW,MYRAW)
C CALL PLOTXY(MXRAW,MYRAW,N)
DO 7 I=1,N
IF(X(I) .GE. 1)GOTO 8
7 CONTINUE
WRITE (5,99)
99 FORMAT (8X,'P/Po',7X,'VOL ADS',5X,'P/V(Po-P)')
2 DO 10 I=1,N
IF(X(I) .GT. 0.25)GOTO 1000
Y(I)=ADS(X,VA,I)
WRITE (5,100)X(I),VA(I),Y(I)
100 FORMAT (3(3X,F9.4))
10 CONTINUE
1000 L = I - 1
IF(L .LT. 2)GOTO 41
C WRITE(*,283)
C 283 FORMAT(' FOR THE BET PLOT ')
C CALL PLOTPREP(X,Y,L,MXBET,MYBET)
C CALL PLOTXY(MXBET,MYBET,L)
CALL STDEV(X,Y,L,STDY,STDY,YCROSS,SLOPE)
WRITE (5,199)
199 FORMAT ('STD DEV FOR X AND Y,INTERCEPT AND SLOPE ARE AS FOLLOWS')
WRITE(5,200)STDY,STDY,YCROSS,SLOPE
200 FORMAT(2(3X,F10.4),2(5X,F10.4))
CALL MONOVOL(YCROSS,SLOPE,VM,C)
WRITE (5,940)VM,C
940 FORMAT ('MONOLAYER VOLUME = ',F8.4,2X,'CC/G C VALUE = ',F9.3)
WRITE (*,299)
299 FORMAT (' TYPE OF GAS? ',/, ' N2 --- 1',/, ' KR1 (0.195) --- 2',/,
* ' KR2 (0.210) --- 3 ',\ )
READ (*,300)KTYPE
300 FORMAT (I10)
BETAREA = AREA(KTYPE,VM)
WRITE (5,399)BETAREA
399 FORMAT (3X,'BET AREA IS - ',F11.6,2X,'M2/G')
GOTO 332
41 WRITE(*,42)
42 FORMAT(' NOT ENOUGH DATA POINTS TO CALCULATE STANDARD DEVIATION,
*SLOPE,INTERCEPT,MONOVOLUME LAYER AND BET')
332 CALL GN2KR(X,N,XI,TEMP)
CALL DP(N,XI,VA,TEMP,YIN,SLOPE,E)
893 WRITE(5,894)TEMP,YIN,SLOPE,E
894 FORMAT (2X,' TEMP = ',F5.0,2X,' Yin = ',F8.3,2X,' SLOPE = ',F9.5,
* 3X,' FREE ENERGY = ',F10.6)
WRITE(*,51)
51 FORMAT(' NEED D-A CALCULATIONS? - YES OR NO ',\ )
READ(*,799)EQN
799 FORMAT(A15)
IF (EQN .EQ. 'NO')GOTO 490
CALL DA(N,XI,VA,TEMP,YIN,Q,CORVAL,SLOPE,E)
922 WRITE(5,921)YIN,Q,CORVAL,SLOPE,E
921 FORMAT(' INTERCEPT = ',F9.4,' POWER VALUE = ',F3.1,/, ' SLOPE = '
*,F9.4,' FREE ENERGY = ',F12.5)
GOTO 490

```

```

      GOTO 490
      8 WRITE(*,129)
      129 FORMAT(' CO2 TEMP PLEASE? - ',/, ' 298 --- 1 ',/, ' 273 --- 2 ',
        */, ' 195 --- 3 ',/\)
      READ(*,*)KTEMP
      CALL CO2(KTEMP,X,N,XI,TEMP)
C
C   DO 3 I=1,N
C   3 XIL(I) = 1.0/XI(I)
C   WRITE(*,383)
C   383 FORMAT(' FOR THE RAW DATA PLOT ')
C   CALL PLOTPREP(XIL,VA,N,MXIL,MVAL)
C   CALL PLOTXY(MXIL,MVAL,N)
C   WRITE(*,943)
C   943 FORMAT(' ANY POINTS TO DELETE? (YES OR NO) - ',/\)
C   READ(*,*)EQN
C   IF(EQN.EQ.'NO')GOTO 824
C   CALL DELETE(XIL,VA,N,XIL2,VAL2,K)
C   IF(K.EQ.0)GOTO 698
C   WRITE(*,483)
C   483 FORMAT(' FOR THE REVISED RAW DATA PLOT ')
C   CALL PLOTPREP(XIL2,VAL2,K,MXIL2,MVAL2)
C   CALL PLOTXY(MXIL2,MVAL2,K)
C   824 CALL DP(N,XI,VA,TEMP,YIN,SLOPE,E)
      WRITE(S,347)
      347 FORMAT(' THE D-P CALCULATIONS ARE AS FOLLOWS ')
      898 WRITE(S,899)TEMP,YIN,SLOPE,E
      899 FORMAT(2X,' TEMP = ',F5.0,2X,' Yin = ',F8.3,2X,' SLOPE = ',F9.5,
        *3X,' FREE ENERGY = ',F10.6)
      CALL COAREA(YIN,C1,C2,C3)
      WRITE(S,454)C1,C2,C3
      454 FORMAT(' SURFACE AREA FOR CO2 CONSTANTS: ',/, ' P = 0.170',3X,
        *' C = ',F11.5,/, ' P = 0.190',3X, ' C = ',F11.5,/, ' P = 0.253',
        *3X, ' C = ',F11.5)
      698 CALL DA(N,XI,VA,TEMP,YIN,Q,CORVAL,SLOPE,E)
      WRITE(S,357)
      357 FORMAT(/' THE D-A CALCULATIONS ARE AS FOLLOWS ')
      902 WRITE(S,901)YIN,Q,CORVAL,SLOPE,E
      901 FORMAT(' INTERCEPT = ',F9.4,' POWER VALUE = ',F3.1,/, ' SLOPE = ',
        *F9.4,' FREE ENERGY = ',F12.5)
      CALL COAREA(YIN,C1,C2,C3)
      WRITE(S,454)C1,C2,C3
      DO 34 I=1,N
      VAL(I) = ALOG(VA(I)*100) - 2.0
      34 XIQ(I) = (ALOG(XI(I)))*Q
C
C   WRITE(*,583)
C   583 FORMAT(' FOR THE D-A PLOT ')
C   CALL PLOTPREP(XIQ,VAL,N,MXIQ,MVALQ)
C   CALL PLOTXY(MXIQ,MVALQ,N)
C   CALL RUNAVG(X,VA,N,XX,VAV,M)
      GOTO 2001
      490 WRITE (*,101)
      101 FORMAT(' CHOOSE THICKNESS EQN ',/,2X,' 1 --- 3.54(1.8777/(-8.77E
        *-3 - Ln P/Po))*0.5',/,2X,' 2 --- 3.54(1.1359/(1.41E-3 - Ln P/Po)
        *)**0.5',/,2X,' 3 --- 3.54(2.6732/(-2.0E-2 - Ln P/Po))*0.5',/,2X,
        *' 4 --- (13.99/(3.4E-2 - Log P/Po))*0.5',/,2X,' 5 --- 3.54(
        *-5.0/Ln P/Po))*0.33',/,2X,' 6 --- 6.1 - (2.47*Ln Po/P)',/,2X,
        *' 7 --- NONE',/,/\)
      READ(*,*)L
      IF(L.EQ.7)GOTO 491
      CALL THICK(XI,N,L,T)
      WRITE(S,629)L
      629 FORMAT(/' THICKNESS EQUATION NO. ',I3,/,5X,' Rp ':,2X,' Vp',10X,' Cum
        * Vp',12X,' SA',10X,' Cum SA')
      CALL CYLINDER(N,T,VA,XI,TEMP,RK,RP,ARK,ARP,AVP,DT,DVL,DVG,DTSUR,
        *ADD,SUR)
C
C   WRITE(*,683)
C   683 FORMAT(' THE AVG PORE RADIUS/CUMULATIVE SURFACE AREA PLOT ')
C   CALL PLOTPREP(ARP,ADD,K,MARP,MSUM)
C   CALL PLOTXY(MARP,MSUM,K)
C   CALL RUNAVG(ARP,ADD,K,RARP,RSUM,J)
C   WRITE(*,783)
C   783 FORMAT(' THE CURVE SMOOTHING FOR AVG RP/CUM SURFACE AREA ')
C   CALL PLOTPREP(RARP,RSUM,J,MRP,MRSUM)
C   CALL PLOTXY(MRP,MRSUM,K)
      GOTO 490
C   491 WRITE(S,493)
C   493 FORMAT(/' SLIT PORE CALCULATIONS ',/,5X,' Dp',12X,' Vp',10X,' Cum Vp'
C   *,12X,' SA',10X,' Cum SA')
      491 CALL SLIT(XI,X,VA,N,RADIUS,DELTA,DELTA,DELTA,SUMV,DELA,SUMA)
      2001 STOP
      END

```

```

SUBROUTINE MONOVOL(YINCPT,RSERUN,VOL,D)
IF(YINCPT.GT. 1.0E-6)GOTO 5
YINCPT = 0.0
5 Q = 1/(YINCPT + RSERUN)
VOL = Q
IF (YINCPT.LT. 1.0E-6)GOTO 2
D = (RSERUN/YINCPT) + 1
RETURN
2 D = 99999.0
RETURN
END
SUBROUTINE GN2KR(A,K,AA,T)
DIMENSION A(K),AA(K)
DO 1 I=1,K
1 AA(I) = 1/A(I)
T = 77.0
RETURN
END

FUNCTION ENERGY(SLOPES,TEMPR)
R = 0.00198
ENERGY = (2.303*R+TEMPR)/EXP(SLOPES)
RETURN
END
FUNCTION RVAL(A2,AA2,M)
DIMENSION A2(M),AA2(M)
INTRINSIC SORT
ASUM = 0.0
AASUM = 0.0
ASUM1=0.0
ASUM2=0.0
DO 5 I=1,M
ASUM1 = ASUM1 + A2(I)**2
ASUM2 = ASUM2 + AA2(I)**2
ASUM = ASUM + A2(I)
AASUM = AASUM + AA2(I)
5 CONTINUE
XYSUM = 0.0
DO 6 I=1,M
6 XYSUM = (A2(I)+AA2(I)) + XYSUM
QP = XYSUM - ((1/M)*ASUM+AASUM)
QR = ASUM1 - ((1/M)*(ASUM**2))
QS = ASUM2 - ((1/M)*(AASUM**2))
RVAL = QP/SORT(QR+QS)
RETURN
END
SUBROUTINE ERROR(Z,R,YOVRX,I,CORMAX,PT,SLP)
DIMENSION Z(100),R(100),YOVRX(100)
IF (ABS(Z(I-1)) .LT. ABS(Z(I)))GOTO 2
CALL SORT(R,I)
CALL SORT(YOVRX,I)
CALL SORT(Z,I)
2 PT = R(I)
SLP = YOVRX(I)
CORMAX = Z(I)
RETURN
END
SUBROUTINE SORT(U,K)
DIMENSION U(K)
HOLD = U(K-1)
U(K-1) = U(K)
U(K) = HOLD.
RETURN
END
SUBROUTINE CO2(KTEMP,A,K,AA,T)
DIMENSION A(K),AA(K)
GOTO(20,30,40),KTEMP
20 P=48250.0
T = 298.0
GOTO 5
30 P=26142.0
T = 273.0
GOTO 5
40 P=793.0
T = 195.0
5 DO 50 I=1,K
AA(I)=P/A(I)
50 CONTINUE
RETURN
END

```

```

FUNCTION ADS(A,B,I)
DIMENSION A(I),B(I)
ADS = A(I)/(B(I)*(1-A(I)))
RETURN
END
SUBROUTINE STDEV(P,Q,K,STDP,STDQ,A,B)
DIMENSION P(K),Q(K)
SUMP=0.0
SUMQ=0.0
DO 50 I=1,K
SUMP=SUMP+P(I)
SUMQ=SUMQ+Q(I)
50 CONTINUE
AVGP=SUMP/K
AVGQ=SUMQ/K
DIFF=0.0
DIFQ=0.0
BSUM=0.0
DO 60 I=1,K
DIFF=DIFF+((P(I) - AVGP)**2)
DIFQ=DIFQ+((Q(I) - AVGQ)**2)
BSUM=BSUM + ((P(I) - AVGP)*(Q(I) - AVGQ))
60 CONTINUE
VARP=DIFF/(K-1)
VARQ=DIFQ/(K-1)
STDP=SQRT(VARP)
STDQ=SQRT(VARQ)
B=BSUM/DIFF
A=AVGQ-(B*AVGP)
RETURN
END
FUNCTION AREA(KGUESS,VOL)
GOTO(10,20,30),KGUESS
10 P = 0.162E-18
GOTO 40
20 P = 0.195E-18
GOTO 40
30 P = 0.210E-18
40 AVO = 6.02E25
V = VOL/22414.0
AREA = V * AVO * P
RETURN
END
SUBROUTINE DP(N,X1,VA,TEMP,YCEPT,RSERUN,E)
DIMENSION XI(N),VA(N),X2(100),VA2(100),X3(100)
DO 5 I = 1,N
X2(I) = ALOG(XI(I))
VA2(I) = ALOG(VA(I))
X2(I) = X2(I)**2
5 CONTINUE
CALL STDEV(X2,VA2,N,STD X2,STDVA2,YCEPT,RSERUN)
E = ENERGY(RSERUN,TEMP)
RETURN
END
SUBROUTINE DA(N,X2,VA2,TEMP,YCEPT,PTMAX,RVMAX,SLP MAX,E)
DIMENSION X2(N),VA2(N),X3(100),P(99),RS(99),RV(99),VA3(99)
W = 1.0
DO 1 K=1,50
P(K) = W
DO 9 I = 1,N
X3(I) = ALOG(X2(I))
VA3(I) = ALOG(VA2(I))
X3(I) = X3(I)**P(K)
9 CONTINUE
CALL STDEV(X3,VA3,N,STD X3,STDVA3,YCEPT,RSERUN)
RS(K)=R SERUN
RV(K)=RVAL(X3,VA3,N)
WRITE (5,10)P(K),RV(K)
10 FORMAT(' THE CORRELATION COEFFICIENT FOR P VALUE ',F3.1,3X,' IS ',
1F10.4)
CALL ERROR(RV,P,RS,K,RVMAX,PTMAX,SLP MAX)
11 W = W + 0.1
IF ( W .GT. 3.0 )GOTO 15
1 CONTINUE
15 WRITE (5,12)PTMAX,RVMAX,SLP MAX
12 FORMAT(' OPTIMUM PARAMETERS ARE: P = ',F4.1,2X,' RVALUE = ',F7.4,
12X,' SLOPE = ',F9.4)
E = ENERGY(SLP MAX,TEMP)
RETURN
END

```

```

SUBROUTINE CYLINDER(K,AT,AVA,AXI,TEMP,ARK,ARP,AVRK,AVRP,AVP,
1 DAT,DAVL,SAVP,DELTS,SUM,S)
DIMENSION AT(100),AVA(100),AXI(100),ARP(100),P(100),Q(100)
2,AVRP(100),DAVA(100),DAT(100),AVRK(100),ARK(100)
DOUBLE PRECISION DAVL(100),AVP(100),DELTS(100),S(100),
*SAVP(100),SUM(100)
SAVE /AVA/,/AXI/,/AT/
CALL DESCEND(AVA,AXI,AT,K)
DO 10 I=1,K
P(I) = ALOG10(AXI(I))
Q(I) = 1.0/P(I)
ARK(I) = 4.15*Q(I)
ARP(I) = ARK(I) + AT(I)
10 CONTINUE
DO 20 I=1,K-1
AVRK(I) = AVG(ARK,I)
AVRP(I) = AVG(ARP,I)
DAVA(I) = DELTA(AVA,I)
DAT(I) = DELTA(AT,I)
20 CONTINUE
DO 30 I=1,K-1
DAVL(I) = DAVA(I)*1.54E-3
30 CONTINUE
SUMS = 0.0
DELTS(1) = 0.0
SAV = 0.0
DO 40 I=1,K-1
AVP(I) = ((AVRP(I)/AVRK(I))**2)*(DAVL(I) - (DELTS(I)*1E-4))
S(I) = (20000.*AVP(I))/AVRP(I)
SUMS = SUMS + S(I)
SUM(I) = SUMS
SAV = SAV + AVP(I)
SAVP(I) = SAV
IF(I .EQ. K-1)GOTO 40
DELTS(I+1) = (DAT(I+1)*1E-10)*SUM(I)
40 CONTINUE
DO 36 I=1,K-1
WRITE(5,627)AVRP(I),AVP(I),SAVP(I),S(I),SUM(I)
627 FORMAT(2X,F8.3,4(3X,D13.6))
36 CONTINUE
RETURN
END
FUNCTION AVG(D,K)
DIMENSION D(K)
AVG = (D(K) + D(K+1))/2
RETURN
END
FUNCTION DELTA(E,K)
DIMENSION E(K)
DELTA = E(K) - E(K+1)
RETURN
END
SUBROUTINE DESCEND(A,B,C,N)
DIMENSION A(N),B(N),C(N)
KASS = N+1
DO 5 L=1,N
K = KASS-L
DO 6 J=2,K
IF( A(J) .LT. A(J-1))GOTO 6
CALL SORT(A,J)
CALL SORT(B,J)
CALL SORT(C,J)
6 CONTINUE
5 CONTINUE
RETURN
END
SUBROUTINE RUNAVG(P,Q,K,R,S,J)
DIMENSION P(K),Q(K),R(K),S(K)
J=K-2
DO 10 I=1,J
R(I) = (P(I) + P(I+1) + P(I+2))/3
S(I) = (Q(I) + Q(I+1) + P(I+2))/3
10 CONTINUE
RETURN
END

```

```

SUBROUTINE SLIT(XA,X,Y,K,DK,DELV,SUMVK,A,DELA)
DIMENSION X(K),Y(K),P(99),Q(99),QP(99),XA(K)
DOUBLE PRECISION TAU(99),T(99),DELV(99),A(99),DELA(99),
1TAUK(99),HT(99),DK(99),PK(99),V(99),AA(99),DY(99),TP(99),
2SUMVK(100),R(99),D(99)
REAL*8 DEL
CALL DESCEND(Y,X,XA,K)
DO 5 I=1,K
5 P(I)=ALOG10(XA(I))
DO 10 I=1,K
TAU(I) = 0.405/P(I)
T(I) = SQRT(0.1399/(P(I)+0.034))
D(I) = TAU(I) + (2*T(I))
R(I) = 1.548E-3 * Y(I)
10 CONTINUE
DO 15 I=1,K-1
QP(I) = AVG(X,I)
PK(I) = ALOG10(1.0/QP(I))
TAUK(I) = 0.405/PK(I)
TP(I) = SQRT(0.1399/(PK(I)+0.034))
DK(I) = TAUK(I) + (2.0*TP(I))
15 CONTINUE
DELA(1)=0.0
SUMVK(1)=0.0
DO 30 J=1,K-1
DY(J) = DEL(R,J)*1.0E-6
HT(J) = DEL(T,J)
WRITE(5,92)DY(J),HT(J)
92 FORMAT(2X,D14.6,2X,D14.6)
30 CONTINUE
DO 20 J=1,K-1
DELV(J) =(DK(J)/(DK(J)-(2.0*T(J+1))))*(DY(J)-(HT(J)+DELA(J)))
SUMVK(J+1) = SUMVK(J) + DELV(J)
A(J) = (2.0*DELV(J))/DK(J)
DELA(J+1) = DELA(J) + A(J)
20 CONTINUE
V(1) = SUMVK(K-1)
AA(1) = DELA(K)
DO 25 J=2,K
V(J) = V(J-1) - DELV(J-1)
AA(J) = AA(J-1) - A(J-1)
25 CONTINUE
DO 35 I=1,K-1
WRITE(5,31)DK(I),DELV(I),SUMVK(I),A(I),DELA(I)
31 FORMAT(2X,D10.5,4(3X,D13.6))
35 CONTINUE
RETURN
END
REAL*8 FUNCTION DEL(Q,K)
DOUBLE PRECISION Q(100)
DEL = Q(K) - Q(K+1)
RETURN
END
SUBROUTINE THICK(XI,K,L,T)
DIMENSION XI(K),T(K),P(100)
DO 11 I=1,K
11 P(I) = 1/XI(I)
GOTO(1,2,3,4,5,6),L
1 DO 10 I=1,K
10 T(I) = 3.54*SQRT(1.8777/((-0.00877)-ALOG(P(I))))
RETURN
2 DO 20 I=1,K
20 T(I) = 3.54*SQRT(1.1359/(0.00141-ALOG(P(I))))
RETURN
3 DO 30 I=1,K
30 T(I) = 3.54*SQRT(2.6732/((-0.020)-ALOG(P(I))))
RETURN
4 DO 40 I=1,K
40 T(I) = SQRT(13.99/(0.034-ALOG10(P(I))))
RETURN
5 DO 50 I=1,K
50 T(I) = 3.54*(((5.0)/ALOG(P(I)))*0.33)
RETURN
6 DO 60 I=1,K
60 T(I) = 6.1-(2.47*ALOG(XI(I)))
RETURN
END

```

```

SUBROUTINE DELETE (ARRAYA, ARRAYB, M, ARRAY1, ARRAY2, J)
DIMENSION ARRAYA (M), ARRAYB (M), ARRAY1 (100), ARRAY2 (100)
DIMENSION IDEL (100)
WRITE (*, 1)
1  FORMAT (' POINTS TO DELETE - ', \)
   READ (*, *) N
   DO 10 K=1, N
   WRITE (*, 2)
2  FORMAT (' ENTER POINT NUMBER AND HIT RETURN - ', \)
   READ (*, *) L
   ARRAYA (L) = 0.0
   ARRAYB (L) = 0.0
   IDEL (K) = L
10  CONTINUE
   J = 0
   DO 20 I=1, M
   IF (ARRAYA (I) .NE. 0.0 .OR. ARRAYB (I) .NE. 0.0) THEN
   J = J + 1
   ARRAY1 (J) = ARRAYA (I)
   ARRAY2 (J) = ARRAYB (I)
   ENDIF
20  CONTINUE
   DO 30 I=1, M
30  WRITE (5, 4) ARRAYA (I), ARRAYB (I)
4  FORMAT (2(2X.F15.6))
   DO 40 I=1, M-N
40  WRITE (5, 5) ARRAY1 (I), ARRAY2 (I)
5  FORMAT (2(3X.F15.6))
   RETURN
   END

SUBROUTINE PLOTPREP (XA, YA, N, MX, MY)
INTEGER X, Y, X1, Y1
DIMENSION XA (N), YA (N), MX (N), MY (N)
X=130
Y=310
X1=640
Y1=50
DO 30 I=1, N
   IF (I .LT. 2) GOTO 30
   XMIN = ZMIN (XA, I)
   YMIN = ZMIN (YA, I)
30  CONTINUE
   DO 40 I=1, N
   IF (I .LT. 2) GOTO 40
   XMAX = ZMAX (XA, I)
   YMAX = ZMAX (YA, I)
40  CONTINUE
   WRITE (*, 7) XMIN, YMIN, XMAX, YMAX
7  FORMAT (' THE MINIMUM VALUES: X = ', F11.4, 2X, ' Y = ', F11.4, /,
* ' THE MAXIMUM VALUES: X = ', F11.4, 2X, ' Y = ', F11.4)
   WRITE (*, 8)
8  FORMAT (' REDEFINE MIN AND MAX VALUES FOR X (REAL # ONLY) ', \)
   READ (*, *) XIN, XAX
   WRITE (*, 9)
9  FORMAT (' REDEFINE MIN AND MAX VALUES FOR Y (REAL # ONLY) ', \)
   READ (*, *) YIN, YAX
   DO 20 I=1, N
   XSCR = SCREEN (I, XA, XIN, XAX, X1, X)
   YSCR = SCREEN (I, YA, YIN, YAX, Y, Y1)
   MX (I) = X + XSCR
   MY (I) = Y - YSCR
20  CONTINUE
   RETURN
   END

```

```

SUBROUTINE PLOTXY(AA,AB,N)
DIMENSION AA(N),AB(N)
EXTERNAL GMODE,CLRSCR,GPAGE,DLINE,PUTPT,PLOT,TMODE
INTEGER A,B,A1,B1,AA,AB
A=130
B=310
A1=640
B1=50
CALL GMODE
CALL CLRSCR
BUFFPAGE=1
CALL GPAGE(BUFFPAGE)
CALL PUTPT(A,B)
CALL DLINE(A1,B)
CALL DLINE(A1,B1)
CALL DLINE(A,B)
CALL DLINE(A,B)
CALL PUTPT(A,B)
CALL PUCMARK(A,B,A1,B1)
MSG='*'
LEN=1
DO 1 I=1,N
CALL PUTPT(AA(I),AB(I))
CALL PLOT(AA(I),AB(I))
CALL TEXTF(AA(I),AB(I),LEN,MSG)
1 CONTINUE
READ(*,*)ANSWER
CALL TMODE
RETURN
END
FUNCTION ZMIN(A,I)
DIMENSION A(I)
IF(A(I) .LT. A(I-1))GOTO 1
CALL SORT(A,I)
1 ZMIN = A(I)
RETURN
END
FUNCTION ZMAX(A,I)
DIMENSION A(I)
IF(A(I) .GT. A(I-1))GOTO 1
CALL SORT(A,I)
1 ZMAX = A(I)
RETURN
END
FUNCTION SCREEN(I,AA,AMIN,AMAX,I.B,I.C)
DIMENSION AA(I)
RANGE = AMAX-AMIN
SCREEN = ((AA(I)-AMIN)/RANGE) - (I B-I C)
RETURN
END
SUBROUTINE PUCMARK(A,B,A1,B1)
INTEGER A,B,A1,B1
M = (A1 - A)/4
LEN = 1
MSG = '*'
DO 1 I = A,A1,M
CALL PUTPT(I,B)
CALL TEXTF(I,B,LEN,MSG)
1 CONTINUE
L = (B - B1)/4
MSG = '---'
LEN = 2
DO 2 I = B1,B1,L
CALL PUTPT(A,I)
CALL TEXTF(A,I,LEN,MSG)
2 CONTINUE
RETURN
END
SUBROUTINE COAREA(VOL,C1,C2,C3)
P = 0.17E-18
C1 = CAREA(P,VOL)
Q = 0.19E-18
C2 = CAREA(Q,VOL)
R = 0.253E-18
C3 = CAREA(R,VOL)
RETURN
END
FUNCTION CAREA(A,VP)
AVO = 6.02E23
V = EXP(VP)/22414.0
CAREA = A*V*AVO
RETURN
END

```

1987 USAF-UES SUMMER FACULTY RESEARCH PROGRAM/
GRADUATE STUDENT SUMMER SUPPORT PROGRAM.

Sponsored by the
AIR FORCE OFFICE OF SCIENTIFIC RESEARCH

Conducted by the
Universal Energy Systems, Inc.

FINAL REPORT

An Advanced Vision System Testbed

Prepared by: Robert G. Trenary, Ph.D.
Louis A. Tamburino, Ph.D.
and William VanValkenburg

Academic Rank: Assistant Professor

Department and University: Computer Science Department,
Western Michigan University

Research Location: AFWAL System Avionics Division/AAAT-3
Wright-Patterson AFB
Dayton, OH 45433

USAF Researcher: Louis A. Tamburino, Ph.D.

Date: September 4, 1987

Contract No: F49620-85-C-0013

REFERENCE DR. TRENARY
SFRP FINAL REPORT NUMBER 125

1987 USAF-UES SUMMER FACULTY RESEARCH PROGRAM/
GRADUATE STUDENT SUMMER SUPPORT PROGRAM

Sponsored by the
AIR FORCE OFFICE OF SCIENTIFIC RESEARCH

Conducted by the
Universal Energy Systems, Inc.

FINAL REPORT

Numerical Calculations of Dopant Diffusion
involving flashlamp heat: g of silicon

Prepared by: Joseph C. Varga
Academic Rank: Research Assistant
Department and Department of Physics
University: Kent State University
Research Location: Wright-Patterson Air Force Base
Air Force Wright Aeronautical Laboratories
Materials Laboratory, Electromagnetic
Materials Division, Laser and Optical
Materials Branch
USAF Researcher Dr. Patrick M. Hemenger
Date: Sept. 30, 1987
Contract No: F49620-85-C-0013

Numerical Calculations of Dopant Diffusion
involving flashlamp heating of silicon

by
Joseph C. Varga

ABSTRACT

Work was begun on finding a solution to the flashlamp heating of a doped semiconductor. A Blackbody spectrum was assumed for the incident radiation. Also, the absorption coefficient was assumed to follow a Lorentzian lineshape. Finite difference techniques were used. The diffusion of dopant through a semiconductor was calculated. A comparison was made between an analytical solution and numerical calculation. The results agreed to within 0.002%.

ACKNOWLEDGEMENTS

The author would like to thank the Air Force Systems Command, the Air Force Office of Scientific Research, and the Materials laboratory, AFWAL for the support and for providing an opportunity to spent a very rewarding summer at the Materials Laboratory, Wright-Patterson AFB, Ohio.

He would also like to thank Dr. Patrick M. Hemenger and Dr. David S. Moroi for suggesting this area of research, and for their collaboration and guidance. He is very grateful to Lt. Craig Stice, Lt. Greg Piesert, and Mr. Jeff Fox for their valuable assistance in the use of the computer facilities.

I. Introduction

Dr. D. S. Moroi, from Kent State, has been doing research at the Materials Laboratory as a visiting scientist. I have been working on by Ph.D at Kent State University. It was at the suggestion of Dr. Moroi that I became involved with the project. As part of my research, I have done extensive computer modeling using various numerical methods. Also, as part of my engineering background, I have worked with the finite difference technique.

The thermal diffusion equation is usually solved by means of a finite difference calculation. Because of my previous experience with numerical methods on the computer, I was approached to work on the flashlamp heating problem at the Materials laboratory.

II. OBJECTIVES OF THE RESEARCH EFFORT:

1. Using finite difference techniques, solve the nonlinear heat conduction equation with a source term appropriate to a flashlamp heating of doped GaAs or Si wafer, and obtain the temperature profile.
2. Determine the precision of the numerical methods used.
3. Compare the numerical calculations with an analytical solution of the dopant diffusion equation being worked out by Dr. Moroi.

III. THERMAL DIFFUSION

Numerical finite difference techniques were applied to the thermal diffusion equation given by

$$\rho c \frac{\partial T}{\partial t} = \frac{\partial}{\partial z} \left(K \frac{\partial T}{\partial z} \right) + \alpha I (1-R) \quad (1)$$

The intensity (I) was assumed to follow the Blackbody radiation law:

$$I = I_0 \frac{1}{\lambda^5} \left(e^{hc/\lambda T} - 1 \right)^{-1} \quad (2)$$

where $T = 5500K$

The absorption coefficient was assumed to follow a Lorentzian distribution:

$$\alpha = \alpha_0 \frac{\Gamma/2}{(\omega - \omega_0)^2 + (\Gamma/2)^2} \quad \text{and} \quad \omega = \frac{2\pi c}{\lambda} \quad (3)$$

Because the intensity of the incident radiation was much lower than in laser annealing, the incident energy had more time to diffuse into the semiconductor. It was thus necessary to go a moderate distance into the substrate to map the temperature profile. Because of the large size of the mesh points, all of the incident radiation was absorbed in the outermost cell of the mesh. This caused stability problems. Although there is a stability criterion that must be met, this criterion alone is not enough. The extra energy being absorbed in the outer cell, but not the one next to it, caused the solution to be unstable. Further work needs to be done to eliminate this problem.

IV. DOPANT DIFFUSION

The dopant diffusion equation is given by:

$$\frac{\partial C}{\partial t} = \frac{\partial}{\partial z} \left(D \frac{\partial C}{\partial z} \right) \quad (4)$$

where D is the dopant diffusion coefficient and C is the concentration.

The function^{1,2}

$$G(z, t) = \frac{1}{2 \sqrt{\pi D t}} \exp \left(-\frac{(z - z_0)^2}{4 D t} \right) \quad (5)$$

is the fundamental solution or the Green's function for the diffusion equation. Physically, the Green's function represents the concentration at a point z at time t due to a unit source at a point z_0 at time zero.

In order to check out the numerical accuracy of the finite difference method, it was necessary to find a problem that had a simple analytical solution. The simplest case occurs when the initial dopant distribution has a gaussian shape. To match the boundary condition of a zero gradient at the surface, it was necessary to consider a unit source inside the substrate and its image source outside the surface. The initial concentration assumed the form:

$$C = C_m \left[\exp \left(-\frac{(z - z_0)^2}{2 s_0^2} \right) + \exp \left(-\frac{(z + z_0)^2}{2 s_0^2} \right) \right] \quad (6)$$

The analytic solution to this problem is just the superposition of two Green's functions:

$$C = \frac{K}{2\sqrt{\pi D(t+t_0)}} \left[\exp\left(\frac{-(Z-Z_0)^2}{4D(t+t_0)}\right) + \exp\left(\frac{-(Z+Z_0)^2}{4D(t+t_0)}\right) \right] \quad (7)$$

Comparing coefficients, it is seen that

$$t_0 = \frac{S_0^2}{2D} \quad K = 2 C_0 S_0 \sqrt{\frac{\pi}{2}} \quad (8)$$

When this analytical solution was compared with the numerical finite difference solution, the two agreed to better than 0.002% for the case of a mesh of 512 points. It was necessary to make this comparison because some other numerical calculations were showing some differences with the analytical results of Dr. Moroi. Figure 1 shows the results of the calculation, and Table 1 gives the relative errors.

VI. RECOMMENDATIONS

1. An analytical solution to the flashlamp heating is still needed.

It is important that this work continue. When it does become available, it will be necessary to compare the analytical result with a finite difference calculation to confirm its accuracy.

2. In the finite difference approach the the flashlamp heating, stability turned out to be a problem. It will be necessary to try a different approach to the boundary condition at the surface in the hope of eliminating the instability.

Table 1. Relative error of finite difference calculation.

distance	analytical	numerical	relative error (%)
0.0	.54227	.54225	.00227
6.0	.63583	.63583	-.00014
12.0	.68309	.68311	-.00158
18.0	.46802	.46802	.00033
24.0	.18881	.18879	.00281
30.0	.04431	.04431	-.00001
36.0	.00604	.00604	-.01743

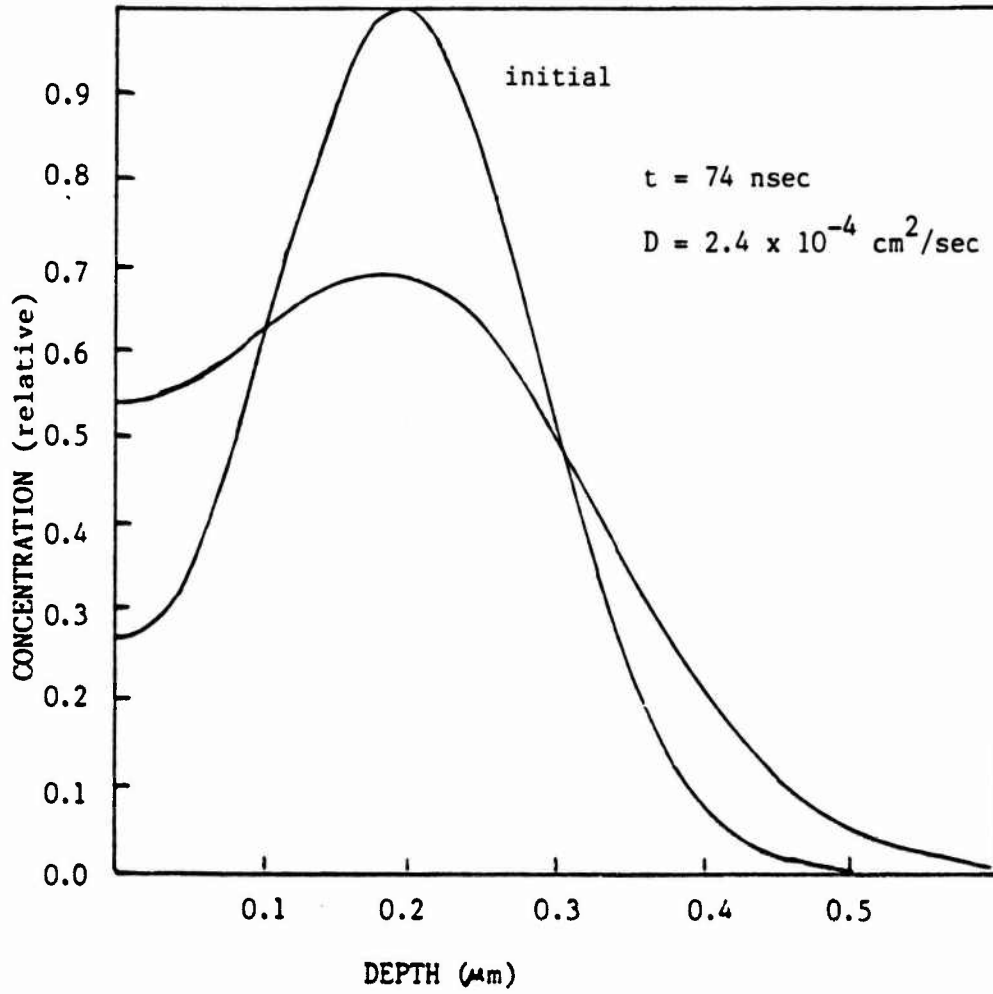


Fig 1. Initial and final dopant distribution

REFERENCES

1. E. C. Young, Partial Differential Equations, (Allyn and Bacon, 1972).
2. J. Crank, The Mathematics of Diffusion, (Clarendon, Oxford, 1956).

1987 USAF-UES SUMMER FACULTY RESEARCH PROGRAM/
GRADUATE STUDENT SUMMER SUPPORT PROGRAM

Sponsored by the
AIR FORCE OFFICE OF SCIENTIFIC RESEARCH

Conducted by
UNIVERSAL ENERGY SYSTEMS, INC.

FINAL REPORT

Scanning Electron Microscopy of PBO, PBT, and
Kevlar Fiber

Prepared By:	Deborah L. Vezie
Academic Rank:	Graduate Student
Department and University:	Chemical, Bio, and Materials Eng. Arizona State University
Research Location:	AFWAL/MLBP
USAF Researcher:	Dr. Wade Adams
Date:	10 September 1987
Contract No.:	F49620-85-C-0013

Scanning Electron Microscopy of PBO, PBT, and Kevlar Fiber

by

Deborah L. Vezie

SUMMARY

Samples of Dow PBO (poly-p-phenylene benzobisoxazole), Celanese PBT (poly-p-phenylene benzobisthiazole), and Dupont Kevlar-PPTA (poly-p-phenylene terephthalamide) fibers were surveyed by scanning electron microscopy in order to correlate fiber structural features with varying processing conditions and varying properties. Different fibers showed minor morphological differences in the fiber surface and the kink band structure, but major differences were found in the liquid nitrogen fracture surfaces. All PBO fiber fracture surfaces showed some "ribbon-like" fibrillar bundles at a scale of 1 to 10 μ m, similar to PPTA, but unlike PBT. Kevlar 49 showed 200-500 nm pleats along the length of the fracture surfaces whereas Kevlar 149 did not, indicating that improved modulus of Kevlar 149 may be due to "straightening out" of pleats.

FINAL REPORT
TO
UNIVERSAL ENERGY SYSTEMS

SLEW-INDUCED DEFORMATIONS
IN A SPACE-BASED
ELECTROMAGNETIC RAIL GUN

BY

JAMES W. WADE

Research conducted at
Kirtland Air Force Base
Albuquerque, New Mexico
Under the
Graduate Student Summer Support Program

ABSTRACT

A space-based rail gun has many possible uses, one of which is a component of a space-based defense network. Stringent pointing requirements are placed on a rail gun to be used for this purpose. Disturbances to the rail gun may significantly affect pointing accuracy. Possible sources of disturbances identified in this study include: on-board equipment, rail vibrations, environmental torques, and slew-induced deformations. Slewing deformations are studied by including the coupling of the slew dynamics with the Bernoulli-Euler beam model. The slewing disturbances are modeled, with control methods suggested to overcome the resulting pointing errors.

1. INTRODUCTION

1.1 Background

An electromagnetic rail gun is a device which transfers electromagnetic energy directly into kinetic energy. The rail gun consists of two parallel rails with a sliding armature between them. A large current travels down one rail, across the armature and back up the other rail, creating a magnetic field. This magnetic field interacts with the current in the armature to create the driving force known as the Lorentz force: see Figure 1.

Rail guns are capable of accelerating masses ranging from a few milligrams to several kilograms with peak velocities currently approaching 10 km/s.¹ Accelerations of over 1,000,000 g's have been attained.² However, most projectiles tend to disintegrate when experiencing accelerations of this magnitude.

Applications of the rail gun are being considered for the acceleration of a variety of projectiles with various purposes. Smaller rail guns which accelerate frozen hydrogen pellets may be used to initiate fusion reactions and re-fuel fusion reactors.³⁻⁵ Larger rail guns which accelerate larger masses may be used in space as reaction engines or as a space-based kinetic energy weapon as part of a space-based defense network.⁶⁻⁸

A rail gun is attractive for these applications since a

higher velocity is attainable than by using conventional mechanical or chemical methods. The higher velocity may also be attained at a lower cost by electromagnetic acceleration than by conventional methods.

1.2 Space-Based Rail Gun

A space-based rail gun could be a component of the space-based ballistic missile defense system, and thus would have several operational and equipment requirements. Some operational requirements include the firing rate, projectile mass and pointing accuracy of the system. Equipment requirements include the rails and projectiles, a current generation source, and target acquisition, tracking and pointing equipment.

The rail gun's effectiveness is dependent upon pointing accuracy, which may be degraded by disturbances. These disturbances may come from the operation of on-board equipment, the firing of the rail gun, oscillations caused by various environmental torques, and slew induced deformations.

These disturbance sources were studied, under the Universal Energy Systems Graduate Student Summer Support Program, in a hierarchical fashion, beginning with the disturbance sources which have a lesser effect on the rail gun and proceeding to those which significantly affect rail gun performance.⁹ The primary disturbance source was found to result from the rapid slewing of the rail gun and, and

therefore is studied in detail in this final report. Any stated graphs in this report may be seen by referencing the previous report.⁹

1.3 Space-Based Rail Gun Design

1.3.1 Performance

Each projectile of a space-based rail gun would have internal sensors and control jets to perform final guidance to the target. The rail gun must have a pointing accuracy of at least 5 milliradians in order to get the projectile close enough for this internal guidance to be effective. The rail gun must also have a slewing capability of 10 degrees per second per second to efficiently fire on expected targets.^{6,7}

1.3.2 Geometry

The rail gun geometry for the following study will consist of the current generation equipment and tracking equipment contained in an axisymmetric "black box" coaxial with the barrel. This geometry will reduce the necessary maneuvering torques as well as symmetrize the slew induced deformations.

1.3.3 Dimensions

Approximate measures for the rail gun barrel and

surrounding accessory assembly are calculated here. From this the overall moments of inertia are then calculated.

The rail gun barrel consists of two parallel rails surrounded by a stiff composite material. The length of the rail is about 50 meters and the diameter about 1 meter. Total mass of the rail and surrounding material is about 30,000 Kg.^{6,7}

Equipment for power generation, tracking and other purposes is contained in a cylinder with an outer diameter of 4 meters, length of 5.5 meters and a mass of about 70,000 Kg. This cylinder surrounds the rail barrel and is located at the barrel mid-point: see Figure 2.

Total moments of inertia may be calculated from the physical dimensions of the rail gun. Along the barrel axis the moment of inertia is 150,000 Kg-m² while the other two axes both have moments of inertia of 6,500,000 Kg-m.²

2. SLEW INDUCED VIBRATIONS

2.1 Background

Rapid repointing of a space-based rail gun is necessary to fire effectively on several targets. Since a rail gun is not a rigid body, slewing causes vibrations along the entire length of the rail gun. Deformations resulting from these vibrations create boresight pointing errors in the rail gun.

These deformations may be calculated by solving the equations of motion for a space-based rail gun. The equations of motion are presented in matrix form to accommodate any number of desired modes of vibration. The rail gun, shown in Figure 2, consists of a central cylinder with two appendages extending in opposite directions.

Only the first mode of vibration is studied to simplify the computations, giving an order of magnitude approximation of the slew induced vibrations.

2.2 Theory

The elastic deflections, $u(s,t)$, at any point on the rail gun barrel are given in terms of generalized coordinates, $z_i(t)$, and the mode shapes, $\phi_i(s)$, of the rail gun barrel.

$$u(s,t) = \sum_{i=1}^{\infty} \phi_i(s) z_i(t) \quad (2.1)$$

By adapting the four-spoke spacecraft model, found on pages 134-170 of Junkins and Turner,¹⁰ to the case of two symmetric fore and aft barrel sections, the kinetic energy may then be found at any point and expressed as:

$$T = 1/2(I_{Hub} + 2I_{App.})\dot{\theta}^2 + 1/2\dot{\theta}^2 \sum_{i,j}^n \sum_{i,j}^n (M_{ij} - M_{ij})\dot{z}_i\dot{z}_j + 1/2 \sum_{i,j}^n \sum_{i,j}^n M_{ij}\dot{z}_i\dot{z}_j + \dot{\theta} \sum_{i,j}^n M_{\theta z}\dot{z}_i \quad (2.2)$$

where $I_{App} = \rho \left[\frac{(r+L)^3}{3} - r^3 \right]$

$$M_{ij} = 2\rho \int_r^{r+L} \phi_i(s) \phi_j(s) ds$$

$$M_{ij} = 2\rho \int_r^{r+L} [(r+L)^2 - s^2] \frac{\partial \phi_i}{\partial s} \frac{\partial \phi_j}{\partial s} ds$$

$$M_{\theta z} = 2\rho \int_r^{r+L} s \phi_i(s) ds$$

r = Distance of the attachment point of each barrel half from the system center of mass

L = Length of each barrel half.

In a similar fashion, the potential energy may be expressed as:

$$V = 1/2 \sum_{i,j}^n \sum_{i,j}^n K_{ij} z_i z_j \quad (2.3)$$

where $K = 2EI \int_r^{r+L} \left[\frac{\partial^2 \phi_i}{\partial s^2} \frac{\partial^2 \phi_j}{\partial s^2} \right] ds$

By elimination of higher order terms, the energies may be simplified and expressed in matrix form,

$$T = 1/2(\dot{x})^T [M^*] (\dot{x}) \quad (2.4)$$

$$V = 1/2(x)^T [K^*] (x) \quad (2.5)$$

where $\{x\} = \begin{Bmatrix} \theta \\ \{z\} \end{Bmatrix}$

$$[M^*] = \begin{vmatrix} I_{Hub} + 2I_{App} & \\ & \{M_{\theta z}\}^T \\ \hline & \{M_{\theta z}\} & \\ & & [M] \end{vmatrix}$$

$$[K] = \begin{vmatrix} \diamond & \\ -\sigma & -[KJ] \end{vmatrix}$$

Another implicit simplification of this configuration is the permissibility of assuming antisymmetric mode shapes for each half of the barrel, as well as no shift of the system center of mass during deformation.

This leads to the linearized equation of motion of the slewing rail gun barrel:

$$[M]\{\ddot{x}\} + [K]\{x\} = [P]\{v\} \quad (2.6)$$

where $\{v\} = \begin{Bmatrix} u_r \\ u_{ei} \\ \vdots \\ u_{ei} \\ F \end{Bmatrix}$

$$[P] = \begin{vmatrix} 1 & 2 & \dots & 2 & 2(r+L) \\ \diamond & 2\phi_{1,x}^1 & \dots & & 2\phi_1 \\ \vdots & \vdots & \vdots & \vdots & \vdots \\ \diamond & 2\phi_{1,x}^1 & 2\phi_{1,x}^1 & & 2\phi_i \end{vmatrix}$$

The vector v is composed of a moment u_r , applied at the center of the rail gun barrel, and r moments applied at locations along the barrel length. The last element, F , is a force at the very end of the barrel applied perpendicularly to the barrel.

The upper right element of the P matrix, $(r+L)$, is the moment arm of the force applied at each end of the barrel.

The ϕ_i of the matrix are the mode shape functions evaluated at the end of the barrel. The ϕ_i^j, x are the derivatives of the mode shapes ("mode slopes") with respect to x , evaluated at the location of the j^{th} moment along the rail gun barrel.

The mode shapes employed ("assumed modes") are the static modes for simplicity, which are determined by solving the general expression for transverse beam vibrations, equation (3.3):

$$EI \frac{d^4 u}{ds^4} + \rho A \frac{d^2 u}{dt^2} = 0 \quad (2.7)$$

The general expression for the spatial factor, $\phi_i(s)$, of equation (2.1) for transverse beam vibrations is given by:

$$\phi_i = C_{1i} \sin b_i L + C_{2i} \cos b_i L + C_{3i} \sinh b_i L + C_{4i} \cosh b_i L \quad (2.8)$$

By applying the end conditions for a cantilever beam to the solution of the general expression, the mode shapes are determined to be:

$$\phi_i = K_i (\cosh b_i x - \cos b_i x) - \frac{(\cos b_i L + \cosh b_i L)}{(\sin b_i L + \sinh b_i L)} (\sinh b_i x - \sin b_i x) \quad (2.9)$$

Values of $b_i L$ are determined by solutions of $\cos(b_i L) : \cosh(b_i L) = -1$. The values for the first four modes of vibration are listed below.

i	$b_i L$
1	1.875
2	4.694
3	7.855
4	10.996

2.3 First Mode Response

Because only the first mode of vibration is studied here, the matrices in the equations of motion become scalars, thereby simplifying the equations of motion.

$$J\ddot{\theta} + M_{\theta z}\ddot{z} = u_r + 50F \quad (2.10)$$

$$M_{\theta z}\ddot{\theta} + M\ddot{z} + Kz = 2\phi_1 F \quad (2.11)$$

To minimize slewing time and permit the use of on-off end thrusters, the torque is applied in the manner known as bang-bang. A constant torque is applied in one direction to create the maximum possible angular acceleration. A reverse torque is then applied in the opposite direction in mid-maneuver, to arrive at the desired pointing angle.

Slew induced deformations and pointing errors are studied for bang-bang control applied by three different techniques. One technique employs only forces at the end of the rail gun barrel. The second technique utilizes a moment at the center of the rail gun length in addition to the end forces. A third method uses structural rate feedback damping forces in addition to the central moment produced by structural acceleration feedback.

2.3.1 Required Performance

Two pointing maneuvers have been investigated. In the first, the angular change for the maneuver is 10 degrees, and in the second, a slew of 1 degree is performed. A 200 millisecond slew time has been chosen, determined by the required firing rate of four shots per second. Each shot lasts about 10 milliseconds, leaving 200 milliseconds between shots for recharging and repointing procedures, with an additional 40 milliseconds buffer, to allow for structural damping.

All graphs referred to are actually composed of two separate graphs: a and b. Graph a refers to plots for a 1 degree slew. Graph b refers to the 10 degree slew.

2.3.2 Slewing with End Forces Only

The application of end forces at the end of the rail gun barrel produces deformations of the barrel. Pointing inaccuracies of the undeformed state of the rail gun barrel also occur depending on the method used to determine the switching time.

A switching time determined by an open-loop method of half the total slew time produces the largest pointing errors. The closed-loop method determines the torque switch by the detected crossing of the optimal switching surface relating angular attitude and rate. For a rest-to-rest slew

the switching surface is obtained by first normalizing state and force amplitude, then using the double integrator solution, such as found on pages 193-201 of Junkins and Turner. The resulting switching surface is:

$$\theta = \frac{J\dot{\theta}^2}{100F_{\max}} \quad (2.12)$$

Since the actual angle and angular rate are used, a smaller pointing error is to be expected, but the feedback approach has not been implemented in the present study.

The equations of motion for the open-loop method may be written as:

$$J\ddot{\theta} + M_{\theta z}\ddot{z} = 50F \quad (2.13)$$

$$\left[M - \frac{M_{\theta z}^2}{J}\right]\ddot{z} + Kz = \left(2\phi_1 - \frac{50M_{\theta z}}{J}\right)F \quad (2.14)$$

where F will have a bang-bang profile for either the open loop or the closed loop approaches. Equation (2.14) may then be solved first, from which the distortion on the boresight dynamics induced by the second term of equation (2.13) can then be computed: see Graph 9.

Plots of the deformation and nominal pointing angle throughout the slewing time, and for 40 milliseconds after the slew is completed, appear in Graphs 10 and 11 respectively.

2.3.3 Slewing with End Forces and Central Moment

Pointing error correction is effected if a central

moment can be applied in addition to the end forces. Such a central moment must be controlled in such a manner as to eliminate the $M_{\Theta z}^T$ term in equation (2.9). If possible, this would be done by commanding a hub torque, given by equation (2.15), by structural accelerometer feedback.

$$u_r = M_{\Theta z}^T z \quad (2.15)$$

The rail gun boresight then follows that of an equivalent rigid body during rotation, with the equations of motion becoming:

$$J\ddot{\Theta} = 50F \quad (2.16)$$

$$M_{\Theta z}\ddot{\Theta} + M\ddot{z} + Kz = 2\phi_1 F \quad (2.17)$$

Plots of the end point deformations and nominal pointing angle appear in Graphs 10 and 11. A plot of the central torque required appears in Graph 12, to determine the required torque magnitude and bandwidth.

2.3.4 Damping Force Application

In either of the previous cases, the line of sight angle, Θ_{LOS} , is given by:

$$\Theta_{LOS} = \Theta^* + \frac{\phi_1(r+L)z}{r+L} \quad (2.18)$$

If the central moment can be applied then the nominal pointing angle, Θ^* , becomes equal to the target angle at the end of the bang-bang control force, and remains so. If only

the bang-bang end control is supplied, then $\theta(t_f)$ is erroneous, as may be seen in Graph 11. In both cases, however, the residual jitter, proportional to the modal deformation rate, distorts the post-slew line of sight: see Graph 13.

Additional structural rate feedback damping forces, F_d , at each end are then needed, given by:

$$F_d = -2T^{-1}\phi_1^{-1}Mz \quad (2.19)$$

Where T is the desired time constant of the residual jitter.

The equivalent equations of motion, for bang-bang end forces and a central torque given by equation (2.14), as well as structural damping forces according to equation (2.18), takes the form:

$$J\ddot{\theta} = 50F \quad (2.20)$$

$$M\ddot{z} + 200M\dot{z} + Kz + M_{\theta z}\ddot{\theta} = 2\phi_1 F \quad (2.21)$$

The desired jitter time constant, T , was chosen to be 10 milliseconds, which is the expected transit time of the projectile in the barrel. The resulting damping end forces appear in Graph 14.

End point deformations appear in Graph 10, along with the results from the previous maneuvering methods. The nominal pointing angle is identical to the case when a central torque is supplied: see Graph 11. The line of sight pointing angle appears in Graph 13 for each of the maneuvering methods investigated.

2.4 Results

The method of applying only end forces, in the open-loop case, produces large steady state pointing errors of approximately 5 milliradians for a 1 degree slew and 50 milliradians for a 10 degree slew, even after settling of the jitter-induced error. The central moment method produces no such steady-state error. However, the required central moment is much larger than could ever be achieved by a hub torque actuator, on the order of 10^7 N-m for a 10 degree slew, and 10^8 N-m for a 1 degree slew.

Since the required hub torque is found to be too large, additional torque actuators may be used along the barrel to distribute the required torque per actuator. A higher dimensional model is then needed, since other structural modes may thereby be significantly excited.

By comparing the results in Graph 10, it is apparent that control with and without a hub torque produce deformations which result in errors on the same order of magnitude as the 5 milliradians allowed for a space-based rail gun.

A 10 degree slew produces end point deformations corresponding to angular errors of approximately 10 milliradians at the end of the slewing maneuver, whether a central torque is applied or not. 40 milliseconds after the

slew is completed, these angular errors become 10 milliradians for the end force only method, and 7 milliradians when the central torque is applied.

For a 1 degree slew, the results are similar, but smaller in magnitude. Angular errors of approximately 1 milliradian exist at the end of the slewing maneuver, whether a central torque is applied or not. 40 milliseconds after the slew is completed, these angular errors become 1 milliradian for the end force method, and .7 milliradians when the central torque is applied.

By applying damping forces, the deformation errors are reduced nearly to zero at the end of the slew. The errors remain nearly zero for all time after the slew is complete. Since the required damping tip forces are very large, as seen in Graph 14, the desirability of additional actuators along the barrel is again evident, to distribute the total damping force per actuator.

2.5 Summary

Pointing errors produced by slew induced vibrations of a space-based rail gun are substantial if only rigid body control is used. When structural control is also applied, the method of applying a central moment together with structural damping control eliminates the line of sight pointing angle errors. This requires, however, a very large central moment correction, and a very large structural rate

damper. This can be alleviated if intermediate structural torque actuators are also used to distribute the required slew torque compensation and structural damping.

A more precise analysis will include natural structural damping, enhanced by proper choice of structural materials, or else by use of passive damping by means of incorporation of viscoelastic coatings.¹¹ This will reduce the active control requirements.

Moreover, since the maximum angular rate in the 10 degree slew case is 1.46 radians/second, the equations of motion should include the "gyroscopic damping" factor, $\dot{\theta}^2$, neglected in the present linearized model.

The slew torque and structural controls, given by equations (2.15) and (2.19), can be replaced by weaker as well as lower bandwidth controls, proportional to the commanded slew jerk rate. This will correct boresight pointing after decay of a transient, as recently proposed.¹²

The passive damping augmentation, slew feedforward control, and nonlinear dynamic model topics mentioned here are beyond the scope of the present investigation.

3. CONCLUSIONS

The rail gun's effectiveness is dependent upon pointing accuracy, which may be degraded by several disturbance sources. Disturbances of increasing magnitude and concern come from: operation of on-board equipment, the firing of the rail gun, oscillations caused by various environmental torques, and by slew induced structural deformations. Disturbances resulting from several of these sources have been found to be either negligible or easily controllable, yet the slew-induced vibrations were seen to require correction.

Negligible disturbances were found to result from the expected equipment operation characteristics, while easily controllable disturbances resulted from firing and environmental torques. The firing vibrations may be prevented by surrounding the rail with a stiff, composite material. Environmental torques were found to be very small, yet produce very large, slow oscillations. These oscillations are of primary concern while the space-based rail gun is in orbit, and are managed by standard spacecraft attitude determination and control methods not discussed here. During rail gun operation, maneuvering torques were found to overpower these environmental torques.

Vibrations which are caused by the rapid slewing of a space-based rail gun were shown to produce large line-of-sight pointing errors, if a rigid body model is used for slew command generation. To prevent these errors, large

correcting torques and forces are required if fast retargeting is attempted. The magnitudes of the correcting torques and forces are not attainable from single actuators. However, the required effort from each actuator can be reduced by distributing several structural actuators throughout the rail gun. The study of distributed actuators, as well as various alternative slew command generation and damping techniques, are topics reserved for further study.

The slew-induced deformations may be graphically seen in the thesis previously mentioned. Deformations for various slewing techniques, slew angle and slew time may be interactively visualized by use of a BASIC program for an Apple computer available at either: Universal Energy Systems, Dayton, Ohio, or ARBC Division, c/o Cpt. Bob Hunt, Air Force Weapons Laboratory (AFWL), Kirtland Air Force Base, Albuquerque, New Mexico. Another interactive program exists on the IRIS Silicon Graphics computer at AFWL/ARBC. Video tapes of the silicon graphics simulation are available at UES and at AFWL/ARBC.

REFERENCES

1. J. Honig and K. Kim, J. Vac. Sci Technol. A 2, 621 (1984).
2. BMS, Physics Today, December, 19 (1980).
3. R. S. Hawke, J. Vac. Sci. Technol. A1 , 969 (1983).
4. S. Usuba, K. Kondo and A. Sawaoka, IEEE Trans. Magn. **MAG-20**, 260 (1984).
5. J. Honig, K. Kim and S. W. Wedge, J. Vac. Sci. Technol. A 4, 1106 (1986).
6. S. Aiken, M. Michnovicz, J. Cremer and C. Hudson, "Space-Based Electromagnetic Launcher Structure and Dynamic Disturbances", TAL-86-024, Titan Systems, Inc., September 1986.
7. T. B. Clark, Editor, "Electromagnetic Launcher and Prime Power Systems", Informal Technical Information Report, CDRL Sequence Number AO12, Ford Aerospace & Communications Corporation, February 1987.
8. D. P. Bauer, J. P. Barber and H. F. Swift, IEEE Trans. Magn. **MAG-18**, 170 (1982).
9. J. W. Wade, M.S Thesis, University of Illinois, 1987.
10. J. L. Junkins and J. D. Turner, Optimal Spacecraft Rotational Maneuvers , Esleveir, New York, 1986.
11. K. E. Smith, "Damping of a Selected Structure", Report No. 87-04-02, CSA Engineering, Inc., Palo Alto, CA, April 1987.
12. T. A. W. Dwyer III, "Pointing and Tracking Maneuvers With Slew-Excited Deformation Shaping", Proc. AIAA Guidance, Navigation and Control Conf. (Monterey, CA, Aug. 17-19, 1987).

1987 USAF-UES SUMMER FACULTY RESEARCH PROGRAM/
GRADUATE STUDENT SUMMER SUPPORT PROGRAM

Sponsored by the
AIR FORCE OFFICE OF SCIENTIFIC RESEARCH

Conducted by the
Universal Energy Systems, Inc.

FINAL REPORT

Hole Diameters in Plates Impacted by Projectiles

Prepared by:	Randall F. Westhoff
Academic Rank:	Master of Science
Department and University:	Department of Mathematics Eastern Washington University
Research Location:	Armament Laboratory Analysis Branch Eglin AFB, FL 32542
USAF Researcher:	George Crews
Date:	4 Sept 87
Contract No:	F49620-85-C-0013

Hole Diameters in Plates Impacted by Projectiles

by

Randall F. Westhoff

ABSTRACT

During my research period at the Armament Laboratory, I evaluated the hole diameter and rod loss models of SPADE, a program designed to calculate the damage to an array of spaced plates impacted by a projectile. Comparison with actual test data showed that the hole diameter model was only accurate under certain impact conditions. Using experimental data and curve fitting techniques, I was able to modify the hole diameter model to achieve greater fidelity over a broad range of test conditions. The only available data on rod loss was from the original report which suggested the rod loss model currently used by SPADE. This report also verifies the accuracy of this model.

ACKNOWLEDGMENTS

I would like to thank the Air Force Systems Command and the Air Force Office of Scientific Research for their sponsorship of this research. I would also like to thank Universal Energy Systems, the Armament Laboratory at Eglin AFB, and the Shalimar office of Science Applications International Corporation (SAIC) for their support of this project. In particular, I would like to acknowledge the support of John Gagliano, George Crews, Dr. Sam Lambert, and David Syse of the Armament Laboratory and a very special thanks to Larry Cohen, Hartley King, Ken Stewart, and Norm Banks of SAIC.

I. INTRODUCTION:

One of the functions of the Analysis Branch of the Armament Laboratory at Eglin AFB is to assess the vulnerability of air, space, ground mobile, and fixed targets under various modes of attack. There is currently a great deal of effort being directed towards estimating kill probabilities for kinetic energy weapons against SDI targets. This requires algorithms like SPADE to calculate the damage to SDI targets when impacted by a projectile. These algorithms use both theoretical and experimentally based models to predict damage to various components of each target. Statistical procedures are then used to generate kill probabilities from these damage estimates. The accuracy of these kill probabilities is directly related to the fidelity of each of the models that goes into the overall algorithm. Therefore, it is necessary to develop models that accurately predict the experimental data available.

My educational background is centered in the area of pure mathematics, especially complex analysis. I have also had several courses in applied areas such as mathematical statistics, numerical analysis, and computer science. These skills made it possible for me to do experimentally

based evaluations and modifications of vulnerability models with only a minimum amount of background study.

II. OBJECTIVES OF THE RESEARCH EFFORT:

My assignment as a participant in the 1987 Graduate Student Summer Support Program (GSSSP) did not carry with it any specific research goals. I was placed under the direction of George Crews, Chief of the Analysis Branch at the Armament Laboratory. For a period of about three weeks, I worked with David Syse of the Vulnerability Assessments group. During this period I became acquainted with the work being done in this area and did some small programming tasks.

For the remainder of my assignment, I was placed under John Gagliano, head of the Space Targets Group of the Analysis Branch. My objective was to evaluate and if necessary modify the hole diameter and rod loss models of SPADE, a program designed to calculate the damage to an array of spaced plates impacted by a projectile. The SPADE algorithm was developed by Science Applications International Corporation (SAIC) so I worked out of their office in Shalimar. After a review of the available data it was found that the hole diameter model was only accurate

under certain impact conditions. Therefore, the improvement of this model became the primary objective of my research effort.

III.

a. In order to evaluate the rod loss and hole diameter models of SPADE, I began by researching the literature and gathering experimental data. The data for rod loss was limited almost exclusively to the report of Baker (1969). This report is also the source of the rod loss model used by SPADE. Over this range of data, the rod loss model suggested by Baker (1969) is reasonably accurate. For this reason no attempt was made to modify SPADE's rod loss model. I was, however, able to obtain a large amount of data on hole diameters in plates impacted at normal angle by a projectile from the reports of Baker (1969) and Payne (1965), and from a database maintained by SAIC. Comparison of this data with SPADE's hole diameter model suggested revisions of the SPADE model would be needed.

The model for hole diameter in plates impacted at normal angle by a projectile currently being used by SPADE is a modified version of the model proposed by Baker (1969) and is given by

$$D/d = 1 + (D_{inf}/d - 1)(1 - \exp(-kt/d)) \quad (1)$$

where D is the hole diameter, d is the projectile diameter, t is the plate thickness, k is a material dependent shape factor, and D_{inf} is the diameter of a crater made under the same impact conditions assuming the plate has semi-infinite thickness. The shape factor k was set to 1.5 independent of materials. The formula for D_{inf} is based on a formula for penetration suggested by Payne (1965) and the assumption that the crater diameter is twice the penetration. This leads to the relationship

$$D_{inf}/d = (p_p/p_t)^{1/3} (p_p v^2 / (.024B))^{1/3} ; D_{inf}/d \geq 1 \quad (2)$$

where p_p is the projectile density (g/cc), p_t is the target density (g/cc), v is the impact velocity (km/sec), and B is the Brinell hardness of the target material.

The overall form of equation (1) seemed theoretically sound in the sense that the hole diameter approaches the projectile diameter for very thin plates and for very thick plates the hole diameter approaches D_{inf} . The exponential variation of the hole diameter with respect to plate thickness also seemed reasonable when compared to actual test data. For these reasons equation (1) was retained with only one modification which shall be explained later.

The model for crater diameter in semi-infinite targets given by equation (2) was found to incorrectly take into account the projectile-to-target density ratio (p_p/p_t). This results from the assumption that the crater diameter is twice the penetration for all impacts when in reality craters are generally only hemispherical for like material impacts of spherical projectiles. Comparison with test data for spherical projectiles from Payne (1965) showed that the formula in equation (2) overpredicted D_{inf}/d when $p_p > p_t$ and underpredicted D_{inf}/d when $p_p < p_t$. This is illustrated in figure 1. Data for long rods from the report of Baker (1969) showed an increase in crater diameter as the length-to-diameter ratio (L/d) of the projectile increased. Taking these factors into account an equation of the form

$$D_{inf}/d = c_1(p_p/p_t)^{c_2} (1.5 L/d)^{c_3} \times (p_p/p_t)^{1/3} (p_p v^2 / (.024B))^{1/3} \quad (3)$$

was found to better predict crater diameters in semi-infinite targets.

Since the SPADE algorithm assumes all projectiles are cylindrical, spheres were modeled as cylinders with $L/d = 2/3$. With this convention equation (3) reduces to the following equation for like material impacts of spherical

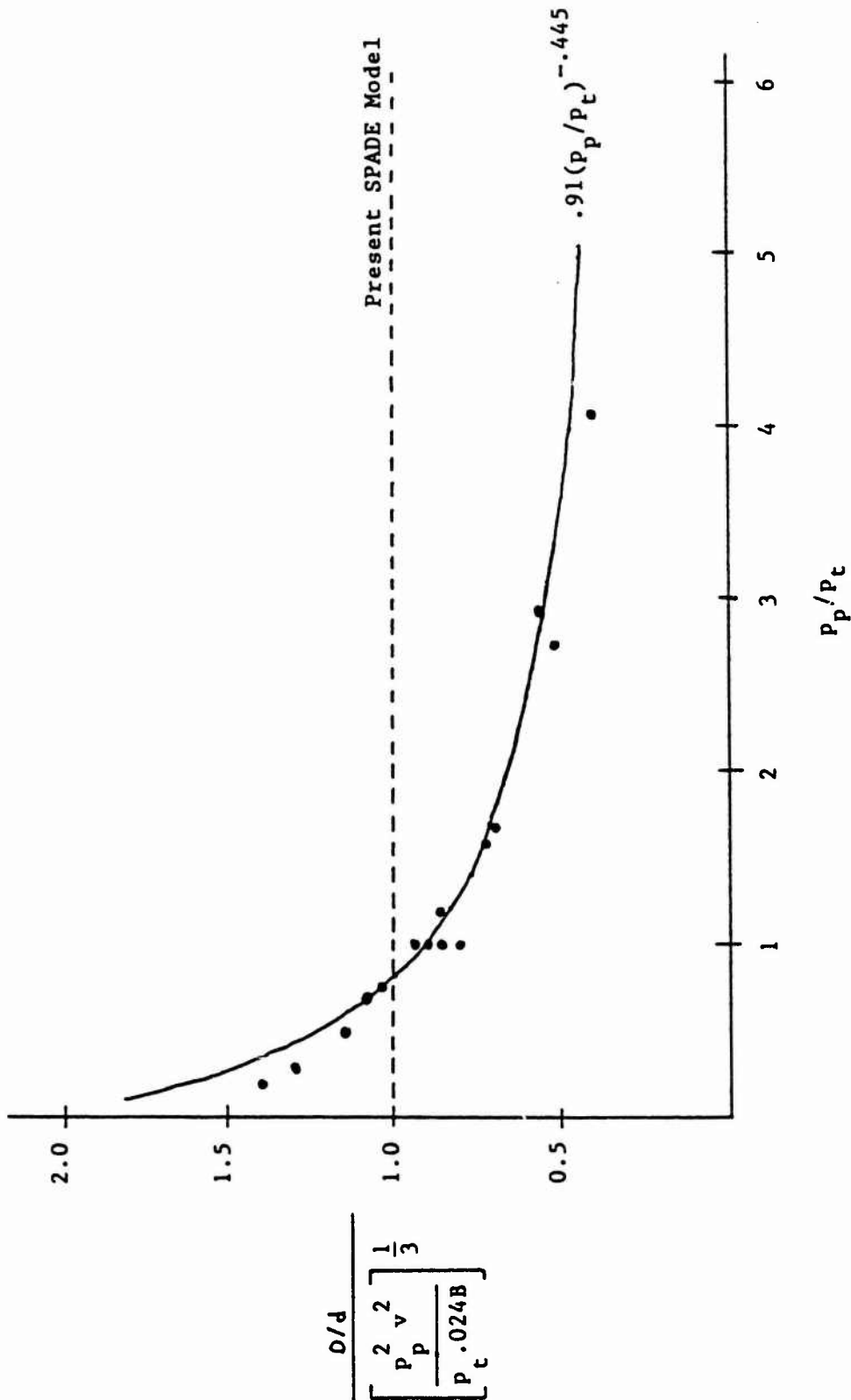


Figure 1: Diameter/SPADE predicted diameter versus projectile/target density for spherical projectiles of stainless steel, titanium, magnesium, aluminum, and lead into semi-infinite targets of aluminum and stainless steel with impact velocities ranging from 4.5 to 8.0 km/sec.

projectiles.

$$D_{inf}/d = c_1(p_p v^2 / (.024B))^{1/3} \quad (4)$$

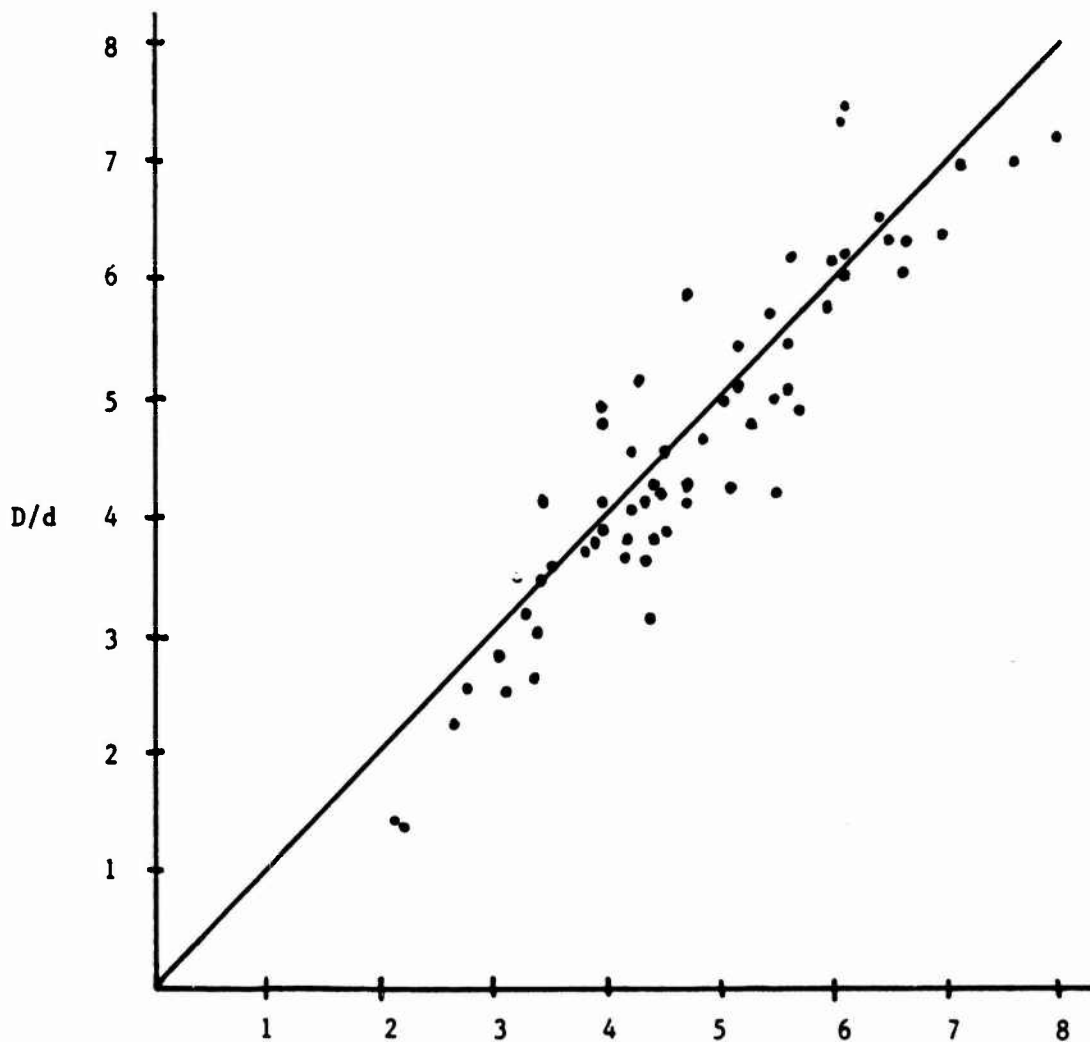
The constant c_1 was set to .91 to bring equation (4) and thus equation (3) in line with data for like material impacts of spherical projectiles. Values for c_2 and c_3 were determined by using curve fitting techniques and experimental data primarily from the reports of Baker (1969) and Payne (1965). This gave the values $c_2 = -0.445$ and $c_3 = 0.2$. With these values equation (3) reduces to the expression

$$D_{inf}/d = .91(p_t/p_p)^{.112} (1.5 L/d)^{.2} (p_p v^2 / (.024B))^{1/3}. \quad (5)$$

Data from impacts involving 11 different projectile materials and 10 different target materials in various combinations were used in the above data fit. A comparison of the crater diameters for these impacts and the values predicted by equation (5) is given in figure 2.

Having established a reasonably accurate formula for crater diameter in semi-infinite targets, I turned my attention to the development of a formula for the material dependent shape factor k in equation (1). Solving for kt/d in equation (1) gives the expression

$$kt/d = -\ln[1 - (D/d - 1)/(D_{inf}/d - 1)]. \quad (6)$$



$$.91 \left[\frac{p_t}{p_p} \right]^{.112} \left[1.5 \frac{L}{d} \right]^{.2} \left[\frac{p_p v^2}{.024B} \right]^{1/3}$$

Figure 2: Diameter versus predicted diameter for a wide variety of projectiles and semi-infinite target materials, velocities ranging from 2.75 to 8.0 km/sec, and length-to-diameter ratios between .08 and 10.

Using the values for D_{inf}/d predicted by equation (5) and data from the report of Baker (1969) and a database maintained by SAIC, it became apparent that the right side of equation (6) was not varying linearly with t/d for data from tests with varying plate thicknesses but the same projectile and target materials. Raising t/d to the $2/3$ power in equations (1) and (6), however, alleviated this problem. I then proceeded to test several formulas for determining k . Using curve fitting techniques and carefully studying trends in the data, it was found that the formula

$$k = .46(B/p_p)^{.29} \quad (7)$$

was the most reliable in predicting values for k with only one exception. For targets of silica phenolic, I recommend using $k = 2$.

In summary, the model developed for hole diameters in plates impacted at normal angle by a projectile is given by the formula

$$D/d = 1 + (D_{inf}/d - 1)(1 - \exp(-k(t/d)^{2/3}) \quad (8)$$

where D_{inf}/d is given by equation (5) and k is given by equation (7).

b. The model for hole diameter described in equation (8) was found to accurately predict test data over a reasonably broad range of impact conditions. A comparison of the data from impacts of 18 different material combinations and the hole diameters predicted by equation (8) is given in figure 3. This represents a significant increase in fidelity over the current SPADE hole diameter model.

IV. RECOMMENDATIONS:

a. I recommend that the hole diameter model described in equation (8) be incorporated into the SPADE algorithm. The convention of modeling spherical projectiles as cylinders with a length-to-diameter ratio of $2/3$ should also be adopted.

b. Although a reasonable amount of experimental data was available for this study, it was not sufficient to cover the desired range of impact conditions. Very little comprehensive data is available for impacts at velocities greater than 6 km/sec, impacts at oblique angles, and impacts with nonzero projectile yaw. Data for a wider variety of target and projectile materials, plate thicknesses, and projectile length-to-diameter ratios would also be useful. A comprehensive test program should be developed to fill these and other gaps in existing data.

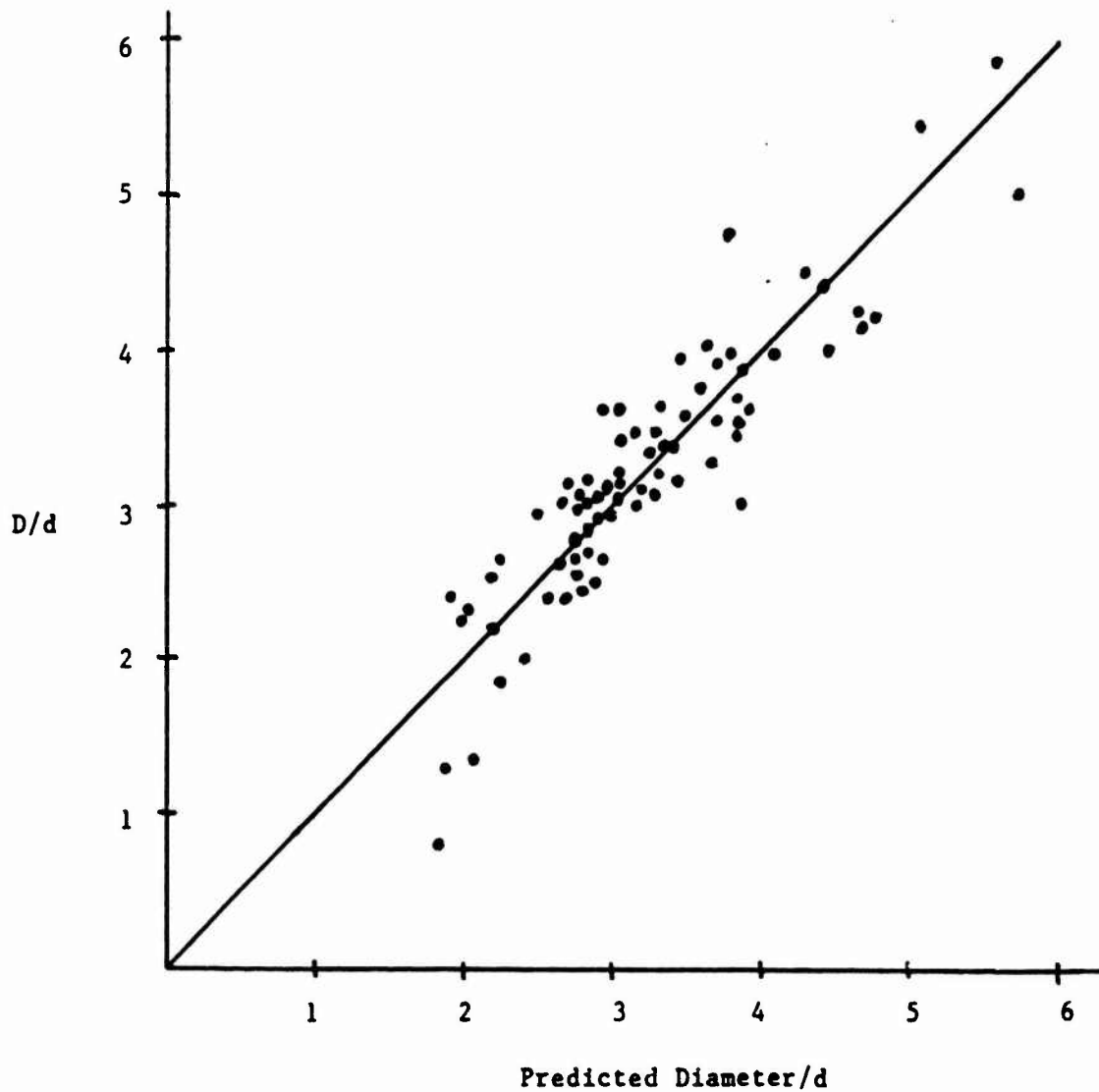


Figure 3: Diameter versus predicted diameter for several projectile and target materials, velocities ranging from 5 to 8 km/sec, plate thicknesses ranging from .25 to 4 (in projectile diameter units), and length-to-diameter ratios between .08 and 10.

REFERENCES

Baker, J. R., "Rod Lethality Studies", NRL 6920, AFATL TR-69-1, Naval Research Lab, Washington, D.C., July 1969.

Payne, J. J., "Impacts of Spherical Projectiles of Aluminum, Stainless Steel, Titanium, Magnesium, and Lead into Semi-Infinite Targets of Aluminum and Stainless Steel", AEDC-TR-65-34, Feb. 1965.

1987 USAF-UES SUMMER FACULTY RESEARCH PROGRAM
GRADUATE STUDENT SUMMER SUPPORT PROGRAM

Sponsored by the
AIR FORCE OFFICE OF SCIENTIFIC RESEARCH

Conducted by the
UNIVERSAL ENERGY SYSTEMS, INC.

FINAL REPORT

HUMAN RESPONSE TO PROLONGED MOTIONLESS SUSPENSION
IN FOUR TYPES OF FULL BODY HARNESSSES

Prepared by: Terri Wilkerson

Academic Rank: Graduate Student

University: Wright State University School of Medicine

Research Location: AAMRL/BBP
Wright-Patterson Air Force Base

USAF Researcher: Major Mary Ann Orzech, M.D.

Date: August 28, 1987

Contract No.: F49620-85-C-0013

HUMAN RESPONSE TO PROLONGED MOTIONLESS SUSPENSION
IN FOUR TYPES OF FULL BODY HARNESSSES

by
Terri Wilkerson

ABSTRACT

The ability to withstand prolonged suspension while being restrained by fall protection harnesses is of vital interest to occupational safety. A fallen worker may be suspended in a fall protection harness for an indefinite period waiting for rescue. This experiment was conducted using volunteers to evaluate the relative capabilities of four types of full body harnesses (FBH) to provide occupant body support and restraint during post-fall suspension. A series of 42 randomized tests were conducted to evaluate the physiological effects and subjective responses to prolonged, motionless suspension in four different designs of FBH. Measured physiological parameters included blood pressure, heart rate, and respiratory rate. Subjects were passively suspended in each of the four harness configurations until subjective tolerance was reached prompting the subject to request termination of the test or until symptoms developed which prompted a medical decision to end test. Nonparametric analysis of the test durations was conducted using Wilcoxon paired-replicate rank test. Subjective symptoms which prompted test termination were analyzed for the relative occurrence frequency in each harness configuration. Based upon suspension duration and subjective response data, the FBH-C appears to be the superior harness configuration. The median duration period in FBH-C was 28.36 min with symptoms of nausea and changes in thermal sensations occurring most frequently as the reason for test termination. FBH-D

suspensions had a median duration of 26.66 min and FBH-B had a median time of 18.36 min, with light-headedness and nausea for both harness designs most often ending a test. Motionless suspension in FBH-A lasted a median duration of 17.05 min with the primary symptoms of nausea, change in vision, and decreased heart rate terminating most tests.

ACKNOWLEDGEMENTS

The author gratefully acknowledges the sponsorship of the Air Force System Command, Air Force Office of Scientific Research and the Biomechanical Protection Branch of the Aeromedical Research Laboratory (AAMRL/BBP) of Wright-Patterson AFB. The author wishes to thank Major Mary Ann Orzech, M.D. for her support and guidance as my research advisor and Sgt Mark McDaniel for scheduling and preparing the subjects prior to each test. Also special thanks to Lt Karin Getschow for functioning as safety monitor during each test and to Mrs. Jeni Blake for preparation of this document.

I. INTRODUCTION

The U.S. Department of Labor, Occupational Safety and Health Administration (OSHA) is now developing new regulations governing the design of fall protection equipment. OSHA has asked the Harry G. Armstrong Aerospace Medical Research Laboratory (AAMRL) to investigate several specific issues where additional data is essential to the establishment of fall protection harness standards. The relative capability of various full body harnesses (FBH) configurations to provide occupant support during prolonged post-fall suspension is currently under study.

The ability to withstand prolonged suspension is of vital interest to occupational safety since a worker may be suspended in a harness for a considerable time period waiting for rescue. Complications stemming from prolonged suspension may range from nausea, light-headedness, changes in vision, respiratory difficulty, and cardiac dysrhythmias in a conscious individual to more serious cardiac dysrhythmias and possibly even death in individuals who have lost consciousness due to suspension or who were unconscious prior to or as a result of the fall.

Research previously conducted in the area of occupant protection during prolonged suspension is limited. The earlier researchers who studied human tolerance to suspension observed similar physiological effects. The effects include: extremity numbness; abdominal, shoulder, or groin pain; respiratory difficulty; nausea; light-

headedness; a variety of cardiac dysrhythmias; and loss of consciousness.

II. OBJECTIVES OF THE RESEARCH EFFORT

This experiment is the second phase of human prolonged suspension studies conducted at AAMRL. The first phase of this study compared the relative capabilities of three extremely different fall protection harness configurations. Analyzed in this initial study was the body belt, chest harness, and full body harness. The full body harness was determined to provide the optimal support and safety to the user. While only minor differences exist among the designs of body belts and chest harnesses commercially produced, major differences exist in full body harness designs available to industry. These FBH configurations differ in strap design, occupant position upon suspension, and load distribution. This current study will analyze four designs of FBH and will determine the optimal configuration in terms of support and safety to the occupant. Motionless suspension was chosen to be evaluated since it would probably be the least tolerated physiologically and have effects that are potentially life threatening. Motionless suspension would occur if the harnessed occupant is unconscious or unable to move his extremities due to injury.

The null hypothesis that was evaluated in the experiment was that there is no difference in the suspension duration tolerated by occupants of the four harness designs.

III. TEST EQUIPMENT

Four types of full-body harnesses were evaluated. The harnesses were coded as FBH-A, FBH-B, FBH-C, and FBH-D. All FBH are similar to the parachute harness design.

FBH-A was manufactured by Research and Trading Corporation, Style No. 425. This harness is constructed of 1 3/4 inch wide straps encircling the torso and the upper thighs. A strap in the back functions as a buttock sling and connects the two thigh straps. A D-ring is used to attach a fall arrest lanyard and is usually located between the shoulder blades of the occupant.

FBH-B was manufactured by Miller Equipment Division, Style No. 8095. This harness was constructed with 1 3/4 inch wide straps with rubber rings at each hip area. All straps: shoulder strap, waist belt, thigh strap, and buttock sling converge at the rubber hip ring. The waist belt fastens in the front with a standard buckle with the posterior section of the belt generally not load bearing. A D-ring is used to attach a fall arrest lanyard.

Rose Manufacturing, Inc. designed the FBH-C (Model 502700). The most striking difference in design of this harness from the others is the shoulder straps (1 3/4 inch width) are continuous as the waist strap. The joint shoulder straps are connected by another strap which crosses itself and enters a metal chest ring. The front shoulder straps also travel down past the axilla to a metal hip ring and around the front to the metal chest ring. A load bearing buttock sling is continuous with the thigh straps. Also the D-ring is attached to the

shoulder straps and the shoulder straps are then configured through a large plastic spreader. This configuration spreads the shoulder straps out the most over the front and back of the occupant as compared to the other harnesses.

FED-D is manufactured by DB Industries, Inc., Style No. LS 1631. The shoulder straps (1 3/4 inch width) travel down the chest and are connected with a non-crossing connecting strap across the chest. Two metal O-rings rest at the hip area and all straps: thigh, buttock sling, anterior and posterior shoulder straps converge at the O-ring on the appropriate side. The thigh straps, continuous with the buttock sling, travel from back to front through the groin area, loop through the O-ring and buckle in the front groin area. A D-ring is used to attach a fall arrest lanyard and is usually located between the shoulder blades of the occupant.

Each harness was snugly fitted to the subject but not to the point where the range of extremity motion or torso movement was restricted. This ensured subject safety as well as meeting work mobility requirements.

An ANSI A10.14-75 approved, six-foot long nylon lanyard with a non-locking snap hook at each end was used to suspend the subjects. One snap hook was attached to the D-ring of the harness and the other was connected to a steel cable of a hoist. A hoist control box was operated by the equipment safety officer to raise and lower the test subject.

IV. TEST PROCEDURES

Nine males and one female voluntarily participated as subjects in this test program. The subjects were all members of the AAMRL Impact Acceleration Stress Panel. All subjects successfully completed an intense medical screening evaluation.

Informed consent was provided by all subjects on an ongoing basis during the test program. Prior to each test the subject was briefed on procedure and potential of medical risks. The subject signed a witnessed consent form plus the medical monitor stressed that any subject was free to withdraw from testing at any time for any reason.

The test conductor for each test completed the following tasks:

1. Inspect harness and hoist mechanism.
2. Conduct manikin trial suspension employing an anthropomorphic dummy designed to represent a 95th percentile (weight) adult male.
3. Prepare data sheet and test instrumentation.
4. Secure the area.
5. Brief the subject on test protocol.
6. Harness subject and ensure mobility.
7. Instrument subject and record baseline physiological values.
8. Complete pre-test photo.
9. Collect baseline physiological data.
10. Initialize voice recorder and Holter EKG system.
11. Suspend subject.

12. Complete test photo.
13. Collect physiological data every two minutes and subjective data every five minutes.
14. End suspension by physician or subject request.
15. Collect post-test data.

Physiological parameters measured included peripheral blood pressure, respiratory rate and EKG. The blood pressure was taken employing an automatic sphygmomanometer which measured systolic/diastolic, mean arterial pressure and heart rate at two minute intervals. The respiratory rate was measured using a nasal thermistor. The EKG data was recorded with redundancy to ensure a comprehensive evaluation of the electrocardiographic waveform. A Holter EKG monitor and a Hewlett-Packard EKG telemetry unit were both used to monitor heart rate and potential cardiac dysrhythmias. The EKG telemetry data were transmitted to a strip-chart recorder and were used primarily by the medical monitor to evaluate the heart rate before, during, and after the test. The Holter EKG monitor recorded data on a cassette tape which were later analyzed by microcomputer.

At five minute intervals in the experiment, the subject's response to a qualifying condition questionnaire were recorded on a cassette tape recorder. The series of questions was designed to provide data on the subject's perception of his fluctuating physiological state and additional physiological data. The questions surveyed the frequency of symptoms of extremity paresthesias (numbness/tingling), nausea, light-headedness, respiratory difficulty, detection of any pain or discomfort and location of strap pressure.

The subjects were instructed to remain motionless during the experiment. The test was terminated when the subject reached his or her subjective tolerance or when symptoms appeared which required a medical decision to end the suspension.

The heart rate data was analyzed by creating data files and producing graphical plots utilizing the Vax computer.

The suspension-duration data were statistically analyzed using the Wilcoxon paired-replicate rank test assuming a 90% confidence level for a two-tailed test.

V. RESULTS

Forty-two experiments with ten volunteers were performed. Table 1 presents the median and range of the suspension duration for each of the harnesses tested. The data shows FBH-C was tolerated for the longest median period of suspension (28.36 min) followed closely by FBH-D (26.66 min). FBH-B and FBH-A observed median times of 18.36 min and 17.05 min respectively. Therefore, the Wilcoxon paired-replicate rank test revealed statistically significant differences in the suspension durations in only two of the pairs: between FBH-A and FBH-C and between FBH-A and FBH-D.

TABLE 1
SUMMARY OF SUSPENSION DURATION DATA

	FBH-A	FBH-B	FBH-C	FBH-D
Total Number of Tests	10	10	10	10
Range of Durations (min)	3.47 to 32.00	5.5 to 37.5	10.2 to 49.8	4.33 to 60.00
Median Duration (min)	17.05	18.36	28.36	26.66

Table 2 lists the symptoms which were primarily responsible for test termination of a particular suspension. The most frequent reason for termination in FBH-A was attributed to the feeling of nausea. Light-headedness, changes in vision, and a decreasing heart rate also frequently ended a FBH-A test. Suspensions in FBH-B were ended most often due to nausea and light-headedness. Tests in FBH-C ended most frequently due to nausea. Nausea also ended the most tests in FBH-D. Suspensions in FBH-D were frequently terminated due to light-headedness as well.

TABLE 2
SYMPTOMS RESPONSIBLE FOR TEST TERMINATION

SYMPTOMS	FBH-A	FBH-B	FBH-C	FBH-D
Test Time Limit (60 min)	0 (0)	0 (0)	0 (0)	1 (10)
Nausea	3 (30)	5 (50)	4 (40)	5 (50)
Light-Headedness	2 (20)	3 (30)	0 (0)	4 (40)
Change in Thermal Sensation	0 (0)	0 (0)	3 (30)	2 (20)
Change in Vision	2 (20)	1 (10)	0 (0)	1 (10)
Strap Pressure: Groin	1 (10)	0 (0)	0 (0)	0 (0)
Strap Pressure: Buttocks	0 (0)	0 (0)	1 (10)	0 (0)
Generalized Discomfort	1 (10)	0 (0)	0 (0)	0 (0)
Muscular Fatigue (Back)	0 (0)	0 (0)	1 (10)	0 (0)
Limb Paresthesias	1 (10)	0 (0)	2 (20)	1 (10)
Lower Limb Discomfort	0 (0)	2 (20)	1 (10)	1 (10)
Respiratory Difficulty	0 (0)	1 (10)	1 (10)	0 (0)
Decreased Heart Rate	2 (20)	2 (20)	2 (20)	1 (10)
Pallor	0 (0)	1 (10)	0 (0)	0 (0)
Drowsiness	1 (10)	0 (0)	0 (0)	0 (0)

NOTE: FBH = Full Body Harness
Data Format = Number of reports (percentage)
Multiple symptoms may have contributed to test termination.

A medical decision to terminate a suspension occurred most frequently in FBH-B while voluntary termination of a test occurred the most in FBH-C. Table 3 presents these findings. A medical decision to end a test was most often due to a decreasing heart rate, nausea, or light-headedness. Primary recurring reason for a subject to request test end was due to nausea.

TABLE 3
 FREQUENCY OF PHYSICIAN OR SUBJECT DECISION TO END SUSPENSION

TYPE OF DECISION	FBH-A	FBH-B	FBH-C	FBH-D*
Medical	4 (40)	7 (70)	3 (30)	3 (30)
Voluntary	6 (60)	3 (30)	7 (70)	6 (60)

*One subject (P5) remained suspended until test time limit of 60 min was achieved.

The suspension duration and the symptoms responsible for test termination are given in Table 4. Also indicated for each test is whether a medical or subject request terminated the test. Note that subject P5 on FBH-D achieved the 60 min mark and suspension ended due to the test time limit. It is most likely that subject P5 could have tolerated the test for a much longer duration. Six of ten suspensions in FBH-A were terminated by subject request. Seventy percent of FBH-B tests were discontinued by a medical decision. In FBH-C, 7 of 10 tests were ended by subject request. Also, 60 percent of all tests in FBH-D were terminated by subject request.

TABLE 4

INDIVIDUAL SUSPENSION DURATIONS AND SYMPTOMS
RESPONSIBLE FOR TEST TERMINATIONS

SUBJECT ID	FBH-A	FBH-B	FBH-C	FBH-D
B1	17.42s (N)	21.65s (O)	40.68s (K)	27.50s (C)
D5	6.08s (F)	11.70m (A,C)	24.83s (A,E,N)	12.83m (C,F)
K3	17.00s (I)	17.10m (C)	43.83s (N)	29.80s (N)
K5	3.47m (D,F)	37.50s (O)	10.2m (D)	4.33m (D,A)
L3	26.42s (L)	24.30m (C,A,F)	31.90s (O,A)	25.83s (A)
M18	5.90s (A)	5.50m (A,G)	14.83s (A,E)	18.70s (A)
P5	17.10m (A)	19.62m (D,A)	38.50s (M)	60.00x
S3	32.00m (D,C)	21.50m (D)	49.80m (D,E)	44.27s (A,E,C)
T4	10.50m (H)	7.00m (B)	22.00m (B)	14.90m (C)
Z2	18.90s (A)	8.23s (A)	15.33s (A,E)	37.33s (A,E,O)

NOTE: Durations given in decimal minutes.

Small case letters: s - indicates subject request
m - indicates medical monitor request
x - indicates test time limit

KEY TO SYMPTOM CODE:

- | | |
|---------------------------------|------------------------------|
| A - Nausea | H - Drowsiness |
| B - Difficulty Breathing | I - Strap Pressure: Groin |
| C - Light-Headedness | J - Strap Pressure: Ribs |
| D - Decreased Heart Rate | K - Strap Pressure: Buttocks |
| E - Change in Thermal Sensation | L - Overall Discomfort |
| F - Change in Vision | M - Muscular Fatigue |
| G - Change in Skin Color | N - Limb Paresthasias |
| | O - Lower Limb Discomfort |

The recurrence of symptoms of light-headedness, nausea, respiratory difficulty, and diaphoresis for the four harnesses is given in Table 5. Diaphoresis occurred with marked frequency in all the harness designs but FBH-C. Nausea presented with high frequency in all but FBH-A. Respiratory difficulty occurred in 3 out of 10 tests. Light-headedness did not present as a symptom in any suspension test of FBH-C and occurred with highest frequency in FBH-D.

TABLE 5
 RECURRENCE OF SELECTED SYMPTOMS DURING EXPERIMENT

SYMPTOM	FBH-A	FBH-B	FBH-C	FBH-D
Light-Headedness	2 (20)	3 (30)	0 (0)	4 (40)
Nausea	3 (30)	5 (50)	5 (50)	5 (50)
Respiratory Difficulty	2 (20)	2 (20)	3 (30)	3 (30)
Diaphoresis	5 (50)	6 (60)	3 (30)	6 (60)

Table 6 indicates the occurrence of numbness and tingling in the limbs or technically defined as extremity paresthesias. Paresthesias occurred with low frequency in the extremities in FBH-C. Upper extremity numbness and tingling occurred most frequently in FBH-B. Also lower extremity numbness presented the most repeatedly in FBH-B. Tingling in the lower extremity recurred repeatedly in FBH-D.

Recurrence of harness pressure at specific body regions is given in Table 7. Note that although strap pressure in the groin area occurred with great frequency in FBH-C it never progressed to the intolerable stage to end a suspension. The buttock sling of FBH-B

delivers considerable pressure in most occupants. FBH-A and FBH-D produced pressure points in the groin region in most users.

TABLE 6
FREQUENCY OF OCCURRENCE OF PARESTHESIAS IN THE EXTREMITIES

SYMPTOMS	FBH-A	FBH-B	FBH-C	FBH-D
Upper Extremity Numbness	4 (40)	4 (40)	2 (20)	3 (30)
Lower Extremity Numbness	6 (60)	7 (70)	6 (60)	6 (60)
Upper Extremity Tingling	4 (40)	7 (70)	3 (30)	5 (50)
Lower Extremity Tingling	6 (60)	5 (50)	5 (50)	9 (90)

TABLE 7
RECURRENCE OF HARNESS PRESSURE AT SPECIFIC BODY REGIONS

	FBH-A	FBH-B	FBH-C	FBH-D
Abdomen	1 (10)	4 (40)	0 (0)	1 (10)
Back	0 (0)	0 (0)	0 (0)	1 (10)
Buttocks	1 (10)	6 (60)	5 (50)	2 (20)
Chest	1 (10)	1 (10)	1 (10)	1 (10)
D-Ring	0 (0)	0 (0)	0 (0)	1 (10)
Groin	9 (90)	2 (20)	7 (70)	6 (60)
Hip	0 (0)	0 (0)	2 (20)	2 (20)
Shoulders	2 (20)	2 (20)	2 (20)	0 (0)

Twice the electrode placement on subject S3 yielded EKG output which was indecipherable and the test was repeated until useful data was acquired. Thus this experiment is based on forty data collections.

Cardiac dysrhythmias that were observed included tachycardia, relative bradycardia, and premature ventricular contractions.

VI. RECOMMENDATIONS

Orzech, Goodwin, and Brinkley (2) defined a plausible mechanism responsible for limiting human tolerance to vertical suspension in the first phase of this study. The additional data from this Phase 2 experiment supports the idea that the skeletal muscle pump is inactivated during motionless suspension and thus cannot maintain circulation or return blood to the heart and central circulation. Another mechanism which can result in the clinical findings associated with motionless suspension is the vasovagal response. During a vasovagal event, patients may experience hypotension, bradycardia, and loss of consciousness in response to environmental stresses. The bradycardia is the result of vagal stimulation. Other symptoms indicating a vasovagal attack are pallor, nausea, sweating, and abdominal discomfort arising from sympathoadrenal and vagal responses. Loss of consciousness occurs as a result of cerebral ischemia from hypotension. The symptoms of light-headedness, dizziness, or feeling faint are attributed to the presence of hypotension are a result of either mechanism described above. When both of these mechanisms are present the effect is additive and can result in a considerable drop in blood pressure. Thus a harness occupant with cardiovascular disease may be at increased risk during motionless suspension.

The symptom of paresthesia of the extremities is a result of decreased blood flow to the extremities and/or direct pressure on the nerves supplying the limbs.

Each subject was asked to identify the most tolerable and least tolerable harness when he/she had completed suspension in all four harnesses. FBH-C was selected by 8 of 10 subjects as most tolerable because it provided even weight distribution. Two of ten subjects considered FBH-D most tolerable due to no outstanding pressure points developing and that they settled on FBH-D immediately with no further slipping. No harness design stood far apart from the rest as the least tolerable. Each harness design received at least one recommendation to make it more tolerable to the suspended occupant. Some of the complaints included asymmetrical weight distributions on the harness straps creating pain and/or decreasing circulation to the extremities, thus increasing the onset of symptoms. Two of the subjects had no preference as to the least tolerable harness design.

From the data acquired and analyzed in this Phase 2 study of prolonged motionless suspension the optimal harness configuration in terms of occupant safety and tolerability would be a full body harness that distributes the strap pressure evenly and symmetrically over bony structures and large areas of the body. A lattice network across the chest connecting the shoulder straps and displacing the load of the shoulder straps over a larger surface area would be advised. FBH-C demonstrated a design similar to this with a single strap crossing the chest between the shoulder straps. The buttock sling is necessary to provide a seat for the buttocks and relieve pressure in the groin area. Decreased pressure in the groin area would alleviate many of the reported symptoms of the lower extremities. The rubber hip ring would be most tolerable by the occupant than the metal hip rings as

FBH-B demonstrated. Finally, the plastic spreader utilized by FBH-C at the shoulder strap/D-ring interface is also desirable to distribute the straps most evenly as in a parachute harness.

The next phase of research in the area of fall protection harnesses should be the study of the human inertial response to tethered fall. This study would provide insight on the location of maximum energy absorption on the human body and the values of these energy impulses.

REFERENCES

1. McClare, J.T., F.H. Dietrich, II, Statistics, San Francisco, Dellent Publishing Company, 1985.
2. Orzech, M.A., M.D. Goodwin, J.W. Brinkely, et al., "Evaluation of Fall Protection Equipment by Prolonged Motionless Suspension of Volunteers," SAFE, Summer Quarter 1987, Vol 17, No. 2, pp. 46-53.
3. Stein, Emanuel, Clinical Electrocardiography, Philadelphia, Len & Febiger Publishers, 1987.

MR. DOUGLAS WISE
FINAL REPORT NUMBER 101
LATE START DATE
REPORT TO BE SUBMITTED LATER